

Fábio Daniel Pedroso de Lima da Conceição

Novel chromene and imidazole derivatives: Synthesis, biological evaluation and computational studies

Uminho | 2021





University of Minho
School of Sciences

Fábio Daniel Pedroso de Lima da Conceição

Novel chromene and imidazole derivatives: Synthesis, biological evaluation and computational studies

November 2021

University of Minho
School of Sciences

Fábio Daniel Pedroso de Lima da Conceição

Novel chromene and imidazole derivatives: Synthesis, biological evaluation and computational studies

Doctoral thesis in Chemistry
Specialization in organic and biological chemistry

Work performed under the supervision of
Professor Maria Fernanda Proença
and of
Professor Concepción González-Bello

November 2021

DIREITOS DE AUTOR E CONDIÇÕES DE UTILIZAÇÃO DO TRABALHO POR TERCEIROS

Esta licença permite que outros remisturem, adaptem e criem a partir do seu trabalho, mesmo para fins comerciais, desde que lhe atribuam o devido crédito e que licenciem as novas criações ao abrigo de termos idênticos. Esta licença costuma ser comparada com as licenças de software livre e de código aberto «copyleft». Todos os trabalhos novos baseados no seu terão a mesma licença, portanto quaisquer trabalhos derivados também permitirão o uso comercial. Esta é a licença usada pela Wikipédia e é recomendada para materiais que seriam beneficiados com a incorporação de conteúdos da Wikipédia e de outros projetos com licenciamento semelhante



Atribuição-SemDerivações CC BY-ND
https://creativecommons.org/licenses/by-nd/4.0/

Acknowledgements

First, I would like to thank my supervisors. To Prof. Maria Fernanda Proença, for all the dedication and patience to teach me and guide me. For the passion that has transmitted me in every single mechanism and «moment of happiness», and the joy with what has always guided me throughout this journey. For all the tolerance and teachings, even in the most complicated moments, and for her availability at any time. To Prof. Concepción González-Bello for all the help and for receiving me in her group with open arms. For all the guidance, tolerance, comprehension, and opportunities that have given me. For all the teachings that passed me, as well as the rigor and clearance of thought that taught me to have.

To Dr. Emílio Lence, for all the help, friendship, and patience to teach me how to perform the calculations and to correct me when I needed, as well as for all the availability to help me throughout the process.

To Drª Marta Costa, I thank the kindness and availability with which always helped me. To her, along with Master Ana Luísa Carvalho, I thank the biological evaluation of the anticancer activity for triple-negative breast cancer treatment, and to Prof. Dr. Maria Fernanda Proença the opportunity to perform them.

To Prof. José António Aínsa (Universidad de Zaragoça), I thank the biological evaluation of the antitubercular activity, and to Prof. Concepción González-Bello for the opportunity to perform them.

To Drª Carla Calçada and her group, I thank the biological evaluation of the antimalarial activity, and to Prof. Dr. Maria Fernanda Proença the opportunity to perform them.

I would also like to acknowledge the financial support from Programa NORTE 2020 - CCDR-N (ref. NORTE-08-5369-FSE-000033; scholarship UMINHO/BD/42/2016) and thank for the opportunity to develop my work and my PhD.

Statement of Integrity

I hereby declare having conducted my thesis with integrity. I confirm that I have not used any plagiarism or any form of falsification of results in the process of the thesis elaboration.

I further declare that I have fully acknowledged the Code of Ethical Conduct of the University of Minho.

Braga, 11th November, 2021



(Fábio Daniel Pedroso de Lima da Conceição)

RESUMO

A investigação de compostos bioactivos que possam levar ao desenvolvimento de novas alternativas terapêuticas para algumas das patologias mais nefastas a nível mundial continua, nos dias de hoje, a ser uma necessidade no ramo da Química Medicinal. Nesta pesquisa, algumas moléculas presentes na natureza são usadas como ponto de partida para o desenvolvimento de novos compostos promissores. Neste âmbito, os cromenos e os imidazóis são amplamente reconhecidos como estruturas interessantes. Estão descritos na literatura vários derivados de cromenos e imidazóis que apresentam actividade biológica no tratamento de uma vasta gama de patologias (p. ex. anticancerígeno, antibiótico, antimicrobiano, antiviral, etc).

Neste trabalho, foi explorada a reactividade de 2*H*- e 4*H*-cromenos, que levou ao desenvolvimento de novos derivados, como por exemplo cromeno[2,3-*d*]pirimidin-4(5*H*)-onas, cromeno[2,3-*d*]pirimidin-4(3*H*)-onas e 5-imino-*N*,2-diaril-5*H*-cromeno[3,4-*c*]piridin-4-aminas. Foram também preparados outros compostos promissores como por exemplo 5-(2-hidroxiaril)-7-arilpirido[2,3-*d*]pirimidin-4(1*H*)-ones e 1-aril-2-(4-(arilamino)-5*H*-cromeno[2,3-*d*]pirimidin-5-il)etanonas, e novos derivados de 5-ciano-1-(2-hidroxibenzil)-1*H*-imidazol-4-carboxamidas. Foi estudado o mecanismo que levou à formação de 5-imino-*N*,2-diaril-5*H*-cromeno[3,4-c]piridin-4-aminas, 5-(2-hidroxiaril)-7-arilpirido[2,3-*d*]pirimidin-4(1*H*)-onas e 5-ciano-1-(2-hidroxibenzil)-1*H*-imidazol-4-carboxamidas e o mecanismo deste último foi também estudado com recurso a metodologias computacionais.

Foi avaliada uma selecção de compostos relativamente ao seu potencial no tratamento do cancro da mama triplo negativo (TNBC), tuberculose (*M.tuberculosis*) e malária (*plasmodium falciparum*), e algumas moléculas apresentaram resultados promissores. Foi ainda realizado um conjunto de estudos de *docking* molecular e de dinâmica molecular, tendo como ponto de partida os resultados de actividade biológica obtidos para as cromeno[2,3-*d*]pirimidin-4(5*H*)-onas contra o cancro da mama triplo negativo, o que permitiu o desenvolvimento de um modelo preliminar de relação estrutura-actividade para este grupo de compostos, nesta patologia.

Palavras-chave: Cromenos; imidazóis; anticancerígeno; antimicrobiano; antimalárico; *in silico*; *docking* molecular; Dinâmica molecular; relação estrutura-atividade.

ABSTRACT

The search for bioactive compounds that can lead to novel therapeutic alternatives to some of the most devastating diseases is still an important research topic in Medicinal Chemistry. In this search, some naturally occurring scaffolds are used as inspiration for the development of new drug candidates and among those, chromenes and imidazoles are widely studied and recognized as interesting scaffolds. Several chromene and imidazole derivatives have been described in the literature, where their biological activity against a wide range of diseases (e.g. anticancer, antibiotic, antimicrobial, antiviral, etc) is identified.

In this work, the reactivity of 2*H*- and 4*H*-chromenes was explored, which led to the development of novel derivatives, such as chromene[2,3-*d*]pyrimidin-4(5*H*)-ones, chromene[2,3-*d*]pyrimidin-4(3*H*)-ones and 5-imino-*N*,2-diaryl-5*H*-chromeno[3,4-c]pyridin-4-amines. Other promising compounds based on other scaffolds, such as 5-(2-hydroxyaryl)-7-arylpyrido[2,3-*d*]pyrimidin-4(1*H*)-ones and 1-aryl-2-(4-(arylamino)-5*H*-chromeno[2,3-*d*]pyrimidin-5-yl)ethanones, as well as 2-substituted 5-cyano-1-(2-hydroxybenzyl)-1*H*-imidazole-4-carboxamides were also prepared. The mechanism that leads to the formation of 5-imino-*N*,2-diaryl-5*H*-chromeno[3,4-c]pyridin-4-amines, 5-(2-hydroxyaryl)-7-arylpyrido[2,3-*d*]pyrimidin-4(1*H*)-ones and 2-substituted 5-cyano-1-(2-hydroxybenzyl)-1*H*-imidazole-4-carboxamides was studied, and for the imidazole derivatives the mechanistic proposal was supported by computational studies.

A selection of the prepared compounds was evaluated for their potential as anticancer agents using triple-negative breast cancer cell lines (TNBC), as antituberculosis agents (*M.tuberculosis*) and as antimalarial agents (*Plasmodium falciparum*), some of them with promising results. Studies on molecular docking and molecular dynamics were also performed, based on the results obtained for the anticancer activity of chromene[2,3-*d*]pyrimidin-4(5*H*)-ones, allowing the development of a preliminary structure-activity relationship (SAR) model for this group of compounds and for this disease.

Keywords: Chromene; imidazole; anticancer; antimicrobial; antimalarial; *in silico*; molecular docking; molecular dynamics; structure-activity relationship.

Index

Acknowledgments iii
Statement of integrity iv
Resumo v
Abstract vi
Index vii
List of abbreviations xi
List of figures xv
List of tables xxiv
List of schemes xxxi

Chapter 1: Introduction 1
1.1 Chromene scaffold 2
1.1.1 Biological importance of the chromene moiety 3
1.1.2 Synthetic approaches for the chromene scaffold 7
1.1.3 Chromenopyridines: synthesis and biological importance 9
1.2 Imidazole scaffold 13
1.2.1 Biological importance of the imidazole moiety 17
References 18

Chapter 2: Synthesis of 2*H*-chromene, 4*H*-chromene and 1*H*-imidazole derivatives 27
2.1 2- and 3-substituted 2*H*- and 4*H*-chromenes 28
2.1.1 Synthesis and reactivity of 2-imino-2*H*-chromene-3-carboxamides 28
Synthesis of chromeno[2,3-*d*]pyrimidin-4(5*H*)-ones and chromeno[2,3-*d*]pyrimidin-4(3*H*)-ones 31
Physical, analytical and spectroscopical characterization 40
Water-soluble salt formation 65

2.1.2 Synthesis and reactivity of 2-imino-2*H*-chromen-3-amines and 2-oxo-2*H*-chromen-3-amines 68

Synthesis of 3-(aryldeneamino)-2*H*-chromen-2-ones and 3-(alkylideneamino)-2*H*-chromen-2-ones 71

Synthesis of 2-(5-methoxy-1,9-dihydrochromeno[2,3-*d*]imidazole-9-yl)malononitrile 76

Physical, analytical and spectroscopical characterization 78

2.1.3 Synthesis and reactivity of 2-amino-4-(2-oxo-2-arylethyl)-4*H*-chromene-3-carbonitriles 83

Synthesis of 2-amino-4-(2-oxo-2-arylethyl)-4*H*-chromene-3-carbonitriles 85

Reactivity of 2-amino-4-(2-oxo-2-arylethyl)-4*H*-chromene-3-carbonitriles in aqueous acidic conditions 87

Reactivity of 2-amino-4-(2-oxo-2-arylethyl)-4*H*-chromene-3-carbonitriles with primary amines: synthesis of novel 6-imino-*N*,9-diaryl-6*H*-benzo[c]chromen-7-amines and 6-oxo-*N*,9-diaryl-6*H*-benzo[c]chromen-7-amines 90

Reactivity of 2-amino-4-(2-oxo-2-arylethyl)-4*H*-chromene-3-carbonitriles in aqueous base 114

Reactivity of 2-amino-4-(2-oxo-2-arylethyl)-4*H*-chromene-3-carbonitriles with phenyl-hydrazine 122

Physical, analytical and spectroscopical characterization 125

2.1.4 Synthesis and reactivity of ethyl *N*-(3-cyano-4-(2-arylethyl)-4*H*-chromen-2 yl)formimidate 162

Synthesis of ethyl *N*-(3-cyano-4-(2-arylethyl)-4*H*-chromen-2-yl)formimidates 163

Reactivity of ethyl *N*-(3-cyano-4-(2-arylethyl)-4*H*-chromen-2-yl)formimidates with primary amines 165

Studies on the reactivity of *N*-(3-cyano-4-(2-arylethyl)-4*H*-chromen-2-yl)formimida-mides 178

Discussion on possible reaction mechanism 186

Reaction of ethyl *N*-(3-cyano-4-(2-arylethyl)-4*H*-chromen-2-yl)formimidates with phenyl hydrazine 199

Reaction of ethyl *N*-(3-cyano-4-(2-arylethyl)-4*H*-chromen-2-yl)formimidates ammonium acetate 201

Physical, analytical and spectroscopical characterization 203

2.2 2-substituted 1*H*-imidazole-4-carboxamides 239

2.2.1 Synthesis of 2-substituted-5-cyano-1-(2-hydroxyaryl)-1*H*-imidazole-4-carboxamides 239

Diaminomaleonitrile as a precursor for substituted imidazoles and pyrazines 239

Synthesis and reactivity of 2-amino-3-(arylideneamino)maleonitriles with aldehydes 243

Synthesis of 2-substituted-5-cyano-1-(2-hydroxyaryl)-1*H*-imidazole-4-carboxamides and cyano-5,6-diaryl-1,6-dihydropyrazine-carboxamides 253

Synthesis of cyano-5,6-diphenyl-1,6-dihydropyrazine-carboxamides 254

Physical, analytical and spectroscopical characterization 255

References 271

Chapter 3: Biological evaluation and computational studies 281

3.1 Triple-negative breast cancer (TNBC) 282

3.1.1 Introduction 282

Cancer – relevance, incidence, and impact on human health 282

Molecular mechanisms and biochemical features of cancer 283

Breast cancer and triple-negative breast cancer 285

Current therapies and treatment 289

3.1.2 Biological evaluation of chromene-based and imidazole-based compounds activity against TNBC cell lines 289

3.1.3 Structure-activity relationship of chromene[2,3-*d*]pyrimidin-4(5*H*)-ones and chromeno[2,3-*d*]pyrimidin-4(3*H*)-ones 2.3 and 2.6 297

3.1.4 *In silico* study of the potential of chromene[2,3-*d*]pyrimidin-4(5*H*)-ones and chromeno[2,3-*d*]pyrimidin-4(3*H*)-ones 2.6 as PARP inhibitors 304

Importance of BRCA genes and PARP inhibition in TNBC 304

Structure-activity relationship in PARP inhibitors 307

Molecular docking studies 310

Molecular dynamics simulations 315

MMPBSA studies 322

3.2 Tuberculosis 324

3.2.1 Tuberculosis – challenges and impact on human health 324

Current therapies and treatment 327

3.2.2 Biological evaluation of chromene-based and imidazole-based compounds activity against *M.tuberculosis* 328

3.3 Malaria 329

3.3.1 Malaria – challenges and impact on human health 329

Current therapies and treatment 330

3.3.2 Biological evaluation of chromene-based and imidazole-based activity compounds against *Plasmodium falciparum* 332

3.4 Computational studies on the reaction mechanism of 2-substituted 5-cyano-1-(2-hydroxybenzyl)-1*H*-imidazole-4-carboxamides 338

3.4.1 Step 1: intramolecular cyclization 341

3.4.2 Step 2: aromatization 346

References 350

Chapter 4: Conclusions and final remarks 359

Chapter 5: Experimental section 366

List of abbreviations

Ac – Acetyl group

AChE – Acetylcholinesterase

AcOH – Acetic acid

ACP – Acyl carrier protein

AIDS – Acquired immunodeficiency syndrome

Akt – Protein Kinase B

BACE – β-site Amyloid Precursor Protein Cleaving Enzyme

BBB – Blood-brain barrier

BCG – Bacillus Calmette–Guérin

BChE – Butyrylcholinesterase

Bcl-2 – B-cell lymphoma 2

BH – Bcl2 homology

Bid – BH-3 interacting-domain death agonist

CDK – Cyclin-Dependent kinase

CSC – Cancer stem cells

CuOTf – Copper(I) trifluoromethanesulfonate

DCM – Dichloromethane

Dec. – Decomposition

DMSO – Dimethyl sulphoxide

DNA – Deoxyribonucleic acid

ED – Effective dose

EGFR – Epidermal growth factor receptor

EMA – European Medicines Agency

ER – Estrogen receptor

ERK – Extracellular signal-regulated kinase

Et – Ethyl group

Et_3N – Triethylamine

EtOAc – Ethyl acetoacetate

EtOH – Ethanol

FADD – Fas-associated Protein with Death Domain

Fas – Fibroblasti-associated cell surface

FasL – Fibroblasti-associated cell surface ligand

FDA – Food and Drug administration

GB – Generalized Born

GLOBOCAN – Global Cancer Observatory

HDI – Human developing index

HDI – Human development index

HER - Human epidermal growth factor receptor

HIV – Human immunodeficiency virus

IC – Inhibitory concentration

IHC – Immuno histocompatibility complex

IR – infrared

IRC – Internal reaction coordinate

IUPAC - International Union of Pure and Applied Chemistry

IUPAC – International Union of Pure and Applied Chemistry

JAK – Janus kinase

K_i – Inhibitory constant

MCR – Multi-component reaction

MD – Molecular Dynamics

MDR – Multi-drug resistant

MDR-TB – Multi-drug resistant tuberculosis

Me – Methyl group

MeCN - Acetonitrile

MEK – Mitogen-activated protein kinase kinase

MeMgCl – Methylmagnesium chloride

MeOH – Methanol

MIC – Minimum inhibitory concentration

MMGBSA – Molecular mechanics with generalised Born and surface area solvation

MMPBSA – Molecular mechanics Poisson-Boltzmann surface area

mTOR – Mammalian target of rapamycin

NAD – Nicotinamide adenine dinucleotide

NMP – *N*-methylpiperazine

NMR – Nuclear magnetic resonance

nRTK – Non-receptor tyrosine kinases

NSAID – Non-steroidal anti-inflammatory drug

OEt – Ethoxyl group

OMe – Methoxyl group

PAR – Poly(ADP-ribose)

PARPi – PARP inhibitors

PB – Poisson-Boltzmann

PES – Potential energy surface

PfPI3K – *Plasmodium falciparum* phosphoinositide 3-kinase

PI3K– Phosphoinositide 3-kinase

pK_a – Acid Dissociation constant

PME – Particle mesh Ewald

PPA – Polyphosphoric Acid

PPTS – Pyridinium p-toluenesulfonate

PR – Progesterone receptor

R&D – Resesrch and development

RHF – Restricted Hartree-Fock

RNA – Ribonucleic acyd

SAR – Structure-activity relationship

SRB – Sulforhodamine B assay

STAT – Signal transducer and activator of transcription proteins

TB – Tuberculosis

***t*-BuOK** – Potassium tert-butoxide

TEOF – Triethyl orthoformate

THF – Tetrahydrofuran

TLC – Thin layer chromatography

$TMSCH_2Li$ – Trimethylsilylmethyllithium

TNBC – Triple-negative breast cancer

TNF – Tumor necrosis factor

TRAIL – TNF-related apoptosis-induced ligand

TS – Transition state

VEGF – Vascular endothelial growth factor

WHO – World health organization

XDR-TB – Extensively drug resistant tuberculosis

List of Figures

Chapter 1

Figure 1: General chemical structures of 1-benzopyrans, 2-benzopyrans and 2*H*- and 4*H*-chromenes...2

Figure 2: Chemical structure of naturally occurring neo-tanshinlactone, asphodelin A and macluraxanthone with biological activity [ref.28] 3

Figure 3: Chemical structures of bioactive gramniphenols **1.1** and **1.2a,b**, extracted from *Arundina gramnifolia* [ref.32] 4

Figure 4: Chemical bioactive gramniphenols **1.3a-c**, chromene-based **1.4**, and compound **1.5** [ref. 33-36]. The MIC values of **1.5** against virulent M. tuberculosis is also included 4

Figure 5: Chemical structure of compounds **1.6** and **1.7**, highlighted by Parthiban *et al* as potential antimalarial agents, with their respective IC_{50} values [ref. 37] 5

Figure 6: Chemical structures of compounds 1.8 and 1.9, highlighted by Patil et al as potentially active gainst melanoma and prostate cancer, and compounds 1.10 and 1.11, developed by Yin et al as PI3K inhibitors [ref.29, 38] 5

Figure 7: Chemical structures of psoralidin and isoscopoletin [ref. 40-42,45].....6

Figure 8: Chemical structures of pavietin and compound 1.12 [ref. 28,55-57].....7

Figure 9: Examples of approved drugs that incorporate a chromenopyridine moiety 9

Figure 10: Examples of chromenopyridines synthesized by Ibrahim et al [adapted from ref. 85].....10

Figure 11: Chemical structure of topoisomerase II inhibitors **1.43a-i** designed by Thapa *et al* and Magdar *et al* [ref. 92-94].....13

Figure 12: Chemical structure of imidazole, guanine, adenine, histidine, and histamine 14

Figure 13: Chemical structure of metronidazole and clotrimazole 17

Figure 14: Chemical structure of bioactive compounds containing the imidazole moiety [ref. 125-129] 18

Chapter 2

Figure 15: Selection of bioactive compounds described by Hadfield *et al*. The corresponding IC_{50} values obtained for each cancer cell line are indicated [adapted from ref.3].....29

Figure 16: ^{1}H NMR (400 MHz, DMSO-d_6, δ ppm) spectrum of compound **2.6a**, in which some relevant signals are highlighted 36

Figure 17: ^{13}C NMR (100 MHz, DMSO-d_6, δ ppm) spectrum of compound **2.6a**, in which some relevant signals are highlighted 36

Figure 18: 1D transient NOE (400 MHz, DMSO-d_6) spectrum obtained after inversion of the signal

δ12.82 ppm in compound **2.6x** (R1=R2=R3=H).....65
Figure 19: Chemical structures of novobiocin, coumermycin A1 and clorobiocin 69
Figure 20: Chemical structure of the synthesized compounds **2.22a** and **2.25a** 70
Figure 21: ^{1}H NMR (400 MHz, DMSO-d_6, δ ppm) spectrum of compound **2.27** in which some signals are highlighted 73
Figure 22: ^{13}C NMR (100 MHz, DMSO-d_6, δ ppm) spectrum of compound **2.27** in which some signals are highlighted 73
Figure 23: ^{1}H NMR (400 MHz, DMSO-d_6, δ ppm) spectrum of compound **2.28** in which some signals are highlighted 74
Figure 24: ^{13}C NMR (100 MHz, DMSO-d_6, δ ppm) spectrum of compound **2.28** in which some signals are highlighted 74
Figure 25: ^{1}H NMR (400 MHz, DMSO-d_6, δ ppm) spectrum of compound **2.29** in which some signals are highlighted 75
Figure 26: ^{1}H NMR spectrum (400 MHz, DMSO-d_6, δ ppm) of a freshly prepared sample of compound **2.29** in DMSO-d_6, taken after obtaining ^{13}C NMR and bidimensional correlation spectra, where compound **2.25a** can be identified 75
Figure 27: ^{1}H NMR (400 MHz, DMSO-d_6, δ ppm) spectrum of compound **2.35** in which some signals are highlighted 77
Figure 28: ^{13}C NMR (100 MHz, DMSO-d_6, δ ppm) spectrum of compound **2.35** in which some signals are highlighted 78
Figure 29: Chemical structure of (4*R*)-2,7,8-triamino-4-(3-bromo-4,5-dimethoxyphenyl)-4*H*-chromene-3-carbonitrile(crolibulin) 84
Figure 30: ^{1}H NMR (400 MHz, DMSO-d_6, δ ppm) spectrum of **2.50a**.....88
Figure 31: Expansion of the ^{1}H NMR (400 MHz, DMSO- d_6, δ ppm) spectrum of **2.50a** between δ5.25-3.50 ppm 89
Figure 32: ^{1}H NMR (400 MHz, DMSO-d_6, δ ppm) spectrum of compound **2.55a**, in which some signals are highlighted 94
Figure 33: ^{13}C NMR (100 MHz, DMSO-d_6, δ ppm) spectrum of compound **2.55a**, in which some signals are highlighted 94
Figure 34: ^{1}H NMR (400 MHz, DMSO-d_6, δ ppm) spectrum of compound **2.56a** in which some signals are highlighted 95
Figure 35: ^{13}C NMR (100 MHz, DMSO-d_6, δ ppm) spectrum of compound **2.56a** in which some signals are highlighted 95

Figure 36: Representation of the expected intramolecular hydrogen bonding interaction between the NH group and the imine group or ketone groups in **2.55a** and **2.56a**, respectively 96

Figure 37: ^{1}H NMR (400 MHz, DMSO-d_6, δ ppm) spectrum of a mixture of compounds **2.39e** and **2.60a**, in which several signals of compound **2.39** (black circles) and of **2.60a** (blue circles) are high-lighted 97

Figure 38: ^{13}C NMR (100 MHz, DMSO-d_6, δ ppm) spectrum of a mixture of compounds **2.39e** and **2.60a**, in which several signals of compound **2.39** (black circles) and of **2.60a** (blue circles) are high-lighted 97

Figure 39: A: ^{1}H NMR (400 MHz, DMSO-d_6,, δ ppm) spectrum of compound **2.61a**, in which several signals are highlighted. **B:** ^{1}H NMR (400 MHz, DMSO-d_6,, δ ppm) spectrum of a mixture of compounds **2.60a** and **2.61a**, generated from a sample of **2.61a**, in DMSO-d_6, while collecting the ^{13}C NMR (100 MHz, DMSO-d_6, δ ppm) spectra, in which several signals of compound **2.60a** (blue circles) and of **2.61a** (red circles) highlighted 101

Figure 40: ^{13}C NMR (100 MHz, DMSO-d_6, δ ppm) spectrum of a mixture of compounds **2.60a** and **2.61a**, generated from a sample of **2.61a**, in DMSO-d_6, in which several signals of compound **2.61a** (red circles) highlighted 102

Figure 41: ^{1}H NMR (400 MHz, DMSO-d_6, δ ppm) spectrum of the crude solid obtained from the reaction described in **Table 38** (entry 5), with the identification of several signals belonging to compounds **2.55x**, **2.56j** and **2.57c** 109

Figure 42: HMBC NMR (100 MHz, DMSO-d_6, δ ppm) spectrum of the crude solid obtained from the reaction described in **Table 38** (entry 5), with the identification of the signals belonging to compounds **2.55x**, **2.56j** and **2.57c** 109

Figure 43: ^{1}H NMR (400 MHz, DMSO- d_6, δ ppm) spectrum recorded form the crude product of the reaction described in entry 6 (**table 39**) after 14.66 h of reaction. Among the observed mixture, it is possible to observe the same pattern belonging to compounds **2.55b'** (blue circles), **2.60d** (red circles) and **2.61b** (black circles circles) 111

Figure 44: ^{1}H NMR (400 MHz, DMSO- d_6, δ ppm) spectrum recorded form the crude product of the reaction described in entry 6 (**table 39**) after 20.66 h of reaction. Among the observed mixture, it is possible to observe the same pattern belonging to compounds **2.55b'** (blue circles), **2.60d** (red circles) and **2.61b** (black circles circles) 112

Figure 45: ^{1}H NMR (400 MHz, DMSO- d_6, δ ppm) spectrum recorded form the crude product of the reaction described in entry 6 (**table 39**) after 26.66 h of reaction. Among the observed mixture, it is possible to observe the same pattern belonging to compounds **2.55b'** (blue circle) and traces of **2.60d** (red circles) 112

Figure 46: ^{1}H NMR (400 MHz, DMSO-d_6, δ ppm) spectrum of compound **2.69a**, in which two signals are highlighted 116
Figure 47: ^{13}C NMR (100 MHz, DMSO-d_6, δ ppm) spectrum of compound **2.69a**, in which several signals are highlighted 117
Figure 48: ^{1}H NMR (400 MHz, DMSO-d_6, δ ppm) spectrum of compound **2.71a**, in which two signals are highlighted 119
Figure 49: ^{13}C NMR (100 MHz, DMSO-d_6, δ ppm) spectrum of compound **2.71a**, in which several signals are highlighted 119
Figure 50: ^{1}H NMR (400 MHz, DMSO-d_6, δ ppm) spectrum of compound **2.82a**, in which several signals are highlighted 124
Figure 51: ^{13}C NMR (100 MHz, DMSO-d_6, δ ppm) spectrum of compound **2.82a**, in which several signals are highlighted 124
Figure 52: ^{1}H NMR (400 MHz, DMSO-d_6, δ ppm) spectrum of compound **2.85a**, in which several signals are highlighted 164
Figure 53: ^{13}C NMR (100 MHz, DMSO-d_6, δ ppm) spectrum of compound **2.85a**, in which several signals are highlighted 164
Figure 54: ^{1}H NMR (400 MHz, DMSO-d_6, δ ppm) spectrum of compound **2.86b**, in which several signals are highlighted 169
Figure 55: ^{13}C NMR (100 MHz, DMSO-d_6, δ ppm) spectrum of compound **2.86b**, in which several signals are highlighted 169
Figure 56: ^{1}H NMR (400 MHz, DMSO-d_6, δ ppm) spectrum of compound **2.87b**, in which the amidine NH and CH signals, for both tautomers, are highlighted.....175
Figure 57: ^{13}C NMR (100 MHz, DMSO-d_6, δ ppm) spectrum of **2.87b**, in which several signals, for both tautomers, are highlighted.....176
Figure 58: ^{1}H NMR (400 MHz, DMSO-d_6, δ ppm) spectrum of compound **2.88a**, in which several signals, are highlighted 180
Figure 59: ^{13}C NMR (100 MHz, DMSO-d_6, δ ppm) spectrum of **2.88a**, in which several signals are highlighted.....181
Figure 60: ^{1}H NMR (400 MHz, DMSO-d_6, δ ppm) spectrum of compound **2.89a**, in which several signals, are highlighted 182
Figure 61: ^{13}C NMR (100 MHz, DMSO-d_6, δ ppm) spectrum of **2.89a**, in which several signals are highlighted.....182
Figure 62: ^{1}H NMR (400 MHz, DMSO-d_6, δ ppm) spectrum of compound **2.90**, in which several signals, are highlighted 183

Figure 63: ^{13}C NMR (100 MHz, DMSO-d_6, δ ppm) spectrum of **2.90**, in which several signals are highlighted.....183

Figure 64: ^{1}H NMR (400 MHz, DMSO-d_6, δ ppm) spectrum of a mixture of compounds **2.55a**, **2.56a** and **2.86c**, obtained after heating an ethanolic solution of compound **2.88b** at 80 °C, for 12.5 hours 186

Figure 65: ^{1}H NMR (400 MHz, DMSO-d_6, δ ppm) spectrum of a mixture of compounds **2.86b** and **2.88a**, obtained after stirring a solution of compound **2.88c** in an (3:1) EtOH/H_2O, at room temperature for 16 h, and additional heating at 50 °C for 12.5 h. Two new doublets were also identified (black circles), along with signals from **2.86b** (blue circles) and **2.88a** (red circles) 187

Figure 66: ^{1}H NMR (400 MHz, DMSO-d_6, δ ppm) spectrum of compounds **2.86b**, obtained after heating the DMSO-d_6 sample containing the mixture, presented in **Figure 65**, at 80°C for 2.5 hours, with three signals highlighted 188

Figure 67: ^{1}H NMR (400 MHz, DMSO-d_6, δ ppm) spectrum of a mixture of compound **2.86c** (blue circles) and an unidentified compound (black circles), obtained after obtained after heating at 50 °C for 5 h of a suspension (100:5) EtOH/H_2O solution of compound **2.88c** in the presence of 0.5 equiv. of AcOH 189

Figure 68: **^{1}**H NMR (400 MHz, DMSO-d_6, δ ppm) spectrum of compounds **2.86c**, obtained after heating, at 80°C for 4 h, the sample containing the mixture, presented in **Figure 67**, in EtOH, with three signals highlighted 190

Figure 69: ^{1}H NMR (400 MHz, DMSO-d_6, δ ppm) spectrum of a mixture of compound **2.88a** (red circles) and an unidentified compound (black circles), obtained after heating a solution of compound **2.88a** in EtOH/H_2O (3:1), and in the presence of 0.5 equivalents of acetic acid at 80 °C for 20 min. 191

Figure 70: ^{1}H NMR (400 MHz, DMSO-d_6, δ ppm) spectrum of a mixture of compound **2.86b** (blue circles) and other unidentified compounds (black and green circles, for unknown n°1 and 2, respectively), obtained after heating a solution of compound **2.88a** in a (3:1) EtOH/H_2O, and in the presence of 0.5 equivalents of acetic acid at 80 °C for 2.33 h. 192

Figure 71: ^{1}H NMR (400 MHz, DMSO-d_6, δ ppm) spectrum of a mixture of compound **2.86b** (blue circles) and other unidentified compound (green circles), obtained after allowing compound **2.88a** to stir, at 80 °C, in an EtOH/ H_2O 3:1 system and in the presence of 0.5 equiv. of AcOH, for 4.33 hours.....193

Figure 72: ^{1}H NMR (400 MHz, DMSO-d_6, δ ppm) spectrum of a mixture of compounds **2.86b** (range circles) and **2.87b** (red and blue circles), obtained after heating a solution of compound **2.87b** in EtOH and in the presence of 0.5 equiv. of AcOH, at 80 °C for 7 h. Several signals are highlighted. 194

Figure 73: ^{1}H NMR (400 MHz, DMSO-d_6, δ ppm) spectrum of a mixture of compounds **2.86b** (blue circles) and an unidentified component (green circles, **unknown nº 2**), obtained after heating a solution

of compound **2.88a** in EtOH and in the presence of 0.5 equiv. of AcOH, at 80 °C for 7 h. Several signals are highlighted. 195

Figure 74: ^{1}H NMR (400 MHz, DMSO-d_6, δ ppm) spectrum collected from the crude product obtained after the addition of 1 equiv. of DBU to a suspension of **2.88a** in EtOH, at 80 °C, that was left stirring for 1.5 hours (400 MHz, DMSO-d_6, δ ppm. 196

Figure 75: ^{1}H NMR (400 MHz, DMSO-d_6, δ ppm) spectrum of compound **2.100a**, in which several signals are highlighted 200

Figure 76: ^{13}C NMR (100 MHz, DMSO-d_6, δ ppm) spectrum of **2.100a**, in which several signals are highlighted 200

Figure 77: ^{1}H and ^{13}C NMR (400 and 100 MHz, DMSO-d_6, δ ppm) spectra of compound **2.105** with H1 and H5 signals highlighted 202

Figure 78: ^{1}H NMR (400 MHz, DMSO-d_6, δ ppm) spectrum for compound **2.109a** 244

Figure 79: ^{13}C NMR (100 MHz, DMSO-d_6, δ ppm) spectrum for compound **2.109a** 245

Figure 80: A: ^{1}H NMR (400 MHz, DMSO-d_6, δ ppm) spectrum of the product obtained from the reaction of **2.109c** with 2-chlorobenzaldehyde (1.2 equiv.), in EtOH and at r.t. (96 h), in the presence of Et_3N (2 equiv.). Several signals were highlighted for compounds **2.112c** (red circles) and compounds **2.113b** and **2.114b** (blue circles) (entry 2 - **Table 105**); **B:** ^{1}H NMR (400 MHz, DMSO-d_6, δ ppm) spectrum of the same product after heating the sample at 80 °C for 0.5 h, with a full conversion to **2.113b** 249

Figure 81: A: ^{1}H NMR (400 MHz, DMSO-d_6, δ ppm) spectrum of the product obtained from the reaction of **2.109g** with 2-chlorobenzaldehyde (1.2 equiv.), in EtOH and at r.t. (96 h), in the presence of Et_3N (2 equiv.). Several signals were highlighted for compounds **2.112d** (red circles) and compounds **2.113c** and **2.114c** (blue circles) (entry 3 - **Table 105**); **B:** ^{1}H NMR (400 MHz, DMSO-d_6, δ ppm) spectrum of the same product after heating the sample in the NMR tube. Several signals were highlighted 250

Figure 82: A: ^{1}H NMR (400 MHz, DMSO-d_6, δ ppm) spectrum of the product obtained for compound **2.113d**, with some signals highlighted (black circles); **B**: ^{13}C NMR (100 MHz, DMSO-d_6, δ ppm) spectrum of the product obtained compound **2.113d**, with two signals highlighted (black circles) 251

Chapter 3

Figure 83: Charts presenting the distribution of cases and deaths for the 10 most common cancers for both sexes in 2020, according to GLOBOCAN 2020 [adapted from ref.2] 282

Figure 84: The cancer hallmarks according to Hananah and Weinberg [adapted from ref.12] 284

Figure 85: Compounds employed in assays with MCF-7 cancer cell lines 293

Figure 86: Ring nomenclature for compounds **2.3** and **2.6** 297

Figure 87: Minimum energy conformations of compounds **2.6j'** (left) and **2.6k'** (right). Note how for

compound **2.6j'** a strong hydrogen bonding between the NH group of the pyrimidinone ring and the oxygen atom of the methoxy substituent at position 2 was identified, which would control the relative arrangement between the rings 302

Figure 88: Minimum energy conformations of compound **2.3i** (left) and its counterpart with C2 being a sp^2 carbon (right). Each compound is represented in sticks (up) and in spheres (down). The carbon atoms of the aryl substituent in position C2 of the chromenepyrimidinone moiety are highlighted in yellow and green colours. Note the significant change in the overall conformation of the compounds when the position C2 change from the sp^3 to sp^2 hybridized forms 303

Figure 89: Positions and type of substituents promoting the activity of chromene[2,3-*d*]pyrimidin-4(5*H*)-one derivatives studied against TNBC cell lines. X= halide 304

Figure 90: Schematic representation of PARP1 biological function. After binding to SSBs, PARP1 transfers the ADP-ribosyl moiety from NAD^+ to acceptor proteins, generating long chains of poly (ADP-ribosyl)ated polymers. This allows for the recruitment of DNA repair proteins such as DNA polymerase b, DNA ligase III, and scaffolding protein XRCC1 to sites of SSBs. PARP may also facilitate homologous recombination via recruitment of factors like ATM, Mre11, and Nbs1 to sites of double-stranded DNA damage and has been shown to interact with the DNA protein kinase complex involved with nonhomologous end-joining. ATM, ataxia telangiectasia-mutated; BER, base excision repair; DNA-PKcs, DNA-protein kinase catalytic subunit; DSB, double-strand break; HR, homologous recombination; Mre11, mitotic recombination 11; Nbs1, Nijmegen breakage syndrome 1; NHEJ, nonhomologous end-joining; PPi, inorganic pyrophosphate; SSB, single-strand break; XRCC1, X-ray cross-complementing protein [Source: ref. 107] 306

Figure 91: Chemical structures of olaparib, rucaparib, niraparib and talazoparib 307

Figure 92: Structural motifs in reported PARP inhibitors 308

Figure 93: Schematic representation of the binding mode of several PARP-1 inhibitors in the nicotinamide binding pocket of PARP1: (A) 5-hydroxy-3,4-dihydroisoquinolin-1(2*H*)-one; (B) rucaparib; (C) quinazoline derivative [Source: ref.123] 308

Figure 94: Pharmacophore model for PARP1 inhibitors [Source: ref.123] 309

Figure 95: Compounds used in the molecular docking studies. The percentage of cell viability in Hs578t cancer cell lines after 72 h of treatment and at 30 μM concentration of the compound is also included..... 311

Figure 96: (A) Comparison of the highest score solutions obtained by molecular docking for compounds **2.6d'** (blue), **2.6h'** (green), **2.6j'** (yellow) and **2.6l'** (magenta) in the nicotinamide binding pocket of PARP1. (B) Superposition of the proposed binding mode for bromide **2.6d'** (blue) and inhibitor FR257517 (orange) as observed in PDB 1UK0. Relevant side chain residues are shown and labelled. The most relevant interactions are indicated as blue (polar) and black (apolar) dashed lines..... 312

Figure 97: Comparison of the highest score solutions obtained by molecular docking for compounds **2.6t** (blue), **2.6x** (yellow) and **2.6b'** (green) in the nicotinamide binding pocket of PARP1. Relevant side chain residues are shown and labelled. The most relevant interactions are indicated as blue (polar) and black (apolar) dashed lines..... 313

Figure 98: Superposition of some of the arrangements for compounds **2.6e** (A) and compound **2.6k** (B) obtained by molecular docking 314

Figure 99: Compounds used for MD simulation studies 316

Figure 100: (**A**) Superposition of several snapshots [0 ns (yellow), 20 ns (pink), 40 ns (green); 60 ns (blue), 80 ns (orange), 100 ns (purple)] from the 100 ns of MD simulation on the **2.6d'**@PARP1 binary complex. (**B**) Overall view of the binding mode of compound **2.6d'** against PARP1 obtained by MD simulation studies. Snapshot taken after 80 ns of simulation. (**C**) Detailed view of the main contacts for **2.6d'** in the **2.6d'**@PARP1 binary complex. The relevant residues and side chains involved are shown and labeled. Hydrogen bonding interactions are indicated as red dashed lines. (**D**) Frequency (%) and enzyme atoms with which the hydrogen bonding interactions between **2.6d'** and PARP1 are observed during whole simulation. Average distances (Å) between the donor/acceptor atoms involved when the hydrogen bond is observed are also shown..... 317

Figure 101: (**A**) Superposition of several snapshots [0 ns (yellow), 20 ns (pink), 40 ns (green); 60 ns (blue), 80 ns (orange), 100 ns (purple)] from the 100 ns of MD simulation on the **2.6j'**@PARP1 binary complex. (**B**) Overall view of the binding mode of compound **2.6j'** against PARP1 obtained by MD simulation studies. Snapshot taken after 80 ns of simulation. (**C**) Detailed view of the main contacts for **2.6j'** in the **2.6j'**@PARP1 binary complex at 50 ns. (**D**) Frequency (%) and enzyme atoms with which the hydrogen bonding interactions between **2.6j'** and PARP1 are observed during whole simulation. Average distances (Å) between the donor/acceptor atoms involved when the hydrogen bond is observed are also shown..... 319

Figure 102: (**A**) Superposition of several snapshots [0 ns (yellow), 20 ns (pink), 40 ns (green); 60 ns (blue), 80 ns (orange), 100 ns (purple)] from the 100 ns of MD simulation on the **2.6e**@PARP1 binary complex. (**B**) Overall view of the binding mode of compound **2.6** against PARP1 obtained by MD simulation studies. Snapshot taken after 80 ns of simulation. (**C**) Detailed view of the main contacts for **2.6e** in the **2.6e**@PARP1 binary complex obtained by MD simulation studies. Snapshot taken after 80 ns of simulation. The relevant residues and side chains involved are shown and labeled. Hydrogen bonding interactions are indicated as red dashed lines. (**D**) Frequency (%) with which the hydrogen bonding interactions between **2.6e** and PARP1 are observed during whole simulation and average distance (Å) between the donor/acceptor atoms involved 321

Figure 103: Schematic representation of the MM/PBSA approach. Thermodynamic cycles for binding free energy calculations for a protein–ligand complex. Solvated systems are shown in blue boxes, while

systems in the gas phase are in white boxes. Free energies that are directly calculated are shown in black, while the free energy of interest is shown in red [adapted from ref.130] 323

Figure 104: Countries (in blue) that had an estimated TB incidence rate of less than 10 per 100 000 population in 2019 [obtained from ref. 132] 326

Figure 105: Global number of people reported to have been treated for TB disease, 2015–2019 (left) and the global number of people reported to have been enrolled on treatment for MDR/RR-TB, 2015–2019 (Global data disaggregated by age are not available for the years before 2018) (right) [obtained from ref. 132] 326

Figure 106: Chemical structure of compounds **2.119e**, **2.119i** and **2.119n** and their *in vitro* [MIC (μg/mL)] activity against virulent *M. tuberculosis*..... 329

Figure 107: Examples of quinine-derived antimalarial drugs, developed between 1820 and the 1980s 330

Figure 108: Examples of artemisinin-derived antimalarial drugs 331

Figure 109: Free energy profiles for the cyclization steps to afford 5- and 6-membered derivatives substituted with 2-, 3- and 4-hydroxylphenyl groups 343

Figure 110: Geometries of the transition states **TS1.0H** (A, C and E) and **TS2.0H** (B, D, F). The ortho (A, B), meta (C, D) and para (E, F) isomers of each TS are shown 345

Figure 111: Geometries of the transition states **TS1.0** (A, C and E) and **TS2.0** (B, D, F). The ortho (A, B), meta (C, D) and para (E, F) isomers of each TS are shown 346

Figure 112: Geometries of the intermediates **B.0H** and **B.0**. Note how for the ortho isomers, no planar arrangements were observed. The phenol/phenolate moieties are located on a suitable arrangement for the removal of one of the hydrogen atoms of the methylene group. The distances between the oxygen atom of the phenol/phenolate group and the methylene hydrogen atom are highlighted 347

Figure 113: Geometry of the **TS4**. The distances (Å) of the formed (blue) and broken (yellow) bond are indicated. 348

Figure 114: Free energy profiles for the formation of 5- and 6-membered derivatives substituted with 2-, 3- and 4-hydroxylphenyl groups. Only the phenolate forms of the starting material, intermediates and TS are considered. 349

List of Tables

Chapter 2

Table 1: Experimental conditions and results obtained for the reaction of **2.1a** with benzaldehyde, under different reaction conditions 33

Table 2: Reaction conditions for the preparation of compounds **2.3d-i** 38

Table 3: Reaction conditions for the preparation of compounds **2.6a-k'** 38

Table 4: Physical and analytical data obtained for 2-imino-2*H*-chromeno-3-carboxamides **2.1a-g** and 2-oxo-2*H*-chromeno-3-carboxamide **2.15a** 40

Table 5: Physical and analytical data obtained for 2-aryl-3*H*-chromeno[2,3-*d*]pyrimidin-4(3*H*)-ones **2.3d-i** 41

Table 6: Physical and analytical data obtained for 2-aryl-3*H*-chromeno[2,3-*d*]pyrimidin-4(5*H*)-ones **2.6a-k'** 42

Table 7: IR spectroscopic data (Nujol, cm^{-1}) obtained for 2-imino-2*H*-chromeno-3-carboxamides **2.1a-g** and 2-oxo-2*H*-chromeno-3-carboxamide **2.15a**.....45

Table 8: IR spectroscopic data (Nujol, cm^{-1}) obtained for 2-aryl-3*H*-chromeno[2,3-*d*]pyrimidin-4(3*H*)- ones **2.3d-i** 45

Table 9: IR spectroscopic data (Nujol, cm^{-1}) obtained for 2-aryl-3*H*-chromeno[2,3-*d*]pyrimidin-4(5*H*)- ones **2.6a-k'** 46

Table 10: ^{1}H NMR (400 MHz, DMSO-d_6, δ ppm) spectroscopic data obtained for 2-imino-2*H*-chromeno-3-carboxamides **2.1a-g** and for 2-oxo-2*H*-chromeno-3-carboxamide **2.15a** 50

Table 11: ^{13}C NMR (100 MHz, DMSO-d_6, δ ppm) spectroscopic data obtained for 2-imino-2*H*-chromeno-3-carboxamides **2.1a-g** and for 2-oxo-2*H*-chromeno-3-carboxamide **2.15a** 51

Table 12: ^{1}H NMR (400 MHz, DMSO-d_6, δ ppm) spectroscopic data obtained for 2-aryl-3*H*-chromeno [2,3-d]pyrimidin-4(3*H*)-ones **2.3d-k** 53

Table 13: ^{13}C NMR (100 MHz, DMSO-d_6, δ ppm) spectroscopic data obtained for 2-aryl-3*H*-chromeno [2,3-d]pyrimidin-4(3*H*)-ones **2.3d-k** 54

Table 14: ^{1}H NMR (400 MHz, DMSO-d_6, δ ppm) spectroscopic data obtained for 2-aryl-3*H*-chromeno [2,3-*d*]pyrimidin-4(5*H*)- ones **2.6a-k'** 55

Table 15: ^{13}C NMR (100 MHz, DMSO-d_6, δ ppm) spectroscopic data obtained for 2-aryl-3*H*-chromeno [2,3-*d*]pyrimidin-4(5*H*)- ones **2.6a-k'** 59

Table 16: ^{1}H NMR (400 MHz, DMSO-d_6, δ ppm) spectroscopic data obtained for 2-aryl-3*H*-chromeno [2,3-*d*]pyrimidin-4(5*H*)- ones **2.6q, 2.6r** and **2.6h'**.....63

Table 17: ^{13}C NMR (100 MHz, DMSO-d_6, δ ppm) spectroscopic data obtained for 2-aryl-3*H*-chromeno [2,3-*d*]pyrimidin-4(5*H*)- ones **2.6q, 2.6r** and **2.6h'** 64

Table 18: Experimental conditions for the preparation of water-soluble sodium salts of **2.6a** and **2.6x** 66

Table 19: Selection of ^{13}C NMR (100 MHz, DMSO-d_6, δ ppm) chemical shifts obtained for **2.6a** (R^1= OMe) and **2.6x** (R^1=H) vs **2.19a** and **2.19x**, respectively 67

Table 20: Reaction conditions and results obtained for the reaction of **2.25a** with aldehydes **2.2**, in ethanol under reflux 71

Table 21: Physical and analytical data obtained for compounds **2.22,2.27-2.29** and **2.35** 79

Table 22: IR spectroscopic data (Nujol, cm^{-1}) obtained for compounds **2.27-2.29** 80

Table 23: ^{1}H NMR (400 MHz, DMSO-d_6, δ ppm) and ^{13}C NMR (100 MHz, DMSO-d_6, δ ppm) spectroscopic data obtained for compounds **2.22a** and **2.25a** 80

Table 24: ^{1}H NMR (400 MHz, DMSO-d_6, δ ppm) and ^{13}C NMR (100 MHz, DMSO-d_6, δ ppm) spectroscopic data obtained for compound **2.27** 81

Table 25: ^{1}H NMR (400 MHz, DMSO-d_6, δ ppm) and ^{13}C NMR (100 MHz, DMSO-d_6, δ ppm) spectroscopic data obtained for compound **2.28** 82

Table 26: ^{1}H NMR (400 MHz, DMSO-d_6, δ ppm) and ^{13}C NMR (100 MHz, DMSO-d_6, δ ppm) spectroscopic data obtained for compound **2.29** 82

Table 27: ^{1}H NMR (400 MHz, DMSO-d_6, δ ppm) and ^{13}C NMR (100 MHz, DMSO-d_6, δ ppm) spectroscopic data obtained for compound **2.35** 83

Table 28: Reaction conditions and yields for the preparation of compounds **2.37** from salicylaldehydes **2.2** and acetophenones **2.36** 86

Table 29: Reaction conditions and yields of synthesis of 4*H*-chromenes **2.39a-i** from α,β-unsaturated ketones **2.37a-i** 86

Table 30: Reaction conditions and results obtained from the treatment of chromenes **2.39** with concentrated H_2SO_4 in aqueous ethanol to afford compounds **2.50** 90

Table 31: Experimental conditions tested, in the reaction of compound **2.39e** with aniline 91

Table 32: Conditions tested for the reaction of compound **2.39e** with aniline, in an EtOH/H_2O system 98

Table 33: Results for the reaction of chromenes **2.39a** with anilines **2.51** (2 equivalents) and acetic acid (0.5 equivalents) in ethanol at 80 °C 103

Table 34: Results for the reaction of chromenes **2.39c** with anilines **2.51** (3-4 equivalents) and acetic acid (0.5 equivalents) in ethanol at 80 °C 104

Table 35: Results for the reaction of chromenes **2.39d** with anilines **2.51** (3-4 equivalents) and acetic

acid (0.5 equivalents) in ethanol at 80 °C 105
Table 36: Results for the reaction of chromenes **2.39e** with anilines **2.51** (2-5 equivalents) and acetic acid (0.5 equivalents) in ethanol at 80 °C 106
Table 37: Results for the reaction of chromenes **2.39f** with anilines **2.51** (2-3 equivalents) and acetic acid (0.5 equivalents) in ethanol at 80 °C 107
Table 38: Results for the reaction of chromenes **2.39g** with anilines **2.51** (3-4 equivalents) and acetic acid (0.5 equivalents) in ethanol at 80 °C.....108
Table 39: Results for the reaction of **2.39h** with anilines **2.51** (2-3 equivalents) and acetic acid (0.5 equivalents) in ethanol at 80 °C 110
Table 40: Results for the reaction of **2.39i** with anilines **2.51** (2-3 equivalents) and acetic acid (0.5 equivalents) in ethanol at 80 °C 113
Table 41: Reaction conditions and results obtained from the reaction of compounds **2.39** with NaOH/MeOH.....115
Table 42: Experimental conditions used to perform the one-pot synthesis of compounds **2.69** 117
Table 43: Physical and analytical data obtained for compounds 3-(2-hydroxyaryl)-1-arylprop-2-en-1-ones **2.37a-i**.....126
Table 44: Physical and analytical data obtained for 4*H*-chromene-3-carbonitriles **2.39** 126
Table 45: Physical and analytical data obtained for 4*H*-chromene-3-carbonitriles **2.50** 128
Table 46: Physical and analytical data obtained for chromenopyridines **2.55**, **2.56** and **2.69**.....129
Table 47: Physical and analytical data obtained for compounds **2.60a**, **2.61a**, **2.68a**,**b**, **2.70a** and **2.71a,b** 132
Table 48: Physical and analytical data obtained for 2-amino-4-(2-aryl-2-(2-phenylhydrazono)ethyl)-4*H*-chromene-3-carbonitriles **2.82a,b**.....133
Table 49: IR spectroscopic data (Nujol, cm^{-1}) obtained for 3-(2-hydroxyaryl)-1arylprop-2-en-1-ones **2.37** 133
Table 50: IR spectroscopic data (Nujol, cm^{-1}) obtained for 4*H*-chromene-3-carbonitriles **2.39**.....134
Table 51: IR spectroscopic data (Nujol, cm^{-1}) obtained for 4*H*-chromene-3-carbonitriles **2.50**.....135
Table 52: IR spectroscopic data (Nujol, cm^{-1}) obtained for 5-imino and 5-oxo-*N*,2-diaryl-5*H*-chromeno[3,4-*c*]pyridin-4-amines **2.55**, **2.56** and **2.69**.....135
Table 53: IR spectroscopic data (Nujol, cm^{-1}) obtained for compounds **2.60a**, **2.61a**, **2.68**, **2.70a** and **2.71** 137
Table 54: IR spectroscopic data (Nujol, cm^{-1}) obtained for 2-amino-4-(2-aryl-2-(2-phenylhydrazono)ethyl)-4*H*-chromene-3-carbonitriles **2.82a** and **2.82b** 138
Table 55: ^{1}H NMR (400 MHz, DMSO-d_6, δ ppm) spectroscopic data obtained for 3-(2-hydroxyaryl)-1 arylprop-2-en-1-ones **2.37** 140

Table 56: ^{13}C NMR (100 MHz, DMSO-d_6, δ ppm) spectroscopic data obtained for 3-(2-hydroxyaryl)-1 arylprop-2-en-1-ones **2.37** 141

Table 57: ^{1}H NMR (400 MHz, DMSO-d_6, δ ppm) spectroscopic data obtained for 4*H*-chromene-3-carbonitriles **2.39** 142

Table 58: ^{13}C NMR (100 MHz, DMSO-d_6, δ ppm) spectroscopic data obtained 4*H*-chromene-3-carbonitriles **2.39** 143

Table 59: ^{1}H NMR (400 MHz, DMSO-d_6, δ ppm) spectroscopic data obtained for 4*H*-chromene-3-carbonitriles **2.50** 144

Table 60: ^{13}C NMR (100 MHz, DMSO-d_6, δ ppm) spectroscopic data obtained for 4*H*-chromene-3-carbonitriles **2.50** 146

Table 61: ^{1}H NMR (400 MHz, DMSO-d_6, δ ppm) spectroscopic data obtained for 5-imino and 5-oxo-*N*,2-diaryl-5*H*-chromeno[3,4-*c*]pyridin-4-amines **2.55**, **2.56** and **2.69** 147

Table 62: ^{13}C NMR (100 MHz, DMSO-d_6, δ ppm) spectroscopic data obtained for 5-imino and 5-oxo-*N*,2-diaryl-5*H*-chromeno[3,4-*c*]pyridin-4-amines **2.55**, **2.56** and **2.69** 152

Table 63: ^{1}H NMR (400 MHz, DMSO-d_6, δ ppm) spectroscopic data obtained for compounds **2.60a**, **2.61a**, **2.68**, **2.70a** and **2.71** 158

Table 64: ^{13}C NMR (100 MHz, DMSO-d_6, δ ppm) spectroscopic data obtained for compounds **2.60a**, **2.61a**, **2.68**, **2.70a** and **2.71** 159

Table 65: ^{1}H NMR (400 MHz, DMSO-d_6, δ ppm) and ^{13}C NMR (100 MHz, DMSO-d_6, δ ppm) spectroscopic data obtained for 2-amino-4-(2-aryl-2-(2-phenylhydrazono)ethyl)-4*H*-chromene-3-carbonitriles **2.82a** and **2.82b** 160

Table 66: Reaction time and isolated yield of chromene-based imidates **2.85** 163

Table 67: Reaction conditions and results of the reaction of compound **2.85a** with aniline 165

Table 68: Reaction conditions and results of the reaction of compound **2.85d** with aniline 167

Table 69: Reaction conditions and results, of the experiments performed with compound **2.85e** and aniline in a dual solvent systems 170

Table 70: Experimental conditions and results for the reaction of imidates **2.85** with amines 171

Table 71: Reaction conditions and results for the reaction of imidates **2.85** with different primary amines, in ethanol 176

Table 72: Results of the heating, at 80 °C in ethanol, of samples of amidines **2.87** also containing spiro derivatives **2.58**/**2.61**, and dihydropyridines **2.59**/**2.60** 177

Table 73: Results of the treatment of amidine **2.87b** with diverse type of bases 178

Table 74: Reaction conditions, and results for the reaction of compounds **2.87** with NaOH (2 M) in EtOH at room temperature 185

Table 75: Reaction conditions and results obtained for the reaction of compounds **2.85d-h** with phenylhydrazine 199
Table 76: Physical and analytical data obtained for imidates **2.85a-h** 203
Table 77: Physical and analytical data obtained for pyridopyrimidines **2.86** 204
Table 78: Physical and analytical data obtained for amidines **2.87** 205
Table 79: Physical and analytical data obtained for compounds **2.88** 207
Table 80: Physical and analytical data obtained for chromenopyridines **2.89** 207
Table 81: Physical and analytical data obtained for compounds **2.90** and **2.105** 208
Table 82: Physical and analytical data obtained for compounds **2.100a,b** 209
Table 83: IR spectroscopic data (Nujol, cm^{-1}) obtained for imidates **2.85a-h** 209
Table 84: IR spectroscopic data (Nujol, cm^{-1}) obtained for imidates **2.86** 210
Table 85: IR spectroscopic data (Nujol, cm^{-1}) obtained for amidines **2.87** 211
Table 86: IR spectroscopic data (Nujol, cm^{-1}) obtained for compounds **2.88a-c** 212
Table 87: IR spectroscopic data (Nujol, cm^{-1}) obtained for chromenopyridines **2.89** 213
Table 88: IR spectroscopic data (Nujol, cm^{-1}) obtained for compounds **2.90** and **2.105** 213
Table 89: IR spectroscopic data (Nujol, cm^{-1}) obtained for compounds **2.100a,b** 214
Table 90: ^{1}H NMR (400 MHz, DMSO-d_6, δ ppm) spectroscopic data obtained for imidates **2.85a-h** ..216
Table 91: ^{13}C NMR (100 MHz, DMSO-d_6, δ ppm) spectroscopic data obtained for imidates **2.85a-h** 217
Table 92: ^{1}H NMR (400 MHz, DMSO-d_6, δ ppm) spectroscopic data obtained for pyridopyrimidines **2.86** 219
Table 93: ^{13}C NMR (100 MHz, DMSO-d_6, δ ppm) spectroscopic data obtained for pyridopyrimidines **2.86** 221
Table 94: ^{1}H NMR (400 MHz, DMSO-d_6, δ ppm) spectroscopic data obtained for amidines **2.87** 223
Table 95: ^{13}C NMR (100 MHz, DMSO-d_6, δ ppm) spectroscopic data obtained for amidines **2.87** 227
Table 96: ^{1}H NMR (400 MHz, DMSO-d_6, δ ppm) spectroscopic data obtained for compounds **2.88a-c** 230
Table 97: ^{13}C NMR (100 MHz, DMSO-d_6, δ ppm) spectroscopic data obtained for compounds **2.88a-c** 232
Table 98: ^{1}H NMR (400 MHz, DMSO-d_6, δ ppm) spectroscopic data obtained for chromenopyridines **2.89** 233
Table 99: ^{13}C NMR (100 MHz, DMSO-d_6, δ ppm) spectroscopic data obtained for chromenopyridines **2.89** 234
Table 100: ^{1}H NMR (400 MHz, DMSO-d_6, δ ppm) and ^{13}C NMR (100 MHz, DMSO-d_6, δ ppm) spectroscopic data obtained for compounds **2.90** and **2.105** 236

Table 101: ^{1}H NMR (400 MHz, DMSO-d_6, δ ppm) and ^{13}C NMR (100 MHz, DMSO-d_6, δ ppm) spectroscopic data obtained for compounds **2.100a,b**.....237

Table 102: Reaction conditions and reagents used for the preparation of eneimines **2.109a-h** from aldehydes **2.2** and DAMN.....244

Table 103: Experimental conditions and results obtained for the reaction of **2.109a,b** with different aldehydes **2.2**.....246

Table 104: Experimental conditions and results obtained for the reaction of imine **2.109d** with benzaldehydes **2.2**, in ethanol and using triethylamine as base.....247

Table 105: Selection of reactions performed with imine **2.109** and 2-chlorobenzaldehyde (2 equiv.), in the presence of triethylamine (2 equiv.), in ethanol and at room temperature for 96 h.....248

Table 106: Reaction conditions for the synthesis of imidazoles **2.119a-q**.....253

Table 107: Physical and analytical data obtained for compounds **2.109a-b**.....255

Table 108: Physical and analytical data obtained for compounds **2.113b,d**.....256

Table 109: Physical and analytical data obtained for compounds **2.119a-q**.....256

Table 110: IR spectroscopic data (Nujol, cm^{-1}) obtained for compounds **2.109a-b**.....259

Table 111: IR spectroscopic data (Nujol, cm^{-1}) obtained for compounds **2.113b,d**.....259

Table 112: IR spectroscopic data (Nujol, cm^{-1}) obtained for compounds **2.119a**.....260

Table 113: IR spectroscopic data (Nujol, cm^{-1}) obtained for compounds **2.119e,p,q**.....261

Table 114: ^{1}H NMR (400 MHz, DMSO-d_6, δ ppm) spectroscopic data obtained compounds **2.109a-b**.....262

Table 115: ^{13}C NMR (100 MHz, DMSO-d_6, δ ppm) spectroscopic data obtained for compounds **2.109a-b**.....263

Table 116: ^{1}H NMR (400 MHz, DMSO-d_6, δ ppm) spectroscopic data obtained compounds **2.113b,d**.....264

Table 117: ^{13}C NMR (100 MHz, DMSO-d_6, δ ppm) spectroscopic data obtained for compounds **2.113b,d**.....264

Table 118: ^{1}H NMR (400 MHz, DMSO-d_6, δ ppm) spectroscopic data obtained compounds **2.119**.....265

Table 119: ^{13}C NMR (100 MHz, DMSO-d_6, δ ppm) spectroscopic data obtained for compounds **2.119**.....267

Table 120: ^{1}H NMR (400 MHz, DMSO-d_6, δ ppm) spectroscopic data obtained compounds **2.119e,p,q**.....269

Table 121: ^{13}C NMR (100 MHz, DMSO-d_6, δ ppm) spectroscopic data obtained for compounds **2.119e,p,q**.....270

Chapter 3

Table 122: Molecular subtypes of breast cancer, according to the St. Gallen Consensus summary [adapted from ref.41] 286

Table 123: Percentage (%) of cell viability, in Hs578t, MDA-MB-231 and MCF-7 breast cancer cell lines, after 72 h of treatment with compounds **2.3** and **2.6** at 10 and 30 μM concentrations..... 290

Table 124: Percentage (%) of cell viability, in Hs578t, MDA-MB-231 and MCF-7 breast cancer cell lines, after 72 h of treatment with compounds **2.50**, **2.55, 2.69b**, **2.86**, **2.87** and **2.90** at 10 and 30 μM concentrations 293

Table 125: Percentage (%) of cell viability, in Hs578t, MDA-MB-231 and MCF-7 breast cancer cell lines, after 72 h of treatment with compounds **2.119** at 10 and 30 μM concentrations..... 295

Table 126: IC_{50} values of compounds **2.6p**, **2.6d'**, **2.6j'**, **2.86g** and **2.90**, doxorubicin and quercetin against Hs578t and MCF-10A cell lines after 72 h of treatment and selectivity index 296

Table 127: Compounds included in group 1 297

Table 128: Compounds included in group 2 298

Table 129: Compounds included in group 3 299

Table 130: Compounds included in group 4 300

Table 131: Compounds included in group 5 301

Table 132: Compounds included in group 6 301

Table 133: Compounds included in group 7 303

Table 134: Calculated binding free energies (kcal mol^{-1}) for compounds **2.6d'**, **2.6j'** and **2.6e** using MM/PBSA method 324

Table 135: Survival rate percentage of *Plasmodium falciparum* (% mean value) parasites after treatment with a selection of compounds **2.3** and **2.6** 332

Table 136: Survival rate percentage of *Plasmodium falciparum* (% mean value) parasites after treatment with a selection of compounds **2.50**, **2.55**, **2.69**, **2.86**, **2.87**, **2.90** and **2.105** 334

Table 137: Survival rate percentage of *Plasmodium falciparum* (% mean value) parasites after treatment with a selection of compounds **2.119**..... 337

List of Schemes

Chapter 1

Scheme 1: Reaction mechanism for Pechmann condensation reaction 7

Scheme 2: Synthetic procedure for the preparation of umbelliferone from formylacetic acid and resorcinol.....8

Scheme 3: Synthetic procedure for the preparation of compounds **1.19** by Michael addition of the phenolic oxygen of 3-ethoxysalicylaldehyde to β-nitrostyrenes **1.18**, as proposed byYin *et al* [ref. 38] 8

Scheme 4: Synthetic procedure for the preparation of compounds **1.22** via a three-component Knoevenagel condensation, as proposed by Evdokimov *et al* [ref.69].....9

Scheme 5: Synthetic pathways for the preparation of chromenopyridines **1.25-1.27**, as proposed by Ibrahim *et al.* [adapted from ref.85] 10

Scheme 6: Synthetic pathways for the preparation of chromenopyridines **1.35***,* as proposed by Dineem *et al* [ref. 86], Epstein *et al* [ref. 87] and Huang *et al* [adapted from ref. 89]. **a)** (i) Cs_2CO_3, CuOTf (cat.), EtOAc (cat.), toluene, 90 °C, then HCl; (ii) H_2SO_4 or PPA, 60-110 °C, 26-85 **b)** (i) MeMgCl, THF, - 10 °C, then PPTS or HCl, or $TMSCH_2Li$, THF, - 78°C, then AcCl; (ii) AgOCN, THF, 0 °C to r.t., then NH_3 THF, 23-53% 11

Scheme 7: Synthetic pathways for the preparation of chromenopyridines **1.39***,* as proposed by Epstein *et al* [ref. 87]. **a)** (i) BBr3, DCM, 96%; **b)** 2-fluoro-3-phenylboronic acid, $Pd(PPh_3)4$, Na_2CO_3, DMF/H_2O, 87%; **c)** *N*-(5-chloro-2-pyridyl)bis-(trifluoromethanesulfonimide)(Commins' reagent), Et_3N, DCM, 84%;**d)**2-(3,6-dihydro-2*H*-pyran-4-yl)-4,4,5,6-tetramethyl-1,3,2-dioxaborolane, $Pd(PPh_3)_4$, Na_2CO_3, DMF/water, 61% 12

Scheme 8: Synthesis of chromenopyridines **1.41** and **1.43**, as proposed by Thapa *et al* [adapted from ref.90,91] 12

Scheme 9: General procedure for the Debus-Radziszewski imidazole synthesis [ref. 100]].....14

Scheme 10: General procedure for the synthesis of imidazolquinolines **1.52**, reported by Guam *et al.* [ref. 102] 15

Scheme 11: Synthetic procedures for the preparation of imidazoles **1.54** [Fang *et al*, ref. 103], **1.57** [Man *et al*, ref. 104] and **1.59** [Wang *et al*, ref. 105] [adapted from ref.101]. a) $R^2B(OH)_2$ (2.0 equiv.), $Ni(PPh_3)_2Br_2$ (10 mol %), Na_2SO_4 (3 equiv.), toluene, 120 °C, 24h, 38 examples, 13-90 %; **b)** Et_3N (2.0 equiv.), thermally, EtOH, 85 °C, 14 h or KOAc (20 mol%), microwave, *t*-BuOH, 125 °C, 20 min. or KOAc (20 mol%), blue light, EtOH, r.t., 2 h; **c)** cyclohexane, 110 °C, 11 h, silica gel, 30 examples, 49-93% 16

Chapter 2

Scheme 12: Synthesis of chromene[2,3-*d*]pyrimidin-4(5*H*)-*ones* **2.3**, as proposed by O'Callaghan [ref.1] 28

Scheme 13: Rearrangement promoted by heat, as proposed by O'Callaghan [ref.2] 28

Scheme 14: Reaction conditions optimized by Borisov *et al* for automated parallel synthesis of compounds **2.6**, **2.7**, **2.9** and **2.10** [adapted from ref.4] 30

Scheme 15: Preparation of 2-imino- **2.1** and 2-oxo-2*H*-chromene-3-carboxamides **2.15**, via Knoevenagel condensation, as proposed by Proença *et al* [adapted from ref.5] 31

Scheme 16: Synthesis of 2-imino-2*H*-chromene-3-carboxamides **2.1a-g** from 2-cyanoacetamide and salicylaldehydes **2.2a-g** 32

Scheme 17: Reaction of chromene **2.1a** with triethyl orthoformate 32

Scheme 18: Proposed mechanism for the synthesis of 9-methoxy-2-phenyl-3*H*-chromeno[2,3-*d*]pyrimidin-4(5*H*)-one **2.6a** 37

Scheme 19: Synthesis of 3-aminochromenes **2.22** and **2.25**, as proposed by Costa *et al* [adapted from ref. 41] 69

Scheme 20: Synthesis of 3-aminocoumarins **2.25** from *N*-acetylglicine and salicylaldehydes **2.2**, as proposed by Das *et al* [adapted from ref. 43] 70

Scheme 21: Proposed mechanism for the formation of compounds **2.27-2.29** 72

Scheme 22: Proposed mechanism for the formation of compounds **2.35** 77

Scheme 23: Synthesis of 4*H*-chromenes **2.39** and **2.40** [adapted from ref.104] 85

Scheme 24: Proposed mechanism for the formation of compound **2.50a** from **2.39a** after treatment with H_2SO_4 (c). The formation of compound **2.44** was not detected 87

Scheme 25: Predicted reaction sequence that would allow the formation of products **2.55** 91

Scheme 26: Proposed mechanism for the formation of compounds **2.55** and **2.56** 102

Scheme 27: Conversion of a mixture of compounds **2.55a**, **2.56a**, **2.60a** and **2.61a** into the desired compound **2.56a** by heating at 80 °C with concentrated H_2SO_4 114

Scheme 28: Synthesis of lactone pyridine **2.69a** by acid-catalysed intramolecular cyclization of pyridine **2.68a** 116

Scheme 29: Synthesis of pyridine **2.71a** from compound **2.37e** and malononitrile 119

Scheme 30: Plausible ANRORC-type mechanism for the formation of compounds **2.68** (R^3=Me), **2.69** (R^3=Et) and **2.70** (R^3=Me) via a three-step procedure involving (i) addition of the nucleophile, ring-opening, and ring-closure; (ii) lactonization; and (ii) aromatization 120

Scheme 31: Plausible mechanism for the formation of compounds **2.71** from chromenes **2.39** by treatment with 2 equivalents of malononitrile and NaOH (3 M) in MeOH, which include chromene ring-opening and retro Michael addition for the regeneration of the α,β-unsaturated ketone **2.37** (**A**),

formation of the intermediate **2.79** (**B**) and pyridine **2.71** synthesis (**C**) 121

Scheme 32: Synthesis of imino chromenepyridines **2.55** from chromenes **2.39** and primary amines in acidic media 122

Scheme 33: Reaction conditions for the preparation of compounds **2.82a-b** 123

Scheme 34: Proposed mechanism for the formation of compounds **2.82** 125

Scheme 35: Selection of correlations, observed by HMBC, for compounds **2.60a**, **2.61a**, **2.68**, **2.70a** and **2.71** 157

Scheme 36: Tautomeric forms for amidines **2.87** observed in DMSO-d_6 175

Scheme 37: Proposed mechanism for the formation of compounds **2.89**, via base-catalysed Dimroth rearrangement 184

Scheme 38: Reaction of **2.88a** in ethanol at 80 °C, for 12.5h 186

Scheme 39: Reaction of **2.88a** in a suspension of EtOH/H_2O (3:1), at r.t for 16h, followed by heating at 50 °C for 12.5 h 187

Scheme 40: Reaction of **2.88a** in a suspension of EtOH/H_2O (20:1), at 50 °C for 5 h, in the presence of 0.5 equivalents of acetic acid 189

Scheme 41: Reaction of **2.88a** in a mixture of EtOH/H_2O (3:1), at 80 °C for 20 min 190

Scheme 42: Reaction of **2.88a** in a mixture of EtOH/H_2O (3:1), at 80 °C for 2 h and 20 min 191

Scheme 43: Reaction of **2.88a** in a mixture of EtOH/H_2O (3:1), at 80 °C for 4 h and 20 min 192

Scheme 44: Reaction of **2.87b** in ethanol and at 80 °C, in the presence of 0.5 equivalents of acetic acid, for 7 h 193

Scheme 45: Reaction of **2.88a** in ethanol and at 80 °C, in the presence of 0.5 equivalents of acetic acid, for 7 h 194

Scheme 46: Reaction of **2.88a** in ethanol and at 80 °C, in the presence of 1 equivalent of DBU, for 1.5h 196

Scheme 47: Summary of the reaction conditions and products for the isolation of compounds **2.86**-**2.90**. The formation of compounds **2.55**, **2.56** and **2.69** was also observed 197

Scheme 48: Proposed mechanism for the evolution of compound **2.87** to generate **2.86** and **2.88**-**2.90** 198

Scheme 49: Proposed mechanism for the formation of compounds **2.100** 201

Scheme 50: Synthesis of compound **2.85a** into **2.105** by treatment with ammonium acetate 201

Scheme 51: Proposed mechanism for the formation of compounds **2.105** from the reaction of **2.85a** with ammonium acetate 202

Scheme 52: Synthesis of imidazoles **2.111** from **DAMN**, as proposed by Ohtsuka *et al* [adapted from ref.147] 239

Scheme 53: Preparation of dihydropyrazines **2.113** and **2.114** from imines **2.109**, as proposed by Ohtsuka *et al* [adapted from ref.148] 240

Scheme 54: Plausible mechanism for the formation of both 1,6-dihydropyrazines **2.113** and **2.114** [adapted from ref.148] 242

Scheme 55: Reaction mechanism for the synthesis of compounds **2.111** and **2.119** from imines **2.109** [adapted from ref. 158] 243

Scheme 56: Theoretical tautomeric forms of *ortho* **2.109a** and *para* substituted imines **2.109g** 252

Scheme 57: Synthesis of dihydropyrazine **2.113d** from imine **2.109e** and 2-chlorobenzaldehyde ..254

Scheme 58: Reaction mechanism for the synthesis of compounds **2.119** and side reaction obtained from hydroxylated derivatives of **2.112** [adapted from ref. 153].....339

Scheme 59: Results obtained from the reaction of **2.109a** (R^1= 2-OH) and **2.109g** (R^1= 4-OH) with 2-chlorobenzaldehyde; **a)** 2-chlorobenzaldehyde (1.2 equiv.), Et_3N (2 equiv.), EtOH, r.t., 96h 339

Scheme 60: Plausible mechanisms studied for the formation of 1H-imidazole **E** and pyrazine derivative **C** from 2-hydroxybenzylidene acrylamide **A**.....341

Scheme 61: Schematic representation of the reaction paths for the formation of 5- and 6-membered compounds **B** and **C**, respectively. The different types of isomers studied are also indicated. The structures in which the phenol group is in the neutral form are indicated as "**.OH**" and with "**.O**" for those using phenolate forms 342

Scheme 62: Schematic representation of the possible conversion of intermediates **B.OH** and **B.O** in imidazoles **E.OH** and **E.O** through [1,3]-hydrogen shift reaction 346

Scheme 63: Schematic representation of the possible conversion of intermediate **B.O** in imidazole **E.O** through an intramolecular hydrogen abstraction and a subsequent proton transfer reaction 348

Scheme 64: Synthetic route for the preparation of compounds **2.3** and **2.6** 360

Scheme 65: Synthetic route for the preparation of compounds **2.27-2.29** and **2.35** 361

Scheme 66: Synthetic route for the preparation of compounds **2.50**, **2.55**, **2.56**, **2.68**, **2.69**, **2.70** and **2.82** 363

Scheme 67: Synthetic route for the preparation of compounds **2.86-2.90**, **2.100** and **2.105**.....364

Scheme 68: Synthetic route for the preparation of imidazoles **2.119**.....365

Chapter 1

Introduction

1.1. Chromene scaffold

Benzopyran is the general terminology used to describe molecules where a benzene ring is fused to a pyran ring. This bicyclic molecule can differ in terms of position of the double bond, as well as the oxygen atom, in the pyran nucleus. According to the position of the oxygen atom, IUPAC defines two distinct structures: **1-benzopyran** and **2-benzopyran** (**Figure 1**). Based on the degree of saturation, benzopyrans are classified as 1*H*, 2*H*, 3*H* or 4*H*-benzopyran, depending on the position of the sp^3 carbon atom in the pyran ring.

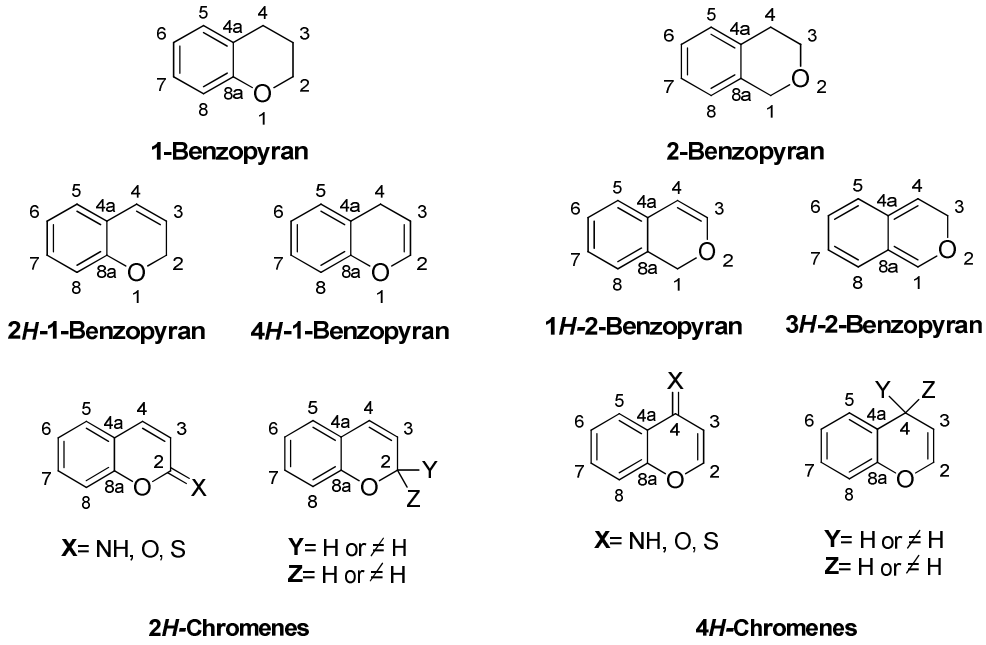


Figure 1: General chemical structures of 1-benzopyrans and 2-benzopyrans and 2*H*- and 4*H*-chromenes

1-Benzopyrans, generally known as **chromenes** (or **chromane** in case of complete saturation of the pyran ring), may also be named as ***2H*-chromenes** (2*H*-1-benzopyran) or ***4H*-chromenes** (4*H*-1-benzopyran) (**Figure 1**). For ***2H*-chromenes**, the double bond is positioned between C3 and C4, while for ***4H*-chromenes** the double bond is located between C2 and C3. For the latter compounds, C2 (2*H*-chromenes) or C4 (4*H*-chromenes) carbon atoms are typically involved in an exocyclic double bond with oxygen (X=O, 2-oxo-2*H*-chromene, commonly known as **coumarin**, or 4-oxo-4*H*-chromene, commonly known as chromenone), nitrogen (X=NH, 2-imino-2*H*-chromene, or 4-imino-4*H*-chromene) or sulfur (X=S, 2*H*-chromene-2-thione, or 4*H*-chromene-4-thione) or alternatively forms two single bonds with different substituents Y, Z (**Figure 1**).

1.1.1. Biological importance of the chromene moiety

There are several applications for compounds incorporating the chromene moiety, from cosmetic to food industries and even biodegradable products for agrochemical usage[1]. However, the chromene moiety is mostly recognized by its biological potential, with hundreds of chromene derivatives being reported for their activity as antibacterial[2–6], anti-inflammatory[7], anti-HIV[8], antioxidant[9,10], anticancer[11–21], antituberculosis[22], anticoagulant[23], monoamine oxidase inhibitors[24,25], cholinesterase inhibitors[26], antileishmanial[27], among many others described in several reviews[1,28–31].

There are many examples of naturally occurring chromenes that showed interesting biological properties. Neo-tanshinlactone (**Figure 2**) can be isolated as a minor component from the ethanol extract of *Salvia miltiorrhiza*, specifically its root[28]. It was tested for antitumor activity against several human breast cancer cell lines of clinical significance, exhibiting low ED_{50} values of 0.45 μg/mL (MCF-7) and 0.18 μg/mL (ZR-75-1)[28]. Asphodelin A (**Figure 2**) could be isolated from the bulbs and roots of *Asphodelus microcarpus*, collected in Egypt. It exhibited interesting antimicrobial activity against *S. aureus, E. coli* and *P.aeruginosa*, with minimal inhibitory concentrations (MIC) of 4-16 μg/mL[28]. Macluraxanthone (**Figure 2**) was isolated from nonpolar fractions of the methanolic extract, from the root bark of *Maclura pomifera*. Its activity as inhibitor of acetylcolinesterase (AChE) and butyrylcholinesterase (BChE) enzymes was investigated, and was concluded that it can specifically inhibit AChE with an IC_{50} value of 8.47 mM and a K_i of 3.43 mM[28].

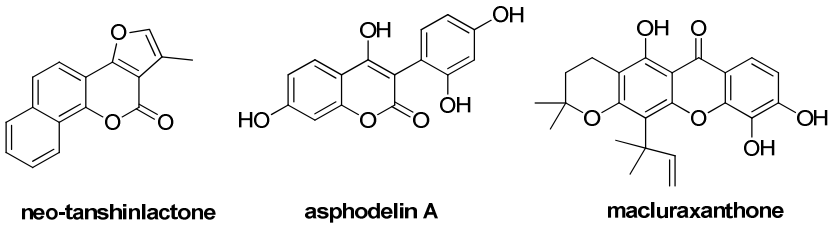


Figure 2: Chemical structure of naturally occurring neo-tanshinlactone, asphodelin A and macluraxanthone with biological activity [ref.28]

Gramniphenols **1.1** and **1.2a,b** (**Figure 3**), isolated from the extracts of *Arundina gramnifolia*, a plant from the orchid family, have also proven to be biologically active[32]. These compounds were tested for their antiviral activity against tobacco mosaic virus, with IC_{50} values of 20.8, 40.8 and 57.7 μM, respectively.

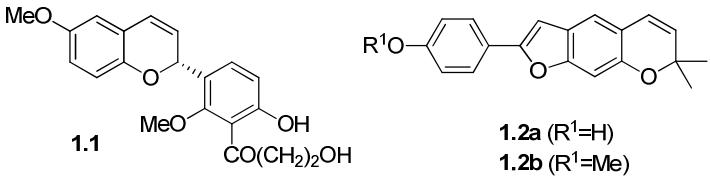


Figure 3: Chemical structure of bioactive gramniphenols **1.1** and **1.2a,b**, extracted from *Arundina gramnifolia* [ref. 32]

Several other natural chromene-based compounds were reported to exhibit anti-inflammatory activity[28]. Compounds **1.3a-c** (**Figure 4**), for example, have been identified from the fruits of *Melicope semecarpifolia*, a low-altitude tree found in the forests of Taiwan and Philippines[33]. They were tested for their anti-inflammatory activity and demonstrated moderate activity (IC_{50} values of 7 and 31 mg/mL) via inhibition of superoxide anion generation and elastase release by human neutrophils. It was also possible to find several publications involving the identification, characterization and evaluation of chromene-based compounds with therapeutical potential against Alzheimer's disease[28]. For example, compounds **1.4** and **1.5** (**Figure 4**) demonstrated AChE inhibitory capacity[34,35], with compound **1.5** being a specific inhibitor of AChE when compared to the *in vitro* results obtained for the BChE enzyme, with a K_i of 3.43 μM and a IC_{50} value of 8.47 μM[35]. Among the synthetic chromenes, designed to search for new biologically active compounds, the number of publications describing promising new synthetic approaches is very ample in the last years. In 2020, Zhao *et al* developed a complete study on the structure-activity relationship between a substituted chromene framework and its antituberculosis activity, describing the synthetic pathway, the *in vitro* and *in vivo* data and the plausible binding mode[36]. From this work, compound **1.5** was highlighted, having moderate activity in acute mouse TB model, favorable mouse and human microsomal stability, low cytotoxicity, and acceptable oral bioavailability (**Figure 4**).

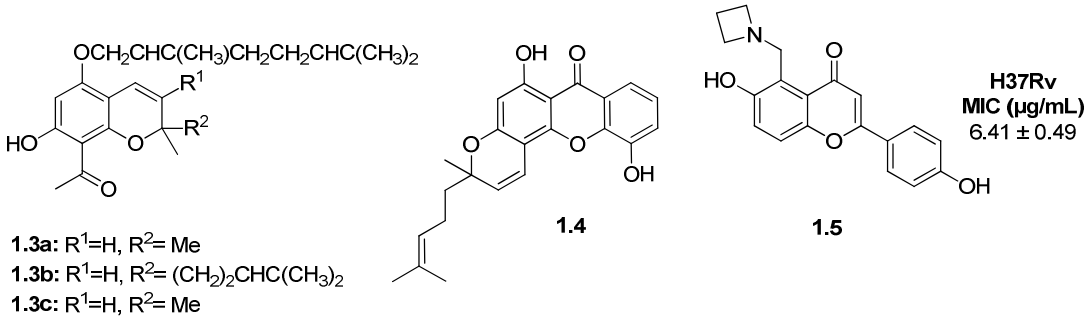
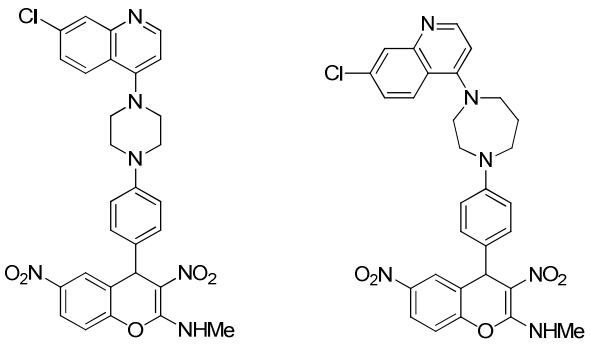


Figure 4: Chemical structure of bioactive gramniphenols **1.3a-c**, chromene-based **1.4**, and compound **1.5** [ref. 33-36]. The MIC values of **1.5** against virulent *M. tuberculosis* is also included

Examples of chromenes with important antimalarial activity has also been reported. In 2015, Parthiban *et al* studied a 2-amino-3-nitro-4*H*-chromene to address the problem of blood-brain barrier (BBB) crossing that is characteristic of the hydrophobic chloroquine derivatives[37]. For this reason, chromene-chloroquine conjugates were developed and tested, resulting in the identification of compounds **1.6** and **1.7** (**Figure 5**).

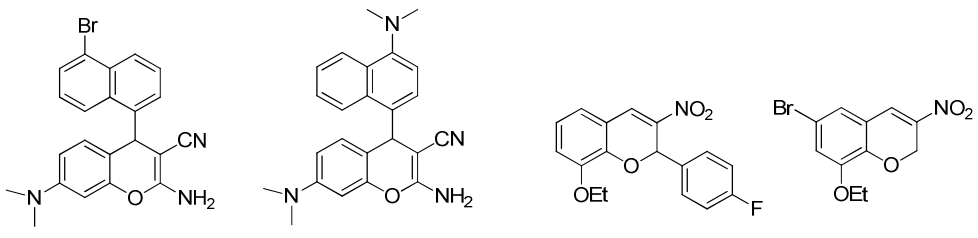


1.6
IC50 (μM)
3D7: 0.62
K1: 1.78

1.7
IC50 (μM)
3D7: 0.29
K1: 0.496

Figure 5: Chemical structure of compounds **1.6** and **1.7**, highlighted by Parthiban *et al* as potential antimalarial agents, with their respective IC_{50} values [ref. 37]

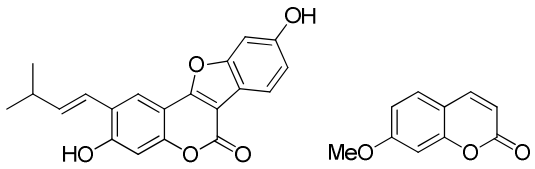
Several synthetic chromene-based compounds with anticancer properties have also been reported. In 2012, Patil *et al* published the synthesis and biological evaluation of new 4*H*-chromenes, which were selected by virtual screening methodologies. The authors showed that compounds **1.8** and **1.9** (**Figure 6**) exhibited promising results against melanoma and prostate cancer[29]. Yin *et al* identified two novel 6-bromo-8-ethoxy-3-nitro-2*H*-chromenes[38], compounds **1.10** and **1.11**, based on 8-ethoxy-2-(4-fluorophenyl)-3-nitro-2*H*-chromene that had previously proved to be a phosphoinositide 3-kinase (PI3K) inhibitor[39]. These new compounds demonstrated to be very active as antiproliferative agents in 12 cancer cell lines, by blocking protein kinase B (Akt) phosphorylation pathway and inducing cell apoptosis (**Figure 6**).



1.8 **1.9** **1.10** **1.11**

Figure 6: Chemical structures of compounds **1.8** and **1.9**, highlighted by Patil *et al* as potentially active against melanoma and prostate cancer, and compounds **1.10** and **1.11**, developed by Yin *et al* as PI3K inhibitors [ref. 29, 38]

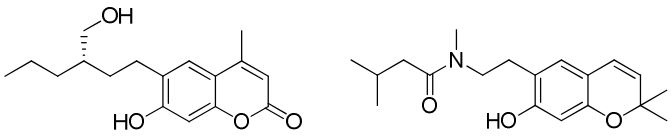
However, among the chromene-based molecular moieties that can be found from both natural and synthetic sources, one of the most important structural motifs in terms of biological activity, is the **coumarin** scaffold. Good examples are: psoralidin (**Figure 7**)[40], isolated from *Psoralea corylifolia,* which showed to have a potent cytotoxic effect on colon, breast and gastric cancer cell lines, as well as antidepressant[41] and antibacterial[42] activities; neo-tanshinlactone[43,44] (**Figure 2**), which was extracted from the root of *Salvia miltiorrhiza,* exhibited low ED_{50} values (0.2-0.6 mg/mL) for both ER+ and ER-/HER-2 overexpressing cell lines; isoscopoletin[45] (**Figure 7**), which was extracted from the roots of *Mallotus resinosus,* was considered a promising starting point for the development of novel anticancer compounds, as it demonstrated to promote DNA cleavage, although with a mild potency. The coumarin scaffold also proved to have multiple and promising pharmacological properties[46], such as anticancer[15,16,18,20], acetilcholinesterase inhibitors[26,47], antitubercular[6,48], antiviral[49–51], antileishmanial[27], anti-HIV[52],antimalarial agents[28], among others.



Psoralidin **Isoscopoletin**

Figure 7: Chemical structures of psoralidin and isoscopoletin [ref.40-42,45]

Examples of coumarin-based compounds with interesting antibacterial activity have also been reported. For instance, a set of 3-amide and 4-aryl-substituted coumarins were evaluated *in vitro* against *Staphylococcus aureus, Escherichia coli, Bacillus cereus, Listeria monocytogenes* and *Salmonella typhi,* among others[53,54]. One example is asphodelin A (**Figure 2**), obtained from bulbs and roots of *Asphodelus microcarpus*, in Egypt. This compound inhibits the growth of *Staphylococcus aureus*, *Escherichia coli* and *Pseudomonas aeruginosa* with a minimal inhibitory concentration (MIC) of 4-16 μg/mL[55]. Another example is pavietin and compound **1.12** (**Figure 8**), isolated from the leaves of *Aesculus pavia* and *Amyris texana*, respectively[56,57]. Pavietin was tested against several fungal pathogens and demonstrated the highest activity against *Guignardia aesculin*, at three different concentrations (50, 100 and 200 μM). Compound **1.12** showed the highest activity against *Botrytis cinerea*, as well as selective algicidal activity against *Planktothrix perornata*, compared with *Selenastrum capricornutum.*

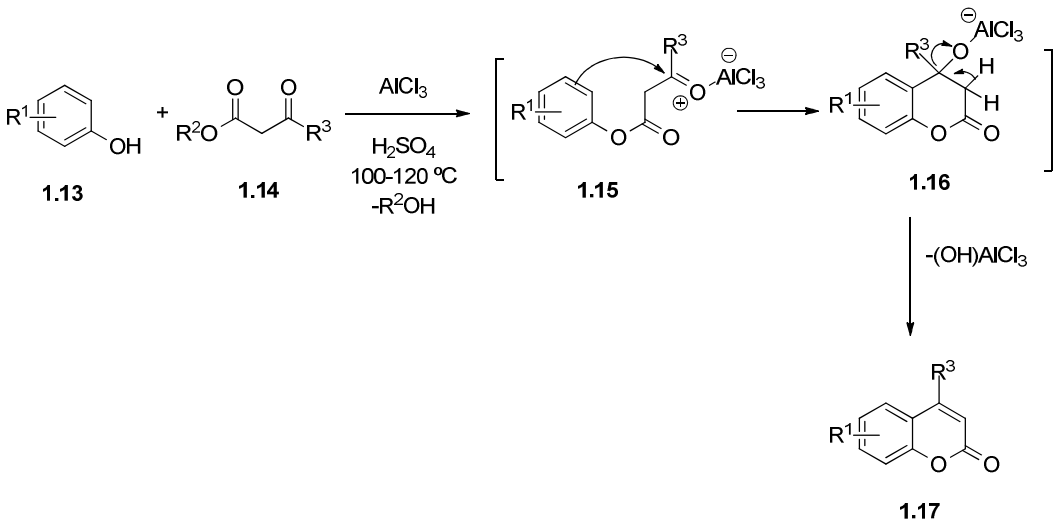


Pavietin **1.12**

Figure 8: Chemical structures of pavietin and compound **1.12** [ref.28,55-57]

1.1.2. Synthetic approaches for the chromene scaffold

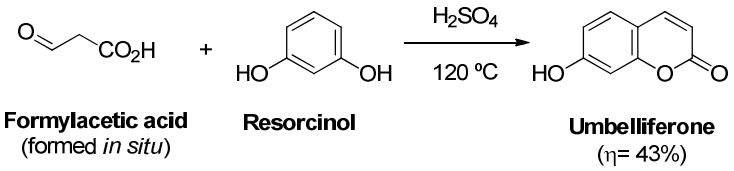
There are several procedures described in the literature for the synthesis of chromene derivatives involving an intramolecular cyclization step[58]. One of the most well-known and applied reactions is the Pechmann reaction (or Pechamnn condensation)[58–60]. This process involves the reaction of a phenol with an ester or carboxylic acid that incorporates a β-carbonyl moiety, and typically requires harsh conditions (depending on the nucleophilicity of the phenol), such as the use of a strong acid (such as H_2SO_4) and high temperatures (100-120 °C). This process occurs in two steps: (i) nucleophilic attack of the phenol moiety to an electrophile (typically an ester); and (ii) Friedel-Crafts cyclization by nucleophilic attack of the aromatic ring to the resulting electrophilic species generated in step (i) (**Scheme 1**). This reaction may involve a Lewis acid (such as $AlCl_3$) to activate the electrophilic species used in the second step (typically ketones, aldehydes or esters)[58].



Scheme 1: Reaction mechanism for Pechmann condensation reaction

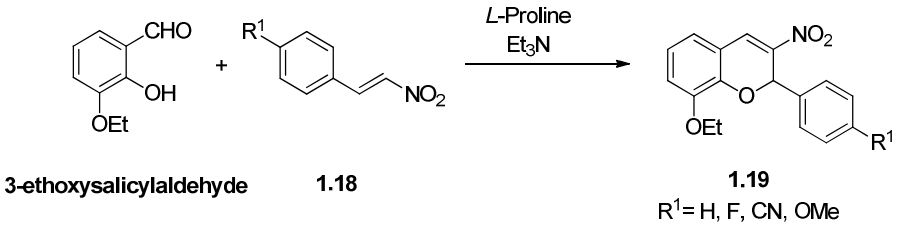
One of the most widely known synthetic products of the Pechmann condensation is umbelliferone and its derivatives[61] (**Scheme 2**). Although a series of catalysts were developed for

the synthesis of the chromene scaffold, the typical Pechmann condensation is still used in the preparation of novel chromene derivatives[62–66].



Scheme 2: Synthetic procedure for the preparation of umbelliferone from formylacetic acid and resorcinol [ref.58]

Other strategies involves the Michael addition of the phenol group of salicylaldehydes to an α,β-unsaturated carbonyl compound[5,38]. For example, by following this approach, in 2013, Yin *et al* reported the synthesis of new promising anticancer agents using 3-ethoxysalicylaldehyde and β-nitrostyrenes **1.18**, in the presence of a catalytic amount of *L*-proline and triethylamine, affording compounds **1.19** in 21-53% yield (**Scheme 3**)[38].

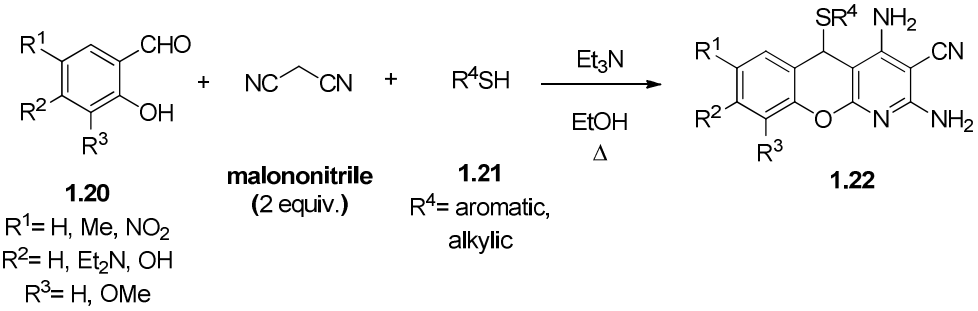


Scheme 3: Synthetic procedure for the preparation of compounds **1.19** by Michael addition of the phenolic oxygen of 3-ethoxysalicylaldehyde to β-nitrostyrenes **1.18**, as proposed by Yin *et al* [ref.38]

However, the Knoevenagel condensation between active methylene compounds to salicylaldehydes, followed by an intramolecular cyclization reaction[31,67] is probably the most widely used procedure for the synthesis of the chromene ring. The reaction typically occurs under basic conditions, and condensation is followed by intramolecular cyclization involving a nucleophilic and an electrophilic species. The Knoevenagel condensation can be performed by a two-component reaction between a salicylaldehyde and an active methylene compound, which generates 2*H*-chromenes, or a three-component reaction between a salicylaldehyde, an active methylene compound and a nucleophile, to generate 4*H*-chromenes.

Since 2000, there have been numerous procedures describing the latter three-component reactions[13,14,67–72]. One of those procedures was reported by Evdokimov *et al*, involving diverse salicylaldehydes (**1.20**), malononitrile and thiols (**1.21**), to generate chromenes **1.22** in good to high yields (**Scheme 4**)[69]. Substituted chromene derivatives were also prepared by modifications on previously synthetized chromene compounds, obtained by the methodologies described

above[20,73,74]. This procedure is usually applied for the preparation of new 5- or 6-membered rings fused to the chromene moiety. This approach promotes a ring expansion or generates dimeric structures, that are frequently used for SAR studies or ligand/target interaction studies.



Scheme 4: Synthetic procedure for the preparation of compounds **1.22** via a three-component Knoevenagel condensation, as proposed by Evdokimov et al [ref.69]

1.1.3. Chromenopyridines: synthesis and biological importance

The chromenopyridine moiety has been widely identified as an interesting scaffold for medicinal chemistry, with several studies reporting their biological activity[75] as antinociceptive[76–78], alpha adrenergic antagonists[79], bronchodilator[80–82], antimicrobial[83] or antibiotic[84], among others. Amlexanon (**Figure 9**), an antiallergic drug that showed clinical effectiveness against atopic diseases, allergic asthma, and rhinitis, is also a molecule with a chromenopyridine sketetal motif. Pranoprofen (**Figure 9**), a non-steroidal anti-inflammatory drug (NSAID) used in ophthalmology, constitutes, in addition to amlexanon, another example of a chromenopyridine-based approved drug.

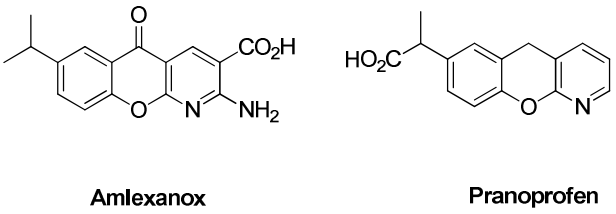
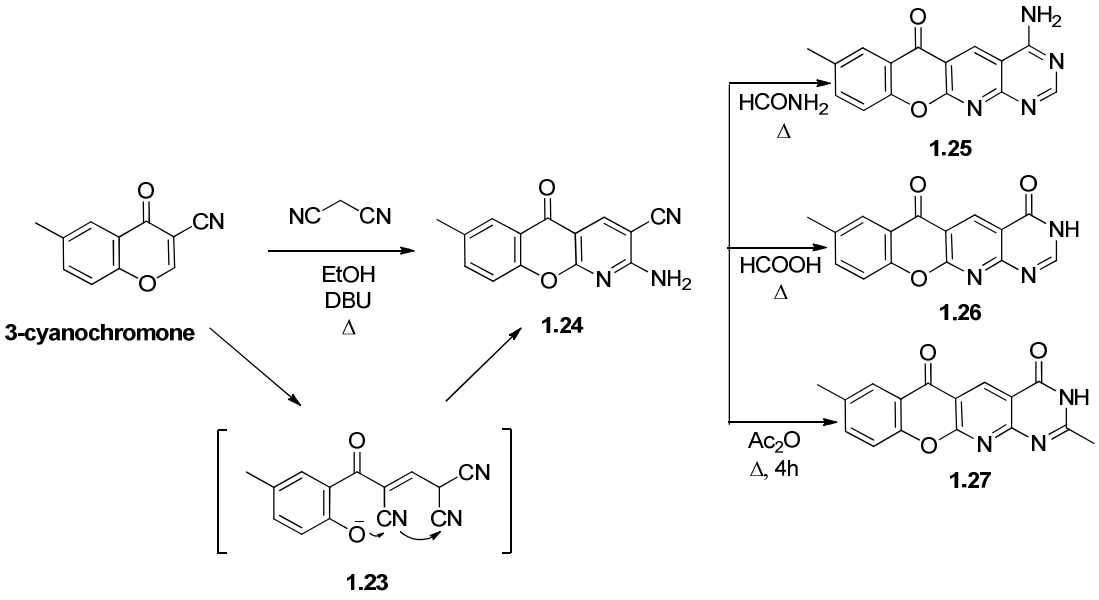


Figure 9: Examples of approved drugs that incorporate a chromenopyridine moiety

Ibrahim *et al* reported the synthesis of diverse chromenopyridines by a cascade process starting from a 3-cyanochromene and involving the pyran ring opening through conjugated addition of the malononitrile anion (**Scheme 5**)[85]. This is followed by intramolecular cyclization, with nucleophilic attack of the phenolate group to one of the nitrile groups generating an imine that cyclizes through nucleophilic attack to the other nitrile group. The reaction was performed in

absolute ethanol, under reflux, using DBU as a base, leading to **1.24**, which was used to prepare the tetracyclic compounds **1.25**, **1.26** and **1.27** by treatment under reflux with formamide, formic acid and acetic anhydride, respectively.



Scheme 5: Synthetic pathways for the preparation of chromenopyridines **1.25-1.27**, as proposed by Ibrahim et al [adapted from ref. 85]

The synthesis of chromenopyridine derivatives **1.28**-**1.30** was also achieved by using the cascade method, starting from 6-methylchromene-3-carbonitrile and diverse activated methylene compounds (**Figure 10**).

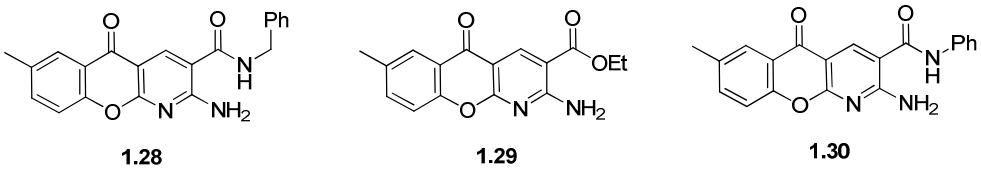
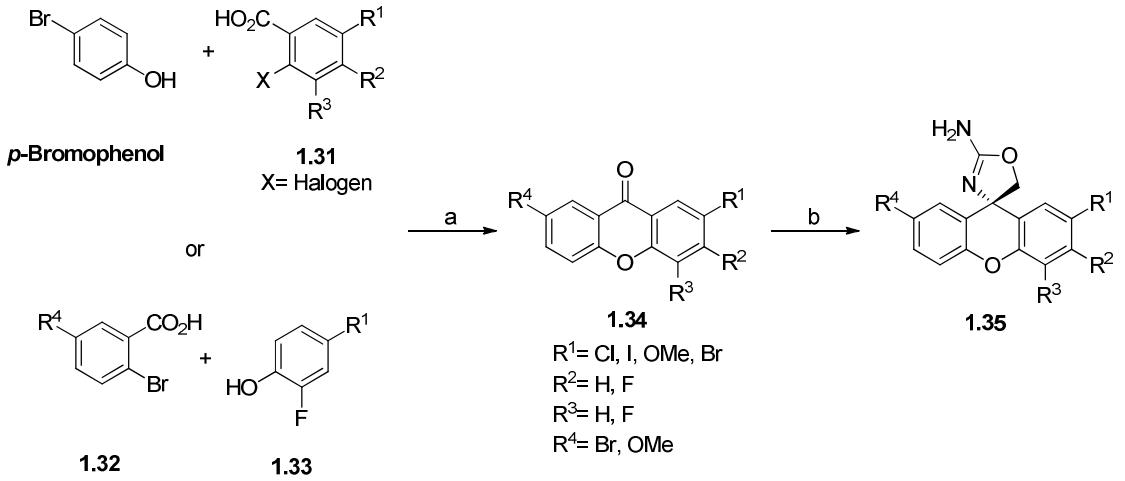


Figure 10: Examples of chromenopyridines synthesized by Ibrahim *et al* [adapted from ref. 85]

Several publications[86–89] on the development of new Inhibitors of β-Site Amyloid Precursor Protein Cleaving Enzyme (BACE1) reported a set of compounds based on the chromenopyridine scaffold. The goal was to improve the selectivity for BACE1 of previously identified products[89], incorporating a nitrogen atom into the xanthene core and to explore the already established SAR studies for BACE1. The chromenopyridine moiety was obtained by condensation of substituted phenols (*p*-bromophenol or **1.32**) with 2-halobenzoic acids **1.31**, in the presence of CuOTf as catalyst, followed by an intramolecular Friedel-Crafts cyclization under acidic conditions, to afford compounds **1.33** (**Scheme 6**)[86,87,89]. The latter compounds were converted into the targeted

aminooxazolines **1.34**, by a two-step procedure. First, an *exo*-olefin was obtained by nucleophilic addition of MeMgCl over the ketone in **1.33**, followed by dehydration of the *in situ* generated tertiary alcohol or through Peterson olefination by treatment with $TMSCH_2Li$, followed by acetyl chloride work-up (**Scheme 6**)[86,87,89].

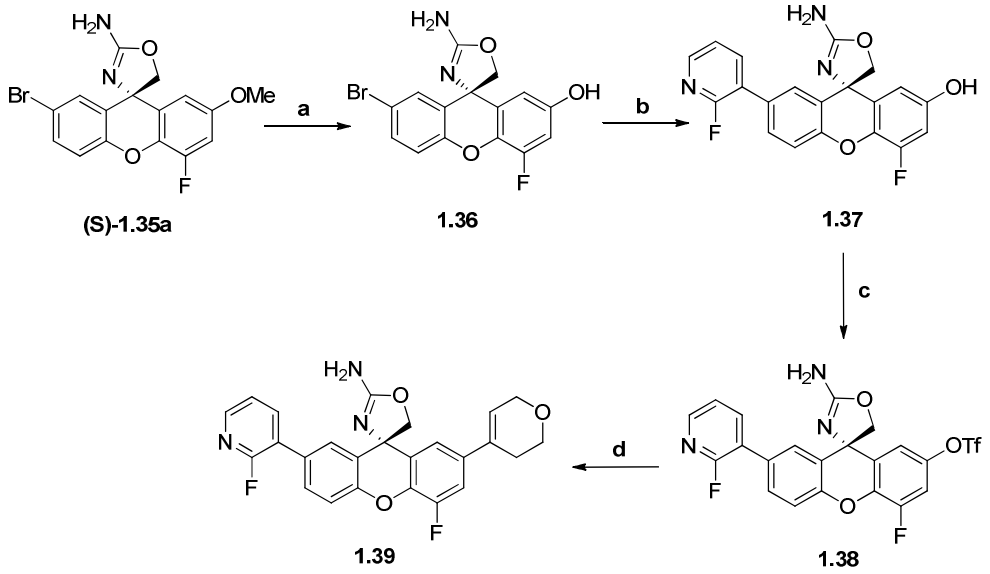


Scheme 6: Synthetic pathways for the preparation of chromenopyridine **1.35**, as proposed by Dineem *et al* [ref. 86], Epstein *et al* [ref. 87] and Huang *et al* [ref. 89]; **a)** (i) Cs_2CO_3, CuOTf (cat.), EtOAc (cat.), toluene, 90 °C, then HCl; (ii) H2SO4 or PPA, 60-110 °C, 26-85 **b)** (i) MeMgCl, THF, - 10 °C, then PPTS or HCl, or $TMSCH_2Li$, THF, -78°C, then AcCl; (ii) AgOCN, THF, 0 °C to r.t., then NH_3, THF, 23-53 %

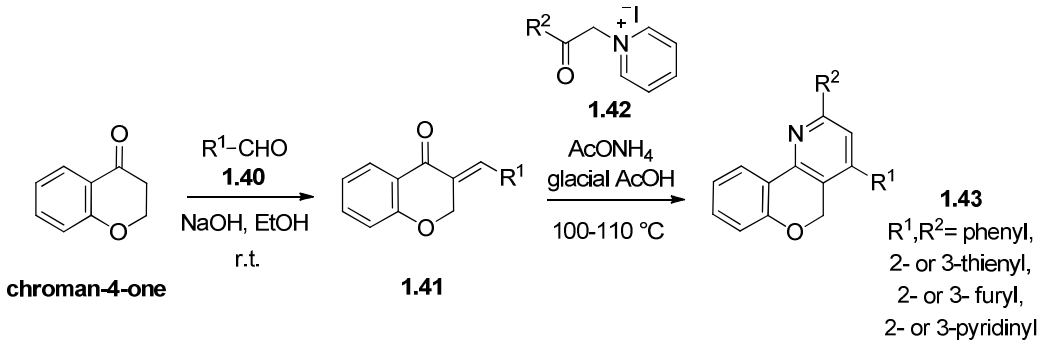
After a series of structure-activity relationship studies using the scaffold **1.35**, compound **1.39** was selected for further evaluation based on its *in vitro* and *in vivo* pharmacodynamic results[87] (**Scheme 7**). The synthetic procedure started by the demethylation of the enantiomer (*S*)-**1.38a** to afford compound **1.36**, which then was used in a Suzuki cross-coupling reaction with 2-fluoro-3-phenylboronic acid to afford compound **1.37** (**Scheme 7**). Compound **1.37** was then used as substrate, in its aryl triflate form (**1.38**), in Pd-catalyzed C-C and C-N coupling reaction with 2-(3,6-dihydro-2*H*-pyran-4-yl)-4,4,5,5-tetramethyl-1,3,2-dioxaborolane to afford compound **1.39**[87] (**Scheme 7**).

Multi-component reactions (MCR), particularly three-component reactions, have been increasingly studied for the synthesis of chromenopyridine derivatives. Thapa *et al*[90,91] developed a new multicomponent reaction to prepare α-terthiophene analogues based on the chromenopyridine moiety, in order to introduce a scaffold rigidity that was predicted to improve its biological activity (**Scheme 8**). Aldol condensation of chroman-4-one with diverse aldehydes **1.40** under basic conditions led to chalcones **1.41**, which were converted into compounds **1.43** by heating at 100 °C with diverse 2-oxoalkylpyridinium iodides **1.42**, in the presence of $AcONH_4$ and

glacial acetic acid. The resulting 2,4-diaryl chromenopyridines **1.43** were tested for their ability as topoisomerases I and II inhibitors, as well as for their cytotoxicity against several human cancer cell lines, with interesting results.



Scheme 7: Synthetic pathways for the preparation of chromenopyridine **1.39**, as proposed by *Epstein et al* [adapted from ref. 87]; **a)** (i) BBr3, DCM, 96%; **b)** 2-fluoro-3-phenylboronic acid, $Pd(PPh_3)4$, Na_2CO_3, DMF/H_2O, 87%; **c)** *N*-(5-chloro-2-pyridyl)bis-(trifluoromethanesulfonimide)(Commins' reagent), Et_3N, DCM, 84%; d) 2-(3,6-dihydro-2*H*-pyran-4-yl)-4,4,5,6-tetramethyl-1,3,2-dioxaborolane, $Pd(PPh_3)_4$, Na_2CO_3, DMF/water, 61%



Scheme 8: Synthesis of chromenopyridines **1.41** and **1.43**, as proposed by Thapa *et al* [adapted from ref.90,91]

As a result of these studies, the same authors described new topoisomerase I and II inhibitors of improved properties based on the chromenopyridine scaffold[92–94]. In particular, chromenopyridines **1.43** in which the R^1 substituent is a phenol group and the R^2 substituent is a thienyl or a phenol group (compounds **1.43a-i**) were the most relevant in terms of selectivity against topoisomerase II (**Figure 11**).

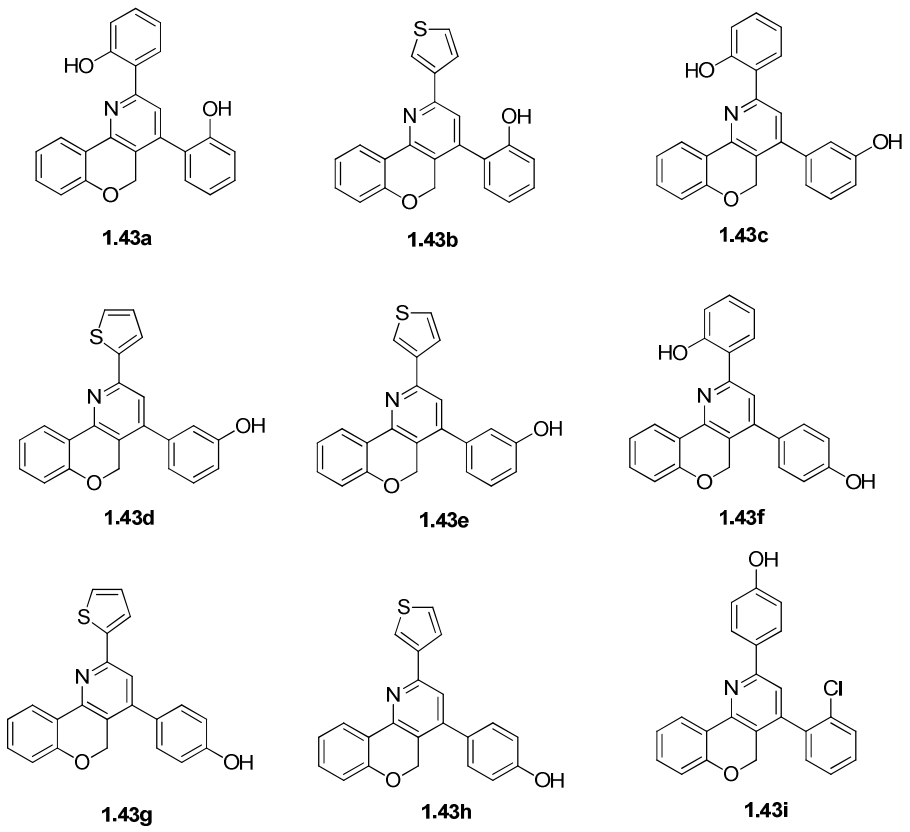
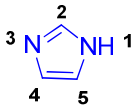


Figure 11: Chemical structure of topoisomerase II inhibitors **1.43a-i** designed by Thapa *et al* and Magdar *et al* [ref. 92-94]

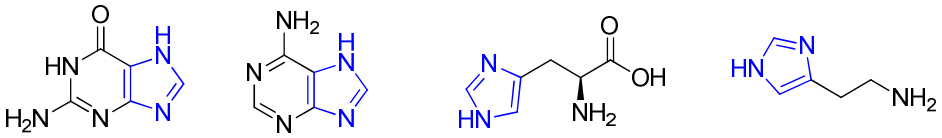
Moreover, this new batch of chromenopyridine derivatives showed interesting and improved results in various cancer cell lines, including breast cancer cell lines T47D. The selectivity between non-tumorigenic cell line MCF10A, and breast cancer cell lines was also noteworthy, which proved to be up to 18-fold higher than the reference for derivative **1.43g** (**Figure 11**). Further SAR studies identified compound **1.43i** (**Figure 11**) with relevant properties[94].

1.2 Imidazole scaffold

Imidazole is a five-membered aromatic molecule that contains two nitrogen atoms, in which one behaves as a pyrrole-type nitrogen and the other as a pyridine-type nitrogen (**Figure 12**)[95]. The systematic IUPAC name is 1,3-diazole, but this terminology is rarely used in the literature. This moiety is present in many highly relevant compounds with important biological properties, such as the DNA nucleotides adenine and guanine, the amino acid histidine, purines and histamines[95–97] (**Figure 12**).



Imidazole

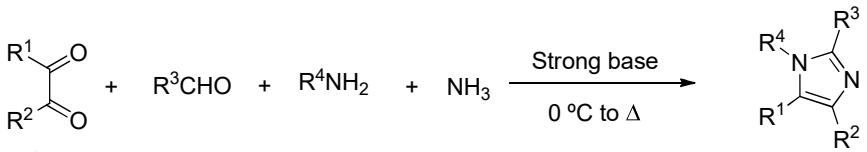


guanine **adenine** **histidine** **histamine**

Figure 12: Chemical structure of imidazole, guanine, adenine, histidine, and histamine

Imidazoles possess an amphoteric behaviour, as they can act as an acid and as a base and are also susceptible to both electrophilic and nucleophilic attacks. This effect leads to two different dissociation constants (pKa) for each nitrogen of the imidazole ring: 7 (conjugated base behaviour of N-3) and 14.9 (conjugated acid behaviour of N-1)[96]. The physical and chemical properties of imidazoles, such as their amphoteric nature, polarity and solubility, together with the synthetic versatility, makes this aromatic structure an interesting scaffold for the development of new compounds for various applications, from biologically active structures to materials science, polymers and catalysts[95,97,98].

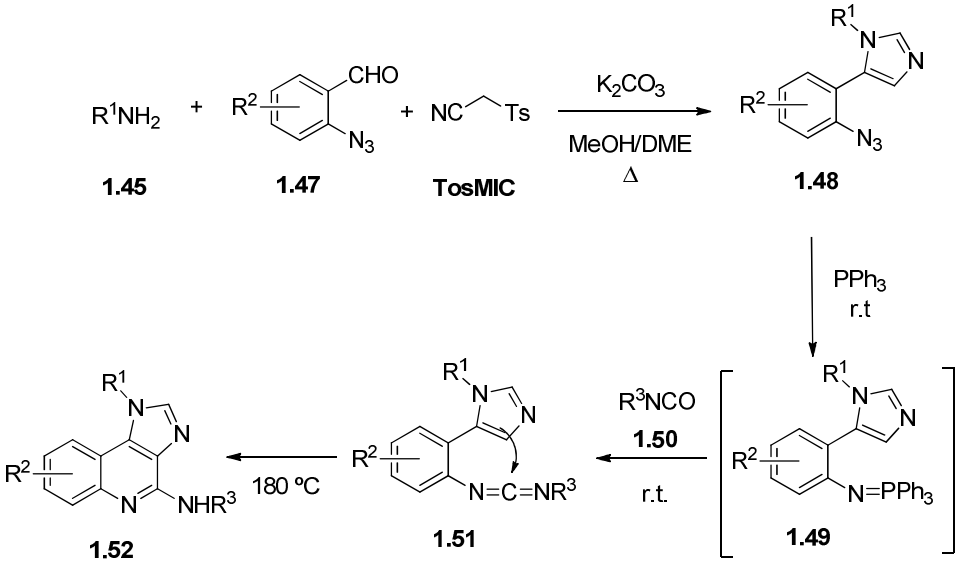
The imidazole ring was first reported by Heinrich Debus in 1858[99], prepared from the reaction of glyoxal with formaldehyde and ammonia, which conferred its first name: glyoxaline. Nowadays, this procedure was optimized and patented (with one equivalent of a primary amine and one equivalent of ammonia instead of the typical two equivalents of ammonia) and is typically known as Debus-Radziszewski imidazole synthesis (**Scheme 9**)[100]. Nevertheless, other methodologies to prepare substituted imidazoles were developed, such as the Wallach synthesis, Marckwald synthesis, and others[96].



1.44 **1.40** **1.45** **ammonia** **1.46**

Scheme 9: General procedure for the Debus-Radziszewski imidazole synthesis [ref. 100]

Moreover, diverse strategies for the synthesis of substituted imidazoles have been reported[98,101]. In particular, the synthetic methods have been evolved to the development of routes that allow the incorporation of the desired substituents in the imidazole moiety rather than the preparation of the 1,3-diazole core and subsequent substitution[96,101]. The available synthetic methodologies typically involve a two-step procedure, with the formation of an open-chain structure and further intramolecular cyclization, a two- or three-component reaction or the rearrangement of other heterocyclic structures such as triazoles or tetrazoles. A good example is the synthesis of imidazoquinolines **1.55** reported by Guan *et al*[102] that involves a stepwise Leusen/Staudinger/aza-Wittig/carbodiimide-mediated cyclization procedure (**Scheme 10**). The approach requires the synthesis of azides **1.51**, which are prepared by three-component reaction involving primary amines **1.48**, 2-azidobenzaldehyde **1.50** and toluenesulfonylmethyl isocyanide (**TosMIC**). Next, Staudinger reaction of the azides **1.51** by treatment with triphenylphosphine and subsequent reaction with isocyanates **1.53** afforded derivatives **1.54**. The imidazoquinolines **1.55** are finally obtained in good to moderate yields by thermal intramolecular cyclization at 180 °C.



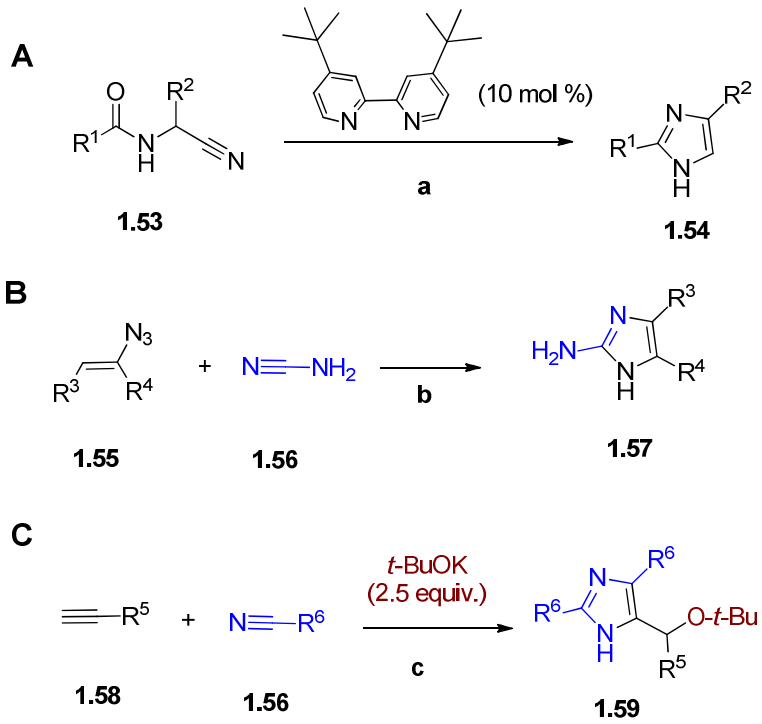
Scheme 10: General procedure for the synthesis of imidazolquinolines **1.52**, reported by Guam *et al* [102]

In an extensive review, published in 2020 by Shabalin and Camp[101], a set of methods for preparing substituted imidazoles are compiled, which are organized by the number of bonds formed during the synthetic process. For one-bond formation procedures, a limited number of recent publications have been described, with a special emphasis to the protocol involving the

intramolecular cyclization between an amine and a nitrile group, as was proposed by Fang *et al*[103] (**Scheme 11**A).

For two-bond formation procedures, a wider variety of protocols have been described. A good example is the method reported by Man *et al*[104] for the synthesis of 2-aminoimidazoles **1.60** involving the reaction of cyanamides with 2*H*-aziridines, which are generated *in situ* from vinylazides **1.58**, followed by reaction with amine **1.59** (**Scheme 11B**).

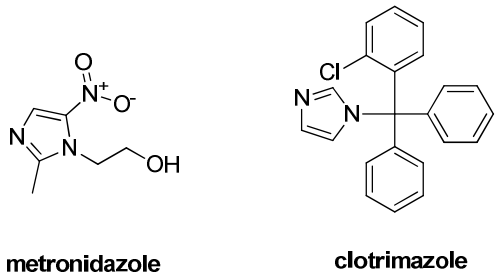
For the three-bond formation approaches, is worth highlighting the synthesis of the trisubstituted imidazoles **1.60** described by Wang *et al*[105]. This method involves the reaction of two equivalents of the nitriles **1.62** with the *in situ* generated acetylide from alkynes **1.63**, in the presence of 2.5 equivalents of *t*-BuOK, which acts as both base and nucleophile (**Scheme 11C**). This methodology allowed the preparation of substituted imidazoles with alkyl, aryl and heteroaryl substituents.



Scheme 11: Synthetic procedures for the preparation of imidazoles **1.54** (Fang *et al*, ref. 103), **1.57** (Man *et al*, ref. 104) and **1.59** (Wang *et al*, ref. 105) [adapted from 101]; **a**) $R^2B(OH)_2$ (2.0 equiv.), $Ni(PPh_3)_2Br_2$ (10 mol %), Na_2SO_4 (3 equiv.), toluene, 120 °C, 24h, 38 examples, 13-90 %; **b)** Et_3N (2.0 equiv.), thermally, EtOH, 85 °C, 14 h or KOAc (20 mol%), microwave, *t*-BuOH, 125 °C, 20 min. or KOAc (20 mol%), blue light, EtOH, r.t., 2 h; **c)** cyclohexane, 110 °C, 11 h, silica gel, 30 examples, 49-93%

1.2.1 Biological importance of the imidazole moiety

The biological importance of the imidazole ring is widely recognized[95–97], with this unit appearing in several compounds showing antibacterial[96,97,106–108], antifungal[109–111], anti-inflammatory[112,113], antiviral[106,114,115], anticancer[97,109,116–119], antihistaminic[109,120,121], among other recognized biological activities[98]. There are already several imidazole-based approved drugs for the treatment of various diseases. For example, metronidazole, a drug approved as antibiotic and antiprotozoal for several microbial infections, is a 1,2,5-trisubstituted imidazole and is widely used in clinical practice[96,122,123] (**Figure 13**). Other example is clotrimazole, an antifungal prescribed for the treatment of fungal skin infections such as athlete's foot and ringworm, that contains an imidazole ring fused to a central sp^3 carbon (**Figure 13**).



metronidazole **clotrimazole**

Figure 13: Chemical structure of metronidazole and clotrimazole

Currently, the imidazole moiety is still being studied for a wide variety of biological applications. Zheng *et al*[125] refer, in a 2020 review article, a series of new imidazole derivatives, prepared using Van Leusen imidazole synthesis. In 2021, Rodríguez-Arévalo *et al*[126] reported the synthesis of novel benzofuranoyl-2-imidazoles that are able to bind and modulate the activity of several imidazoyl-I_2 receptors, whose deregulation is associated with a series of physiological conditions, including Alzheimer's disease. The most promising compound, LSL60101 (**Figure 14**), which presented the most relevant pharmacokinetics profile, was able to penetrate the blood-brain-barrier and demonstrated to be able to reduce the FADD protein content in *in vivo* models.

Also in 2021, Beltran-Hortelano *et al*[127] prepared a series of imidazoles and benzimidazoles by base-catalysed Michael addition of the appropriate imidazole/benzimidazole to the previously prepared vinyl ketones. These studies allowed for the identification of compound **1.60** (**Figure 14**) that proved to be active against Chagas disease. This derivative was selected for having the most trypanocidal activity throughout the distinct life stages of the parasite, not possessing host cell genotoxicity and rapidly acting at low administered concentrations (micromolar range).

Ammazzalorso *et al*[128] reported a series of novel inhibitors of the aromatase enzyme, which is involved in the biosynthesis of estrogens, that possess either an imidazole or a triazole nucleus. These new compounds, which were developed for the development of new anticancer therapies, coordinate to the iron core of the heme group, the substrate of the aromatase enzyme, and therefore block the estrogen biosynthesis. Among the reported compounds, derivatives **1.61** and **1.62** (**Figure 14**) were highlighted, with the imidazole-based compounds having lower IC_{50}, in human breast cancer cells MCF-7, than any of the triazole derivatives tested.

In 2018, Dubovis *et al* reported the synthesis of novel substituted1-(1*H*-imidazole-4-yl)-1*H*-1,2,3-triazoles **1.63** (**Figure 14**)[129]. These compounds were tested for their antifungal activity by assessing the mycelium radius growth of a series of different fungal species and comparing with a standard (Triadimefon). The results demonstrated that several compounds presented satisfactory growth inhibition percentages and could be used as starting materials for the preparation of new antifungal agents.

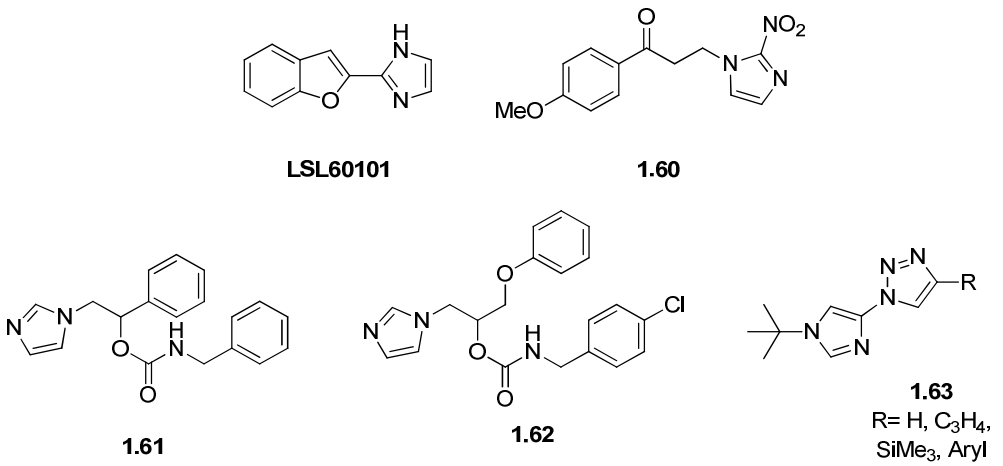


Figure 14: Chemical structure of bioactive compounds containing the imidazole moiety [125-129]

REFERENCES:

[1] Kaur, N. Six-membered O,O-heterocycles in metal- and nonmetal-Assisted synthesis of six-membered heterocycles. 351–412 (2020). doi:10.1016/B978-0-12-820282-1.00007-5.

[2] Musicki, B. *et al.* Improved antibacterial activities of coumarin antibiotics bearing 5′, 5′-dialkylnoviose : biological activity of RU79115. *Bioorg. Med. Chem. Lett* **10**, 1695–1699 (2000).

[3] Alt, S. *et al*. An artificial pathway to 3,4-dihydroxybenzoic acid allows generation of new aminocoumarin antibiotic recognized by catechol transporters of E. coli. *Chem. Biol.* **18**, 304–313 (2011).

[4] Vahabi, V. & Hatamjafari, F. Microwave assisted convenient one-pot synthesis of coumarin derivatives via Pechmann condensation catalyzed by FeF3 under solvent-free conditions and antimicrobial activities of the products. *Molecules* **19**, 13093–13103 (2014).

[5] Angelova, V. T. *et al.* Antimycobacterial activity of novel hydrazide-hydrazone derivatives with 2H-chromene and coumarin scaffold. *Bioorg Med. Chem. Lett.* **27**, 223–227 (2017).

[6] Hu, Y. Q. *et al.* Recent developments of coumarin-containing derivatives and their anti-tubercular activity. *Eur. J. Med. Chem.* **136**, 122–130 (2017).

[7] Konstantina C. Fylaktakidou *et al.* Natural and Synthetic Coumarin Derivatives with Anti-Inflammatory / Antioxidant Activities. *Curr. Pharm. Des.* **10**, (2004).

[8] Kostova, I. *et al.* Structure-activity relationships of synthetic coumarins as HIV-1 inhibitors. *Bioinorg. Chem. Appl.* **2006**, (2006).

[9] Kostova, I. Synthetic and Natural Coumarins as Antioxidants. *Mini-Reviews Med. Chem.* **6** (2006).

[10] Subbareddy, C. V. Subashini, R. & Sumathi, S., Synthesis of substituted 2H-chromenes by a three-component reaction as potential antioxidants. *Mol. Divers.* **21**, 841–848 (2017).

[11] Anthony, S. P. *et al.* EPC2407, a new beta-tubulin vascular disrupting agent with potent apoptosis and cell growth inhibition. *J. Clin. Oncol.* **25**, 14043 (2007).

[12] Donnelly, A. C. *et al.* The design, synthesis, and evaluation of coumarin ring derivatives of the novobiocin scaffold that exhibit antiproliferative activity. *J. Org. Chem.* **73**, 8901–8920 (2008).

[13] Alblewi, F. F. *et al.* Antiproliferative effect, cell cycle arrest and apoptosis generation of novel synthesized anticancer heterocyclic derivatives based 4*H*-benzo[h]chromene. *Bioorg. Chem.* **87**, 560–571 (2019).

[14] Patil, S. A. *et al.* New substituted 4*H*-chromenes as anticancer agents. *Bioorg. Med. Chem. Lett.* **22**, 4458–4461 (2012).

[15] Emami, S. & Dadashpour, S. Current developments of coumarin-based anti-cancer agents in medicinal chemistry. *Eur. J. Med. Chem.* **102**, 611–630 (2015).

[16] Thakur, A., Singla, R. & Jaitak, V. Coumarins as anticancer agents: A review on synthetic strategies, mechanism of action and SAR studies. *Eur. J. Med. Chem.* **101**, 476–495 (2015).

[17] Halawa, A. H. *et al.* Synthesis, biological evaluation and molecular docking studies of 4*H*-benzo[h]chromenes, 7*H*-benzo[h]chromeno[2,3-d]pyrimidines as antitumor agents. *Lett. Drug Des. Discov.* **13**, 77–88 (2016).

[18] Bisi, A. *et al.* Coumarin derivatives as potential antitumor agents: Growth inhibition, apoptosis induction and multidrug resistance reverting activity. *Eur. J. Med. Chem.* **127**, 577–585 (2017).

[19] Mbaba, M. *et al.* Ferrocenyl and organic novobiocin derivatives: Synthesis and their in vitro biological activity. *J. Inorg. Biochem.* **172**, 88–93 (2017).

[20] Elshemy, H. A. H. & Zaki, M. A. Design and synthesis of new coumarin hybrids and insight into their mode of antiproliferative action. *Bioorgan. Med. Chem.* **25**, 1066–1075 (2017).

[21] Li, H. *et al.* Anticancer carbazole alkaloids and coumarins from Clausena plants: A review. *Chin. J. Nat. Med.* **15**, 881–888 (2017).

[22] Correia, C., Carvalho, M. A. & Proença, M. F. Synthesis and in vitro activity of 6-amino-2,9-diarylpurines for Mycobacterium tuberculosis. *Tetrahedron* **65**, 6903–6911 (2009).

[23] Abdelhafez, O. M. *et al.* Synthesis, anticoagulant and PIVKA-II induced by new 4-hydroxycoumarin derivatives. *Bioorgan. Med. Chem.* **18**, 3371–3378 (2010).

[24] Patil, P. O. *et al.* A comprehensive review on synthesis and designing aspects of coumarin derivatives as monoamine oxidase inhibitors for depression and Alzheimer's disease. *Bioorgan. Med. Chem.* **21**, 2434–2450 (2013).

[25] Matos, M. J. *et al.* Novel (coumarin-3-yl)carbamates as selective MAO-B inhibitors: Synthesis, in vitro and in vivo assays, theoretical evaluation of ADME properties and docking study. *Eur. J. Med. Chem.* **63**, 151–161 (2013).

[26] de Souza, L. G., Rennã, M. N. & Figueroa-Villar, J. D. Coumarins as cholinesterase inhibitors: A review. *Chem. Biol. Interact.* **254**, 11–23 (2016).

[27] Gonçalves, G. A. *et al.* Natural and synthetic coumarins as antileishmanial agents: a review. *Eur. J. Med. Chem.* **203**, (2020).

[28] Costa, M., Dias, T. A., Brito, A. & Proença, F. Biological importance of structurally diversified chromenes. *Eur. J. Med. Chem.* **123**, 487–507 (2016).

[29] A Patil, S. *et al.* Chromenes: potential new chemotherapeutic agents for cancer. *Futur. Med. Chem.* **5**, 1647–1660 (2013).

[30] Raj, V. & Lee, J. 2*H*/4*H*-Chromenes—A Versatile Biologically Attractive Scaffold. *Front. Chem.* **8**, 1–23 (2020).

[31] Borges, F. *et al.* Simple Coumarins and Analogues in Medicinal Chemistry: Occurrence, Synthesis and Biological Activity. *Curr. Med. Chem.* **12**, 887–916 (2005).

[32] Hu, Q. F. *et al.* Antiviral phenolic compounds from Arundina gramnifolia. *J. Nat. Prod.* **76**, 292–296 (2013).

[33] Chen, J. J. *et al.* Benzoic acid derivatives, acetophenones, and anti-inflammatory constituents from Melicope semecarpifolia. *J. Nat. Prod.* **71**, 71–75 (2008).

[34] Brühlmann, C. *et al.* Screening of Non-Alkaloidal Natural Compounds as Acetylcholinesterase Inhibitors. *Chem. Biodivers.* **1**, 819–829 (2004).

[35] Khan, M. T. H. *et al.* Cholinesterase inhibitory activities of some flavonoid derivatives and chosen xanthone and their molecular docking studies. *Chem. Biol. Interact.* **181**, 383–389 (2009).

[36] Zhao, W. *et al.* Design, synthesis, and biological evaluation of novel 4*H*-chromen-4-one derivatives as antituberculosis agents against multidrug-resistant tuberculosis. *Eur. J. Med. Chem.* **189**, 112075 (2020).

[37] Parthiban, A. *et al.* Synthesis, in vitro and in silico antimalarial activity of 7-chloroquinoline and 4*H*-chromene conjugates. *Bioorganic Med. Chem. Lett.* **25**, 4657–4663 (2015).

[38] Yin, S. Q. *et al.* Preparation of S14161 and its analogues and the discovery of 6-bromo-8-

ethoxy-3-nitro-2*H*-chromene as a more potent antitumor agent in vitro. *Bioorgan. Med. Chem. Lett.* **23**, 3314–3319 (2013).

[39] Mao, X. *et al.* A small-molecule inhibitor of D-cyclin transactivation displays preclinical efficacy in myeloma and leukemia via phosphoinositide 3-kinase pathway. *Blood* **117**, 1986–1997 (2011).

[40] Mar, W., Je, K. H. & Seo, E. K. Cytotoxic constituents of Psoralea corylifolia. *Arch. Pharm. Res.* **24**, 211–213 (2001).

[41] Yi, L. T. *et al.* Antidepressant-like effects of psoralidin isolated from the seeds of Psoralea Corylifolia in the forced swimming test in mice. *Prog. Neuro-Psychopharmacology Biol. Psychiatry* **32**, 510–519 (2008).

[42] Khatune, N. A. *et al.* Antibacterial compounds from the seeds of Psoralea corylifolia. *Fitoterapia* **75**, 228–230 (2004).

[43] Dong, Y., Morris-Natschke, S. L. & Lee, K. H. Biosynthesis, total syntheses, and antitumor activity of tanshinones and their analogs as potential therapeutic agents. *Nat. Prod. Rep.* **28**, 529–542 (2011).

[44] Wang, X. *et al.* Anti-Breast Cancer Activity of Neo-tanshinlactone from Salvia miltiorrhiza. *J. Med. Chem.* **47**, 5816–5819 (2004).

[45] Ma, J., Jones, S. H. & Hecht, S. M. A coumarin from Mallotus resinosus that mediates DNA cleavage. *J. Nat. Prod.* **67**, 1614–1616 (2004).

[46] Kumar, K. A. *et al.* Comprehensive review on coumarins: Molecules of potential chemical and pharmacological interest. *J. Chem. Pharm. Res.* **7**, 67–81 (2015).

[47] Song, M. qiu *et al.* Design, synthesis and biological evaluation of new carbazole-coumarin hybrids as dual binding site inhibitors of acetylcholinesterase. *J. Mol. Struct.* **1229**, 129784 (2021).

[48] Reddy, D. S. Kongot, M. & Kumar, A., Coumarin hybrid derivatives as promising leads to treat tuberculosis: Recent developments and critical aspects of structural design to exhibit anti-tubercular activity. *Tuberculosis* **127**, 102050 (2021).

[49] Li, Z. *et al.* Pharmacological perspectives and molecular mechanisms of coumarin derivatives against virus disease. *Genes Dis.* 103307 (2021) doi:10.1016/j.gendis.2021.03.007.

[50] Hu, Y. *et al.* Synthesis and antiviral activity of coumarin derivatives against infectious hematopoietic necrosis virus. *Bioorganic Med. Chem. Lett.* **29**, 1749–1755 (2019).

[51] Mishra, S., Pandey, A. & Manvati, S. Coumarin: An emerging antiviral agent. *Heliyon* **6**, e03217 (2020).

[52] Xu, Z. *et al.* Coumarin-based derivatives with potential anti-HIV activity. *Fitoterapia* **150**, 104863 (2021).

[53] Jaswal, S. *et al.* Recent advancements in the medicinal chemistry of bacterial type II topoisomerase inhibitors. *Bioorg. Chem.* **104**, 104266 (2020).

[54] Mani Chandrika, K. V. S. & Sharma, S. Promising antifungal agents: A minireview. *Bioorgan. Med. Chem.* **28**, 115398 (2020).

[55] El-Seedi, H. R. Antimicrobial arylcoumarins from Asphodelus microcarpus. *J. Nat. Prod.*

70, 118–120 (2007).

[56] Curir, P. *et al.* Pavietin, a coumarin from Aesculus pavia with antifungal activity. *J. Nat. Prod.* **70**, 1668–1671 (2007).

[57] Meepagala, K. M. *et al*. New class of algicidal compounds and fungicidal activities derived from a chromene amide of amyris texana. *J. Agric. Food Chem.* **58**, 9476–9482 (2010).

[58] Katritzky, A. R. *et al*. 4.4 - Synthesis of Bicyclic Ring Systems Without Ring Junction Heteroatoms. in *Handbook of Heterocyclic Chemistry (Third Edition)* (eds. Katritzky, A. R., Ramsden, C. A., Joule, J. A. & Zhdankin, V. V), 797–871 (Elsevier, 2010). doi:https://doi.org/10.1016/B978-0-08-095843-9.00015-X.

[59] Pechmann, V. H. Neue Bildungsweise der Cumarine. Synthese des Daphnetins. I. *Berichte der Dtsch. Chem. Gesellschaft* **17**, 929–936 (1884).

[60] S. Zambare, A. *et al*. Recent Advances in the Synthesis of Coumarin Derivatives via Pechmann Condensation. *Curr. Org. Chem.* **20**, 798–828 (2015).

[61] Ahluwalia, V. K. *et al*. *Intermediates for Organic Synthesis*. (I. K. International Publishing House, 2005).

[62] Anand, A. *et al.* A click chemistry approach for the synthesis of mono and bis aryloxy linked coumarinyl triazoles as anti-tubercular agents. *Eur. J. Med. Chem.* **105**, 194–207 (2015).

[63] Salehian, F. *et al.* A review: Biologically active 3,4-heterocycle-fused coumarins. *Eur. J. Med. Chem.* **212**, 113034 (2021).

[64] Azelmat, J. *et al.* Synthesis and evaluation of antibacterial and anti-inflammatory properties of naturally occurring coumarins. *Phytochem. Lett.* **13**, 399–405 (2015).

[65] Pornsatitworakul, S. *et al.* The coumarin synthesis: a combined experimental and theoretical study. *Monatshefte fur Chemie* **148**, 1245–1250 (2017).

[66] Manhas, M. S. *et al*. Microwave initiated reactions: Pechmann coumarin synthesis, Biginelli reaction, and acylation. *Tetrahedron Lett.* **47**, 2423–2425 (2006).

[67] Wang, H. *et* al. Regioselective synthesis and evaluation of 2-amino 3-cyano chromene-chrysin hybrids as potential anticancer agents. *Bioorg. Med. Chem. Lett.* **30**, 127087 (2020).

[68] Dige, N. C. *et al.* Synthesis and characterization of new 4*H*-chromene-3-carboxylates ensuring potent elastase inhibition activity along with their molecular docking and chemoinformatics properties. *Bioorg. Chem.* **100**, 103906 (2020).

[69] Evdokimov, N. M. *et al.* One-step synthesis of heterocyclic privileged medicinal scaffolds by a multicomponent reaction of malononitrile with aldehydes and thiols. *J. Org. Chem.* **72**, 3443–3453 (2007).

[70] Okasha, R. M. *et al.* Design of new benzo[h]chromene derivatives: antitumor activities and structure-activity relationships of the 2,3-positions and fused rings at the 2,3-positions. *Molecules* **22**, (2017).

[71] Dinh, N. *et al.* Efficient click chemistry towards novel 1*H*-1,2,3-triazole-tethered 4*H*-chromene-*D*-glucose conjugates: Design, synthesis and evaluation of in vitro antibacterial, MRSA and antifungal activities. *Eur. J. Med. Chem.* **167**, 454–471 (2019).

[72] Tashrifi, Z. *et al*. Synthesis and pharmacological properties of polysubstituted

2 - amino-4H-pyran-3-carbonitrile derivatives. *Mol. Divers.* **24**, 1385–1431 (2020).

[73] Chitreddy, S. V & Shanmugam, S. Solvent free-synthesis of highly functionalized 4*H*-chromene-3-carboxamide derivatives using cerium ammonium nitrate and their antioxidant, antibacterial and solvatochromism studies. *J. Mol. Liq.* **243**, 494–502 (2017).

[74] Chaudhari, H. K., Pahelkar, A. & Takale, B. S. Preparative-scale synthesis of amino coumarins through new sequential nitration and reduction protocol. *Tetrahedron Lett.* **58**, 4107–4110 (2017).

[75] J. Nunez-Vergara, L. *et al.* Chromenopyridines: promising scaffolds for medicinal and biological chemistry. *Curr. Med. Chem.* **18**, 4761–4785 (2011).

[76] Razdan, K. K. *et al*. Steroidal Analog of a Tetrahydrocannabinol. *J. Med. Chem.* **11**, 377–378 (1968).

[77] Pars, H. G. *et al*. Physiologically Active Nitrogen Analogs of Tetrahydrocannabinols, Tetrahydrobenzopyrano[3,4-d]pyridines. *J. ofthe Am. Chem. Soc.* **88**, 3664–3665 (1966).

[78] Pars, H. G. *et al.* Drugs Derived from Cannabinoids. 1. Nitrogen Analogs, Benzopyranopyridines and Benzopyranopyrroles. *J. Med. Chem.* **19**, (1976).

[79] Meyer, M.D., Altenbach, R. J. Basha, F., Carroll, W.A., Drizin, I., Kerwin, J. F., Wendt, M.D., Haight, A. R., and Zhang, W. Preparation of Benzopyranopyrrole and Benzopyranopyridine as alpha-1 Adrenergic Antagonists. WO9824791, 1 (1998).

[80] Brown, R.E.; Puchalski, C.; Shavel, J. Jr. Novel substituted benzopyranopyridine. U.S. Patent 3,962,266, May, 1 (1975).

[81] Connor, D. T. *et al.* Synthesis of 1,2,3,4-tetrahydro-5*H*-[1]benzopyrano[3,4-c]pyridin-5-ones. II. Substitution at the 3-position with 2-aminoethyl and 2-aminopropyl side chains. *J. Heterocyclic Chem.* **21**, 1561–1564 (1984).

[82] Connor, D. T. *et al.* Synthesis of 1,2,3,4-tetrahydro-5H-[1]benzopyrano[3,4-c]pyridin-5-ones. I. 3-unsubstituted compounds. *J. Heterocyclic Chem.* **21**, 1557–1559 (1984).

[83] Stojanovic, G., Vukic, R. & Radulovic, N. New 3 ,4-annelated coumarin derivatives : synthesis , antimicrobial activity, antioxidant capacity, and molecular modeling. *Monatsh. Chem.* **137,** 1477–1486 (2006). https://doi.org/10.1007/s00706-006-0537-6

[84] Dawane, B. S., Konda, S. G. & Bodade, R. G. An efficient one-pot synthesis of some new 2 , 4-diaryl pyrido[3,2-c]coumarins as potent antimicrobial agents. *J. Heterocyclic Chem.* 237 (2010) doi:10.1002/jhet.

[85] Ibrahim, M. A. *et al*. Synthesis of some novel heteroannelated chromones by basic rearrangement of 6-methylchromone-3-carbonitrile. *Chem. Heterocycl. Compd.* **50**, 1624–1633 (2015).

[86] Dineen, T. A. *et al.* Inhibitors of β-site amyloid precursor protein cleaving enzyme (BACE1): Identification of (*S*)-7-(2-fluoropyridin-3-yl)-3-((3-methyloxetan-3-yl)ethynyl)-5′*H*-spiro [chromeno [2,3- *b*]pyridine-5,4′-oxazol]-2′-amine (AMG-8718). *J. Med. Chem.* **57**, 9811–9831 (2014).

[87] Epstein, O. *et al.* Lead optimization and modulation of hERG activity in a series of aminooxazoline xanthene β-site amyloid precursor protein cleaving enzyme (bace1) inhibitors. *J. Med. Chem.* **57**, 9796–9810 (2014).

[88] Cheng, Y. *et al.* An orally available BACE1 inhibitor that affords robust CNS Aβ reduction without cardiovascular liabilities. *ACS Med. Chem. Lett.* **6**, 210–215 (2015).

[89] Huang, H. *et al.* Structure- and property-based design of aminooxazoline xanthenes as selective, orally efficacious, and cns penetrable BACE inhibitors for the treatment of alzheimers disease. *J. Med. Chem.* **55**, 9156–9169 (2012).

[90] Thapa, U. *et al.* Synthesis of 2,4-diaryl chromenopyridines and evaluation of their topoisomerase I and II inhibitory activity, cytotoxicity, and structure e activity relationship. *Eur. J. Med. Chem.* **46**, 3201–3209 (2011).

[91] Thapa, P. & Lee, E. 2,4-Diaryl-5,6-dihydro-1,10-phenanthrolines with furyl or thienyl moiety at 4-position : Synthesis, Topoisomerase I and II Inhibitory Activity, and Cytotoxicity. *B. Kor. Chem. Soc.* **33**, 5, 1769-1772 (2012).

[92] Thapa, P. *et al.* Design and synthesis of conformationally constrained hydroxylated 4-phenyl-2-aryl chromenopyridines as novel and selective topoisomerase II-targeted antiproliferative agents. *Bioorgan. Med. Chem.* **23**, 6454–6466 (2015).

[93] Kwon, H. B. *et al.* A series of novel terpyridine-skeleton molecule derivants inhibit tumor growth and metastasis by targeting topoisomerases. *J. Med. Chem.* **58**, 1100–1122 (2015).

[94] Magar, T. B. T. *et al.* Synthesis and SAR study of new hydroxy and chloro-substituted 2,4-diphenyl 5*H*-chromeno[4,3-*b*]pyridines as selective topoisomerase IIα-targeting anticancer agents. *Bioorgan. Med. Chem.* **26**, 1909–1919 (2018).

[95] Ross Grimmett, M. Imidazoles. *Compr. Heterocycl. Chem. II A Rev. Lit. 1982-1995* **3**, 77–220 (2009).

[96] Siwach, A. & Verma, P. K. Synthesis and therapeutic potential of imidazole containing compounds. *BMC Chem.* **15**, 1–69 (2021).

[97] Verma, A., Joshi, S. & Singh, D. Imidazole: Having versatile biological activities. *J. Chem.* **2013**, (2013).

[98] Daraji, D. G., Prajapati, N. P. & Patel, H. D. Synthesis and applications of 2-substituted imidazole and Its derivatives: a review. *J. Heterocycl. Chem.* **56**, 2299–2317 (2019).

[99] Debus, H. Ueber die einwirkung des ammoniaks auf glyoxal. *Justus Liebigs Ann. Chem.* **107**, 199–208 (1858).

[100] Saxer, S., Marestin, C., Mercier, R. & Dupuy, J. The multicomponent Debus–Radziszewski reaction in macromolecular chemistry. *Polym. Chem.* **9**, 1927–1933 (2018).

[101] Shabalin, D. A. & Camp, J. E. Recent advances in the synthesis of imidazoles. *Org. Biomol. Chem.* **18**, 3950–3964 (2020).

[102] Guan, Z. R., Liu, Z. M. & Ding, M. W. New efficient synthesis of 1*H*-imidazo-[4,5-*c*]quinolines by a sequential Van Leusen/Staudinger/aza-Wittig/carbodiimide-mediated cyclization. *Tetrahedron* **74**, 7186–7192 (2018).

[103] Fang, S. *et al.* Nickel-catalyzed construction of 2,4-disubstituted imidazoles via C–C coupling and C–N condensation cascade reactions. *Adv. Synth. Catal.* **361**, 3312–3317 (2019).

[104] Man, L., Copley, R. C. B. & Handlon, A. L. Thermal and photochemical annulation of vinyl

azides to 2-aminoimidazoles. *Org. Biomol. Chem.* **17**, 6566–6569 (2019).

[105] Wang, Q. *et al*. Base-promoted nitrile-alkyne domino-type cyclization: a general method to trisubstituted imidazoles. *Org. Lett.* **21**, 9874–9877 (2019).

[106] Sharma, D. *et al.* Synthesis, antimicrobial and antiviral evaluation of substituted imidazole derivatives. *Eur. J. Med. Chem.* **44**, 2347–2353 (2009).

[107] Khan, M. S. *et al.* Antibacterial activity of synthesized 2,4,5-trisubstituted imidazole derivatives. *Chem. Biol. Drug Des.* **72**, 197–204 (2008).

[108] Fan, Y. L. *et al.* Recent advances of imidazole-containing derivatives as anti-tubercular agents. *Eur. J. Med. Chem.* **150**, 347–365 (2018).

[109] Zhang, L. *et al*. Comprehensive Review in Current Developments ofImidazole-Based Medicinal Chemistry. *Med. Res. Rev.* **34**, 340–437 (2014).

[110] Ribeiro, A. I. *et al.* Synthesis and antimicrobial activity of novel 5-aminoimidazole-4-carboxamidrazones. *Bioorg. Med. Chem. Lett.* **24**, 4699–4702 (2014).

[111] Rani, N. *et al*. R. Imidazoles as potential antifungal agents: a review. *Mini-Rev. Med. Chem.* **13**, 1626–1655 (2015).

[112] Selig, R. *et al.* A frozen analogue approach to aminopyridinylimidazoles leading to novel and promising p38 MAP kinase inhibitors. *J. Med. Chem.* **55**, 8429–8439 (2012).

[113] Gising, J. *et al.* Trisubstituted imidazoles as mycobacterium tuberculosis glutamine synthetase inhibitors. *J. Med. Chem.* **55**, 2894–2898 (2012).

[114] Ren, J. *et al.* Binding of the second generation non-nucleoside inhibitor S-1153 to HIV-1 reverse transcriptase involves extensive main chain bonding hydrogen. *J. Biol. Chem.* **275**, 14316–14320 (2000).

[115] Zhan, P. *et al.* Synthesis and biological evaluation of imidazole thioacetanilides as novel non-nucleoside HIV-1 reverse transcriptase inhibitors. *Bioorgan. Med. Chem.* **17**, 5775–5781 (2009).

[116] Bellina, F. *et al*. Imidazole analogues of resveratrol: synthesis and cancer cell growth evaluation. *Tetrahedron* **71**, 2298–2305 (2015).

[117] Li, L. *et al.* Design, synthesis, and biological evaluation of 1-substituted -2-aryl imidazoles targeting tubulin polymerization as potential anticancer agents. *Eur. J. Med. Chem.* **184**, 111732 (2019).

[118] Sharma, G. V. M. *et al.* Imidazole derivatives show anticancer potential by inducing apoptosis and cellular senescence. *Medchemcomm.* **5**, 1751–1760 (2014).

[119] Ali, I., Lone, M. N. & Aboul-Enein, H. Y. Imidazoles as potential anticancer agents. *Medchemcomm* **8**, 1742–1773 (2017).

[120] Kitbunnadaj, R. *et al.,* Identification of 4-(1*H*-Imidazol-4(5)-ylmethyl)pyridine(Immethridine) as a novel, potent, and highly selective histamine H3 receptor agonist. *J. med. chem.* **47**, 2414–2417 (2004).

[121] Motawaj, M. & Arrang, J. M., Ciproxifan, a histamine H3-receptor antagonist/inverse agonist, modulates methamphetamine-induced sensitization in mice. *Eur. J. Neurosci.* **33**, 1197–1204 (2011).

[122] Khabnadideh, S. *et al*. Synthesis of metronidazole derivatives as antigiardiasis agents. *Daru* **15**, 17–20 (2007).

[123] NHS. Metronidazole. *NHS*. URL: https://www.nhs.uk/medicines/metronidazole (2018), last accessed on 20th September 2021.

[124] EMA. *Losec*. *EMA*. URL: https://www.ema.europa.eu/en/medicines/human/referrals/losec (2021), last acessed on 20th September 2021.

[125] Zheng, X., Ma, Z. & Zhang, D. Synthesis of imidazole-based medicinal molecules utilizing the van Leusen imidazole synthesis. *Pharmaceuticals* **13**, (2020).

[126] Rodriguez-Arévalo, S. *et al.* Benzofuranyl-2-imidazoles as imidazoline I2 receptor ligands for Alzheimer's disease. *Eur. J. Med. Chem.* **222**, 113540 (2021).

[127] Beltran-Hortelano, I. *et al.* Design and synthesis of Mannich base-type derivatives containing imidazole and benzimidazole as lead compounds for drug discovery in Chagas Disease. *Eur. J. Med. Chem.* **223**, 113646 (2021).

[128] Ammazzalorso, A. *et al.* Design, synthesis and biological evaluation of imidazole and triazole-based carbamates as novel aromatase inhibitors. *Eur. J. Med. Chem.* **211**, 113115 (2021).

[129] Dubovis, M. V. *et al.* A new method of synthesis of substituted 1-(1*H*-imidazole-4-yl)-1*H*-1,2,3-triazoles and their fungicidal activity. *Tetrahedron* **74**, 672–683 (2018).

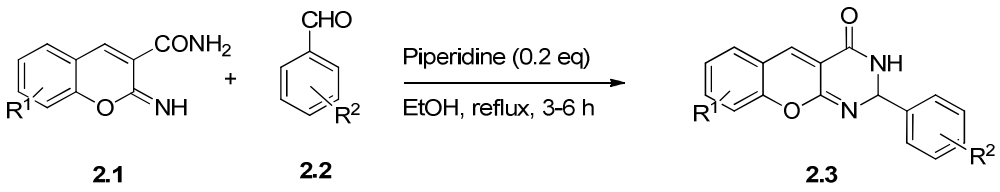
Chapter 2

Synthesis of 2*H*-chromene, 4*H*-chromene and 1*H*-imidazole derivatives

2.1. 2 and 3-substituted 2*H*- and 4*H*-chromenes

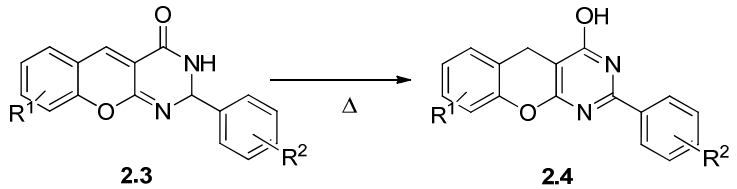
2.1.1 Synthesis and reactivity of 2-imino-2*H*-chromene-3-carboxamides

The synthesis of chromene[2,3-*d*]pyrimidin-4(5*H*)-ones was reported in 1973[1] and 1980[2] by O'Callaghan. In this work, the author prepared a set of compounds by reacting 2-imino-2*H*-chromene-3-carboxamides **2.1** with various aldehydes, to generate the desired product **2.3** (**Scheme 12**). The synthesis was performed in ethanol and with piperidine catalysis. The author also referred that these compounds presented biological activity against P388 lymphocytic leukemia, without further development of this topic. O'Callaghan also referred that a prolonged refluxing time "causes rearrangement to take place with formation of the high-melting insoluble isomers"[2], here represented by structure **2.4** (**Scheme 13**).



2.1 **2.2** **2.3**

Scheme 12: Synthesis of chromene[2,3-d]pyrimidin-4(5H)-ones **2.3**,as proposed by O'Callaghan [ref.1]



2.3 **2.4**

Scheme 13: Rearrangement promoted by heat, as proposed by O'Callaghan [ref.2]

Later, in 1999, Hadfield *et al* prepared a library of compounds with the core structure **2.3** in order to evaluate their biological activity against several cancer cell lines, including P388 Lymphocytic Leukemia and for their ability to alter cell cycle kinetics[3]. The compounds reported were like those obtained by O'Callaghan, but also some derivatives were identified as having structure **2.4** (**Figure 15**). After evaluating the IC_{50} values against diverse cancer cell lines, specifically K562 (human chronic myelogenous leukemia), P388 (murine lymphocytic leukemia) and A2780 (human ovarian cell lines), compound **2.3a** was selected (**Figure 15**) for further studies on different cancer cell lines as this was the only compound that presented relevant activity in the ovarian cancer cell line A2780.

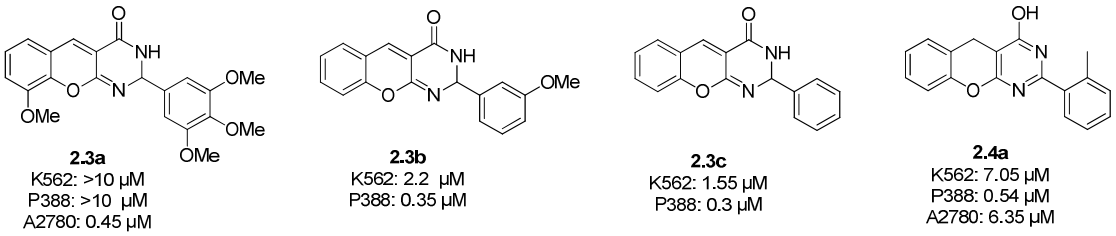
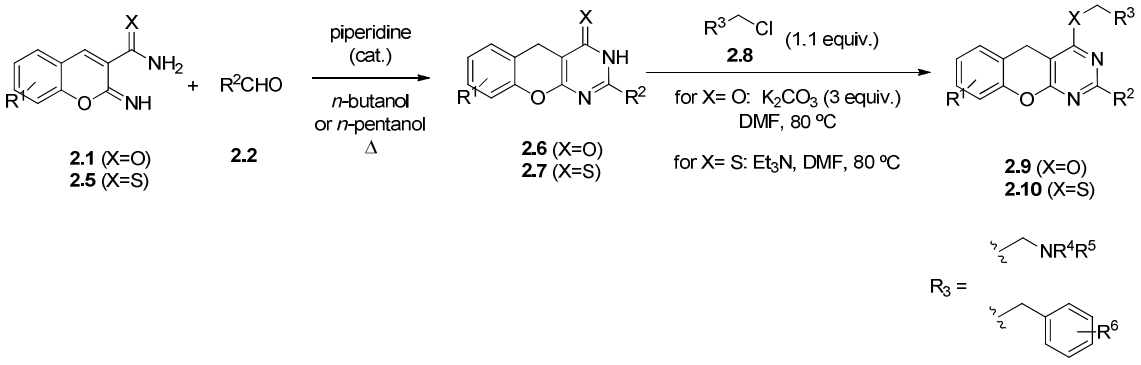


Figure 15: Selection of bioactive compounds described by Hadfield *et al.* The corresponding IC_{50} values obtained for each cancer cell line are indicated [adapted from ref. 3]

Compound **2.3a** was then tested in several ovarian and non-ovarian cancer cell lines, specifically A549 (adenocarcinomic human alveolar basal epithelial cell line), H460 (epithelial lung large cell cancer cell line), and the ovarian cancer cell lines Ovca5 and Ovca433. Consistently with previous results, this compound proved to be more active against ovarian cancer cell lines than against other type of cancer cell lines, although the IC_{50} values were not as promising as those obtained for the A2780 cancer cell line. To understand if this was due to hormone-derived effects, compound **2.3a** was tested in estrogen-positive MCF7 and estrogen-negative BT20 human breast carcinoma cell lines. This hypothesis was finally discarded as no relevant cytotoxic activity was observed. Among many other pyrimidinones tested, some presented strong cytotoxic ability towards K562, P388 and A2780 cancer cell lines, as it is the case for compounds **2.3a-c**. A small number of compounds displayed the ability to arrest cells in the G_2/M phase of the cell cycle.

In 2007, Borisov *et al* described new protocols for the reaction of 2-imino-2*H*-chromene-3-carboxamides **2.1** and 2-imino-2*H*-chromene-3-(thio)carboxamides **2.5** with a variety of aldehydes **2.2**, to afford derivatives **2.6** and **2.7** (**Scheme 14**)[4]. Also, new procedures for the preparation of O- and S-alkylated derivatives **2.9** and **2.10**, respectively, were reported, taking advantage of the tautomeric equilibrium of compounds **2.6** and **2.7** and their corresponding phenolic and thiophenolic forms, initially proposed by O'Callaghan[2]. Through these methodologies, the authors prepared a set of compounds derived from structures **2.6**, **2.7**, **2.9** and **2.10** using an automated parallel synthesis methodology. To improve the reaction yield maintaining the automated parallel process, the authors used higher boiling alcohols, namely *n*-pentanol (for reactions involving **2.1**) and *n*-butanol (for reactions involving **2.5**), and piperidine as catalyst. Compounds **2.9** and **2.10** were prepared from **2.6** and **2.7** upon reaction with a slight molar excess of the appropriate halide (benzyl chloride or alkyl iodide), in DMF, at 80 °C and in the presence of 3 equiv. of K_2CO_3 (oxo analogues) or an excess of triethylamine (thio analogues).



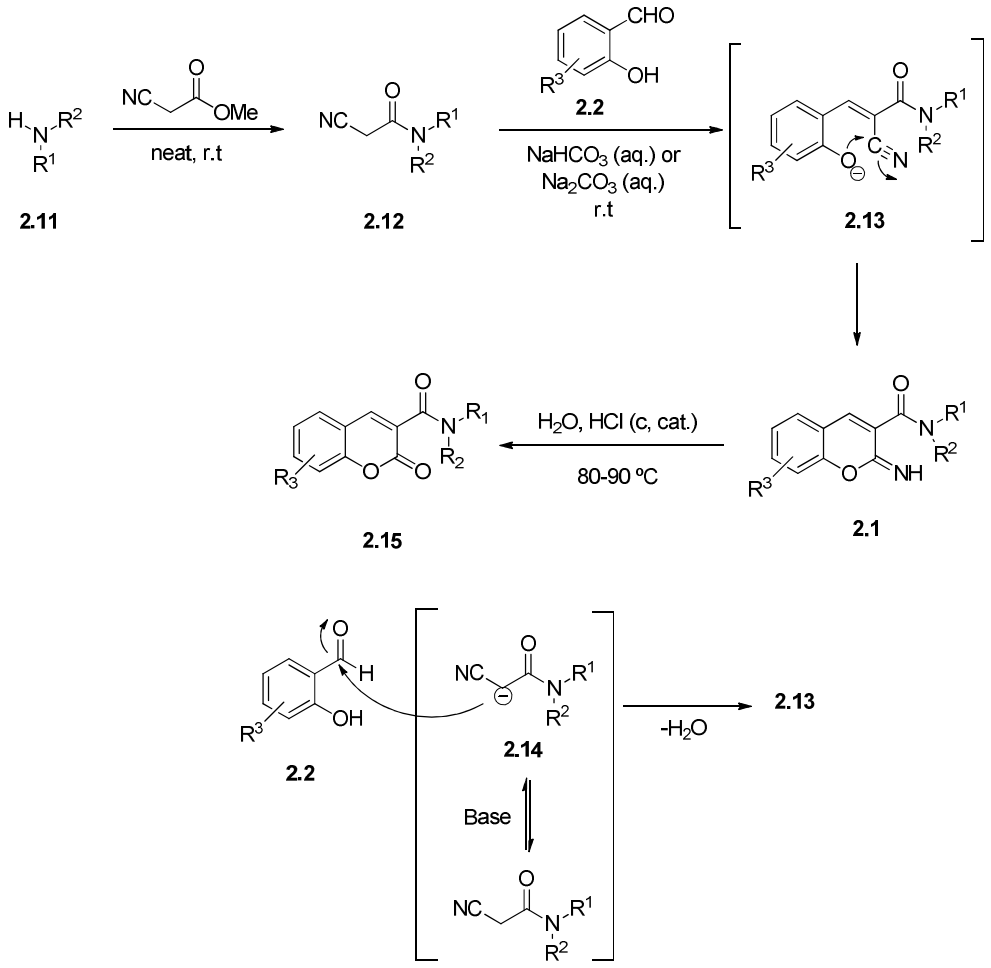
Scheme 14: Reaction conditions optimized by Borisov *et al* for automated parallel synthesis of compounds **2.6**, **2.7**, **2.9** and **2.10** [adapted from ref. 4]

The present work was a follow-up of these studies. By making use of the vast experience, in our research group, two main objectives were established:

1) Avoid the usage of high boiling solvents, which are more difficult to handle and less readily available, and obtain a laboratorial-scale process to prepare a library of chromene[2,3-*d*]pyrimidin-4(5*H*)-ones to be tested for their biological activity as anticancer (triple negative breast cancer) and antituberculosis agents.
2) Obtain a structure-activity relationship (SAR) model that could supply information on possible structural modifications that could improve their activity.

Our research group have previously reported[5] a simple and eco-friendly synthetic route for the preparation of 2-imino and 2-oxo-2*H*-chromene-3-carboxamides. This procedure started with the synthesis of *N*-substituted cyanoacetamides **2.12** by direct combination of primary or secondary amines **2.11** with ethyl acetoacetate, in a solventless reaction (**Scheme 15**). These compounds were prepared at room temperature and isolated by filtration after adding a few drops of diethyl ether. The synthesis of compounds **2.1** occurred when cyanoacetamides **2.13** were combined with the appropriate salicylaldehyde **2.2** in aqueous sodium carbonate or hydrogen carbonate solutions, at room temperature (**Scheme 15**). This reaction occurred via a Knoevenagel condensation, with the nucleophilic addition of the active methylene compound to the carbonyl moiety of **2.14**, followed by an intramolecular cyclization reaction promoted by nucleophilic attack of the hydroxyl group to the nitrile group. The Knoevenagel product precipitated from the reaction mixture and was isolated as the pure compound **2.1** by simple filtration. This methodology afforded a simple and ecological way to prepare 2-imino–2*H*-chromene-3-carboxamides **2.1** in high yields,

which can be easily transformed into 2-oxo-2*H*-chromene-3-carboxamides **2.15** by acid catalyzed hydrolysis at 80-90 °C (**Scheme 15**).



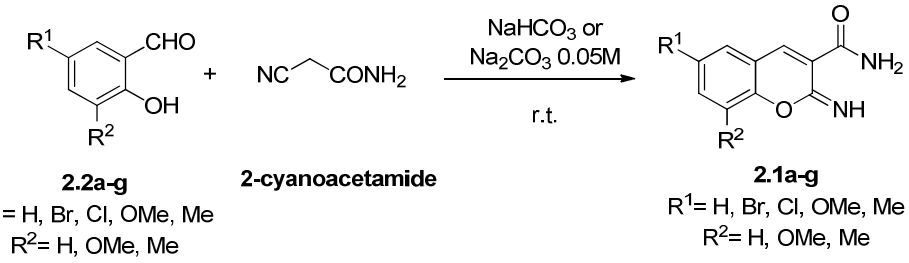
Scheme 15: Preparation of 2-imino- **2.1** and 2-oxo-2*H*-chromene-3-carboxamides **2.15**, via Knoevenagel condensation, as proposed by Proença et al. [adapted from ref. 5]

Synthesis of chromeno[2,3-*d*]pyrimidin-4(5*H*)-ones and chromeno[2,3-*d*]pyrimidin-4(3*H*)-ones

One of the aims of this PhD thesis was to select the best reaction conditions to prepare chromene[2,3-*d*]pyrimidin-4(5*H*)-ones **2.3** and **2.6** in good synthetic yield, while avoiding the use of alcohols of high boiling as solvents. Following the procedure developed in our group[5], a series of 2-imino-2*H*-chromene-3-carboxamides **2.1** were prepared using 2-cyanoacetamide and several salicylaldehydes **2.2a-g**, in high to almost quantitative yield for most cases (**Scheme 16**).

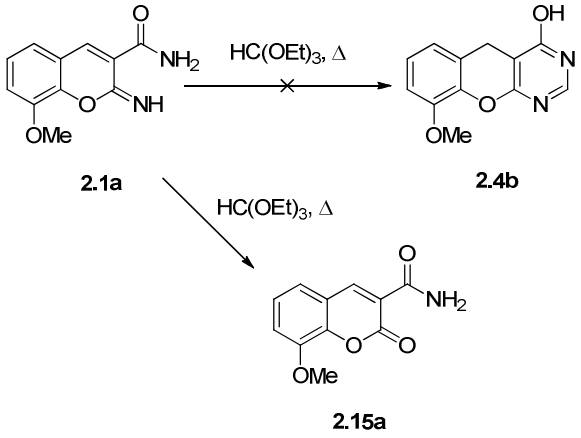
The potential of 2-imino-2*H*-chromene-3-carboxamides **2.1** for the synthesis of complex fused heterocycles was then explored. First, the utility of **2.1** for the synthesis of chromene[2,3-*d*]pyrimidin-4(5*H*)-ones was studied (**Scheme 17**). The presence of a methoxyl group in **2.1a** (R^1= H, R^2= OMe) allowed a simple method to follow the reaction by ^{1}H NMR and to understand

the formation of different products incorporating this unit. Moreover, IR monitoring of the changes in the carbonyl stretching band in **2.1a** (around 1710 cm^{-1}) was used to understand the global evolution of the process.



Scheme 16: Synthesis of 2-imino-2*H*-chromene-3-carboxamides **2.1a-g** from 2-cyanoacetamide and salicylaldehydes **2.2a-g**

The heating at 100 °C for 15 h of a solution of 2-iminochromene **2.1a** in triethyl ortoformate and in the presence of acetic acid did not afford the desired tricyclic compound **2.4b** (**Scheme 17**). Under these conditions, 2-oxochromene **2.15a** was obtained with a 67% yield. When the reaction was performed using 1.2 equivalents of triethyl ortoformate, in the presence of acetic acid and heating under reflux for 2.5 h, mainly no reaction was obtained. The addition of an additional 3.3 equivalents of triethyl ortoformate and another 4h of reflux, once again provided chromene-based lactone **2.15a** with a 61% yield.

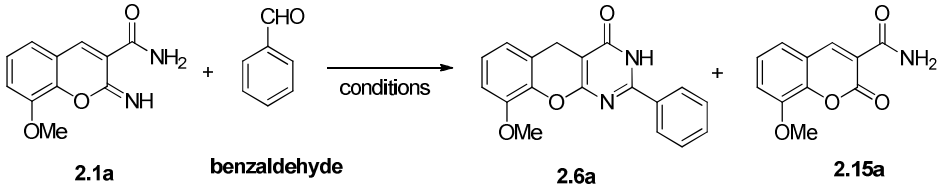


Scheme 17: Reaction of chromene **2.1a** with triethyl orthoformate

The identification of the chemical structure of **2.15a** was carried out by comparison of the ^{1}H NMR and IR signals for this product and the starting material **2.1a**. Thus, the absence in the ^{1}H NMR spectrum of **2.15a** of the NH signal, at δ8.97 ppm, corroborated the transformation of the imino group in **2.15a**. The IR spectra allowed to distinguish both compounds by their C=O

stretching vibration, which was an intense signal at 1710 cm^{-1} for **2.15a**, masking the signal at 1700 cm^{-1} for the C=O stretching vibration of the amide carbonyl group visible in the IR spectrum of **2.1a**. Next, the reaction of 2-iminochromene **2.1a** with benzaldehyde to obtain chromene-based pyrimidinone **2.6a** was analyzed under different experimental conditions, which are summarized in **Table 1**.

Table 1: Experimental conditions and results obtained for the reaction of **2.1a** with benzaldehyde, under different reaction conditions



2.1a **benzaldehyde** **2.6a** **2.15a**

Entry	PhCHO (equiv.)	base/ acid (equiv.)	solvent	T (°C)	t (h)	results
1	1.2	TFA (1.1)	EtOH	100	15	**2.15a** (η=50%)
2	1.2	-	AcOH	100	15	**2.15a** (η=50%)
3	1.2	AcOH (1.2)	-	r.t.	22.5	**2.15a** (η=56%)
4	1.2	$NaHCO_3$	$NaHCO_3$ 0.05 M	70	24	**2.1a + 2.15a**
5	1.2	NMP (1.1)	MeCN	100	30	complex mixture
6	1.2	NMP (1.1)	EtOAc	70	18	**2.1a** (16%) **+** mixture (by IR)
7	1.2	NMP (1.1)	EtOH	70	18	**2.6a** (η< 2%)
8	1.2	-	EtOH	70	24	**2.1a** + by-products
9	1.2	NMP (1.1)	EtOH	100	8	**2.6a** (η= 19%)
10	1.2	NMP (1.1)	MeOH	reflux	8	**2.6a** (η= 17%)
11	1.2	NMP (1.1)	EtOH	100	24	**2.6a** + impurities
12	1.2	pyridine (1.1)	EtOH	100	24	complex mixture
13	1.2	piperidine (1.1)	EtOH	100	32.25	**2.6a** (η= 39%)
14	3	piperidine (1.1)	EtOH	100	3	**2.6a** (η= 35%)

The reaction was initially carried out under acidic conditions. The use of 1.2 equivalents of benzaldehyde and 1.1 equivalents of trifluoroacetic acid (TFA) in ethanol at 100 °C (entry 1– **Table 1**), afforded the chromene-based lactone **2.15a** with a 50% yield. A similar result was obtained when the same amount of acetic acid was used (entry 2– **Table 1**). The same reaction, performed at room temperature for 22.5h (entry 3– **Table 1**), also afforded chromene **2.15a** with 56% yield. Thus, it was concluded that performing this reaction under acidic conditions the hydrolysis of the imino group in **2.1a** takes place by an acid-catalyzed process, similarly to what was described in the literature[5] for the reaction with concentrated HCl.

The reaction was then performed under basic conditions using aqueous $NaHCO_3$ solution. Conducting this reaction at 70 °C for 24 h afforded a mixture of the starting material **2.1a** and **2.15a**, as confirmed by IR spectroscopy (entry 4– **Table 1**). To avoid hydrolysis of the imine function in the starting material, the reaction was carried out in the presence of an organic base and a non-aqueous solvent. The use of *N*-methylpiperazine (1.1 equivalents) in acetonitrile with heating at 100 °C for 30 h, resulted in a black complex mixture that could not be characterized (entry 5– **Table 1**). Replacing acetonitrile for ethyl acetate, reducing the reaction time to 18 h and heating at 70 °C, provided a mixture of products that contained the starting material **2.1a** as revealed its IR spectra (entry 6 – **Table 1**).

When the same reaction was carried out in ethanol, heating at 70 °C for 18 h (entry 7– **Table 1**) an orange solid was collected and identified as the desired product **2.6a**, in very low yield (< 2%). A complex mixture was also isolated, after concentrating the reaction mixture in the rotary evaporator. Carrying out the reaction in ethanol, in the absence of base (entry 8– **Table 1**) confirmed that its presence is imperative for the reaction to occur, as compound **2.1a** was collected along with several by-products, most likely due to chromene ring-opening that is known to occur under prolonged heating.

From the solvents tested, ethanol showed to be the best, and its performance was compared with that of methanol, using *N*-methylpiperazine as base (entries 9 and 10– **Table 1**). Compound **2.1a** was treated with benzaldehyde for 8 h in both ethanol and methanol, with heating conditions. In both cases, the chromene **2.1a** was added in two portions, to avoid the formation of side products and thus improve the reaction yield. In both cases, the resulting product, chromene-based pyrimidinone **2.6a**, was isolated in comparable yields (17% for the reaction in methanol, 19% for the reaction in ethanol). These results prompted us to select ethanol as the best solvent in terms of safety concerns and the remaining assays were performed in ethanol. To assess

the effect of the organic base, three experiments were designed where a suspension of chromene **2.1a** in ethanol was heated at 100 °C in the presence of *N*-methylpiperazine (24h, entry 11– **Table 1**), pyridine (24h, entry 12– **Table 1**) and piperidine (32h, entry 13– **Table 1**). The use of pyridine resulted in a complex mixture while with *N*-methylpiperazine the desired product **2.6a** was isolated, although in poor yield and contaminated with by-products. Fortunately, in the presence of piperidine, the desired compound **2.6a** was isolated in 39% yield. At this point, it became clear that piperidine was the best base for this reaction, as it allowed the pure compound **2.6a** to be collected in an acceptable yield.

This study led us to conclude that: (i) the best experimental conditions required the use of ethanol as solvent and piperidine as base; (ii) performing the reaction with benzaldehyde for longer periods of time did not affect the isolated yield of the product; and (iii) the observed impurities must be due to temperature-induced evolution of the side products formed in this reaction, since no starting material was detected after 3 h at 100 °C (entry 14– **Table 1**). Therefore, the optimized reaction conditions, summarized in **Table 1**, entry 14, were adopted as standard conditions for this process.

The spectroscopic characterization of **2.6a** will be used to illustrate the structural features of this compound family. The ^{1}H NMR spectrum (**Figure 16**) shows two distinct singlets, one at δ12.82 ppm, corresponding to the NH group of the pyrimidinone ring, and other at δ3.73 ppm, assigned to the methylene group. In the ^{13}C NMR spectrum (**Figure 17**) the carbonyl group generates a signal at δ164 ppm, which although not visible in the ^{13}C NMR spectrum presented, could be identified in the HMQC and HMBC correlation spectra. The methylene carbon led to a signal at δ21.86 ppm.

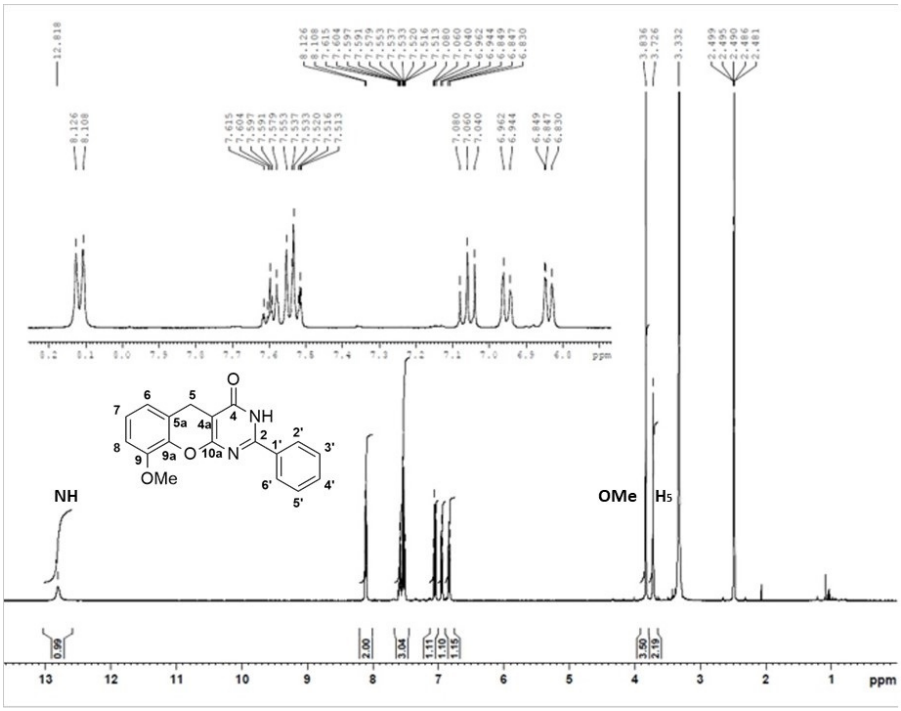


Figure 16: ^{1}H NMR (400 MHz, DMSO-d$_6$, δ ppm) spectrum of compound **2.6a**, in which some relevant signals are highlighted

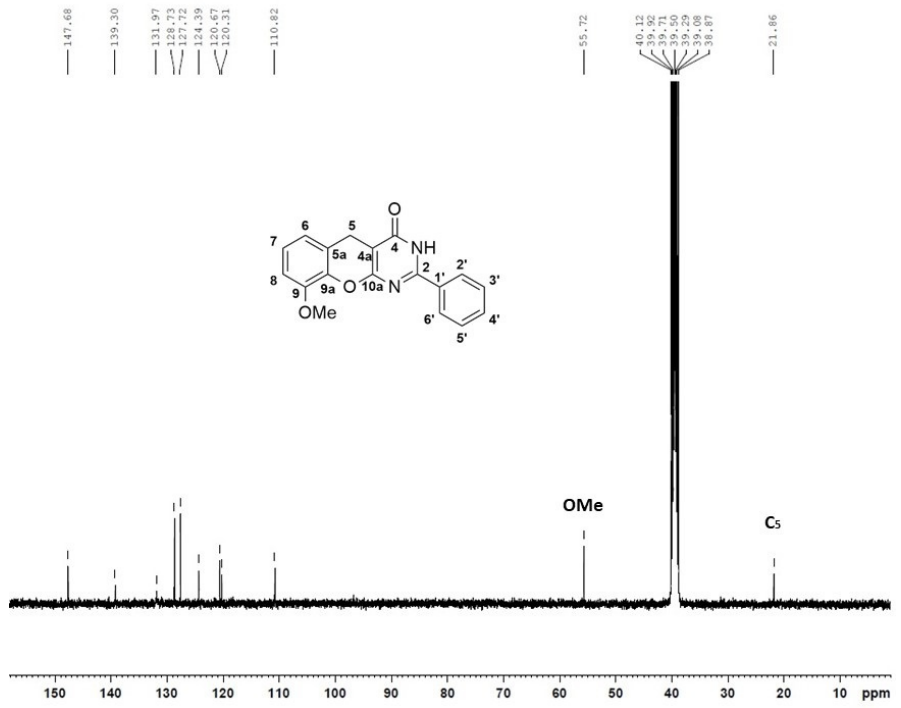
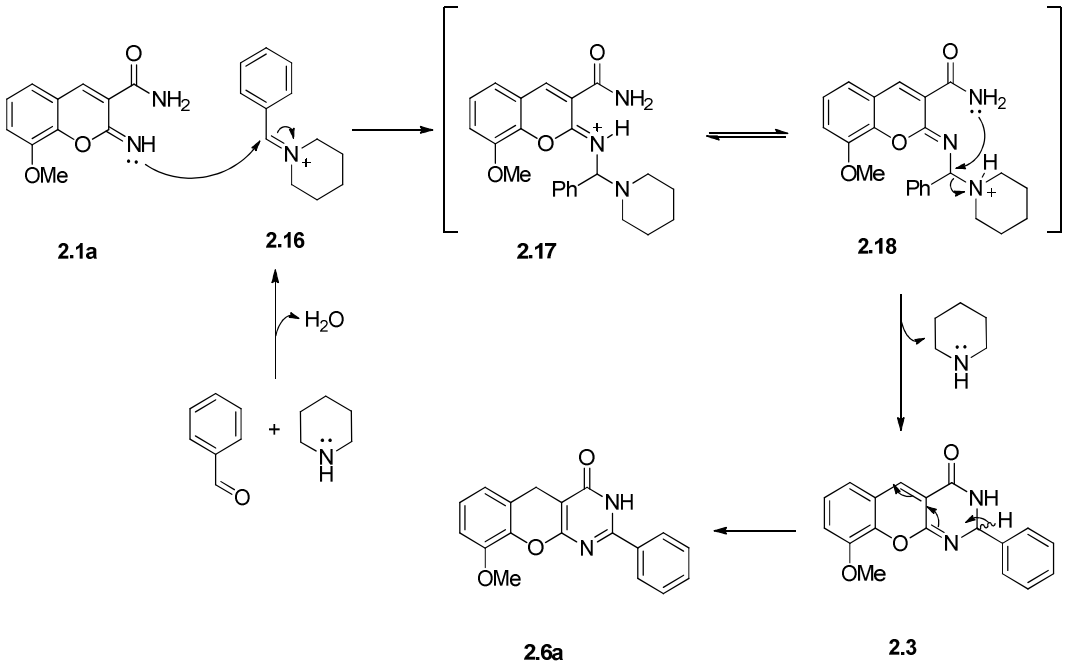


Figure 17: ^{13}C NMR (100 MHz, DMSO-d$_6$, δ ppm) spectrum of compound **2.6a**, in which some relevant signals are highlighted

A proposal for the reaction mechanism is presented in **Scheme 18**. Benzaldehyde is activated through conjugation with *N*-methylpiperazine, which facilitates the nucleophilic attack of the imine group. Intramolecular cyclization, involving the amide group, affords compound **2.6a**.

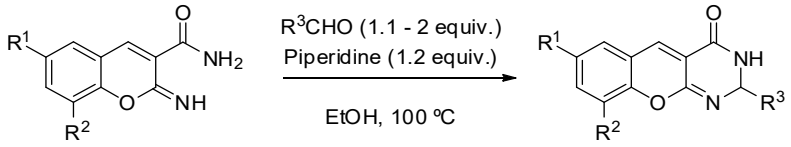


Scheme 18: Proposed mechanism for the synthesis of 9-methoxy-2-phenyl-3*H*-chromeno[2,3-*d*]pyrimidin-4(5*H*)-one **2.6a**

After exploring the optimal reaction conditions, a library of chromene-based pyrimidinones was prepared, starting from diverse 2-imino-2*H*-chromene-3-carboxamides **2.1** and aldehydes and the results are presented in **Tables 2** and **3**. For most cases, some solubilization of the partially soluble reagents was observed, which typically included imines **2.1** but, in some cases, also aldehydes (for most of the solid aldehydes used). The desired products tend to precipitate after some time at 100 °C, most likely shifting the reaction equilibrium to the formation of the product. The use of *ortho*-disubstituted aromatic aldehydes (**Table 2**) resulted in the isolation of compounds **2.3** instead of the **2.6** isomer. It is possible that this is due to steric hindrance that shields the proton on the sp^3 carbon, hindering its removal and a favorable orbital overlap that would allow tautomerization to **2.6**, as depicted in **Scheme 18**.

It was identified a selection of aldehydes that did not provide good results for the synthesis of tricyclic structures **2.3** or **2.6**, particularly morpholine-4-carbaldehyde, 4-cyanobenzaldehyde, 2.6-difluorbenzaldehyde and 4-nitrobenzaldehyde. Thus, the use of morpholine-4-carbaldehyde resulted in a mixture of five products, including the starting material, after 12 h in ethanol, at 100 °C. 4-Cyanobenzaldehyde and 2,6-difluorbenzaldehyde afforded oily mixtures that could not be identified, and 4-nitrobenzaldehyde, gave a red solid that revealed to be a non-identifiable complex mixture by IR and ^{1}H NMR.

Table 2: Reaction conditions for the preparation of compounds **2.3d-i**



2.1 **2.3**

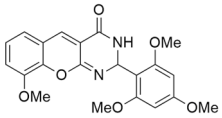
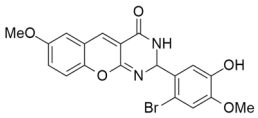
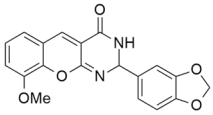
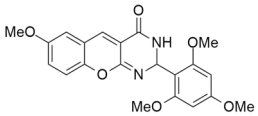
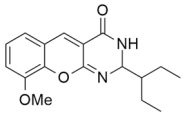
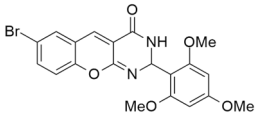
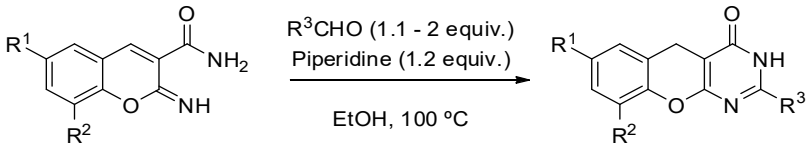
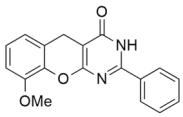
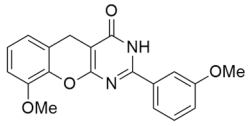
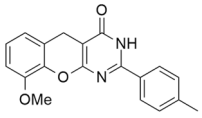
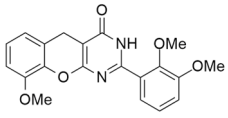
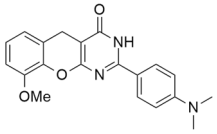
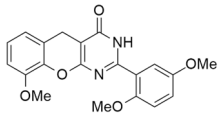
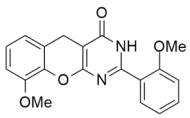
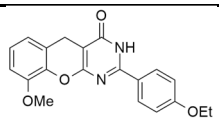
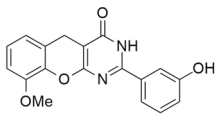
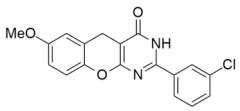
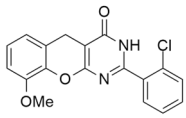
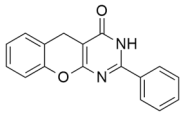
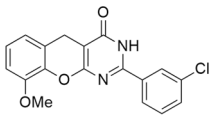
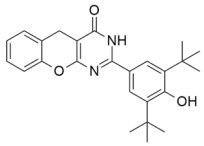
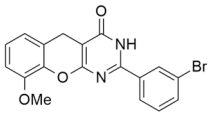
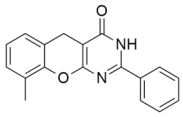
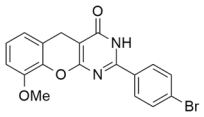
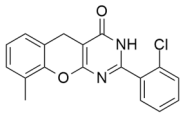
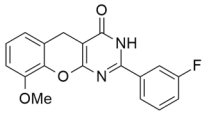
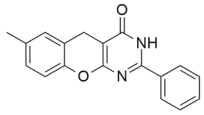
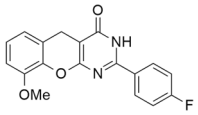
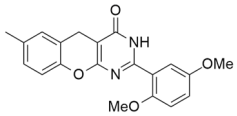
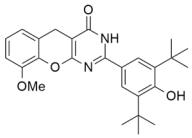
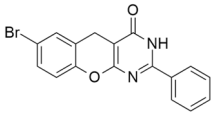
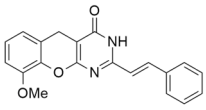
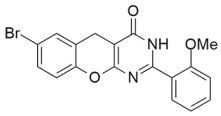
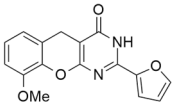
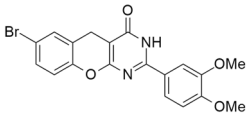
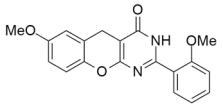
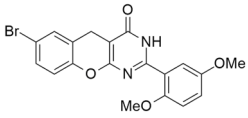
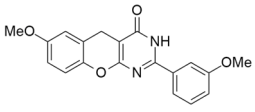
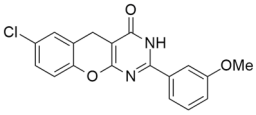
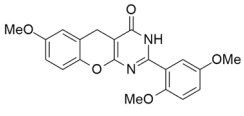
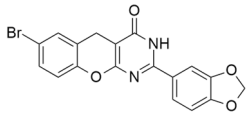
Product	structure	t(h)	η (%)	Product	structure	t(h)	η (%)
2.3d		3.5	63	**2.3g**		4	48
2.3e		2.5	31	**2.3h**		1.5	79
2.3f		6.5	25	**2.3i**		10.33	28

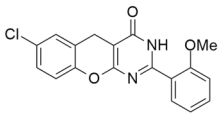
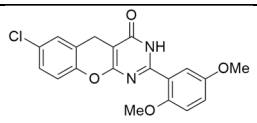
Table 3: Reaction conditions for the preparation of compounds **2.6a-k'**



2.1 **2.6**

Product	structure	t(h)	η (%)	Product	structure	t(h)	η (%)
2.6a		3	35	**2.6e**		3.5	34
2.6b		3.33	42	**2.6f**		3.6	59*
2.6c		28	45	**2.6g**		4.33	59
2.6d		3.5	63	**2.6h**		17	38

2.6i		10	54	**2.6v**		2.5	39
2.6j		9	36	**2.6x**		5	39
2.6k		16	27	**2.6y**		5	21
2.6l		14	22	**2.6z**		5	56
2.6m		16	39	**2.6a'**		17.66	33
2.6n		8	17	**2.6b'**		4.75	62
2.6o		2.5	23	**2.6c'**		4.75	73
2.6p		7.5	21	**2.6d'**		5.5	22
2.6q		4	17	**2.6e'**		3.66	25*
2.6r		1.83	33	**2.6f'**		12	24
2.6s		1.33	81	**2.6g'**		11	44
2.6t		1.33	65	**2.6j'**		3.5	32
2.6u		4	79	**2.6h'**		5.5	21

2.6i'		3.66	65	**2.6k'**		3.66	62

*****Yield after recrystallization

The reaction with polyhydroxylated aldehydes was also troublesome, as none of the attempts provided pure isolated products. When 2,4,6-trimethoxybenzaldehyde and piperonal were employed, the final tautomerization involving positions 2 and 5 was not observed, affording tricyclic products **2.3**, with a tetrahedral rearrangement (sp^3) at position 2 (**Scheme 19**). Typically, these compounds could be recognized by a shift in two signals: (i) the NH group in the pyrimidinone ring shifts from a singlet at δ12-13 ppm (**2.6**) to a singlet or broad doublet at about δ6.4-6.9 ppm (**2.3**); and (ii) the methylene group in **2.6**, which typically present a singlet at around δ3–4 ppm, shifts to a small doublet at about δ7.2-7.8 ppm, which corresponds to the alkene moiety of the 2,3-dihydropyrimidin-4(5*H*)-ones **2.3**.

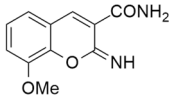
Physical, analytical, and spectroscopic characterization

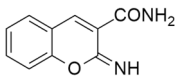
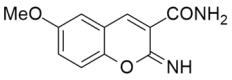
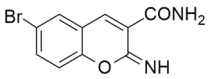
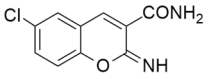
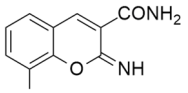
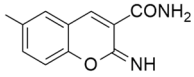
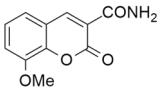
The chemical structure of compounds **2.1, 2.15a**, **2.6** and **2.3** was assigned based on physical, analytical, and spectroscopic data (elemental analysis, melting point, IR, ^{1}H and ^{13}C NMR).

Physical and analytical characterization

The molecular formula and molecular weight were calculated based on the predicted structure and the information obtained from the elemental analysis. The melting point intervals (°C) were also measured, and the data is referred in the following **Tables 4-6**. Compound **2.15a** has been previously characterized in the literature[6].

Table 4: Physical and analytical data obtained for 2-imino-2*H*-chromeno-3-carboxamides **2.1a-g** and 2-oxo-2*H*-chromeno-3-carboxamide **2.15a**

Comp.	**structure**	**Mp(°C)**	**Molecular formula/ Mass (M)**	**calculated /obtained values (%)**			
				C	H	N	O
2.1a[1]		—	$C_{11}H_{10}N_2O_3$/ 218.21	60.55 –	4.62 –	12.84 –	22.00 –

2.1b		185-188	$C_{10}H_8N_2O_2$/188.18	63.82 63.95	4.28 4.27	14.89 14.84	17.00 –
2.1c		200-202	$C_{11}H_{10}N_2O_3$/ 218.21	60.55 60.7	4.62 4.5	12.84 12.9	22.00 –
2.1d		202-204	$C_{10}H_7BrN_2O_2$/267.08	44.97 44.87	2.64 2.64	10.49 10.33	11.98 –
2.1e		192-194	$C_{10}H_7ClN_2O_2$/ 222.63	53.95 53.65	3.17 3.16	12.58 12.62	14.37 –
2.1f		191-193	$C_{11}H_{10}N_2O_2$/ 202.21	65.34 65.38	4.98 4.98	13.95 13.99	15.82 –
2.1g		222-224	$C_{11}H_{10}N_2O_2$/ 202.21	65.34 65.31	4.98 4.93	13.95 13.94	15.82 –
2.15a[a]		–	$C_{11}H_9NO_4$/ 219.19	60.27 –	4.14 –	6.39 –	29.20 –

[a]Commercial product

Table 5: Physical and analytical data obtained for 2-aryl-3*H*-chromeno[2,3-*d*]pyrimidin-4(3*H*)-ones **2.3d-i**

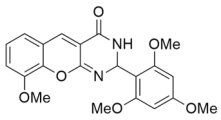
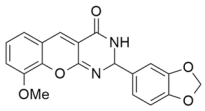
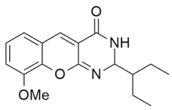
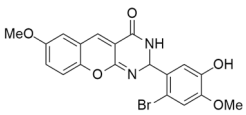
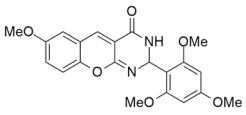
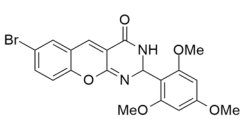
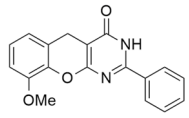
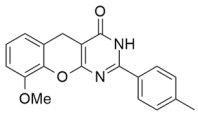
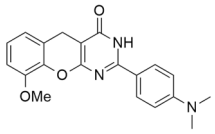
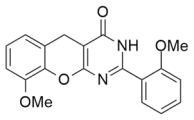
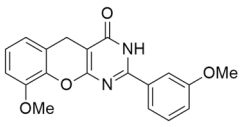
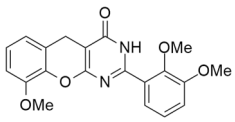
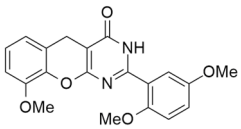
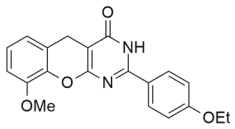
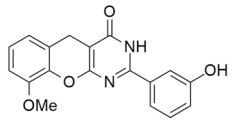
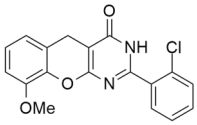
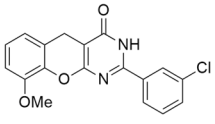
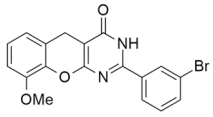
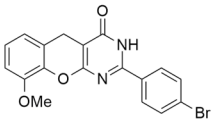
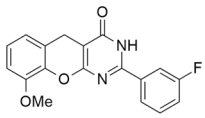
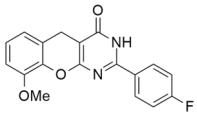
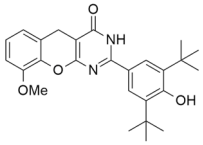
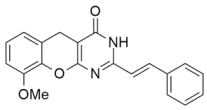
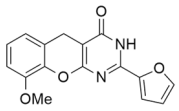
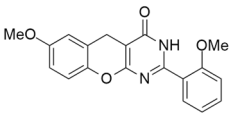
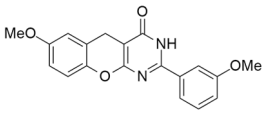
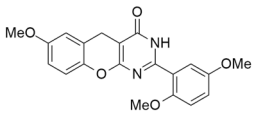
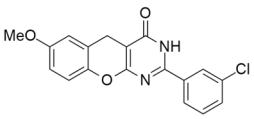
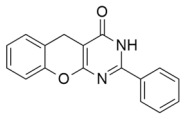
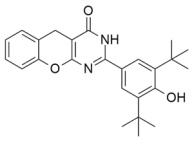
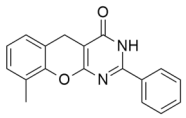
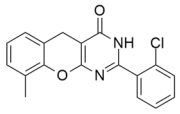
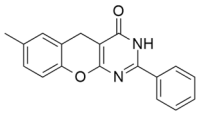
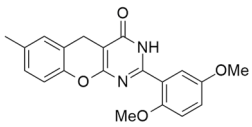
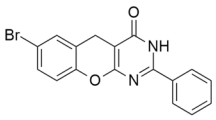
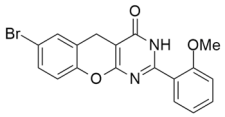
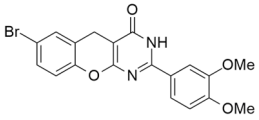
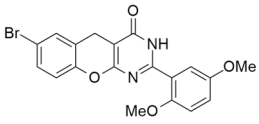
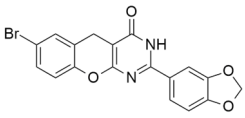
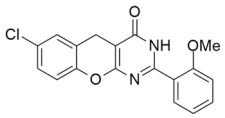
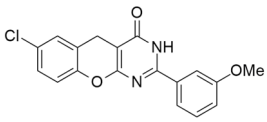
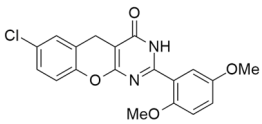
Comp.	Structure	Mp (°C)	Molecular formula/ Mass (M)	calculated /obtained values (%)			
				C	H	N	O
2.3d		270-271	$C_{21}H_{20}N_2O_6$/396.39	63.63 63.92	5.09 5.08	7.07 7.27	24.22 –
2.3e		>300	$C_{19}H_{14}N_2O_5$/350.32	65.14 65.54	4.03 4.14	8.00 8.25	22.84 –
2.3f		260-262	$C_{17}H_{20}N_2O_3$/300.35	67.98 67.74	6.71 6.53	9.33 9.54	15.98 –
2.3g		270 (dec.)	$C_{19}H_{15}BrN_2O_5$. 0,25H_2O/431.24	52.36 52.36	3.55 3.61	6.43 6.31	19.29 –
2.3h		252-254	$C_{21}H_{20}N_2O_6$/396.39	63.63 64.04	5.09 5.13	7.07 7.39	24.22 –
2.3i		248-250	$C_{20}H_{17}BrN_2O_5$/ 445.26	53.95 53.49	3.85 3.86	6.29 6.36	17.97 -

Table 6: Physical and analytical data obtained for 2-aryl-3*H*-chromeno[2,3-*d*]pyrimidin-4(5*H*)-ones **2.6a-k'**

Comp.	Structure	Mp (°C)	molecular formula/ mass (M)	Calculated /obtained values (%)			
				C	H	N	O
2.6a		dec (270)	$C_{18}H_{14}N_2O_3$/ 306.32	70.58 70.3	4.61 4.5	9.15 9.0	15.67 –
2.6b		>300	$C_{19}H_{16}N_2O_3$/ 320.34	71.24 71.11	5.03 5.07	8.74 8.78	14.98 –
2.6c		297-300	$C_{20}H_{19}N_3O_3$/ 349.38	68.75 –	5.48 –	12.03 –	13.74 –
2.6d		260-262	$C_{19}H_{16}N_2O_4$/ 336.34	67.85 68.22	4.79 4.81	8.33 8.42	19.03 –
2.6e		296-300	$C_{19}H_{16}N_2O_4.0,2H_2O$/339.94	67.1 66.8	4.8 4.6	8.2 8.3	19.7 –
2.6f		255-257	$C_{20}H_{18}N_2O_5$/ 366.37	65.57 –	4.95 –	7.65 –	21.84 –
2.6g		297-300	$C_{20}H_{18}N_2O_5$/ 366.37	65.57 65.22	4.95 5.03	7.65 7.79	21.84 -
2.6h		295-297	$C_{20}H_{18}N_2O_4$/ 350.37	68.56 68.52	5.18 5.05	8.00 8.21	18.27 –
2.6i		298-302	$C_{18}H_{14}N_2O_4$/ 322.31	67.07 66.86	4.38 4.66	8.69 8.66	19.88 –
2.6j		262-264	$C_{18}H_{13}ClN_2O_3$/ 340.76	63.44 63.70	3.85 3.95	8.22 8.54	14.09 –
2.6k		>300	$C_{18}H_{13}ClN_2O_3$/ 340.76	63.44 63.24	3.85 3.78	8.22 8.30	14.09 –

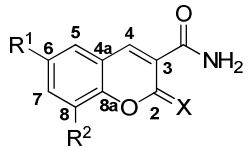
2.6l		>300	$C_{18}H_{13}BrN_2O_3$ .0,2H_2O/388.81	55.51 55.41	3.44 3.45	7.20 7.32	13.17 –
2.6m		>300	$C_{18}H_{13}BrN_2O_3$/ 385.21	56.12 56.52	3.40 3.43	7.27 7.27	12.46 –
2.6n		270-273	$C_{18}H_{13}FN_2O_3$/ 324.31	66.66 –	4.04 –	8.64 –	14.80 –
2.6o		>300	$C_{18}H_{13}FN_2O_3$/ 324.31	66.66 66.98	4.04 3.97	8.64 8.91	14.80 –
2.6p		>300	$C_{26}H_{18}N_2O_4$/ 434.53	71.87 71.96	6.96 6.86	6.45 6.75	14.73 –
2.6q		dec. (275)	$C_{20}H_{16}N_2O_3$/ 332.35	72.28 72.15	4.85 5.16	8.43 8.75	14.44 –
2.6r		>300	$C_{16}H_{12}N_2O_4$ .0,2H_2O/299.88	64.02 64.33	4.13 4.40	9.33 9.55	22.40 –
2.6s		246-248	$C_{19}H_{16}N_2O_4$/ 336.34	67.85 67.79	4.79 4.86	8.33 8.54	19.03 –
2.6t		268-270	$C_{19}H_{16}N_2O_4$/ 336.34	67.85 67.56	4.79 4.76	8.33 8.56	19.03 –
2.6u		205-207	$C_{20}H_{18}N_2O_5$/ 366.37	65.57 65.79	4.95 4.87	7.85 7.76	21.84 –
2.6v		278 (dec.)	$C_{18}H_{13}ClN_2O_3$/ 340.76	63.44 63.48	3.85 3.88	8.22 8.33	14.09 –
2.6x		dec. (298)	$C_{17}H_{12}N_2O_2$/ 276.29	73.90 74.01	4.38 4.48	10.14 10.09	11.58 –
2.6y		dec. (300)	$C_{25}H_{28}N_2O_3$/ 404.50	74.23 73.95	6.98 6.84	6.93 7.19	11.87 –

2.6z		>300	$C_{18}H_{14}N_2O_2$/ 290.32	74.47 74.35	4.86 4.98	9.65 9.65	11.02 –
2.6a'		262-265	$C_{18}H_{13}ClN_2O_2$/ 324.76	66.57 –	4.03 –	8.63 –	9.85 –
2.6b'		300-303	$C_{18}H_{14}N_2O_2$/ 290.32	74.47 74.36	4.86 5.00	9.65 9.60	11.02 –
2.6c'		207-209	$C_{20}H_{18}N_2O_4$/ 350.37	68.56 68.78	5.18 5.17	8.00 8.07	18.27 –
2.6d'		290-292	$C_{17}H_{11}BrN_2O_2$. $2H_2O$/374.80	52.19 52.31	3.86 4.12	7.16 7.16	20.42 –
2.6e'		288 (dec.)	$C_{18}H_{13}BrN_2O_3$/ 385.21	56.12 55.92	3.40 3.41	7.27 7.29	12.46 –
2.6f'		>300	$C_{19}H_{15}BrN_2O_4$/ 415.24	54.96 54.86	3.64 3.52	6.75 7.06	15.41 –
2.6g'		218-221	$C_{19}H_{15}BrN_2O_4$/ 415.24	54.96 —	3.64 –	6.75 –	15.41 –
2.6h'		>300	$C_{18}H_{11}BrN_2O_4$/ 399.19	54.16 54.55	2.78 2.73	7.02 7.11	16.03 –
2.6i'		274-276	$C_{18}H_{13}ClN_2O_3$/ 340.76	63.54 63.59	3.75 3.96	8.22 8.55	14.09 –
2.6j'		290 (dec.)	$C_{18}H_{13}ClN_2O_3$/ 340.76	63.54 63.95	3.75 3.79	8.22 8.58	14.09 –
2.6k'		260-262	$C_{19}H_{15}ClN_2O_4$.1,5 H_2O/397.79	57.31 57.51	4.52 4.13	7.03 6.92	22.12 –

IR spectroscopy

IR spectroscopy allowed to distinguish both compounds **2.1** and **2.15** by the C=O stretching band, which occurs at 1692 cm^{-1} for **2.15a**. For compound **2.1a**, the C=O stretching vibration of the amide carbonyl group appears at 1700 cm^{-1}, while for **2.15a** appears at 1706 cm^{-1}. For compounds **2.1**, the N-H stretching vibration can also be observed around 3200-3300 cm^{-1}, while for **2.15** are observed at 3392 and 3275 cm^{-1} (**Table 7**).

As expected, the IR spectra for compounds **2.3** and **2.6** shares some similarities. In both cases, the C=O stretching vibration band is identified around 1630-1700 cm^{-1}, and the N-H stretching vibration band of the amide group is observed around 3000 cm^{-1}. The latter band is often broad and tends to show a low intensity (**Tables 8** and **9**).

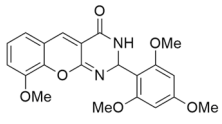


2.1 (X=NH)
2.15a (X=O, R^1=H, R^2=OMe

Table 7: IR spectroscopic data (Nujol, cm^{-1}) obtained for 2-imino-2*H*-chromeno-3-carboxamides **2.1a-g** and 2-oxo-2*H*-chromeno-3-carboxamide **2.15a**

Compound	R^1	R^2	4000-3000	1700-1500
2.1a	H	OMe	3293s, 3149m	1700s (C=O)
2.1b	H	H	3280m, 3130m	1681s (C=O), 1603m, 1567m
2.1c	OMe	H	3278s, 3145m	1678s (C=O), 1600m,1575m
2.1d	Br	H	3278s, 3132m	1684s (C=O), 1611m, 1592sh, 1563m
2.1e	Cl	H	3272m, 3175m	1675s (C=O), 1596m, 1564m
2.1f	H	Me	3274m, 3126m	1681s (C=O), 1602m, 1577m
2.1g	Me	H	3276s, 3154m	1675s (C=O), 1599m, 1577m
2.15a	H	OMe	3392m, 3275m	1706s (C=O), 1647m, 1612m, 1591m, 1577m

Table 8: IR spectroscopic data (Nujol, cm^{-1}) obtained for 2-aryl-3*H*-chromeno[2,3-*d*]pyrimidin-4(3*H*)- ones **2.3d-i**

Compound	Structure	4000-3000	1700-1500
2.3d		3155w	1699s, 1658s (C=O), 1625sh, 1603s

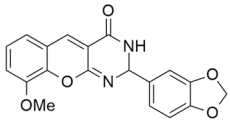
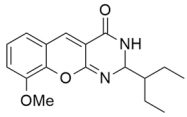
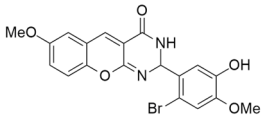
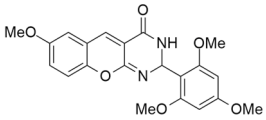
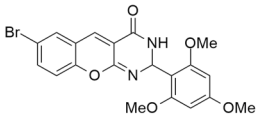
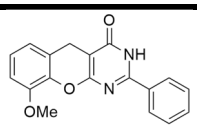
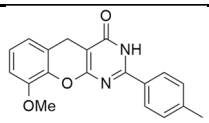
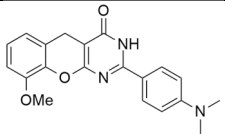
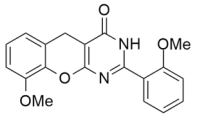
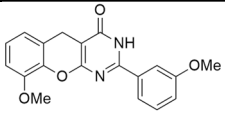
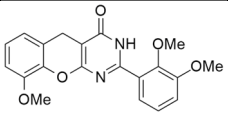
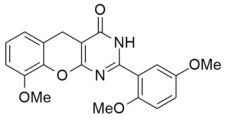
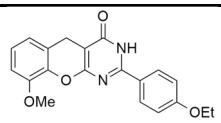
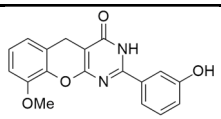
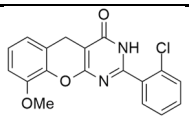
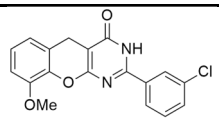
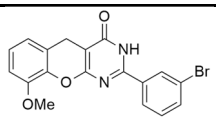
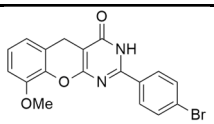
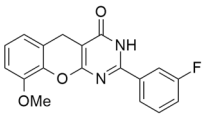
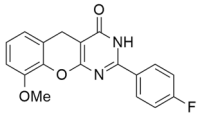
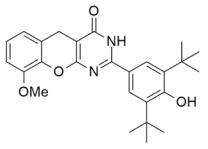
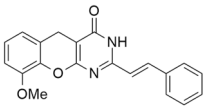
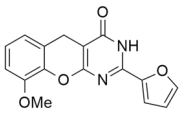
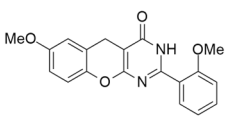
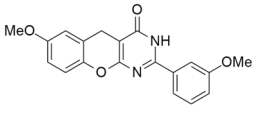
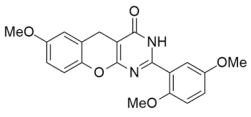
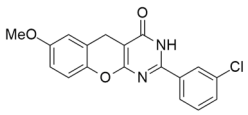
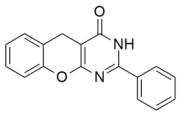
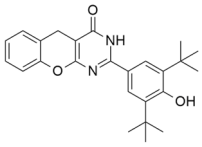
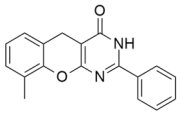
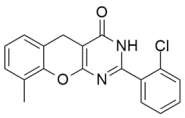
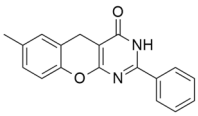
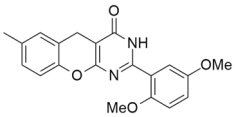
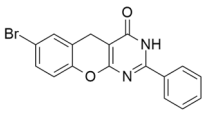
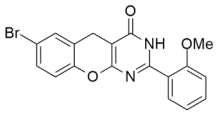
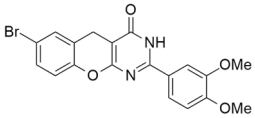
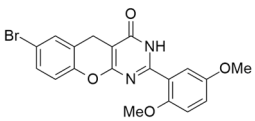
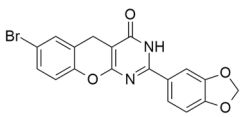
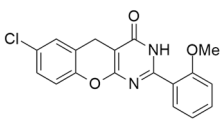
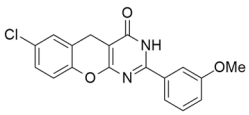
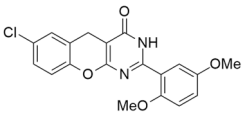
2.3e		3151m	1686m, 1649s (C=O), 1649sh, 1606m, 1564s, 1517sh
2.3f		3172m, 3040i	1688s, 1653s (C=O), 1619s, 1609s, 1580m
2.3g		3358m, 3153m, 3026m	1692s, 1643s (C=O), 1619sh, 1579s
2.3h		3146m	1694s, 1656s (C=O), 1603s, 1584s
2.3i		3150m	1697s, 1657s (C=O), 1625sh, 1604sh, 1592s, 1564sh

Table 9: IR spectroscopic data (Nujol, cm^{-1}) obtained for 2-aryl-3*H*-chromeno[2,3-*d*]pyrimidin-4(5*H*)-ones **2.6a-k'**

Compound	Structure	4000-3000	1700-1500
2.6a		3150m, 3067m	1637s (C=O), 1609sh, 1579s
2.6b		3151m, 3070m	1649s (C=O), 1601m, 1577s, 1554sh
2.6c		3150m, 3074m	1650s (C=O), 1601m, 1577s, 1556sh
2.6d		3314s	1661s (C=O), 1608sh, 1577s, 1558sh
2.6e		3195m, 3090m	1643s (C=O), 1621s, 1606sh, 1573s, 1555s, 1511sh
2.6f		-	1637s (C=O), 1611sh, 1582s
2.6g		3282s, 3026m	1665s (C=O), 1617sh, 1603m, 1572s, 1526sh

2.6h		3075m	1649s (C=O), 1612sh, 1579s, 1559sh, 1524m
2.6i		3493m, 3076w	1671sh, 1642s (C=O), 1609sh, 1582m, 1561m, 1515m
2.6j		-	1642s (C=O), 1608m, 1599sh, 1580s
2.6k		3060w	1659s (C=O), 1607m, 1579s, 1564s, 1505w
2.6l		3088w	1654s (C=O), 1607m, 1578s, 1533m, 1511w
2.6m		3139w, 3066m	1649s (C=O), 1602m, 1578s, 1552m, 1510m
2.6n		3070w	1650s (C=O), 1607sh, 1573s, 1512w
2.6o		3156w, 3082m	1650s (C=O), 1612m, 1576s, 1524m
2.6p		3638m, 3622m	1657s (C=O), 1607m, 1580s, 1565s
2.6q		3160w, 3068m, 3040m	1648s (C=O), 1575s, 1565sh, 1541sh
2.6r		3124m	1650s(C=O), 1602m, 1577s, 1546sh
2.6s		3208m	1660m (C=O), 1617m, 1589sh, 1578m, 1546m
2.6t		3142w, 3077m	1631s (C=O), 1599sh, 1582sh,1556m
2.6u		3206m	1662s (C=O), 1618sh, 1590sh, 1578sh, 1553s

2.6v		3058m	1662s (C=O), 1614sh, 1581sh, 1568m
2.6x		3154w, 3073w	1646s (C=O), 1617sh, 1592m, 1575m, 1554m, 1518m, 1504w
2.6y		3635m, 3625sh, 3611sh	1638s (C=O), 1607sh, 1576s, 1566s
2.6z		3150w, 3073m	1651s (C=O), 1605sh, 1585m, 1555m, 1514w
2.6a'		-	1653s (C=O), 1607m, 1583m, 1565sh, 1503w
2.6b'		3151w, 3070m	1644s (C=O), 1619sh, 1590sh, 1557m, 1505sh
2.6c'		3331m	1667s (C=O), 1620m, 1578sh, 1560s
2.6d'		3167w, 3060m	1667s (C=O), 1611m, 1570m, 1558m, 1511w
2.6e'		3223w, 3170w, 3088w	1650s (C=O), 1614m, 1602m, 1584m, 1567s, 1556s
2.6f'		3151w, 3073w	1641s (C=O), 1603w, 1572m, 1530m
2.6g'		3285m	1679s (C=O), 1614m, 1601m, 1586m, 1567s
2.6h'		3154w, 3066w	1650s (C=O), 1574m, 1518m
2.6i'		3271m	1663s (C=O), 1623m, 1602sh, 1584m, 1545s,

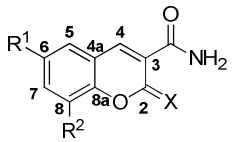
2.6j'		3133w, 3055m	1658s (C=O), 1619sh, 1566s, 1509m
2.6k'		3293m	1672s (C=O), 1614sh, 1606m, 1586sh, 1568s

NMR Spectroscopy

Compounds **2.1** and **2.15a** (**Table 10**) have characteristic spectroscopic signals. By ^{1}H NMR, it is possible to identify compounds **2.1** from the displacement of the NH_2 protons of the amide moiety (δ9.87-7.75 ppm), which occurs more intensely than in **2.15a** (δ8.06-7.91 ppm), probably due to the nature of the interaction between the amide protons and imine (**2.1**) and oxo (**2.15a**) groups.

The ^{1}H NMR spectra of **2.15a** also corroborates the absence of the imino group as the characteristic signal at δ9.01 ppm corresponding to the NH group in **2.1** was obtained. As referred by O'Callaghan[7], there is an observable ring-opening phenomenon in DMSO-d_6, with an extent varying from 0 to 89% depending on the substituents present in the chromene ring. The ^{1}H and ^{13}C NMR characterization of compounds **2.1a**, **2.1c** and **2.1e** was performed considering to the information currently described in the literature[7]. The most distinctive features in the ^{13}C NMR spectra are the amide carbonyl signal, which appears around δ164-162 ppm, and the C4 signal between δ142-140 ppm (except for compound **2.1c**, in which appears at δ119 ppm) (**Table 11**).

It is possible to observe the chromene ring-opening of compounds **2.1** in DMSO-d_6, but for the present work, such structures are not characterized by NMR spectroscopy, as they are not relevant for the matter and because, for most of the chromenes **2.1** described in this work, there is already an identification of both these structures and the ratio of the substituent-dependent ring-closed/ring-opened structures[7]. For some compounds, another small, broad signal appeared at δ12.7-12.5 ppm,



2.1 (X=NH)
2.15a (X=O, R^1=H, R^2=OMe

Table 10: ^{1}H NMR (400 MHz, DMSO-d_6, δ ppm) spectroscopic data obtained for 2-imino-2*H*-chromeno-3-carboxamides **2.1a-g** and for 2-oxo-2*H*-chromeno-3-carboxamide **2.15a**

Comp.	R^1	R^2	H4	Ar (H5-8)	NH	$CONH_2$	OMe/ Me
2.1a[1]	H	OMe	8.38 (s, 1H)	7.32 (t, J= 7.9 Hz, 1H, H6), 7.30 (dd, J_1= 7.9Hz, J_2= 1.0 Hz, 1H, H7), 7.25 (d, J= 7.9 Hz, 1H, H5)	9.01 (s, 1H)	9.61 (s, 1H) and 7.90 (s, 1H)	3.89 (s, 3H)
2.1b[1]	H	H	8.42 (s, 1H)	7.76 (dd, J_1=7.5 Hz, J_2=1.3 Hz, 1H, H5), 7.58 (dt, J_1= 7.5 Hz, J_2=1.3 Hz, 1H, H7), 7.26 (t, J= 7.5 Hz, 1H, H6), 7.22 (d, J= 7.5 Hz, 1H, H8)	8.90 (s, 1H)	9.87 (s, 1H) and 8.03 (s, 1H)	-
2.1c[1]	OMe	H	8.43 (s, 1H)	7.36 (d, J= 3.0 Hz, 1H, H5), 7.16 (d, J= 8.9 Hz, 1H, H8), 7.13 (dd, J_1= 3.0 Hz, J_2= 8.9 Hz, 1H, H7)	9.01 (s, 1H)	9.87 (s, 1H) and 8.03 (s, 1H)	3.80 (s,3H)
2.1d	Br	H	8.36 (s, 1H)	7.96 (d, J= 2.4 Hz, 1H, H5), 7.64 (dd, J_1= 8.8 Hz, J_2= 2.8 Hz, 1H, H7), 7.13 (d, J= 8.4 Hz, 1H, H8)	9.00 (s, 1H)	9.48 (s, 1H) and 7.81 (s, 1H)	-
2.1e[1]	Cl	H	8.40 (s, 1H)	7.81 (d, J= 2.5 Hz, 1H, H5), 7.55 (dd, J_1= 8.8 Hz, J_2= 2.5 Hz, 1H, H7), 7.23 (d, J= 8.8 Hz, 1H, H8)	9.02 (s, 1H)	9.51 (s, 1H) and 7.80 (s, 1H)	-
2.1f	H	Me	8.35 (d, J= 1.6 Hz, 1H)	7.53 (d, J= 7.6 Hz, 1H, H5), 7.40 (dd, J_1= 7.6 Hz, J_2 = 0.8 Hz, 1H, H7), 7.17 (t, J= 7.6 Hz, 1H, H6)	8.84 (s, 1H)	9.71 (s, 1H) and 7.75 (s, 1H)	2.32 (s, 3H)
2.1g	Me	H	8.31 (s, 1H)	7.49 (s, 1H, H5), 7.33 (dd, J_1= 8.4 Hz, J_2= 2.0 Hz, 1H, H7), 7.07 (d, J= 8.4 Hz, 1H, H8)	8.64 (s, 1H)	9.48 (s, 1H) and 7.75 (s, 1H)	2.31 (s, 3H)
2.15a[2]	H	OMe	8.83 (s, 1H)	7.49 (dd, J_1= 7.5, J_2= 1.5 Hz, 1H, H5), 7.42 (dd, J_1= 8.2 Hz, J_2= 1.5, 1H, H7), 7.35 (t, J= 7.8 Hz, 1H, H6)	-	8.06 (s, 1H) and 7.91 (s, 1H)	3.88 (s, 3H)

[1]Data obtained from ref. 7; performed using Bruker MSL 400 instrument

[2]Data obtained from ref. 6; performed using Bruker MSL 400 instrument; Commercial product

Table 11: ^{13}C NMR (400 MHz, DMSO-d_6, δ ppm) spectroscopic data obtained for 2-imino-2*H*-chromeno-3-carboxamides **2.1** and for 2-oxo-2*H*-chromeno-3-carboxamide **2.15a**

Comp.	R^1	R^2	C2	C3	C4	Ar (C4a-8a)	$CONH_2$	OMe/ Me
2.1a[1]	H	OMe	155.1	128.3	141.1	145.8 (C8), 145.7 (C8a), 123.8 (C5), 121.0 (C6), 119.0 (C4a), 115.4 (C7)	162.9	55.9
2.1b[1]	H	H	155.5	120.9	141.0	153.6 (C8a), 132.9 (C7), 129.8 (C5), 124.0 (C6), 118.5 (C4a), 114.8 (C8)	162.9	-
2.1c[1]	OMe	H	156.2	121.4	119.1	155.5 (C6), 152.5 (C5), 148.3 (C8a), 120.1 (C7), 119.1 (C4a), 116.1 (C8)	163.3	56.1
2.1d	Br	H	156.94	121.90	139.75	152.68 (C8a), 135.01 (C7), 115.26 (C6), 131.73 (C5), 121.04 (C4a), 117.05 (C8)	162.41	-
2.1e[1]	Cl	H	157.1	122.7	142.1	154.6 (C8a), 134.5 (C7), 130.4 (C6), 129.1 (C5), 122.3 (C4a), 119.0 (C8)	164.7	-
2.1f	H	Me	155.68	120.43	141.32	151.78 (C8a), 134.00 (C7), 127.46 (C5), 123.84 (C4a), 123.44(C6), 118.08 (C8)	162.99	14.41
2.1g	Me	H	155.60	120.76	140.64	151.54 (C8a), 133.24 (C7), 129.22 (C5), 127.90(C6), 117.99 (C4a), 114.32 (C8)	162.67	19.75
2.15a[2]	H	OMe	-	-	-	-		

[1]Data obtained from ref. 7; performed using Bruker MSL 400 instrument

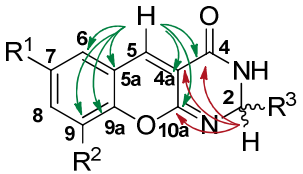
[2]Data obtained from ref. 6; performed using Bruker MSL 400 instrument; Commercial product

The most relevant features of the ^1H and ^{13}C NMR spectra of compounds **2.3** are (**Tables 12** and **13**): (i) the existence of a singlet between δ7.99-7.50 ppm and a small doublet at δ6.6-6.3 ppm, attributed to H5 and H2, respectively; (ii) the strong displacement to low field of the NH signal of the pyrimidinone group, when comparing to what is observed for compounds **2.6**; (iii) two signals, one between δ130-133 ppm (C5) and another between δ62-70 ppm (C2). For all the

compounds, the complete assignation of the signals in the ^{13}C NMR spectrum was performed by two-dimensional correlation spectra (HMQC, HMBC). The most relevant cross peaks identified were between H4 and C4, C4a, C5a, C6, C9, C9a, C10a and, in some cases, also with C2, as well as the correlation between H2 with C1', C4, C4a, C10a and, in some cases, C5.

The most relevant features of the ^{1}H and ^{13}C NMR spectra of compounds **2.6** are (**Tables 14-17**): (i) a singlet between δ3-4 ppm, integrating for two protons, which was assigned to H5; (ii) a broad singlet at around δ12.93-12.06 ppm region corresponding to the NH group of the pyrimidinone moiety; (iii) two signals at around δ161-163 ppm, belonging to both C4 and C10a; (iv) a signal at around δ 155-156 ppm corresponding to C2. HMBC correlation spectra showed relevant cross peaks, for example between C2' and C6', and between the methylene group at C5 and C4, C4a, C5a, C6, C9a, C10a and in some cases, C7.

Table 12: ^{1}H NMR (400 MHz, DMSO-d$_6$, δ ppm) spectroscopic data obtained for 2-aryl-3*H*-chromeno[2,3-d]pyrimidin-4(3*H*)-ones **2.3d-k**



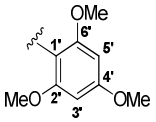
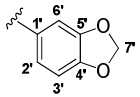
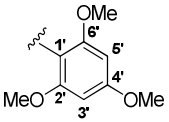
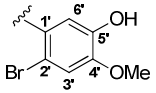
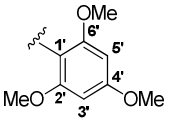
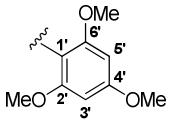
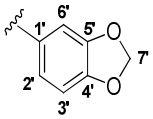
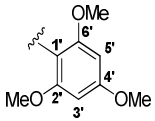
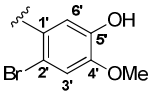
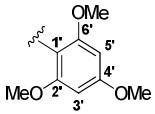
Comp.	R^1	R^2	R^3	H2	H5	H6-9	H2'-6'	NH
2.3d	H	OMe		6.52 (s, 1H)	7.93 (s, 1H)	7.17 (d, *J*= 8.4 Hz, 1H, H6), 7.16 (d, *J*= 8.4 Hz, 1H, H8), 7.11 (t, *J*= 8-0 Hz, 1H, H7), 3.81 (s, 3H, OMe)	6.20 (s, 2H, H3'+H5'), 3.74 (OMe), 3.73 (br s, 6H, 2x OMe)	8.48 (d, *J*= 1.6 Hz, 1H)
2.3e	H	OMe		6.13 (s, 1H)	7.93 (s, 1H)	7.21 (t, *J*= 7.2 Hz, 1H, H7), 7.20 (d, *J*= 7.2 Hz, 1H, H8), 7.13 (d, *J*= 8.0 Hz, 1H, H6), 3.83 (s, 3H, OMe)	6.88 (t, *J*= 1.6 Hz, 1H, H3'), 6.86 (s, 1H, H6'), 6.81 (dd, J_1= 8.0, J_2= 1.6 Hz, 1H, H2'), 6.98 (s, 2H, H7')	8.91 (d, *J*= 1.2 Hz, 1H)
2.3f	H	OMe		5.27 (s, 1H)	7.81 (d, *J*= 1.2 Hz, 1H)	7.21 (dd, J_1= 1.6 Hz, J_2= 7.6 Hz, 1H, H8), 7.16 (dd, J_1= 1.6 Hz, J_2= 7.6 Hz, 1H, H6), 7.11 (t, *J*= 7.6 Hz, 1H, H7), 3.85 (OMe)	1.42-1.33 (m, 3H), 1.08 (q, J_1= 2Hz, J_2= 7.2 Hz, J_3= 14 Hz, 2H), 0.89 (t, *J*= 7.6 Hz, 1H), 0.83 (t, *J*= 7.6 Hz, 1H)	8.49 (s, 1H)
2.3g	OMe	H		6.52 (dd, J_1= 0.4 Hz, J_2= 1.6 Hz, 1H)	7.86 (s, 1H)	7.25 (d, *J*= 2.8 Hz, 1H, H6), 7.09-7.02 (m, 2H, H8+H9),	6.21 (s, 2H, H3'+ H5'), 3.76 (s, 3H, OMe), 3.75 (br s, 6H, 2x OMe)	8.48 (d, *J*= 1.6 Hz, 1H)
2.3h	OMe	H		6.34 (s, 1H)	7.99 (s, 1H)	7.26 (d, J= 2.8 Hz, 1H, H9), 7.11 (s, 1H, H6), 7.09 (d, *J*= 2.8 Hz, 1H, H8),	7.07 (s, 1H, H3'), 6.73 (s, 1H, H6')	8.89 (s, 1H)
2.3i	Br	H		6.53 (s, 1H)	7.89 (s, 1H)	7.89 (s, 1H, H6), 7.60 (dd, J_1= 8.8 Hz, J_2= 2.4 Hz, 1H, H8), 7.11 (d, *J*= 8.8 Hz, 1H, H9),	6.21 (s, 2H, H3'+H5'), 3.75 and 3.64 (s, 9H, 3x OMe)	8.56 (s, 1H)

Table 13: ^{13}C NMR (400 MHz DMSO-d_6, δ ppm) spectroscopic data obtained for 2-aryl-3*H*-chromeno[2,3-*d*]pyrimidin-4(3*H*)-ones **2.3d-k**

Comp.	R^1	R^2	R^3	C2	C5	C4a-10a	C1'-7'	$CONH_2$
2.3d	H	OMe		63.02	130.99	154.65 (C10a), 146.47 (C9), 142.68 (C9a), 123.95 (C7), 121.03 (C6), 119.08 (C5a), 116.73 (C4a), 115.54 (C8), 56.22 (OMe)	161.03 (3C, C2'+C4'+C6'), 109.27 (C1'), 91.46 (C3'+C5'), 56.00 (OMe), 55.33 (2C, 2x OMe)	159.90
2.3e	H	OMe		70.84	133.60	154.36 (C10a), 146.51 (C9), 142.73 (C9a), 124.20 (C7), 121.24 (C6), 119.65 (C5a), 116.08 (C8), 114.77 (C4a)	147.59 (C4'), 147.11 (C5'), 136.45 (C1'), 119.90 (C2'), 108.25 (C6'), 106.98 (C3'), 101.29 (C7')	159.06
2.3f	H	OMe		70.50	132.70	157.45 (C10a), 146.55 (C9), 142.82 (C9a), 124.32 (C7), 121.23 (C6), 119.72 (C5a), 116.00 (C8), 115.45 (C4a), 56.30 (OMe)	48.73 (C1'), 20.67 (C2'), 12.32 (C3')	160.23
2.3g	OMe	H		62.83	130.56	155.15 (C7), 154.72 (C10a), 147.61 (C9a), 119.51 (C5a), 118.81 (C9), 116.78 (C4a), 116.40 (C8), 112.75 (C6), 56.06 (OMe)	160.79 (3C, C2'+ C4'+ C6'), 109.24 (C1'), 91.29 (C3'+C5'), 55.80 (OMe), 55.68 (OMe), 55.34 (OMe)	159.61
2.3h	OMe	H		70.90	133.54	155.95 (C7), 154.90 (C10a), 147.80 (C9a), 119.93 (C9), 119.57 (C5a), 116.83 (C6), 114.93 (C4a), 113.03 (C8), 56.28 (OMe)	148.62 (C4'), 146.67 (C5'), 132.49 (C1'), 116.19 (C3'), 114.91 (C6'), 109.66 (C2')	159.44
2.3i	Br	H		62.93	129.40	154.23 (C10a), 152.61 (C9a), 134.70 (C8), 131.50 (C6), 121.31 (C5a), 117.84 (C9), 117.42 (C4a), 115.29 (C7)	160.96 (C2'+ C4'+ C6'), 108.84 (C1'), 91.32 (C3'+ C5'), 55.82 and 55.41(3x OMe)	159.32

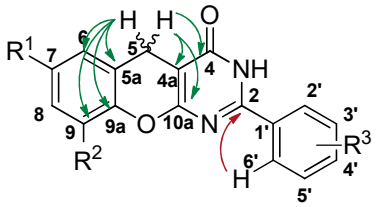


Table 14: ^{1}H NMR (400 MHz, DMSO-d_6, δ ppm) spectroscopic data obtained for 2-aryl-3*H*-chromeno[2,3-*d*] pyrimidin-4(5*H*)-ones **2.6a-k'**

Comp.	R^1	R^2	R^3	H5	Ar(H6-9)	Ar(H2'-6')	NH
2.6a	H	OMe	H	3.73 (s, 2H)	7.06 (t, *J*= 8.0 Hz, 1H, H7), 6.96 (dd, J_1= 8.0, J_2= 1.2 Hz, 1H, H8), 6.84 (dd, J_1= 7.6, J_2= 1.6 Hz, 1H, H6), 3.83 (s, 3H, OMe)	8.18 (d, *J*= 7.6 Hz, 2H, H2'+H6'), 7.60 (dt, J_1= 8.4, J_2= 1.2 Hz, 1H, H4'), 7.54 (dt, J_1= 8.0 Hz, J_2= 1.6 Hz, 2H, H3'+ H5'),	12.82 (s, 1H)
2.6b	H	OMe	4'-Me	3.71 (s, 2H)	7.05 (t, *J*= 8.0 Hz, 1H, H7), 6.94 (dd, J_1= 8.0 Hz, J_2= 0.8 Hz, 1H, H8), 6.83 (dd, J_1= 7.6 Hz, J_2= 1.2 Hz, 1H, H6), 3.83 (s, 3H, OMe)	8.02 (dt, *J*= 8.0 Hz, 2H, H2'+6'), 7.33 (d, *J*= 8.0 Hz, 2H, H3'+ H5'), 2.38 (s, 3H, CH_3)	12.74 (s, 1H)
2.6c	H	OMe	4'-N(Me)$_2$	3.70 (s, 2H)	7.04 (t, *J*= 8.0 Hz, 1H, H7), 6.79 (dd, J_1= 7.6, J_2= 0.8 Hz, 1H, H8), 6.83 (dd, J_1= 8.8, J_2= 2.0 Hz, 1H, H6), 3.86 (OMe)	8.03 (dt, J_1=8.8, J_2= 2.0 Hz, 2H, H2' + H6'), 6.79 (dd, J_1= 8.8, J_2= 2.0 Hz, 2H, H3'+ H5'), 3.02 (s, 6H, 2x Me)	12.08 (s, 1H
2.6d	H	OMe	2'-OMe	3.70 (s, 2H)	7.06 (t, *J*= 8.0 Hz, 1H, H7), 6.95 (dd, J_1= 8.0 Hz, J_2= 1.2 Hz, 1H, H8), 6.83 (dd, J_1= 7.6 Hz, J_2= 1.6 Hz, 1H, H6), 3.82 (s, 3H, OMe)	8.05 (d, *J*= 8.4 Hz, 2H, H2' + H6'), 7.37 (d, *J*= 8.4 Hz, 2H, H3'+ H5'), 2.68 (q, *J*= 7.6 Hz, 2H, CH2), 1.21 (t, *J*= 7.6 Hz, 3H, CH3)	12.18 (s, 1H)
2.6e	H	OMe	3'-OMe	3.72 (s, 2H)	7.06 (t, *J*= 8.0 Hz, 1H, H7), 6.94 (d, *J*= 7.2 Hz, 1H, H8), 6.83 (d, *J*= 7.6 Hz, 1H, H6), 3.83 (s, 3H, OMe)	7.71 (dd, J_1= 7.6 Hz, J_2=1.6 Hz, 1H, H6'), 7.67 (t, *J*= 1.2 Hz, 1H, H2'), 7.44 (t, *J*= 8 Hz, 1H, H5'), 7.14 (dd, J_1= 8.0 Hz, J_2= 2.0 Hz, 1H, H4'), 3.84 (s, 3H, OMe)	12.79 (s, 1H)
2.6f	H	OMe	2'-OMe, 3'-OMe	3.71 (s, 2H)	7.06 (t, *J*= 8.0 Hz, 1H, H7), 6.94 (dd, J_1= 8.4, J_2= 1.2 Hz, 1H, H8), 6.84 (dd, J_1= 7.6, J_2= 0.8 Hz, 1H, H6), 3.81 (s, 3H, OMe)	7.25 (d, J_1= 6.4, J_2= 4.0 Hz, 1H, H4'), 7.21-7.17 (m, 2H, H5' + H6'), 3.86 (s, 3H, C3'-OMe), 3.76 (s, 3H, C2'-OMe	12.36 (s, 1H)

2.6g	H	OMe	2'-OMe, 5'-OMe	3.71 (s, 2H)	7.06 (t, J= 8.0 Hz, 1H, H7), 6.94 (d, J= 7.2 Hz, 1H, H8), 6.83 (d, J= 7.6 Hz, 1H, H6), 3.84 (s, 3H, OMe)	7.28 (d, J= 2.4 Hz, 1H, H6'), 7.15-7.12 (d, J= 2.4 Hz, 2H, H3' + H4'), 3.82 (s, 3H, C3'-OMe), 3.77 (S, 3H, C5'-OMe)	12.12 (s, 1H)
2.6h	H	OMe	4'-OEt	3.69 (s, 2H)	7.04 (t, J= 8.0 Hz, 1H, H7), 6.93 (d, J= 7.6 Hz, 1H, H8), 6.82 (d, J= 7.2 Hz, 1H, H6), 3.83 (s, 3H, OMe)	8.09 (d, J= 8.8 Hz, 2H, H2' + H6'), 7.04 (d, J= 8.8 Hz, 2H, H3'+ H5'), 4.11 (q, J= 7.6 Hz, 2H, CH2), 1.34 (t, J= 7.2 Hz, CH3)	12.62 (s, 1H)
2.6i	H	OMe	3'-OH	3.72 (s, 2H)	7.06 (t, J= 8.0 Hz, 1H, H7), 6.94 (d, J= 8.4 Hz, 1H, H8), 6.83 (dd, J_1= 7.6 Hz, J_2= 1.2 Hz, 1H, H6), 3.84 (S, 3H, OMe)	9.78 (s, 1H, OH), 7.56 (d, J= 6.4 Hz, 1H, H6'), 7.55 (s, 1H, H2'), 7.32 (t, J= 8.4 Hz, 1H, H5'), 6.92 (dd, J_1= 9.6 Hz, J_2= 2.0 Hz, 1H, H4')	12.68 (s, 1H)
2.6j	H	OMe	2'-Cl	3.73 (s, 2H)	7.07 (t, J= 7.6 Hz, 1H, H7), 6.95 (t, J= 7.6 Hz, 1H, H8), 6.85 (d, J= 7.2 Hz, 1H, H6), 3.80 (S, 3H, OMe)	8.18 (d, J= 7.6 Hz, 2H, H2' + H6'), 7.64-7.60 (m, 2H, H3' + H6'), 7.56 (dt, J_1= 8.0 Hz, J_2= 1.6 Hz, 1H, H4')	12.93 (s, 1H)
2.6k	H	OMe	3'-Cl	3.75 (s, 2H)	7.05 (t, J= 7.6 Hz, 1H, H7), 6.94 (d, J= 7.6 Hz, 1H, H8), 6.84 (d, J= 7.2 Hz, 1H, H6), 3.85 (S, 3H, OMe)	8.17 (t, J=1.2 Hz, 1H, H2'), 8.09 (dt, J_1= 8.0 Hz, J_2= 1.2 Hz, 1H, H6'), 7.63 (dq, J_1= 8.0 Hz, J_2= 2.0 Hz, J_3= 1.2 Hz, 1H, H4'), 7.55 (t, J= 8 Hz, 1H, H5')	12.83 (s, 1H)
2.6l	H	OMe	3'-Br	3.72 (s, 2H)	7.06 (t, J= 8.0 Hz, 1H, H7), 6.94 (d, J= 7.2 Hz, 1H, H8), 6.83 (d, J= 7.6 Hz, 1H, H6), 3.83 (s, 3H, OMe)	8.31 (t, J=1.6 Hz, 1H, H2'), 8.12 (d, J= 8 Hz, 1H, H6'), 7.78 (dd, J_1= 8.0 Hz, J_2= 0.8 Hz, 1H, H4'), 7.49 (t, J= 8.0 Hz, 1H, H5')	12.86 (s, 1H)
2.6m	H	OMe	4'-Br	3.72 (s, 2H)	7.06 (t, J= 8.0 Hz, 1H, H7), 6.94 (d, J= 6.8 Hz, 1H, H8), 6.83 (d, J= 6.8 Hz, 1H, H6), 3.83 (s, 3H, OMe)	8.06 (d, 2H, J=8.4 Hz, H2' + H6'), 7.38 (d, 2H, J= 8.4 Hz, H3'+ H5')	12.58 (s, 1H)
2.6n	H	OMe	3'-F	3.74 (s, 2H)	7.07 (t, J= 7.6 Hz, 1H, H7), 6.96 (d, J= 7.2 Hz, 1H, H8), 6.84 (d, J= 6.4 Hz, 1H, H6), 3.84 (S, 3H, OMe)	7.99 (d, J= 8.0 Hz, 1H, H6'), 7.93 (dd, J_1= 10.0, J_2= 2.4 Hz, 1H, H2'), 7.58 (q, J= 8.0 Hz, 1H, H5'), 7.45 (dt, J_1= 8.4, J_2= 2.0 Hz, 1H, H4')	12.88 (s, 1H)
2.6o	H	OMe	4'-F	3.72 (s, 2H)	7.06 (t, J= 8.0 Hz, 1H, H7), 6.95 (d, J= 6.8 Hz, 1H, H8), 6.84 (d, J= 6.8 Hz, 1H, H6), 3.83 (s, 3H, OMe)	8.18 (dd, 2H, J_1=8.8 Hz, J_2= 5.2 Hz, H3'+ H5'), 7.37 (dt, 2H, J_1= 8.8 Hz, J_2 =2.0 Hz, H2' + H6')	12.83 (s, 1H)

2.6p	H	OMe	3',5'-*t*-Bu, 4'-OH	3.70 (s, 2H)	7.07 (t, J= 8 Hz, 1H, H7), 6.95 (d, J= 6.8 Hz, 1H, H8), 6.83 (d, J= 6.8 Hz, 1H, H6), 3.83 (s, 3H, OMe)	7.83 (s, 2H, H2' + H6'), 7.65 (s, 1H, OH), 1.43 (s, 9H, C3' or C5'-*t*Bu), 1.35 (s, 9H, C3' or C5'-*t*Bu)	12.76 (s, 1H)
2.6s	OMe	H	2'-OMe	3.72 (s, 2H)	7.02 (d, J= 9.2 Hz, 1H, H9), 6.84 (d, J= 2.8 Hz, 1H, H6), 6.79 (dd, J_1= 8.8 Hz, J_2= 2.8 Hz, 1H, H8), 3.86 (s, 3H, OMe)	7.69 (d, 1H, J_1= 8.0 Hz, J_2= 2.0 Hz, H6'), 7.53 (dt, 1H, J_1= 7.2 Hz, J_2= 2.0 Hz, H4'), 7.19 (d, 1H, J= 8.4 Hz, H3'), 7.07 (dt, 1H, J_1= 7.2 Hz, J_2 =0.8 Hz, H5')	12.15 (s, 1H)
2.6t	OMe	H	3'-OMe	3.72 (s, 2H)	7.14 (dd, J_1= 8.0 Hz, J_2= 2.0 Hz, 1H, H8), 7.07 (d, J= 8.0 Hz, 1H, H9), 6.87 (d, J= 3.2 Hz, 1H, H6), 3.74 (s, 3H, OMe)	7.70 (d, J= 7.6 Hz, 1H, H6'), 7.67 (s, 1H, H2'), 7.43 (t, J= 8.0 Hz, 1H, H5'), 6.83 (dd, J_1=8.8 Hz, J_2= 2.8 Hz, 1H, H4'), 3.84 (s, 3H, OMe)	12.79 (s, 1H)
2.6u	OMe	H	2'-OMe, 5'-OMe	3.67 (s, 2H)	7.14 (dd, J_1= 8.0 Hz, J_2= 2.0 Hz, 1H, H8), 7.07 (t, J= 8.0 Hz, 1H, H9), 6.87 (d, J= 3.2 Hz, 1H, H6), 3.73 (s, 3H, OMe)	7.26 (dd, J_1= 2.4 Hz, J_2= 0.8 Hz, 1H, H4'), 7.12 (d, J= 2.4 Hz, 1H, H3'), 7.12 (s, 1H, H6'), 3.82 (s, 3H, C6'-OMe), 3.75 (S, 3H, C2'-OMe)	12.15 (s, 1H)
2.6v	OMe	H	3'-Cl	3.76 (s, 2H)	7.06 (d, J= 8.8 Hz, 1H, H9), 6.86 (d, J= 2.6 Hz, 1H, H6), 6.81 (dd, J_1= 8.8 Hz, J_2= 2.4 Hz, 1H, H8), 3.73 (s, 3H, OMe)	8.16 (t, J= 1.6 Hz, 1H, H2'), 8.07 (d, J= 7.6 Hz, 1H, H6'), 7.65 (dd, J_1= 8.0 Hz, J_2= 1.2 Hz, 1H, H4'), 7.56 (t, J= 8 Hz, 1H, H5')	12.84 (s, 1H)
2.6x	H	H	H	3.73 (s, 2H)	7.30 (dd, J_1= 8.0 Hz, J_2= 1.6 Hz, 1H, H6), 7.26 (dt, J_1= 7.6 Hz, J_2= 1.2 Hz, 1H, H8), 7.14-7.11 (m, 2H, H7+ H9)	8.11 (dd, J_1= 8.0, J_2= 1.2 Hz, 2H, H2' + H6'), 7.59 (dt, J_1= 7.2 Hz, J_2= 1.2 Hz, 1H, H4'), 7.52 (dt, J_1= 1.2 Hz, J_2= 6.8 Hz, 2H, H3'+ H5')	12.82 (s, 1H)
2.6y	H	H	3',5'-*t*-Bu, 4-OH	3.73 (s, 2H)	7.28 (d, J= 7.6 Hz, 1H, H6), 7.25 (t, J= 6.4 Hz, 1H, H8), 7.14 (d, J= 8.0 Hz, 1H, H9), 7.12 (t, J= 7.6 Hz, 1H, H7)	7.85 (s, 2H, H2' + H6'), 7.65 (s, J= 7.6 Hz, 1H, OH), 1.42 (s, 18H, 2x *t*Bu)	12.77 (s, 1H)
2.6z	H	Me	H	3.75 (s, 2H)	7.10 (d, J= 7.6 Hz, 2H, H7 + H9), 7.01 (t, J= 8.0 Hz, 1H, H8), 2.32 (s, 3H, Me)	8.13 (dd, J_1= 8.0 Hz, J_2= 1.2 Hz, 2H, H2' + H6'), 7.53 (dt, J_1= 8.0 Hz, J_2= 2.8 Hz, 1H, H5'), 7.53 (dt, J_1= 7.6 Hz, J_2= 1.6 Hz, 2H, H3'+ H5')	12.47 (s, 1H)

2.6a'	H	Me	2'-Cl	3.72 (s, 2H)	7.06 (br d, J= 8.0 Hz, 2H, H6 + H8), 7.01 (t, J= 8.0 Hz, 1H, H7), 2.32 (s, 3H, Me)	7.59 (br dt, J_1= 7.2 Hz; J_2= 1.6 Hz, 2H, H3'+ H6'), 7.56 (dt, J_1= 7.6 Hz, J_2= 1.6 Hz, 1H, H4'), 7.48 (d, J= 7.6 Hz, 1H, H5')	12.98 (s, 1H)
2.6b'	Me	H	H	3.68 (s, 2H)	7.09 (d, J= 1.6 Hz, 1H, H6), 7.04 (dd, J_1= 7.6, J_2= 1.6 Hz, 1H, H8), 7.01 (d, J= 7.6 Hz, 1H, H9), 2.25 (s, 3H, Me)	8.10 (d, J= 7.2 Hz, 2H, H2'+ H6'), 7.82 (t, J= 7.6 Hz, 1H, H5'), 7.59 (dt, J_1= 7.2, J_2= 1.2 Hz, 2H, H3'+ H5')	12.79 (s, 1H)
2.6c'	Me	H	2'-OMe, 5'-OMe	3.58 (s, 2H)	7.00 (dd, J_1= 8.8 Hz, J_2 = 0.8 Hz, 1H, H8), 6.94 (dd, J_1= 8.4 Hz, J_2= 1.6 Hz, 1H, H6), 6.91 (d, J= 8.0 Hz, 1H, H9), 2.17 (s, 3H, Me)	7.17 (dd, J_1= 2.4 Hz, J_2= 0.8 Hz, 1H, H6'), 7.03 (d, J= 3.2 Hz, 1H, H3'), 7.03 (dd, J_1= 3.2 Hz, J_2= 0.8 Hz, 1H, H4'), 3.74 (s, 3H, C6'-OMe), 3.67 (S, 3H, C3'-OMe)	12.06 (s, 1H)
2.6d'	Br	H	H	3.75 (s, 2H)	7.58 (d, J= 2.4 Hz, 1H, H6), 7.42 (dd, J_1= 8.8, J_2= 2.4 Hz, 1H, H8), 7.11 (d, J= 8.4 Hz, 1H, H9)	8.10 (dd, J_1= 7.6, J_2= 1.2 Hz, 2H, H2'+ H6'), 7.59 (dt, J_1= 7.2, J_2= 1.2 Hz, 1H, H4'), 7.54 (dt, J_1= 6.0, J_2= 3.2 Hz, 2H, H3'+ H5')	12.84 (s, 1H)
2.6e'	Br	H	2'-OMe	3.73 (s, 2H)	7.54 (d, J= 2.4 Hz, 1H, H6), 7.41 (dd, J_1= 7.6 Hz, J_2= 2.4 Hz, 1H, H8), 7.07 (d, J= 7.6 Hz, 1H, H9)	7.66 (dd, J_1= 7.6 Hz, J_2=1.6 Hz, 1H, H6'), 7.54 (dt, J_1= 7.6 Hz, J_2=2.4 Hz, 1H, H4'), 7.18 (d, J= 8 Hz, 1H, H3'), 7.08 (dt, J_1= 7.6 Hz, J_2=0.8 Hz, 1H, H5'), 3.85 (s, 3H, OMe)	12.25 (s, 1H)
2.6f'	Br	H	3',4'-OMe	3.72 (s, 2H)	7.52 (d, J= 2.4 Hz, 1H, H6), 7.40 (dd, J_1= 8.4 Hz, J_2= 2.4 Hz, 1H, H8), 7.10 (d, J= 8.4 Hz, 1H, H9)	7.79 (dd, J_1= 8.4 Hz, J_2= 2.0 Hz, 1H, H6'), 7.74 (d, J= 2.4 Hz, 1H, H5'), 7.08 (dd, J_1= 8.8, J_2= 1.2 Hz, 1H, H2'), 3.87 (s, 3H, C4'-OMe), 3.85 (s, 3H, C3'-OMe)	12.71 (s, 1H)
2.6g'	Br	H	2'.5'-OMe,	3.74 (s, 2H)	7.52 (d, J= 2.4 Hz, 1H, H6), 7.41 (dd, J_1= 8.8 Hz, J_2= 2.8 Hz, 1H, H8), 7.09 (d, J= 8.0 Hz, 1H, H9)	7.25 (dd, J_1= 2.4 Hz, J_2= 0.8 Hz, 1H, H6'), 7.12 (d, J= 2.4 Hz, 2H, H3' + H4'), 3.82 (s, 3H, C2'-OMe), 3.75 (s, 3H, C5'-OMe)	12.12 (s, 1H)
2.6i'	Cl	H	2'-OMe	3.72 (s, 2H)	7.40 (s, 1H, H6), 7.28 (dd, J_1= 8.8 Hz, J_2 = 2.4 Hz, 1H, H8), 7.13 (d, J= 8.8 Hz, 1H, H9)	7.67 (dd, J_1= 7.6 Hz, J_2= 1.6 Hz, 1H, H6'), 7.54 (dt, J_1= 8.8 Hz, J_2= 1.6 Hz, 1H, H4'), 7.18 (d, J= 8.4 Hz, 1H, H3'), 7.08 (t, J= 7.6 Hz, 1H, H5'), 3.86 (s, 3H, OMe)	12.25 (s, 1H)

2.6j'	Cl	H	3'-OMe	3.76 (s, 2H)	7.39 (t, J= 2.4 Hz, H6), 7.28 (dd, J_1= 8.8 Hz, J_2= 2.4 Hz, 1H, H8), 6.87 (d, J= 3.2 Hz, 1H, H9)	7.72 (d, J= 8.4 Hz, 1H, H6'), 7.68 (t, J= 2.0 Hz, 1H, H2'), 7.43 (t, J= 8.0 Hz, 1H, H5'), 7.14 (dd, J_1= 8.0 Hz, J_2= 2.4 Hz, 1H, H4'), 3.85 (s, 3H, OMe)	12.86 (s, 1H)
2.6k'	Cl	H	2',5'-OMe	3.72 (s, 2H)	7.41 (d, J=2.8 Hz, 1H, H6), 7.29 (dd, J_1= 8.8 Hz, J_2= 2.8 Hz, 1H, H8), 7.12 (d, J= 8.8 Hz, 1H, H9)	7.25 (dd, J_1= 2.4 Hz, J_2= 1.2 Hz, 1H, H4'), 7.16 (s, 1H, H6'), 7.12 (d, J= 6.8 Hz, 1H, H3'), 3.82 (s, 3H, C2'-OMe), 3.75 (s, 3H, C5'-OMe)	12.12 (s, 1H)

Table 15: ^{13}C NMR (400 MHz, DMSO-d_6, δ ppm) spectroscopic data obtained for 2-aryl-3*H*-chromeno[2,3-*d*]pyrimidin-4(5*H*)-ones **2.6a-k'**

Comp.	R^1	R^2	R^3	C5	C2-10a	C1'-6'	C=O
2.6a	H	OMe	H	21.86	161.61 (C10a), 147.68 (C9), 139.30 (C9a), 124.39 (C7), 120.67 (C6), 120.31 (C2), 120.31 (C5a), 110.82 (C8), 96.83 (C4a), 55.72 (C9-OMe)	131.97 (C4'), 128.73 (C2'+C6'), 127.72 (C3'+C5')	163.72
2.6b	H	OMe	4'-Me	21.84	161.51 (C10a), 155.21 (C2), 147.65 (C9), 139.30 (C9a), 124.29 (C7), 120.31 (C5a), 120.63 (C6), 110.75(C8), 94.41 (C4a), 55.67 (C9-OMe)	142.14 (C4'), 129.28 (C3'+C5'), 127.62 (C2'+C6'), 20.98 (Me)	163.59
2.6c	H	OMe	4'-N(Me)$_2$	21.54	161.48 (C10a), 154.93 (C2), 147.49 (C9), 139.57 (C9a), 123.58 (C7), 120.42 (C5a), 120.38 (C6), 110.86(C8), 94.12 (C4a), 55.61 (C9-OMe)	154.43 (C4'), 128.56 (C2'+C6'), 117.55 (C1'), 110.89 (C3'+C5'), 30.60 (2x Me)	163.13
2.6d	H	OMe	2'-OMe	21.87	161.56 (C10a), 154.68 (C2), 147.70 (C9), 139.31 (C9a), 124.43 (C7), 120.97 (C5a), 120.72 (C6), 110.86(C8), 96.82 (C4a), 55.76(C9-OMe)	157.25 (C2'), 133.01 (C4'), 130.44 (C6'), 120.63 (C5'), 120.35 (C1'), 112.08 (C3'), 55.92 (C2'-OMe)	162.55
2.6e	H	OMe	3'-OMe	21.87	161.46 (C10a), 154.68 (C2), 147.66 (C9), 139.27 (C9a), 124.36 (C7), 120.65 (C6), 120.28 (C5a), 110.77 (C8), 96.62 (C4a), 55.67 (C9-OMe)	159.39 (C3'), 133.01 (C1'), 129.86 (C5'), 120.05 (C6'), 118.33 (C4'), 112.19 (C2'), 55.41 (C3'-OMe)	163.59

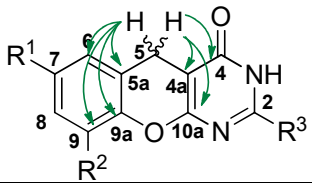
2.6f	H	OMe	2'-OMe, 3'-OMe	21.83	161.33 (C10a), 154.71 (C2), 147.65 (C9), 139.25 (C9a), 124.39 (C7), 120.67 (C6), 120.30 (C5a), 110.85 (C8), 97.05 (C4a), 55.73 (C9-OMe)	152.36 (C3'), 146.75 (C2'), 127.01 (C1'), 124.18 (C5'), 121.19(C6'), 115.61 (C4'), 56.02 (C3'-OMe)	162.52
2.6g	H	OMe	2'-OMe, 5'-OMe	21.82	161.40 (C10a), 154.27 (C2), 147.62 (C9), 139.23 (C9a), 124.34 (C7), 120.64 (C6), 120.28 (C5a), 110.76 (C8), 96.88 (C4a), 55.67 (C9-OMe)	152.91 (C5'), 151.35 (C2'), 121.18 (C1'), 118.60 (C4'), 114.63 (C6'), 113.41 (C3'), 56.24 (C2'-OMe), 55.65 (C5'-OMe)	162.34
2.6h	H	OMe	4'-OEt	21.62	161.59 (C10a), 154.92 (C2), 147.64 (C9), 139.58 (C9a), 124.04 (C7), 123.64 (C5a), 120.53 (C6), 111.11 (C8), 95.55 (C4a), 55.79 (C9-OMe)	161.44 (C4'), 129.28 (C2'+C6'), 120.36 (C1'), 114.42 (C3'+C5'), 63.40 (CH2), 14.16 (CH3)	163.37
2.6i	H	OMe	3'-OH	21.87	147.67 (C9), 139.30 (C9a), 124.34 (C7), 120.66 (C6), 120.32 (C5a), 110.79 (C8), 96.67 (C4a), 55.72 (C9-OMe)	157.59 (C3'), 132.64 (C1'), 119.02 (C4'), 118.22 (C6'), 114.46 (C2')	-
2.6j	H	OMe	2'-Cl	21.81	161.28 (C10a), 155.11 (C2), 147.70 (C9), 139.20 (C9a), 124.56 (C7), 120.72 (C6), 120.27 (C5a), 110.94 (C8), 97.66 (C4a), 55.79 (C9-OMe)	132.63 (C2'), 132.07 (C4'), 131.29 (C1'), 130.85 (C6'), 129.79 (C3'), 127.34 (C5')	162.82
2.6k	H	OMe	3'-Cl	21.58	161.62 (C10a), 154.43 (C2), 147.61 (C9), 139.45 (C9a), 124.11 (C7), 120.48 (C6), 120.17 (C5a), 111.16 (C8), 96.88 (C4a), 55.76 (C9-OMe)	134.00 (C3'), 133.33 (C1'), 131.10 (C4'), 130.18 (C5'), 127.15 (C2'), 126.02 (C6')	163.47
2.6l	H	OMe	3'-Br	21.86	154.59 (C10a), 147.70 (C9), 139.25 (C9a), 124.47 (C7), 120.48 (C6), 120.17 (C5a), 111.16 (C8), 96.88 (C4a), 55.76 (C9-OMe), C2 not seen	134.51 (C4'), 130.90 (C5'), 130.33 (C2'), 126.75 (C6'), 121.98 (C3'), C1' not seen	161.59
2.6m	H	OMe	4'-Br	21.52	161.48 (C10a), 154.72 (C2), 147.53 (C9), 139.40 (C9a), 123.96 (C7), 120.38 (C6), 120.12 (C5a), 111.05 (C8), 96.54 (C4a), 55.67 (C9-OMe)	131.25 (C3'+C5'), 129.45 (C1'), 129.34 (C2'+C6'), 123.96 (C4')	163.43

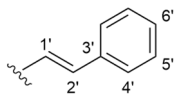
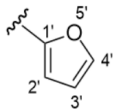
2.6n	H	OMe	3'-F	21.88	160.53 (C10a), 147.67 (C9), 147.66 (C2), 139.24 (C9a), 124.44 (C7), 120.66 (C6), 120.23 (C5a), 110.84 (C8), 97.36 (C4a), 55.71 (C9-OMe)	160.87 (d, J= 242 Hz, C3'), 130.89 (d, J= 8.1 Hz, C5'), 123.91 (d, J= 0.7 Hz, C6'), 118.40 (d, J= 20.0 Hz, C4'), 114.45 (d, J= 23.7 Hz, C2'), C1' not seen	163.65
2.6o	H	OMe	4'-F	21.88	161.63 (C10a), 147.74 (C9), 139.33 (C9a), 124.59 (C7), 120.73 (C6), 120.34 (C5a), 110.89 (C8), 96.75 (C4a), 55.78 (C9-OMe), C2 not seen	164.40 (d, J= 248.9 Hz, C4'), 130.50 (d, J= 9.2 Hz, C3'+C5'), 128.24 (C1'), 115.87 (d, J= 21.9 Hz, C2'+C6')	163.16
2.6p	H	OMe	3',5'-*t*Bu, 4'-OH	21.85	161.55 (C10a), 156.02 (C2), 147.62 (C9), 139.33 (C9a), 124.24 (C7), 120.64 (C6), 120.42 (C5a), 110.64 (C8), 95.45 (C4a), 55.59 (C9-OMe)	157.63 (C4'), 138.68 (C3'+C5'), 124.79 (C2'+C6'), 122.60 (C1'), 34.73 (C(CH3)3), 30.20 and 30.13 (CH3)	163.71
2.6s	OMe	H	2'-OMe	22.20	161.81 (C10a), 155.99 (C2), 154.70 (C7), 120.47 (C5a), 117.50 (C9), 113.83 (C6+C8), 96.33 (C4a), 55.92 (C7-OMe)	157.27 (C2'), 133.01 (C4'), 130.39 (C6'), 121.01 (C1'), 120.66 (C5), 112.11 (C3')	162.61
2.6t	OMe	H	3'-OMe	22.18	161.66 (C10a), 155.90 (C7), 154.98 (C2), 143.78 (C10), 120.35 (C5a), 118.28 (C8), 117.44 (C9), 113.73 (C6), 96.39 (C4a), 55.38 (C7-OMe)	159.37 (C3'), 132.93 (C1'), 129.84 (C5'), 119.99 (C6'), 113.73 (C4'), 112.77 (C2'), 55.43 (C3'-OMe)	163.61
2.6u	OMe	H	2'-OMe, 5'-OMe	22.19	161.70 (C10a), 155.97 (C7), 154.30 (C2), 143.79 (C9a), 120.42 (C5a), 117.48 (C9), 113.81 (C8), 113.80 (C6), 96.43 (C4a), 55.50 (C7-OMe)	152.98 (C2'), 151.45 (C5'), 121.17 (C1'), 118.66 (C3'), 114.67 (C4'), 113.52 (C6'), 56.33 (C5'-OMe), 55.71 (C2'-OMe)	162.48
2.6v	OMe	H	3'-Cl	22.16	161.74 (C10a), 155.95 (C7), 143.73 (C9a), 120.30 (C5a), 117.45 (C9), 113.80 (C6), 113.77 (C8), 96.78 (C4a), 55.46 (C7-OMe), C2 not seen	133.53 (C3'), 131.57 (C4'), 130.64 (C5'), 127.42 (C2'), 126.32 (C6'), C1' not seen	Not seen
2.6x	H	H	H	21.75	161.62 (C10a), 155.43 (C2), 149.98 (C9a), 129.62 (C6), 128.06 (C8), 124.59 (C7), 119.57 (C5), 116.58 (C9), 96.97 (C4a)	131.68 (C4'), 131.66 (C1'), 128.72 (C3'+C5'), 127.68 (C2'+C6')	163.63

2.6y	H	H	3',5'-*t*Bu, 4-OH	21.74	161.65 (C10a), 156.16 (C2), 150.09 (C9a), 129.59 (C6), 128.00 (C8), 124.48 (C7), 119.70 (C5a), 116.59 (C9), 95.62 (C4a)	157.67 (C4'), 138.86 (C3'+C5'), 124.81 (C2'+C6'), 122.49 (C1'), 34.74 (C3'-*t*Bu or C5'-*t*Bu), 30.13 (C3'-*t*Bu or C5'-*t*Bu)	163.77
2.6z	H	Me	H	21.60	162.27 (C10a), 161.58 (C2), 148.14 (C9a), 128.86 (C8), 126.55 (C6), 125.01 (C9), 123.56 (C7), 118.99 (C5a), 96.59 (C4a), 15.04 (Me)	155.29 (C1'), 131.31 (C4'), 128.19 (C3'+C5'), 127.32 (C2'+C6')	163.19
2.6a'	H	Me	2'-Cl	22.11	161.78 (C10a), 155.55 (C2), 148.36 (C9a), 129.76 (C8), 127.45 (C6), 125.77 (C9), 124.63 (C7), 119.31 (C5a), 98.26 (C4a), 15.88 (Me)	132.85 (C2'), 132.45 (C4'), 131.54 (C1'), 131.02 (C3'), 130.04 (C6'), 127.72 (C5')	163.32
2.6b'	Me	H	H	21.74	161.65 (C10a), 155.24 (C2), 147.84 (C9a), 129.72 (C6), 128.48 (C8), 119.09 (C7), 117.43 (C5a), 116.31 (C9), 96.81 (C4a), 20.21 (Me)	133.61 (C1'), 131.90 (C4'), 128.69 (C3'+C5'), 127.64 (C2'+C6')	163.64
2.6c'	Me	H	2'-OMe, 5'-OMe	21.73	161.56 (C10a), 154.26 (C2), 147.80 (C9a), 133.61 (C7), 129.72 (C8), 128.47 (C6), 119.09 (C5a), 116.28 (C9), 96.92 (C4a), 20.21 (Me)	152.91 (C2'), 151.37 (C5'), 121.14 (C1'), 118.56 (C4'), 114.62 (C6'), 113.42 (C3'), 56.26 (C5'-OMe), 55.64 (C2'-OMe)	162.37
2.6d'	Br	H	H	21.62	161.43 (C10a), 155.60 (C2), 149.32 (C9a), 132.02 (C6), 130.79 (C8), 122.42 (C5a), 118.78 (C9), 116.07 (C7), 96.71 (C4a),	132.02 (C4'), 128.72 (C3'+C5'), 127.68 (C2'+C6')	163.54
2.6e'	Br	H	2'-OMe	21.63	161.26 (C10a),154.89 (C2), 149.28 (C9a), 132.03 (C6), 130.76 (C8), 122.45 (C5a), 118.75 (C9), 116.06 (C7), 99.69 (C4a)	157.16 (C2'), 132.96 (C4'), 130.71 (C6'), 120.90 (C1'), 120.55 (C5'), 112.03 (C3'), 55.86 (OMe)	162.33
2.6f'	Br	H	3',4'-OMe	21.31	161.14 (C10a), 154.84 (C2), 149.22 (C9a), 131.55 (C6), 130.33 (C8), 122.25 (C5a), 118.32 (C9), 115.59 (C7), 95.32 (C4a),	152.04 (C4'), 148.61 (C3'), 123.59 (C1'), 121.16 (C6'), 111.63 (C2'), 111.03 (C5'), 55.66 (C4'-OMe), 55.56 (C3'-OMe)	163.06

2.6g'	Br	H	2',5'-OMe,	21.76	161.40 (C10a), 154.65 (C2), 149.39 (C9a), 132.17 (C6), 130.99 (C8), 122.51 (C5a), 118.96 (C9), 116.30 (C7), 96.99 (C4a), 21.76 (C5)	153.09 (C5'), 151.59 (C2'), 120.99 (C1'), 118.96 (C4'), 114.75 (C6'), 113.67 (C3'), 56.46 (C2'-OMe), 55.83 (C5'-OMe)	162.51
2.6i'	Cl	H	2'-OMe	21.79	162.46 (C10a), 154.97 (C2), 148.88 (C9a), 129.20 (C6), 128.21 (C7), 127.98 (C8), 122.03 (C5a), 118.47 (C9), 96.69 (C4a), 55.95 (OMe)	157.28 (C2'), 133.11 (C4'), 130.40 (C6'), 120.89 (C1'), 120.67 (C5'), 112.13 (C3')	161.41
2.6j'	Cl	H	3'-OMe	21.48	161.69 (C10a), 148.70 (C9a), 128.72 (C6), 127.90 (C7), 127.53 (C8), 121.72 (C5a), 118.03 (C9), 96.33 (C4a), 55.19 (OMe)	159.24 (C3'), 132.82 (C1'), 129.45 (C5'), 119.78 (C6'), 117.97 (C4'), 112.28 (C2'), 55.43 (C3'-OMe)	Not seen
2.6k'	Cl	H	2',5'-OMe,	21.74	161.25 (C10a), 154.52 (C2), 148.80 (C9a), 129.13 (C6), 128.13 (C7), 127.89 (C8), 121.95 (C5a), 113.47 (C9), 96.74 (C4a), 21.74 (C5)	152.93 (C5'), 151.40 (C2'), 121.05 (C1'), 118.68 (C3'), 118.40 (C6'), 114.63 (C4'), 56.28 (C5'-OMe), 55.67 (C2'-OMe)	Not seen

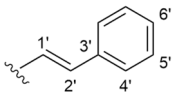
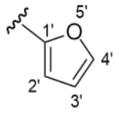
Table 16: ^{1}H NMR (400 MHz, DMSO-d$_6$, δ ppm) spectroscopic data obtained for 2-aryl-3*H*-chromeno[2,3-*d*]pyrimidin-4(5*H*)-ones **2.6q, 2.6r** and **2.6h'**



Comp.	R^1	R^2	R^3	H5	Ar(H6-9)	H1'-7'	NH
2.6q	H	OMe		3.69 (s, 2H)	7.05 (t, *J*= 8.0 Hz, 1H, H7), 6.94 (dd, J_1= 8.8 Hz, J_2= 0.8 Hz, 1H, H8), 6.82 (dd, J_1= 7.6 Hz, J_2= 1.2 Hz 1H, H6), 3.83 (s, 3H, OMe)	7.91 (d, *J*= 16.0 Hz, 1H, H2'), 7.64 (dd, J_1= 8.4 Hz, J_2= 1.6 Hz, 2H, H4'+ H8'), 7.48-7.42 (m, 3H, H5' + H 6' + H 7'), 6.82 (d, *J*= 16.0 Hz, 1H, H1')	12.55 (s, 1H)
2.6r	H	OMe		3.69 (s, 2H)	7.05 (t, *J*= 8.0 Hz, 1H, H7), 6.95 (dd, J_1= 8.4 Hz, J_2= 1.2 Hz, 8.8 Hz, 1H, H8), 6.83 (d, *J*= 7.6 Hz, 1H, H6), 3.83 (s, 3H, OMe)	7.99 (d, 1H, *J*=1.2 Hz, H4'), 7.56 (d, 1H, *J*= 3.6 Hz, H3'), 6.74 (d, *J*= 31.6 Hz, 1H, H4')	12.35 (s, 1H)

2.6h'	Br	H	3.72 (s, 2H)	7.49 (dd, J_1= 3.2 Hz, $J2$= 0.8 Hz, 1H H6), 7.40 (dd, J_1= 8.8 Hz, J_2= 0.8 Hz, 1H, H8), 7.06 (d, J= 8.4 Hz, 1H, H9)	7.74 (dd, J_1= 8.0 Hz, J_2= 1.6 Hz, 1H, H2'), 7.63 (d, J= 1.6 Hz, 1H, H6'), 7.00 (d, J= 8.4 Hz, 1H, H3'), 6.13 (s, 2H, H7')	12.66 (s, 1H)

Table 17: ^{13}C NMR spectroscopic data (400 MHz, DMSO-d$_6$, δ ppm) obtained for 2-aryl-3*H*-chromeno[2,3-*d*]pyrimidin-4(5*H*)-ones **2.6q, 2.6r** and **2.6h'**

Comp.	R^1	R^2	R^3	C5	C2-10a	C1'-7'	$CONH_2$
2.6q	H	OMe		21.96	161.54 (C10a), 154.13 (C2), 147.68 (C9), 139.33 (C9a), 124.32 (C7), 120.65 (C6), 120.34 (C5a), 110.78 (C8), 96.42 (C4a), 55.72 (OMe)	139.60 (C2'), 134.62 (C3'), 130.14 (C5' + C7'), 129.12 (C6'), 127.84 (C4' + C8'), 119.41 (C1')	162.91
2.6r	H	OMe		21.89	163.15 (C10a), 159.87 (C2), 147.65 (C9), 139.26 (C9a), 124.33 (C7), 120.63 (C6), 120.30 (C5a), 110.81 (C8), 96.54 (C4a), 55.72 (OMe)	146.90 (C4'), 145.74 (C1'), 115.20 (C2'), 112.76 (C3'),	161.46
2.6h'	Br	H		21.27	161.22 (C10a), 154.97 (C2), 149.23 (C9a), 131.48 (C6), 130.33 (C8), 122.21 (C5a), 118.28 (C9), 115.62 (C7), 95.49 (C4a)	150.18 (C4'), 147.46 (C5'), 125.43 (C1'), 122.71 (C2'), 107.85 (C3'), 107.07 (C6'), 101.48 (C7')	163.11

1D Nuclear Overhauser effect (NOE) experiments with compound **2.6x** were carried out to elucidate the two plausible tautomeric forms of the compounds **2.6** in DMSO-d_6, thus amide *vs* phenol forms. Positive cross peaks (with different sign to the inverted signal) were observed, as expected for a small molecule tumbling rapidly in solution (**Figure 18**). It was found that the inversion of the signal at δ12.82 ppm enhanced H2' and H6' signals (24%). These results clearly show that: (i) fast rotation of the aryl substituent around the C2-C1´ bond is taking place in solution; and (ii) the proton studied is located close to the C2-C1´ bond, which is only compatible with the amide tautomeric form.

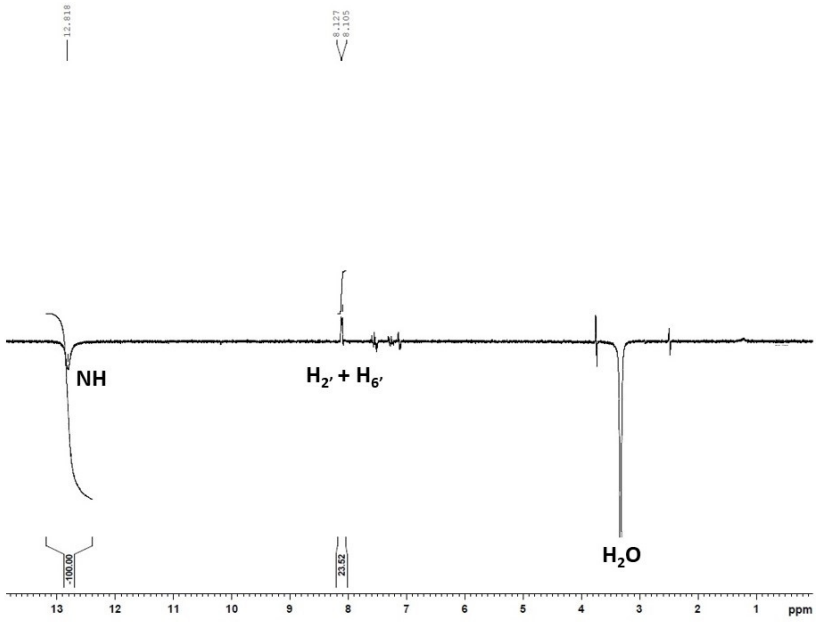


Figure 18: 1D transient NOE (400 MHz, DMSO-d_6) spectrum obtained after inversion of the signal δ12.82 ppm in compound **2.6x** (R^1=R^2=R^3=H)

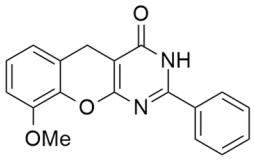
Water-soluble salt formation

In order to prepare water soluble forms of chromene-base pyrimidinones **2.6**, the removal of the NH proton in compounds **2.6a** and **2.6x** were studied by using NaOH (3 M) under the experimental conditions described in **Table 18**.

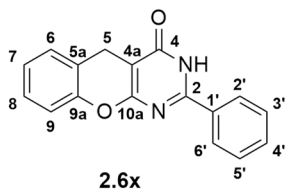
The treatment of pyrimidinone **2.6a** with 1 equivalent of NaOH (3 M) in ethanol at room temperature for 30 min. converted the initial white suspension into orange (entry 1, **Table 18**). The resulting light orange precipitate was collected, and the formation of the sodium salt was confirmed by spectroscopic data (η= 11%, isolated yield). For compound **2.6x**, two simultaneous

experiments (entries 2 and 3 - **Table 18**) were performed. For both experiments, 1 equivalent of NaOH (3 M) was employed, while stirring at room temperature in DMSO.

Table 18: Experimental conditions for the preparation of water-soluble sodium salts of **2.6a** and **2.6x**



2.6a



2.6x

Entry	compound	Experimental conditions	precipitation solvent	observations	η (sodium salt of 2.6)
1	**2.6a**	EtOH/ NaOH (1 equiv., 3 M), r.t., 19h	EtOH	orange suspension	11%
2	**2.6x**	DMSO/ NaOH (1 equiv., 3 M), r.t., 19h	-	orange suspension	83%
3	**2.6x**	DMSO/ NaOH (1 equiv., 3 M), r.t., 19h	MeOH	orange suspension	35%

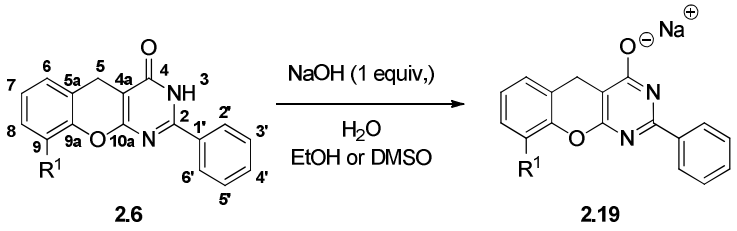
In both entries 2 and 3 (**Table 18**), the white suspension turned orange after the addition of NaOH. After 5 min., the orange colour of the solid gradually evolved to yellow. After 30 min. of stirring at room temperature, MeOH was added to the reaction (entry 3), while no solvent was added to the suspension in entry 2 and both samples were kept at -9°C overnight. Both samples in entries 2 and 3 generated a yellow and a brown suspension, respectively. The solid products were filtered and washed with cold MeOH and H_2O, respectively. A second crop of the same product was collected by addition of diethyl ether to the filtrate from entry 2, resulting in a total yield of the salt of 83%.

The IR spectra of the resulting salts revealed that no significant differences between the neutral and deprotonated forms of compound **2.6a**. It was theorized that the removal of the NH proton of the pyrimidinone ring would lead to a negatively charged nitrogen, generating a tautomeric equilibrium with the vicinal carbonyl moiety, delocalizing the electron pair throughout the amide bond, and that this phenomenon should lead to a shift in the carbonyl signal in IR spectroscopy, but this fact could not be verified. By ^{1}H NMR spectroscopy, the disappearance of the NH signal (δ12.82 ppm), as well as a shift of the methylene signal, at C5, from δ 3.73 ppm to δ 3.58 ppm was considered indicative of the formation of the salt. There was also a significant

shift in several ^{13}C signals: C2 shifted from δ155.37 ppm to δ160.46; C4 shifted from δ 163.72 ppm to δ 174.50 ppm; C4a shifted from δ96.83 ppm to δ92.95 ppm; and C10a shifted from δ161.61 to δ162.44 (**Table 19**).

For the reactions involving compound **2.6x**, the products obtained for entries 2 and 3 were characterized by IR and NMR spectroscopy, showing a similar pattern: C2 NMR signal shifted from δ155.43 ppm to δ159.62; C4 NMR signal shifted from δ 163.63 ppm to δ 172.68 ppm; C4a NMR signal shifted from δ96.97 ppm to δ93.91 ppm; and C10a NMR signal shifted from δ161.62 to δ162.39 ppm. From these results, it was concluded that the corresponding anion **2.19** could be formed, under the basic conditions used (**Table 19**). This could explain the deshielding effect on the *ipso* and *meta* positions, and the shielding effect on the *ortho* and *para* positions of the newly formed enolate group.

Table 19: Selection of ^{13}C NMR (100 MHz, DMSO-d_6, δ ppm) chemical shifts obtained for **2.6a** (R^1=OMe) and **2.6x** (R^1=H) vs **2.19a** and **2.19x**, respectively



2.6 **2.19**

Compound	C2	C4	C4a	C10a
2.6a	155.37	163.72*	96.83	161.61*
2.19a	160.46	174.50	92.95	162.44
2.6x	155.43	163.63*	96.97	161.62*
2.19x	159.62	172.68	93.91	162.39

*Interchangeable

Although requiring more studies, which include further adjustments in the experimental conditions, these results point out that it is possible to develop a generic protocol to prepare the sodium pyrimidinolate salts **2.19** from the respective pyridiminone **2.6** in good to high yields. Also, the results are pointing out that a DMSO/H_2O or DMSO/MeOH system for salting out is less adequate than the DMSO/Et_2O mixture, probably because of the increased solubility that is obtained with the salt form.

2.1.2 Synthesis and reactivity of 2-imino-2*H*-chromen-3-amines and 2-oxo-2*H*-chromen-3-amines

The 2-imino-2*H*-chromen-3-amine and 2-oxo-2*H*-chromen-3-amine moiety has been extensively studied, mainly due to their biological importance observed in diverse chromene products[8–14], as well as in synthetic ones, such as anticancer[15–18], anti-inflammatory[19], antituberculosis[20–22], antiviral[23–26], cannabinoid receptor agonist[27] or antiprotozoarian activity[28], among many others.

As previously demonstrated, the benzopyran ring has proven to be a very interesting building block for the synthesis of new bioactive compounds, with a series of diversified biological activities and several coumarin-based compounds used in clinical practice. Among the chromene family, the coumarin ring has attracted particular interest. A review article[29] resumed the most relevant existing synthetic methods for preparing coumarins and noted their wide distribution in plants for various functions. In 1994, a review[30] covering all literature articles about natural coumarins between 1988 and 1994 reported a series of extraction methods for coumarins from their natural products and a few synthetic pathways as well.

In the last decades, several articles summarizing the most relevant approaches for the synthesis of coumarins have been reported[5,31,40–49,32,50,33–39], in which appeared as the main building block for several new biologically active compounds[49,51,52], including anticancer[48,53,62,54–61], antibacterial[21,63–69], antioxidant[70–74] and others[75–77]. There was an increasing scientific interest towards novobiocin, coumermycin A1 and clorobiocin (**Figure 19**). These compounds were obtained from their natural sources and proved to be effective as antimicrobial agents against several infectious sources, in particular novobiocin[78,79]. Their activity was associated with the capacity to inhibit the B subunit of the DNA Gyrase[80]. Since its identification and clinical approval, DNA Gyrase inhibitors based on the aminocoumarin scaffold have been extensively studied, to better understand the interaction with HSP90 and other molecular targets[56,81] or to develop new novobiocin-based HSP90 inhibitors[53,82,83], as well as for the development of novel anticancer agents against several cancer cell lines[54,84,93,85–92].

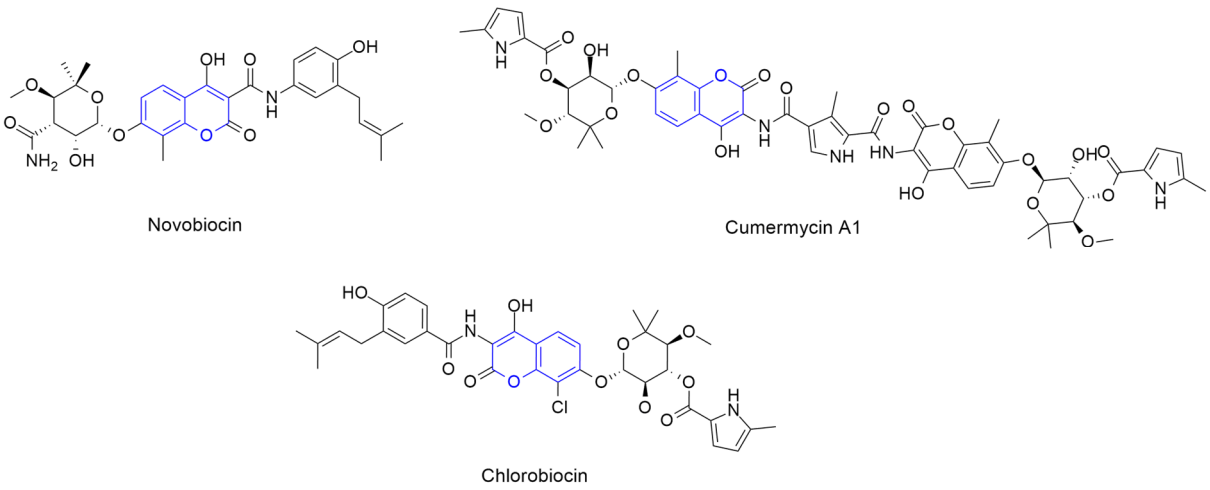
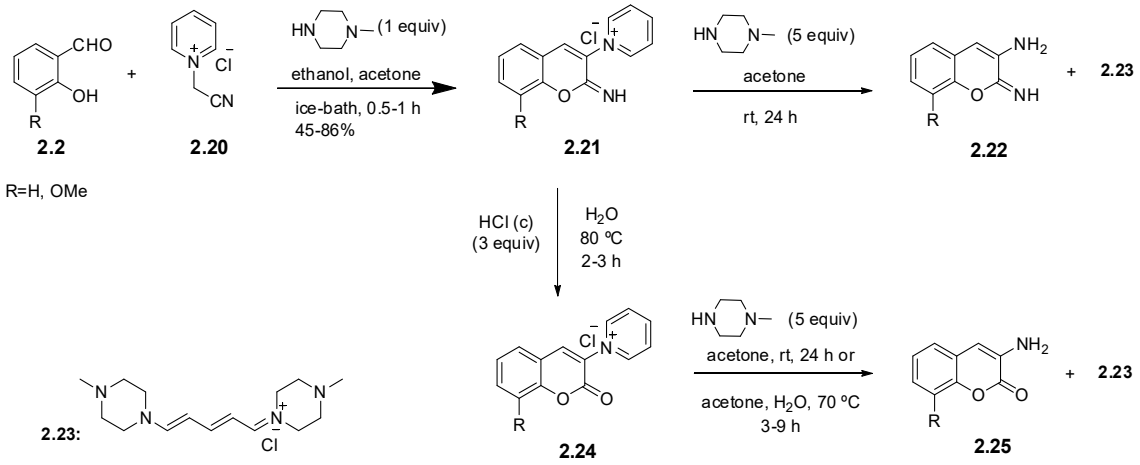


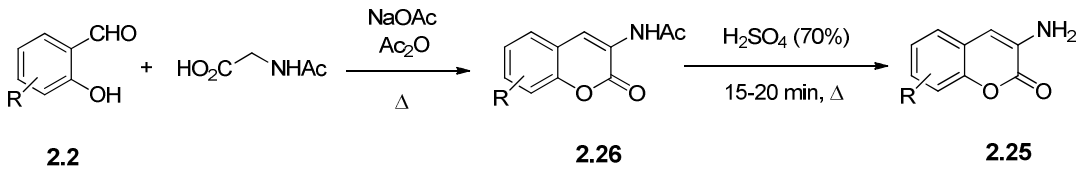
Figure 19: Chemical structures of novobiocin, coumermycin A1 and clorobiocin

There are only a few methods available for preparing the 3-aminocoumarin scaffold. The first reported method was attributed to Linch[94], and since then there have been several attempts to improve this synthetic process[83,84,88,92,93,95–97]. In 2014, Costa *et al*[41] reported a new protocol involving 1-(imino-2*H*-chromen-3-yl)pyridine-1-ium chlorides **2.21** (**Scheme 19**) as the key intermediate. This compound is obtained by the reaction of an appropriate salicylaldehyde with the prepared 1-(-cyanomethyl)pyridinium chloride **2.20**. Moreover, compound **2.21** is transformed into 2-imino-3-aminochromenes **2.22** by pyridine ring-opening by treatment at room temperature with 5 equivalents of *N*-methylpiperazine. A similar approach is employed for the synthesis of 3-amino-2-oxocoumarins **2.25**, but in this case, it is first required the hydrolysis of the imino group in compound **2.21** to give the coumarin **2.24**.



Scheme 19: Synthesis of 3-aminochromenes **2.22** and **2.25**, as proposed by Costa et al [adapted from ref. 41]

Also in 2014, Das *et al*[43] reported the two-step synthesis of the 3-aminocoumarins **2.25** from salicylaldehydes **2.2** and *N*-acetylglycine (**Scheme 20**). This involves the formation of the 3-amidocoumarins **2.26**, followed by hydrolysis via treatment with H_2SO_4 (70%) (**Scheme 20**).



2.2 **2.26** **2.25**

Scheme 20: Synthesis of 3-aminocoumarins **2.25** from *N*-acetylglicine and salicylaldehydes **2.2**, as proposed by Das et al [adapted from ref.43]

In this work, the goal was to prepare new compounds based on 2-imino-3-aminochromenes **2.22** and 3-aminocoumarins **2.25**, in a continuation of the previous exploratory work performed in our research group and following the methodology also developed in the group[41]. In the article, the authors explore the reactivity of compounds **2.22** and **2.25** with a group of electrophiles, to unravel new compounds via a simple and efficient synthetic methodology. The 2-imino-3-aminochromenes **2.22** and 3-aminocoumarins **2.25** were prepared via the methodology previously unravelled by our research group[41]. It starts with the preparation of pyridinium salts **2.20** by refluxing 2-chloroacetonitrile and pyridine, which precipitate during the reaction and was isolated by simple filtration as a light-brown solid after 10-15 min (**Scheme 20**). Then, the treatment of the pyridinium salts **2.20** with diverse salicylaldehydes **2.2** afforded 1-(2-imino-2*H*-chromen-3-yl)pyridin-1-ium chlorides **2.21**. From this point, compounds **2.21** can either react with *N*-methylpiperazine to afford the appropriate 2-imino-3-aminochromene **2.22** or be converted into 1-(2-oxo-2*H*-chromen-3-yl)pyridin-1-ium chlorides **2.24** by acid-catalyzed hydrolysis and subsequent treatment with *N*-methylpiperazine to afford the oxo counterpart **2.25**. For the presented study, only compounds **2.22a** and **2.25a** were synthesized (**Figure 20**). This choice was related not only to the presence of the methoxy group, that possesses a characteristic ^{1}H NMR singlet that can aid in the identification of the number of chromeno units present in the isolated products or mixtures, but also to the fact that both compounds were already fully characterized.



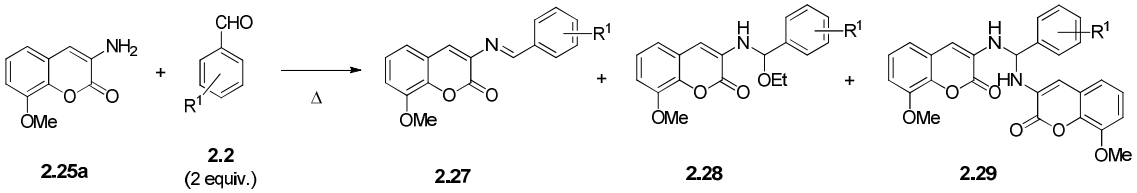
2.22a **2.25a**

Figure 20: Chemical structure of the synthesized compounds **2.22a** and **2.25a**

Synthesis of 3-(aryldeneamino)-2*H*-chromen-2-ones and 3-(alkylideneamino)-2*H*-chromen-2-ones

It was proposed that the amino group of both compounds **2.22a** and **2.25a** (**Figure 20**) could react as nucleophiles and thus be involved in nucleophilic additions with electrophiles such as aldehydes. It was theoretically proposed that, due to the presence of the 2-oxo moiety, compounds **2.25** would only react with one equivalent of aldehyde, with less probability of generating side products. For this reason, and to explore this reactivity, a series of reactions were performed involving only compound **2.25a**. The reactions were performed in ethanol, in a closed vial, under reflux conditions (**Table 20**).

Table 20: Reaction conditions and results obtained for the reaction of **2.25a** with aldehydes **2.2**, in ethanol under reflux



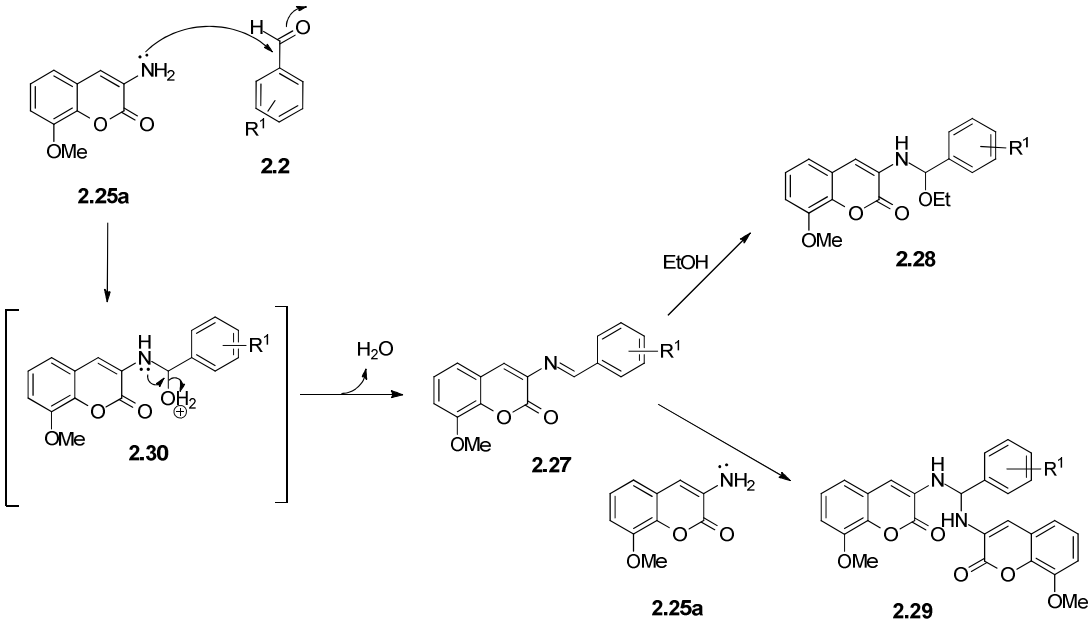
2.25a **2.2** (2 equiv.) **2.27** **2.28** **2.29**

Entry	R^1	t (h)	results		η (%)
			product	ratio	
1	2-OMe	2	**2.27**		30
2	2,4-OH,3-Me	5	**2.2a**/**2.25a**/**2.27**[1]	3.5/2.3/1	-
3	2,3,4,5,6-F	4	**2.28**		51
4	4-Br	1	**2.29**		13
5	4-CF_3	8	**2.25a**/**2.2b**[1]	1/1	-

[1] by ^{1}H NMR

The heating under reflux of a solution of coumarin **2.25a** in ethanol with aldehydes **2.2** provided three distinct reaction products (entries 1,3 and 4 - **Table 20**): compounds **2.27**, **2.28** and **2.29**. When using 2-methoxybenzaldehyde, the expected imine derivative **2.27** was obtained with a 30% yield. On the contrary, when more electrophilic aldehydes were employed, such as 4-bromobenzaldehyde and pentafluorobenzaldehyde, further nucleophilic addition reactions in the imine moiety were observed, which would be promoted by the inductive effect of the electron-withdrawing substituents of the phenyl ring (**Scheme 21**). Thus, by using 4-bromobenzaldehyde, compound **2.29** was isolated in a poor yield, which would result from the nucleophilic attack of

the remaining starting material. By using pentafluorobenzaldehyde, only compound **2.28** could be isolated as a pure product. The formation of the latter could be explained by nucleophilic attack of the solvent over the imine group.



Scheme 21: Proposed mechanism for the formation of compounds **2.27-2.29**

Compounds **2.27** can be easily identified by ^{1}H NMR spectroscopy by a singlet at around δ9.20 ppm corresponding to the imino moiety (**Figure 21**). The structure of compound **2.28** was supported by the presence of two correlated doublets at δ6.66 ppm and δ6.08 ppm (J= 8.0 Hz), corresponding to the NH and the CH groups, respectively (**Figure 23**). Compounds **2.29** possess a very distinctive triplet signal at about δ6.15 ppm (J= 8.8 Hz), attributed to the methylidene group, as well as the doublet (J= 8.8 Hz), integrating for two protons, which correspond to the two NH groups (**Figure 25**). However, during the collection of the ^{13}C and correlation NMR spectra in DMSO-d_6, the sample evolved to regenerate the starting material **2.25a** (**Figure 26**).

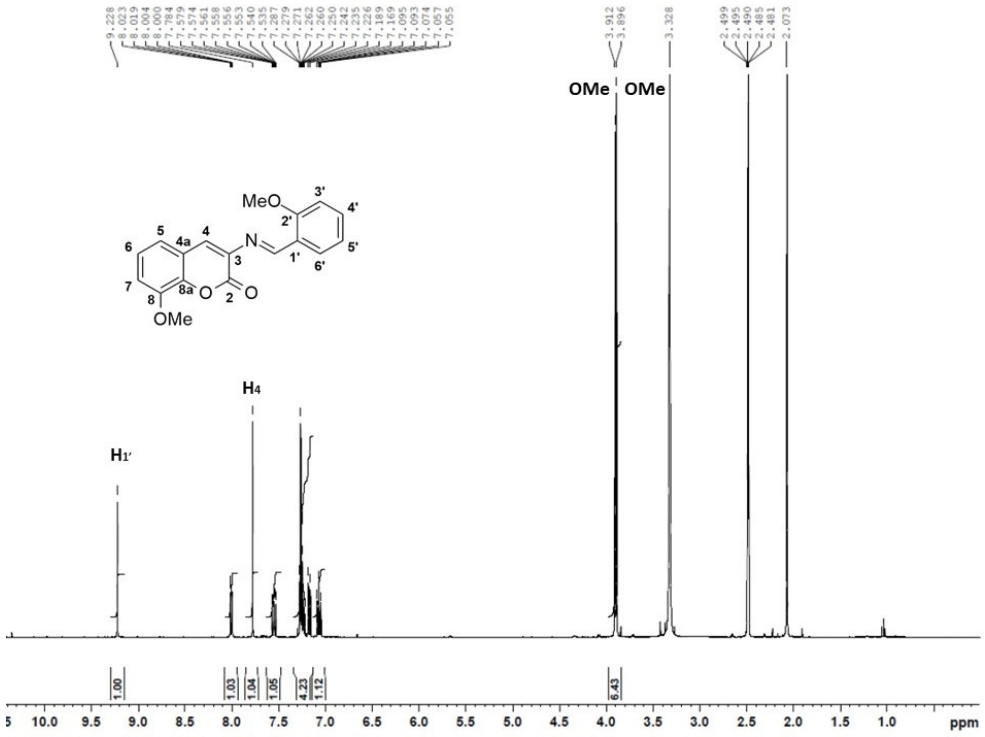


Figure 21: ^{1}H NMR (400 MHz, DMSO-d$_6$, δ ppm) spectrum of compound **2.27** in which some signals are highlighted

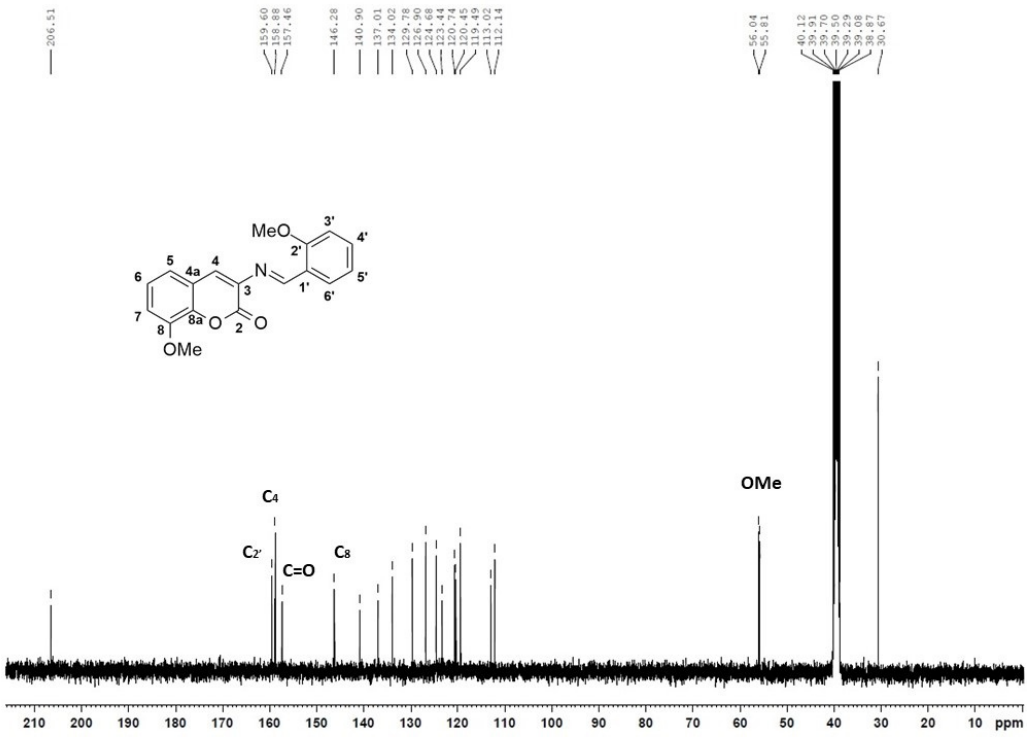


Figure 22: ^{13}C NMR (100 MHz, DMSO-d$_6$, δ ppm) spectrum of compound **2.27**, in which some signals are highlighted

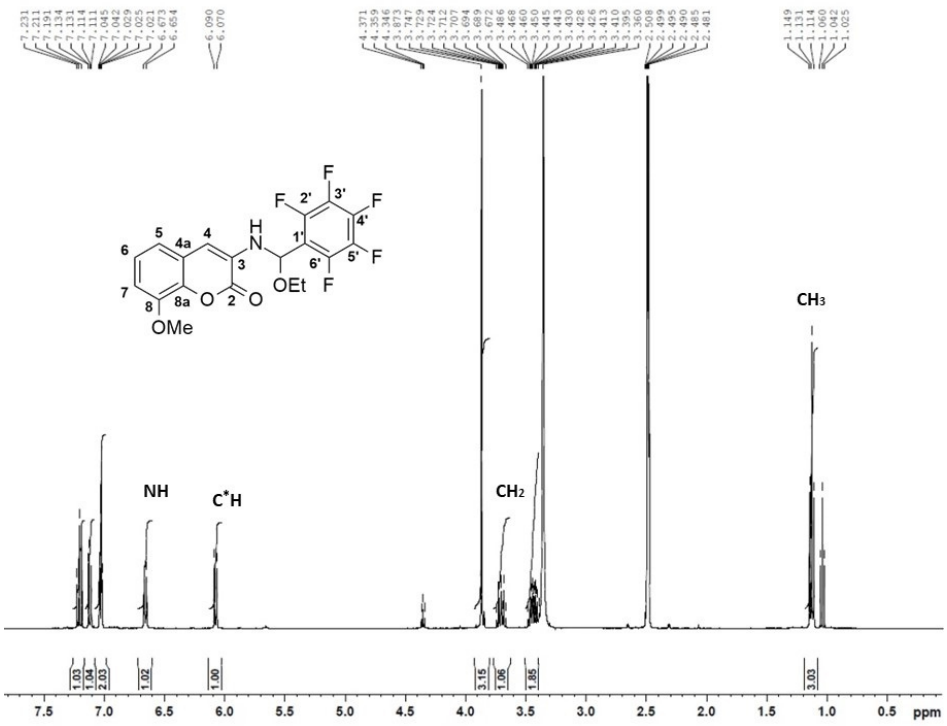


Figure 23: ^{1}H NMR spectrum (400 MHz DMSO-d$_6$, δ ppm) of compound **2.28** in which some signals highlighted

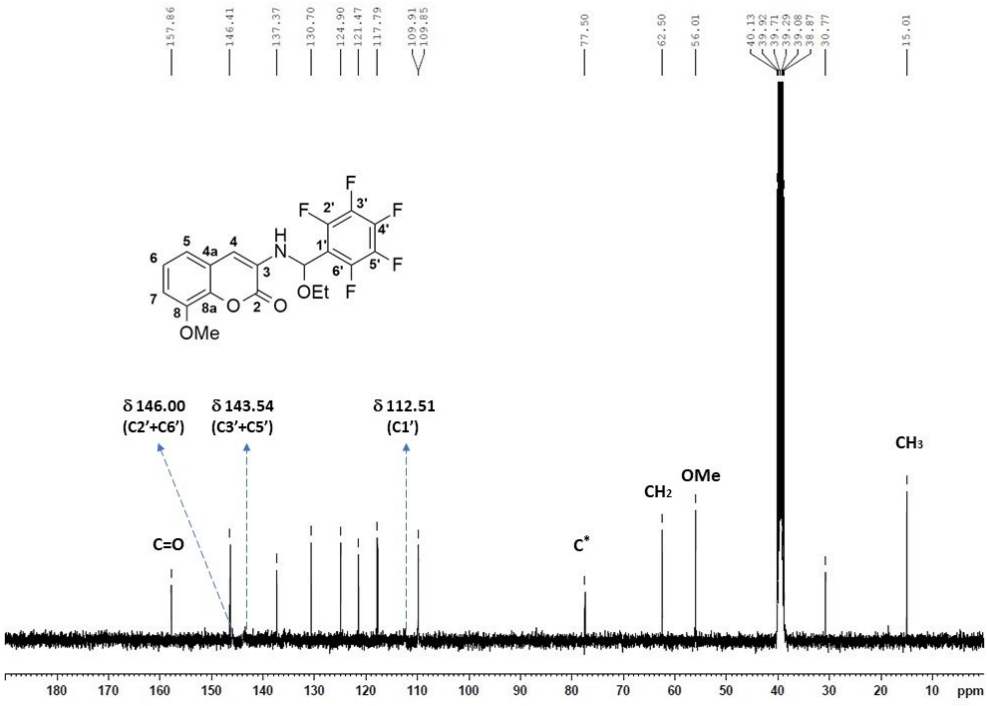


Figure 24: ^{13}C NMR spectrum (100 MHz, DMSO-d$_6$, δ ppm) of compound **2.28** in which some signals highlighted

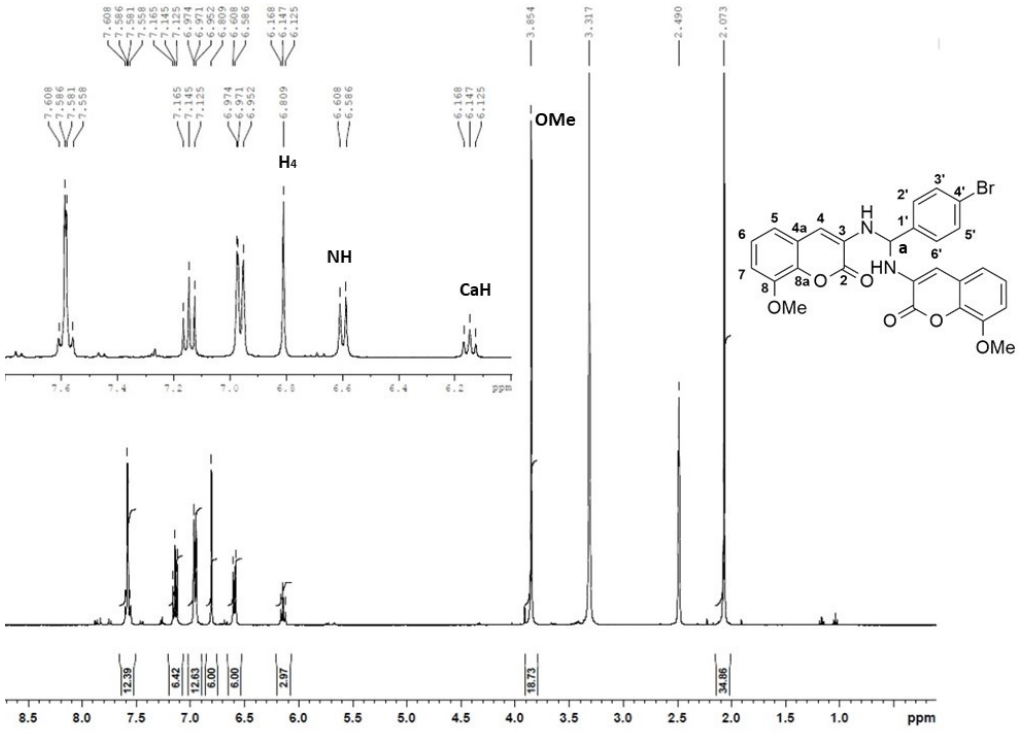


Figure 25: ^{1}H NMR spectrum (400 MHz, DMSO-d$_6$, δ ppm) of compound **2.29** in which some signals are highlighted

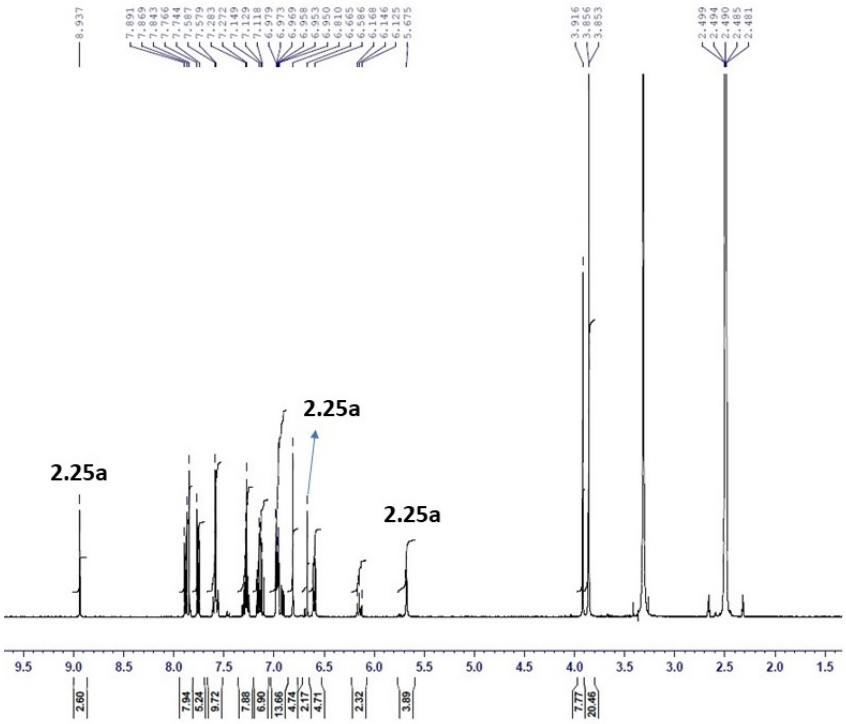


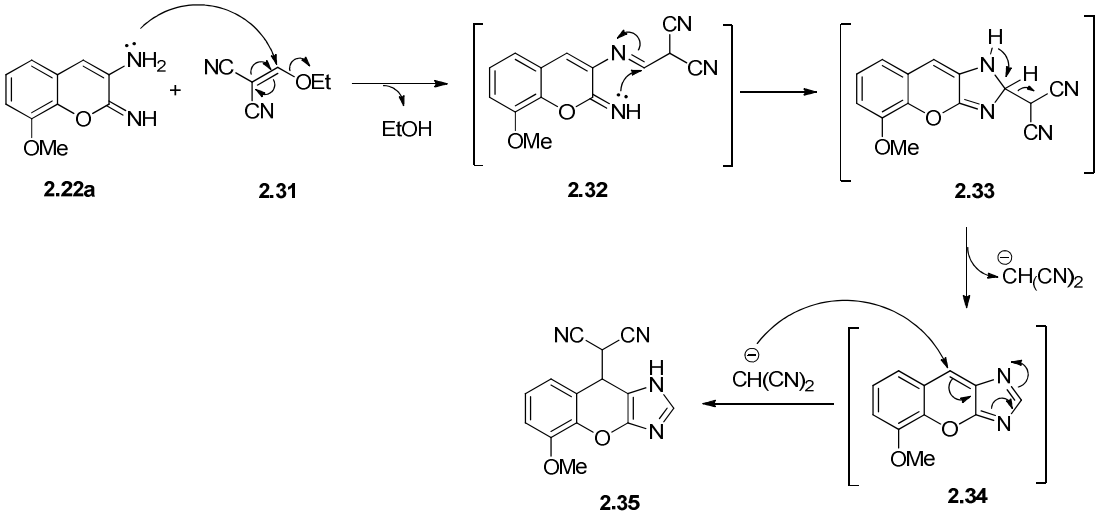
Figure 26: ^{1}H NMR spectrum (400 MHz, DMSO-d$_6$, δ ppm) of a freshly prepared sample of compound **2.29** in DMSO-d$_6$, taken after obtaining ^{13}C NMR and bidimensional correlation spectra, where compound **2.25a** can be identified

Although the selected approach afforded a simple and efficient method for developing the desired compound **2.27** it is possible that, with appropriate conditions, the formation of **2.28** and **2.29** can also be prepared with broader extent. These studies were abandoned due to the relative instability of compounds in solution, namely DMSO-d_6. In fact, there was a clear evolution in DMSO-d_6 in a period of just a few days, which was recurrent in several of the obtained compounds. As the main objective of the synthesis of new coumarin derivatives was to assess their biological activity, and the samples for such assays are prepared in a small amount of DMSO, the low stability of these discourages further work on the reaction with aldehydes.

Synthesis of 2-(5-methoxy-1,9-dihydrochromeno[2,3-*d*]imidazol-9-yl)malononitrile

The reactivity of the 2-imino-3-aminochromenes was further investigated with the reaction of compound **2.22a** and (ethoxymethylene)malononitrile (**2.31**) (**Scheme 22**). It was hypothesized that once the Michael addition have taken place and therefore the imine **2.32** was formed, the amino group in **2.32** would undergo an intramolecular nucleophilic addition to the imidate moiety with the subsequent elimination of malononitrile. To test this hypothesis, 1 molar equivalent of (ethoxymethylene)malononitrile (**2.32**) was added to a suspension of compound **2.22a** in acetonitrile, at room temperature and stirred for 5 days. Under these conditions, the product isolated was identified as compound **2.35** (η= 31%). The formation of this product can be explained via 1,4-nucleophilic addition to **2.31** with elimination of ethanol, to afford the imine intermediate **2.32** (**Scheme 22**). Intramolecular cyclization of **2.32** with concomitant elimination of malononitrile would afford intermediate **2.34**. Finally, nucleophilic attack of the released malononitrile anion would lead to the isolated product, identified as **2.35**.

The ^{1}H NMR spectra of compound **2.35** presented a very distinctive set of signals (**Figure 27**). In particular, a singlet at δ12.07 ppm, which was attributed to the NH group, and another at δ7.53 ppm, corresponding to the C-H group of the imidazole ring (**Figure 27**). Also remarkable are two doublets at δ5.25 ppm and δ5.20 ppm (J= 2.8 Hz), each integrating for one hydrogen, corresponding to the other methylene groups (H1 and H1´hydrogens) in **2.35**. In the ^{13}C NMR spectra of **2.35** highlighted the two peaks at δ 117.85 and δ 118.05 ppm corresponding to the nitrile groups linked to C1' (**Figure 28**). The signals for C1 and C1' carbons were assigned to δ36.90 and δ31.92 ppm, respectively. The signal corresponding to C9 appears at δ 132.93 ppm.



Scheme 22: Proposed mechanism for the formation of compound **2.35**

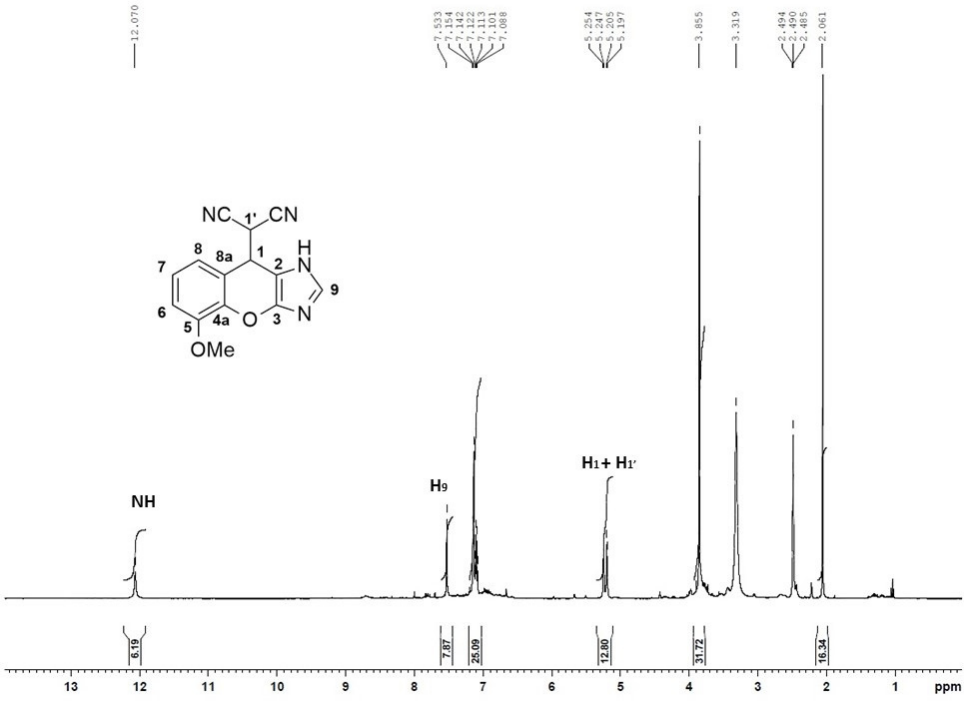


Figure 27: ^{1}H NMR (400 MHz, DMSO-d_6, δ ppm) spectrum of compound **2.35** with three signals highlighted

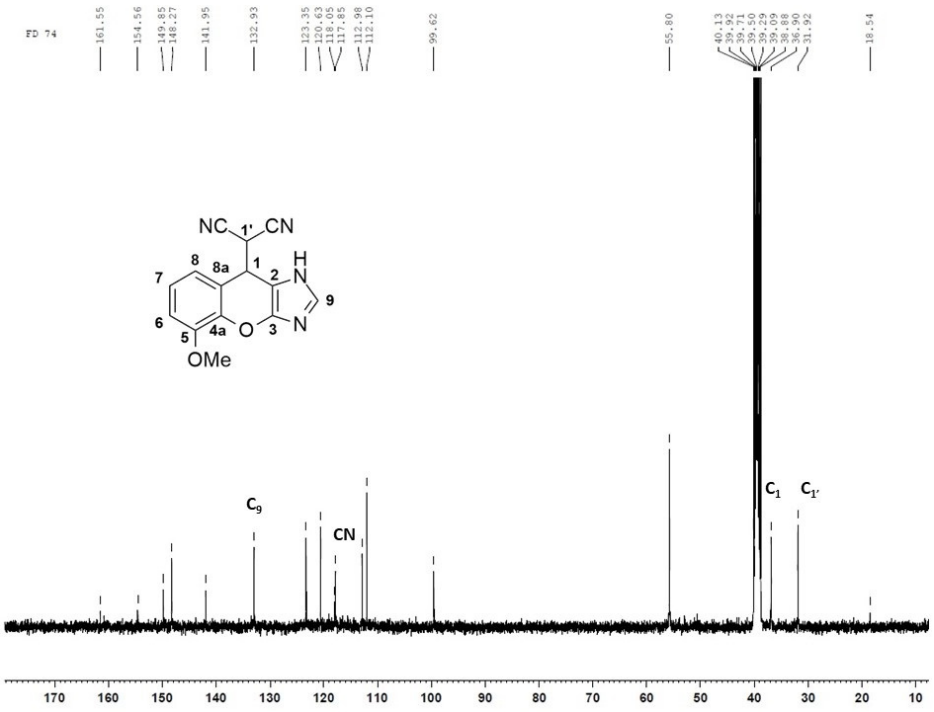


Figure 28: ^{13}C NMR (100 MHz, DMSO-d_6, δ ppm) spectrum of compound **2.35** with some signals highlighted

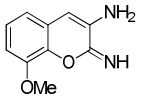
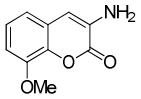
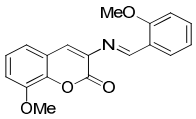
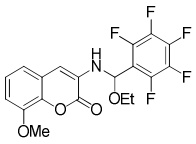
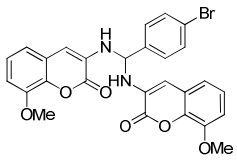
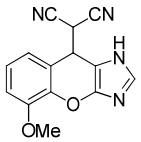
Physical, analytical, and spectroscopic characterization

The structure of compounds **2.27**, **2.28**, **2.29** and **2.35** was determined in consonance with physical, analytical, and spectroscopic data (elemental analysis, meting point, IR, ^{1}H and ^{13}C NMR). This information is presented in the following section. Complete analytical and spectroscopic characterization of compounds **2.22a** and **2.25a** is available in previously published literature[41].

Physical and analytical characterization

The molecular formula and molecular weight were calculated based on the predicted structure and the information obtained from the elemental analysis. The melting point intervals (°C) were also measured, and all the data is referred in the following **Table 21**.

Table 21: Physical and analytical data obtained for compounds **2.22,2.27-2.29** and **2.35**

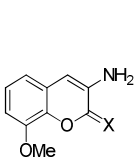
Comp.	Structure	Mp (°C)	molecular formula/ mass (M)	calculated /obtained values (%)			
				C	H	N	O
2.22a[1]		115-117	$C_{10}H_{10}N_2O_2$/ 190.20	63.16 63.20	5.26 5.27	14.74 14.74	16.82 –
2.25a[1]		128-129	$C_{10}H_9NO_3$/ 191.18	62.83 62.81	4.71 4.95	7.33 7.05	25.11 –
2.27		220-222	$C_{18}H_{15}NO_4$. 0.2 H_2O/312.92	69.02 69.03	4.92 5.30	4.47 4.54	21.47 -
2.28		168-170	$C_{19}H_{14}FNO_4$/ 415.31	54.95 54.73	3.40 3.68	3.37 3.21	15.41 -
2.29		193-194	$C_{27}H_{21}BrN_2O_6$. 0.4H_2O/556.00	58.27 58.36	3.92 4.00	5.03 4.88	18.41 -
2.35		—	$C_{14}H_{10}N_4O_2$/ 266.25	63.15 —	3.79 –	21.04 –	12.02 -

[1]Data obtained from ref. 41

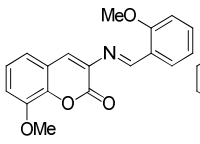
IR spectroscopy

The IR spectra of compound **2.27** corroborated the transformation of the amino group in the starting material as no signals were observed in the 4000-3000 cm^{-1} region. In addition, an intense band centred at 1719 cm^{-1}, corresponding to the C=O carbonyl stretching vibration, confirmed the formation of the imine group. The IR spectra of compound **2.28** highlighted a medium intensity band centred at 3365 cm^{-1}, corresponding to the N-H stretching vibration. The IR spectra of compound **2.29** presents four distinct signals centred at 3409, 3369, 3330 and 3056 cm^{-1}, attributed to the N-H stretching vibration (**Table 22**).

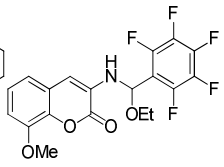
Table 22: IR spectroscopic data (Nujol, cm^{-1}) obtained for compounds **2.27-2.29**



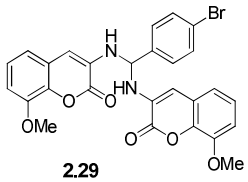
2.22a (X=NH)
2.25a (X=O)



2.27



2.28



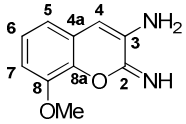
2.29

Compound	4000-3000	1720-1500
2.22a[1]	3453, 3362	1706, 1635, 1612, 1573
2.25a[1]	3422, 3235-3078 (br)	1645, 1620, 1557
2.27	-	1719s (C=O), 1682sh, 1613s, 1601sh, 1582m, 1562s
2.28	3365m	1694s (C=O), 1655w, 1629m, 1606w, 1578m, 1504s
2.29	3409m, 3369m, 3330m	1697s (C=O), 1630m, 1616m, 1578m, 1507sh

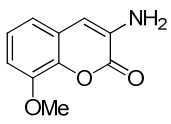
[1]Data obtained from ref. 41

NMR Spectroscopy

All NMR spectroscopic data obtained for compounds **2.22**, **2.25**, **2.27**-**2.29** and **2.35** is presented in **Tables 23-27**. The most relevant signal of the ^{1}H NMR spectra of compound **2.27** is a singlet at δ9.23 ppm (s, 1H), attributed to the imine hydrogen (**Table 24**). In the ^{13}C NMR spectra highlights the peaks at δ157.46 ppm, δ129.78 ppm and δ158.88 ppm, corresponding to C2, C4 and imine group, respectively. The structure of compound **2.27** was further confirmed by HMBC, in which highlights the cross peak between the imine group at δ9.23 ppm and the peaks corresponding to C1', C2', C6' and C3.



2.22a



2.25a

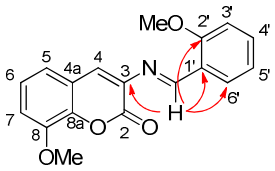
Table 23: ^{1}H NMR and ^{13}C NMR (100 MHz, DMSO-d_6, δ ppm) spectroscopic data obtained for compounds **2.22a** and **2.25a**

		OMe	Ar(2-8a)	NH_2	H4/C4	NH/ C=O
2.22a[1]	**^{1}H**	3.81 (s, 3H)	6.79-6.74 (m, 2H), 6.95 (t, *J*= 8.1 Hz, 1H)	5.43 (s, 2H)	6.18 (s, 1H)	8.30 (s, 1H)
	^{13}C	55.5	153.4, 137.2, 134.8, 123.1, 123.0, 116.3, 107.8, 100.9	-	145.8	-

2.25a[1]	**^{1}H**	3.85 (s, 3H)	7.12 (t, J= 8.0 Hz, 1H), 6.96 (dd, J_1= 7.6, J_2= 1.2 Hz, 1H), 6.91 (dd, J_1= 8.2, J_2= 1.2 Hz, 1H)	5.68 (s, 2H)	6.67 (s, 1H)	-
	^{13}C	55.8	136.9, 133.5, 124.4, 122.4, 116.6, 108.2, 107.7	-	146.2	158.3

[1]Data obtained from ref.41; compound **2.22a** was determined using 400 MHz, DMSO-d_6, δ ppm for ^{1}H NMR and 100 MHz, DMSO-d_6, δ ppm for ^{13}C, while compound **2.25a** was determined using 300 MHz, DMSO-d_6, δ ppm for ^{1}H NMR and 75 MHz, DMSO-d_6, δ ppm for ^{13}C

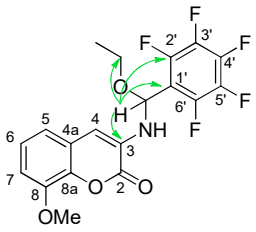
Table 24: ^{1}H NMR (400 MHz, DMSO-d_6, δ ppm) and ^{13}C NMR (100 MHz, DMSO-d_6, δ ppm), spectroscopic data obtained for compound **2.27**



	OMe	**Ar(2-8a)**	**Ar(1'-6')**	**imine**
^{1}H	3.91 (s, 3H, C8-OMe), 3.90 (s, 3H, C2'-OMe)	7.78 (s, 1H, H4), 7.29-7.23 (m, 3H, H5+ H6+ H7)	8.01 (dd, J_1= 7.6 Hz, J_2= 1.6 Hz, 1H, H6'), 7.57 (dt, J_1= 7.2 Hz, J_2= 2.0 Hz, J_3= 1.2 Hz, 1H, H4'), 7.17 (d, J= 8 Hz, 1H, H3'), 7.07 (t, J= 8.4 Hz, 1H, H5')	9.23 (s, 1H)
^{13}C	56.04 (C8-OMe), 55.81 (C2'-OMe)	157.46 (C2), 146.28 (C8), 140.90 (C8a), 137.01 (C3), 129.78 (C4), 124.68 (C6), 120.45 (C4a), 119.49 (C5), 113.02 (C7)	159.60 (C2'), 134.02 (C4'), 126.80 (C6'), 123.44 (C1'), 120.74 (C5'), 112.14 (C3')	158.88

The ^{1}H and ^{13}C NMR spectra of compound **2.28** highlighted the signals corresponding to the generated methylidene group, specifically a doublet at δ6.08 ppm integrating for one hydrogen atom and the signal at δ77.50 ppm, respectively (**Table 25**). Also relevant is the doublet in the ^{1}H NMR spectrum at δ6.66 ppm integrating for one hydrogen atom corresponding to NH group. In the ^{13}C NMR spectrum also stands out the signals corresponding to C2 (δ157.76 ppm) and C4 (δ109.81 ppm). The carbon atoms for the pentafluorbenzene ring are not evident in the spectrum, due to extensive coupling with the fluorine atoms in the *ipso*, *ortho*, *meta* and *para* positions. Nevertheless, some of the carbon signals identified by HMBC through correlation between the CH group of the imino acetal moiety and signals at δ 112.51, δ 143.54 and δ 146.41 ppm, were tentatively assigned to C1', C2'/C6' and C3'/C5', respectively.

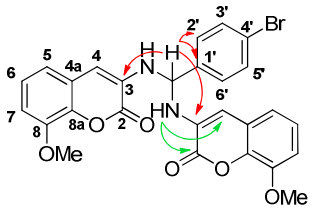
Table 25: ^{1}H NMR (400 MHz, DMSO-d_6, δ ppm) and ^{13}C NMR (100 MHz, DMSO-d_6, δ ppm) spectroscopic data obtained for compound **2.28**



	OMe	OEt	Ar (2-8a)	Ar (1'-6')	C*	N-H
^{1}H	3.87 (s, 3H, OMe)	3.44 and 3.71 (dq, J_1= 7.2 Hz, J_2= 2.0 Hz, 2H, CH_2), 1.13 (t, J= 7.2 Hz, 3H, CH_3)	7.21 (t, J= 8 Hz, 1H, H6), 7.12 (dd, J_1= 8.0 Hz, J_2= 1.2 Hz, 1H, H5), 7.02 J_1= 8.0 Hz, J_2= 1.6 Hz, 1H, H7), 7.02 (s, 1H, H4)	-	6.08 (d, J= 8.0 Hz 1H)	6.66 (d, J= 8.0 Hz 1H)
^{13}C	56.01	62.50 (CH_2), 15.01 (CH_3)	157.86 (C2), 146.41 (C8), 137.37 (C8a), 130.70 (C3), 124.90 (C6), 121.47 (C4a), 117.79 (C5), 109.91 (C4), 109.58 (C7)	146.00 (C2'+ C6'), 143.54 (C3'+ C5'), 112.45 (C1'), C4' not seen	77.50	-

In the ^{1}H and ^{13}C NMR spectra of compound **2.29** stands up the signals at δ6.13 ppm (t, J= 8.4 Hz 1H) and δ 63.61 ppm, respectively, attributed to the methylidene group, as well as by the doublet at δ6.59 corresponding to the NH group (**Table 26**). In the ^{13}C NMR spectra stands out the peaks at δ157.28 ppm and δ107.72 ppm corresponding to C2 and C4, respectively. The proposed structure was further determined by HMBC, thus, cross peaks between the methylidene group and C1', C2'/C6' and C3, and between the NH group and C2 and C4 were observed.

Table 26: ^{1}H NMR (400 MHz, DMSO-d_6, δ ppm) and ^{13}C NMR (100 MHz, DMSO-d_6, δ ppm) spectroscopic data obtained for compound **2.29**



	OMe	Ar (2-8a)	Ar (1'-6')	C-H	N-H
^{1}H	3.86 (s, 3H)	7.96 (dd, J_1= 8.0, J_2= 1.2 Hz, 1H, H5), 7.95 (d, J= 8.0 Hz, 1H, H7), 7.15 (t, J= 8.0 Hz, 1H, H6), 6.81 (s, 1H, H4)	7.59 (d, J= 8.8 Hz, 2H, H3' + H5'), 7.57 (d, J= 8.8 Hz, 2H, H2' + H6')	6.13 (t, J= 8.4 Hz, 1H)	6.59 (d, J= 8.8 Hz, 2H)
^{13}C	55.88	157.28 (C2), 146.32 (C8), 130.95 (C3), 130.69 (C8a), 124.86 (C6), 121.72 (C4a), 117.17 (C5), 109.10 (C7), 107.72 (C4)	138.69 (C1'), 131.49 (C3' + C5'), 129.06 (C2' + C6'), 121.38 (C4')	63.61	-

The most relevant signals in the ^{1}H NMR spectra of compound **2.35** are two singlets at δ12.07 ppm and δ7.53 ppm, attributed to the NH and H9 groups, respectively, and a doublet at δ5.22 ppm attributed to both the H1 and the H1' hydrogens (**Table 27**). By HMBC, cross peaks between H9 with both C2 and C3, and between H1 and C2, C3, C4a, C8a, C8 and the $CH(CN)_2$ moiety were identified.

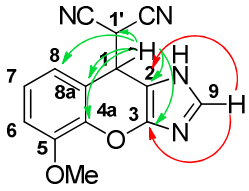


Table 27: ^{1}H NMR (400 MHz, DMSO-d_6, δ ppm) and ^{13}C (100 MHz, DMSO-d_6, δ ppm) spectroscopic data obtained for compound **2.35**

	OMe	Ar (1-8a)	C9/H9	CH(CN)2	N-H
1H	3.86 (s, 3H)	7.15-7.05 (m, 3H, H6-8), 5.22 (dd, J_1= 19.6 Hz, J_2= 2.8 Hz, H1), 5.22 (dd, J_1= 19.6 Hz, J_2= 2.8 Hz, H1)	7.53 (s, 1H)	5.22 (dd, J_1= 19.6 Hz, J_2= 2.8 Hz)	12.07 (s, 1H)
13C	55.80	149.85 (C3), 148.27 (C5), 141.95 (C4a), 123.35 (C6), 120.64 (C7), 112.98(C8a), 112.10 (C8), 99.62 (C2), 36.90 (C1)	132.93	117.85 and 118.05 (CN), 31.92 (C1')	-

2.1.3 Synthesis and reactivity of 2-amino-4-(2-oxo-2-arylethyl)-4*H*-chromene-3-carbonitriles

As was previously mentioned, the chromene moiety is present in several biologically important compounds with interesting chemical and biological properties and can afford a versatile and stable scaffold for the synthesis of new structures. 4*H*-chromenes, in particular, are well described in the literature for several biological and pharmacological activities[98,99], as diverse as antibacterial[100–102], anticancer[103–106], antihyperglycemic[107], antialzheimer[108], antioxidant[102], among others[109]. In combination with cisplatin, crolibulin (**Figure 29**), which is a substituted 4*H*-chromene with anticancer activity, is currently in phase I/II of clinical trials for the treatment of solid tumors with a focus on anaplastic thyroid cancer[110]. Its biological activity is related to tubulin inhibition, leading to induction of apoptosis, disruption of neovascular endothelial cells and disruption of blood flow to the tumor[104].

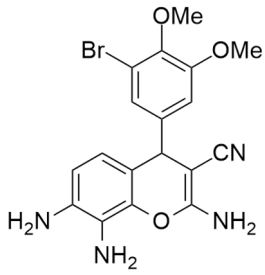
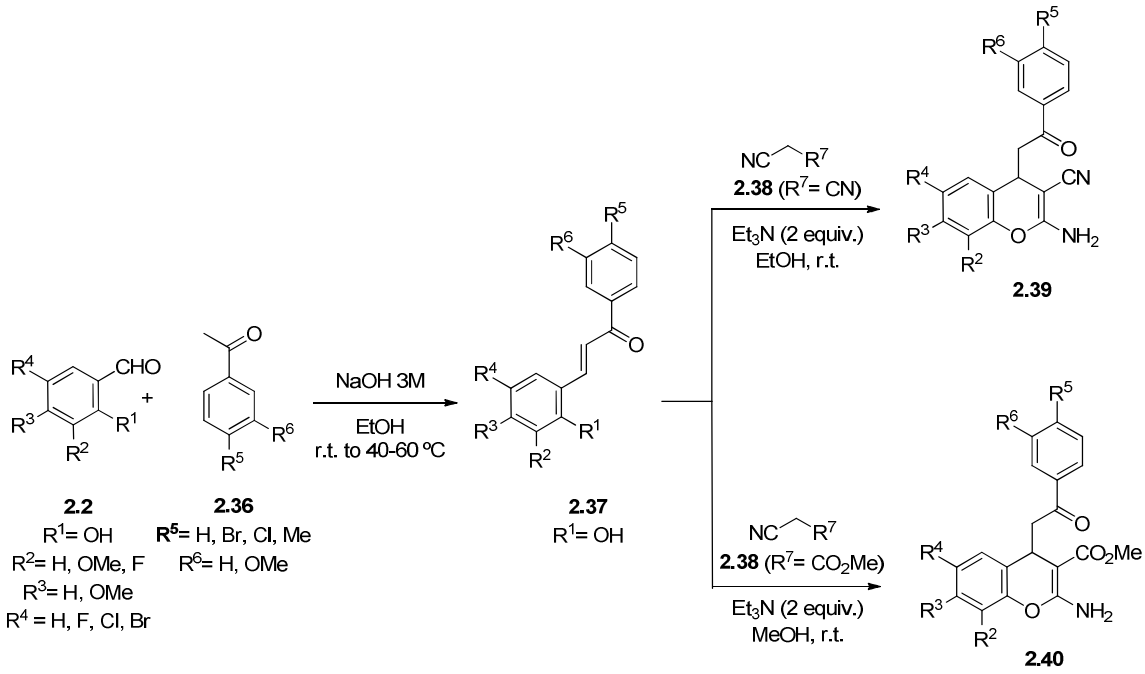


Figure 29: Chemical structure of (4*R*)-2,7,8-triamino-4-(3-bromo-4,5-dimethoxy phenyl)-4*H*-chromene-3-carbonitrile (crolibulin)

Some procedures for the synthesis of chromenes involving α,β-unsaturated carbonyl compounds have been reported[104,111,112]. In the research group, a series of new 4*H*-chromenes has been recently described[104] via a two-step eco-friendly approach, involving α,β-unsaturated carbonyl compounds (**Scheme 23**). The first step involves the base-catalysed aldol condensation between salicylaldehydes **2.2** and acetophenones **2.36**, which are carried out by treatment, at room temperature or under mild heating, with aqueous NaOH (3M) in ethanol as solvent. Under these conditions, compounds **2.3** are isolated in yields ranging from 46% to 100%. The second step consists on the treatment of α,β-unsaturated ketones **2.37** with active methylene compounds, such as methyl malononitrile or cyanoacetate, in the presence of triethylamine as a base and using either methanol or ethanol as solvent, to afford 4*H*-chromenes **2.39** and **2.40**, respectively, in yields ranging from 12% to 94%. This study allowed the identification of some compounds of general structure **2.37**, **2.39** and **2.40** with relevant anticancer activity against MCF-7, Hs578t and MCF10A cancer cell line[104].

Several findings encouraged us to explore the synthesis of new analogues based on this scaffold, in particular: (i) 2-amino-3-cyano-4*H*-chromenes are frequently referred in the literature as biologically active for a series of diseases[106,113]; (ii) the *o*-aminonitrile moiety can participate in several reactions involving both nucleophiles and electrophiles, including the formation of new 6-membered heterocyclic rings[114–117]; and (iii) the presence of a carbonyl group in compounds **2.39** and **2.40** can envisage a broader spectrum of possibilities.



Scheme 23: Synthesis of 4*H*-chromenes **2.39** and **2.40** [adapted from ref.104]

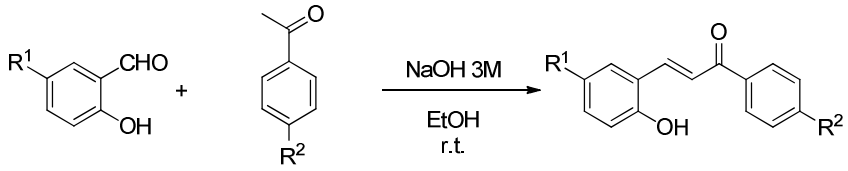
For this reason, the work on 2-amino-3-cyano-4*H*-chromenes **2.39** presented in this chapter, stands on two main objectives:

1) Explore the reactivity of the *o*-aminonitrile moiety of 2-amino-3-cyano-4*H*-chromenes **2.39** under different reaction conditions, including in the formation of new heterocyclic rings.
2) Inspect the potential anticancer, antimicrobial, and/or antimalarial activity of the newly prepared heterocyclic compounds.

Synthesis of 2-amino-4-(2-oxo-2-arylethyl)-4*H*-chromene-3-carbonitriles

Using the previously reported methodology[104], compounds **2.38a-l** were prepared with good to high yields (**Table 28**). Compounds **2.37c**, **2.37e**, **2.37h** and **2.37i**, which were obtained in the first step of the synthetic approach, were slightly contaminated with the corresponding salicylaldehyde **2.2**, and were used without further purifications in the following steps involving formation of chromenes **2.39** (**Table 29**).

Table 28: Reaction conditions and yields for the preparation of compounds **2.37** from salicylaldehydes **2.2** and acetophenones **2.36**



2.2c (R^1= H)
2.2d (R^1= Br)
2.2e (R^1= Cl)

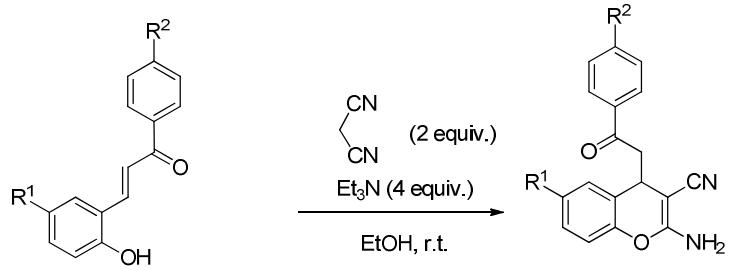
2.36a (R^2= H)
2.36b (R^2= Me)
2.36c (R^2= Br)
2.36d (R^2= Cl)

2.37a (R^1= H, R^2= H)
2.37b (R^1= H, R^2= Me)
2.37c (R^1= H, R^2= Br)
2.37d (R^1= H, R^2= Cl)
2.37e (R^1= Br, R^2= H)
2.37f (R^1= Br, R^2= Me)
2.37g (R^1= Br, R^2= Br)
2.37h (R^1= Br, R^2= Cl)
2.37i (R^1= Cl, R^2= H)

Comp.	R^1	R^2	t (h)	η(%)	ratio 2.2: 2.38	Comp.	R^1	R^2	t (h)	η(%)	ratio 2.2.:2.38
2.37a	H	H	24	62*	-	**2.37f**	Br	Me	3	53	-
2.37b	H	Me	30	68	-	**2.37g**	Br	Br	1.66	64	-
2.37c	H	Br	72	-	0.17:1[a]	**2.37h**	Br	Cl	3	-	0.6:1[a]
2.37d	H	Cl	22	53	-	**2.37i**	Cl	H	24	81	traces[a]
2.37e	Br	H	3	69	-						

[a]Slightly contaminated with aldehyde

Table 29: Reaction conditions and yields of synthesis of 4*H*-chromenes **2.39a-i** from α,β-unsaturated ketones **2.37a-i**



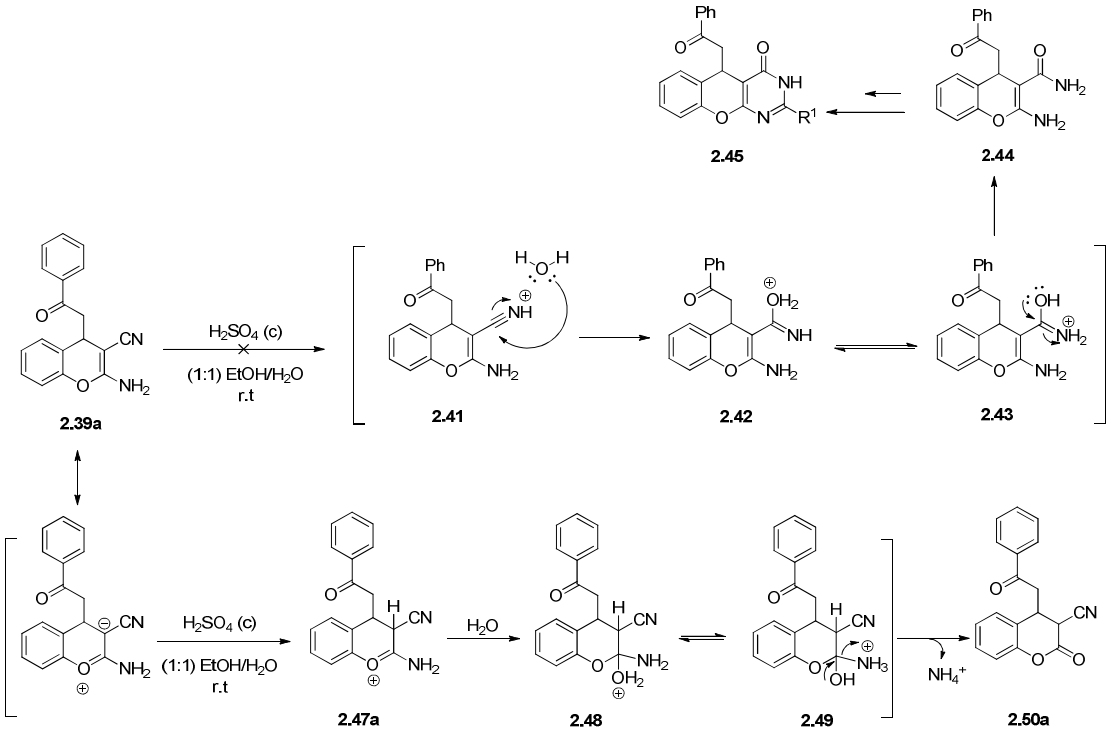
2.37a (R^1= H, R^2= H)
2.37b (R^1= H, R^2= Me)
2.37c (R^1= H, R^2= Br)
2.37d (R^1= H, R^2= Cl)
2.37e (R^1= Br, R^2= H)
2.37f (R^1= Br, R^2= Me)
2.37g (R^1= Br, R^2= Br)
2.37h (R^1= Br, R^2= Cl)
2.37i (R^1= Cl, R^2= H)

2.39a (R^1= H, R^2= H)
2.39b (R^1= H, R^2= Me)
2.39c (R^1= H, R^2= Br)
2.39d (R^1= H, R^2= Cl)
2.39e (R^1= Br, R^2= H)
2.39f (R^1= Br, R^2= Me)
2.39g (R^1= Br, R^2= Br)
2.39h (R^1= Br, R^2= Cl)
2.39i (R^1= Cl, R^2= H)

Compound	R^1	R^2	t (h)	η (%)	Compound	R^1	R^2	t (h)	η (%)
2.41a	H	H	2	30	**2.41f**	Br	Me	1.5h	46
2.41b	H	Me	1.33	50	**2.41g**	Br	Br	1h	40
2.41c	H	Br	3.33	45	**2.41h**	Br	Cl	3h	42
2.41d	H	Cl	5.5	53	**2.41i**	Cl	H	1h	51
2.41e	Br	H	1h	54					

Reactivity of 2-amino-4-(2-oxo-2-arylethyl)-4*H*-chromene-3-carbonitrile in aqueous acidic conditions

With compounds **2.39** in our hands, we explored the acid-catalysed hydrolysis of its nitrile group to afford the amides **2.44** (**Scheme 24**). To attempt this reaction, compound **2.39a** was suspended at room temperature in a mixture of (1:1) EtOH/H_2O in the presence of a catalytic amount of H_2SO_4 (c). After stirring for 4 h, a new beige suspension was obtained and filtered. Unfortunately, the desired product **2.44** could not be identified, but instead a new set of signals were assigned to product **2.50a** (η= 61% crude product (entry 1 – **Table 30**). The formation of compound **2.50a** could be explained by nucleophilic attack of a water molecule to position 2 of the chromene ring, transforming C3 into a chiral carbon (**Scheme 24**). The process evolved with the elimination of ammonia that is present in solution as ammonium chloride. No evidence of the formation of the expected amide **2.44** was observed.



Scheme 24: Proposed mechanism for the formation of compound **2.50a** from **2.39a** after treatment with H_2SO_4 (c). The formation of compound **2.44** was not detected

The chemical structure of compound **2.50a** was determined based on its spectroscopic data. **Figure 30** shows the ^{1}H NMR spectrum of **2.50a**, where two sets of signals between δ3.5 5.5 ppm, assigned to H3, H4 and Ha, were considered indicative of two diastereomers in a 2.1:1 ratio.

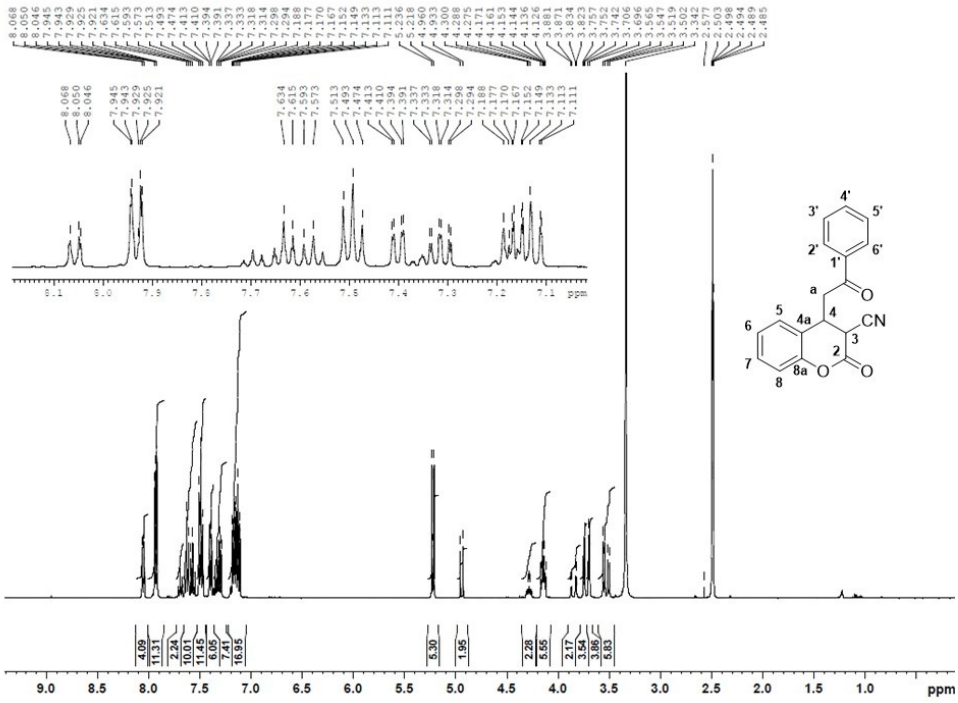


Figure 30: ^{1}H NMR (400 MHz, DMSO-d$_6$, δ ppm) spectrum of **2.50a**

After two-dimensional correlation spectroscopic analysis, the major isomer was identified by a doublet centred at δ5.22 ppm (J= 7.2 Hz) and the multiplet centred at δ4.14 ppm, assigned to the H3 and H4, respectively, and a doublet of doublets centred at approximately δ3.54 ppm (J_1= 6.8 Hz; J_2= 18.4 Hz) and δ3.73 ppm (J_1= 4.0 Hz; J_2= 18.4 Hz), assigned to both protons of Ha (**Figure 31**). The minor isomer was identified by the presence of a doublet centred at δ4.95 ppm (J= 10.8 Hz) and of a multiplet centred at δ4.29 ppm, assigned to the H3 and H4, respectively, and by the presence of a doublet of doublets centred at approximately δ3.72 ppm (J could not be calculated) and δ3.85 ppm (J_1= 4.0 Hz; J_2= 18.8 Hz), assigned to both Ha protons.

Based on the Karplus equation, which allows the prediction of the relative dihedral torsion angles using the $^{3}J_{HH}$ constants[118,119], a calculation was made using the $^{3}J_{HH}$ values of H3 and H4, for both isomers. Thus, the C-H3 signal of the major isomer (**2.50aMaj**) would have a dihedral angle of 41° or 134° with C-H4. For the minor isomer (**2.50amin**), the dihedral angle of C-H3 with C-H4 should be 24° or 148°.

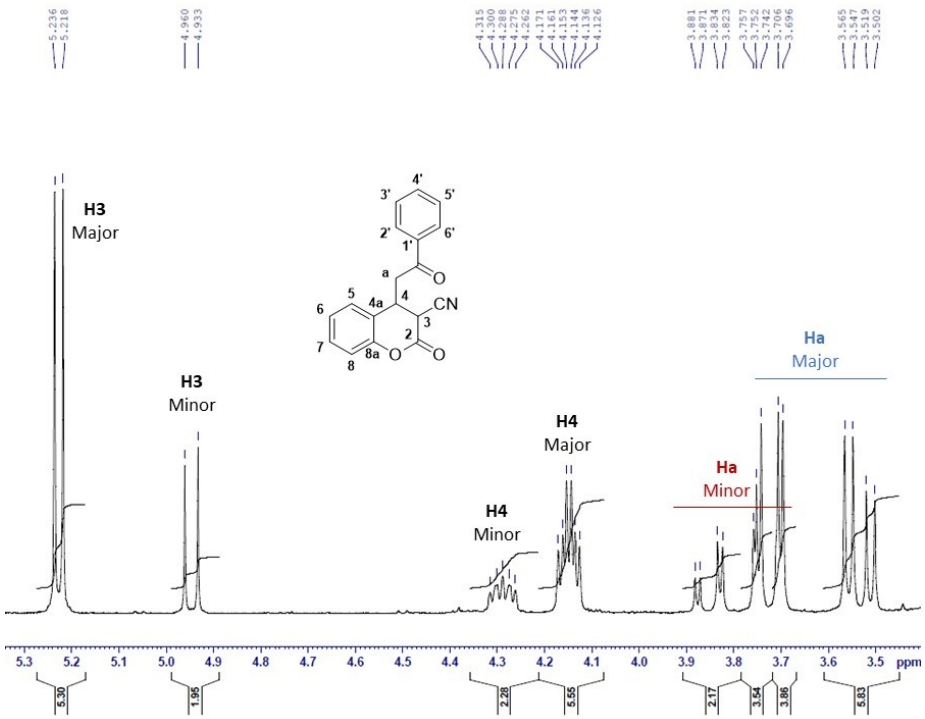


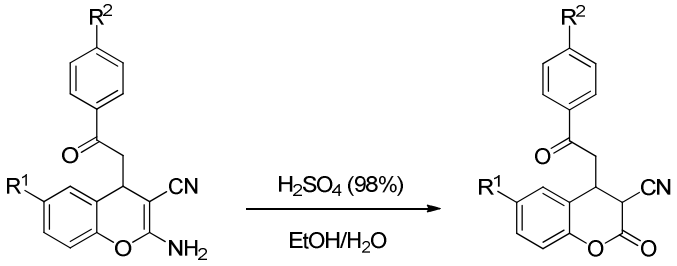
Figure 31: Expansion of the ^{1}H NMR (400 MHz, DMSO-d_6, δ ppm) spectrum of **2.50a** between δ5.25-3.50 ppm

The proposed chemical structure for compound **2.50a** was also supported by IR spectroscopy, in which two intense bands centred at 1769 and 1681 cm^{-1}, assigned to the C=O stretching vibration of both carbonyl groups, were identified. The nitrile stretching vibration shifted from 2179 cm^{-1} in **2.39a** to 2259 cm^{-1} in **2.50a**, accompanied by a change in intensity from medium to weak.

Compounds **2.50b-f** could be prepared using the conditions described in **Table 30**. The results showed that the isomeric ratio does not vary significantly with the presence of different substituents in the starting material. Lower reaction yields were obtained as the number of equivalents of H_2SO_4 (98%) w. as increased. However, additional experiments are needed to confirm, including using other R^1 and R^2 substituents.

In summary, a synthetic procedure was designed and optimized for the preparation of lactones **2.50** in good to high yields. By suspending the appropriate 2-aminochromene **2.39** in aqueous ethanol in the presence of concentrated H_2SO_4 at room temperature, diastereoisomeric mixtures of lactones **2.50** could be isolated.

Table 30: Reaction conditions and results obtained from the treatment of chromenes **2.39** with concentrated H_2SO_4 in aqueous ethanol to afford compounds **2.50**



2.39a (R^1= H, R^2= H)
2.39b (R^1= H, R^2= Me)
2.39c (R^1= H, R^2= Br)
2.39e (R^1= Br, R^2= H)
2.39g (R^1= Br, R^2= Br)
2.39h (R^1= Br, R^2= Cl)

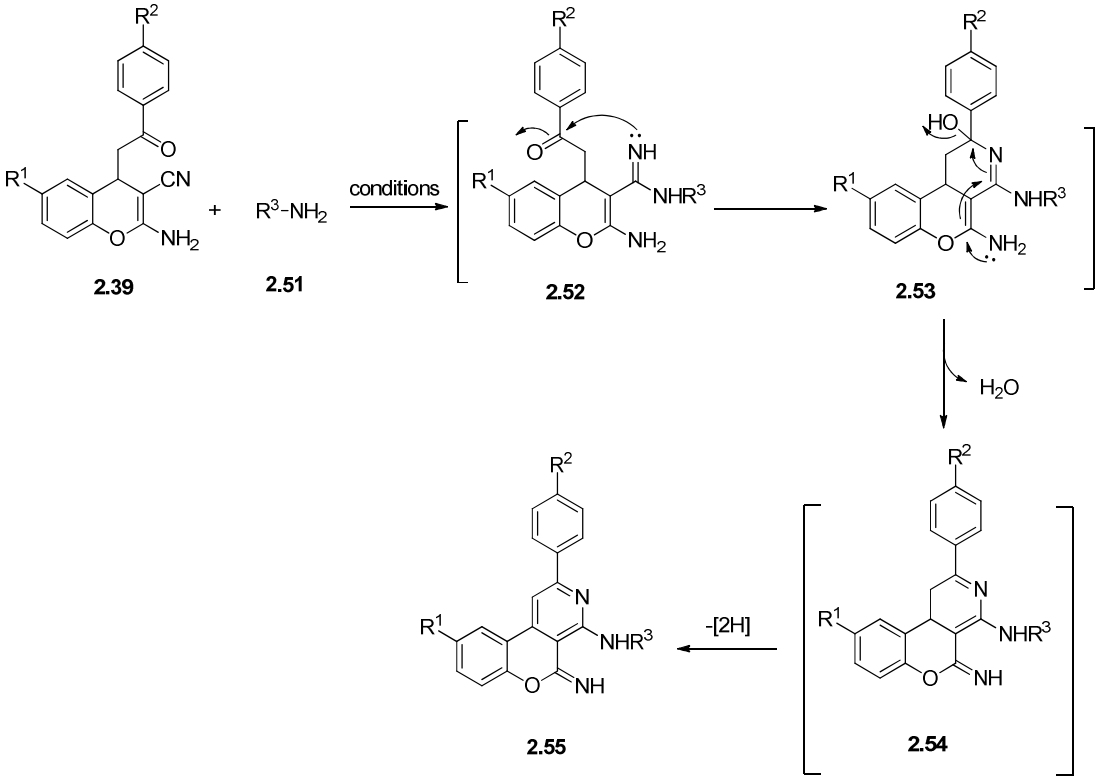
2.50a (R^1= H, R^2= H)
2.50b (R^1= H, R^2= Me)
2.50c (R^1= H, R^2= Br)
2.50d (R^1= Br, R^2= H)
2.50e (R^1= Br, R^2= Br)
2.50f (R^1= Br, R^2= Cl)

Entry	2.39		solvent	H_2SO_4					isomeric
	R^1	R^2	EtOH/H_2O	(equiv.)	T (°C)	t (h)	η (%)	product	ratio
1	H	H	1:1	1.7	r.t.	4	61	**2.50a**	2.1/1
2	H	Me	1:1	1.7	r.t.	4	84	**2.50b**	2.5/1
3	H	Br	1:4	3.7	50	1	78	**2.50c**	2.7/1
4	Br	H	1:1	3	r.t	4	57	**2.50d**	2.7/1
5	Br	Br	1:1	4.5	r.t.	2	17	**2.50e**[1]	2.9/1
6	Br	Cl	1:1	4	r.t.	2	17	**2.50f**[1]	2.9/1

[1]Identified by ^{1}H NMR and IR spectroscopy; evolved during ^{13}C and bidimensional NMR spectra collection

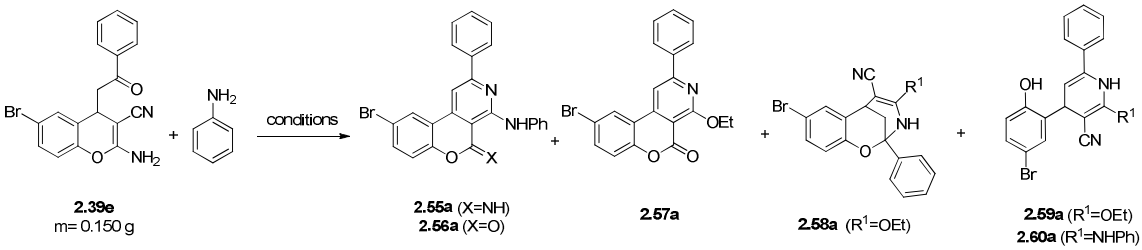
Reactivity of 2-amino-4-(2-oxo-2-arylethyl)-4*H*-chromene-3-carbonitriles with primary amines: synthesis of novel 6-imino-*N*,9-diaryl-6*H*-benzo[*c*]chromen-7-amines and 6-oxo-*N*,9-diaryl-6*H*-benzo[*c*]chromen-7-amines

The reactivity of 2-amino-4-(2-oxo-2-arylethyl)-4*H*-chromene-3-carbonitriles **2.39** with a selection of primary amines was also studied. The goal was to introduce a 6-membered ring in the scaffold by transforming the nitrile group in **2.39** into an amidine moiety able to promote an intramolecular cyclization with the ketone group, as represented in **Scheme 25**. To this end, compound **2.39e** was employed as a model to study and optimize the reaction conditions, with aniline as the amine. The experiments performed were summarized in **Table 31**.



Scheme 25: Predicted reaction sequence that would allow the formation of products **2.55**

Table 31: Experimental conditions tested, in the reaction of compound **2.39e** with aniline



Entry	aniline (equiv.)	conditions					results		
		solvent	AcOH (equiv.)	H_2SO_4 (equiv.)	T (°C)	t (h)	product[a]	ratio	yield (%)
1	1.2	EtOH	-	-	80	92	complex mixture	-	-
2	-	EtOH	0.5	-	80	22	**2.58a** + **2.59a**	1/4	-
3	1.2	EtOH	0.5	-	80	22	**2.56a** + **2.57a** + **2.60a**	2/9/2	-
4	2	MeCN	0.5	-	80	22	**2.55a** + **2.39e**	1/9	-

5	2	Dioxane	0.5	-	80	22	**2.39e**	-	[b]
6	2	EtOAc	0.5	-	80	22	**2.39e**	-	35
7	2	EtOH	0.5	-	80	22	**2.55a** + **2.56a**	9/1	-
8	2	EtOH	-	-	80	22	**2.39e**	-	70
9	2	EtOH	1	-	80	22	**2.55a**	-	18
10	3	EtOH	0.5	-	80	22	**2.55a**	-	25
11	3	EtOH	0.5	-	80	63	**2.55a** + **2.56a**	9/1	-
12	2	EtOH	0.5	-	50	70	**2.55a** + **2.60a**	1/4	-
13	2	EtOH	-	0.5	80	0.33	**2.60a**	-	[b]
14	2	EtOH	-	0.5	80	22	**2.55a** + **2.56a** + $PhNH_3Cl$	5/1/4	-

[a] By ^1H NMR
[b] slightly contaminated product; no yield was calculated

Observing the results from **Table 31**, a series of conclusions can be noted:

- Performing the reaction without an acid catalyst results in a complex mixture after 92 h of reaction (entry 1).
- The absence of aniline led to the formation of products **2.58a** and **2.59a**, where ethanol acted as nucleophile (entry 2), while adding 1.2 equivalents of aniline led to the formation of products **2.56a**, **2.57a** and **2.60a** (entry 3).
- When comparing the reactions performed using different solvents (entries 3-7), it is observable that ethanol was the best solvent to perform this reaction (entry 7), with acetonitrile affording a mixture of **2.55a** and **2.39e** of 1/9 (entry 4) and both dioxane and ethyl acetate leading to the isolation of the starting material **2.39e** (entries 5 and 6).
- When comparing the reactions performed in ethanol for 22 h (entries 7-10), it is possible to conclude that the addition of 1 equivalent of acetic acid (entry 9) improves the isolation yield of **2.55a** (18%) and without the presence of impurities, when compared with the use of 0.5 equivalents of acetic acid (entry 7). However, the best results were obtained when 0.5 equivalents of acetic acid and 3 equivalents of aniline were used (entry 10), which afforded the

isolation of **2.55a** with 25% yield. Removing the acetic acid from the reaction leads to the isolation of the starting material **2.39e** with 70% yield (entry 8).

- Comparing the reactions where 3 equivalents of aniline were used (entries 10 and 11), which differ in the reaction time, it is possible to observe that prolonging the reaction time from 22 h (entry 10) to 63 h (entry 11) leads to the isolation of a mixture of **2.55a** with **2.56a**, which indicates that prolonging the reaction might lead to the hydrolysis of **2.55** into **2.56**.
- Comparing the reactions where sulfuric acid was used (entries 13 and 14), it is possible to observe that the reaction occurred at an accelerated rate when comparing with the ones where acetic acid was used, as after 20 min. of reaction, compound **2.60a** was isolated as a slightly contaminated product (entry 13). However, performing the reaction for 22 h (entry 11) led to a faster hydrolysis rate of **2.55a**, as compound **2.56a** was detected in the mixture in a 5/1 ratio with **2.55a**, which is a higher proportion when comparing to entry 7 where acetic acid was used.
- It was also possible to identify a set of signals attributed to anilinium salt, which was formed due to the presence of a strong acid such as sulfuric acid (entry 14). This might be responsible for a decrease in the formation of **2.55a** by decrease of the availability of aniline to act as a nucleophile.

The chemical structures of the products described in **Table 31** were determined by NMR spectroscopy. The ^{1}H NMR spectra of compound **2.55a** possesses distinctive singlets at δ12.78 (C4-NHPh), δ 9.32 (C5=NH) and δ8.14 ppm (C1-H) (**Figures 32** and **33**). Compound **2.56a** presents several peaks that possess similar chemical shifts to those observed for **2.55a**, with the main difference being the absence of the singlet at δ9.32 ppm and the presence of a new singlet at δ10.75 ppm (**Figure 34**), which was attributed to the C4-NHPh after HMBC and HMQC correlation studies. ^{13}C NMR spectra of compound **2.56a** presents a group of signals with similar chemical shifts to those presented by **2.55a**, with the distinction of C5 (δ155.46 ppm) (**Figure 35**).

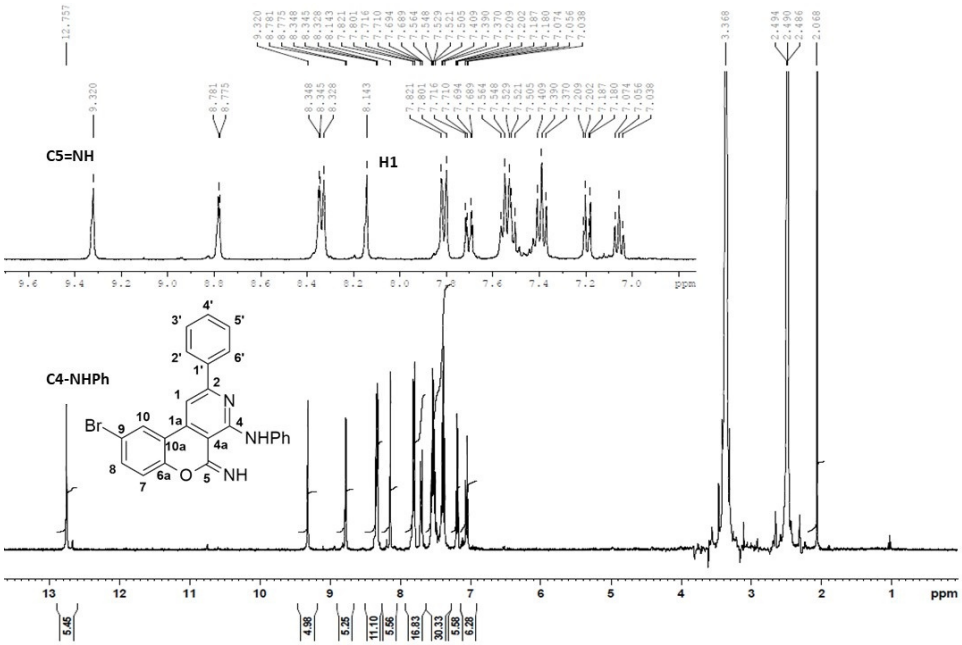


Figure 32: ^{1}H NMR (400 MHz, DMSO-d$_6$, δ ppm) spectrum of compound **2.55a**, in which three signals are highlighted

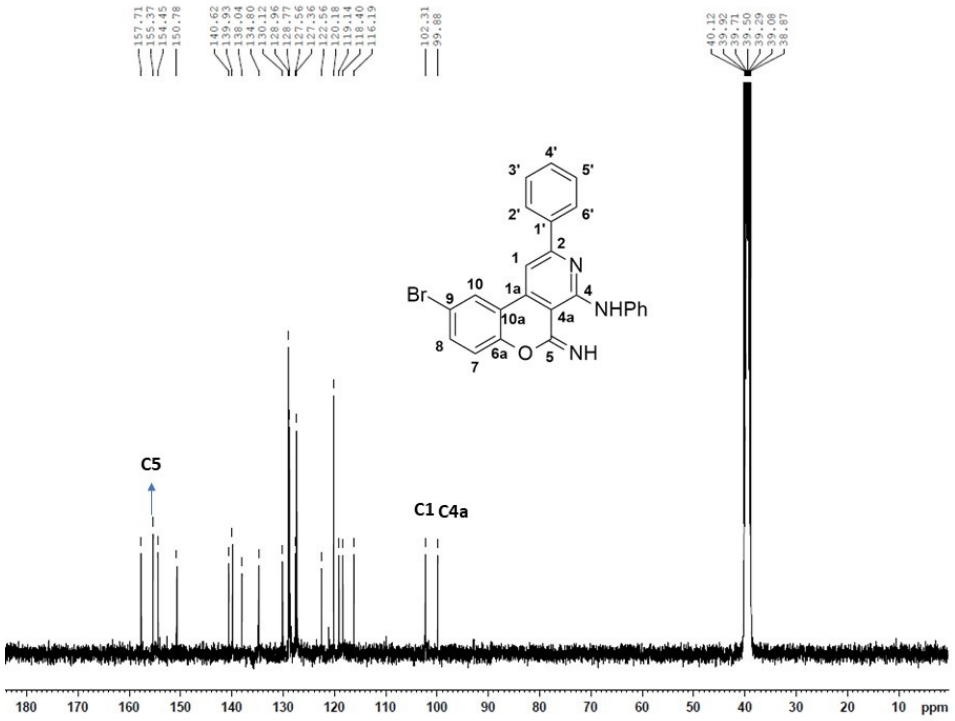


Figure 33: ^{13}C NMR (100 MHz, DMSO-d$_6$, δ ppm) spectrum of compound **2.55a**, in which three signals are highlighted

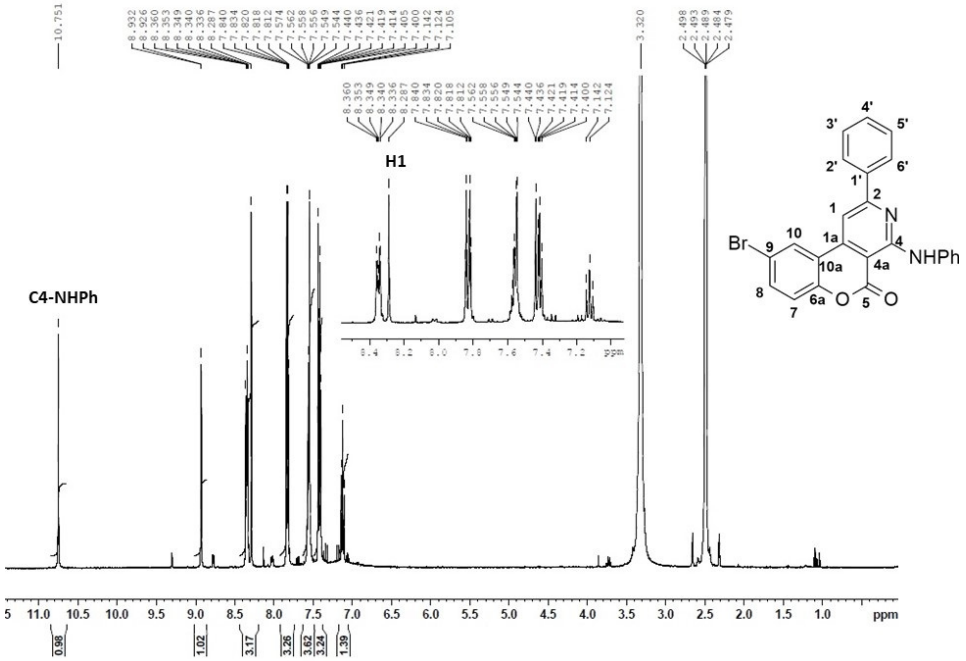


Figure 34: ^{1}H NMR (400 MHz, DMSO-d$_6$, δ ppm) spectrum of compound **2.56a**, in which two signals are highlighted

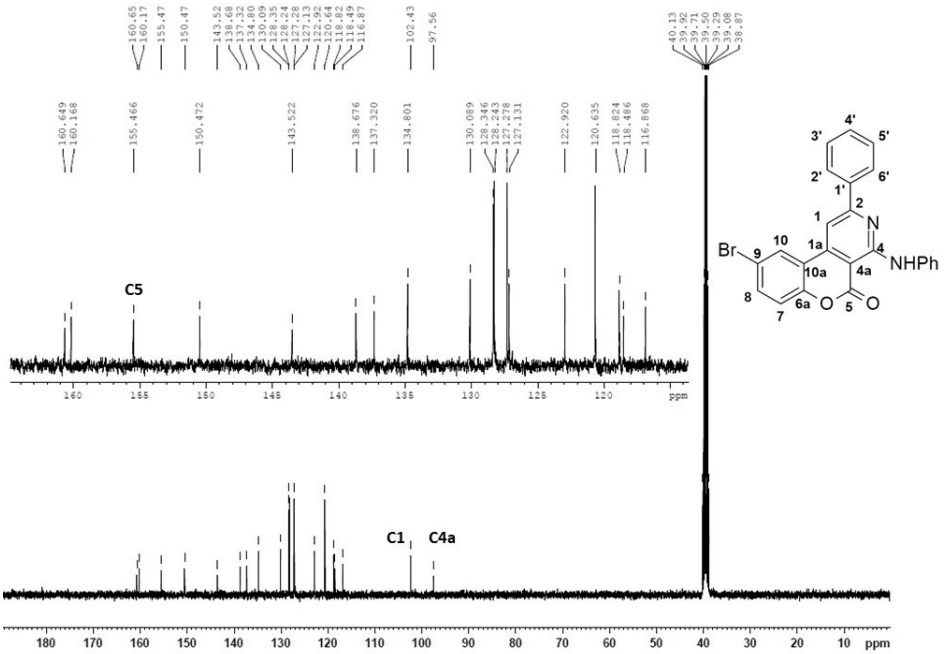


Figure 35: ^{13}C NMR (100 MHz, DMSO-d$_6$, δ ppm) spectrum of compound **2.59a**, in which three signals are highlighted

It is worth highlighting that the chemical shifts of the NH groups in compounds **2.55** and **2.56** showed to be highly different, specifically the singlets appearing at δ12.74 ppm and δ10.73 ppm, respectively. This may be explained by the strength of the expected intramolecular hydrogen

bonding interaction between the NH group and the imine and ketone groups in compounds **2.55** and **2.56**, respectively, which are disposed in a 6-membered ring fashion (**Figure 36**).

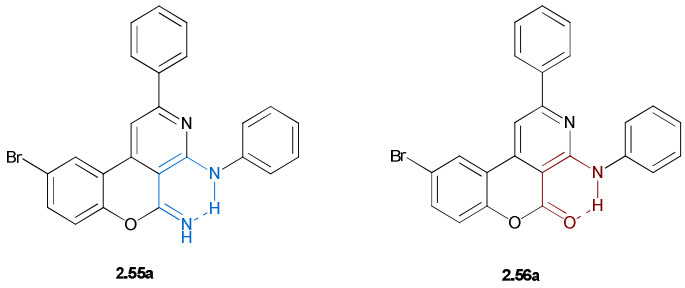


Figure 36: Representation of the expected intramolecular hydrogen bonding interaction between the NH group and the imine group or ketone groups in **2.55a** and **2.56a**, respectively

The identification of compound **2.60a** was performed by ^{1}H and ^{13}C NMR spectroscopy on a mixture of compounds **2.60a** and **2.39e** (**Figures 37** and **38**) considering the NMR signals previously obtained from the pure compound **2.39e**. The characterization of compound **2.60a** was based on the presence of a doublet centred at δ4.68 ppm (J= 5.6 Hz) corresponding to H4 hydrogen atom, the double doublet at δ5.26 ppm (J_1= 1.2 Hz; J_2= 5.6 Hz) assigned to H5 hydrogen atom, and three singlets, one attributed to the pyridine NH group (δ 8.81 ppm), the second to the exocyclic amine (δ8.51 ppm) and the third to the hydroxy group (δ9.94 ppm), respectively.

The studies on the reaction of **2.39e** with aniline, summarized in **Table 31**, showed that performing the reaction in ethanol, at 80 °C, and in the presence of acetic acid afforded compound **2.55a** after 22 h. It was then theorized that compounds **2.55**, **2.56**, **2.58** and **2.59** could be selectively obtained by controlling the reaction conditions. Also, the isolation of compounds **2.58** and **2.59** when performing the reaction in the absence of aniline (entry 2 – **Table 31**) led to the hypothesis that these compounds were being generated in a stepwise fashion, with compound **2.58a** being a precursor of compound **2.59a**.

Additionally, the isolation of compound **2.60a** by using 2 equivalents of aniline, in a reaction performed in the presence of 0.5 equivalents of sulfuric acid, in ethanol and at 80 °C, for 20 min. (entry 13- **Table 31**), could mean that there could exist a precursor of **2.60a** whose structure would be analogue to **2.58a**, but that had incorporated aniline instead of ethanol. It was also theorized that compound **2.60a** could be a precursor of compound **2.55a**, which could generate compound **2.56a** by hydrolysis.

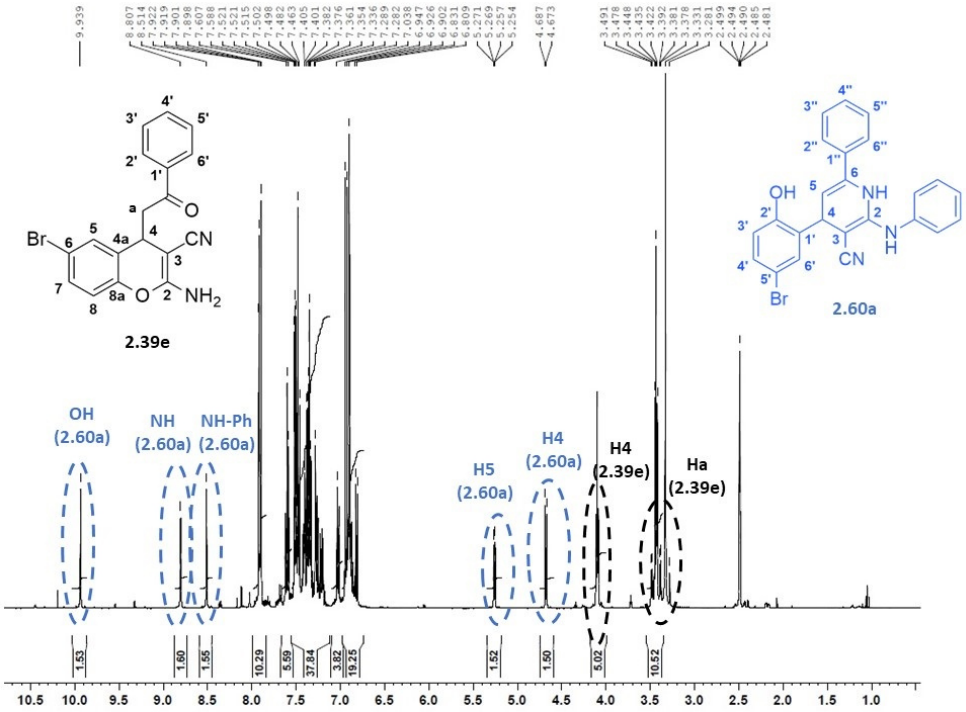


Figure 37: ^{1}H NMR (400 MHz, DMSO-d_6, δ ppm) spectrum of a mixture of compounds **2.39e** and **2.60a**, in which several signals of compound **2.39e** (black circles) and of **2.60a** (blue circles) are highlighted

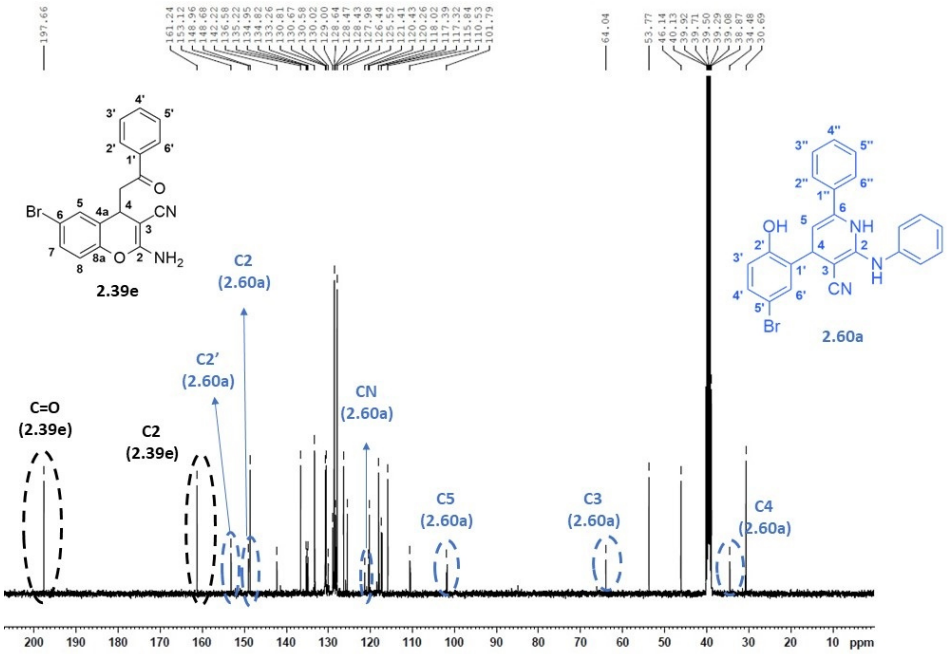
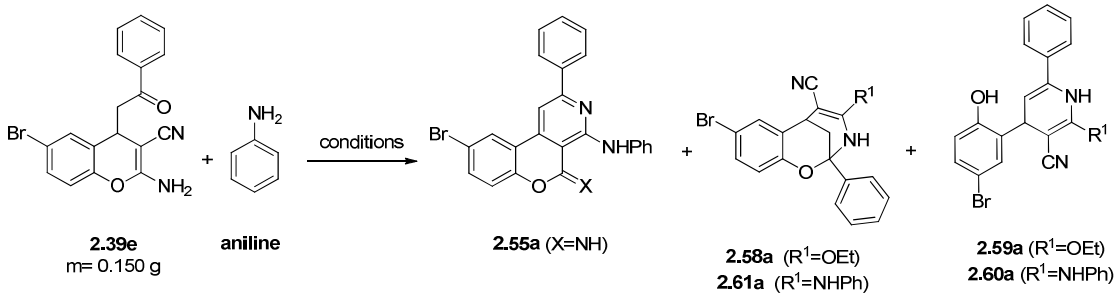


Figure 38: ^{13}C NMR (400 MHz, DMSO-d_6, δ ppm) spectrum of a mixture of compounds **2.39e** and **2.60a**, in which several signals of compound **2.39e** (black circles) and of **2.60a** (blue circles) highlighted

In search of the optimal conditions for the isolation of each of these compounds, a series of experiments were performed using these conditions in an EtOH/H_2O system to promote a solubility-controlled reaction in which the products reacted while in suspension (**Table 32**).

Table 32: Conditions tested for the reaction of compound **2.39e** with aniline, in an EtOH/H_2O system



2.39e m= 0.150 g | **aniline** | **2.55a** (X=NH) | **2.58a** (R^1=OEt) **2.61a** (R^1=NHPh) | **2.59a** (R^1=OEt) **2.60a** (R^1=NHPh)

Entry	aniline (equiv.)	AcOH (equiv.)	t (h)	products[a]	ratio[a]	yield (%)
1	2	0.25	0.5	**2.60a** + **2.39e**	1/5	-
2	2	0.25	1	**2.60a** + **2.61a** + **2.39e**	1/1/3	-
3	2	0.25	1.5	**2.61a** + **2.39e**	1/3	-
4	2	0.5	1.5	**2.61a**	-	65
5	2	1	1.5	**2.60a** + **2.61a**	1/9	-
6	2	2	1.5	**2.55a** + **2.61a**	1/4	-
7	2	0.5	15.5	**2.55a** + **2.61a**	1/4	-
8	2	1	15.5	**2.55a** + **2.61a**	1/4	-
9	2	2	15.5	**2.55a** + **2.61a**	1/4	-
10	1.2	0.5	22	**2.55a** + **2.60a** + **2.61a**	1/1/8	-
11	2	0.5	22	**2.55a** + **2.61a**	1/4	-
12	3	0.5	63	**2.55a** + **2.61a**	1/1	-

[a]By ^{1}H NMR

From the results presented in **Table 32**, a series of conclusions can be pointed out as well:

- When 0.25 equivalents of acetic acid were used (entries 1-3), longer reaction times favoured the formation of compounds **2.60a** and **2.61a**.
- When fixing the reaction time in 1.5 h (entries 3-6), an increase in the acetic acid equivalents resulted in the isolation of different products mixed with **2.61a**. The order of identification of these different products follows the previously proposed stepwise order of formation for compounds **2.55a**, **2.60a** and **2.61a**, which corroborate the theory that **2.61a** is the precursor of **2.60a**, which in turn is the precursor of **2.55a**.
- When the reaction time was fixed in 15.5 h (entries 7-9), it was verified that an increase in the acetic acid equivalents did not result in any change of the isolated mixture of **2.55a** and

2.61a, as the ratio was the same for all three experiments (1/4). This might indicate that, at this point, the reaction may be mainly controlled by other variables other than the amount of acetic acid in solution.

- Fixing the reaction time in 22 h (entries 10 and 11) and varying the aniline equivalents, while fixing the amount of acetic acid in 0.5 equivalents, showed that the amount of aniline bears an important role in the reaction, as the use of 1.2 equivalents (entry 10) led to the isolation of a mixture of 3 products (**2.55a**, **2.60a** and **2.61a**) in a 1/1/8 ratio, while the use of 2 equivalents increased the ratio of the product **2.55a** in relation to **2.61a** (entry 11).
- When the reaction time and aniline equivalents were increased to 63 hours and 3 equivalents, respectively, it was verified that a mixture of **2.55a** and **2.61a** was still present, in a ratio of 1/1.

From the results presented in **Table 32**, it was possible to confirm that compounds **2.61a**, **2.60a** and **2.55a** are being generated in a stepwise fashion. The reaction is promoted by acetic acid catalysis, but an increase in the amount of acetic acid is not directly proportional to an increase in the formation of **2.55a**. An increase in the reaction time is not directly related to an increment in the formation **2.55a** as well, as a ratio of **2.55a** and **2.61a** of 1/4 was found in entry 6 (2 equivalents of aniline, 2 equivalents of acetic acid, 1.5 hours), entry 9 (2 equivalents of aniline, 2 equivalents of acetic acid, 15.5 h) and entry 11 (2 equivalents of aniline, 0.5 equivalents of acetic acid, 22 h).

These findings suggested that the newly formed product **2.61a** would be quite insoluble in the aqueous ethanol (50%) employed in the reaction, thus facilitating the evolution of the reaction to the formation of compound **2.55a**. Therefore, this solvent mixture does not seem to be suitable for preparing compounds **2.55**, **2.56** and **2.60**, but an option for the synthesis of compounds **2.61**, as provided compound **2.61a** with a 65% yield (entry 4). It is important to note that, for entry 4, **2.61a** was found after 1.5 h of reaction, while for 0.5 h of reaction time (entry 1) compound **2.60a** was found; this can be explained considering the evolution that compounds **2.61a** suffers in DMSO-d_6, generating **2.60a**, which could have occurred during the collection of the ^{1}H NMR spectrum in entry 1. For this reason, the percentages of both compounds **2.60a** and **2.61a** that were identified in the crude mixtures must be analysed with a certain caution, as even though the collection of the ^{1}H NMR spectrum was readily performed after the preparation of the sample, the conversion of **2.60a** into **2.61a** rapidly occurs in DMSO-d_6.

Compound **2.61a** was identified by ^{1}H NMR as a pure product (**Figure 39A).** However, an evolution of **2.61a** into **2.60a** was observed in the NMR tube (DMSO-d_6 solution) during the collection of the ^{13}C NMR spectra (**Figure 39B**). As compound **2.60a** had been previously characterized, the ^{13}C NMR signals for compound **2.61a** could be assigned (**Figure 40**). In the ^{1}H NMR spectra of compound **2.61a** stands out two doublet of doublets at around δ2.16 and δ2.41 ppm (J_1= 9.2 Hz; J_2= 3.2 Hz), which correspond to the H3 hydrogen atoms. It also possesses a triplet at around δ3.72 ppm (J= 2.8 Hz), corresponding to H4, and two distinct singlets at δ8.02 and δ8.12 ppm, which are attributed to the NH-Ph and the endocyclic NH groups, respectively. Compounds **2.58a** and **2.59a** could be identified due to the presence of the characteristic signals previously identified for **2.60q** and **2.61a**, by ^{1}H NMR, and for the existence of an additional triplet and quartet, typical of the methyl and methylene groups of ethoxyl groups.

The results pointed to the involvement of dihydropyridine **2.60** and spiro derivative **2.61** in the formation of imine derivative **2.55**, with **2.61** being a precursor of **2.60**, which in turn is a precursor of **2.55**. These findings led us to review the mechanism proposed in **Scheme 25**, suggesting that the reaction occurs through path **B** (**Scheme 26**) as a possible reaction mechanism for the formation of imino chromenopyridine **2.55** and lactone chromenopyridine **2.56**, instead of path **A** (**Scheme 26**). It is expected that prolonging the reaction time after compound **2.55** is formed will lead to an increased hydrolysis rate, and thus generating **2.56** from **2.55 (Scheme 26**). As observed in **Table 31**, compound **2.57a** was found when the amount of aniline was decreased from 2 to 1.2 equivalents or removed. Therefore, it was concluded that the formation of the lactone **2.57** would follow a similar pathway to that proposed for imine **2.55**, competing with the added nucleophile (anilines in the present study) for the attack at C2. This will tend to occur when less amount of amine is used, or a less nucleophilic amine is chosen. Dihydropyridines **2.59** and **2.60** are expected to have been generated during the formation of lactones **2.57**, following a similar reaction mechanism than that presented in **Scheme 26**.

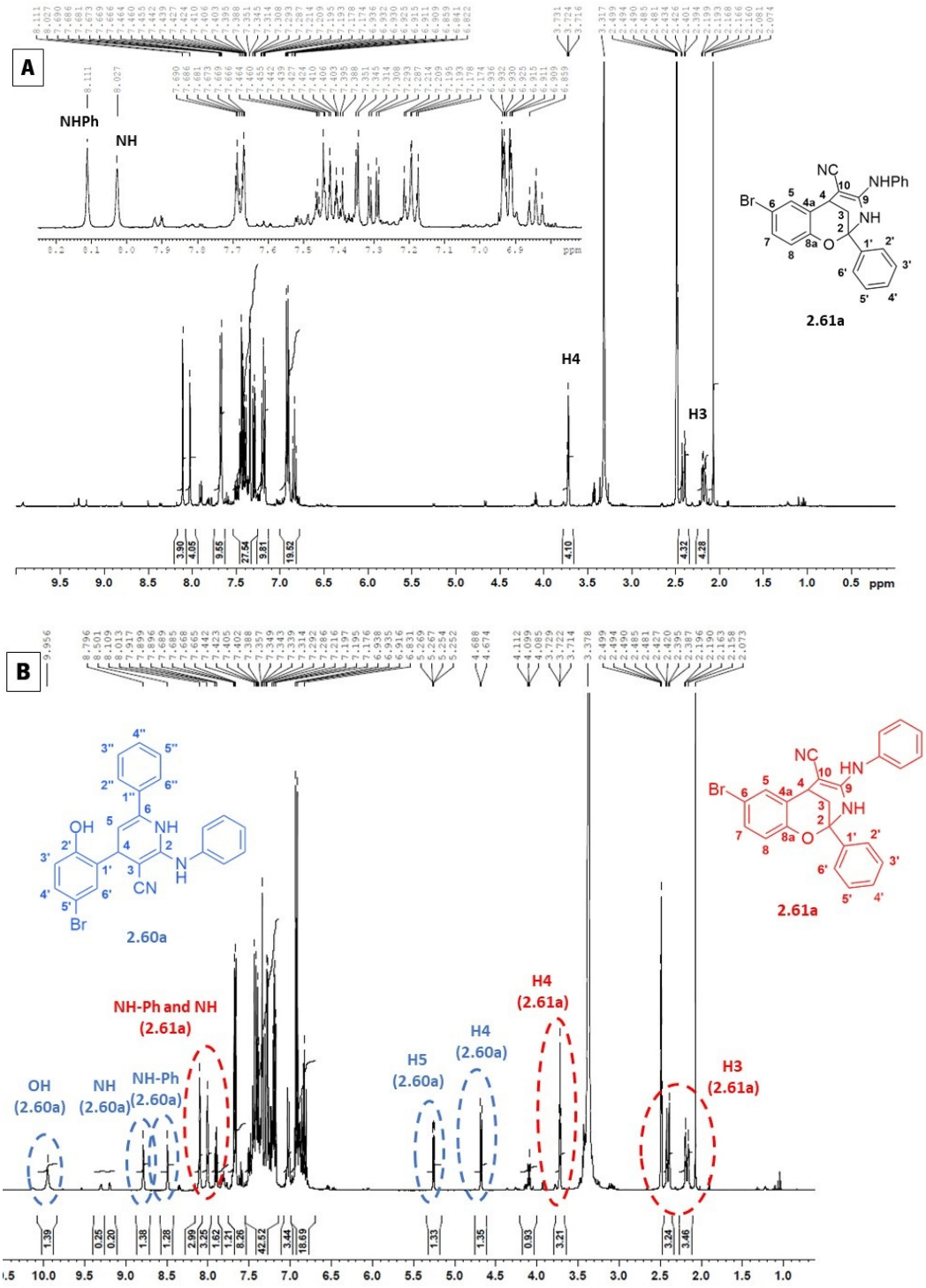


Figure 39: **A:** ^{1}H NMR (400 MHz, DMSO-d$_6$, δ ppm) spectrum of compound **2.61a**, in which several signals are highlighted. **B:** ^{1}H NMR (400 MHz, DMSO-d$_6$, δ ppm) spectrum of a mixture of compounds **2.60a** and **2.61a**, generated from a sample of **2.61a,** in DMSO-d$_6$, while collecting the ^{13}C NMR (100 MHz, DMSO-d$_6$, δ ppm) spectra, in which several signals of compound **2.60a** (blue circles) and of **2.61a** (red circles) highlighted

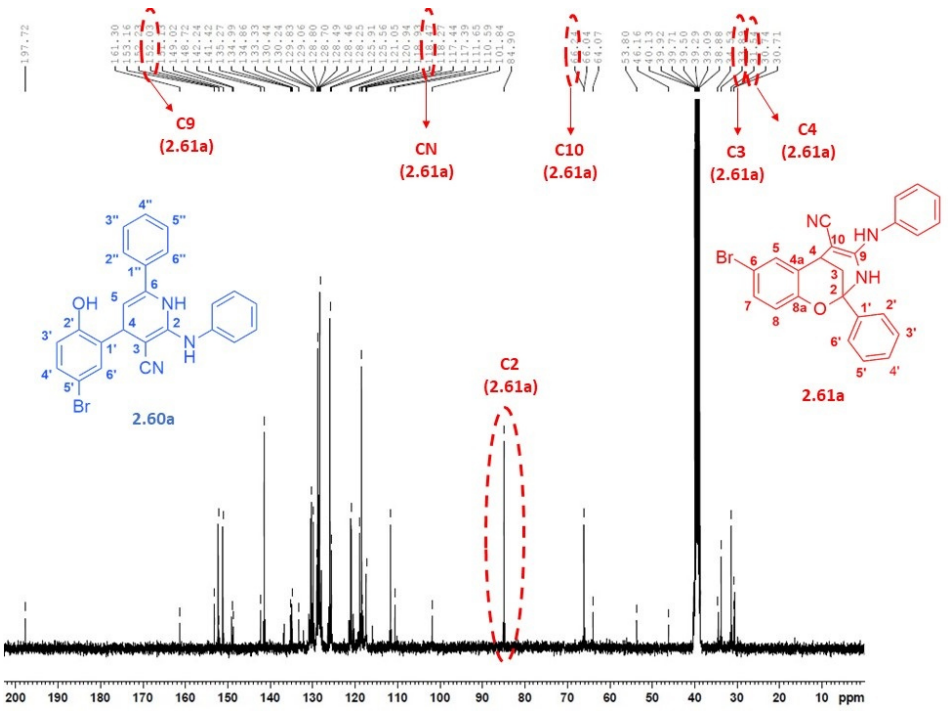
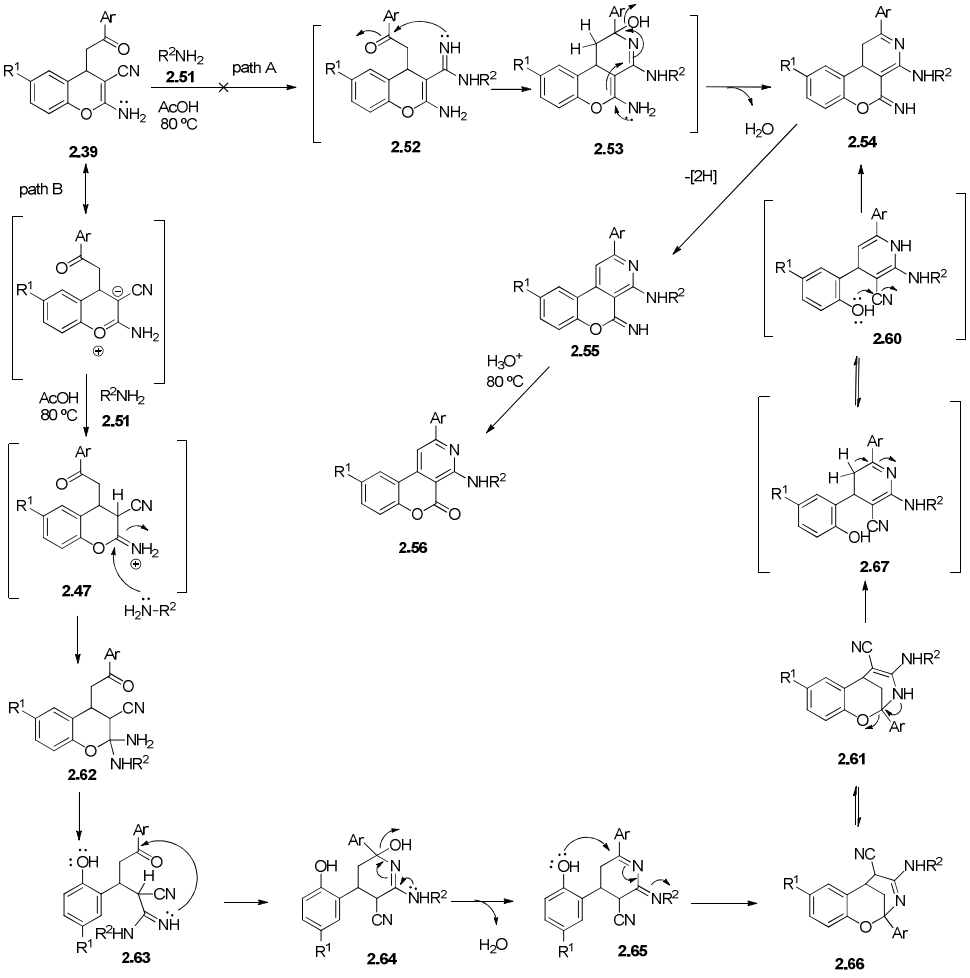


Figure 40: ^{13}C NMR (100 MHz, DMSO-d_6, δ ppm) spectrum of a mixture of compounds **2.60a** and **2.61a**, generated from a sample of **2.61a**, in DMSO-d_6, in which several signals of compound **2.61a** (red circles) highlighted

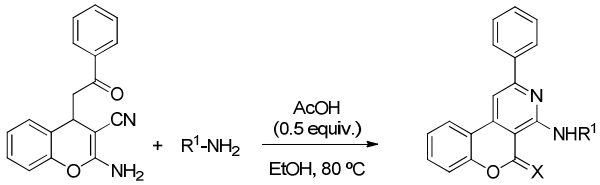


Scheme 26: Proposed mechanism for the formation of compounds **2.55** and **2.56**

Since reactions carried out using 50% aqueous ethanol did not enhanced the formation of imines **2.55**, the reactivity of the chromenes **2.39** with diverse anilines **2.51** using ethanol as sole solvent was then explored (**Tables 33-40**).

The treatment of chromene **2.39a** (R^1= H, R^2= H) with aniline, 4-toluidine, 4-methoxyaniline and 4-bromoaniline provided the imines **2.55**, which were isolated as light-yellow solids in yields ranging from 48% to 68% (**Table 33**). The reaction starts as a suspension that gradually solubilizes and later leads to a new suspension that is filtered. For the reactions involving *p*-toluidine (entry 2) and 3-bromoaniline (entry 4), a slight contamination with the 5-oxo derivative **2.58** was obtained (below 5% of the total amount).

Table 33: Results for the reaction of chromenes **2.39a** with anilines **2.51** (2 equivalents) and acetic acid (0.5 equivalents) in ethanol at 80 °C



2.39a **2.51** (2 equiv.) **2.55** (X=NH) **2.56** (X=O)

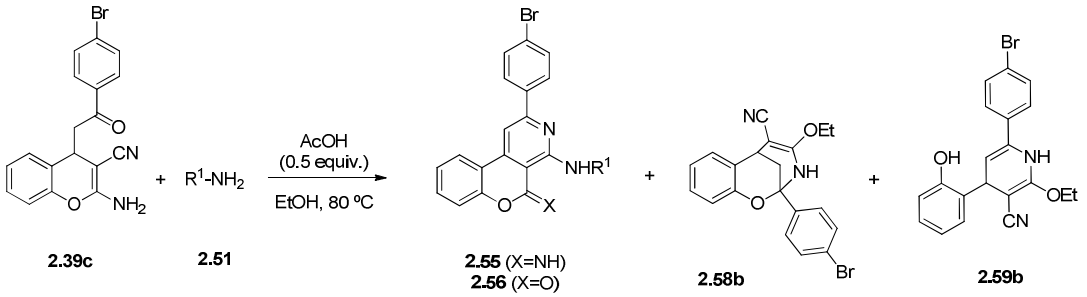
Entry	R^1	t (h)	results			
			products[a]	yield (%)	contamination[a]	%
1	Ph	22	**2.55b**	61	-	
2	4-MeC_6H_4	22.66	**2.55c**	66	**2.56b**	3.6
3	4-OMeC_6H_4	22.25	**2.55d**	68	-	
4	3-BrC_6H_4	22	**2.55e**	48	**2.56c**	4.8

[a]By ^{1}H NMR

The results of the reactions carried out with compound **2.41c** (R^1= H, R^2= Br) are summarized in **Table 34**. This compound showed to be more soluble in EtOH. To accelerate the reaction conditions and therefore avoiding the conversion of the desired imino chromenopyridine **2.55** into lactone chromenopyridine **2.56**, 3 or 4 equivalents of aniline, 4-toluidine, 4-methoxyaniline and 4-aminobenzonitrile were employed. In contrast to compound **2.39a**, the reaction mixture started as a thin suspension that quickly solubilized and resuspended. In this case, a small amount of a yellow solid precipitated after 3 days at -9 °C. However, the higher degree of solubility of chromene **2.39c** seems to be promoting the formation of other products, leading to the formation of complex reaction mixtures. Performing the reaction with 4-

aminobenzonitrile, for 30.25 h, afforded a complex mixture, from where it was possible to identify a set of signals that could be assigned to intermediates **2.58b** and **2.59b.**

Table 34: Results for the reaction of chromenes **2.39c** with anilines **2.51** (3-4 equivalents) and acetic acid (0.5 equivalents) in ethanol at 80 °C



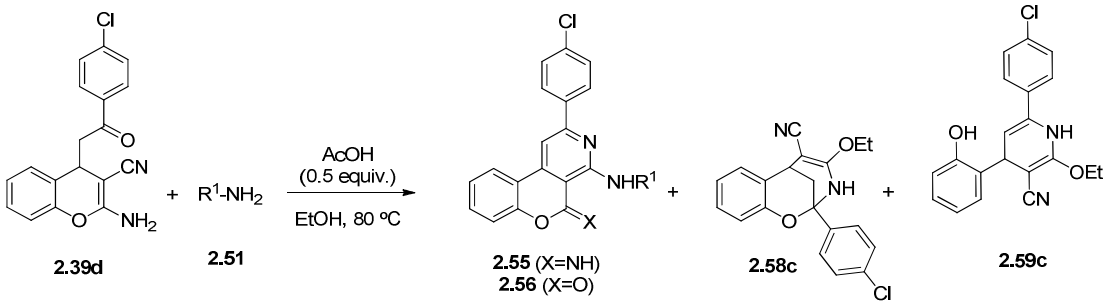
2.39c **2.51** **2.55** (X=NH) **2.56** (X=O) **2.58b** **2.59b**

Entry	R^1	amine (equiv.)	t (h)	results		
				products[a]	ratio[a]	yield (%)
1	Ph	3	14	**2.55f**	-	<5
2	4-MeC_6H_4	3	22	complex mixture	-	-
3	4-$OMeC_6H_4$	3	14h	**2.55g**	-	22
4	4-CNC_6H_4	4	30.25	mixture containing **2.58b** + **2.59b**[a]	7:5/4:4	-

[a]By ^{1}H NMR

The reaction of chromene **2.39d** (R^1= H, R^2= Cl) with aniline, 4-toluidine, 4-methoxyaniline and 4-aminobenzonitrile led to very similar results to those obtained for chromene **2.39c** (**Table 35**). When the desired product **2.55** was isolated, its formation occurred in very low yields and the product was often contaminated with unknown impurities. When 4-methoxyaniline was employed (entry 3), imino chromenopyridine **2.55g** was obtained by simple filtration, with 22% yield. The filtrate was concentrated and resuspended in a small amount of EtOH/Et_2O. After filtering the suspended orange solid, an ^{1}H NMR spectrum was obtained from which lactone choromenopyridine **2.56d** was identified, as well as to the respective precursors **2.61c** and **2.60c**. A subset of signals, related to minor products, are also present, but remain unidentified. This strongly indicates the possible formation of other unidentified side products, which could explain the low isolated yield of **2.55g**. For the reaction involving 4-aminobenzonitrile (entry 4), the ^{1}H NMR spectrum of the collected solid was comparable to that obtained for the reaction with chromene **2.39c** with the same aniline, which indicates that a similar phenomenon is occurring.

Table 35: Results for the reaction of **2.39d** with anilines **2.51** (3-4 equivalents) and acetic acid (0.5 equivalents) in ethanol at 80 °C



2.39d **2.51** **2.55** (X=NH) **2.56** (X=O) **2.58c** **2.59c**

Entry	R^1	amine (equiv.)	t (h)	results			
				products[a]	yield (%)	contamination[a]	%
1	Ph	3	31	**2.55h**	13	**2.56d**	12.5
2	4-MeC_6H_4	3	6.5	**2.55i**	<5	**2.56e**	17
3	4-$OMeC_6H_4$	3	6.5	**2.55j**	8	-	-
4	4-CNC_6H_4	4	25	mixture containing **2.58c** + **2.59c**	-	-	-

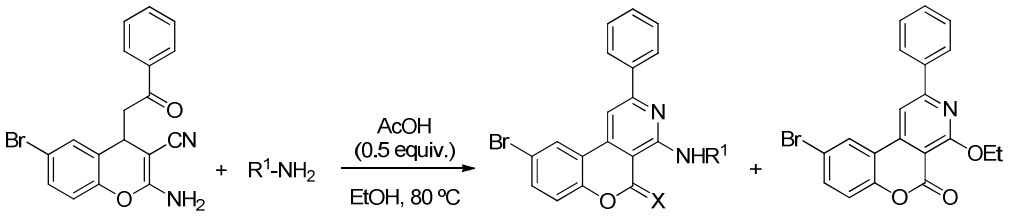
[a] By ^1H NMR

The reactivity of compound **2.39e** (R^1= Br, R^2= H) against a selection of anilines (aniline, *p*-toluidine, 4-methoxyaniline, 4-chloroaniline and 3-bromoaniline) and aliphatic amines such as 2-aminoethan-1-ol under acidic conditions was also studied (**Table 36**). It was expected that the higher nucleophilicity of aliphatic amines would accelerate the reaction, and precipitation of the product from the reaction medium would avoid its permanence, and subsequent evolution, in solution. Unfortunately, the formation of the desired products was not observed. For this reason, the use of aliphatic amines may require further adjustments of the reaction conditions, but this possibility was not further explored.

The results obtained for the more nucleophilic anilines, such as *p*-toluidine and in particular 4-methoxyaniline, not only when chromene **2.39e** was used but as a rule for all compounds **2.39**, confirm that they lead to better yields of the desired imino chromenopyridine **2.55l**. The use of *p*-toluidine led to a mixture of compounds **2.55k** and **2.57a**, in a similar ratio even when the number of equivalents were increased from 2 to 5 and the reaction time was expanded from 22 h to 47 h (entries 4 and 5, Table 35). 4-chloroaniline, in which the chloride would act as an electron-

withdrawing substituent by inductive effect, more than it can contribute as an electron-donating substituent by resonance effect, led to a complex mixture (entry 7, **Table 36**).

Table 36: Results for the reaction of **2.39e** with amines **2.51** (2-5 equivalents) and acetic acid (0.5 equivalents) in ethanol at 80 °C



2.39e **2.51** **2.55** (X=NH) **2.56** (X=O) **2.57a**

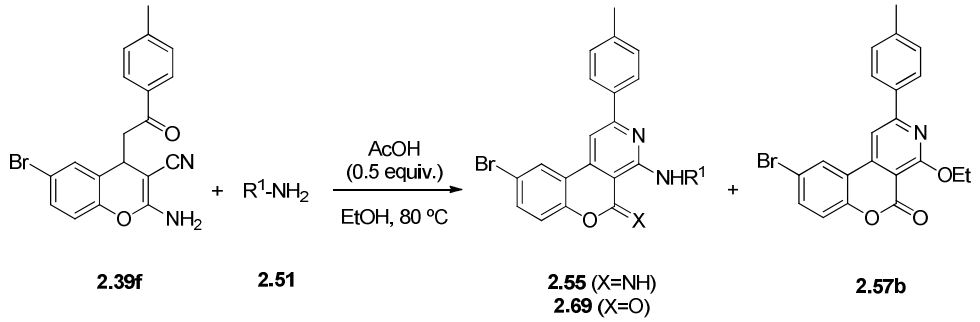
Entry	R^1	amine (equiv.)	t (h)	results				
				products[a]	ratio[a]	yield (%)	contamination[a]	%
1	$(CH_2)_2OH$	2	24	complex mixture	-	-	-	-
2	$(CH_2)_5OH$	2	2	**2.39e**	-	24	-	-
3	Ph	3	22	**2.55a**	-	25	-	-
4	4-MeC_6H_4	3	22	**2.55k + 2.57a**	1/1.2	-	-	-
5	4-MeC_6H_4	5	47	**2.55k + 2.57a**	1/1.3	-	-	-
6	4-$OMeC_6H_4$	2	22	**2.55l**	-	55	**2.56f**	traces
7	4-ClC_6H_4	2	22	complex mixture	-	-	-	-
8	3-BrC_6H_4	2	19	**2.55m**	-	19	-	-

[a]By ^1H NMR

The results of the reaction of chromene **2.39f** (R^1= Br, R^2= Me) with aniline, *m*-toluidine, *p*-toluidine, 4-methoxyaniline, and 3-methoxyaniline, under the aforementioned reaction conditions, afforded the imino chromenopyridines **2.55** in yields ranging from 17% and 37% (**Table 37**). Only the reaction involving *m*-toluidine led to lactone chromenopyridine **2.57b** as the major product and imino chromenopyridine **2.55o** as the minor product (entry 3). For the reactions involving aniline (entry 1) and *p*-toluidine (entry 4), a small contamination with lactone

chromenopyridine **2.56g** for the first case and a small unidentified contamination was observed for the latter.

Table 37: Results for the reaction of **2.39f** with anilines **2.51** (2-3 equivalents) and acetic acid (0.5 equivalents) in ethanol at 80 °C



2.39f **2.51** **2.55** (X=NH) **2.69** (X=O) **2.57b**

Entry	R^1	amine (equiv.)	t (h)	results				
				products[a]	ratio[a]	yield (%)	contamination[a]	%
1	Ph	2	22	**2.55n**	-	17	**2.56g**	6
2	Ph	2	15	**2.55n**	-	15	-	-
3	3-MeC_6H_4	2	21.25	**2.55o + 2.57b**	1/2	-	-	-
4	4-MeC_6H_4	2	21.25	**2.55p**	-	34	unknown	-
5	4-MeC_6H_4	3	22	**2.55p**	-	37	-	-
6	4-$OMeC_6H_4$	2	17.25	**2.55q**	-	32	-	-
7	3-$OMeC_6H_4$	2	21.25	**2.55r**	-	31	-	-

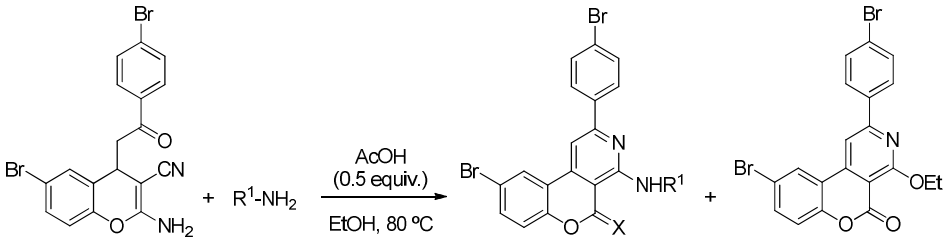
[a]By ^{1}H NMR

Similar results were also obtained for compound **2.39g** (R^1= Br, R^2= Br) with aniline, *p*-toluidine, 4-methoxyaniline, and 3-methoxyaniline (**Table 38**). Thus, for less nucleophilic anilines, such as 3-methoxyaniline (entry 5) and 4-bromoaniline (entry 6), a complex mixture or a mixture containing imino chromenopyridine **2.39x**, traces of lactone pyridines **2.56j** and **2.57c** were obtained. It should be noted that the most prevalent contamination observed for these reactions involved the formation of lactone chromenopyridine **2.57c**, where ethanol is competing as a nucleophile. Compound **2.57c** was identified from the mixture obtained from the reaction described in entry 5. The structural identification, by NMR, of compound **2.57c** from this mixture

allowed for the confirmation that the ethoxy group is indeed part of the structure and was neither solvent traces nor co-crystallized ethanol molecules, as the CH_2 moiety correlates, by HMBC NMR spectroscopy, with C4 (δ ppm) (**Figures 41** and **42**).

Compounds **2.57** are much likely formed due to nucleophilic competition between the aniline **2.51** used and ethanol, which seems to be occurring more extensively when the solubility of the used chromene **2.39** decreases. This competition may also be favoured when less nucleophilic or less soluble anilines **2.51** are employed. The possible replacement of the existing secondary aniline at position C4 in either imino chromenopyridines **2.55** and/or lactone pyridines **2.56** by nucleophilic reagents such as ethanol, or vice-versa, was not further explored.

Table 38: Results for the reaction of **2.39g** with anilines **2.51** (2-3 equivalents) and acetic acid (0.5 equivalents) in ethanol at 80 °C



2.39g **2.51** **2.55** (X=NH) **2.56** (X=O) **2.57c**

Entry	R^1	amine (equiv.)	t (h)	results				
				products[a]	ratio[a]	yield (%)	contam.[a]	%
1	Ph	2	72	**2.55s** + **2.56h** **2.57c**	2/0.11/0.33	-	-	-
2	4-MeC_6H_4	2	22	**2.55t** + **2.56i** + **2.57c**	4.4/0.4/0.5	-	-	-
3	4-MeC_6H_4	3	35.25	**2.55u**	-	17	-	-
4	4-$OMeC_6H_4$	2	22	**2.55v**	-	56	**2.57c**	11
5	3-$OMeC_6H_4$	2	39	**2.55x + 2.56j + 2.57c**	1/traces/0.7	-	-	-
6	4-BrC_6H_4	2	22	complex mixture	-	-	-	-

[a]By ^{1}H NMR

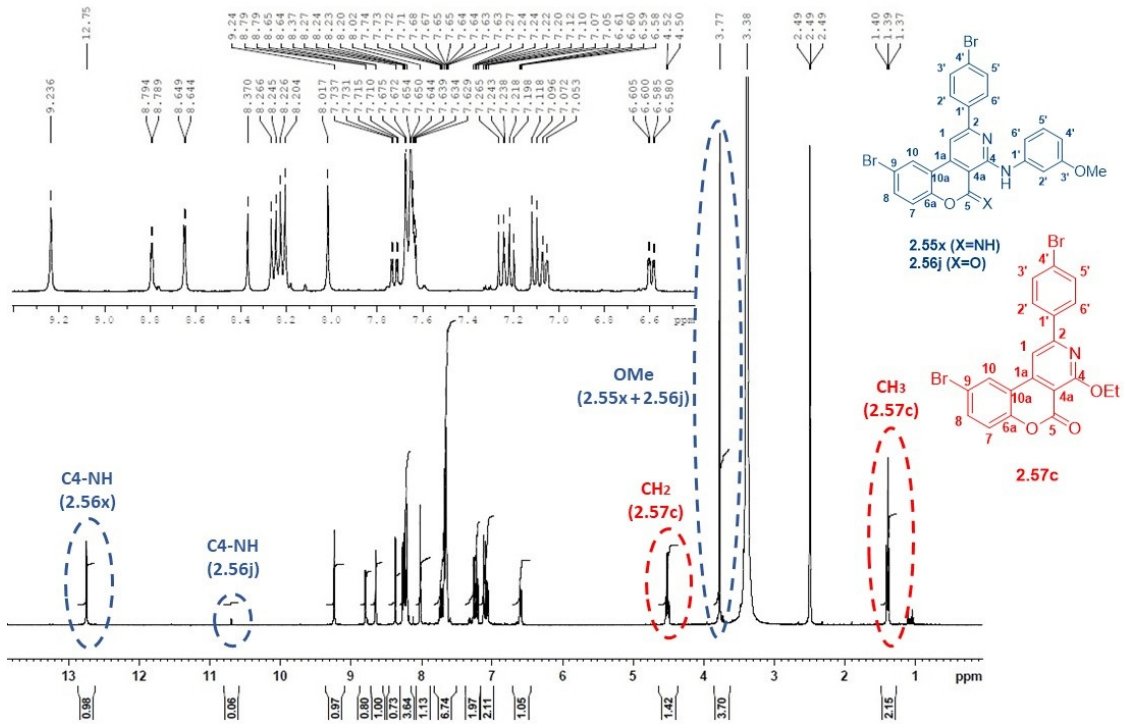


Figure 41: ^{1}H NMR (400 MHz, DMSO-d$_6$, δ ppm) spectrum of the crude solid obtained from the reaction described in **Table 38** (entry 5), with the identification of several signals belonging to compounds **2.55x**, **2.56j** and **2.57c**

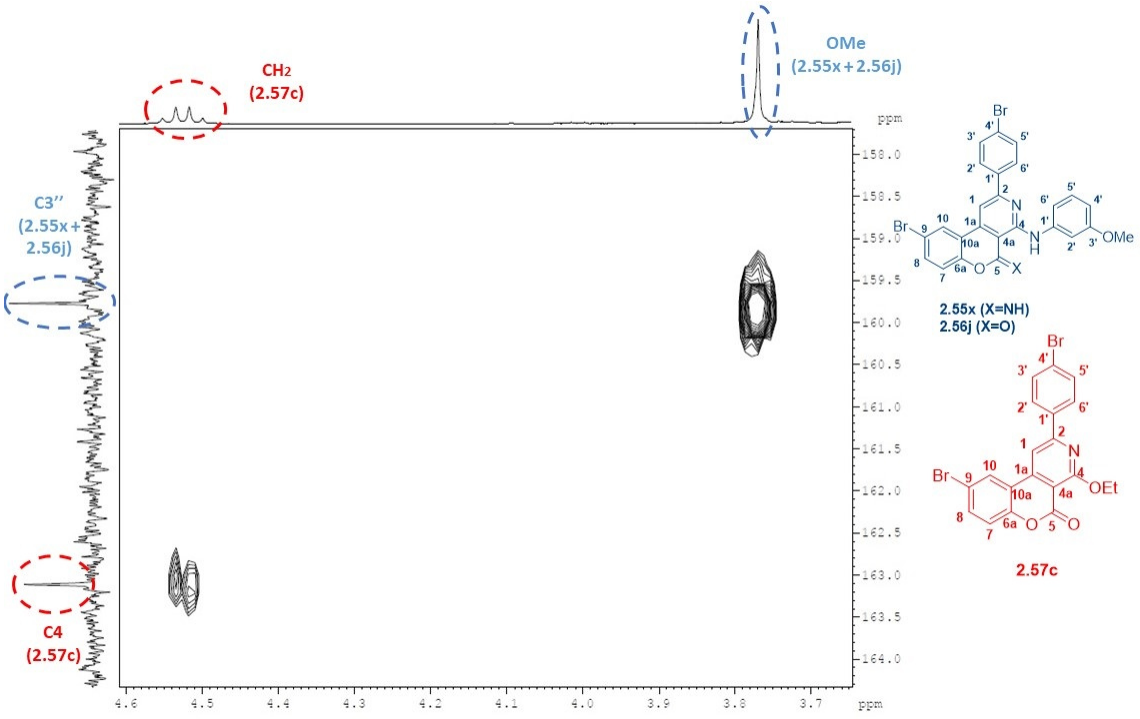
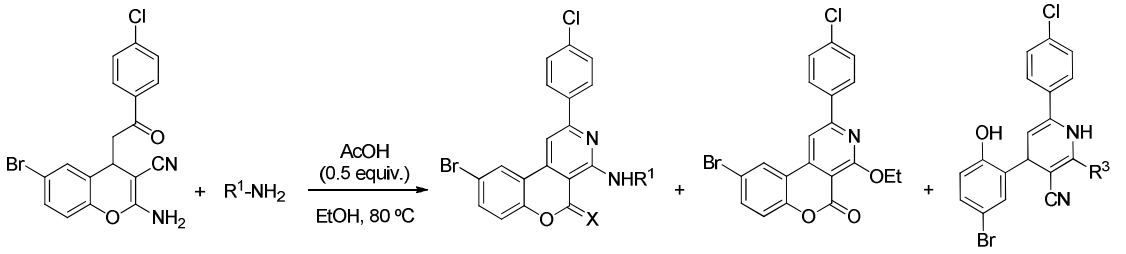


Figure 42: HMBC NMR (100 MHz, DMSO-d$_6$, δ ppm) spectrum of the crude solid obtained from the reaction described in **Table 38** (entry 5), with the identification of the signals belonging to compounds **2.55x**, **2.56j** and **2.57c**

Chromene **2.39h** (R^1= Br, R^2= Cl) was also used in the reaction with aniline, *p*-toluidine, *m*-toluidine, 4-methoxyaniline, and 3-methoxyaniline (**Table 39**). For most of the reactions performed (entries 1-5), a mixture of the desired imino chromenopyridine **2.55** was identified in a mixture with either its corresponding precursor dihydropyridine **2.60** or with lactone chromenopyridine **2.57d**, formed by the nucleophilic attack of ethanol. This indicates that an extensive nucleophile competition may be occurring when 2 equivalents of the aniline derivative are used, specifically with aniline (entry 1) and *p*-toluidine (entry 3). The reaction was also performed with 3 equivalents of aniline (entry 2) and *p*-toluidine (entry 5), with similar results. When comparing the same amine (*p*-toluidine, entries 4 and 5), in the reactions where 2 equivalents were used in a reaction that lasted for 48 h (entry 4) and 3 equivalents were used in a reaction that lasted for 20 h (entry 5), it is possible to observe that the ratios of formation of imino chromenopyridine **2.55a'** and lactone chromenopyridine **2.57d**, collected in the mixture and analysed by ^{1}H NMR, were comparable.

Table 39: Results for the reaction of **2.39h** with anilines **2.51** (2-3 equivalents) and acetic acid (0.5 equivalents) in ethanol at 80 °C



2.39h **2.51** **2.55** (X=NH) **2.57d** **2.60** (R^3=NHR^3)

Entry	R^1	amine (equiv.)	t (h)	results				
				products[a]	ratio[a]	yield (%)	contamin.[a]	%
1	Ph	2	38	**2.55y** + **2.57d**	2/1.6	-	-	-
2	Ph	3	27	**2.55y** + **2.60b**	2/1.6	-	-	-
3	3-MeC_6H_4	2	21	**2.55z** + **2.57d**	1.7/1	-	-	-
4	4-MeC_6H_4	2	48	**2.55a'** + **2.60c**	1/3	-	-	-
5	4-MeC_6H_4	3	20	**2.55a'** + **2.60c**	2/2.4	-	-	-

6	4-$OMeC_6H_4$	2	14.66 + 6.5 + 6[b]	**2.55b'**	-	21	**2.60d**	traces
7	3-$OMeC_6H_4$	2	39	**2.55c'**	-	<5	-	-

[a]By ^{1}H NMR; [b]The reaction was stopped two times, with the suspended product being filtered and an ^{1}H NMR spectrum was collected from the crude product. Then, the reaction continued for an additional period of time.

The experiment described in entry 6 was performed differently from those presented up to this point: (i) after stirring at 80 °C for 14.66 h, the suspended solid was isolated, and a sample of the obtained crude product was analysed by ^{1}H NMR (**Figure 43**); (ii) the solid was resuspended in the filtrate and proceeded to stir at 80 °C for an additional 6 h. After this time, the suspended solid was isolated, and a sample of the obtained crude product was once again analysed by ^{1}H NMR (**Figure 44**); (iii) the solid was resuspended in the filtrate and proceeded to stir at 80 °C for an additional 6 h. After this time, the suspended solid was isolated, and a sample of the obtained crude product was analysed by ^{1}H NMR a third time (**Figure 45**). The ^{1}H NMR spectra demonstrate that the reaction was not completed neither after 14.66 h (**Figure 43**) nor after 6 additional hours (**Figure 44**), with a mixture of imino chromenopyridines **2.55b'**, dihydropyridine **2.60d** and spiro derivative **2.61b** being identified in both cases. The product collected after 26.66 h of reaction appeared, by ^{1}H NMR spectroscopy, as a sole product, identified as imino chromenopyridines **2.55b'** (η= 21%), with traces of dihydropyridine **2.60d** (**Figure 45**).

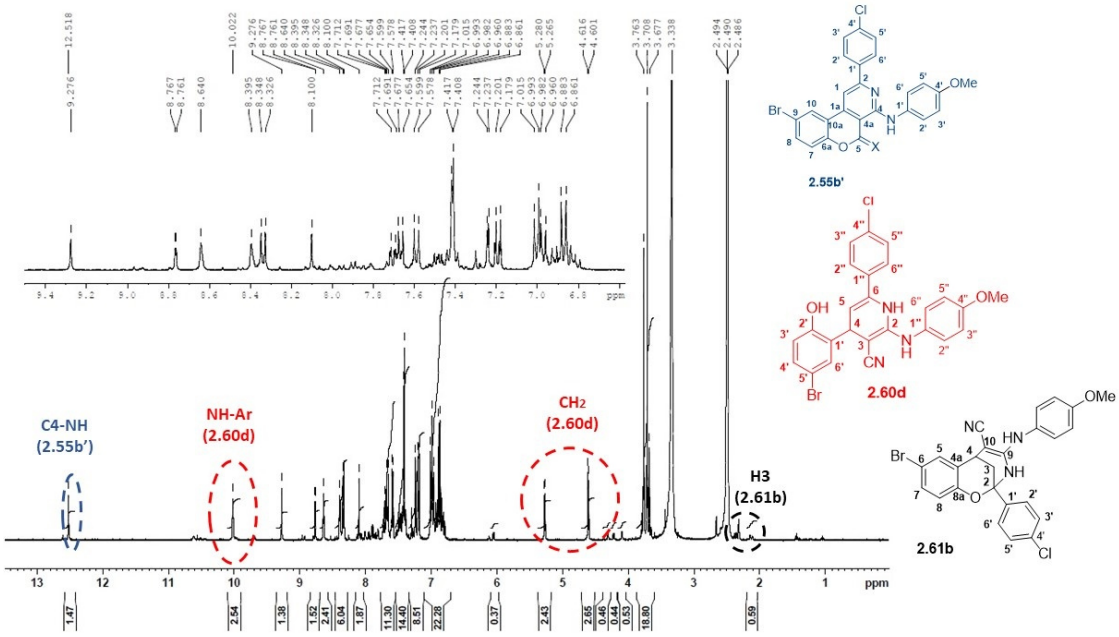


Figure 43: ^{1}H NMR (400 MHz, DMSO-d_6, δ ppm) spectrum recorded form the crude product of the reaction described in entry 6 (**table 39**) after 14.66 h of reaction. Among the observed mixture, it is possible to observe the same pattern belonging to compounds **2.55b'** (blue circles), **2.60d** (red circles) and **2.61b** (black circles circles)

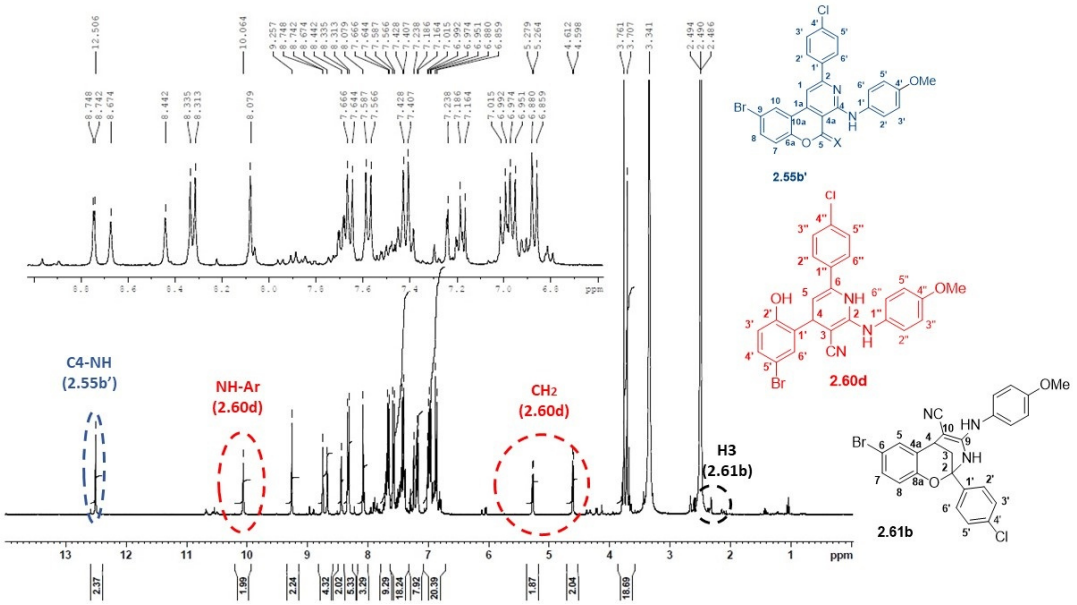


Figure 44: ^{1}H NMR spectrum (400 MHz, DMSO-d$_6$, δ ppm) recorded form the crude product of the reaction described in entry 6 (table 39) after 20.66 h of reaction. Among the observed mixture, it is possible to observe the same pattern belonging to compounds **2.55b'** (blue circles), **2.60d** (red circles) and **2.61b** (black circles circles)

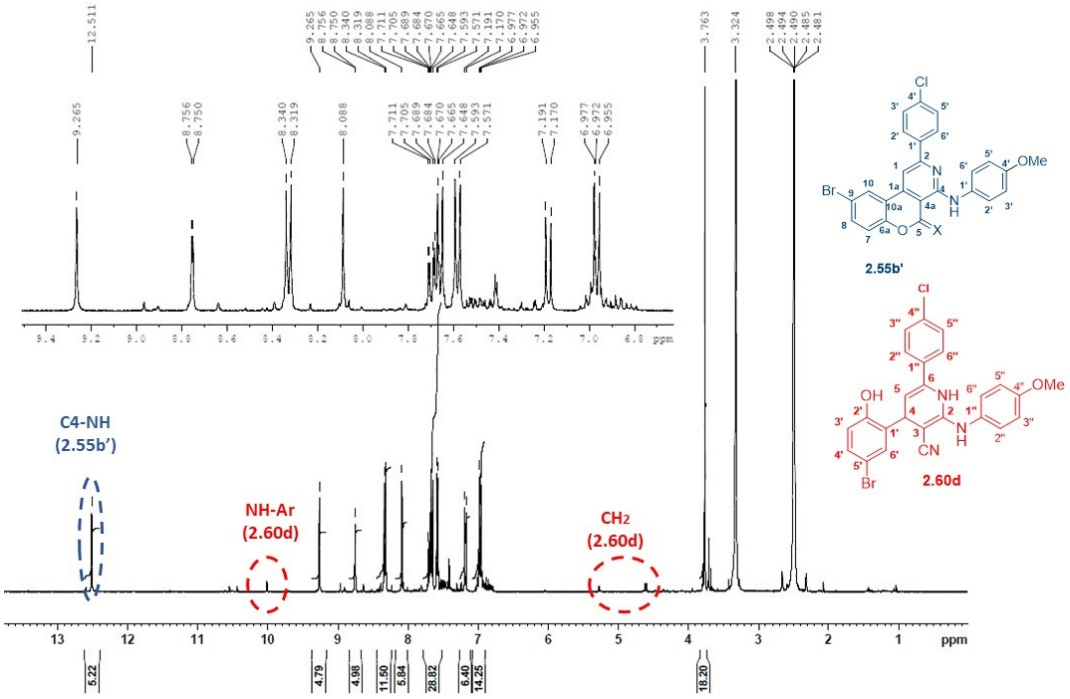
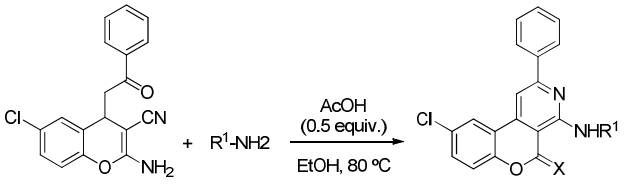


Figure 45: ^{1}H NMR (400 MHz, DMSO-d$_6$, δ ppm) spectrum recorded form the crude product of the reaction described in entry 6 (table 39) after 26.66 h of reaction. Among the observed mixture, it is possible to observe the same pattern belonging to compounds **2.55b'** (blue circle) and traces of **2.60d** (red circles)

In general, the reactions involving compound **2.39i** (R^1= Cl, R^2= H) with aniline, *p*-toluidine, *m*-toluidine, 4-methoxyaniline, and 3-bromoaniline afforded good results, with a series of imino chromenopyridines **2.55** being synthesized with yields ranging from 16-55% and with minor impurities (**Table 40**). In general, similar results to those obtained for compounds **2.39b** and **2.39f**, where a series of chromenopyridines **2.55** derivatives could also be prepared with minor or no contamination. This seems to reinforce the idea that the solubility of the starting materials greatly influences the course of the reaction.

Table 40: Results for the reaction of **2.39i** with anilines **2.51** (2-3 equivalents) and acetic acid (0.5 equivalents) in ethanol at 80 °C

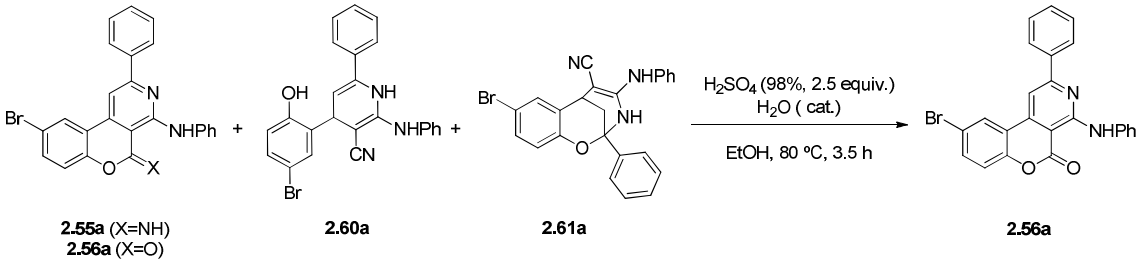


2.39i **2.51** **2.55** (X=NH) **2.56** (X=O)

Entry	R^1	amine (equiv.)	t (h)	results				
				product[a]	ratio[a]	yield (%)	contamination[a]	%
1	Ph	2	88	**2.55d'**	-	16	**2.56k**	6
2	Ph	3	22	**2.55d'**	-	55	-	-
3	4-MeC_6H_4	2	22.25	**2.55e'** + **2.56l**	1.5/1	-	-	-
4	4-MeC_6H_4	3	21	**2.55f'**	-	22	-	-
5	4-$OMeC_6H_4$	2	39.25	**2.55g'**	-	55	-	-
6	3-BrC_6H_4	2	15h	complex mixture	-	-	-	-

[a]By ^{1}H NMR

The best reaction conditions for the selective preparation of the lactone pyridines **2.56** from imino chromenopyridines **2.55** was also explored. The use of concentrated H_2SO_4 as catalyst, instead of AcOH, was also attempted but led to the formation of complex mixtures. Remarkably, when a mixture containing compounds **2.55a**, **2.56a**, **2.60a** and **2.61a** was used the reaction was successful. Thus, the heating at 80 °C for 3.5 h of a solution of the mixture in ethanol in the presence of approximately 2.5 equivalents of concentrated H_2SO_4 and a catalytic amount of water afforded compound **2.56a**, by simple filtration, with 26% yield (**Scheme 27**).



2.55a (X=NH) **2.56a** (X=O) **2.60a** **2.61a** **2.56a**

Scheme 27: Conversion of a mixture of compounds **2.55a**, **2.56a**, **2.60a** and **2.61a** into the desired compound **2.56a** by heating at 80 °C with concentrated H_2SO_4.

In conclusion, it is possible to affirm that:

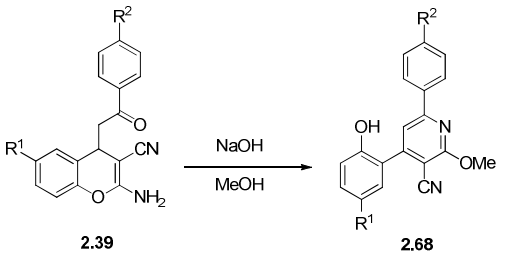
1) A new synthetic method for the preparation of novel 5-imino-2-aryl-*N*-substituted-5*H*-chromeno[3,4-*c*]pyridin-4-amines **2.55**, with yields ranging from 5-68%, has been discovered.
2) The best reaction conditions to afford imino chromenopyridines **2.55** involved the use of 2-4 equivalents of the appropriate aniline, 0.5 equivalents of AcOH, ethanol as solvent and heating at 80 °C.
3) The reaction mechanism for the synthesis of **2.55** would involve spiro derivatives **2.61** and dihydropyridines **2.60** in a sequential fashion, with these compounds have been successfully identified by NMR spectroscopy.
4) It is possible to generate the lactone pyridine **2.56** by a two-step procedure involving the formation of a mixture of imino chromopyridines **2.55** and lactone pyridines **2.56** with their precursors dihydropyridine **2.60** and spiro derivatives **2.61**, followed by heating at 80 °C with concentrated H_2SO_4.

Reactivity of 2-amino-4-(2-oxo-2-arylethyl)-4*H*-chromene-3-carbonitriles in aqueous base

The observed competition between nucleophiles (anilines *vs* ethanol), during the formation of imino chromenopyridines **2.55**, brought the idea of developing new synthetic pathways involving other types of nucleophiles as a way to expand the chemical space. It was then proposed that compounds **2.39** could also engage in ring-opening processes, under basic conditions, and that the nucleophile could be the used solvent itself, in a similar mechanism to that verified when aromatic amines were used (**Scheme 26**, page 103). To test this possibility, a selection of reactions was performed under various experimental conditions, and the results are presented in

Table 41. The goal was to study the effect of a nucleophilic solvent (namely MeOH or EtOH) on the evolution of **2.39** to different products that incorporate the solvent.

Table 41: Reaction conditions and results obtained from the reaction of compounds **2.39** with NaOH/MeOH



2.39 **2.68**

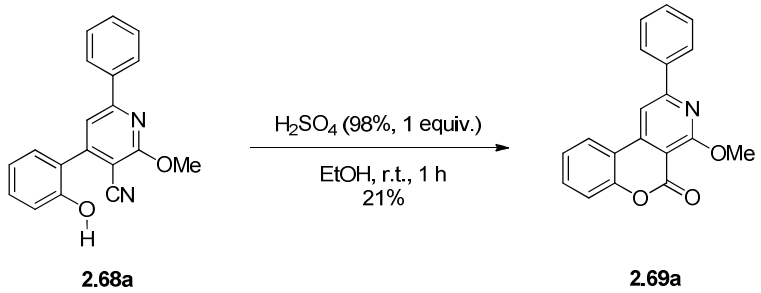
Entry	2.39			NaOH (equiv.)	Ratio (NaOH/MeOH)	T (°C)	t (h)	results	
	R^1	R^2	C(M)[a]					product	η (%)
1	H	H	0.5	0.1	1/1	r.t.	99	**2.39a**	80
2	H	H	0.35	5.8	1/1	r.t.	17.5	**2.68a**	10
3	H	H	0.22	4.6	1/2	r.t.	64	**2.68a**	21
4	Br	H	0.20	9.8	1/1	80	0.25	degradation	-
5	Br	H	0.20	9.8	1/1	r.t.	27	**2.68b**	35
6	Br	H	0.20	9.8	1/1	r.t.	41	**2.68b**	46

[a]Concentration of the starting material

From the results presented in **Table 41**, there are some conclusions that can be drawn:

- Among the reactions performed with chromene **2.39a** (entries 1-3), it can be concluded that using lower NaOH equivalents (0.1 equivalents, entry 1 vs 5.8 and 4.6, entries 2 and 3), even for a longer reaction time than the other two experiments (99 h vs 17.5 and 64 h), is not sufficient to promote the conversion of chromene **2.39a** into the desired pyridine **2.68a**, as mainly no reaction was observed and the starting material **2.39a** was isolated with 80% yield. However, by increasing the equivalents of NaOH the desired product **2.68a** can be obtained in low yields (entries 2 and 3).
- Comparing the reaction that involved **2.39e** (entries 4-6), the best results are obtained when the reaction is performed at room temperature and using 9.8 equivalents of NaOH. Under these conditions, the desired product **2.68b** can be obtained up to 46% yield. High temperatures (80 °C) mainly provided product degradation after 0.25 h of reaction (entry 4). Longer reaction times slightly increased the reaction from 35% (entry 5) to 46% (entry 6).

It was found that pyridines **2.68a** can be transformed into lactone pyridine **2.69a** by acid-catalysed intramolecular cyclization with a yield of 21% (**Scheme 28**).



2.68a **2.69a**

Scheme 28: Synthesis of lactone pyridine **2.69a** by acid-catalysed intramolecular cyclization of pyridine **2.68a**

The formation of lactone pyridine **2.69a** was corroborated by NMR spectroscopy (**Figures 46 and 47**). The ^{1}H NMR spectrum of **2.69a** possesses two distinctive singlets at about δ4.14 ppm and δ8.48 ppm, attributed to the H1 hydrogen atom and the methoxy group, respectively (**Figure 46**). The most characteristic signals in its ^{13}C NMR spectrum are the signals at δ163.63 ppm (C4), δ158.35 ppm (C2) and δ155.86 ppm (C5) (**Figure 47**).

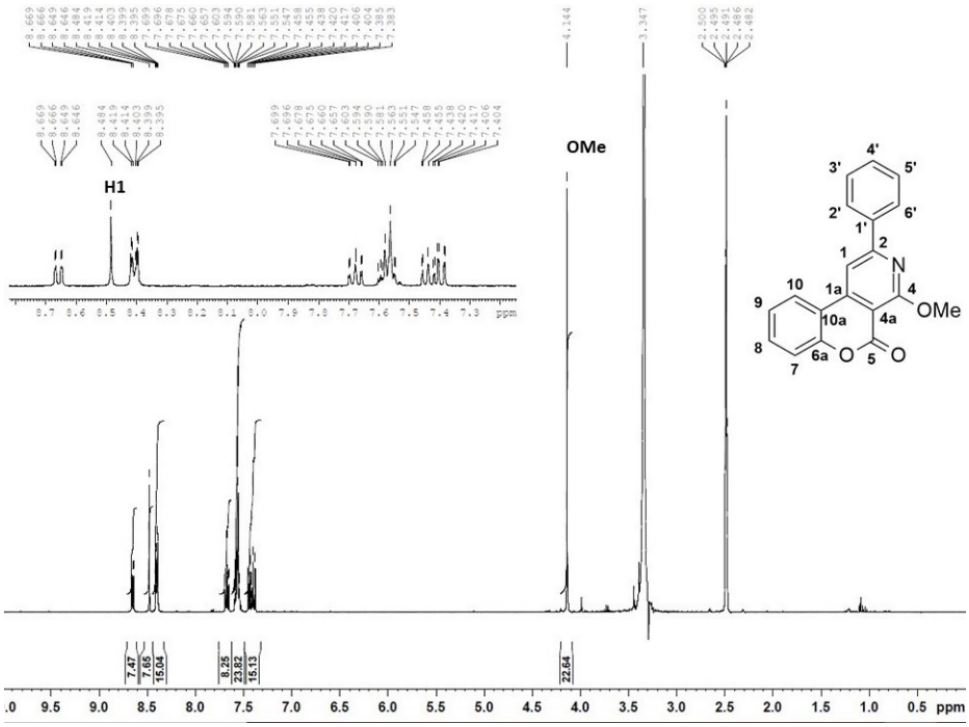


Figure 46: ^{1}H NMR (400 MHz, DMSO-d_6, δ ppm) spectrum of compound **2.69a**, in which two signals are highlighted

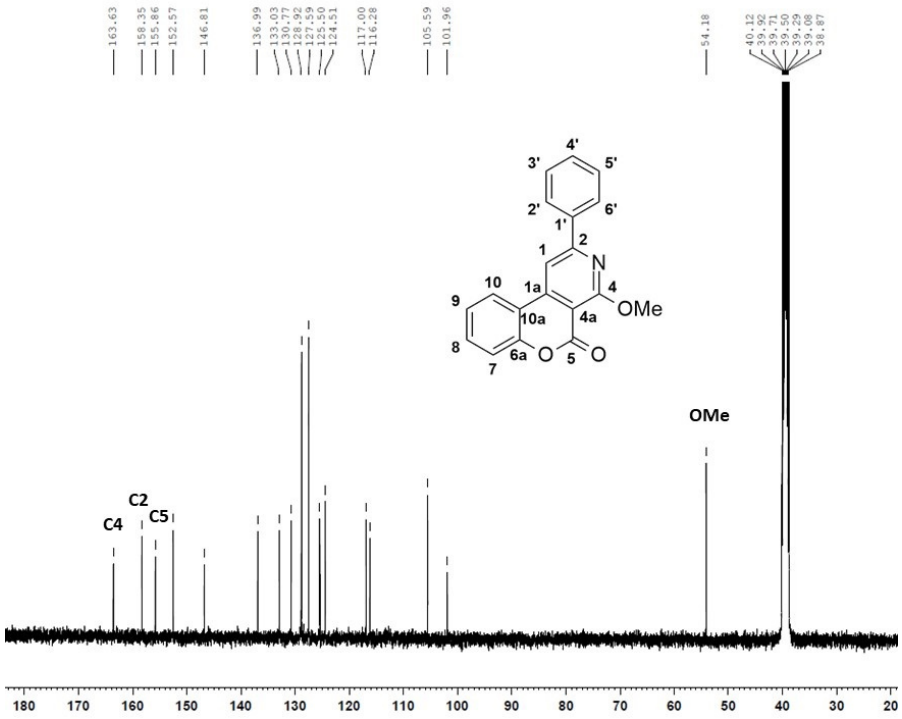
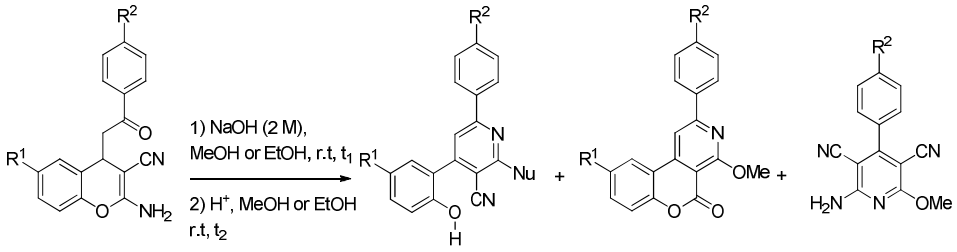


Figure 47: ^{13}C NMR (100 MHz, DMSO-d_6, δ ppm) spectrum of compound **2.69a**, in which several signals are highlighted

To attempt the development of a one-pot methodology that afforded lactone pyridines **2.69** from chromenos **2.39** by a two-step procedure, involving (i) chromene ring-opening in aqueous basic conditions, and subsequent (ii) acid-catalysed chromene ring-closing step, a series of experiments were performed (**Table 42**).

Table 42: Experimental conditions used to perform the one-pot synthesis of compounds **2.69**



2.39 | **2.68** (Nu= OMe) **2.70** (Nu= OEt) | **2.69** | **2.71**

Entry	2.39		solvent	Nu	reaction time		results[a]		
	R^1	R^2			t_1	t_2		ratio	η(%)[b]
1	H	H	MeOH	MeO	0.75	4	**2.68a** + **2.71a**	3/1	-
2	H	Me	MeOH	MeO	3.75	4	**2.71b**	-	10

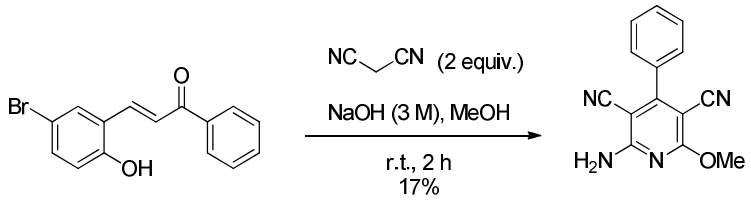
3	H	Br	MeOH	MeO	5.25	7	mixture containing **2.68c** and **2.71c**	-	-
4	Br	H	MeOH	MeO	62	26	complex mixture	-	-
5	Br	H	MeOH	MeO	1.33	0.33	**2.69b**	-	38
6	Br	Me	MeOH	MeO	15	3.5	**2.68d** + **2.71d**	3/2	-
7	Br	Br	MeOH	MeO	5.25	7	**2.68e** + **2.71e**	2/1	-
8	Br	Cl	MeOH	MeO	2	1	**2.68f** + **2.71f**	7/4	-
9	Br	Cl	MeOH	MeO	5.25	7	**2.68g** + **2.71g**	2/1	-
10	Cl	H	MeOH	MeO	14	3.66	complex mixture	-	-
11	Cl	H	EtOH	EtO	2	1.2	**2.70a**	-	84

[a]By ^{1}H NMR; [b]Post-recrystalyzation yield (EtOH/n-hexane 1:1)

The results presented in **Table 42** show that:

- The tandem process is less efficient than the stepwise process, affording in most of the assays mixtures of the base-hydrolysed compounds, pyridines **2.68**, and a new compound identified as pyridine **2.71**.
- The yields are generally poor and a careful selection of the reaction conditions (concentration of NaOH, volume ratio of base/alcohol and reaction time) is required and should be optimized for each starting material **2.39**.

The formation of pyridines **2.71**, containing the acetophenone moiety in the starting material, led us to propose that these pyridines could have been generated through other reaction pathways in which the α,β-unsaturated carbonyl compounds **2.37** could be involved (**Scheme 29**). For this reason, in a separate experiment, compound **2.71a** was prepared by treatment of compound **2.37e** (R^1= Br, R^2= H) with 2 equivalents of malononitrile in a (1:6) mixture of NaOH (3 M)/MeOH and stirring for 2 h at room temperature to afford pyridine **2.71a** as a white solid by simple filtration (η= 17%) (**Scheme 29**). The formation of this compound was corroborated by NMR (**Figures 48** and **49**), which confirms the structure previously assigned to the product detected in the experiments described in **Table 42**.



2.37e **2.71a**

Scheme 29: Synthesis of pyridine **2.71a** from compound **2.37e** and malononitrile

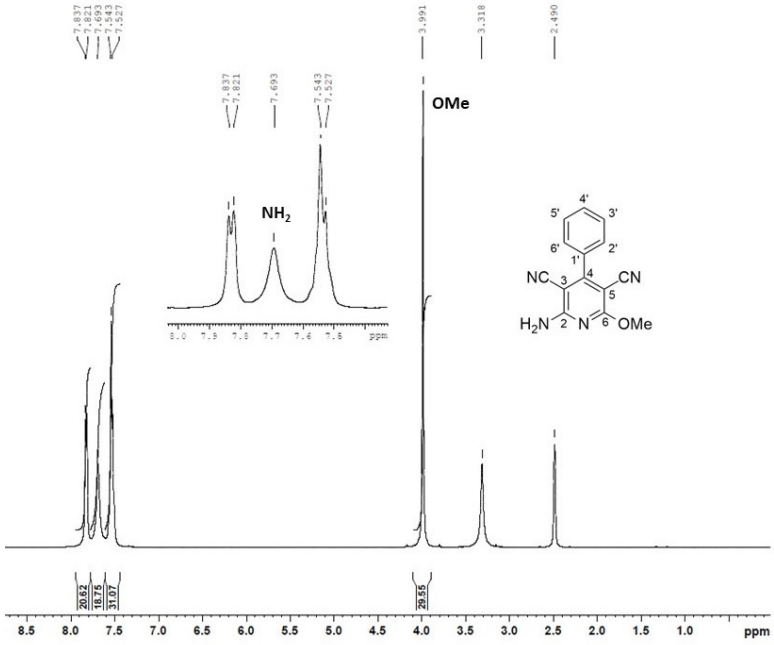


Figure 48: ^{1}H NMR (400 MHz, DMSO-d$_6$, δ ppm) spectrum of compound **2.71a**, in which two signals are highlighted

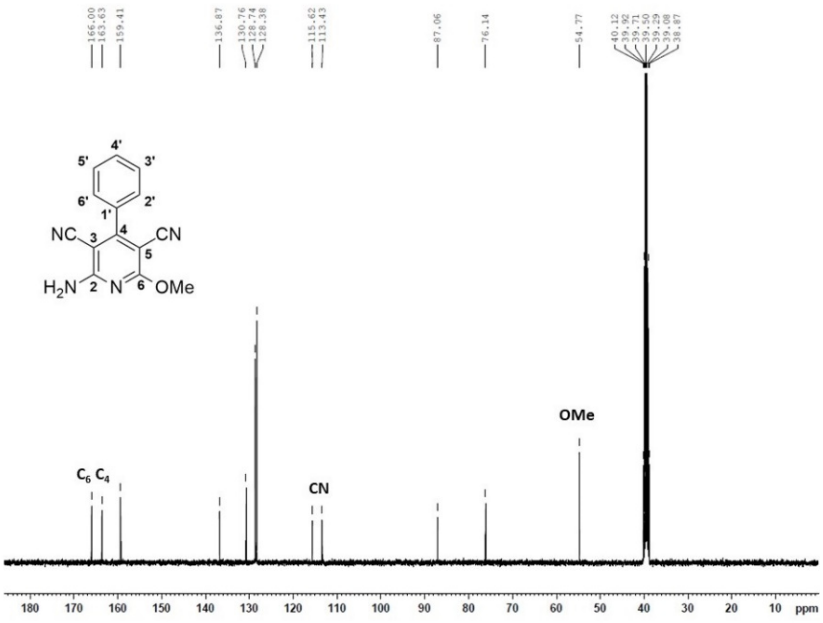
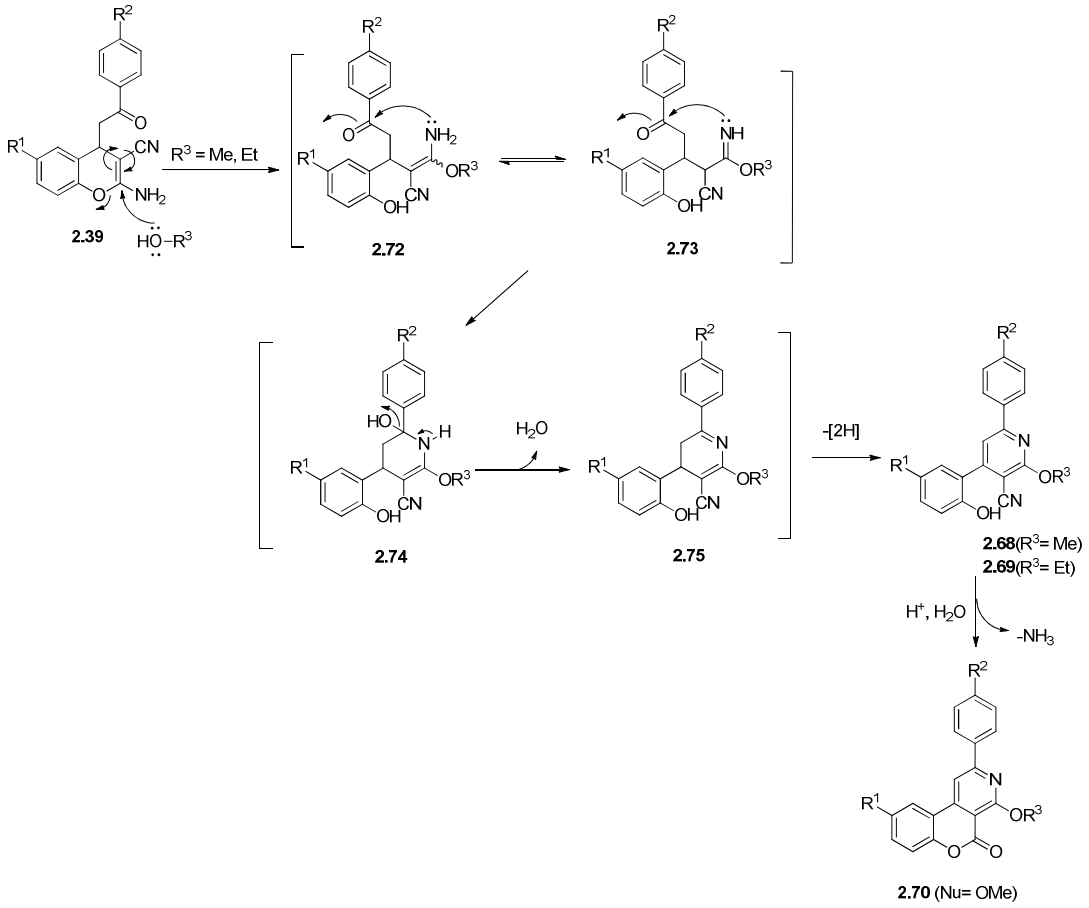


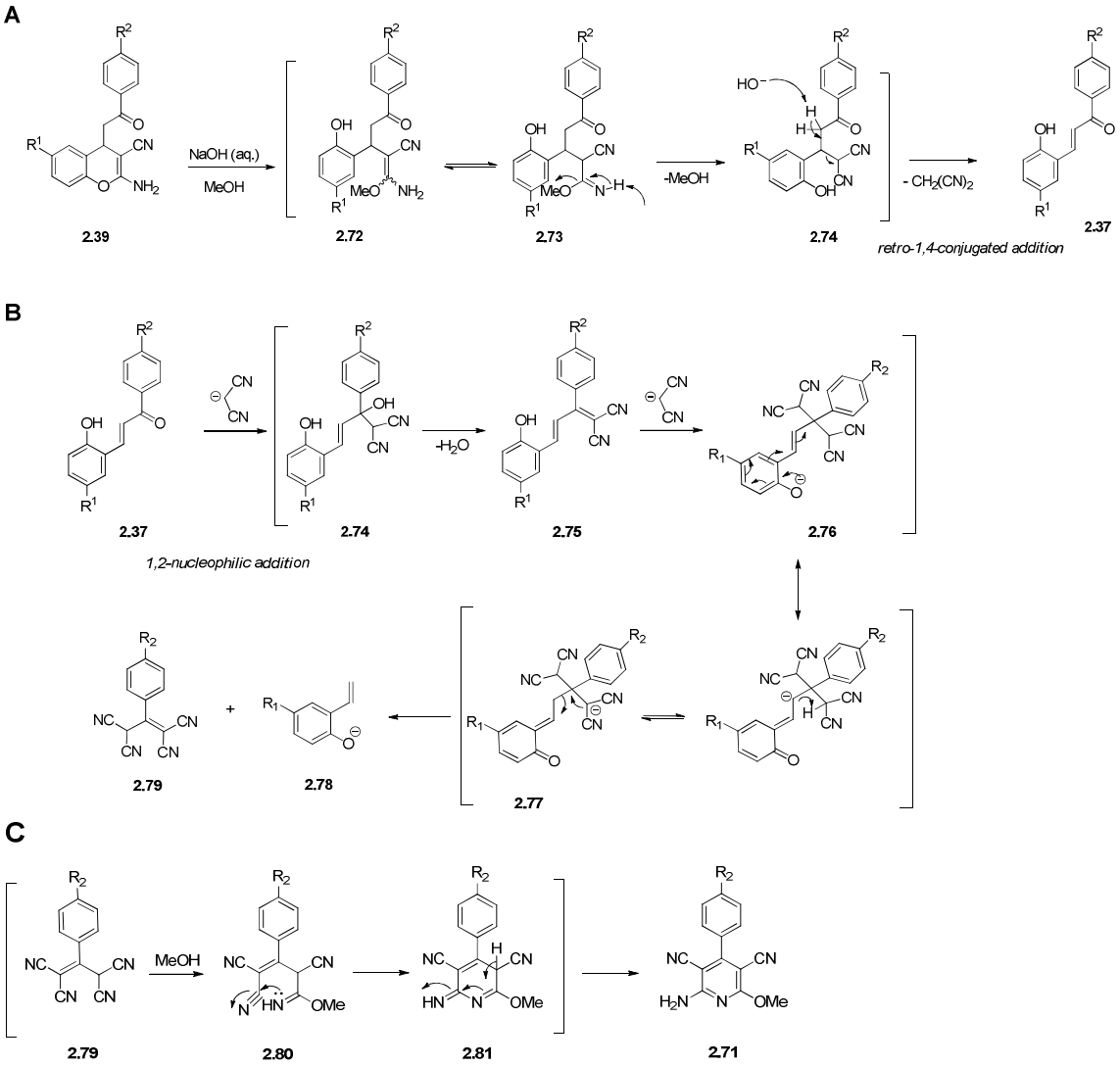
Figure 49: ^{13}C NMR (100 MHz, DMSO-d$_6$, δ ppm) spectrum of the isolated compound **2.71a**, in which several signals highlighted

The formation of compounds **2.68-2.70** proceeds through an ANRORC-type (Addition of the Nucleophile, Ring Opening and Ring Closure) mechanism (**Scheme 30**).



Scheme 30: Plausible ANRORC-type mechanism for the formation of compounds **2.68** (R^3=Me), **2.69** (R^3=Et) and **2.70** (R^3=Me) via a three-step procedure involving (i) addition of the nucleophile, ring-opening, and ring-closure; (ii) lactonization; and (ii) aromatization.

Compounds **2.71** result from a more complex reaction pathway, where the ring-opening process that follows nucleophilic attack at C2 of chromene **2.39**, culminates with the elimination of malononitrile. Two equivalents are required for the formation of **2.79** from the α,β-unsaturated carbonyl compound **2.37**, through an elaborate mechanism, which finally leads to the formation of pyridine **2.71** (**Scheme 31**). The formation of complex reaction mixtures often observed when temperature or reaction time were increased suggests that compound **2.37** may evolve through different reaction pathways in the presence of aqueous base, generating other unidentified products.



Scheme 31: Plausible mechanism for the formation of compounds **2.71** from chromenes **2.39** by treatment with 2 equivalents of malononitrile and NaOH (3 M) in MeOH, which include chromene ring-opening and retro Michael addition for the regeneration of the α,β-unsaturated ketone **2.37** (**A**), formation of the intermediate **2.79** (**B**) and pyridine **2.71** synthesis (**C**)

In conclusion:

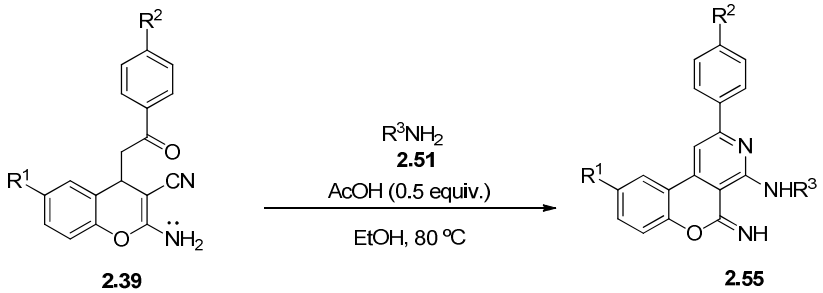
1) Chromenes **2.39** react in aqueous NaOH/alcoholic systems to originate diverse reaction products that, to the best of our knowledge, involve ring-opening and ring-closing processes involving its carbonyl group of the 4-(2-oxo-2-arylethyl) moiety.
2) The mechanism proposed in **Scheme 31** was supported by the results obtained when performing the reaction of α,β-unsaturated carbonyl compound **2.37e** with 2 equivalents of malononitrile in aqueous NaOH/MeOH mixture, where pyridine **2.71a** was isolated. This strongly points to the possibility of compounds **2.39** following several reaction pathways when

in the presence of NaOH, and possibly generating several other unidentified products (apart from compounds **2.71**).

3) Nevertheless, compounds **2.68a-b**, **2.69a-b**, **2.70a** and **2.71-ab** were isolated as pure products and underwent physical, analytical and spectroscopical characterization.
4) To successfully design a synthetic procedure for selectively produce compounds **2.68** and/or **2.69**, further development of the reaction conditions is necessary. In particular, the balance between solubility and reaction rate, which is delicate, must be carefully controlled to avoid the formation of side products.
5)

Reactivity of 2-amino-4-(2-oxo-2-arylethyl)-4*H*-chromene-3-carbonitriles with phenylhydrazine

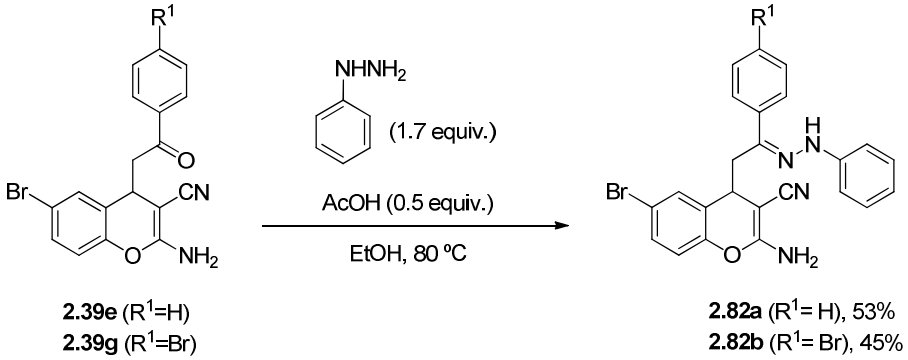
In an attempt to prepare imino chromomenopyridines **2.55** and lactone pyridines **2.56** from chromenes **2.39** using hydrazines as nucleophile, instead of amines as described in previous sections, compounds **2.39** were reacted with phenylhydrazine under similar conditions to those tested for other primary aromatic amines (**Scheme 32**).



Scheme 32: Synthesis of imino chromenepyridines **2.55** from chromenes **2.39** and primary amines in acidic media

Compound **2.39e** was selected to explore this reaction (**Scheme 33**). The first assays were carried out following our previously developed protocol, thus, treatment with 1.7 equivalents of phenylhydrazine and 0.5 equivalents of acetic acid using ethanol as solvent and heating at 80 °C. An orange suspension was obtained immediately after the addition of phenylhydrazine to the beige suspension of **2.39e** in EtOH. After 8 min., the suspension was fully converted into a light orange solution and one hour later, a yellow solid started to resuspend from the orange solution. After 2 h, all the starting material had been consumed [by TLC, (1:1) EtOAc/*n*-hexane], and the beige solid that was isolated could be identified as compound **2.88a** (η= 53%). Using the same

reaction conditions, compound **2.88b** was also prepared (**Scheme 33**), being isolated as a pure product with 45% yield after 1 h of reaction. In contrast to the reaction of chromenes **2.39** with primary amines, no formation of chromenepyridine-base compounds was observed.



Scheme 33: Reaction conditions for the preparation of compounds **2.82a-b**

The spectroscopic data of compounds **2.82** corroborated its formation. Thus, IR spectra of compounds **2.82** showed five bands centred at 3484, 3465, 3370, 3360 and 3305 cm^{-1}, which were assigned to the N-H stretching vibrations, and an intense band centred at 2185 cm^{-1}, attributed to the CN stretching vibration. The carbonyl stretching signal of **2.39e**, at 1674 cm^{-1}, was absent.

The ^{1}H NMR spectra of **2.82** shows two characteristic singlets, one at δ 9.21 ppm, corresponding to the NH group of the hydrazine moiety, and other at δ 6.84 ppm corresponding to the NH_2 group (**Figure 50**). The peak corresponding to the methylene group appear at about δ 3.15 ppm, while the methylidene group appear at around δ 3.85 ppm. The ^{13}C NMR spectra of **2.82** corroborate the transformation of the carbonyl group, which appears at δ197.91 ppm in the starting material **2.39e**, which is shifted to high field in **2.82a** appearing at δ140.39 ppm (**Figure 51**).

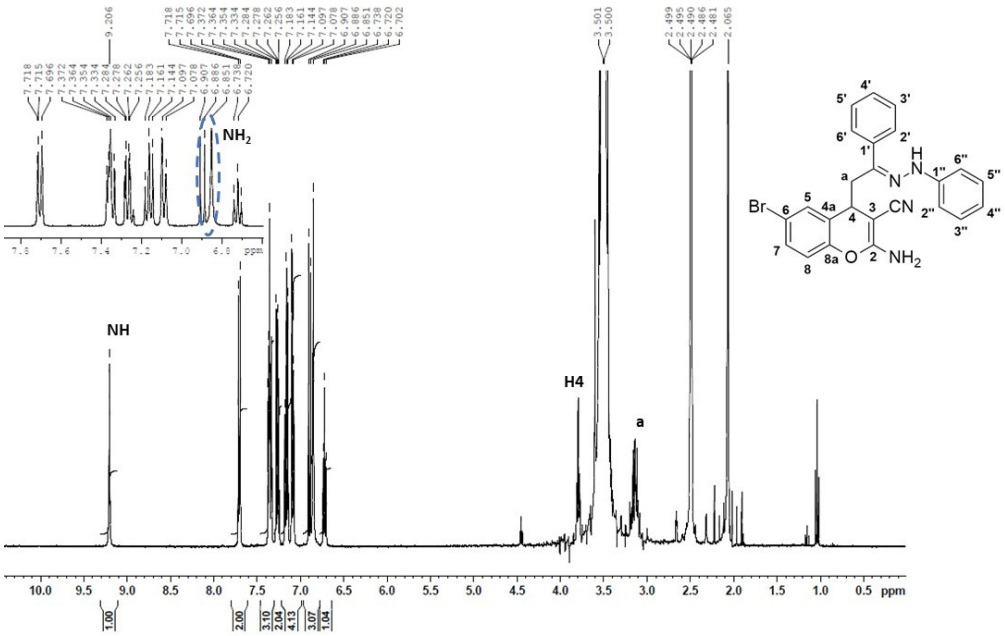


Figure 50: ^{1}H NMR (400 MHz, DMSO-d_6, δ ppm) spectrum of compound **2.82a**, in which several signals are highlighted

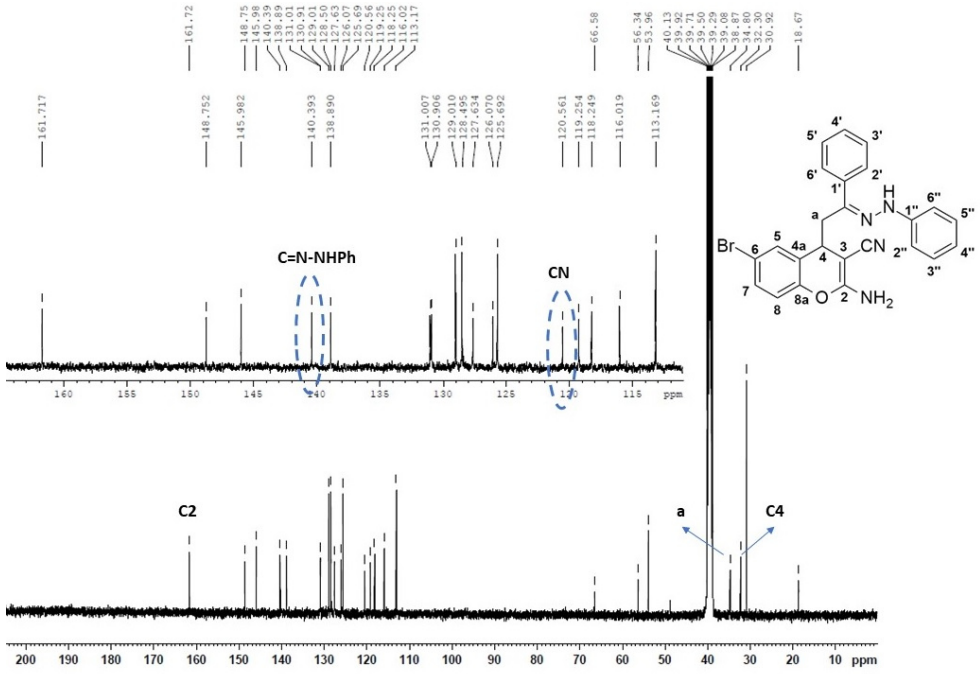
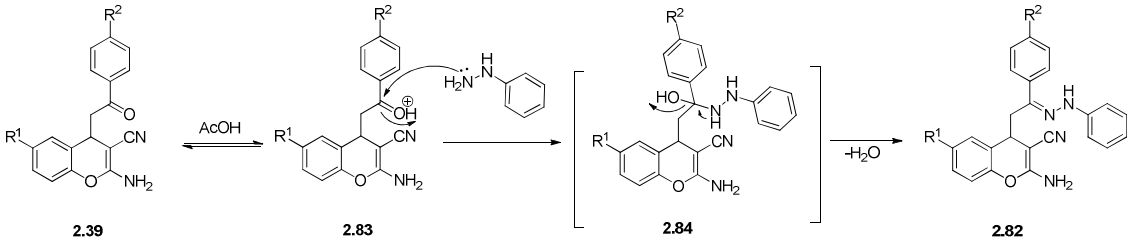


Figure 51: ^{13}C NMR (100 MHz, DMSO-d_6, δ ppm) spectrum of compound **2.82a**, in which several signals are highlighted

Altogether, the treatment of chromenes **2.39** with phenylhydrazine in acidic media does not provide access to chromenopyridine derivatives, instead the expected hydrazone derivatives are obtained. A new synthetic method for the development of novel 2-amino-4-(2-aryl-2-(2-phenylhydrazono)ethyl)-4*H*-chromene-3-carbonitriles **2.82a** and **2.82b** was developed via a

simple, rapid, and easily controlled procedure. The selectivity towards nucleophilic attack to the ketone group instead of the C2 position of the chromene moiety is probably due to the high nucleophilicity of hydrazines, mainly due to the alpha effect[120]. The alpha effect states that nucleophiles that possess a second lone pair on the atom in the alpha position relative to the nucleophilic centre, tend to have abnormally increased nucleophilicity when compared to their amine counterparts (phenylhydrazine *vs* aniline, for example). The mechanism for the formation of compounds **2.82** may involve a simple nucleophilic attack to the carbonyl group of **2.39**, generating an imine through acid-catalysed elimination of a water molecule (**Scheme 34**).



Scheme 34: Proposed mechanism for the formation of compounds **2.82**

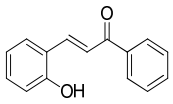
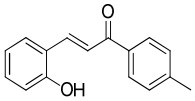
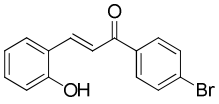
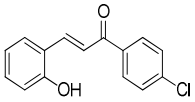
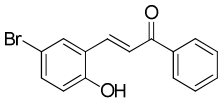
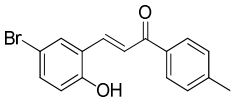
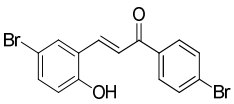
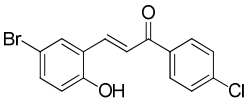
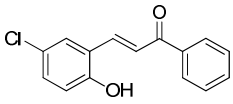
Physical, analytical, and spectroscopic characterization

The chemical structure of compounds **2.37, 2.39, 2.50, 2.55, 2.56, 2.60a, 2.61a, 2.68**, **2.69a**, **2.70**, **2.71** and **2.82** was assigned in consonance with physical, analytical, and spectroscopic data (elemental analysis, meting point, IR, ^{1}H and ^{13}C NMR). This information is presented in the following section. Complete characterization of compounds **2.37a, c** and **e-i**, as well as **2.39a, f** and **g**, were already described in the literature[104].

Physical and analytical characterization

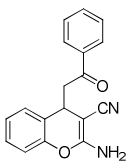
The molecular formula and molecular weight were calculated based on the predicted structure and the information obtained from the elemental analysis, the melting point intervals (°C) were also measured, and all the data is referred in **Tables 43-48**.

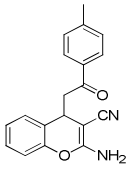
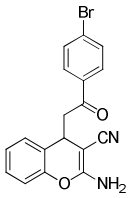
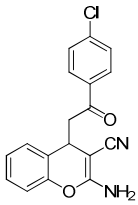
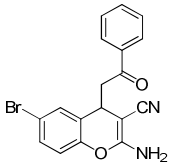
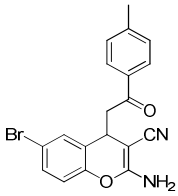
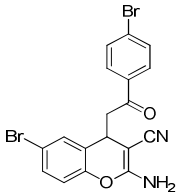
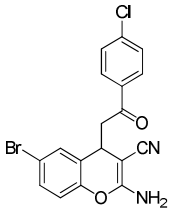
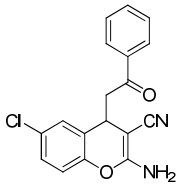
Table 43: Physical and analytical data obtained for 3-(2-hydroxyaryl)-1-arylprop-2-en-1-ones **2.37a-i**

Comp.	structure	Mp (°C)	molecular formula/ mass (M)	calculated /obtained values (%)			
				C	H	N	O
2.37a		169-171	$C_{15}H_{12}O_2$/ 224.25	79.61 79.64	6.25 6.22	- -	- -
2.37b		161-162	$C_{16}H_{14}O_2$/238.28	80.65 –	5.92 –	– –	13.43 –
2.37c[2]		-	$C_{15}H_{11}BrO_2$/303.15	59.43 –	3.66 –	– –	10.56 -
2.37d		155-156	$C_{15}H_{11}ClO_2$/258.70	69.64 –	4.29 –	– –	12.37 –
2.37e[1,2]		-	$C_{15}H_{11}BrO_2$/303.15	59.43 –	3.66 –	– –	10.56 –
2.37f[1]		191-193	$C_{16}H_{13}BrO_2$/317.18	60.20 59.93	4.75 4.77	– –	10.09 –
2.37g[1]		171-173	$C_{15}H_{10}Br_2O_2$/382.05	46.90 47.12	3.16 3.10	– –	– –
2.37h[1,2]		-	$C_{15}H_{10}BrClO_2$/ 337.60	53.37 –	2.99 –	– –	9.48 –
2.37i[1,2]		-	$C_{15}H_{11}ClO_2$/258.70	69.64 –	4.29 –	– –	12.37 –

[1]data obtained from ref. 104; [2]The product was contaminated with aldehyde according to ^{1}H NMR data and was used as starting material in the next step, without furtherpurification

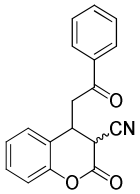
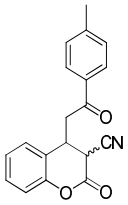
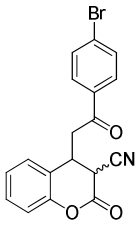
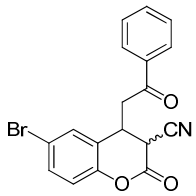
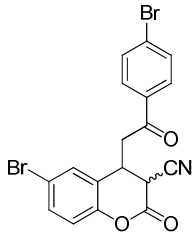
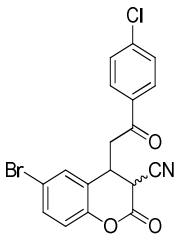
Table 44: Physical and analytical data obtained for 4*H*-chromene-3-carbonitriles **2.39**

Compound	structure	Mp (°C)	molecular formula/ mass (M)	calculated /obtained values (%)			
				C	H	N	O
2.39a[1]		136-138	$C_{18}H_{14}N_2O_2$/ 290.32	74.47 74.18	4.87 4.77	9.65 9.91	11.02 –

2.39b		150-152	$C_{19}H_{16}N_2O_2$/ 304.34	74.98 —	5.30 —	9.20 —	10.51 —
2.39c		198-200	$C_{18}H_{13}BrN_2O_2$/ 369.21	58.56 –	3.55 –	7.59 –	8.67 –
2.39d		147-149	$C_{18}H_{13}ClN_2O_2$/ 324.76	66.57 —	4.03 —	8.63 —	9.85 —
2.39e		192-194	$C_{18}H_{13}BrN_2O_2$/ 369.21	58.56 58.48	3.55 3.44	7.59 7.48	8.67 –
2.39f[1]		183-185	$C_{19}H_{15}BrN_2O_2$/ 383.24	59.55 59.39	3.95 3.96	7.31 7.38	8.35 -
2.39g[1]		186-188	$C_{18}H_{12}Br_2N_2O_2$/ 448.11	52.31 52.35	2.93 2.69	6.78 6.53	7.14 -
2.39h		183-185	$C_{18}H_{12}BrClN_2O_2$/ 403.66	53.56 –	3.00 –	6.94 –	7.93 –
2.39i		184-186	$C_{18}H_{13}ClN_2O_2$/ 324.76	66.57 —	4.03 —	8.63 —	9.85 —

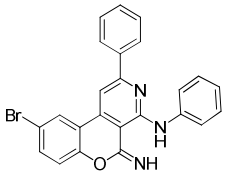
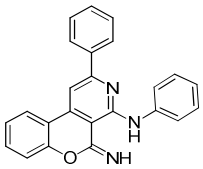
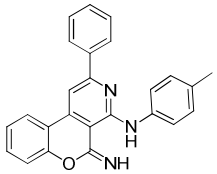
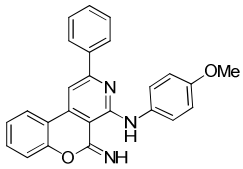
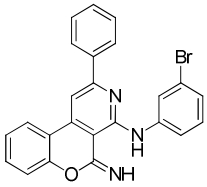
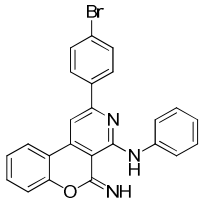
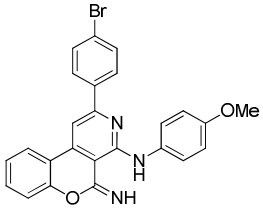
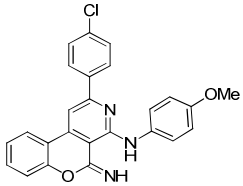
[1]Data obtained from ref. 104

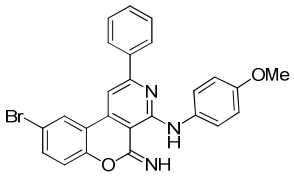
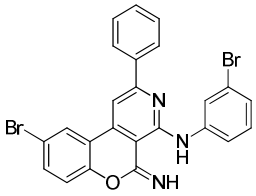
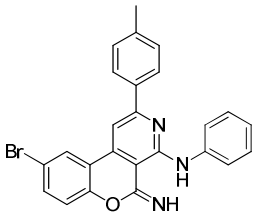
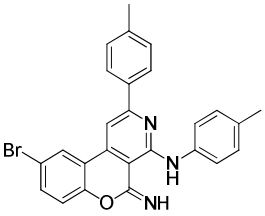
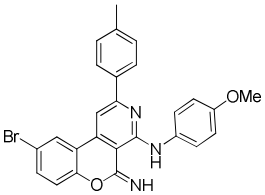
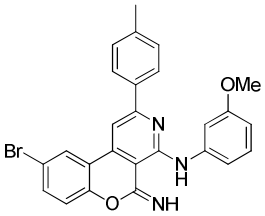
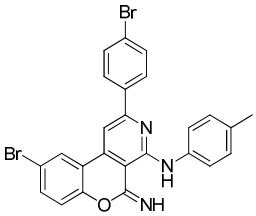
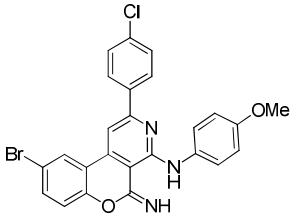
Table 45: Physical and analytical data for 4*H*-chromene-3-carbonitriles **2.50**

Compound	structure	Mp (°C)	molecular formula/ mass (M)	calculated /obtained values (%)			
				C	H	N	O
2.50a		195-197	$C_{18}H_{13}NO_3$/ 291.30	74.22 –	4.50 –	4.81 –	16.48 –
2.50b[1]		106-108	$C_{19}H_{15}NO_3$/ 305.33	74.74 –	4.95 –	4.59 –	15.72 –
2.50c		158-160	$C_{18}H_{12}BrNO_3.0,5H_2O$/ 379.20	57.01 57.1	3.46 3.2	3.69 3.9	14.77 –
2.50d		115-117	$C_{18}H_{12}BrNO_3.0,5H_2O$/ 370.20	57.01 56.8	3.46 3.4	3.69 3.7	14.77 –
2.50e		220 (dec.)	$C_{18}H_{11}Br_2NO_3$/ 449.09	48.14 –	2.47 –	3.12 –	10.69 –
2.50f		108-110	$C_{18}H_{11}BrClNO_3$/ 404.64	53.43 –	2.74 –	3.46 –	11.86 –

[1]Degradation in the solid form

Table 46: Physical and analytical data for chromenopyridines **2.55**, **2.56** and **2.69**

Comp.	structure	Mp (°C)	molecular formula/ mass (M)	calculated /obtained values (%)			
				C	H	N	O
2.55a		200-202	$C_{24}H_{16}BrN_3O$/ 442.31	65.17 –	3.65 –	9.50 –	3.62 –
2.55b		>300	$C_{24}H_{17}N_3O$/ 363.41	79.32 –	4.72 –	11.56 –	4.40 –
2.55c		>300	$C_{25}H_{19}N_3O$/ 377.44	79.55 –	5.07 –	11.13 –	4.24 –
2.55d		>300	$C_{25}H_{19}N_3O_2$/ 393.44	76.32 –	4.87 –	10.68 –	8.13 –
2.55e		>300	$C_{24}H_{16}BrN_3O$/ 442.31	65.17 –	3.65 –	9.50 –	3.62 –
2.55f		221-223	$C_{24}H_{16}BrN_3O$/ 442.31	65.17 –	3.65 –	9.50 –	3.62 –
2.55g		205-206	$C_{25}H_{18}BrN_3O_2$/ 472.33	63.57 –	3.84 –	8.90 –	6.77 –
2.55j		199-201	$C_{25}H_{18}ClN_3O_2$/ 427.88	70.18 –	4.24 –	9.82 –	7.48 –

2.55i		225-227	$C_{25}H_{18}BrN_3O_2$/ 472.33	63.57 –	3.84 –	8.90 –	6.77 –
2.55m		>300	$C_{24}H_{15}Br_2N_3O$/ 521.20	55.31 –	2.90 –	8.06 –	3.07 –
2.55n		>300	$C_{25}H_{18}BrN_3O$/ 456.33	65.80 –	3.98 –	9.21 –	3.51 –
2.55p		239-241	$C_{26}H_{20}BrN_3O$/ 470.36	66.39 –	4.29 –	8.93 –	3.40 –
2.55q		212-214	$C_{26}H_{20}BrN_3O_2$/ 486.36	64.21 –	4.14 –	8.64 –	6.58 –
2.55r		>300	$C_{26}H_{20}BrN_3O_2$/ 486.36	64.21 –	4.14 –	8.64 –	6.58 –
2.55u		292-294	$C_{25}H_{17}Br_2N_3O$/ 535.23	56.10 –	3.20 –	7.85 –	2.99 –
2.55b'		222-224	$C_{25}H_{17}BrClN_3O_2$/ 506.78	59.25 –	3.38 –	8.29 –	6.31 –

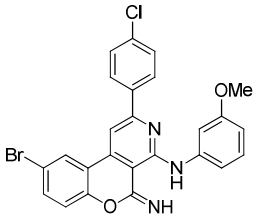
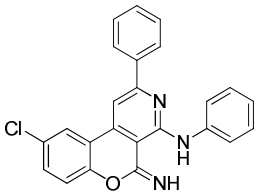
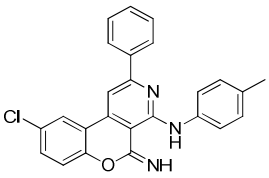
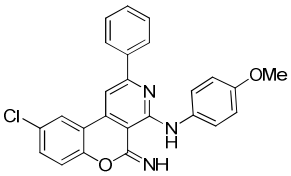
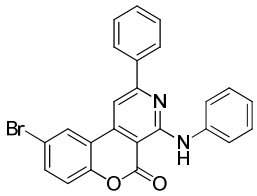
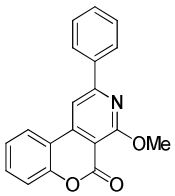
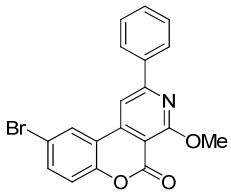
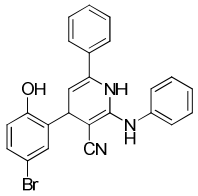
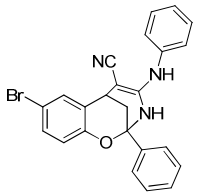
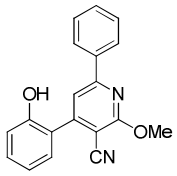
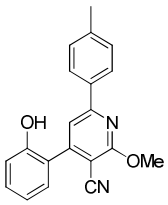
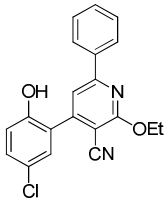
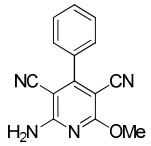
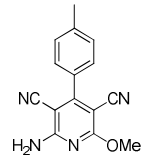
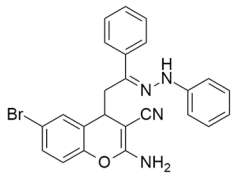
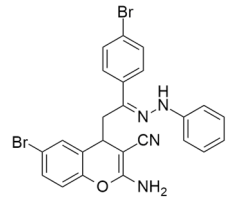
2.55c'		–	$C_{25}H_{17}BrClN_3O_2$/ 506.78	59.25 –	3.38 –	8.29 –	6.31 –
2.55d'		198-200	$C_{24}H_{16}ClN_3O$/ 397.86	72.45 –	4.05 –	10.56 –	4.02 –
2.55f'		228-229	$C_{25}H_{18}ClN_3O$. 0,4H_2O/419.08	71.58 71.70	4.48 4.41	10.02 9.87	5.34 –
2.55g'		226-228	$C_{25}H_{18}ClN_3O_2$/ 427.88	70.18 –	4.24 –	9.82 –	7.48 –
2.56a		268-270	$C_{24}H_{16}BrN_2O_2$/ 443.29	65.05 –	3.41 –	6.32 –	7.22 –
2.69a		>300	$C_{20}H_{15}NO_3$/ 317.34	75.70 –	4.76 –	4.41 –	15.13 –
2.69b		>300	$C_{20}H_{14}BrNO_3$/ 396.23	60.62 –	3.56 –	3.53 –	12.11 –

Table 47: Physical and analytical data for compounds **2.60a, 2.61a**, **2.68a,b, 2.70a** and **2.71a,b**

Compound	structure	Mp (°C)	molecular formula/ mass (M)	calculated /obtained values (%)			
				C	H	N	O
2.60a[1]		—	$C_{24}H_{16}BrN_3O$/ 442.31	65.17 —	3.65 —	9.50 —	3.62 —
2.61a		159-161	$C_{24}H_{18}BrN_3O$/ 444.32	64.88 –	4.08 –	9.46 –	3.60 –
2.68a		—	$C_{19}H_{14}N_2O_2$/ 302.33	75.48 —	4.67 —	9.27 —	10.58 —
2.68b		—	$C_{20}H_{16}N_2O_2$/ 316.35	75.93 —	5.10 —	8.86 —	10.11 —
2.70a		>300	$C_{20}H_{15}ClN_2O_2$/ 350.80	68.48 –	4.31 –	7.99 –	9.12 –
2.71a		220-222	$C_{14}H_{10}N_4O$/ 250.26	67.19 –	4.03 –	22.39 –	6.39 –
2.71b		>300	$C_{15}H_{12}N_4O$/ 264.28	68.14 –	4.58 –	21.20 –	6.05 –

[1]Could not be isolated as a pure product

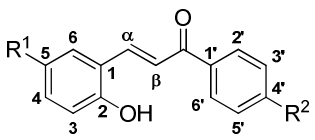
Table 48: Physical and analytical data obtained for 2-amino-4-(2-aryl-2-(2-phenylhydrazono)ethyl)-4*H*-chromene-3-carbonitriles **2.82a,b**

Compound	structure	Mp (°C)	molecular formula/ mass (M)	calculated /obtained values (%)			
				C	H	N	O
2.82a		212-214	$C_{24}H_{19}BrN_4O$/ 459.34	62.75 –	4.17 –	12.20 –	3.48 –
2.82b		210-212	$C_{24}H_{18}Br_2N_4O$/ 538.23	53.56 –	3.37 –	10.41 –	2.97 –

IR spectroscopy

A group of key patterns in the IR spectra could be identified for each of the synthesized compounds. Compounds **2.37** show a characteristic band for the O-H stretching vibration around 3300 cm^{-1}, as well as for the C=O stretching vibration signal of the carbonyl group of the α,β-unsaturated system, at around 1640-1650 cm^{-1} (**Table 49**). The N-H stretching vibration signals of the amino group in **2.39** give rise to multiple signals in the 3190-3460 cm^{-1} region. The carbonyl group also shifts to values between 1670-1690 cm^{-1} (**Table 50**). The stretching vibration for the cyano groups is always present as a medium intensity band in the 2179-2194 cm^{-1} region. Most of the information relating to compounds **2.37**, as well as some for chromenes **2.39**, has already been previously published[121].

Table 49: IR spectroscopic data (Nujol, cm^{-1}) obtained for 3-(2-hydroxyaryl)-1arylprop- 2-en-1-ones **2.37**



Compound	R^1	R^2	4000-3000	1700-1500
2.37a[1]	H	H	3364m	1655s (C=O), 1598m; 1586s; 1569w
2.37b	H	Me	3265w	1649s (C=O), 1607m; 1585s; 1563w
2.37c	H	Br	3223m	1642s (C=O), 1595s; 1585s; 1551m

2.37d	H	Cl	3326w	1643s (C=O), 1595sh; 1581s; 1561s
2.37e[1,2]	Br	H	-	-
2.37f[1]	Br	Me	3375w	1644s (C=O), 1606m; 1559s
2.37g[1]	Br	Br	3285m	1645s (C=O), 1593s; 1568s; 1554w
2.37h[1,2]	Br	Cl	-	-
2.37i[1,2]	Cl	H	-	-

[1]data obtained from ref. 104; [2]The IR spectrum was not registered as the product was slightly contaminated with aldehyde according to ^{1}H NMR data. The solid was used as starting material in the next step, without further purification

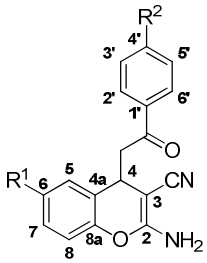


Table 50: IR spectroscopic data (Nujol, cm^{-1}) obtained for 4*H*-chromene-3-carbonitriles **2.39**

Compound	R^1	R^2	4000-3000	CN	1700-1500
2.39a[1]	H	H	3409m; 3325w; 3204w	2182m	1689s (C=O); 1649m; 1609m; 1579s
2.39b	H	Me	3458m; 3328m; 3238w; 3204w	2179m	1679s C=(O); 1645s; 1607m;1580m
2.39c	H	Br	3463m; 3324m; 3240w; 3198w	2189m	1687s (C=O); 1641s; 1608m; 1580m
2.39d	H	Cl	3467m; 3321m; 3237w; 3197w	2191m	1687s (C=O); 1642s; 1606m; 1588sh; 1579m
2.39e	Br	H	3459m; 3320m; 3279w; 3232w; 3191w	2194m	1673s (C=O); 1650s; 1603m; 1566w
2.39f[1]	Br	Me	3461w; 3320w	2193m	1668s(C=O); 1649m; 1602m; 1568s
2.39g[1]	Br	Br	3463w; 3320w	2193m	1677s(C=O); 1650s; 1600m; 1568s
2.39h	Br	Cl	3463w; 3320w; 3280w; 3235w; 3189w	2193m	1678s(C=O); 1651s; 1599m; 1598sh; 1567m
2.39i	Cl	H	3462m; 3320m; 3278w; 3232w; 3192w	2193m	1674s(C=O); 1650s; 1603m; 1572s

[1]data obtained from ref. 104

Compounds **2.50** were identified by their two intense C=O stretching vibration bands: one in the 1765-1770 cm^{-1} region and another in the 1676-1868 cm^{-1} region. The cyano group leads to a weak band around 2260 cm^{-1} (**Table 51**).

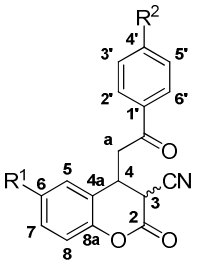
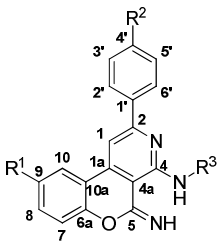


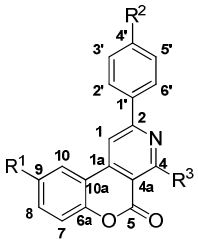
Table 51: IR spectroscopic data (Nujol, cm^{-1}) obtained for 4*H*-chromene-3-carbonitriles **2.50**

Compound	R^1	R^2	CN	1700-1500
2.50a	H	H	2259w	1769s (C=O); 1681s (C=O); 1612sh; 1590m
2.50b	H	Me	2259w	1765s (C=O); 1676s(C=O); 1609m
2.50c	H	Br	2258w	1767s (C=O); 1682s(C=O); 1610m; 1586s
2.50d	Br	H	2260w	1776s (C=O); 1678s(C=O); 1595m
2.50e	Br	Br	2262w	1774s (C=O); 1686s(C=O); 1587m
2.50f	Br	Cl	2261w	1772s (C=O); 1683s(C=O); 1588m

The IR spectra of compounds **2.55** and **2.56** show a small signal for the N-H stretching vibration at around 3300-3400 cm^{-1}, and a set of signals ranging from around 1550-1630 cm^{-1}, which correspond mainly to the C=C stretching vibration of the aromatic rings and the N-H bending signals (**Table 52**). In the IR spectra of compounds **2.56** and **2.69** stand out the presence of intense bands at 1701 cm^{-1} (for **2.56a**) or around 1740 cm^{-1} (for **2.69a** and **2.69b**), corresponding to their carbonyl groups.



2.55



2.56/2.69

Table 52: IR spectroscopic data (Nujol, cm^{-1}) obtained for 5-imino and 5-oxo-*N*,2-diaryl-5*H*-chromeno[3,4-*c*]pyridin-4-amines **2.55**, **2.56** and **2.69**

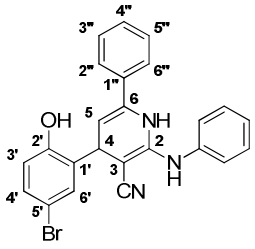
Comp.	R^1	R^2	R^3	4000-3000	1650-1450
2.55a	Br	H	C_6H_5	3311w	1642m; 1629m; 1602m; 1579w; 1549m
2.55b	H	H	C_6H_5	3349w; 3313w	1638m; 1608m; 1578w; 1559m; 1507w
2.55c	H	H	4-MeC_6H_4	3443w; 3349w	1634m; 1609m; 1575w; 1553m; 1510w

2.55d	H	H	4-OMeC_6H_4	3440w; 3348w; 3328w	1637m; 1606m; 1578w; 1555m; 1509s
2.55e	H	H	3-BrC_6H_4	3439w; 3350w; 3310w; 3288w	1636m; 1610m; 1592w; 1572w; 1547m
2.55f	H	Br	C_6H_5	3312w	1629m; 1608m; 1579w; 1556m; 1542sh
2.55g	H	Br	4-OMeC_6H_4	3307w	1635m; 1610m; 1582w; 1561m; 1510s
2.55j	H	Cl	4-OMeC_6H_4	3308w	1638m; 1610m; 1582m; 1563m; 1510s
2.55l	Br	H	4-OMeC_6H_4	3290m	1629m; 1600sh; 1559m; 1508m;
2.55m	Br	H	3-BrC_6H_4	3298w	1629m; 1600w; 1577sh; 1574w; 1548m; 1487m
2.55n	Br	Me	C_6H_5	3315w	1636m; 1601m; 1578w; 1549m
2.55p	Br	Me	4-MeC_6H_4	3318w	1630m; 1596w; 1575w; 1551m; 1511m
2.55q	Br	Me	4-OMeC_6H_4	3319w	1632m; 1598w; 1580w; 1558m; 1509m
2.55r	Br	Me	3-OMeC_6H_4	3315w	1638m; 1603w; 1596w; 1581w; 1559w; 1548sh; 1495m
2.55u	Br	Br	4-MeC_6H_4	3317w	1631m; 1601w; 1574w; 1551m; 1512m
2.55b'	Br	Cl	4-OMeC_6H_4	3319w; 3304w; 3277w	1637m; 1613m; 1604sh; 1582w; 1556m; 1509m
2.55c'	Br	Cl	3-OMeC_6H_4	3303w	1636m; 1595w; 1582w; 1557w; 1543w
2.55d'	Cl	H	C_6H_5	3310w	1630m; 1599w; 1577w; 1533m
2.55f'	Cl	H	4-MeC_6H_4	3318w	1630m; 1603w; 1576w; 1551m; 1511m
2.55g'	Cl	H	4-OMeC_6H_4	3289w	1632m; 1608sh; 1557w; 1509m
2.56a	Br	H	NHC_6H_5	3305w; 3281w	1701s; 1650w; 1602s; 1576sh; 1552m; 1532sh
2.69a	H	H	OMe	-	1741s; 1602m; 1597m; 1550m
2.69b	Br	H	OMe	-	1742s; 1603m; 1591m; 1547m

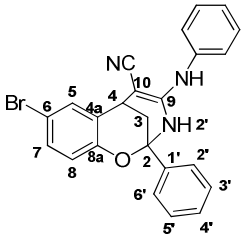
Compounds **2.60a** could not be characterized by IR spectroscopy because it was obtained as a mixture with **2.39e** and most of the signals are superimposed, preventing a correct identification. The IR spectra of compound **2.61** presents a NH stretching vibration band at 3388 cm^{-1} and a CN stretching vibration band at 2195 cm^{-1}. The IR spectra of compounds **2.68** and **2.70a** present bands for the OH stretching vibration at around 3300-3600 cm^{-1}, with compound **2.70a** presenting a broad band at 3261 cm^{-1}. The CN stretching vibration band was also observed,

close to 2230 cm^{-1}. The IR spectra of compounds **2.71** show either one or two bands for the CN stretching vibration, also in the 2195-2239 cm^{-1} region, as well as the N-H stretching vibration (**Table 53**).

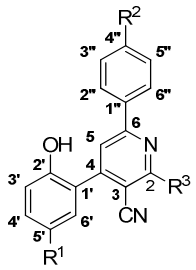
Table 53: IR spectroscopic data (Nujol, cm^{-1}) obtained for compounds **2.60a**, **2.61a**, **2.68**, **2.70a** and **2.71**



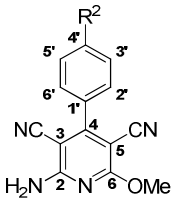
2.60a



2.61a



2.68 (R^3= OMe)
2.70 (R^3= OEt)



2.71

Comp.	R^1	R^2	4000-3000	CN	1700-1500
2.60a[1]	Br	H	-	-	-
2.61a	Br	H	3388m	2195m	1635s, 1603m, 1551w
2.68a	H	H	3441m, 3352s, 3271w, 3193w	2212m	1638s, 1607s, 1588sh, 1550m, 1518m
2.68b	Br	H	3614m, 3578m, 3341m, 3199w	2230m	1654m, 1584m, 1574sh, 1551m, 1526m
2.70a	Cl	H	3261br	2239m	1589m, 1580sh, 1546m
2.71a	H	H	3400m, 3335m, 3244m	2216m	1651m, 1585sh, 1559s
2.71b	H	Me	3407m, 3348m, 3254m	2223m, 2212m	1661m, 1571m, 1556sh

[1]Could not be isolated as a pure product

Compounds **2.82** can easily be identified by the presence of the NH stretching vibration in the IR spectra, with two distinct pairs of weak bands and another with medium intensity (Table 54). A strong CN stretching band at around 2185 cm^{-1} for the nitrile group was also identified. The IR spectra of **2.82** also corroborate the absence of the carbonyl group because no C-O stretching vibration band as for compound **2.39**, at around 1670-1680 cm^{-1}, was identified (**Table 54**).

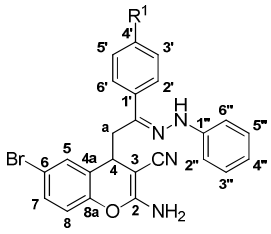


Table 54: IR spectroscopic data (Nujol, cm^{-1}) obtained for 2-amino-4-(2-aryl-2-(2-phenylhydrazono)ethyl)-4*H*-chromene-3-carbonitriles **2.82a** and **2.82b**

Compound	R^1	4000-3000	CN	1700-1500
2.82a	H	3482w; 3465w; 3372sh; 3360m; 3305m	2185s	1646s; 1600m; 1582m; 1569sh
2.82b	Br	3476w; 3467w; 3369sh; 3362m; 3306m	2184s	1648s; 1599s; 1572m; 1556sh; 1514w

NMR spectroscopy

All the NMR spectroscopic data for the compounds of this section is presented in **Tables 55-65**. Compounds **2.37** can be identified for the singlet around δ10.6-10.3 ppm (hydroxyl group) and for the C-H signals of the alkene group that appear as doublets with J= 16 Hz (**Table 55**). In the ^{13}C NMR spectra, the signals of the carbonyl group appear at around δ 188-189 ppm, while Cα and Cβ appear at around δ137-140 and δ120-122 ppm, respectively (**Table 56**). Two-dimensional correlation experiments allowed to identify the remaining carbon signals. H α proton correlates with both C1 and Hβ and Hβ proton correlates with both Hα and the carbonyl carbon atom. A correlation between the OH group and C1 and C3 carbon atoms was identified.

Compounds **2.39** (**Tables 57** and **58**) can be readily identified in their ^1H NMR spectra through their characteristic NH_2 signals, which appear as a singlet at around δ6.80-6.90 ppm, and for their H4 and Ha signals at around δ 4.10 and 3.30-3.50 ppm, respectively. In the ^{13}C NMR spectra of compounds **2.39** stand out the peak at around δ 197 ppm corresponding to the carbonyl group, as well as two peaks, at around δ 46 ppm and δ 30-31 ppm corresponding to Ca and C4, respectively. Full characterization of the NMR signals was achieved by two-dimensional correlation experiments. Thus, cross peaks between H4 and C2, C3, CN, C=O, CH2, C4a, C5 and C8a were identified. Haα and Haβ also correlate with the carbonyl carbon atom, with C1', C3 and with C4a.

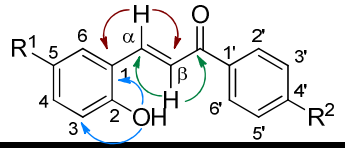
The ^1H NMR spectra of compounds **2.50** present a correlation between H3 and C2, C4 and Ca. It also presents two characteristic sets of signals, one for each isomer (*cis* and *trans*)

(**Table 59**). It is possible to distinguish both isomers through the coupling constant between H3 and H4. For the minor isomer, the signal corresponding to the H3 hydrogen atom appears as a doublet at δ4.91-4.95 ppm with a coupling constant of approximately 11 Hz, while for the major isomer, H3 appears as a doublet around δ5.20-5.22 ppm with a coupling constant of approximately 7 Hz. The signals corresponding to the H4 and Ha hydrogen atoms also differ from the starting material, which appear as a multiplet at around δ 4.10-4.40 ppm, and a doublet of doublets at around δ 3.82-3.49 ppm, respectively, for the major isomer and around δ 3.85-3.65 ppm for the minor isomer. The most relevant signals in the ^{13}C NMR spectra (**Table 60**) are the existence of a new peak at around δ 161-162 ppm corresponding to the carbonyl group at C2, the signals between 37.43 and 36.95 ppm (major isomer) and between δ 37.65 and 37.17 ppm (minor isomer) corresponding to C3 and C4, as well as Ca between δ 40.95 and 40.58 ppm (major isomer) and between δ 39.76 and 38.85 ppm (minor isomer). All the presented compounds had a clear tendency of evolution in DMSO-d_6, to a non-identified mixture.

As expected for the structural similarity, no relevant differences in the NMR spectra of compounds **2.55**, **2.56a** and **2.69** were identified (**Tables 61** and **62**). The signals corresponding to the NH-R^3 group in compounds **2.55** appears as a small singlet in the δ12.30-13.10 ppm region and the imino group around δ9.10-9.30 ppm, while for compound **2.56a** the NH-R^3 group appears as a singlet at δ 10.68 ppm. The ^{13}C NMR signals for C5 are located between δ150-160 ppm for **2.55** and δ160-170 ppm for **2.56** and **2.69**.

Compounds **2.55**, **2.56** and **2.69** present very similar two-dimensional C-H correlation patterns. For compounds **2.55**, the spectra revealed that the imines NH group correlate with C4a and C5 in a regular basis, but for some derivatives, it can also correlate with C10a. The NH-R3 proton can correlate with C1'' and C2'' and C6'' of the R^3 substituent (when R^3 is an aromatic ring), but also with C2 and C4a. In some cases, it also correlates with C4. H2 can correlate with C2, C4a, C6a, C10 and C10a, and in some cases with C1a. The spectra of compounds **2.56** present the same correlations, except for the imine NH correlation that is absent. As for compounds **2.69**, they also exhibit the same H2 correlations as **2.55** and **2.56**, and none of the additional correlations. A correlation between the hydrogen atoms of the methoxy group with C4 is also observed. Compound **2.55e** was evolved in DMSO-d_6 during the collection of the ^{13}C NMR spectra, which did not allow for a correct attribution of its ^{1}H and ^{13}C NMR signals.

Table 55: ^{1}H NMR (400 MHz, DMSO-d_6, δ ppm) spectroscopic data obtained for 3-(2-hydroxyaryl)-1 arylprop-2-en-1-ones **2.37**



Compound	R^1	R^2	H3-6	C2'-6'	Hα, Hβ
2.37a	H	H	10.29 (s, 1H, OH), 7.84 (dd, J_1=8.0, J_2=1.6 Hz, 1H, H6), 7.27 (td, J_1= 7.2, J_2=1.6 Hz, 1H, H4), 6.95 (dd, J_1= 8.0, J_2= 0.8 Hz, 1H, H3), 6.87 (t, J= 7.6 Hz, 1H, H5)	7.56 (t, J= 7.2 Hz, 2H, H2'+H6'), 7.79 (d, J=8.8 Hz, 2H, H3'+ H5')	8.02 (d, J=16.0 Hz, Hα), 7.86 (d, J=16.0 Hz, Hβ)
2.37b	H	Me	10.45 (s, 1H, OH), 7.82 (dd, J_1=8.0, J_2=1.6 Hz, 1H, H6), 7.24 (td, J_1=7.2, J_2= 2.0 Hz, 1H, H4), 7.02 (d, J= 8.0 Hz, 1H, H3), 6.84 (td, J_1=7.6, J_2= 0.8 Hz, 1H, H5)	7.89 (d, J= 8.0 Hz, 2H, H2'+H6'), 7.35 (d, J=8.0 Hz, 2H, H3'+ H5'), 2.39 (s, 3H, Me)	7.99 (d, J=16.0 Hz, Hα), 7.81 (d, J=16.0 Hz, Hβ)
2.37c[2]	H	Br	10.32 (s, 1H, OH), 7.85 (dd, J_1=8.0, J_2=2.0 Hz, 1H, H6), 7.27 (td, J_1=7.2, J_2= 2.0 Hz, 1H, H4), 6.95 (d, J= 8.0 Hz, 1H, H3), 6.86 (td, J_1=7.6, J_2= 0.8 Hz, 1H, H5)	8.02 (dd, J_1= 8.8 Hz, J_2= 1.6 Hz, 2H, H2'+H6'), 7.77 (dd, J_1= 8.8 Hz, J_2= 2.4 Hz, 2H, H3'+ H5')	8.06 (d, J=16.0 Hz, Hα), 7.84 (d, J=16.0 Hz, Hβ)
2.37d	H	Cl	10.41 (s, 1H, OH), 7.84 (dd, J_1=7.6, J_2=1.6 Hz, 1H, H6), 7.26 (td, J_1=7.2, J_2=1.2 Hz, 1H, H4), 6.96 (dd, J_1=8.0, J_2= 1.6 Hz, 1H, H3), 6.86 (dt, J_1= 8.0, J_2= 0.8 Hz, 1H, H5)	8.09 (dd, J_1= 8.8 Hz, J_2= 1.6 Hz, 2H, H2'+H6'), 7.60 (dd, J_1= 8.8 Hz, J_2= 2.4 Hz, 2H, H3'+ H5')	8.04 (d, J=16.0 Hz, Hα), 7.81 (d, J=16.0 Hz, Hβ)
2.37e[1,2]	Br	H	10.45 (s, 1H, OH), 8.15 (d, J= 4.8 Hz, 1H, H6), 7.56 (t, J= 6.4 Hz, 1H, H5), 7.42 (dd, J_1= 8.8, J_2= 2.4 Hz, 1H, H4), 6.90 (d, J= 8.8 Hz, 1H, H3)	8.13 (d, J= 4.8 Hz, 2H, H2'+H6'), 7.92 (d, J= 8.0 Hz, 2H, H3'+ H5'), 6.40 (dd, J_1= 8.8, J_2= 2.4 Hz, 1H, H4')	7.97 (d, J= 16.0 Hz, Hα), 7.95 (d, J= 16.0 Hz, Hβ)
2.37f[1]	Br	Me	10.55 (s, 1H, OH), 8.13 (d, J= 2.4 Hz, 1H, H6), 7.56 (t, J= 6.4 Hz, 1H, H5), 7.40 (dd, J_1=8.8, J_2= 2.4 Hz, 1H, H4), 6.89 (d, J= 8.8 Hz, 1H, H3)	8.06 (d, J= 8.0 Hz, 2H, H2+H6'), 7.37 (d, J= 8.0 Hz, 2H, H3'+ H5'), 2.40 (s, 3H, Me)	7.94 (d, J= 16.0 Hz, Hα), 7.93 (d, J= 16.0 Hz, Hβ)
2.37g[1]	Br	Br	10.49 (s, 1H, OH), 8.04 (d, J= 2.4 Hz, 1H, H6), 7.56 (t, J= 6.4, Hz, 1H, H5), 7.31 (dd, J_1=8.8, J_2= 2.4 Hz, 1H, H4), 6.79 (d, J= 8.8 Hz, 1H, H3)	7.98 (d, J= 6.4 Hz, 2H, H2'+H6'), 7.67 (d, J= 6.8 Hz, 2H, H3'+ H5')	7.86 (d, J= 16.0 Hz, Hα), 7.83 (d, J= 16.0 Hz, Hβ)

2.37h[1,2]	Br	Cl	10.49 (s, 1H, OH), 7.56 (t, J= 6.4 Hz, 1H, H5), 7.63 (dd, J_1= 8.4, J_2= 2.0 Hz, 1H, H6), 7.27 (dd, J_1= 8.8, J_2= 2.0 Hz, 1H, H4), 6.84 (d, J= 8.4 Hz, 1H, H3)	8.18 (d, J= 8.8 Hz, 2H, H3'+ H5'), 7.95 (d, J= 7.6 Hz, 2H, H2'+H6')	7.97 (d, J= 15.6 Hz, Hα), 7.93 (d, J= 15.6 Hz, Hβ)
2.37i[1,2]	Cl	H	10.57 (s, 1H, OH), 7.56 (t, J= 6.4, Hz, 1H, H5), 7.65 (t, J= 7.2 Hz, 1H, H4), 7.30 (dd, J_1= 8.8, J_2= 2.8 Hz, 1H, H6), 6.96 (d, J= 8.0 Hz, 1H, H3)	8.14 (d, J= 8.8 Hz, 2H, H3'+ H5'), 6.40 (dd, J_1= 8.8, J_2= 2.4 Hz, 1H, H4'), 7.56 (t, J= 7.6 Hz, 2H, H2'+H6')	7.97 (d, J= 16.0 Hz, Hα), 7.94 (d, J= 16.0 Hz, Hβ)

[1]data obtained from ref. 104; [2]The product was slightly contaminated with aldehyde according to ^{1}H NMR data and was used as starting material in the next step, without further purification

Table 56: ^{13}C NMR (100 MHz, DMSO-d_6, δ ppm) spectroscopic data obtained for 3-(2-hydroxyaryl)-1arylprop-2-en-1-ones **2.37**

Compound	R^1	R^2	C1-6	C1'-6'	C=O	Cα, Cβ
2.37a[1]	H	H	157.25 (C2), 132.03 (C4), 128.70 (C6), 121.33 (C1), 119.38 (C5), 116.22 (C3)	137.90 (C1'), 132.86 (C4), 128.75 (C3' + C5'), 128.31 (C2' + C6')	189.50	139.54 (Cα), 120.92 (Cβ)
2.37b	H	Me	157.38 (C2), 131.87 (C4), 128.69 (C6), 121.36 (C1), 119.28 (C5), 116.34 (C3)	143.27 (C4'), 135.38 (C1'), 129.34 (C3' + C5'), 128.48 (C2' + C6'), 21.18 (Me)	188.98	139.30 (Cα), 120.88 (Cβ)
2.37c[2]	H	Br	-	-	-	-
2.37d	H	Cl	157.47 (C2), 132.30 (C4), 128.84 (C6), 121.32 (C1), 119.48 (C5), 116.37 (C3)	137.92 (C4'), 136.61 (C1'), 130.31 (C2' + C6'), 128.94 (C3' + C5')	188.49	140.15 (Cα), 120.58 (Cβ)
2.37e[1,2]	Br	H	-	-	-	-
2.37f[1]	Br	Me	156.28 (C2), 134.06 (C4), 130.26 (C6), 123.75 (C1), 118.28 (C3), 110.83 (C5)	143.51 (C4'), 134.09 (C1'), 129.30 (C3' + C5'), 128.66 (C2' + C6'), 21.17 (Me)	188.59	137.11(Cα), 122.01 (Cβ)
2.37g[1]	Br	Br	156.43 (C2), 134.38 (C4), 130.34 (C6), 123.56 (C1), 118.33 (C3), 110.15 (C5)	136.59 (C1'), 131.80 (C3' + C5'), 130.55 (C2' + C6'), 127.25 (C4')	188.24	137.94 (Cα), 121.56 (Cβ)
2.37h[1,2]	Br	Cl	-	-	-	-
2.37i[1,2]	Cl	H	-	-	-	-

[1]data obtained from ref. 104; [2]The product was slightly contaminated with aldehyde according to ^{1}H NMR data, and the ^{13}C NMR spectrum was not registered

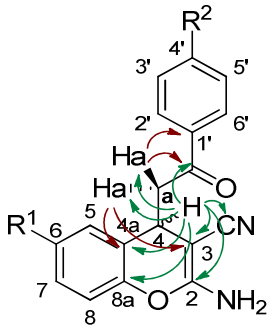


Table 57: ^{1}H NMR (400 MHz, DMSO-d_6, δ ppm) spectroscopic data obtained for 4*H*-chromene-3-carbonitriles **2.39**

Comp.	R^1	R^2	H5-8	H2'-6'	H4	Ha	NH_2
2.39a[1]	H	H	7.23 (m, 2H, H5 + H6), 7.05 (td, J_1= 7.2, J_2= 1.2 Hz, 1H, H7), 6.98 (dd, J_1= 8.0, J_2= 0.8 Hz, 1H, H8)	7.90 (dd, J_1= 8.4, J_2= 1.2 Hz, 2H, H2'+ H6'), 7.60(tt, J_1= 7.6, J_2= 1.2 Hz, 1H, H4'), 7.47 (t, J= 8.0 Hz, 2H, H3' + H5')	4.10 (t, J= 5.6Hz, 1H)	3.36 (m, 2H)	6.82 (s, 2H)
2.39b	H	Me	7.22 (dt, J_1= 7.6, J_2= 1.2 Hz, 1H, H7), 7.19 (dd, J_1= 7.6, J_2= 1.6 Hz, 1H, H5), 7.05 (dt, J_1= 7.2, J_2= 1.2 Hz, 1H, H6), 6.96 (dd, J_1= 8.0, J_2= 1.2 Hz, 1H, H8)	7.80 (dd, J_1= 8.0, J_2= 1.2 Hz, 2H, H2' + H6'), 7.27 (d, J= 8.0 Hz, 2H, H3' + H5'), 2.10 (s, 3H, Me)	4.10 (t, J= 6.0 Hz, 1H)	3.31 (m, 2H)	6.84 (s, 2H)
2.39c	H	Br	7.25 (dt, J_1= 7.6, J_2= 1.2 Hz, 1H, H7), 7.20 (dd, J_1= 8.0, J_2= 1.2 Hz, 1H, H5), 7.06 (dt, J_1= 7.2, J_2= 1.2 Hz, 1H, H6), 6.96 (dd, J_1= 8.0, J_2= 0.8 Hz, 1H, H8)	7.83 (dd, J_1= 7.6, J_2= 2.0 Hz 2H, H2' + H6'), 7.67 (dd, J_1= 8.4, J_2=1.6 Hz, 2H, H3' + H5')	4.10 (t, J= 5.6 Hz, 1H)	3.35 (m, 2H)	6.85 (s, 2H)
2.39d	H	Cl	7.26 (dd, J_1= 7.6, J_2= 1.6 Hz, 1H, H5), 7.21 (dt, J_1= 8.0, J_2= 1.6 Hz, 1H, H7), 7.06 (dt, J_1= 7.6, J_2= 1.2 Hz, 1H, H6), 6.96 (dd, J_1= 8.0, J_2= 0.8 Hz, 1H, H8)	7.91 (dd, J_1= 8.4, J_2= 2.0 Hz 2H, H2' + H6'), 7.53 (dd, J_1= 8.8, J_2=2.4 Hz, 2H, H3' + H5')	4.10 (t, J= 5.6 Hz, 1H)	3.61 (m, 2H)	6.84 (s, 2H)
2.39e[1]	Br	H	7.46 (dd, J_1= 2.4, J_2= 0.8 Hz, 1H, H5), 7.35 (dd, J_1= 8.8, J_2= 2.4 Hz, 1H, H7), 6.94 (d, J= 8.8 Hz, 1H, H8),	7.88 (dd, J_1=8.4, J_2= 1.2 Hz, 2H, H2'+ H6'), 7.60 (dt, J_1= 8.8, J_2= 1.2 Hz, 1H, H4'), 7.48 (t, J=7.6 Hz, 2H, H3' + H5')	4.10 (t, J= 5.6 Hz, 1H)	3.42 (m, 2H)	6.78 (s, 2H)

2.39f[1]	Br	Me	7.38 (dd, J_1= 8.8, J_2= 2.4 Hz, 1H, H7), 7.23 (dd, J_1= 2.4, J_2= 0.8 Hz, 1H, H5), 6.94 (d, J= 8.8 Hz, 1H, H8)	7.81 (dd, J_1= 6.4, J_2= 1.6 Hz, 2H, H2' + H6'), 7.28 (d, J= 8.0 Hz, 2H, H3' + H5'), 2.35 (s, 3H, Me)	4.08 (t, J= 5.6 Hz, 1H)	3.43 (m, 2H)	6.89 (s, 2H)
2.39g[1]	Br	Br	7.52 (d, J= 2.4 Hz, 1H, H5), 7.38 (dd, J_1= 8.8, J_2= 2.4 Hz, 1H, H7), 6.92 (d, J= 8.4 Hz, 1H, H8)	7.84 (d, J= 8.8 Hz, 2H, H2' + H6'), 7.70 (d, J= 8.8 Hz, 2H, H3' + H5')	4.08 (t, J= 5.6 Hz, 1H)	3.45 (m, 2H)	6.90 (s, 2H)
2.39h[1]	Br	Cl	7.52 (d, J= 2.4 Hz, 1H, H5), 7.37 (dd, J_1= 8.4, J_2= 3.2 Hz, 1H, H7), 6.93 (d, J= 8.4 Hz, 1H, H8),	7.92 (dd, J_1= 9.2, J_2= 2.4 Hz, 2H, H2' + H6'), 7.54 (d, J_1= 9.2, J_2= 2.4 Hz, 2H, H3' + H5')	4.08 (t, J= 5.6 Hz, 1H)	3.42 (m, 2H)	6.91 (s, 2H)
2.39i[1]	Cl	H	7.39 (d, J= 2.4 Hz, 1H, H5), 7.24 (dd, J_1= 7.2, J_2= 2.8 Hz, 1H, H7), 6.99 (d, J= 8.8 Hz, 1H, H8),	7.91 (dd, J_1=7.2, J_2= 0.8 Hz, 2H, H2'+ H6'), 7.61 (dt, J_1=7.2, J_2= 1.2 Hz, 1H, H4'), 7.48 (t, J= 8.0 Hz, 2H, H3' + H5')	4.09 (t, J= 5.2 Hz, 1H)	3.42 (m, 2H)	6.91 (s, 2H)

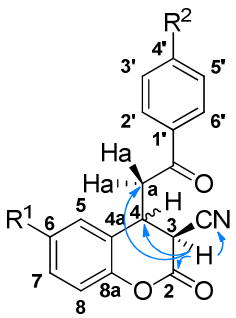
[1]data obtained from ref. 104

Table 58: ^{13}C NMR (100 MHz, DMSO-d_6, δ ppm) spectroscopic data obtained for 4*H*-chromene-3-carbonitriles **2.39**

Comp.	R^1	R^2	C2-8a	C1'-6'	Ca	CN	C=O
2.39a[1]	H	H	161.64 (C2), 149.35 (C8a), 128.11 (C5), 128.10 (C6), 124.54 (C7), 123.92 (C4a), 115.94 (C8), 54.18 (C3), 31.09 (C4)	136.74 (C1'), 133.34 (C4'), 128.76 (C3' + C5'), 128.08 (C2' + C6')	46.90	120.64	197.94
2.39b	H	Me	161.50 (C2), 149.25 (C8a), 128.03 (C7), 127.95 (C5), 124.40 (C6), 123.95 (C4a), 115.83 (C8), 54.15 (C3), 31.10 (C4)	143.57 (C4'), 134.24 (C1'), 129.18 (C3' + C5'), 128.13 (C2' + C6'), 21.10	46.81	120.51	197.26
2.39c	H	Br	161.54 (C2), 149.26 (C8a), 128.06 (C7), 128.02 (C5), 124.43 (C6), 123.74 (C4a), 115.83 (C8), 53.96 (C3), 31.08 (C4)	135.64 (C1'), 131.68 (C3' + C5'), 130.05 (C2' + C6'), 127.35 (C4')	46.88	120.48	197.13
2.39d	H	Cl	161.56 (C2), 149.28 (C8a), 128.08 (C5), 128.04 (C7), 124.45 (C6), 123.75 (C4a), 115.85 (C8), 53.97 (C3), 31.10 (C4)	138.15 (C4'), 135.35 (C1'), 129.97 (C2' + C6'), 128.75 (C3' + C5')	46.90	120.50	196.96

2.39e[1]	Br	H	161.45 (C2), 148.83 (C8a), 130.88 (C7), 130.67 (C5), 126.51 (C4a), 118.25 (C8), 116.03 (C6), 53.90 (C3), 30.87 (C4)	136.71 (C1′), 133.49 (C4′), 128.85 (C3′ + C5′), 128.12 (C2′ + C6′)	46.90	120.47	197.91
2.39f[1]	Br	Me	161.64 (C2), 149.35 (C8a), 128.11 (C5), 128.10 (C6), 124.54 (C7), 123.92 (C4a), 115.94 (C8), 54.18 (C3), 31.09 (C4)	136.74 (C1′), 133.34 (C4′), 128.76 (C3′ + C5′), 128.08 (C2′ + C6′), 21.12 (Me)	46.90	120.64	197.94
2.39g[1]	Br	Br	161.62 (C2), 148.67 (C8a), 130.72 (C7), 130.61 (C5), 126.30 (C4a), 118.04 (C8), 115.86 (C6), 53.62 (C3), 30.76 (C4)	135.58 (C1′), 131.69 (C3′ + C5′), 130.05 (C2′ + C6′), 127.41 (C4′)	46.20	120.22	197.01
2.39h[1,2]	Br	Cl	161.27 (C2), 148.67 (C8a), 130.72 (C7), 130.61 (C5), 126.30 (C4a), 118.05 (C8), 115.86 (C6), 53.62 (C3), 30.77 (C4)	138.19 (C4′), 135.26 (C1′), 129.96 (C2′ + C6′), 128.74 (C3′ + C5′)	46.23	120.23	196.80
2.39i[1,2]	Cl	H	161.20 (C2), 148.22 (C8a), 127.90 (C6), 127.81 (C7), 127.70 (C5), 126.00 (C4a), 117.67 (C8), 53.70 (C3), 30.78 (C4)	136.59 (C1′), 133.29 (C4′), 128.66 (C3′ + C5′), 127.99 (C2′ + C6′)	46.12	120.28	197.68

[1]data obtained from ref. 104



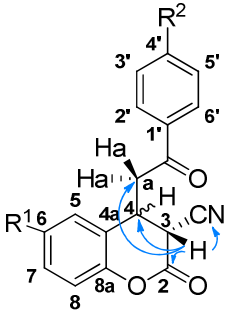


Table 59: ^{1}H NMR (400 MHz, DMSO-d$_6$, δ ppm) spectroscopic data for 4*H*-chromene-3-carbonitriles **2.50**

			Major isomer				Minor isomer			
Comp.	**R^1**	**R^2**	**H5-8, H2'-6'**	**H3**	**H4**	**Ha**	**H5-8, H2'-6'**	**H3**	**H4**	**Ha**
2.50a	H	H	7.93 (d, J= 7.6 Hz, 2H, H2' + H6'), 7.48 (t, J= 7.6 Hz, 1H, H4'), 7.60 (t, J= 7.6 Hz, 2H H3' + H5'), 7.40 (dd, J_1= 7.2, J_2=	5.22 (d, J= 7.2 Hz, 1H)	4.14 (m, 1H)	3.73 (dd, J_1= 18.4, J_2= 4.0 Hz, 1H), 3.54 (dd, J_1= 18.4, J_2= 6.8 Hz, 1H)	8.04 (d, J= 7.2 Hz, 2H, H2' + H6'), 7.69 (t, J= 7.6 Hz, 1H, H4'), 7.56 (t, J= 7.6 Hz, 2H, H3' + H5'), 7.35 (dd, J_1=7.2, J_2= 0.8	4.95 (d, J= 10.8 Hz, 1H)	4.29 (m, 1H)	3.85 (dd, J_1= 18.8, J_2= 4.0 Hz, 1H), 3.72 (dd, 1H)

			0.8 Hz, 1H, H5), 7.20-7.10 (m, 2H, H6, H7)				Hz, 1H, H5), 7.20-7.10 (m, 2H, H6, H7)				
2.50b	H	Me	7.81 (d, J= 8.4 Hz, 2H H3' + H5'), 7.51-7.0 (m, 6H, H2 + H6', H5, H6, H7, H8)	5.20 (d, J= 6.8 Hz, 1H)	4.12 (m, 1H)	3.65 (dd, J_1= 18.0, J_2= 4.0 Hz, 1H), 3.49 (dd, J_1= 18.0, J_2= 6.0 Hz, 1H),	7.94 (d, J= 8.0 Hz, 2H H3' + H5'), 7.51-7.0 (m, 6H, H2 + H6', H5, H6, H7, H8)	4.91 (d, J= 10.8 Hz, 1H)	4.34 (m, 1H)	3.72 (dd, J_1= 18.4, J_2= 4.0 Hz, 1H), 3.65 (dd, 1H)
2.50c	H	Br	7.81 (dd, J_1= 8.8, J_2= 1.2 Hz, 2H, H2' + H6'), 7.70 (dd, J_1= 6.4, J_2= 1.6 Hz, 2H, H3' + H5') 7.38 (dd, J_1= 7.6, J_2= 1.6 Hz, 1H, H5), 7.18-7.10 (m, 3H, H6, H7, H8)	5.20 (d, J= 6.8 Hz, 1H)	4.14 (m, 1H)	3.69 (dd, J_1= 18.4, J_2= 4.0 Hz, 1H), 3.51 (dd, J_1= 7.2, J_2= 18.4 Hz, 1H)	7.97 (d, J= 8.8 Hz, 2H H2' + H6'), 7.78 (d, J= 8.4 Hz, 2H H3' + H5'), 7.30 (dd, J_1= 8.0, J_2= 0.8 Hz, 1H H5) 7.18-7.10 (m, 3H, H6, H7, H8)	4.92 (d, J= 11.2 Hz, 1H)	4.26 (m, 1H)	3.82 (dd, J_1= 18.4, J_2= 4.4 Hz, 1H), 3.67 (dd, 1H)
2.50d	Br	H	7.94 (dd, J_1= 8.0, J_2= 0.8 Hz, 2H, H2' + H6'), 7.64 (t, J= 9.2 Hz, 1H, H4'), 7.57 (t, J_1= 8.0 Hz, 1H, H7), 7.52 (m, 1H, H5), 7.50 (t, J= 8.4 Hz, 2H, H3' + H5'), 7.10 (d, J= 8.8 Hz, 1H, H8)	5.22 (d, J= 7.2 Hz, 1H)	4.15 (m, 1H)	3.82 (dd, J_1= 18.8, J_2= 4.0 Hz, 1H), 3.57 (dd, J_1= 18.8, J_2= 6.4 Hz, 1H)	8.04 (dd, J_1= 8.4, J_2= 1.2 Hz, 2H, H2' + H6'), 7.69 (dt, J_1= 7.2, J_2= 1.2 Hz, 1H, H7), 7.64 (t, J= 9.2 Hz, 1H, H4'), 7.52 (m, 1H, H5), 7.50 (t, J= 8.4 Hz, 2H, H3' + H5'), 7.16 (d, J= 8.8 Hz, 1H, H8)	4.94 (d, J= 10.8 Hz, 1H)	4.30 (m, 1H)	3.97 (dd, J_1= 19.2, J_2= 4.4 Hz, 1H), 3.82 (dd, 1H)
2.50e[1]	Br	Br	7.87 (d, J= 8.8 Hz, 2H, H2' + H6'), 7.71 (d, J= 8.8 Hz, 2H, H3' + H5'), 7.63 (d, J= 2.4 Hz, 1H, H5), 7.49 (dd, J_1= 8.4, J_2= 2.4 Hz, 1H, H7), 7.10 (d, J= 8.4 Hz, 1H, H8)	5.20 (d, J= 7.6 Hz, 1H)	4.14 (m, 1H)	3.76 (dd, J_1= 18.8, J_2= 4.0 Hz, 1H), 3.53 (dd, J_1= 18.8, J_2= 6.8 Hz, 1H)	7.96 (d, J= 8.4 Hz, 2H, H2' + H6'), 7.78 (d, J= 8.8 Hz, 2H, H3' + H5'), 7.63 (d, J= 2.4 Hz, 1H, H5), 7.54 (dd, J_1= 8.8, J_2= 2.4 Hz, 1H, H7), 7.15 (d, J= 8.4 Hz, 1H, H8)	4.91 (d, J= 10.8 Hz, 1H)	4.28 (m, 1H)	3.86 (dd, J_1= 18.8, J_2= 4.0 Hz, 1H), 3.76 (dd, 1H)
2.50f[1]	Br	Cl	7.95 (d, J= 8.4 Hz, 2H, H2' + H6'), 7.64 (m, 1H, H5), 7.57 (d, J= 8.4 Hz, 2H, H3' + H5'), 7.50 (dd, J_1= 8.4, J_2= 2.4 Hz, 1H, H7), 7.10 (d, J= 8.8 Hz, 1H, H8)	5.21 (d, J= 7.2 Hz, 1H)	4.15 (m, 1H)	3.82 (dd, J_1= 19.2, J_2= 4.0 Hz, 1H), 3.57 (dd, J_1= 18.8, J_2= 6.8 Hz, 1H)	8.04 (d, J= 8.4 Hz, 2H, H2' + H6'), 7.64 (m, 1H, H5), 7.57 (d, J= 8.4 Hz, 2H, H3' + H5'), 7.53 (dd, J_1= 8.8, J_2= 2.4 Hz, 1H, H7), 7.15 (d, J= 8.4 Hz, 1H, H8)	4.92 (d, J= 10.8 Hz, 1H)	4.29 (m, 1H)	3.92 (dd, J_1= 19.2, J_2= 4.8 Hz, 1H), 3.79 (dd, 1H)

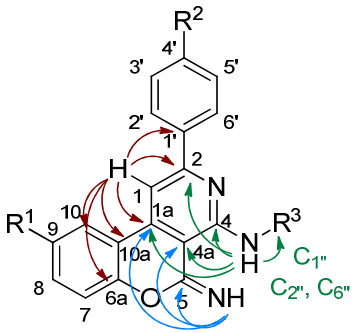
Table 60: ^{13}C NMR (100 MHz, DMSO-d_6, δ ppm) spectroscopic data for 4*H*-chromene-3-carbonitriles **2.50**

			Major isomer					Minor isomer				
Compound	**R^1**	**R^2**	**C2-8a**	**C1'-6'**	**C3/C4/a**	**CN**	**C=O**	**C2-8a**	**C1'-6'**	**C3/C4/a**	**CN**	**C=O**
2.50a	H	H	161.13 (C2), 150.19 (C8a), 129.07 (C5), 126.75 (C6), 124.73 (C7), 122.71 (C4a), 116.67 (C8)	144.31 (C4'), 133.32(C1'), 129.28 (C3' + C5'), 128.21 (C2' + C6')	37.37 (C3), 32.75 (C4), 40.71 (Ca)	115.31	196.79	161.14 (C2), 150.13 (C8a), 129.18 (C5), 126.84 (C6), 125.05 (C7), 123.53 (C4a), 116.67 (C8)	144.31 (C4'), 133.58 (C1'), 129.34 (C3' + C5'), 128.02 (C2' + C6')	37.59 (C3), 33.17 (C4), 38.85 (Ca)	115.60	196.79
2.50b	H	Me	161.22 (C2), 150.21 (C8a), 129.06 (C5), 126.93 (C6), 124.54 (C7), 123.51 (C4a), 116.76 (C8)	135.68 (C1'), 133.88 (C4'), 128.83 (C3' + C5'), 128.16 (C2' + C6')	37.43 (C3), 33.17 (C4), 40.95 (Ca)	115.38	197.44	161.55 (C2), 150.27 (C8a), 129.18 (C5), 127.96 (C6), 125.13 (C7), 122.69 (C4a), 116.76 (C8)	136.06 (C1'), 133.88 (C4'), 128.91 (C3' + C5'), 128.16 (C2' + C6')	37.65 (C3), 32.51 (C4), 39.76 (Ca)	115.67	197.30
2.50c	H	Br	161.20 (C2), 150.16 (C8a), 129.05 (C5), 126.90 (C6), 124.81 (C7), 122.70 (C4a), 116.74 (C8)	134.68 (C1'), 128.00 (C4'), 131.84 (C3' + C5'), 130.17 (C2' + C6')	37.42 (C3), 33.08 (C4), 40.58 (Ca)	115.28	196.55	161.43 (C2), 150.21 (C8a), 129.19 (C5), 126.90 (C6), 125.08 (C7), 123.40 (C4a), 116.74 (C8)	135.05 (C1'), 127.94 (C4'), 131.92 (C3' + C5'), 130.17 (C2' + C6')	37.58 (C3), 32.69 (C4), 38.86 (Ca)	115.58	196.63
			160.65 (C2), 149.48 (C8a),					160.95 (C2), 149.64 (C8a),		37.17 (C3),		

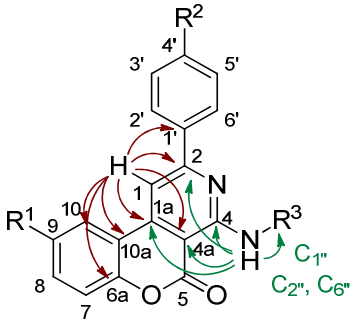
2.50d	Br	H	131.80 (C7), 131.63 (C5), 124.99 (C4a), 118.93 (C8), 116.31 (C6)	135.48 (C1'), 133.90 (C4'), 128.81 (C3' + C5'), 128.16 (C2' + C6')	36.95 (C3), 32.74 (C4), 40.77 (Ca)	115.04	197.49	131.70 (C7), 129.58 (C5), 126.07 (C4a), 118.93 (C8), 116.87 (C6)	136.01 (C1'), 133.78 (C4'), 128.77 (C3' + C5'), 128.16 (C2' + C6')	32.62 (C4), 38.87 (Ca)	115.37	197.22
2.50e[1]	Br	Br	-	-	-	-	-	-	-	-	-	-
2.50f[1]	Br	Cl	-	-	-	-	-	-	-	-	-	-

[1]Identified by ^{1}H NMR and IR spectroscopy; the sample evolved during ^{13}C and two-dimensional NMR spectra collection

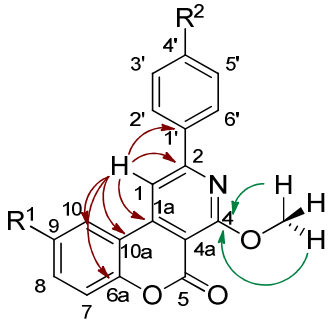
Table 61: ^{1}H NMR (400 MHz, DMSO-d$_6$, δ ppm) spectroscopic data obtained for 5-imino and 5-oxo-*N*,2-diaryl-5*H*-chromeno[3,4-*c*]pyridin-4-amines **2.55, 2.56a** and **2.69**



2.55



2.56



2.69

Compound	R^1	R^2	R^3	H7-10	H2'-6'	R^3 (H2''-6')	H1	NH-Ar	NH	OMe/Me
2.55a	Br	H	C_6H_5	8.77 (d, *J*= 2.4 Hz, 1H, H_{10}), 7.70 (dd, J_1= 8.0, J_2= 1.2 Hz, 1H, H_8), 7.19 (d, *J*= 8.0 Hz, 1H, H_7)	7.80 (d, *J*= 7.6 Hz, 2H, H2'' + H6''), 7.57-7.37 (m, 5H, H3' +H5', H4', H3'' +H5''), 7.05 (t, *J*= 8.0 Hz, 1H, H4'')		8.13 (s, 1H)	12.75 (s, 1H)	9.31 (s, 1H)	-

2.55b	H	H	C_6H_5	8.51 (dd, J_1= 8.0, J_2= 1.2 Hz, 1H, H10), 8.30 (dd, J_1= 8.0, J_2= 1.6 Hz, 2H, H2' + H6'), 7.83 (dd, J_1= 8.8, J_2= 1.2 Hz, 2H, H2'' + H6''), 7.60-7.32 (m, 4H, H8, H4', H3' + H5'), 7.40 (t, J= 7.6 Hz, 2H, H3'' + H5''), 7.34 (dt, J_1= 7.6, J_2= 1.2 Hz, 1H, H8), 7.26 (dd, J_1= 8.0, J_2= 1.2 Hz, 1H, H7), 7.04 (dt, J_1= 7.2, J_2= 1.2 Hz, 1H, H4'')			8.10 (s, 1H)	12.84 (s, 1H)	9.26 (s, 1H)	-
2.55c	H	H	4-MeC_6H_4	8.50 (dd, J_1= 8.0, J_2= 1.2 Hz, 1H, H10), 8.30 (dd, J_1= 8.0, J_2= 1.6 Hz, 2H, H2' + H6'), 7.69-7.48 (m, 4H, H8, H3' + H5', H4'), 7.33 (dt, J_1= 8.4, J_2= 1.2 Hz, 1H, H9), 7.24 (dd, J_1= 8.0, J_2= 0.8 Hz, 1H, H7),	7.70 (d, J= 7.6 Hz, 2H, H2'' + H6''), 7.20 (d, J= 8.4 Hz, 2H, H3'' + H5'')		8.07 (s, 1H)	12.72 (s, 1H)	9.21 (s, 1H)	2.90 (s, 3H)
2.55d	H	H	4-$OMeC_6H_4$	8.49 (dd, J_1= 8.0, J_2= 1.2 Hz, 1H, H10), 8.28 (dd, J_1= 8.0, J_2= 1.6 Hz, 2H, H2' + H6'), 7.59-7.46 (m, 4H, H8, H3' + H5', H4'), 7.33 (dt, J_1= 8.4, J_2= 1.2 Hz, 1H, H9), 7.23 (dd, J_1= 8.4, J_2= *1.2* Hz, 1H, H7)	7.72 (dd, J_1= 6.4, J_2= 2.0 Hz 2H, $H_{2''}$ + $H_{6''}$), 6.97 (dd, J_1= 6.8, J_2= 2.0 Hz, 2H, $H_{3''}$ + $H_{5''}$)		8.08 (s, 1H)	12.59 (s, 1H)	9.17 (s, 1H)	3.77 (s, 3H)
2.55e	H	H	3-BrC_6H_4	8.53 (dd, J_1= 7.6, J_2= 1.2 Hz, 1H, H10), 8.52 (d, J= 2.0 Hz, 1H, H6''), 8.31 (dd, J_1= 7.6, J_2= 2.0 Hz, 2H, H2' + H6'), 7.60-7.52 (m, 5H, H8, H3' + H5', H4', H2''), 7.32 (dt, J_1= 8.4, J_2= 1.2 Hz, 1H, H9), 7.31 (d, J= 8.0 Hz, 1H, H4'), 7.23 (dd, J_1= 8.0, J_2= 0.8 Hz, 1H, H7), 7.22 (dd, J_1= 8.0, J_2= 0.8 Hz, 1H, H3'')			8.16 (s, 1H)	13.03 (s, 1H)	9.31 (s, 1H)	-
2.55f	H	Br	C_6H_5	8.48 (dd, J_1= 8.4, J_2= 1.6 Hz, 1H, H10), 7.57 (dt, J_1= 8.4, J_2= 1.2 Hz, 1H, H8), 7.33 (dt, J_1= 7.6, J_2= 1.2 Hz, 1H, H9), 7.23 (dd, J_1= 8.4, J_2= 1.2 Hz, 1H, H7)	8.24 (dd, J_1= 8.8, J_2= 2.4 Hz, 2H, H2' + H6'), 7.74 (dd, J_1= 8.8, J_2= 2.0 Hz, 2H, H3' + H5')	7.79 (dd, J_1= 8.8, J_2= 1.2 Hz, 2H, H2'' + H6''), 7.38 (dt, J_1= 7.6, J_2= 0.8 Hz, 2H, H3'' + H5''), 7.06 (dt, J_1= 7.6, J_2= 1.2 Hz, 1H, H4'')	8.08 (s, 1H)	12.81 (s, 1H)	9.24 (s, 1H)	-

2.55g	H	Br	4-$OMeC_6H_4$	8.45 (dd, J_1= 8.0, J_2= 1.2 Hz, 1H, H10), 7.56 (dt, J_1= 7.2, J_2= 1.2 Hz, 1H, H8), 7.33 (dt, J_1= 7.2, J_2=1.2 Hz, 1H, H9), 7.22 (dd, J_1= 8.4, J_2= 1.2 Hz, 1H, H7)	8.21 (dd, J_1= 8.8, J_2= 2.0 Hz, 2H, H2' + H6'), 7.72 (dd, J_1= 6.8, J_2= 1.6 Hz, 2H, H3' + H5')	7.68 (dd, J_1= 6.8, J_2= 2.0 Hz, 2H, H2'' + H6''), 6.96 (dd, J_1= 9.2, J_2= 2.4 Hz, 2H, H3'' + H5'')	8.02 (s, 1H)	12.53 (s, 1H)	9.17 (s, 1H)	3.76 (s, 3H)
2.55j	H	Cl	4-$OMeC_6H_4$	8.44 (dd, J_1= 8.0, J_2= 1.2 Hz, 1H, H10), 7.56 (dt, J_1= 8.8, J_2= 0.8 Hz, 1H, H8), 7.32 (dt, J_1= 8.0, J_2= 0.8 Hz, 1H, H9), 7.22 (dd, J_1= 8.0, J_2= 0.8 Hz, 1H, H7)	8.27 (dd, J_1= 6.8, J_2= 2.0 Hz, 2H, H2' + H6'), 7.58 (dd, J_1= 8.4, J_2= 1.6 Hz, 2H, H3' + H5')	7.67 (dd, J_1= 6.8, J_2= 2.0 Hz, 2H, H2'' + H6''), 6.96 (dd, J_1= 8.8, J_2= 2.0 Hz, 2H, H3'' + H5'')	8.00 (s, 1H)	12.57 (s, 1H)	9.17 (s, 1H)	3.76 (s, 3H)
2.55l	Br	H	4-$OMeC_6H_4$	8.71 (d, J= 2.4 Hz, 1H, H10), 8.29 (dd, J_1= 8.0, J_2= 1.6 Hz, 2H, H2' + H6'), 7.69-7.65 (m, 3H, H8, H2'' + H6''), 7.56-7.44 (m, 3H, H3' + H5'', H4'), 7.15 (d, J= 8.0 Hz, 1H, H7), 6.96 (dd, J_1= 9.2, J_2= 1.2 Hz, 2H, H3'' + H5'')			8.03 (s, 1H)	12.49 (s, 1H)	9.13 (s, 1H)	3.75 (s, 3H)
2.55m	Br	H	3-BrC_6H_4	8.78 (d, J= 2.4 Hz, 1H, H10), 7.70 (dd, J_1= 8.8, J_2= 2.4 Hz, 1H, H8), 7.18 (d, J= 8.8 Hz, 1H, H7)	8.32 (dd, J_1= 8.0, J_2= 1.2 Hz, 2H, H2' + H6'), 7.90 (dd, J_1= 8.8, J_2= 2.0 Hz, 2H, H4'' + H6''), 7.57-7.51 (m, 5H, H3' + H5', H4', H2'', H5'')		8.32 (s, 1H)	12.86 (s, 1H)	9.36 (s, 1H)	-
2.55n	Br	Me	C_6H_5	8.71 (d, J= 2.4 Hz, 1H, H10), 7.68 (dd, J_1= 8.8, J_2= 2.4 Hz, 1H, H8), 7.18 (d, J= 8.4 Hz, 1H, H7)	8.20 (d, J= 7.6 Hz, 2H, H2' + H6'), 7.58 (dd, J_1= 8.4, J_2= 1.6 Hz, 2H, H3' + H5')	7.78 (dd, J_1= 8.4, J_2= 0.8 Hz, 2H, H2'' + H6''), 7.37 (dt, J_1= 7.2, J_2= 1.6 Hz, 2H, H3'' + H5''), 7.05 (dt, J_1= 7.6, J_2= 1.2 Hz, 1H, H4'')	8.05 (s, 1H)	12.71 (s, 1H)	9.22 (s, 1H)	2.37 (s, 3H)
2.55p	Br	Me	4-MeC_6H_4	8.75 (d, J= 2.4 Hz, 1H, H10), 7.68 (dd, J_1= 8.8, J_2= 2.4 Hz,	8.22 (d, J= 8.0 Hz, 2H, H2' + H6'), 7.33 (d, J=	7.67 (d, J= 8.4 Hz, 2H, H2'' + H6''), 7.18 (d, J= 8.4 Hz, 2H, H3'' + H5'')	8.09 (s, 1H)	12.62 (s, 1H)	9.23 (s, 1H)	2.38 (s, 3H, $C_{4'}$-Me), 2.29 (s, 3H, $C_{4''}$-Me)

			1H, H8), 7.17 (d, J= 8.8 Hz, 1H, H7)	8.4 Hz, 2H, H3' + H5')						
2.55q	Br	Me	4-$OMeC_6H_4$	8.65 (d, J= 2.4 Hz, 1H, H10), 7.65 (dd, J_1= 9.2, J_2= 2.0 Hz, 1H, H8), 7.14 (d, J= 8.4 Hz, 1H, H7)	8.15 (d, J= 8.4 Hz, 2H, H2' + H6'), 7.29 (d, J= 8.0 Hz, 2H, H3' + H5')	7.64 (dd, J_1= 8.8, J_2= 2.0 Hz, 2H, H2'' + H6''), 6.94 (dd, J_1= 8.8, J_2= 2.0 Hz, 2H, H3'' + H5'')	7.95 (s, 1H)	12.44 (s, 1H)	9.10 (s, 1H)	3.74 (s, 3H)
2.55u	Br	Br	4-MeC_6H_4	8.75 (d, J= 2.0 Hz, 1H, H10), 7.70 (dd, J_1= 9.2, J_2= 2.0 Hz, 1H, H8), 7.18 (d, J= 8.8 Hz, 1H, H7)	8.26 (d, J= 8.4 Hz, 2H, H2' + H6'), 7.72 (d, J= 8.8 Hz, 2H, H3' + H5')	7.64 (d, J= 8.0 Hz, 2H, H2'' + H6''), 7.18 (d, J= 8.4 Hz, 2H, H3'' + H5'')	8.11 (s, 1H)	12.63 (s, 1H)	9.29 (s, 1H)	2.29 (s, 3H)
2.55b'	Br	Cl	4-$OMeC_6H_4$	8.70 (d, J= 2.4 Hz, 1H, H10), 7.65 (dd, J_1= 8.8, J_2= 2.4 Hz, 1H, H8), 7.12 (d, J= 8.8 Hz, 1H, H7)	8.28 (dd, J_1= 8.8, J_2= 2.0 Hz 2H, H3' + H5'), 7.54 (dd, J_1= 8.8, J_2= 2.0 Hz, 2H, H2' + H6')	7.53 (dd, J_1= 9.2, J_2= 2.0 Hz, 2H, H2'' + H6''), 6.93 (dd, J_1= 9.2, J_2= 2.4 Hz, 2H, H3'' + H5'')	8.00 (s, 1H)	12.46 (s, 1H)	9.19 (s, 1H)	3.75 (s, 3H)
2.55c'	Br	Cl	3-$OMeC_6H_4$	8.54 (d, J= 2.4 Hz, 1H, H10), 7.65 (dd, J_1= 8.4, J_2= 2.4 Hz, 1H, H8), 7.15 (d, J= 8.8 Hz, 1H, H7)	8.26 (dd, J_1= 8.4, J_2= 2.0 Hz, 2H, H3' + H5'), 7.53 (dd, J_1= 8.8, J_2= 2.0 Hz, 2H, H2' + H6')	7.61 (t, J= 2.4Hz, 1H, H2''), 7.24 (t, J= 8 Hz, 1H, H5''), 7.16 (dd, J_1= 8.0, J_2= 0.8 Hz, 1H, H6''), 6.63 (dd, J_1= 8.0, J_2= 1.2 Hz, 1H, H4'')	7.95 (s, 1H)	12.56 (s, 1H)	8.92 (s, 1H)	3.79 (s, 3H)
2.55d'	Cl	H	C_6H_5	8.56 (d, J= 2.4 Hz, 1H, H10), 8.28 (dd, J_1= 8.4, J_2= 2.0 Hz, 2H, H2' + H6'), 7.77 (d, J_1= 8.4, J_2= 1.2 Hz, 2H, H2''+ H6''), 7.55-7.49 (m, 4H, H8, H3'+H5', H4'), 7.37(dt, J_1= 8.4, J_2= 1.6 Hz, 2H, H3''+H5''), 7.10 (d, J= 8.0 Hz, 1H, H7), 7.04 (dt, J_1= 7.6, J_2= 0.8 Hz, 1H, H4'')			8.05 (s, 1H)	12.70 (s, 1H)	9.21 (s, 1H)	-

2.55f'	Cl	H	4-MeC_6H_4	8.60 (d, J= 2.4 Hz, 1H, H10), 7.56 (dd, J_1= 8.8, J_2= 2.4 Hz, 1H, H8), 7.24 (d, J= 8.8 Hz, 1H, H7)	8.29 (dd, J_1= 8.4, J_2= 2.0 Hz, 2H, H2' + H6'), 7.54-7.48 (m, 3H, H3' + H5'', H4')	7.66 (dd, J_1= 8.4, J_2= 2.0 Hz, 2H, H2'' + H6''), 7.18 (d, J= 8.4 Hz, 2H, H3'' + H5'')	8.06 (s, 1H)	12.60 (s, 1H)	9.22 (s, 1H)	2.28 (s, 3H)
2.55g'	Cl	H	4-$OMeC_6H_4$	8.58 (d, J= 2.4 Hz, 1H, H10), 7.53 (dd, J_1= 8.8, J_2= 2.4 Hz, 1H, H8), 7.19 (d, J= 8.8 Hz, 1H, H7)	8.27 (dd, J_1= 8.0, J_2= 1.6 Hz, 2H, H2' + H6'), 7.52-7.48 (m, 3H, H3' + H5'', H4')	7.67 (dd, J_1= 9.2, J_2= 2.0 Hz, 2H, H2'' + H6''), 6.95 (dd, J_1= 9.2, J_2= 2.4 Hz, 2H, H3'' + H5'')	8.01 (s, 1H)	12.49 (s, 1H)	9.17 (s, 1H)	3.75 (s, 3H)
2.56a	Br	H	C_6H_5	8.79 (d, J= 2.4 Hz, 1H, H10), 7.78 (dd, J_1= 8.8, J_2= 2.0 Hz, 1H, H8), 7.36 (d, J= 8.8 Hz, 1H, H7)	8.29 (dd, J_1= 8.8 Hz, 2H, H2' + H6'), 7.79 (d, J= 7.6 Hz, 2H, H2'' + H6''), 7.55-7.51 (m, 3H, H3' +H5', H4'), 7.40 (dt, J_1= 7.2, J_2= 2.0 Hz, 2H, H3'' + H5''), 7.12 dt, J_1= 7.2, J_2= 0.8 Hz, 1H, H4'')		8.17 (s, 1H)	10.68 (s, 1H)	-	-
2.69a	H	H	-	8.65 (dd, J_1= 8.0, J_2= 1.2 Hz, 1H, H10), 7.68 (dt, J_1= 7.6, J_2= 1.2 Hz, 1H, H8), 7.43 (dt, J_1= 8.0, J_2= 0.8 Hz, 1H, H9), 7.39 (dd, J_1= 8.0, J_2= 1.2 Hz, 1H, H7)	8.40 (dd, J_1= 8.0, J_2= 2.0 Hz, 2H, H2' + H6'), 7.60-7.53 (m, 3, H3' + H5', H4')	-	8.48 (s, 1H)	-	-	4.14 (s, 3H)
2.69b	Br	H	-	8.60 (d, J= 2.0 Hz, 1H, H9), 7.80 (dd, J_1= 8.8, J_2= 2.4 Hz, 1H, H8), 8.65 (dd, J_1= 8.0, J_2= 1.2 Hz, 1H, H10), 7.34 (d, J= 8.0 Hz, 1H, H7)	8.41 (dd, J_1= 8.0, J_2= 2.0 Hz, 2H, H2' + H6'), 7.60-7.55 (m, 3, H3' + H5', H4')	-	8.50 (s, 1H)	-	-	4.14 (s, 3H)

Table 62: ^{13}C NMR (100 MHz, DMSO-d_6, δ ppm) spectroscopic data for 5-imino and 5-oxo-*N*,2-diaryl-5*H*-chromeno[3,4-*c*]pyridin-4-amines **2.55, 2.56a** and **2.69**

Compound	R^1	R^2	R^3	C2-10a	C1'-6'	R^3(C1''-6'')	C1	C5	OMe/Me
2.55a	Br	H	C_6H_5	157.71 (C2), 154.45 (C4), 150.78 (C6a), 140.62 (C1a), 134.80 (C8), 127.56 (C10), 119.14 (C10a), 118.40 (C7), 116.19 (C9), 99.88 (C4a)	138.04 (C1'), 128.77 (C4'), 130.12 (C3' + C5'), 127.36 (C2' + C6')	139.93 (C1''), 128.96 (C3'' + C5''), 122.56 (C4''), 120.18 (C2'' + C6'')	102.31	155.37	-
2.55b	H	H	C_6H_5	157.49 (C2), 154.53 (C4), 151.61 (C6a), 141.66 (C1a), 132.36 (C8), 125.22 (C10), 124.00 (C9), 116.84 (C10a), 116.10 (C7), 99.93 (C4a)	138.18 (C1'), 128.80 (C4'), 129.98 (C3' + C5'), 127.21 (C2' + C6')	140.01 (C1''), 128.92 (C3'' + C5''), 122.41 (C4''), 120.07 (C2'' + C6'')	102.04	155.85	-
2.55c	H	H	4-MeC_6H_4	157.48 (C2), 155.86 (C4), 151.61 (C6a), 141.60 (C1a), 132.31 (C8), 125.19 (C10), 123.98 (C9), 116.88 (C10a), 116.09 (C7), 99.71 (C4a)	138.21 (C1'), 128.77 (C3' + C5'), 129.85 (C4'), 127.18 (C2' + C6')	140.01 (C1''), 131.35 (C4''), 128.92 (C3'' + C5''), 120.17 (C2'' + C6'')	102.04	155.85	20.44
2.55d	H	H	4-$OMeC_6H_4$	157.51 (C2), 154.60 (C4), 151.61 (C6a), 141.55 (C1a), 133.24 (C8), 125.16 (C10), 123.93 (C9), 116.89 (C10a), 116.06 (C7), 99.71 (C4a)	138.23 (C1'), 128.72 (C3' + C5'), 129.88 (C4'), 127.16 (C2' + C6')	154.84 (C4''), 133.05 (C1''), 121.79 (C2'' + C6''), 114.05 (C3'' + C5'')	102.04	155.86	55.22
2.55e	H	H	3-BrC_6H_4	157.29 (C2), 154.16 (C4), 151.59 (C6a), 141.59 (C1a), 132.47 (C8), 125.26 (C10), 124.04 (C9), 116.73 (C10a), 116.12 (C7), 100.39 (C4a)	138.01 (C1'), 128.79 (C4'), 130.12 (C3' + C5'), 127.20 (C2' + C6')	141.77 (C1''), 130.77 (C5''), 124.60 (C4''), 122.21 (C6''), 121.77 (C3''), 118.66 (C2'')	102.73	155.76	54.93
2.55f	H	Br	C_6H_5	156.24 (C2), 154.49 (C4), 151.63 (C6a), 141.81 (C1a), 132.41 (C8), 125.21 (C10), 123.98 (C9), 116.78 (C10a), 116.11 (C7), 100.23 (C4a)	137.38 (C1'), 131.74 (C3' + C5'), 129.21 (C2' + C6'), 134.70 (C4')	139.90 (C1''), 128.94 (C3'' + C5''), 122.50 (C4''), 120.13 (C2'' + C6'')	102.05	155.80	-

2.55g	H	Br	4-$OMeC_6H_4$	156.25 (C2), 154.56 (C4), 151.63 (C6a), 141.71 (C1a), 132.30 (C8), 125.16 (C10), 123.92 (C9), 116.83 (C10a), 116.07 (C7), 99.74 (C4a)	137.43 (C1'), 131.67 (C3' + C5'), 129.17 (C2' + C6'), 134.70 (C4')	154.90 (C4''), 132.92 (C1''), 121.89 (C2'' + C6''), 114.06 (C3'' + C5'')	101.37	155.81	55.20
2.55j	H	Cl	4-$OMeC_6H_4$	156.16 (C2), 155.82 (C4), 151.63 (C6a), 141.69 (C1a), 132.29 (C8), 125.15 (C10), 123.92 (C9), 116.84 (C10a), 116.08 (C7), 99.70 (C4a)	137.07 (C1'), 134.70 (C4'), 128.91 (C2' + C6'), 128.74 (C3' + C5')	154.91 (C4''), 132.94 (C1''), 121.90 (C2'' + C6''), 114.06 (C3'' + C5'')	101.39	154.57	55.22
2.55l	Br	H	4-$OMeC_6H_4$	157.67 (C2), 154.46 (C4), 150.72 (C6a), 140.43 (C1a), 134.60 (C8), 127.29 (C10), 119.15 (C10a), 118.28 (C7), 116.09 (C9), 99.33 (C4a)	138.08 (C1'), 128.63 (C4'), 129.95 (C3' + C5'), 127.46 (C2' + C6')	154.88 (C4''), 132.96 (C1''), 121.84 (C2'' + C6''), 114.03 (C3'' + C5'')	101.59	155.34	55.23
2.55m	Br	H	3-BrC_6H_4	157.69 (C2), 154.19 (C4), 150.78 (C6a), 140.69 (C1a), 134.89 (C8), 127.60 (C10), 119.06 (C10a), 118.43 (C7), 116.23 (C9), 100.18 (C4a)	137.89 (C1'), 128.83 (C4'), 130.18 (C3' + C5'), 127.41 (C2' + C6')	139.27 (C1''), 131.69 (C5''), 131.19 (C2''), 122.05 (C4'', C6''), 113.83 (C3'')	102.78	155.33	-
2.55n	Br	Me	C_6H_5	157.89 (C2), 155.59 (C4), 150.88 (C6a), 140.63 (C1a), 134.90 (C8), 127.59 (C10), 119.26 (C10a), 118.57 (C7), 116.31 (C9), 99.67 (C4a)	140.08 (C4'), 135.41 (C1'), 127.42 (C2' + C6'), 129.09 (C3' + C5')	140.12 (C1''), 129.09 (C3'' + C5''), 122.68 (C4''), 120.27 (C2'' + C6'')	101.96	154.55	21.12
2.55p	Br	Me	4-MeC_6H_4	157.63 (C2), 154.35 (C4), 150.70 (C6a), 140.38 (C1a), 134.59 (C8), 127.47 (C10), 119.17 (C10a), 118.26 (C7), 116.07 (C9), 99.29 (C4a)	139.76 (C4'), 135.30 (C1'), 129.25 (C3' + C5'), 127.23 (C2' + C6')	137.37 (C1''), 131.31 (C4''), 129.25 (C3'' + C5''), 120.12 (C2'' + C6'')	101.48	155.32	20.94 (C4'-Me), 20.44 (C4'-Me)

2.55q	Br	Me	4-$OMeC_6H_4$	157.90 (C2), 154.60 (C4), 150.86 (C6a), 140.48 (C1a), 134.74 (C8), 127.52 (C10), 119.31 (C10a), 118.49 (C7), 116.25 (C9), 99.16 (C4a)	139.97 (C4'), 135.48 (C1'), 129.45 (C3' + C5'), 127.38 (C2' + C6')	155.02 (C4''), 133.17 (C1''), 122.00 (C2'' + C6''), 114.18 (C3'' + C5'')	101.28	155.62	55.41
2.55u	Br	Br	4-MeC_6H_4	156.36 (C2), 154.38 (C4), 150.76 (C6a), 140.69 (C1a), 134.76 (C8), 127.55 (C10), 119.07 (C10a), 118.32 (C7), 116.12 (C9), 99.96 (C4a)	137.20 or 137.24 (C1'), 131.64 (C3' + C5'), 129.30 (C2' + C6'), 123.74 (C4')	137.20 or 137.24 (C1''), 131.54 (C4''), 129.33 (C3'' + C5''), 120.26 (C2'' + C6'')	101.13	155.26	20.48
2.55b'	Br	Cl	4-$OMeC_6H_4$	156.21 (C2), 154.34 (C4), 150.68 (C6a), 140.51 (C1a), 134.60 (C8), 127.46 (C10), 119.03 (C10a), 118.21 (C7), 116.06 (C9), 99.55 (C4a)	136.83 (C1'), 134.80 (C4'), 128.58 (C3' + C5'), 128.97 (C2' + C6')	154.88 (C4''), 132.80 (C1''), 121.85 (C2'' + C6''), 113.98 (C3'' + C5'')	101.15	155.21	55.19
2.55c'	Br	Cl	3-$OMeC_6H_4$	156.39 (C2), 154.24 (C4), 150.47 (C6a), 140.29 (C1a), 134.37 (C8), 126.96 (C10), 118.71 (C10a), 117.97 (C7), 115.77 (C9), 99.92 (C4a)	136.77 (C1'), 134.66 (C4'), 128.66 (C3' + C5'), 128.22 (C2' + C6')	159.70 (C3''), 140.84 (C1''), 129.07 (C5''), 112.46 (C6''), 108.54 (C4''), 105.75 (C2'')	101.94	155.25	54.93
2.55d'	Cl	H	C_6H_5	157.82 (C2), 154.54 (C4), 150.41 (C6a), 140.72 (C1a), 132.08 (C8), 128.46 (C9), 127.56 (C10), 118.73 (C10a), 118.19 (C7), 99.93 (C4a)	138.13 (C1'), 128.89 (C4'), 130.24 (C3' + C5'), 127.44 (C2' + C6')	140.03 (C1''), 129.06 (C3'' + C5''), 122.68 (C4''), 120.29 (C2'' + C6'')	102.33	155.57	-
2.55f'	Cl	H	4-MeC_6H_4	157.88 (C2), 154.61 (C4), 150.46 (C6a), 140.77 (C1a), 132.05 (C8), 128.47 (C9), 127.79 (C10), 118.81 (C10a), 118.26 (C7), 99.77 (C4a)	138.18 (C1'), 128.92 (C4'), 130.27 (C3' + C5'), 127.42 (C2' + C6')	137.46 (C1''), 131.73 (C4''), 129.50 (C3'' + C5''), 120.42 (C2'' + C6'')	102.04	155.61	20.65

2.55g'	Cl	H	4-OMeC$_6$H$_4$	157.62 (C2), 154.41 (C4), 150.24 (C6a), 140.44 (C1a), 131.68 (C8), 128.19 (C9), 124.61 (C10), 118.67 (C10a), 117.90 (C7), 99.30 (C4a)	138.05 (C1'), 128.59 (C4'), 129.90 (C3' + C5'), 127.25 (C2' + C6')	154.84 (C4''), 132.95 (C1''), 121.77 (C2'' + C6''), 113.98 (C3'' + C5'')	101.56	155.33	55.20
2.56a	Br	H	C$_6$H$_5$	160.17 (C2), 160.65 (C4), 150.47 (C6a), 143.52 (C1a), 134.80 (C8), 127.13 (C10), 118.49 (C10a), 118.24 (C7), 116.87 (C9), 97.54 (C4a)	137.32 (C1'), 128.44 (C4'), 130.09 (C3' + C5'), 127.28 (C2' + C6')	138.68 (C1''), 128.35 (C3'' + C5''), 122.92 (C4''), 120.64 (C2'' + C6'')	102.43	155.47	-
2.69a	H	H	-	163.63 (C4), 158.35 (C2), 152.57 (C6a), 146.81 (C1a), 133.03 (C8), 125.50 (C10), 124.51 (C9), 119.49 (C7), 118.61 (C10a), 101.96 (C4a)	136.99 (C1'), 130.77 (C4'), 128.92 (C3' + C5'), 127.59 (C2' + C6')	-	105.59	155.86	-
2.69b	Br	H	-	163 .76(C4), 158.88 (C2), 151.86 (C6a), 145.94 (C1a), 135.69 (C8), 127.96/127.90 (C10), 119.49 (C7), 118.61 (C10a), 117.00 (C9), 101.99 (C4a)	137.02 (C1'), 131.17 (C4'), 129.12 (C3' + C5'), 127.96/127.90 (C2' + C6')	-	106.02	155.82	-

Compounds **2.60a**, **2.61a**, **2.68**, **2.70a** and **2.71** spectroscopic data is described in **Tables 62** and **63**. Compound **2.60a** can be identified, by ^{1}H NMR, by its double doublet at δ 5.26 ppm (H4), its doublet at δ 4.68 ppm (H5), and its singlets at δ 8.81 (N1-H), 8-51 (NH-R^{3}) and 9.94 (OH) ppm. In the ^{13}C NMR spectra, the most relevant signals correspond to the dihydropyridine ring, which are observed at δ 148.96 (C2), 134.95 (C6), 101.19 (C5), 64.04 (C3) and 34.48 ppm (C4) (**Scheme 35**).

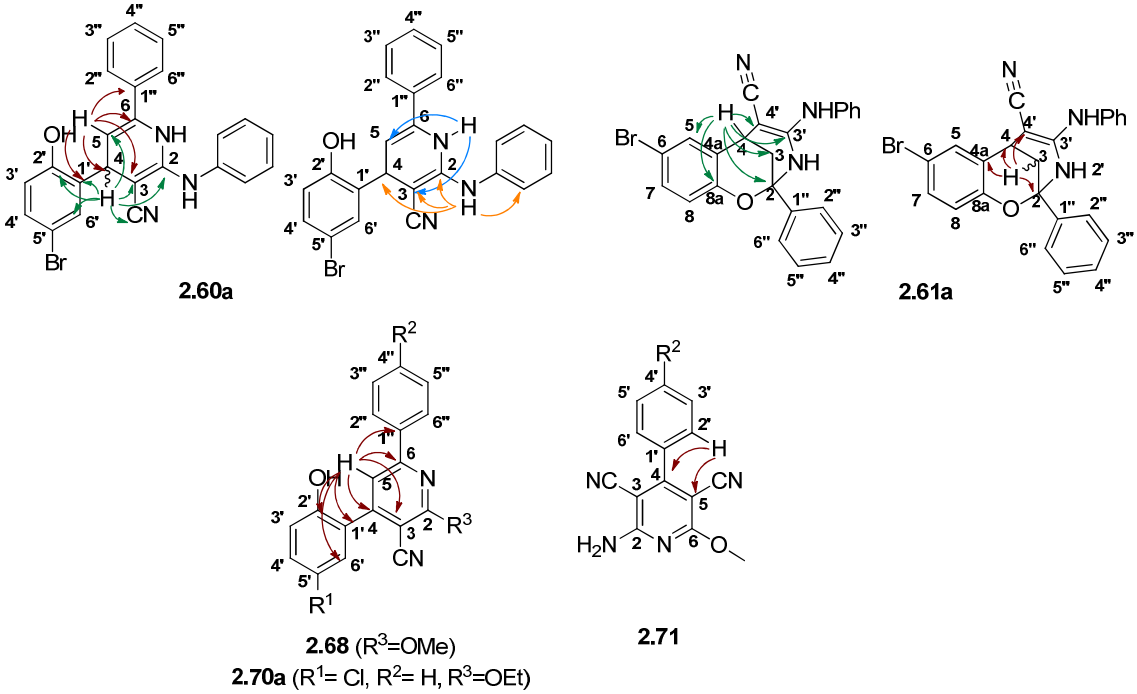
Compound **2.61a** has a group of distinctive signals: two singlets at δ 8.12 (NH-R^{3}) and δ 8.02 (N3-H) ppm corresponding to the NH groups, a triplet at δ 3.72 ppm (H4) and two double doublets at δ 2.41 and 2.17 ppm (H3). The most relevant signals in the ^{13}C NMR spectra are at δ 33.89 (C3), 21.54 (C4), 152.02 (C3'), 66.24 (C4') and 118.93 ppm (CN). The two-dimensional correlation spectra of compound **2.61a** revealed several important correlations, between H4 and C2, C3, C4a, C8a, C3' and C4', and H3 correlating with C2, C4, C4a and C4' (**Scheme 35**).

Compounds **2.68** and **2.70a** can be recognized by ^{1}H NMR signals at δ 7.65 (**2.68a**), δ7.95 (**2.68b**) and δ 7.66 ppm (**2.70a**), which belong to the aromatic hydrogen atom in the pyridine ring (H5), as well as by the singlets corresponding to the MeO groups (δ4.12 ppm for **2.68a**, δ 4.08 ppm for **2.68b**) or by the typical signals of a OEt group, thus a quartet [∼δ 4.60 ppm (CH_2)] and a triplet [∼δ 1.41 ppm (CH_3)]. In the ^{13}C NMR spectra, the signals corresponding to the pyridine ring are easily identifiable for all three compounds, with the nitrile groups' signals appearing at δ 115.37 ppm (**2.68a**), δ 116.14 ppm (**2.68b**) and δ 115.45 ppm (**2.70a**) (**Scheme 35**).

The ^{1}H NMR spectra of compounds **2.71** present two characteristic singlets, one corresponding to the NH group δ 7.66 ppm (**2.71a**) and δ 7.69 (**2.71b**), and the second belonging to the OMe group at δ 3.99 ppm (**2.71a** and **2.71b**). By ^{13}C NMR, compounds **2.71** are recognizable by the pyridine pattern, very similar between both compounds, with C3 and C5 signals proving the presence of different substituents at C2 and C6 [δ 86.93 ppm (C5) and 75.91 ppm (C3) for **2.71a**; δ 87.06 ppm (C5) and 76.14 ppm (C3) for **2.71b**]. Two-dimensional correlation experiments showed that H2' and H6' correlate with C4, C3 and C5 (**Scheme 35**).

Compounds **2.60a, 2.68** and **2.70a** detain a similar HMBC pattern to chromenopyridines **2.55**, **2.56** and **2.69**, thus, H1 correlates with C3 and C5 and the exocyclic

NH proton with the aromatic ring C2 and C6 (for **2.60a**) (**Scheme 35**). The CH hydrogen atoms of the MeO group correlate with C2 (for **2.68** and **2.70**).



Scheme 35: Selection of correlations, observed by HMBC, for compounds **2.60a**, **2.61a**, **2.68**, **2.70a** and **2.71**

Compounds **2.82** can be mainly recognized by two singlets in the ^{1}H NMR spectra attributed to its NH groups: δ9.33 and 9.21 ppm (N=C-NH) and δ 6.85 (NH_2), as well as for the triplet at δ3.82 ppm and the multiplet at δ3.12 ppm corresponding to H4 and Ha, respectively (**Table 65**). The most characteristic signals of these compounds in the ^{13}C NMR corresponds to C4 (δ32.30 and 32.08 ppm), Ca (δ 34.80 and 34.39 ppm), nitrile (δ120.56 and 120.31 ppm) and C=N-N (δ140.39 and 139.07 ppm). The correlation experiments showed that H4 and Ha possess a similar pattern to compounds **2.39** Ha and H4, to which is added the correlation of the hydrazines' NH proton with C1'', C6'' and the imines' carbon atom (**Table 66**).

Table 63: ^{1}H NMR (400 MHz, DMSO-d_6, δ ppm) spectroscopic data obtained for compounds **2.60a**, **2.61a**, **2.68a-b**, **2.70a** and **2.71a-b**

Compound	R^1	R^2	R^3	H2-8	H2'-6'	H2''-6''	NH-Ar (H2'''-6''')	NH	OH	OMe/OEt
2.60a	-	-	-	5.26 (dd, J_1= 5.6, J_2= 1.2 Hz, 1H, H4), 4.68 (d, J= 5.6 Hz, 1H, H5)	7.62 (d, J= 2.4 Hz, H6'), 7.21 (dd, J_1= 8.8, J_2= 2.8 Hz, 1H, H4'), 6.82 (d, J= 8.8 Hz, 1H, H3')	7.43-7.27 (m, 8H, H2'' + H6'', H3'' + H5'', H4'', H3''' + H5''', H4'''), 7.02 (J_1= 8.4, J_2= 0.8 Hz, H2''' + H6''')		8.81 (s, 1H, N1-H), 8.51 (s, 1H, NHR^3)	9.94 (s, 1H)	-
2.61a	-	-	-	7.67 (dd, J_1= 8.8, J_2= 1.6 Hz, 2H, H2'' + H6''), 7.51-7.34 (m, 5H, H7, H3' + H5', H3''' + H5'''), 7.30 (dd, J_1= 7.2, J_2= 2.4 Hz, 1H, H5), 7.20 (t, J= 8.0 Hz, 1H, H4'''), 6.92 (d, J= 7.6 Hz, 3H, H8, H2' + H6'), 6.85 (t, J= 7.6 Hz, 1H, H4'), 3.72 (t, J= 2.8 Hz, 1H, H4), 2.41 (dd, J_1= 9.2, J_2= 3.2 Hz, 1H, H3a), 2.17 (dd, J_1= 9.2, J_2= 3.2 Hz, 1H, H3a)			8.12 (s, 1H, NHR^3), 8.02 (s, 1H, H1)	-	-
2.68a	H	Me	OMe	7.65 (s, 1H, H5)	8.10 (d, J= 8.4 Hz, 1H, H6'), 7.31 (d, J= 8.4 Hz, 5H, H3', H2'' + H6'', H3'' + H5''), 7.00 (d, J= 8.0 Hz, 1H, H3'), 6.94 (dt, $J1$= 7.6, $J2$= 1.2 Hz, 1H, H5'), 2.36 (s, 3H, Me)			-	10.04 (s, 1H)	4.12 (s, 3H)
2.68b	Br	H	OMe	7.95 (s, 1H, H5)	7.23 (d, J= 2.8 Hz, 1H, H3'), 6.97 (dd, J_1= 8.8, J_2= 2.8 Hz, 1H, H4'), 6.35 (d, J= 8.8 Hz, 1H, H6')	8.12 (dd, J_1= 8.4, J_2= 2.0 Hz, 2H, H2'' + H6''), 7.52-7.46 (m, 3H, H3'' + H5'', H4'')	-	-	-	4.08 (s, 3H)
2.70a	H	Cl	OEt	7.66 (s, 1H, H5),	7.39 (t, J= 2.4 Hz, 1H, H4'), 7.35 (d, J= 2.4 Hz, 1H, H6'), 7.00 (d, J= 8.8 Hz, 1H, H3')	8.17 (dd, J_1= 7.6, J_2= 2.0 Hz, 2H, H2'' + H6'), 7.52-7.50 (m, 3H, H3', + H5', H4'')	-	-	10.49 (s, 1H)	4.60 (q, J= 7.2 Hz, 2H, CH_2), 1.41 (t, J= 7.2 Hz, 3H, CH_3)
2.71a					7.82 (dd, J_1= 7.6, J_2= 1.6 Hz, 2H, H2'' + H6''), 7.58-			7.69 (s, 2H)		3.99 (s, 3H)

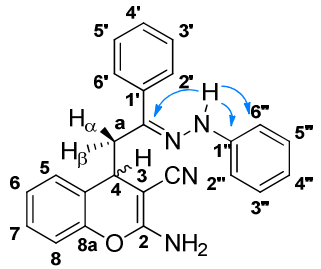
	-	H	-	-	7.51 (m, 3H, H3'' + H5'', H4'')	-	-		-	
2.70b	-	Me	-	-	7.65 (dd, J_1= 8.0, J_2=1.6 Hz, 2H, H3'+H5'), 7.34 (d, J= 8.0 Hz, 2H, H2'+H6'), 2.38 (s, 3H, Me)	-	-	7.66 (s, 2H)	-	3.99 (s, 3H)

Table 64: ^{13}C NMR (100 MHz, DMSO-d_6, δ ppm) spectroscopic data obtained for compounds **2.61, 2.76**, **2.77** and **2.78**

Compound	R^1	R^2	R^3	C1-10	C1'-6'	C1''-6''	NH-Ar(C2'''-6''')	CN	OMe/OEt
2.63a	-	-	-	148.96 (C2), 134.95 (C6), 101.19 (C5), 64.04 (C3), 34.48 (C4)	153.12 (C2'), 134.82 (C1'), 130.51 (C6'), 130.02 (C4'), 117.32 or 117.39 (C3'), 115.84 (C5')	135.22 (C1''), 128.47 (C3'' + C5''), 128.43 (C2'' + C6''), 125.25 (C4'')	142.22 (C1'''), 129.00 (C3'' + C5''), 120.43 (C4''), 117.32 or 117.39 (C2'' + C6'')	121.41	-
2.64a	-	-	-	151.13 (C8a),130.44 (C4a), 130.24 (C5), 129.84 (C7), 118.93 (C8), 84.90 (C2), 33.89 (C3), 21.54 (C4)	152.02 (C3'), 66.24 (C4')	141.42 (C1''), 128.46 (C4''), 128.28 (C3'' + C5''), 125.91 (C2''+ C6'')	152.23 (C1'''), 128.80 (C3''' + C5'''), 120.94 (C4'''), 118.47 (C2''' + C6''')	118.93	-
2.67a	H	Me	OMe	163.69 (C2), 156.78 (C4), 154.82 (C6), 114.50 (C5), 94.04 (C3)	154.39 (C2'), 129.54 (C4'), 127.25 (C6'), 123.36 (C1'), 119.18 (C5'), 116.04 (C3')	140.47 (C4''), 134.03 (C1''), 130.04 (C3'' + C5''), 129.54 (C2'' + C6''), 20.95 (Me)	-	115.37	54.80
2.67c	Br	H	OMe	164.04 (C2), 155.06 (C4), 154.82 (C6), 114.50 (C5), 94.04 (C3)	156.90 (C2'), 133.14 (C4'), 131.44 (C6'),	137.50 (C1''), 129.91 (C4''), 128.78 (C3'' +	-	116.14	53.94

				126.40 (C5'), 124.62 (C1'), 122.77 (C3')	C5''), 127.04 (C2'' + C6'')				
2.68a	H	Cl	OEt	163.59 (C2), 157.46 (C6), 153.56 (C4), 114.84 (C5), 94.73 (C3)	153.56 (C2'), 130.96 (C6'), 129.81 (C4'), 125.26 (C1'), 122.98 (C5'), 117.96 (C3')	136.93 (C1''), 130.98 (C4''), 129.30 (C3'' + C5''), 128.59 (C2'' + C6'')	-	115.45	63.39 (CH2), 14.63 (CH3)
2.78a	-	H	-	166.00 (C6), 163.63 (C4), 159.41 (C2), 130.78 (C1), 87.06 (C5), 76.14 (C3)	136.87 (C1'), 130.76 (C4'), 128.74 (C3' + C5'), 128.38 (C2' + C6')	-	-	113.43, 115.62	54.77
2.78b	-	Me	-	165.91 (C6), 163.52 (C4), 159.42 (C2), 86.63 (C5), 75.91 (C3), 20.97 (Me)	140.86 (C4'), 134.03 (C1'), 128.94 (C2' + C6'), 128.73 (C3' + C5')	-	-	113.44, 115.70	54.70

Table 65: ^{1}H (400 MHz, DMSO-d$_6$, δ ppm) and ^{13}C NMR (100 MHz, DMSO-d$_6$, δ ppm) spectroscopic data obtained for 2-amino-4-(2-aryl-2-(2-phenylhydrazono)ethyl)-4*H*-chromene-3-carbonitriles **2.82a** and **2.82b**



Compound		**R^1**	**R^2**	**H5-8**	**H2'-6'**	**H2''-6''**	**NH**	**NH$_2$**	**H4**	**Ca**
2.82a	**^{1}H**	Br	H	7.35 (d, *J*= 2.8 Hz, 1H, H5), 7.26 (dd, J_1= 7.2, J_2= 2.0 Hz, 1H, H7), 6.89 (d, *J*= 8.8 Hz, 1H, H8)	7.69 (d, *J*= 7.6 Hz, 2H, H2' + H6'), 7.35 (t, *J*= 7.6 Hz, 2H, H3' + H5'), 7.26 (t. *J*= 7.6 Hz, 1H, H4')	7.16 (t, *J*= 8.8 Hz, 2H, H3'' + H5''), 7.08 (d, *J*= 7.6 Hz, 2H, H2'' + H6''), 6.72 (dt, J_1= 7.2, J_2= 0.8 Hz, 1H, H4'')	9.21 (s, 1H)	6.85 (s, 1H)	3.82 (t, *J*= 7.2 Hz, 1H)	3.12 (m, 2H)

2.82a		**R^1**	**R^2**	**C2-8a**	**C1'-6'**	**C1''-6''**	**C4**	**Ca**	**CN**	**C=N-N**
	^{13}C	Br	H	161.72 (C2), 148.75 (C8a), 131.01 (C7), 130.91 (C5), 126.07 (C4a), 118.25 (C8), 116.02 (C6), 53.56 (C3)	138.89 (C1'), 128.50 (C3' + C5'), 127.63 (C4'), 125.69 (C2' + C6'),	145.98 (C1''), 129.01 (C3'' + C5''), 119.25 (C4''), 113.17 (C2'' + C6'')	32.30	34.80	120.56	140.39
2.82b		**R^1**	**R^2**	**H5-8**	**H2'-6'**	**H2''-6''**	**NH**	**NH_2**	**H4**	**Ca**
	^{1}H	Br	Br	7.46 (d, J= 2.4 Hz, 1H, H5), 7.29 (dd, J_1= 8.8, J_2= 2.4 Hz, 1H, H7), 6.90 (d, J= 8.8 Hz, 1H, H8)	7.66 (dd, J_1= 8.4, J_2= 1.6 Hz, 2H, H2' + H6'), 7.51 (dd, J_1= 8.8, J_2= 2.0 Hz, 2H, H3' + H5')	7.17 (dt, J_1= 7.2, J_2= 1.2 Hz, 2H, H3'' + H5''), 7.11 (dd, J_1= 8.8, J_2= 1.2 Hz, 2H, H2'' + H6''), 6.74 (dt, J_1= 7.2, J_2= 1.2 Hz, 1H, H4')	9.33 (s, 1H)	6.85 (s, 1H)	3.82 (t, J= 7.2 Hz, 1H)	3.13 (d, J= 7.2 Hz, 2H)
		R^1	**R^2**	**C2-8a**	**C1'-6'**	**C1''-6''**	**C4**	**Ca**	**CN**	**C=N-N**
	^{13}C	Br	Br	161.58 (C2), 148.65 (C8a), 130.88 (C5), 130.84 (C7), 126.10 (C4a), 118.05 (C8), 115.87 (C6), 53.55 (C3)	131.08 (C1'), 131.08 (C3' + C5'), 127.54 (C2' + C6'), 120.51 (C4')	145.64 (C1''), 128.26 (C3'' + C5''), 119.26 (C4''), 113.10 (C2'' + C6'')	32.08	34.39	120.31	139.07

2.1.4 Synthesis and reactivity of ethyl *N*-(3-cyano-4-(2-arylethyl)-4*H*-chromen-2-yl)formimidate

There are several examples in the literature where triethyl orthoformate is used to prepare imidates, which are suitable precursors for the synthesis of diverse heterocyclic compounds[122]. In addition, chromenes bearing an *o*-aminonitrile moiety have been successfully employed for the synthesis of new formimidate chromene derivatives, which were used as precursors in the preparation of new chromene-based heterocyclic compounds. For example, in the research group, it was possible to synthesize a diaminomaleonitrile imidate by reaction of diaminomaleonitrile (DAMN) with triethyl orthoformate under reflux conditions, and this compound was a versatile starting material for the preparation of imidazoles[123,124], dihydropurines[125], purines[126], triazepines[127], oxazoles[127], oximes[128], pyrroles[129], among others. In the synthesis of chromene derivatives, there have been some studies that involve chromenes bearing an *o*-aminonitrile moiety to generate new formimidate derivatives, that are used as precursors in the formation of new heterocyclic rings fused to the chromene skeleton[130–133].

However, to the best of our knowledge, none of the chromene derivatives reported includes a 2-oxo-2-arylethyl moiety at C4, but rather, quite frequently, these chromenes possess an aromatic ring linked to C4. This fact encouraged us to explore the reactivity of this functionality in the 2-amino-4-(2-oxo-2-arylethyl)-4*H*-chromene-3-carbonitriles **2.39**, with triethyl orthoformate and, subsequently, with nucleophiles, and thus expanding the chemical space of this scaffold. The carbonyl moiety offered a new reactive point for intramolecular and intermolecular reactions.

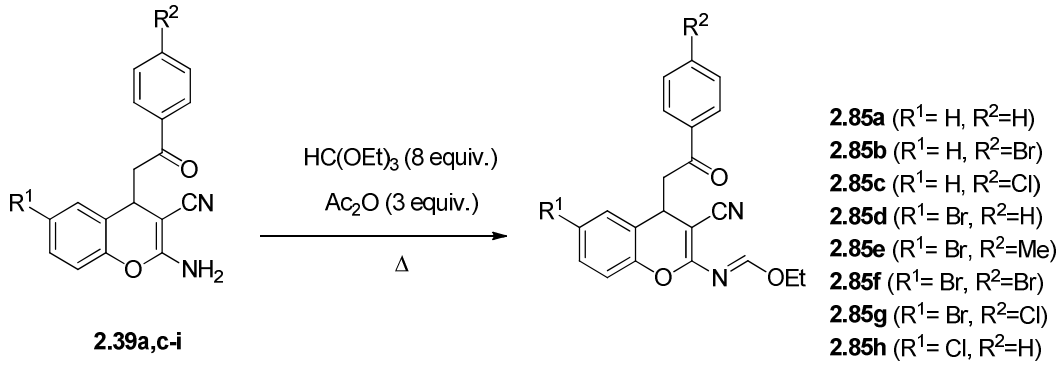
For this reason, the main objectives that were proposed for this topic were:

1) Develop a facile and scalable process to prepare ethyl *N*-(3-cyano-4-(2-oxo-2-arylethyl)-4*H*-chromen-2-yl)formimidates.
2) Explore the reactivity of ethyl *N*-(3-cyano-4-(2-oxo-2-arylethyl)-4*H*-chromen-2-yl)formimidates with nucleophiles, under several reaction conditions.
3) Evaluate the biological potential of the newly prepared heterocyclic structures.

Synthesis of ethyl *N*-(3-cyano-4-(2-oxo-2-arylethyl)-4*H*-chromen-2-yl)formimidates

For the preparation of compounds **2.85**, the procedure previously described by our research group to generate this type of imidate moiety in the synthesis of adenine derivatives was employed[134]. To this end, 2-amino-3-nitrile chromenes **2.39** were heated under reflux in excess of triethyl orthoformate (8 molar equivalents) and acetic anhydride (3 molar equivalents) to led to the desired chromeno-based imidates **2.85** in excellent yields (**Table 66**).

Table 66: Reaction time and isolated yield of chromene-based imidates **2.85**



2.39a,c-i

Compound	t (min)	η (%)	Compound	t (min)	η (%)
2.85a	40	95	**2.85e**	40	86
2.85b	30	89	**2.85f**	30	91
2.85c	30	95	**2.85g**	12	91
2.85d	35	96	**2.85h**	40	87

The spectroscopic data of compounds **2.85** confirmed its formation. Thus, the IR spectra of compounds **2.85** corroborated the absence of the NH stretching vibration, which is present in the synthetic precursors **2.39**. The ^{1}H and ^{13}C NMR spectra showed signals at around δ 8.59 ppm (singlet) and δ 163.52 ppm (for **2.85d**), respectively, attributed to the imidate C-H group, as well as the typical quartet (about δ 4.30 ppm and δ 63.97 ppm, respectively) and triplet (about δ 1.30 ppm and 13.90 ppm, respectively) signals for an ethoxy group (**Figures 52** and **53**).

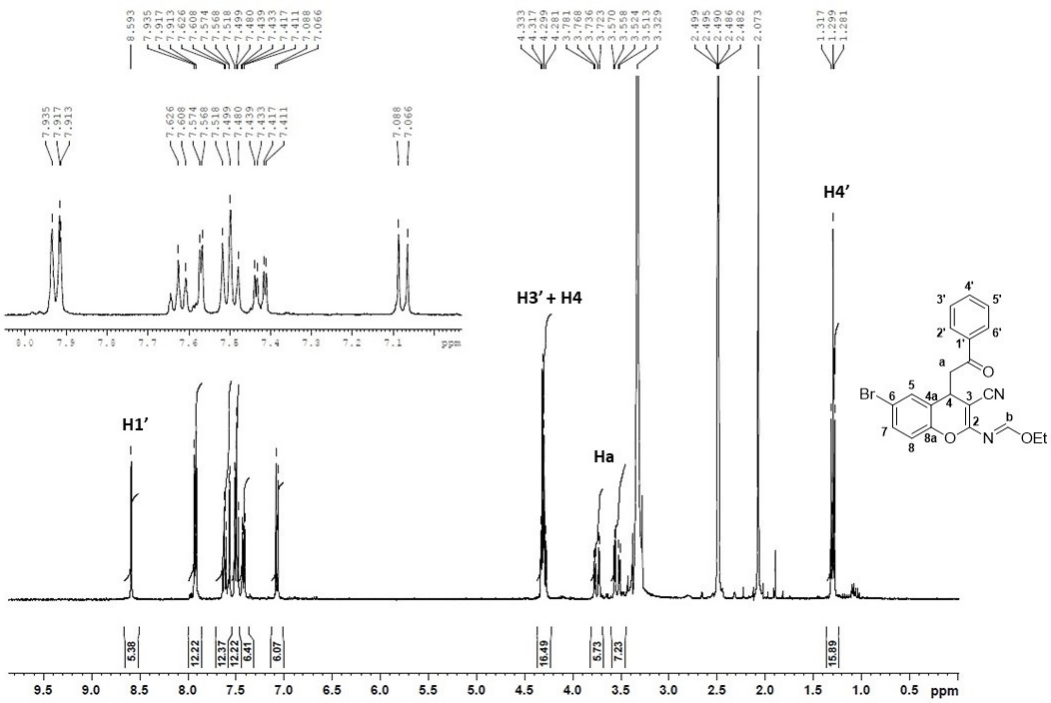


Figure 52: ^{1}H NMR (400 MHz, DMSO-d$_6$, δ ppm). spectrum of compound **2.85d**, in which several signals are highlighted

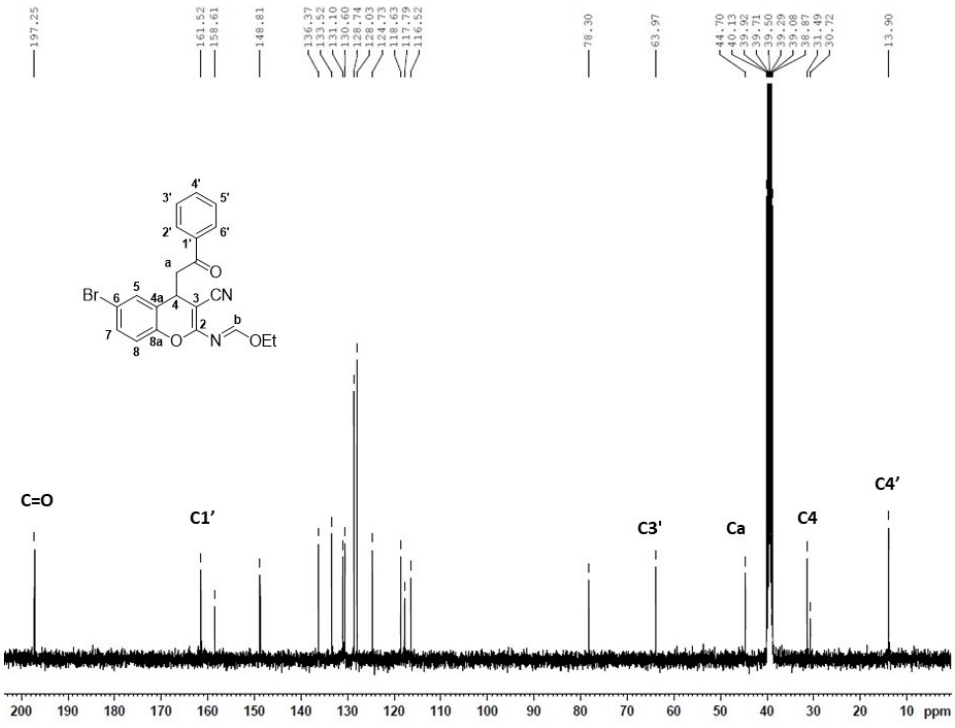
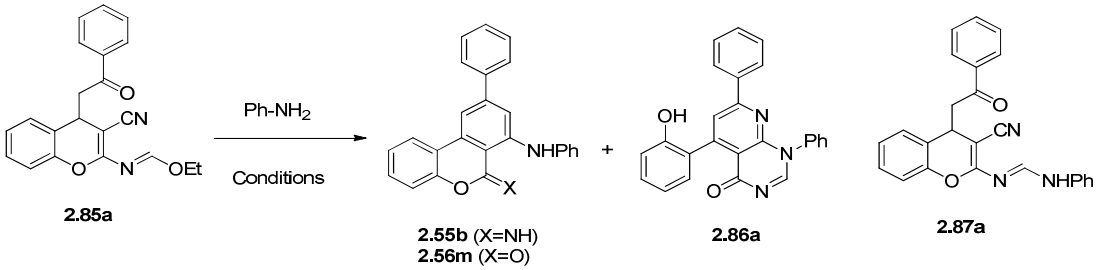


Figure 53: ^{13}C NMR (100 MHz, DMSO-d$_6$, δ ppm) spectrum of compound **2.85d**, in which several signals are highlighted

Reactivity of *N*-(3-cyano-4-(2-oxo-2-arylethyl)-4*H*-chromen-2-yl)-*N*-arylformimidamides with primary amines

The reactivity of compounds **2.85** against diverse anilines was then explored. The best reaction conditions were explored using compound **2.85a** and aniline, which results are summarized in **Table 67**.

Table 67: Reaction conditions and results of the reaction of compound **2.85a** with aniline



2.85a | **2.55b** (X=NH) **2.56m** (X=O) | **2.86a** | **2.87a**

Entry	solvent		aniline (equiv.)	additives	T °C)	t (h)	product	η (%)
1	DMSO	Ph	1.5	-	r.t.	18.5	**2.85a**	28
2	dioxane	Ph	1.2	-	40	120	**2.85a**	44
3	MeOH	Ph	1.5	$PhNH_3Cl$ (cat.)	r.t.	18.5	**2.86a**	51
4	MeOH	Ph	1.5	$PhNH_3Cl$ (cat.)	50	18.5	**2.87a**	15
5	EtOH	Ph	1	-	r.t 80	30 17	**2.86a**	23
6	EtOH	Ph	1.5	-	40	142	**2.86a**	41
7	EtOH	Ph	1.2	H_2SO_4 (0.2 equiv.)	r.t.	3	complex mixture	-
8	EtOH	Ph	1.2	AcOH (0.5 equiv.)	80	1.66	**2.86a**	14
9	EtOH	Ph	1.2	AcOH (0.5 equiv.)	80	6	**2.86a**	29

When the reaction was performed in DMSO and at room temperature for 18.5 h, a mixture of reaction products could be observed by TLC, from which only the starting material **2.85a** could be collected by simple filtration (η= 28%) (entry 1 – **Table 67**). A similar result was obtained by performing the reaction in dioxane with mild heating (40 °C) for 120 h, in which case the starting material **2.85a** was recovered in 44% yield (entry 2 – **Table 67**), or by using methanol at room

temperature in the presence of a catalytic amount of anilinium chloride for 18.5 h (entry 3 **– Table 67**), which provided **2.85a** in 51% yield. For the latter case, performing the reaction at 50 °C led to amidine **2.87a** in 15% yield.

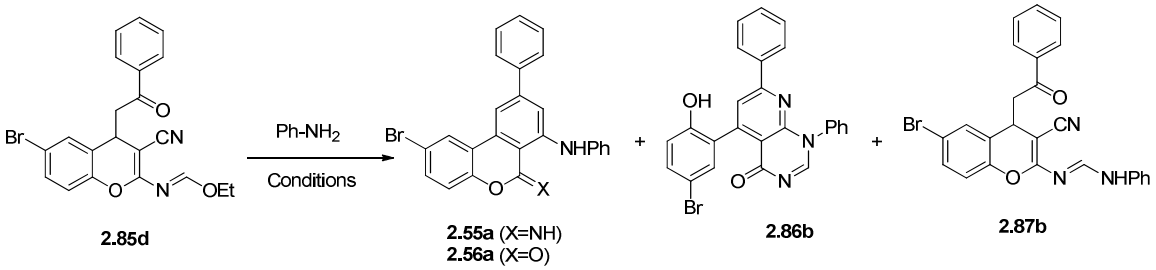
Fortunately, more positive results were achieved by using ethanol as solvent (entries 5-9 – **Table 67**). Thus, while using 1 equivalent of aniline and after 30 h stirring at room temperature mainly gave no reaction, the heating of the reaction mixture at 80 °C for 17 h afforded compound **2.86a** in 23% isolated yield (entry 5 – **Table 67**). The yield of the reaction was increased up to 41% by using 1.5 equivalents of aniline under mild heating (40 °C) for an extended period of 142 h (entry 6 – **Table 67**).

To try to improve the reaction yield, the effect of the presence of acid was explored. The results showed that 0.2 equivalents of sulfuric acid resulted in the formation of a polymeric black mixture (entry 7 – **Table 67**). Better results were obtaining using 0.5 equivalents of acetic acid, although without involving an improvement in the reaction yield. Thus, using 1.2 equivalents of aniline in ethanol and heating at 80 °C for either 1.66 h (entry 8 – **Table 67**) or 6 h (entry 9 – **Table 67**) afforded compound **2.86a** in 14% and 29% isolated yield, respectively. It became evident that increasing the reaction temperature to 80 °C and the reaction time, resulted in higher yields of **2.86a**. Nevertheless, the isolated yield never surpassed 50%.

The isolation of these new derivatives supported the assumption that different side reactions could occur, involving both compound **2.85a** and its synthetic precursor 2-amino-3-nitrile chromene **2.39a** that can be formed by hydrolysis of the imidate moiety in **2.85**. These reactions may even occur in the absence of a catalytic amount of acid.

To the best of our knowledge, no such compounds were described in the literature. To better understand this reactivity, to explore the scope of the reaction, as well as to improve the reaction yield, a set of experiments was performed using chromene-based imidate **2.85d** and aniline. The conditions, and results, are summarized in **Table 68**.

Table 68: Reaction conditions and results of the reaction of compound **2.85d** with aniline



2.85d | **2.55a** (X=NH), **2.56a** (X=O) | **2.86b** | **2.87b**

Entry	solvent	aniline (equiv.)	conditions			results		
			AcOH (equiv.)	T (ºC)	t (h)	product	ratio	yield (%)
1	EtOH	2	-	50	9	**2.85d**	-	72
2	EtOH	2	0.5	50	9	**2.87b**	-	67
3	EtOH	1.2	-	50	60	**2.87b**	-	28
4	MeOH	1.2	-	50	60	**2.87b**	-	<2
5	EtOH	1.2	-	80	96	**2.55a** + **2.56a**	2/3	-
6	EtOH	1.5	0.5	80	96	**2.55a** + **2.56a**	1/1	-
7	EtOH	1.5	0.5	80	2	**2.87b**	-	46
8	EtOH	1.5	0.5	80	4.66	**2.86b**	.	16
9	ACN	1.5	0.5	80	4.66	**2.87b**	.	51
10	EtOH	2	0.5	80	2	**2.87b**	-	55

Based on the results obtained with chromene-based imidate **2.85a** showing that temperature was a key feature to induce a chemical transformation, the initial assays were performed at 50 °C (entries 1-4- **Table 68**). Unfortunately, no reaction was observed by using 2 equivalents of aniline for 9 h, and ethanol as solvent, affording the starting material **2.85d** in 72% yield (entry 1-**Table 68**). However, reproducing these conditions but in the presence of 0.5 equivalents of acetic acid led to the formation of compound **2.87b** in 67% yield (entry 2-**Table 68**). However, in the absence of acetic acid, the aniline equivalents reduced to 1.2 and when the reaction time was increased to 60 h, only 28% yield of compound **2.87b** was obtained (entry 3-

Table 68). The use of methanol as solvent (entry 4-**Table 68**) resulted in a further reduction of the isolated yield (<2%). The latter results highlighted that the formation of compound **2.87b** requires acid-catalysed conditions.

A series of assays were then performed at 80 °C (entries 5-10-**Table 68**). Only good results were obtained when 1.5-2 equivalents of aniline were used and short reaction times, since a mixture of imino chromenepyridine **2.55a** and oxo chromenepyridine **2.56a** were isolated when 1.2 equivalents and long reaction periods were employed (entries 5-6-**Table 68**). However, short reaction times (2 h), a greater excess of aniline (1.5-2 equivalents) in the presence of 0.5 equivalents of acetic acid, whether using ethanol or acetonitrile as solvent, favored the formation of **2.87b** (entries 7-10-**Table 68**), which was obtained in yields ranging from 46% to 55%. Remarkably, compound **2.86b** was obtained in 16% yield when longer reaction times (4.66 h) were used (entry 8). Therefore, the best reaction conditions for the synthesis of compound **2.87b** from chromene-based imidate **2.85e** could be the use of 0.5 equivalents of acetic acid, 2 equivalents of aniline, in ethanol as solvent, either heating at 50 °C for 9 h or at 80 °C for 2 h.

Compounds **2.86** were identified by IR and NMR spectroscopy. In the IR spectra, a broad band appears at around 3300 cm^{-1} (O-H stretching), together with a sharp, medium intensity, peak at 1670-1640 cm^{-1}, corresponding to the C=O stretching vibration. For compound **2.86b**, these values are 3305 cm^{-1} (OH) and 1682 cm^{-1} (C=O). The most characteristic signals in the ^{1}H NMR spectra of **2.86b** are three singlets at δ10, δ 8.5 and δ 7.8 ppm corresponding to the hydroxyl group and the two CH groups of the pyridopyrimidinone core (H2 and H6), respectively (**Figure 54**). For compound **2.86b**, these three singlets appear at δ 10.05, δ 8.63 and δ 7.88 ppm, respectively. In the ^{13}C NMR spectra stand out the signals for the carbonyl, C2 and C6 carbons, which are distinctive of this scaffold. For compound **2.86b**, these signals are at δ 167.84 ppm (carbonyl, C4), δ 153.30 ppm (C2) and δ 121.22 ppm (C6) (**Figure 55**).

The results presented in **Tables 67** and **68** led us to conclude that amidines **2.87** can generate pyrido-pyrimidinones **2.86** under the reaction conditions used. However, the isolation yield of compounds **2.86** is still unsatisfactory. Also, the isolation of a mixture of chromenopyridines **2.55** and **2.56** led us to conclude that the reaction conditions used can parallelly promote the cleavage of either the imidate or the amidine moiety of compounds **2.85** and/or **2.86**. For this reason, a new approach was explored, involving the optimization and preparation of amidines **2.87** to further use as starting material for the preparation of **2.86**.

Attempts to understand the reaction mechanism that leads to the formation of compounds **2.86** would allow to adjust the experimental conditions leading to its selective formation. This new strategy will be discussed in the following sections.

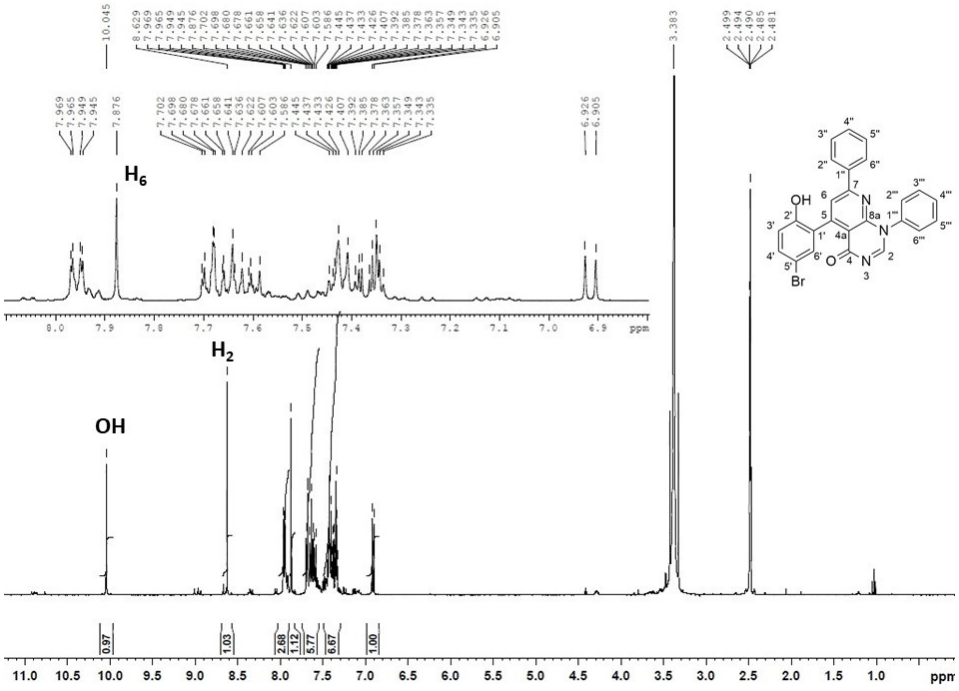


Figure 54: ^{1}H NMR (400 MHz, DMSO-d$_6$, δ ppm) spectrum obtained for compound **2.86b**, in which three signals are highlighted

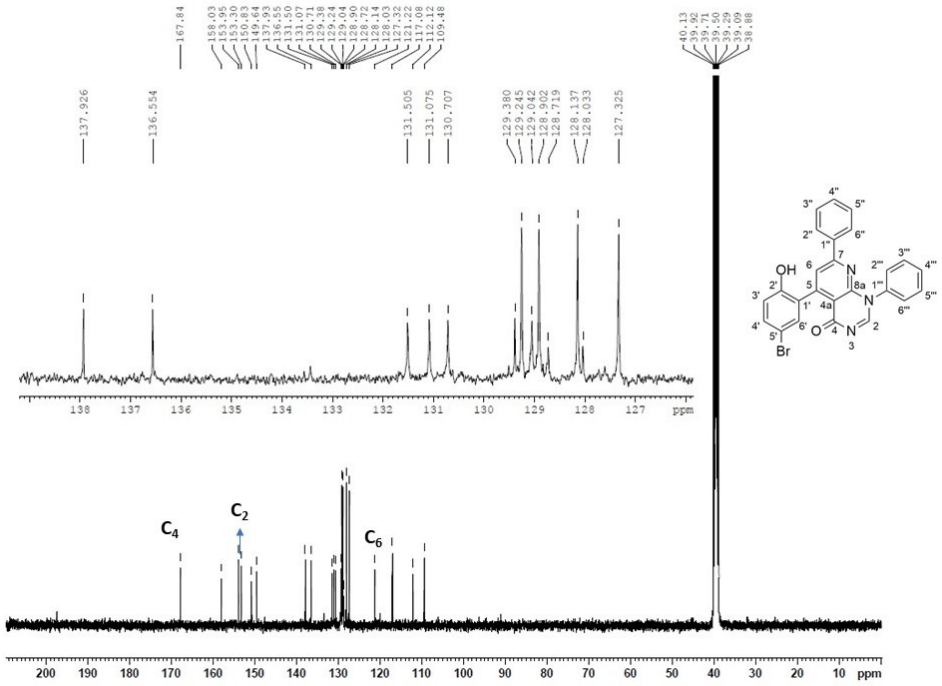
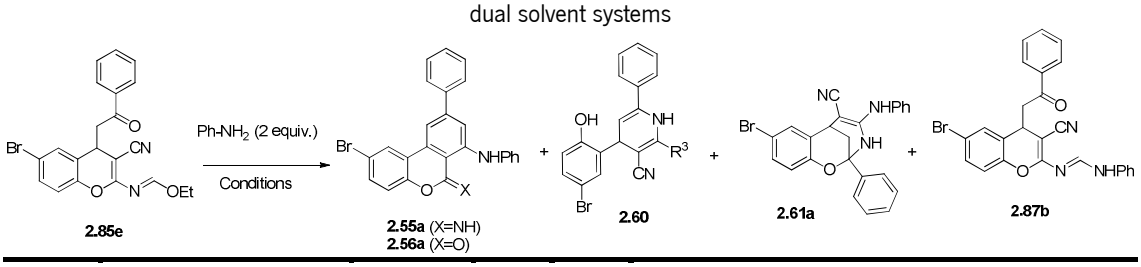


Figure 55: ^{13}C NMR (100 MHz, DMSO-d$_6$, δ ppm) spectrum obtained for compound **2.86b**, in which three signals are highlighted

To further optimize the reaction conditions that lead to the formation of compounds **2.86**, the synthetic method to obtain amidines **2.87** was investigated. This study started by testing a dual solvent system in the reaction of **2.85d** with aniline to induce the removal of compound **2.87b** from the reaction mixture (**Table 69**). Five assays were performed at 80 °C (entries 1-5- **Table 69**) and two at 100 °C (entries 6 and 7- **Table 69**). In entries 1-4, only the reaction time was allowed to vary (3, 5, 15.5 and 48 h for entries 1, 2, 3 and 4, respectively), with 2 equivalents of aniline, 0.5 equivalents of acetic acid and a (1:1) EtOH:H_2O. The results clearly show that 5 h is the optimal reaction time to isolate amidine **2.93** and that above this threshold, the reaction starts to progress to the formation of compounds **2.55/2.56**.

The fact that, after 3 and 5 h of reaction (entries 1 and 2, respectively - **Table 69**), no traces of compound **2.91e** can be found, and that amidine **2.93b** was isolated in good to excellent yield (77% for entry 1, 85% for entry 2- **Table 69**), supports the assumption that cleavage of the amidine moiety is responsible for the formation of the starting material **2.39**, and not cleavage of the imidate unit.

Table 69: Reaction conditions and results, of the experiments performed with compound **2.85e** and aniline in a dual solvent systems



2.85e | **2.55a** (X=NH) **2.56a** (X=O) | **2.60** | **2.61a** | **2.87b**

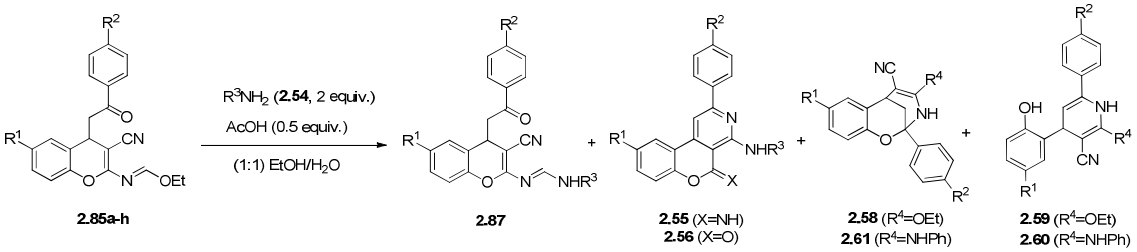
Entry	solvents (ratio)			AcOH (equiv.)	T (°C)	t (h)	results		
	EtOH	ACN	H_2O				product	ratio	η(%)
1	1	-	1	0.5	80	3	**2.87b**	-	77
2	1	-	1	0.5	80	5	**2.87b**	-	85
3	1	-	1	0.5	80	15.5	**2.55a** + **2.56a** + **2.61a**	1.2/1/2.8	-
4	1	-	1	0.5	80	48	**2.55a** + **2.56a** + **2.61a** + **2.87b**	1/1.6/2.1/ 2.7	-
5	-	1	1	0.5	80	5	**2.55a** + **2.56a** + **2.87b**	1.8/1/20	-
6	1	-	1	0.5	100	6	**2.55a** + **2.56a** + **2.61a**	1/1.5/1.6	-

7	1	-	1	1	100	6	**2.55a** + **2.56a** + **2.61a** + **2.60a**	2.4/3.9/7.3/1	-

Replacing ethanol by acetonitrile, in the dual solvent system (entry 5 – **Table 69**) led to the isolation of a mixture of compounds **2.55a**, **2.56a** and **2.87b** in a 1.8:1:20 ratio. Although present as a minor contaminant, the isolation of chromenopyridines **2.55a** and **2.56a** after 5 hours of reaction suggests that the use of acetonitrile as a reaction solvent, in this dual system, tends to lead to the cleavage of the amidine moiety in compound **2.87b** with a higher extent than that observed when ethanol was used, (by comparison with entry 2– **Table 69**). Heating at 100 °C (entries 6 and 7 – **Table 69**) led to the formation of a mixture of products, with compounds **2.55a**, **2.56a**, **2.61a** being isolated in a 1:1.5:1.6 ratio (entry 6) or compounds **2.55a**, **2.56a**, **2.61a** and **2.60a** being isolated in a 2.4:3.9:7.3:1 ratio (entry 7). Performing the reaction under these temperature conditions increases the extent of the amidine cleavage in amidine **2.87b** and its evolution to the spiro compound **2.61a**.

The best reaction conditions identified in **Table 69** for the preparation of amidine **2.87b** [aniline (2 equiv.), acetic acid (0.5 equiv.), (1:1) EtOH:H_2O, 80 °C, 5 h] were used as a starting point for the preparation of new formamidine derivatives. The conditions and results obtained for each imidate **2.85**, as well as for each amine used, are described in **Table 70**. The percentage of contamination in the starting material, detected by ^{1}H NMR, was registered together with the corresponding ratio when the contaminant was identifiable by NMR. The evolution of the reaction was followed by TLC.

Table 70: Experimental conditions and results for the reaction of imidates **2.85** with amines



Entry	2.85			T (°C)	t (min)	results		
	R^1	R^2	R^3			main product	contamination[a] (%)	η (%)
1	H	H	C_6H_5	60	25	**2.87a**	-	33

2	H	H	4-MeC_6H_4	60	25	**2.87c**	-	56
3	H	H	4-$OMeC_6H_4$	60	40	**2.87d**	**2.85a** (5)	47[b]
4	H	Br	C_6H_5	60	45	**2.87b**	-	40
5	H	Br	4-MeC_6H_4	60	120	**2.87e**	**2.85b** (7)	67
6	H	Br	4-$OMeC_6H_4$	60	120	complex mixture	-	-
7	H	Cl	C_6H_5	60	120	**2.87f**	-	77
8	H	Cl	4-MeC_6H_4	60	120	complex mixture	-	-
9	Br	H	4-MeC_6H_4	50	20	**2.87g**	-	68
10	Br	H	4-$OMeC_6H_4$	50	120	**2.87h**	-	77
11	Br	H	3-MeC_6H_4	50	100	**2.87i**	-	77
12	Br	H	3-$OMeC_6H_4$	80	30	**2.87j**	unknown contaminant	-
13	Br	H	4-BrC_6H_4	80	8	**2.87k**	**2.58b/2.61c** + **2.59b /2.60e** (60)	-
14	Br	H	4-ClC_6H_4	80	20	**2.87l**	-	67
15	Br	H	4-CNC_6H_4	80	50	**2.87m**	unknown contaminant	-
16	Br	Me	C_6H_5	60	100	**2.87n**	-	48
17	Br	Me	4-MeC_6H_4	80	50	**2.87o**	**2.85f** (14)	
18	Br	Br	C_6H_5	80	120	**2.87p**	unknown contaminant	-
19	Br	Br	4-MeC_6H_4	80	120	**2.87q**	unknown contaminant	-
20	Br	Br	4-$OMeC_6H_4$	80	120	**2.87r**	unknown contaminant	-
21	Br	Br	4-ClC_6H_4	80	60	**2.87s**	unknown contaminant	-
22	Br	Br	3-ClC_6H_4	80	60	**2.87t**	**2.58c /2.61d** + **2.59c/2.60f** (53)	-
23	Br	Br	4-CNC_6H_4	60	140	**2.87f**	-	63
24	Br	Cl	C_6H_5	60	80	**2.87u**	unknown contaminant	
25	Br	Cl	4-MeC_6H_4	60	80	**2.87v**	**2.86g** (11)	-

26	Br	Cl	4-$OMeC_6H_4$	60	70	**2.87x**	**2.85g** + **2.59d/2.60g** (21)	-
27	Br	Cl	3-BrC_6H_4	80	930	**2.87y**	-	57
28	Cl	H	C_6H_5	60	190	**2.87z**	-	75
29	Cl	H	4-MeC_6H_4	60	180	**2.87a'**	-	59
30	Cl	H	4-$OMeC_6H_4$	60	120	**2.87b'**	**2.85h + 2.59e/2.60h** (25)	-
31	Cl	H	3-MeC_6H_4	60	130	**2.87c'**	unknown contaminant	-
32	Cl	H	4-CNC_6H_4	60	120	**2.87d'**	unknown contaminant	-

[a]Slightly contaminated; [b]By ^{1}H NMR; [c]Yield of the crude product

When imidate **2.85a** (R^1=R^2=H) was used as starting material (entries 1-3 – **Table 70**), amidines **2.87a,b** and **c** could be prepared in good yields, with only a slight contamination with **2.85a** (5%) when the reaction was performed with 4-methoxyaniline (entry 3). The reactions carried out with **2.85b** (R^1=R^2=Br; entries 4-6– **Table 70**) could only lead to the formation of the corresponding amidine **2.87e** (with 7% contamination of **2.85b**) when 4-methylaniline was used, in a reaction kept at 60 °C for 120 minutes (entry 5– **Table 70**). Using **2.85c** (R^1=R^2=Cl; entries 7 and 8– **Table 70**) led to the formation of amidine **2.87f** with good yield (77%), when the reaction was performed with aniline, at 60 °C for 120 minutes (entry 7).

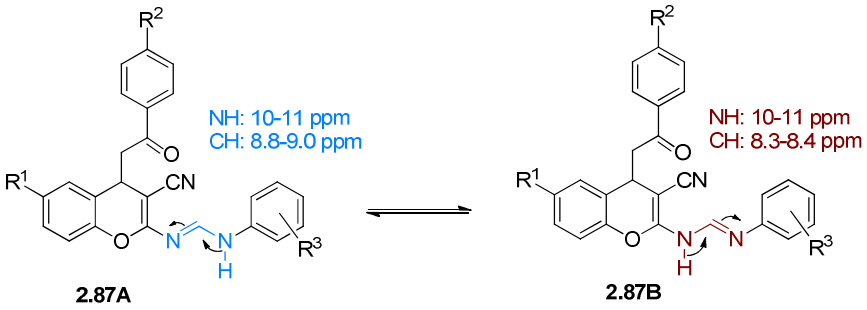
The reaction of imidate **2.85d** (R^1=Br;R^2=H) with 4-methylaniline led to amidine **2.87g** (68% isolated yield) when the reaction was performed at 50 °C (entry 9– **Table 70**) for 20 minutes. Compound **2.87h** was prepared using 4-methoxyaniline and reacting at 50 °C and performing the reaction for 120 minutes (entry 10– **Table 70**). Compound **2.87i** was prepared by using 3-methylaniline and reacting at 50 °C for 100 minutes (entry 11– **Table 70**). Compound **2.87l** was prepared by reacting 4-chloroaniline at 80 °C for 20 minutes (entry 14– **Table 70**). The remaining amidines **2.87j,k** and **m** were obtained as a mixture with other products, such as compounds **2.55**, **2.56** and **2.58-2.61**, in variable ratios (entries 12, 13 and 15). Imidate **2.85h** (R^1=Cl; R^2=H) led to the isolation of pure amidines when the reaction was performed with aniline, at 60 °C for 190 minutes (**2.87z**, 75% yield, entry 28– **Table 70**), and with 4-methylaniline, at 60 °C for 180 minutes (**2.87a'**, 59% yield, entry 29– **Table 70**).

The most insoluble imidates in the ethanol/water mixture were compounds **2.85e-g**. Using **2.85e** (R^1=Br;R^2=Me), the pure amidine **2.87n** was isolated when the reaction with aniline was performed at 60 °C for 100 minutes (48% yield, entry 16– **Table 70**). Using imidate **2.85f** (R^1=Br;R^2=Br) , amidine **2.87q** was obtained in the reaction with 4-methylaniline for 120 minutes and at 80 °C, with a slight contamination with an unknown contaminant (entry 19– Table 70). For the reactions involving **2.85g** (R^1=Br;R^2=Cl), only when 3-bromoaniline was used, in a reaction performed at 80 °C for 930 minutes, could the pure amidine, **2.87y**, be isolated (57% yield, entry 27).

These studies indicate that the best reaction conditions must be adjusted for each imidate **2.85** used and for each amine and are most likely related to the solubility of these compounds in ethanol/water. For the most soluble imidates used, compounds **2.85a-d**, the best results are typically involved lower temperatures (50-60°C) and shorter reaction times (15-40 min.). For the less soluble imidates, derivatives **2.85e-h**, the best results are obtained at 80 °C and longer reaction times (100-930 min.). However, when a mixture was collected, the contaminants contained products that were formed through the hydrolysis of the amidine moiety of **2.87**. It also became clear that, although the EtOH/H_2O system is theoretically helping the formation of amidines **2.87** by keeping imidates **2.85** in suspension throughout the reaction and precipitating amidines **2.87** as they were generated, there seems to be some residual fraction that remains soluble enough to reverse its formation, regenerating the *o*-aminonitrile **2.39**, as expected for a reaction carried out with large amounts of water and acidic conditions. Under this scenario, the resulting *o*-aminonitrile **2.39** is known to react with nucleophiles, either amines or ethanol, to give compounds **2.58/2.61** and/or **2.59/2.60**, which was discussed in section 2.1.3. This appears to happen even without the full consumption of the starting material **2.85**, as is the case of experiments reported in entries 26 and 30 (**Table 70**). The experiments performed using the EtOH/H_2O solvent system allowed to develop a novel synthetic procedure for the preparation of amidines **2.87**, as well as a better understanding on how to adjust the reaction conditions.

The chemical structure of amidines **2.87** was identified by ^{1}H and ^{13}C NMR spectroscopy, including two-dimensional correlation experiments. In the ^{1}H NMR spectra of **2.87** (**Figure 56**), four characteristic signals can be highlighted, that correspond to the NH/CH groups of the amidine fragment, present as two different tautomeric forms, namely **2.87A** and **2.87B** (**Scheme 36**). These signals typically appear between δ 8.5-11 ppm as four doublets, two for each tautomer. The

signals corresponding to the H4 and Ha hydrogen atoms typically appear as a single set of signals, superimposed in the δ 4.0-4.5 ppm (H4) and δ 3.4-3.8 ppm (Ha) region.



Scheme 36: Tautomeric forms for amidines **2.87** observed in DMSO-d_6

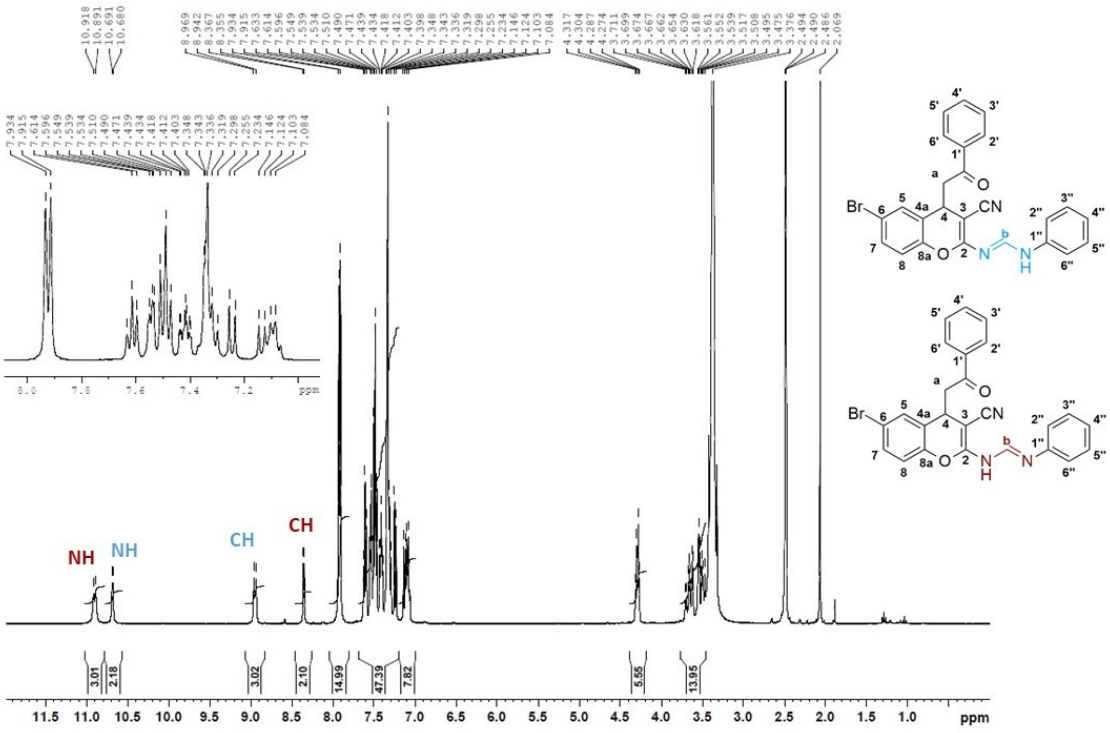


Figure 56: ^{1}H NMR (400 MHz, DMSO-d_6, δ ppm) spectrum obtained for compound **2.87b**, in which the amidine NH and CH signals, for both tautomers, are highlighted

The most relevant signals in the ^{13}C NMR spectra of **2.87** (**Figure 57**), illustrated for compound **2.87b**, are the peaks corresponding to the carbonyl group (δ 197.46 ppm), C2 (δ 160.63 and 160.43 ppm), Cb (δ 151.27 and 149.21 ppm), C3 (δ 74.23 and 73.63 ppm), Ca (δ 45.37 and 45.30 ppm) and C4 (δ 31.95 and 31.67 ppm).

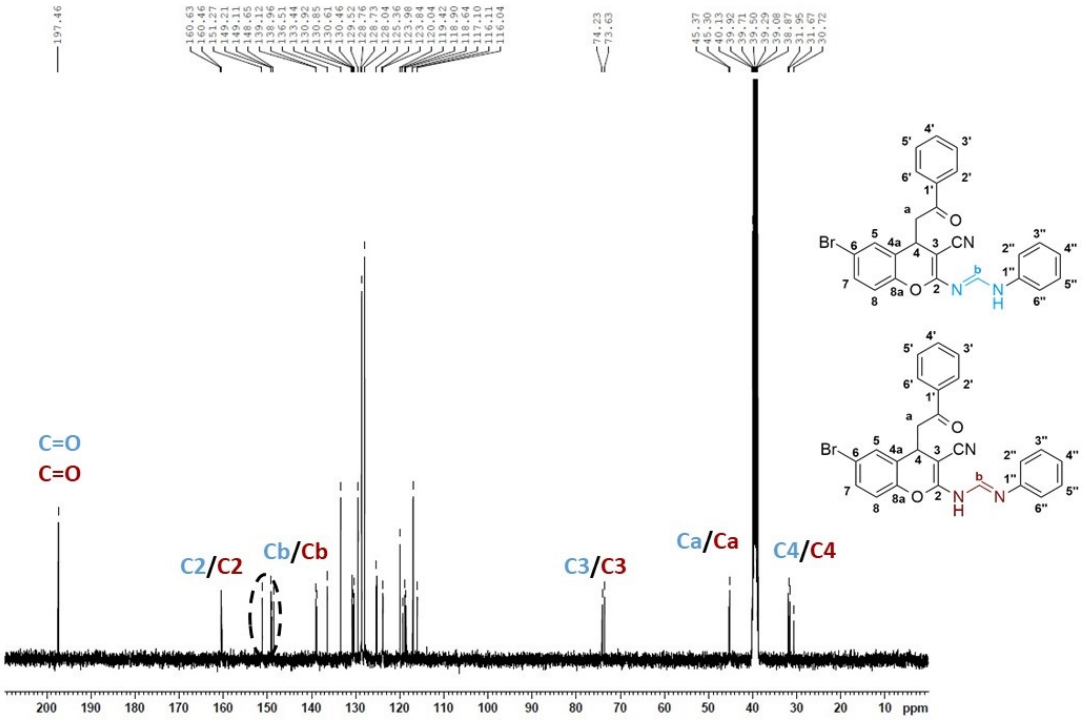
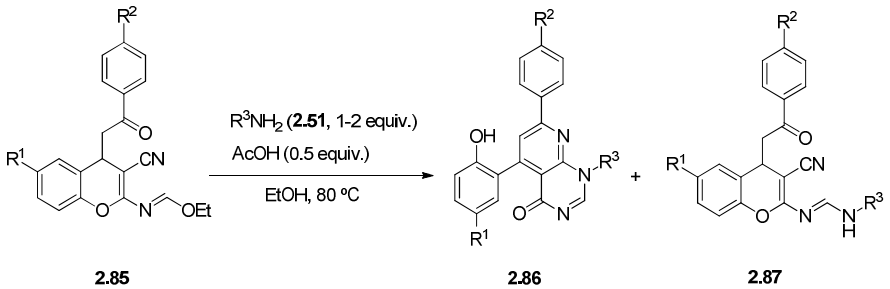


Figure 57: ^{13}C NMR (100 MHz, DMSO-d$_6$, δ ppm) spectrum obtained for compound **2.87b**, in which several signals, for both tautomers, are highlighted

Pyridopyrimidines **2.86b-h** could also be prepared in low yields from imidates **2.85** and primary aromatic amines (**Table 71**). Thus, the treatment of imidates **2.85** with 1-2 equivalents of primary amines **2.51** and 0.5 equivalents of acetic acid in ethanol and heating at 80 °C for 1.5-22 h afforded compounds **2.86** in yields ranging from 16% to 28%.

Table 71: Reaction conditions and results for the reaction of imidates **2.85** with different primary amines, in ethanol



2.85 **2.86** **2.87**

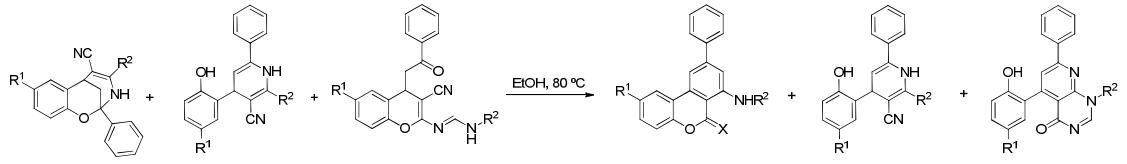
Entry	2.85		2.51		additive	t (h)	results	η (%)
	R^1	R^2	R^3	equiv.				
1	H	H	$CH_2C_6H_5$	1	-	5.5	**2.86c**	19
2	H	H	3-MeC_6H_4	1.2	-	2.25	**2.86d**	27
3	Br	H	C_6H_5	1.5	-	4.66	**2.86b**	16
4	Br	H	4-MeC_6H_4	1.2	-	3.5	**2.86e**	28

5	Br	Br	4-OMeC$_6$H$_4$	2	-	2	**2.86f**	26
6	Br	Cl	4-MeC$_6$H$_4$	1.5	-	22	**2.86g**	27
7	Br	Cl	4-OMeC$_6$H$_4$	1.5	-	1.5	**2.86h**	22
8	Br	H	3-BrC$_6$H$_4$	2	-	7	**2.86i** + **2.87e'** (0.83: 2.87)	-
9	Br	Br	3-MeC$_6$H$_4$	1 + 0.2[a]	H_2O (cat.)	8.5 + 3[a]	**2.86j** + unknown contaminant	-

[a]The reaction was performed for 8 hours in the presence of 1 equivalent of *m*-methylaniline, after which an additional 0.2 equivalents of *m*-methylaniline were added, and the reaction was left at 80 +C for 3 h.

Amidines **2.87** were also converted into pyridopyrimidinones **2.86** by heating at 80 °C in ethanol (**Table 72**). This conversion was explored either using amidines **2.87** as a pure product or combined with spiro derivatives **2.58**/**2.61** and dihydropyridines **2.59**/**2.60**, which were present in <20%. When **2.87** was not used as a pure product, the reaction yields presented were calculated considering that **2.87** was pure (entries 2-5 - **Table 72**). Under these conditions, compounds **2.86k** and **2.86l** were obtained with yields of about 49% and 17% (entries 2 and 3 – **Table 72**). For some experiments, amidines **2.87g**,**z** and **m'** were recovered as a pure product, and it might be necessary to increase the reaction time in order to obtain the respective compound **2.86** (entries 1, 4 and 5– **Table 72**). Moreover, the assays performed with mixtures that did not contain spiro derivatives **2.59**/**2.60**, only amidines **2.87** were only obtained (entries 3, 4 and 7– **Table 72**). Most compounds **2.58**-**2.61** were soluble in ethanol, and this may explain their absence in the isolated products.

Table 72: Results of the heating, at 80 °C in ethanol, of samples of amidines **2.87** also containing spiro derivatives **2.58**/**2.61**, and dihydropyridines **2.59**/**2.60**



2.58 (R^2=OEt) **2.61** (R^2=NHR^3) | **2.59** (R^2=OEt) **2.60** (R^2=NHR^3) | **2.87** | **2.55** (X=NH) **2.56** (X=O) | **2.59** (R^2=OEt) **2.60** (R^2=NHR^3) | **2.86**

Entry	**2.87**				additive	t (h)	results	η (%)[b]
	R^1	**R^2**	**reagents (%)[a]**	**m (g)**				
1	Br	4-MeC$_6$H$_4$	**2.87g**	0.117	H_2O (cat.)	3	**2.87g**	63
2	Br	4-OMeC$_6$H$_4$	**2.87h** (81) + **2.58a**/**2.61e** (12) + **2.59a**/**2.60i** (7)	0.121	-	18.25	**2.86k**	49*

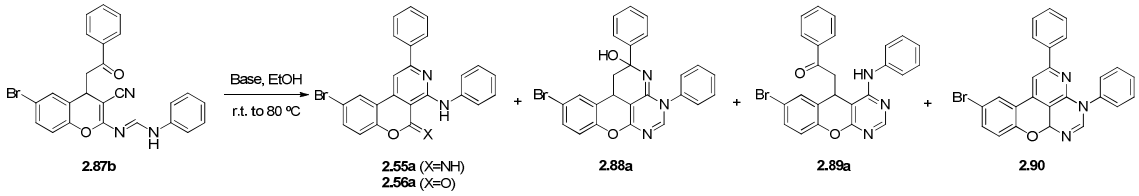
3	Br	4-ClC_6H_4	**2.87l** (94) + **2.86d** (6)	0.087	-	14.66	**2.86l**	13
4	Cl	C_6H_5	**2.87z** (83) + **2.59c/2.60j** (17%)	0.133	H_2O (cat.)	4	**2.87z**	67
5	Cl	4-MeC_6H_4	**2.87a'**	0.117	H_2O (cat.)	2.5	**2.87m'**	61
6	Cl	4-$OMeC_6H_4$	**2.87b'** (92) + **2.59d/2.60k** (8)	0.175	H_2O (cat.)	5	**2.86m**	65

[a]By ^1H NMR; [b]For the cases where mixtures were used, the yields were calculated assuming that the used compound **2.87** is pure

Studies on the reactivity of *N*-(3-cyano-4-(2-oxo-2-arylethyl)-4*H*-chromen-2-yl)-*N*-aryl-formimidamides

The reactivity of *N*-(3-cyano-4-(2-oxo-2-arylethyl)-4*H*-chromen-2-yl)-*N*-aryl-formimidamides **2.87**, under basic conditions, was also studied. To understand the effect of both the nature and concentration of the base in the reaction, amidine **2.87b** was used as a model. The experiments and results are summarized in **Table 73**.

Table 73: Results of the treatment of amidine **2.87b** with diverse type of bases



Entry	[2.87b] (M)	base	equiv.	T (°T)	t (h)	results: product	ratio	η(%)
1	0.20	$NaHCO_3$ 0.05 M	0.12	r.t.	45	**2.88a** + **2.89a**	1.4/1	-
2	0.20	NaOH 2M	0.25	r.t	7.5	**2.89a**	-	53
3	0.20	DBU	1	80	1.5	**2.55a + 2.56a + 2.90**	3/1/3	-
4	0.17	Et_3N	1	r.t.	23	**2.88a**	-	43
5	0.16	DBU	1	r.t.	13.5	**2.88a**	-	51
6	0.14	DBU	1	r.t.	19.5	**2.88a**	.	60
7	0.10	DBU	1	50	5 + 1.5 [a]	**2.88a** + **2.89a**	5/1	-
8	0.13	DBU	1	60	6.33	**2.89a + 2.90**	14/1	-

9	0.13	DBU	1	80	3 + 1.5[a]	**2.55a + 2.56a + 2.90**	3.5/1.4/1	-
10	0.10	DBU	1	80	4 + 2.5[a]	**2.90**	-	42
11	0.14	DBU	cat.	80	5.66 + 1.5[a]	**2.90**	-	27

[a] The addition of DBU occurred after stirring for a certain period of time; after the addition, the mixture was left stirring for an additional period

From these results presented in **Table 73**, the following conclusions were drawn:

1) At room temperature, two competing intramolecular cyclization reactions between the phenylformimidamide moiety and the cyano group to give rise to the 5*H*-chromeno [2,3-*d*]pyrimidine core were observed. One path provided derivatives **2.89a**, and the other evolved further to a second condensation reaction involving the ketone group to afford derivatives **2.88a**. Under these conditions, organic bases favoured the formation of chromenopyrimidine **2.88a** as a single isolated product, while with aqueous inorganic bases derivative **2.89a** was the major compound in the reaction (entries 1-2 *vs* 4-6).
2) Increasing the reaction temperature up to 80 °C, which was only explored with organic bases, led to further intramolecular condensation between the ketone and the aniline substituent in chromenopyrimidine **2.88a** took place to afford a polycyclic derivative **2.90**. The latter compound is obtained in higher yield when 1 equivalent of DBU is employed instead of a catalytic amount (entries 10 *vs* 11). In both cases, DBU was added after an initial stirring in ethanol, at 80°C.
3) The treatment of a solution of imidamide **2.87b** in ethanol with one equivalent of DBU at room temperature for 19.5 h affords chromenopyrimidine **2.88a** with 60% yield as a sole reaction product. On the contrary, as expected, under the same reaction conditions but heating at 80 °C, compound **2.88a** undergoes a second cyclization reaction to afford a polycyclic derivative **2.90** in a 42% yield.

Compound **2.88a** was identified by IR and NMR spectroscopy. In the IR spectrum highlights the small and broad band centred at 3185 cm^{-1}, assigned to the stretching vibration of the hydroxyl group. In addition, the typical band for the ketone group, at 1680-1670 cm^{-1}, is absent. In the ^{1}H NMR spectroscopy, there are two sets of signals for the structure due to the formation of a diastereoisomeric mixture, in virtue of the two chiral centres present in the molecule (Ca and C11b) (**Figure 58**). It is recognizable by its singlets at δ 8.10 and δ 8.04 ppm (H5, major and

minor isomers); its singlets at δ 5.80 and δ 5.61 ppm (hydroxyl groups, major and minor isomers); doublet of doublets, attributed to H1 (α and β) at δ 4.21 (J_1= 12.4, J_2= 4.8 ppm) and δ 2.72 21 (J_1= 12.8, J_2= 4.8 ppm) for the major isomer, and at δ 3.43 and δ 2.80 ppm, respectively, with the same coupling constants, for the minor isomer; two triplets at δ 1.76 (J= 12.8 Hz, minor isomer) and δ 1.30 ppm (J= 12.4 Hz, major isomer), assigned to H11b.

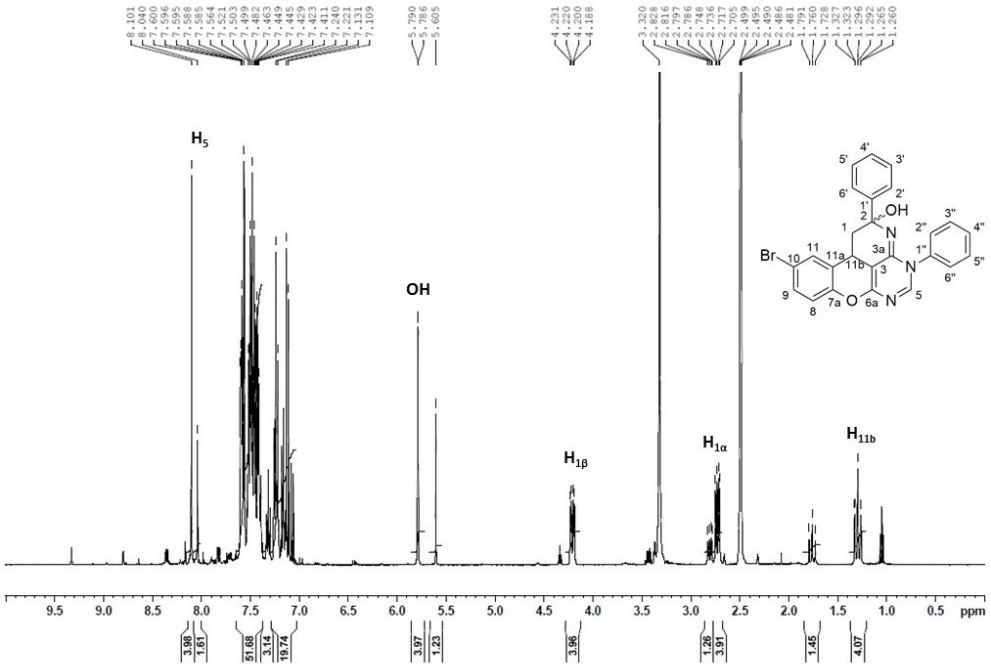


Figure 58: ^{1}H NMR (400 MHz, DMSO-d_6, δ ppm) spectrum obtained for compound **2.88a**, in which several signals are highlighted

The ^{13}C NMR spectrum of **2.88a** highlight two signals at 151.07 and δ 150.76 ppm, which correspond to the C5 minor and major signals, respectively, as well as its C1 and C11a carbon signals, which appear at δ 38.49 and δ 38.30 ppm (C1, major and minor isomers), and δ 27.41 and δ 26.40 for both C11b (minor and major) (**Figure 59**).

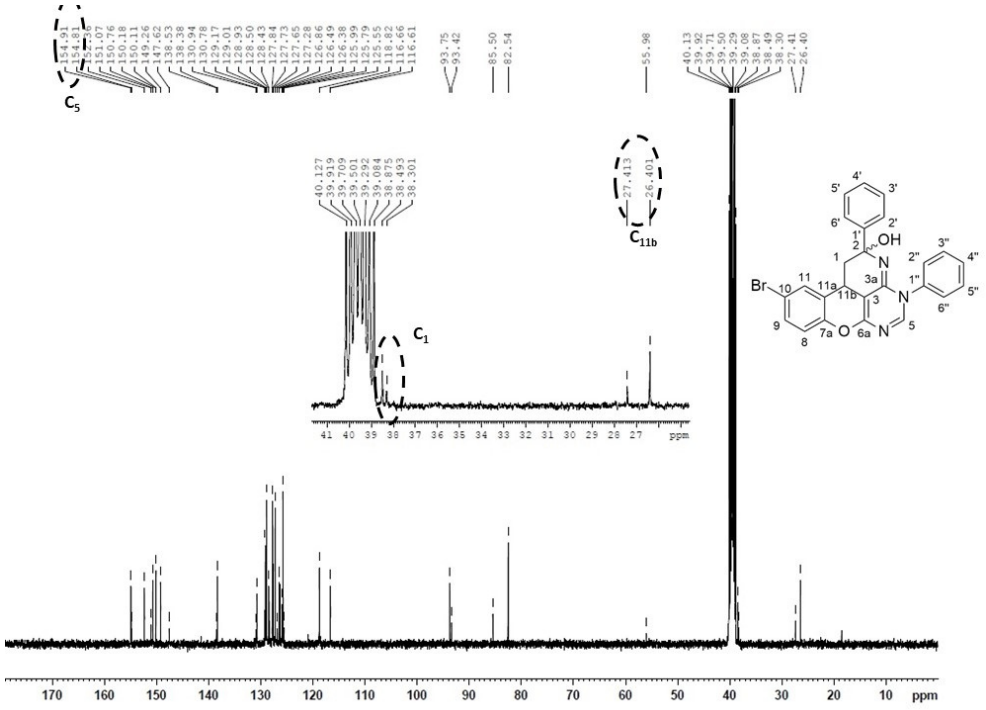


Figure 59: ^{13}C NMR (100 MHz, DMSO-d_6, δ ppm) spectrum obtained for compound **2.88a**, in which three signals are highlighted

Compound **2.89a** was identified by IR and NMR spectroscopy In the IR spectrum highlights a sharp, medium intensity band centred at 3399 cm^{-1}, corresponding to the stretching vibration of the exocyclic NH group, and a strong and sharp carbonyl C=O stretching vibration band, very similar to the signal presented in the starting material, at 1673 cm^{-1}. In the ^{1}H NMR spectrum (**Figure 60**), and using compound **2.89a** as example, two singlets, one at δ 8.96 ppm corresponding to the NH proton, and another at δ 8.23 ppm that corresponds to the H2 hydrogen atom of the pyrimidine ring, can be highlighted. The C5 and Ca signals, also present in the starting material, remain almost unaltered, with only the H4 signal shifting to δ5.00 ppm (t, *J*= 4.8 Hz) and the Ha multiplet remaining at around δ 3.66 ppm. The most remarkable signals in the ^{13}C NMR spectrum are the carbonyl signal at δ197.85, the C2 signal at δ 155.87 ppm and the Ca and C5, of the 4-(2-oxo-2-arylethyl) moiety, at δ44.18 ppm and δ28.80 ppm, respectively (**Figure 61**).

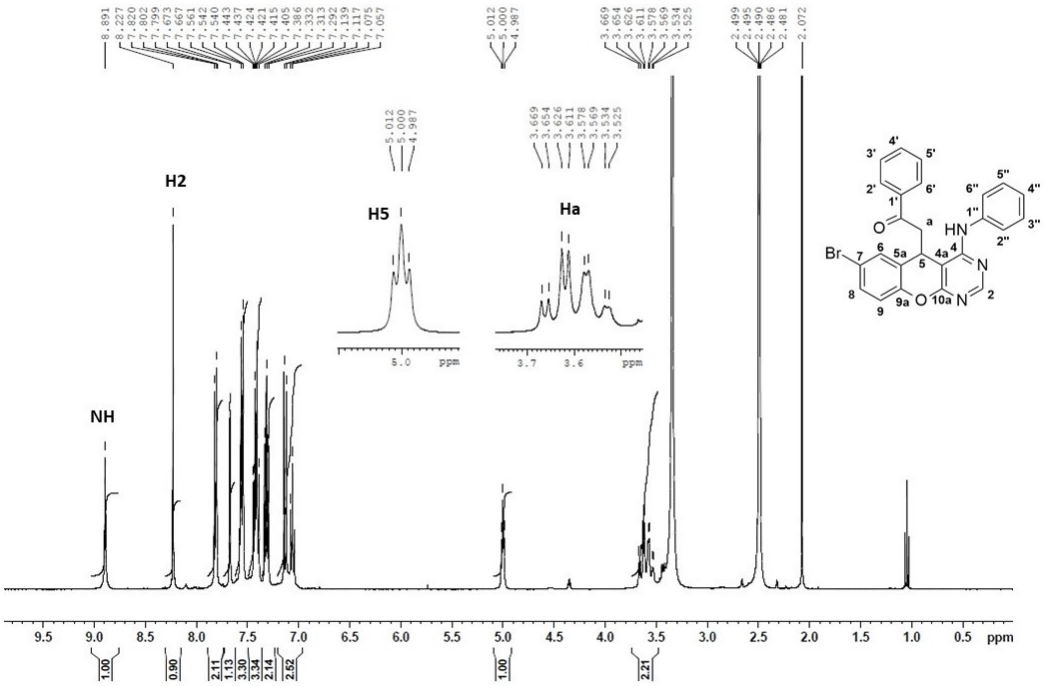


Figure 60: ^{1}H NMR (400 MHz, DMSO-d$_6$, δ ppm) spectrum obtained for compound **2.89a**, in which several signals highlighted

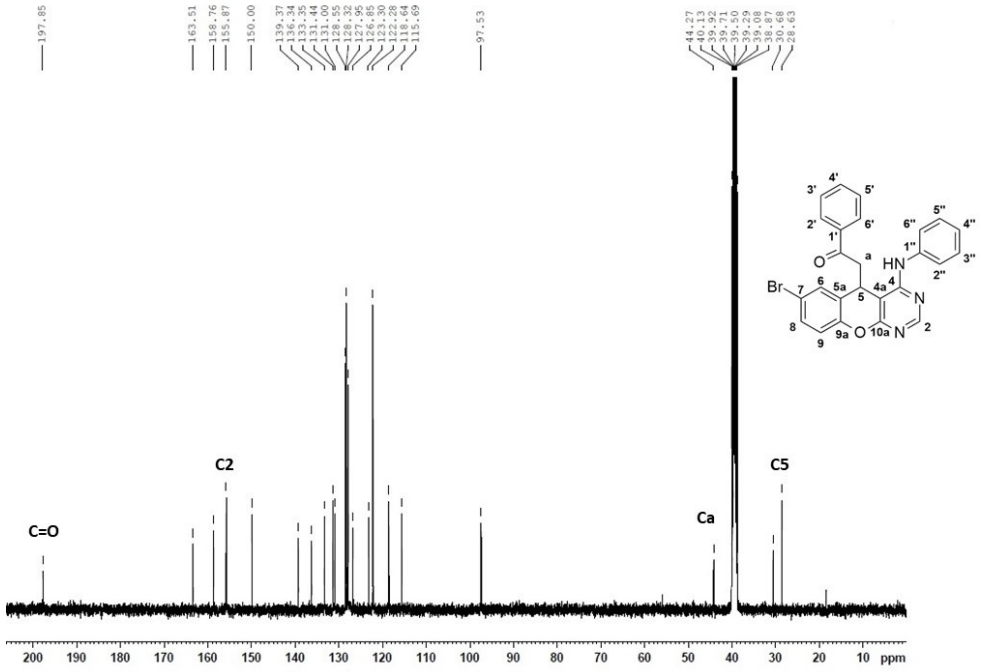


Figure 61: ^{13}C NMR (100 MHz, DMSO-d$_6$, δ ppm) spectrum obtained for compound **2.89a**, in which several signals highlighted

Compound **2.90** was also identified by IR and NMR spectroscopy In the IR spectrum a group of signals in the 1650-1630 cm^{-1} region, assigned mainly to the aromatic C-H stretching vibrations are identified. The most characteristic signals in its ^{1}H NMR spectrum are two doublets

at δ 8.43 ppm and at δ 6.77 ppm, corresponding to H5 and H6a, as well as a singlet at δ 8.22 corresponding to H1 (**Figure 62**). In the ^{13}C spectrum stands out the signals corresponding to C5 (δ 154.91 and 154.81 ppm), C1 (δ 38.49 and 38.30 ppm) and C11a (δ 27.41 and 26.40 ppm), as they appear duplicated (**Figure 63**).

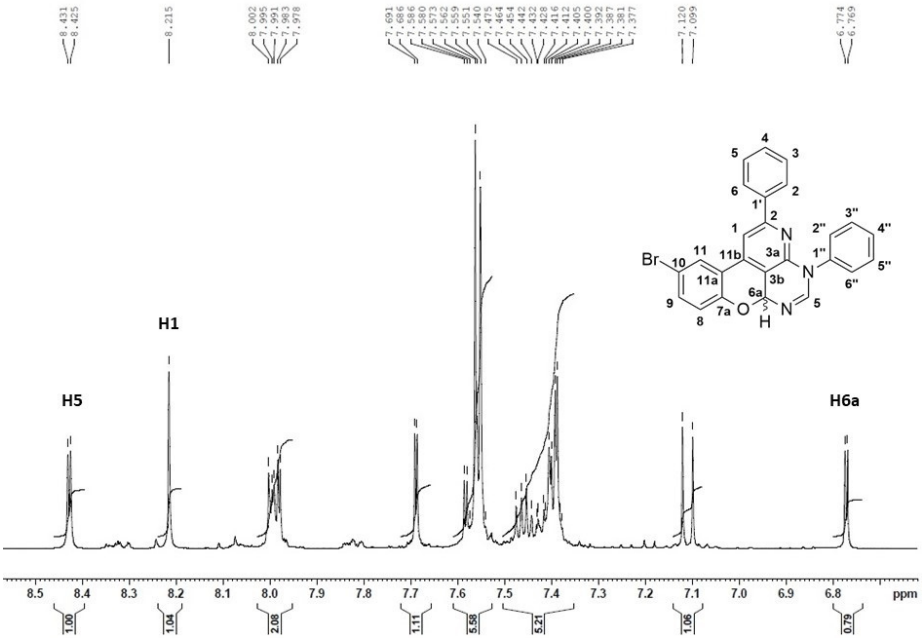


Figure 62: ^{1}H NMR (400 MHz, DMSO-d_6, δ ppm) spectrum obtained for compound **2.90**, in which several signals highlighted

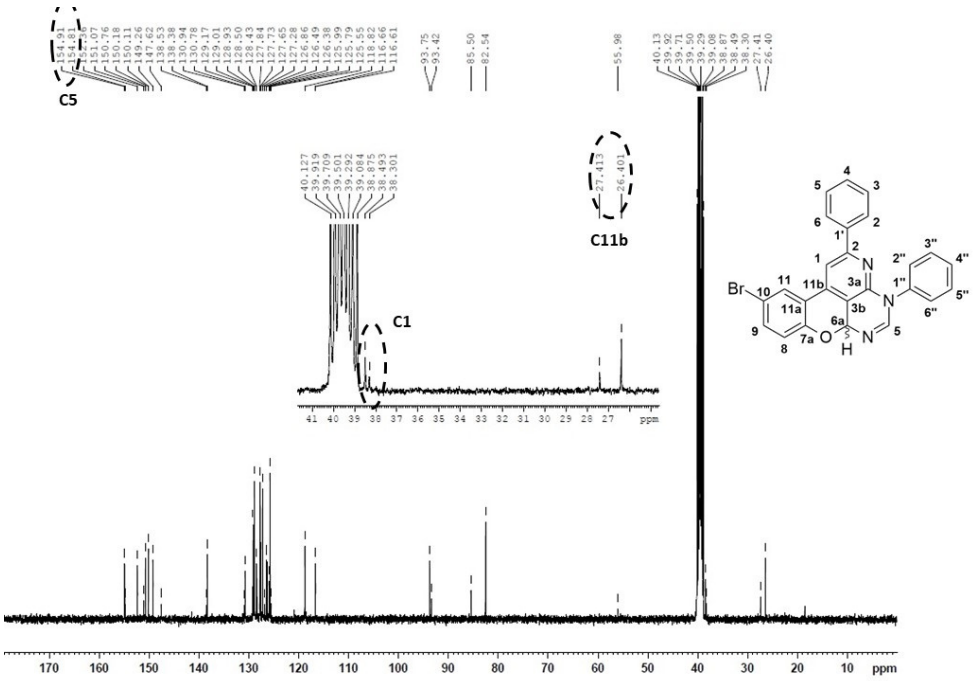
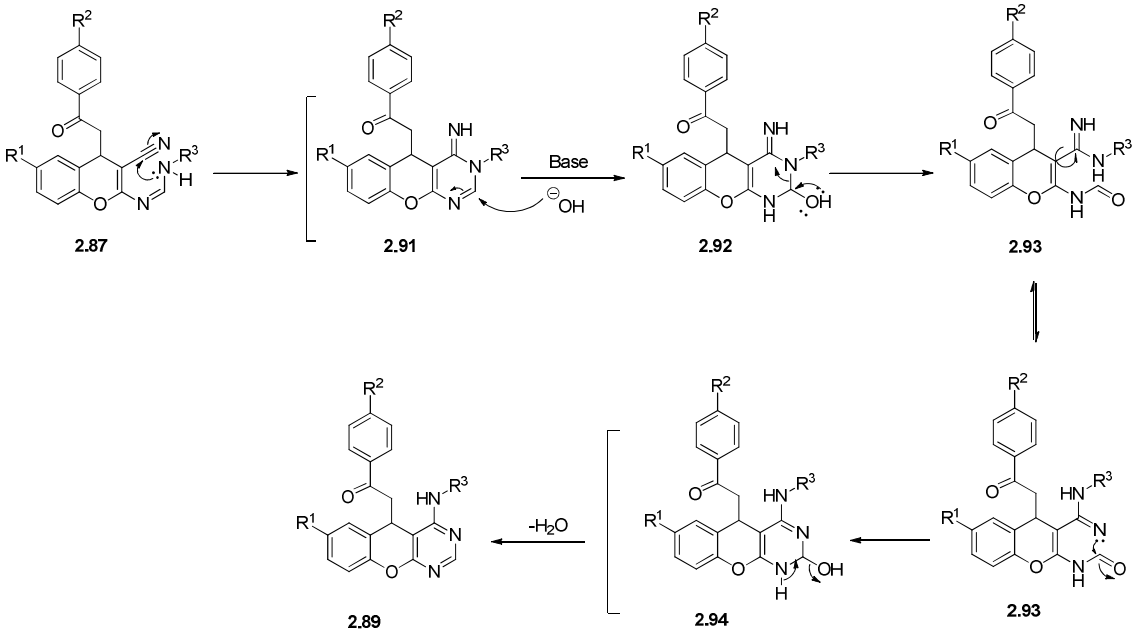


Figure 63: ^{13}C NMR (100 MHz, DMSO-d_6, δ ppm) spectrum obtained for compound **2.90**, in which several signals highlighted

The formation of compounds **2.89** can be explained by intramolecular cyclization followed by a base catalysed Dimroth rearrangement (**Scheme 37**). The latter reaction is well-known[135–138], having examples of acid[137] or base catalysed processes[139,140]. In this case, the rearrangement occurs via a base-catalysed ring opening of intermediate **2.91**, followed by bond rotation and nucleophilic attack of the imine moiety generated, to promote ring closure. Final aromatization of the dihydropyrimidin-2-ol intermediate **2.94** resulted by elimination of a water molecule, providing chromenopyrimidine **2.89**.

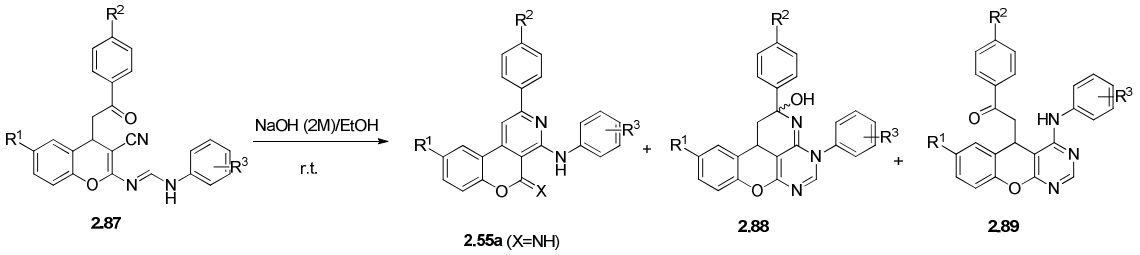


Scheme 37: Proposed mechanism for the formation of compounds **2.89**, via base-catalysed Dimroth rearrangement

Compound **2.89a** was also isolated from the reaction of **2.88a** with (1:3) NaOH (2M)/ethanol, at room temperature, for 14 h and 40 min. The product was isolated in 73% yield, which is higher than when amidine **2.87b** was used (73% vs 53%). Nevertheless, the overall isolated yield is superior when the reaction is performed using amidine **2.87**, as it does not involve the previous formation of compound **2.88**, which adds one step further to the procedure.

For this reason, the standard procedure that was adopted for the preparation of compounds **2.89** uses amidines **2.87** as starting material, in NaOH (2M)/ethanol, at room temperature. The experimental conditions and results are described in **Table 74.** Compounds **2.89** could be isolated as a pure product (entries 1, 3, 4, 8, 10, 11) or as a major product in a mixture containing **2.55** (entries 2, 5, 6, 7, 9).

Table 74: Reaction conditions, and results for the reaction of compounds **2.87** with NaOH (2 M) in EtOH at room temperature



2.87 **2.55a** (X=NH) **2.88** **2.89**

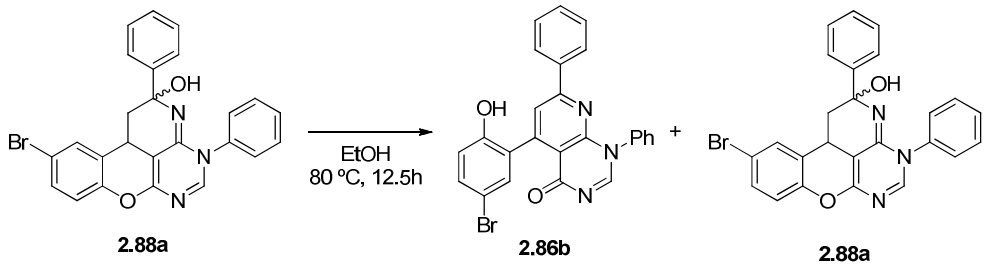
Entry	2.87			NaOH (equiv.)	t (h)	results	ratio	η (%)
	R^1	R^2	R^3					
1	H	H	H	9	16	**2.89b**	-	17
2	H	H	4-Me	5.6	3	**2.55c +2.88b**	1/12.5	-
3	Br	H	4-Me	21	14.33	**2.89c**	-	65[1]
4	Br	Me	H	18.5	13.5	**2.89d**	-	42
5	Br	Br	H	9.2	4	**2.55s +2.89e**	1/20	-
6	Br	Br	4-Me	12.5	14.33	**2.55u +2.89f**	1/12.6	-
7	Br	Br	4-OMe	10.5	13	**2.55v + 2.89g**	1/1.5	-
8	Br	Br	4-CN	18.2	14	**2.89h**	-	23[1,2]
9	Br	Cl	3-Me	6.5	4.33	**2.55z + 2.89i**	1/10	-
10	Cl	H	H	5	1.66	**2.89j**	-	62
11	Cl	H	4-Me	8.2	15	**2.89k**	-	53[1]

[1]Starting material was a crude mixture of **2.87** and other minor contaminants; [2]Yield after recrystalyzation

The results presented in **Table 74** were performed using an NaOH 2M/EtOH ratio according to the amount of ethanol needed to solubilize the used amidine **2.87**. Compounds **2.89c**, **d**, **j** and **k** were obtained with good yields (42-65%), using 5-21 equivalents of NaOH. For amidines **2.87** containing two halogen atoms (entries 5-9), the reactions led to the isolation of a mixture of the corresponding chromenopyridine **2.55** and **2.89**, in variable ratios, except when a crude mixture containing the 4-cyano substituted amidine was used (entry 8), which led to the isolation of **2.89h** after recrystallization. These results show that the conditions used (NaOH equivalents, amount of ethanol, time) must be adjusted for each amidine used, in order to maximize the results. Nevertheless, compounds **2.89a-k** were prepared with low to good yields (17-65%).

Discussion of possible reaction mechanism

With the intent of understanding the reaction pathway that leads to the formation of compounds **2.86**, a series of experiments were carried out with the polycyclic derivative **2.88a** (R^1= Br, R^2= H, R^3= Ph). First, a suspension of compound **2.88a** in ethanol was heated at 80 °C for 12.5 h, and the reaction was followed by TLC (**Scheme 38**). The formation of a yellow solid was observed, which was filtered and washed with cold ethanol, and the collected product was studied by ^{1}H NMR. The spectrum of the solid revealed the presence of pyridopyrimidinone **2.86b** as the major component of a mixture, along with chromenopyridines **2.55a** and **2.56a**, in a 5.7/1/1.7 ratio, respectively (**Figure 64**).



Scheme 38: Reaction of **2.88a** in ethanol at 80 °C, for 12.5h

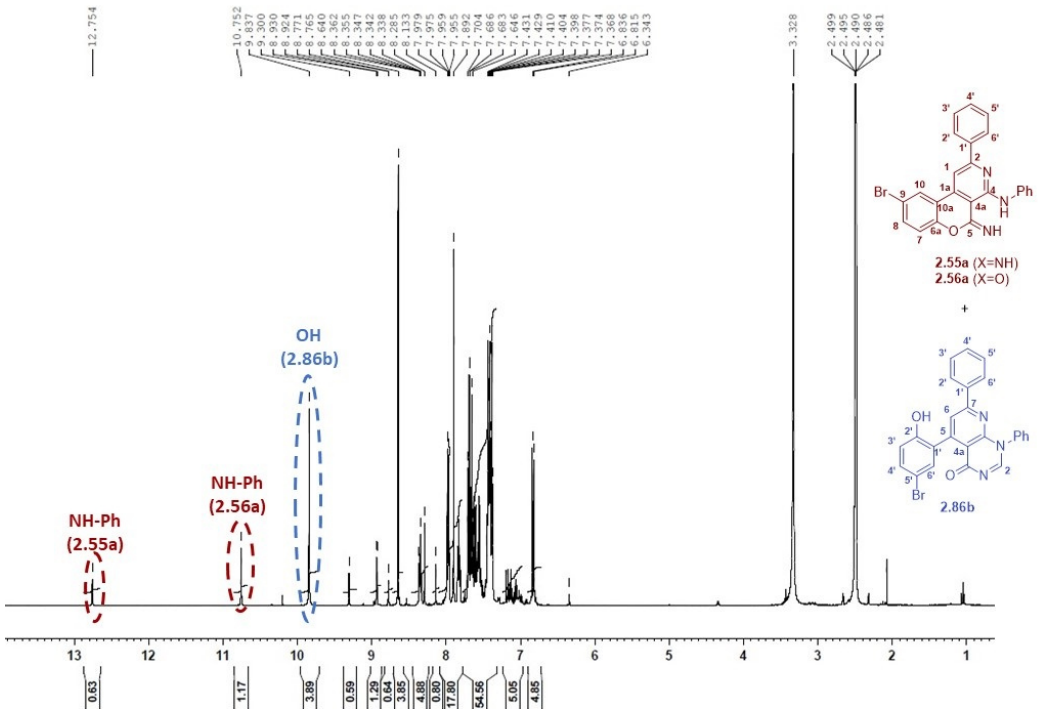
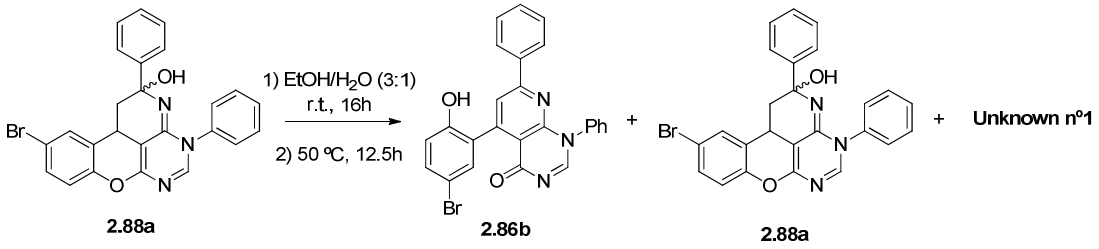


Figure 64: ^{1}H NMR (400 MHz, DMSO-d_6, δ ppm) spectrum of a mixture of compounds **2.55a**, **2.56a** and **2.86c**, obtained after heating an ethanolic solution of compound **2.88b** at 80 °C, for 12.5 hours

In a separate experiment, a suspension of compound **2.88a** in a mixture of EtOH/H_2O (3:1) was stirred at room temperature, and the reaction was followed by TLC (**Scheme 39**). As no evolution was observed after 16 h, the mixture was heated to 50 °C for 12.5 h. The yellow solid was filtered and washed with cold ethanol and studied by ^{1}H NMR, which revealed the formation of pyridopyrimidine **2.86b**, together with compound **2.88a** as a diastereoisomeric mixture, and an unidentified compound (**unknown nº1**) (**Figure 65**). The most relevant signals of the latter compound are two doublets, centred at δ6.44 ppm (*J*= 8.4 Hz) and δ 6.98 ppm (*J*= 8.4 Hz).



Scheme 39: Reaction of **2.88a** in a suspension of EtOH/H_2O (3:1), at r.t for 16h, followed by heating at 50 °C for 12.5 h

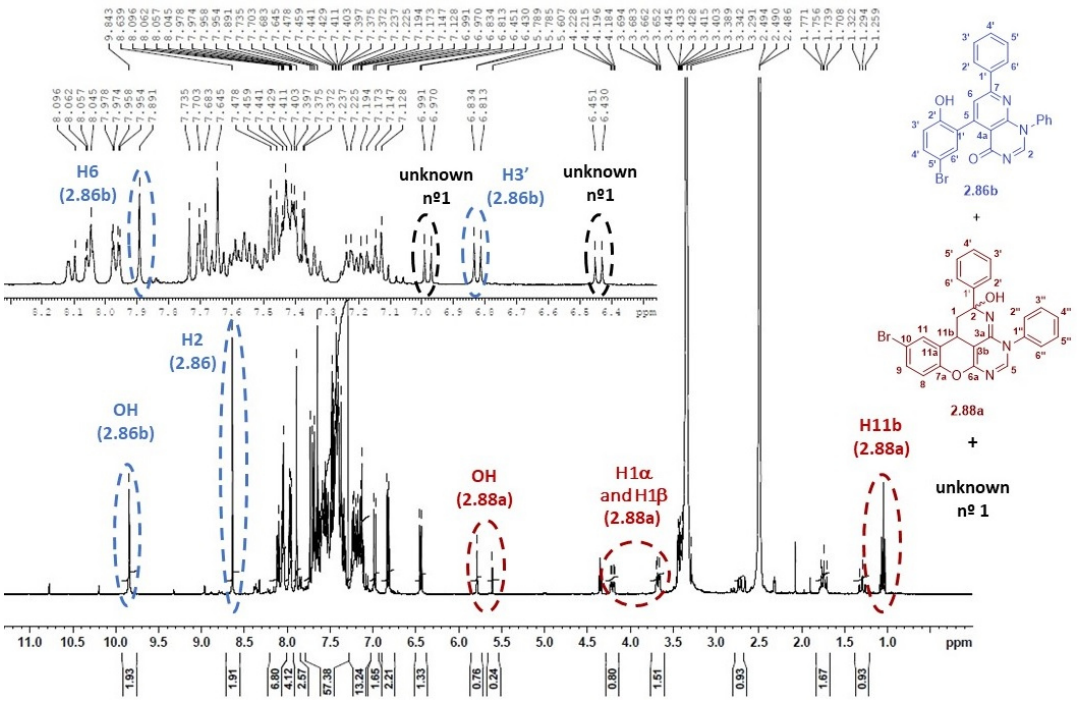


Figure 65: ^{1}H NMR (400 MHz, DMSO-d_6, δ ppm) spectrum of a mixture of compounds **2.86b** and **2.88a**, obtained after stirring a solution of compound **2.88c** in an (3:1) EtOH/H_2O, at room temperature for 16 h, and additional heating at 50 °C for 12.5 h. Two new doublets were also identified (black circles), along with signals from **2.86b** (blue circles) and **2.88a** (red circles)

Moreover, the ^{1}H NMR spectrum of this DMSO-d_6 sample recorded after heating at 80 °C for 2.5 h, revealed a complete conversion of the previous mixture into compound **2.86b**, with very little contamination, confirming that **2.88** is indeed a precursor of **2.86** (**Figure 66**). The identification is possible due to the presence of the characteristic singlets for OH, H2 and H6 that appear at δ 9.84, δ 8.64 and δ 7.89 ppm, respectively.

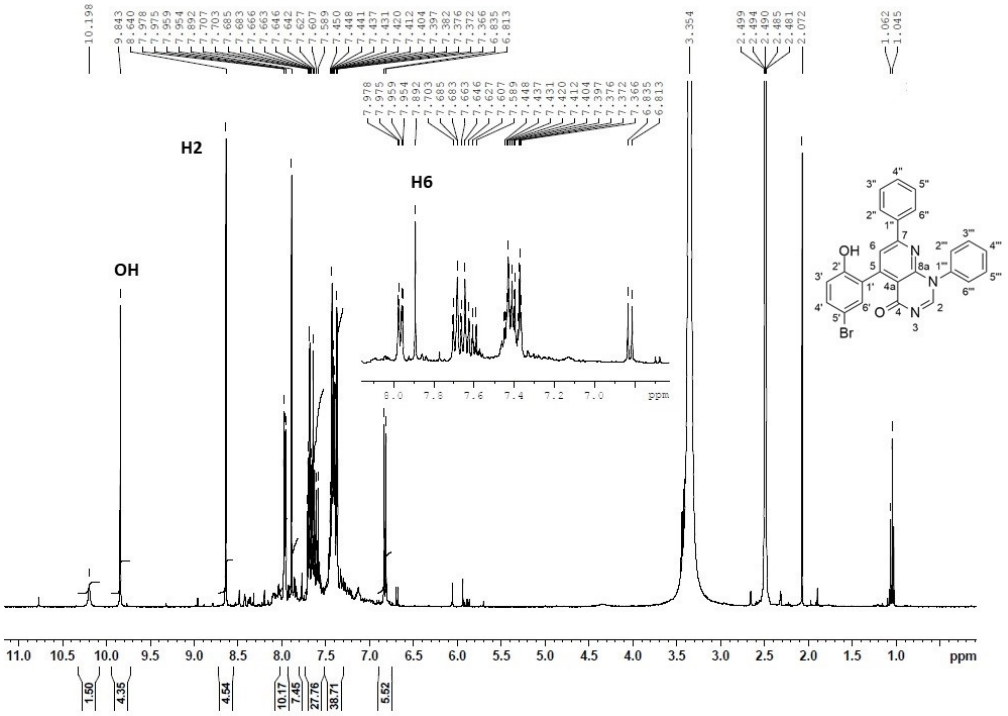
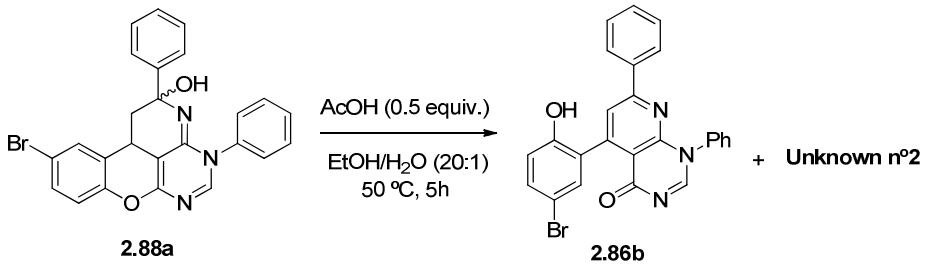


Figure 66: ^{1}H NMR (400 MHz, DMSO-d_6, δ ppm) spectrum of compounds **2.86b**, obtained after heating the DMSO-d_6 sample containing the mixture, presented in **Figure 65**, at 80°C for 2.5 hours, with three signals highlighted

Another experiment consisted in heating at 50 °C, for 5h, a suspension of compound **2.94a** in a EtOH/H_2O (20:1) mixture, in the presence of 0.5 equivalents of acetic acid. The resulting yellowish solid was filtered, washed with cold ethanol, and studied by ^{1}H NMR (**Scheme 40** and **Figure 67**). In this case, the spectrum revealed the formation of a mixture of pyridopyrimidinone **2.86b** with another unidentified compound (**unknown nº2**), which has two characteristic signals [the singlet at δ 10.77 ppm and the small doublet at δ 8.95 ppm (*J*= 2.0 Hz)].



Scheme 40: Reaction of **2.88a** in a suspension of EtOH/H_2O (20:1), at 50 °C for 5 h, in the presence of 0.5 equivalents of acetic acid

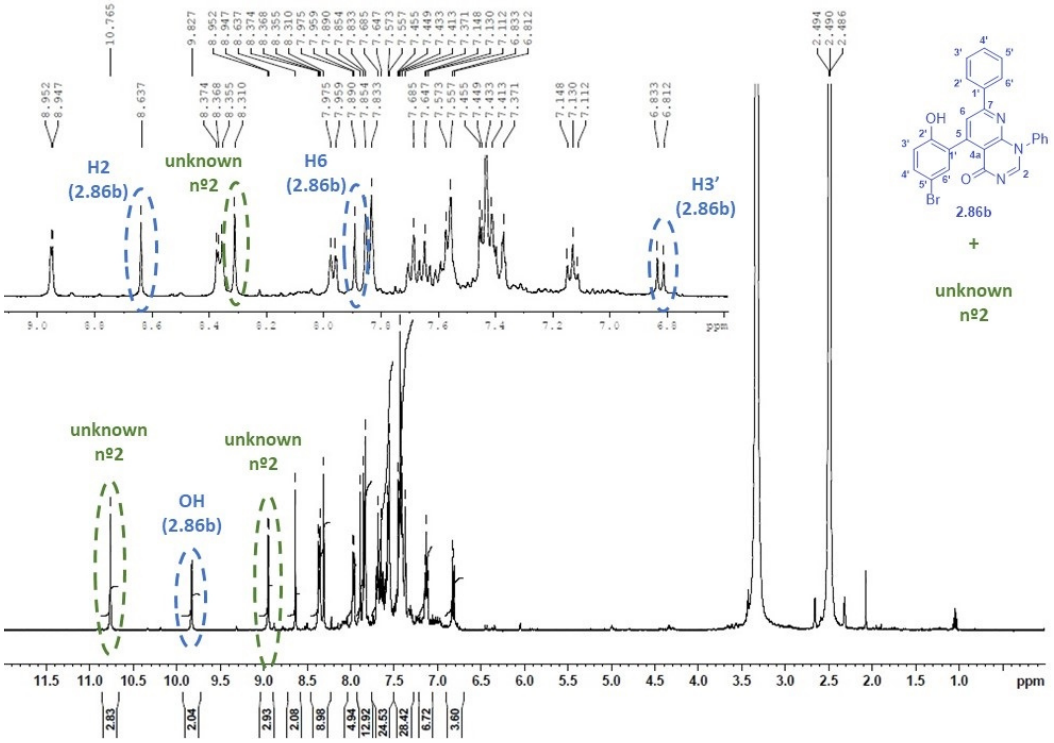


Figure 67: ^{1}H NMR (400 MHz, DMSO-d_6, δ ppm) spectrum of a mixture of compound **2.86c** (blue circles) and an unidentified compound (black circles), obtained after obtained after heating at 50 °C for 5 h of a suspension (100:5) EtOH/H_2O solution of compound **2.88c** in the presence of 0.5 equiv. of AcOH

The yellow solid collected in the previous reaction was solubilized in ethanol and heated at 80 °C for 4 h. A new NMR spectrum of the reaction revealed the complete conversion of the latter compound into pyridopyrimidinone **2.86c** (**Figure 68**).

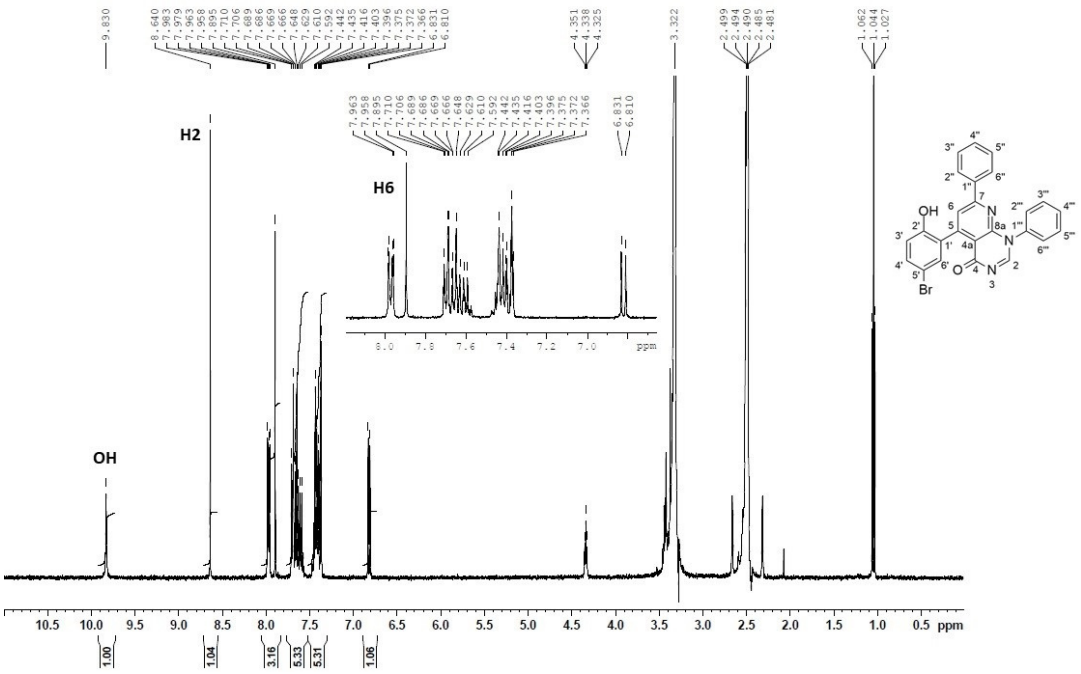
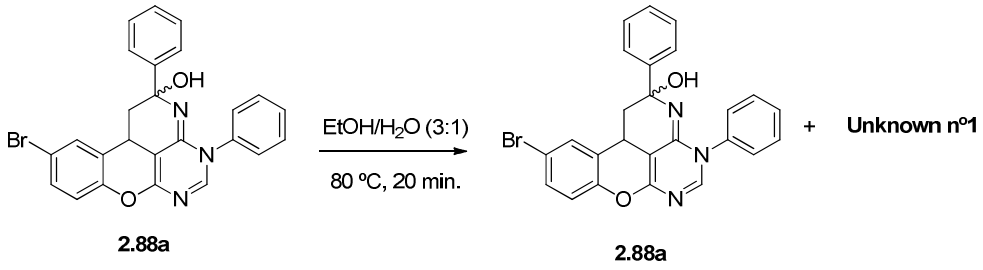


Figure 68: ^{1}H NMR (400 MHz, DMSO-d_6, δ ppm) spectrum of compounds **2.86c**, obtained after heating, at 80°C for 4 h, the sample containing the mixture, presented in **Figure 67**, in EtOH, with three signals highlighted

To get an insight into the chronological formation of the previously unidentified compounds, a solution of amidine **2.87a** in a mixture of EtOH/H_2O (3:1), and in the presence of 0.5 equivalents of acetic acid, was heated at 80 °C, and the reaction was stopped at three different times [after 20 min (**Scheme 41**), 2 h and 30 minutes (**Scheme 42**) and 4 h and 20 minutes (**Scheme 43**)]. The resulting suspension was filtered, washed with cold ethanol, and analysed by ^{1}H NMR. After 20 min, no starting material was observed, but rather another product that contains the two previously identified doublets at δ6.98 (*J*= 8.4 Hz) and δ 6.44 ppm (*J*= 8.4 Hz) was identified (**Figure 69**).



Scheme 41: Reaction of **2.88a** in a mixture of EtOH/H_2O (3:1), at 80 °C for 20 min.

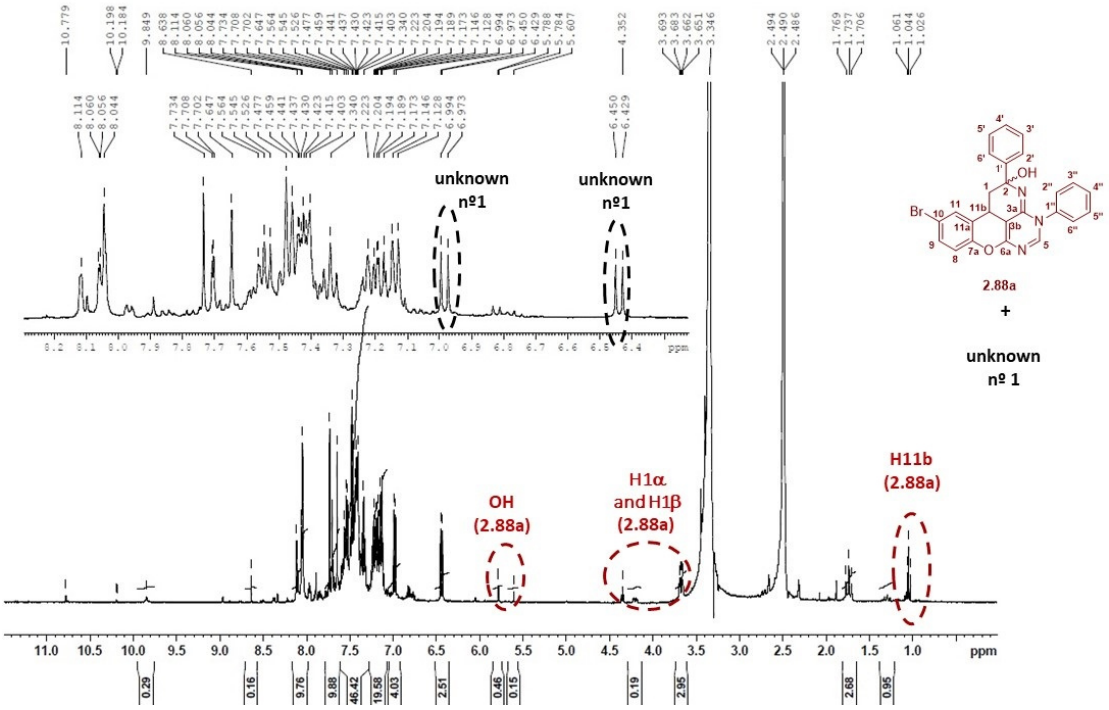
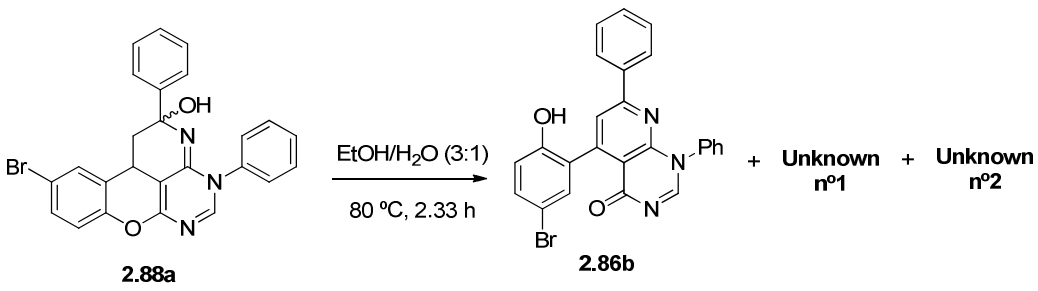


Figure 69: ^{1}H NMR (400 MHz, DMSO-d_6, δ ppm) spectrum of a mixture of compound **2.88a** (red circles) and an unidentified compound (black circles), obtained after heating a solution of compound **2.88a** in EtOH/H_2O (3:1), and in the presence of 0.5 equivalents of acetic acid at 80 °C for 20 min.

After 2 h and 20 minutes, pyridopyrimidine **2.86b** becomes visible in the crude mixture. The aforementioned doublets at δ6.44 (J= 8.4 Hz) and δ6.98 ppm (J= 8.4 Hz) remained, although in a slightly smaller proportion, and the three signals, at δ 10.77 ppm (s), δ 8.95 ppm (d, J= 2.0 Hz) and at δ 8.31 ppm (s) also appear in the spectrum (**Figure 70**).



Scheme 42: Reaction of **2.88a** in a mixture of EtOH/H_2O (3:1), at 80 °C for 2 h and 20 min

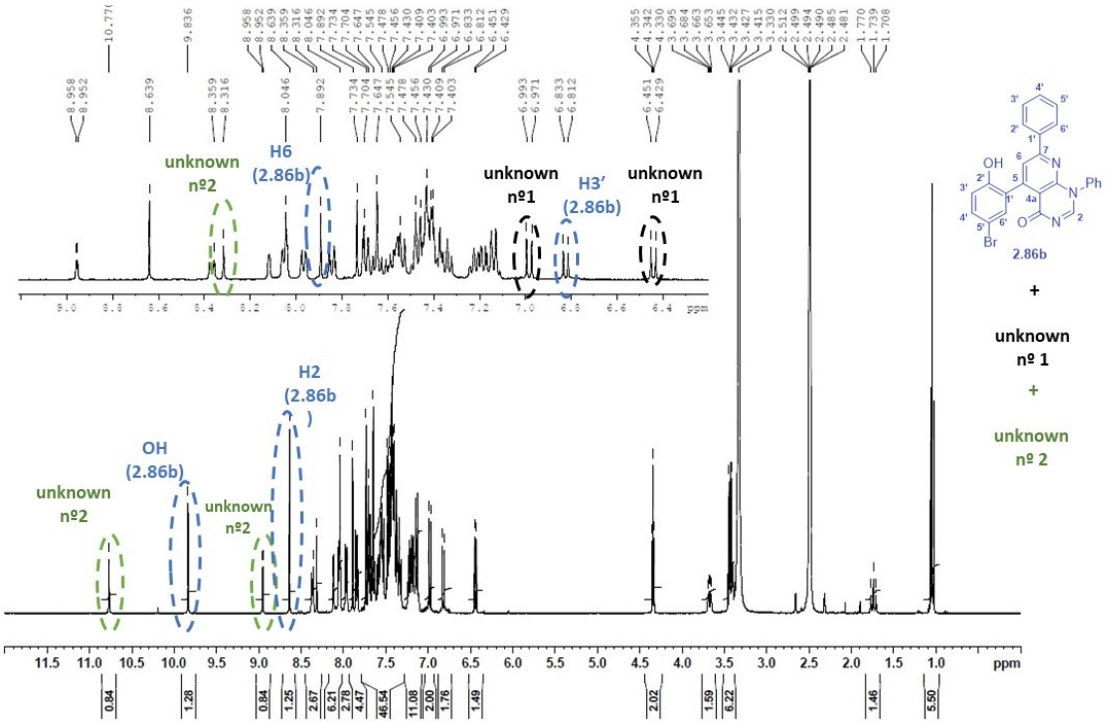
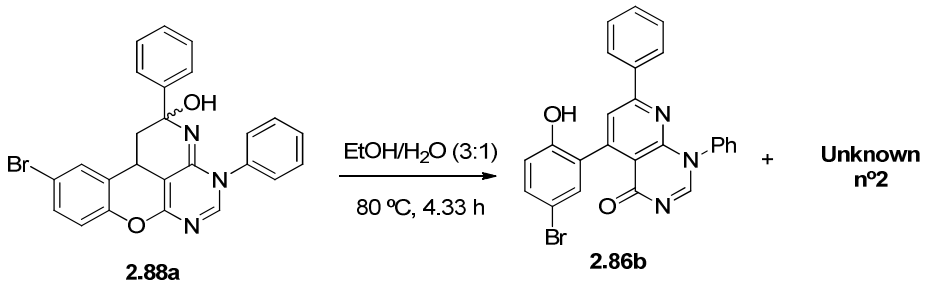


Figure 70: ^{1}H NMR (400 MHz, DMSO-d_6, δ ppm) spectrum of a mixture of compound **2.86b** (blue circles) and other unidentified compounds (black and green circles, for unknown n°1 and 2, respectively), obtained after heating a solution of compound **2.88a** in a (3:1) EtOH/H_2O, and in the presence of 0.5 equivalents of acetic acid at 80 °C for 2.33 h

After 4 h and 20 minutes, the ^{1}H NMR spectrum revealed complete disappearance of the two doublets at δ 6.44 and δ 6.98 ppm was observed, as well as a proportional increase in the remaining unidentified signals at δ 10.77 ppm, δ 8.95 ppm and at δ 8.31ppm. The signals assigned to compound **2.86b** also increased (**Figure 71**).



Scheme 43: Reaction of **2.88a** in a mixture of EtOH/H_2O (3:1), at 80 °C for 4 h and 20 min.

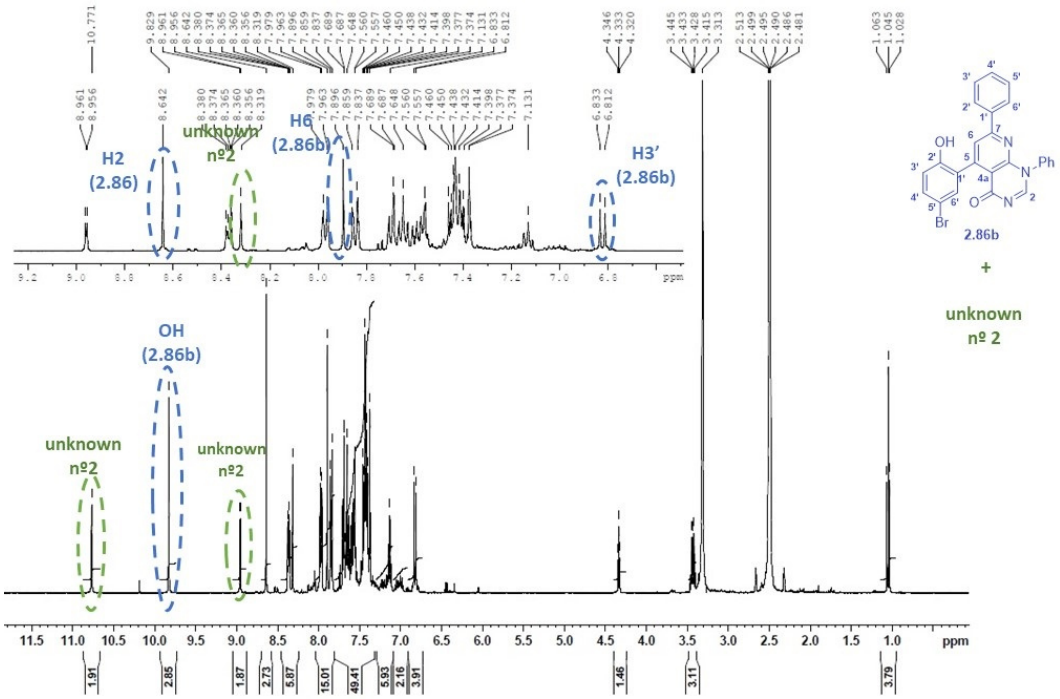
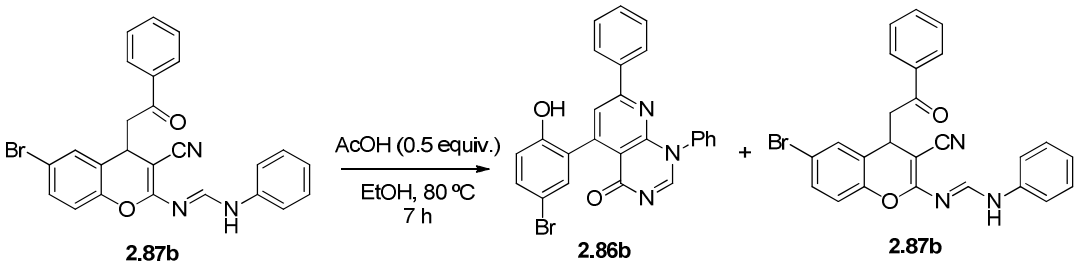


Figure 71: ^{1}H NMR (400 MHz, DMSO-d_6, δ ppm) spectrum of a mixture of compound **2.86b** (blue circles) and other unidentified compound (green circles), obtained after allowing compound **2.88a** to stir, at 80 °C, in an EtOH/ H_2O 3:1 system and in the presence of 0.5 equiv. of AcOH, for 4.33 hours

Finally, two experiments were performed simultaneously, and under the same experimental conditions, but using amidine **2.87b** (**Scheme 44**) and polycyclic derivative **2.88a** (**Scheme 45**). In both reaction, 0.5 equivalents of acetic acid, in an ethanolic solution, were used, and the mixtures were heated at 80 °C for 7 h. For amidine **2.87b**, almost no reaction was observed. However, it appears to have a mixture with pyridopyrimidinone **2.88c** and possibly with one of the previously detected, but still unidentified, products that possess the δ10.77 ppm, δ 8.95 ppm and at δ 8.31 ppm signals (**unknown nº1 and nº2** - **Figure 72**).



Scheme 44: Reaction of **2.87b** in ethanol and at 80 °C, in the presence of 0.5 equivalents of acetic acid, for 7 h

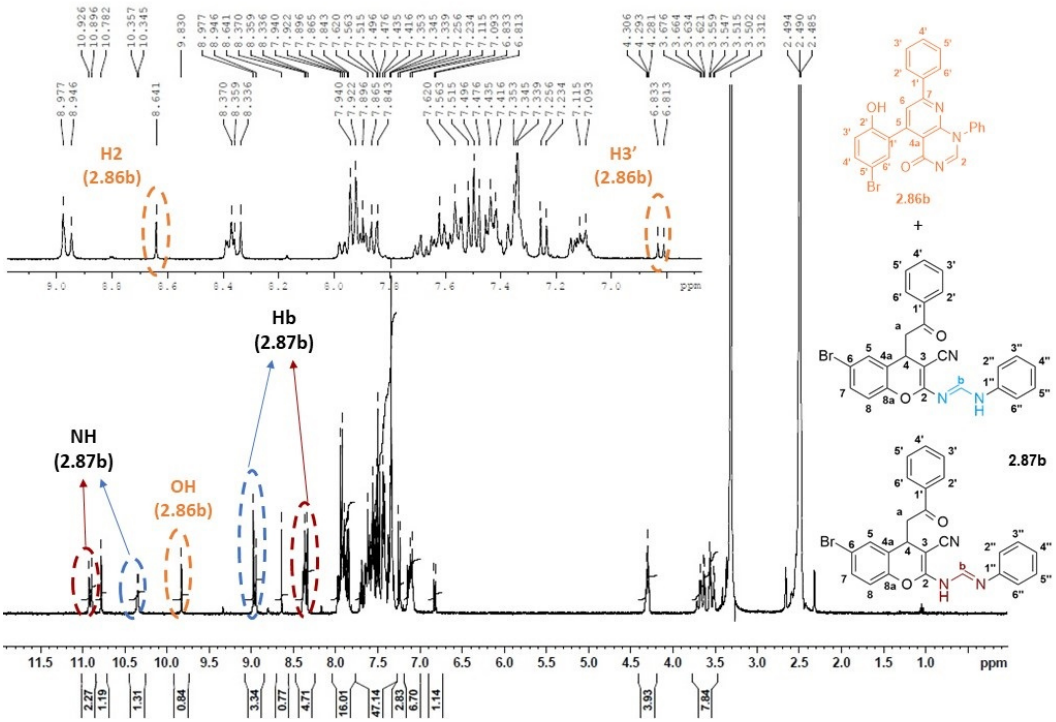
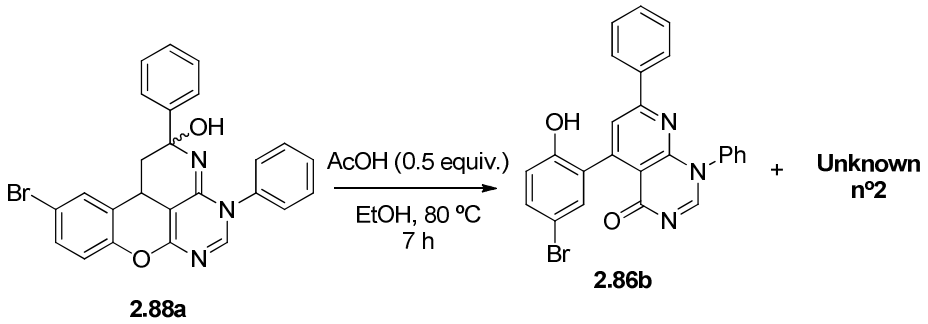


Figure 72: ^{1}H NMR (400 MHz, DMSO-d_6, δ ppm) spectrum of a mixture of compounds **2.86b** (range circles) and **2.87b** (red and blue circles), obtained after heating a solution of compound **2.87b** in EtOH and in the presence of 0.5 equiv. of AcOH, at 80 °C for 7 h. Several signals are highlighted

For the experiment where polycyclic derivative **2.88a** was used, compound **2.86b** was detected as the major product, with the set of three signals, at δ 10.77 ppm, δ 8.95 ppm and at δ 8.31ppm, being detected once more, in a (1:4) ratio with **2.86b** as the major product (**Figure 73**).



Scheme 45: Reaction of **2.88a** in ethanol and at 80 °C, in the presence of 0.5 equivalents of acetic acid, for 7 h

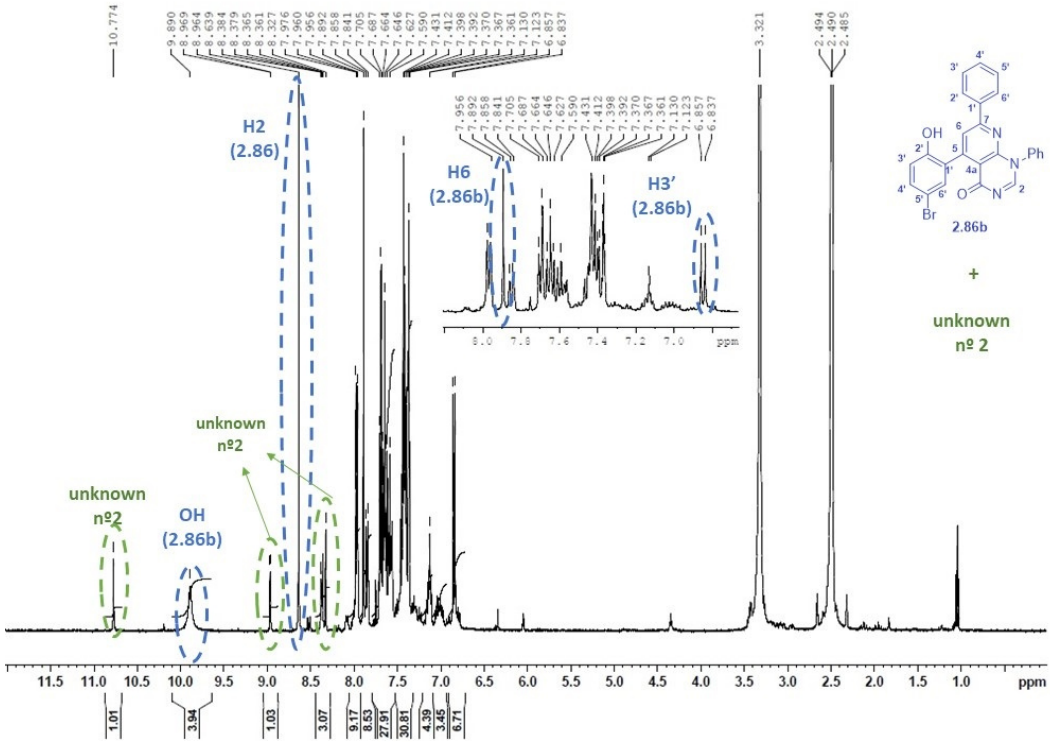


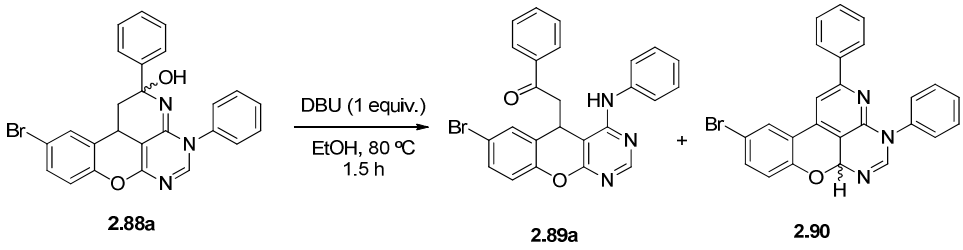
Figure 73: ^{1}H NMR (400 MHz, DMSO-d$_6$, δ ppm) spectrum of a mixture of compounds **2.86b** (blue circles) and an unidentified component (green circles, **unknown nº 2**), obtained after heating a solution of compound **2.88a** in EtOH and in the presence of 0.5 equiv. of AcOH, at 80 °C for 7 h. Several signals are highlighted

The described experiments demonstrated that:

1) Polycyclic derivative **2.88** is indeed a precursor of pyridopyrimidinone **2.86.**
2) The ring-opening and subsequent oxidation of **2.88** to generate **2.86** occurs easilunder heating in ethanol.
3) Depending on the experimental conditions, the formation of pyridopyrimidinone **2.86** can be accompanied by the formation of **2.55** and/or **2.56.**
4) The evolution of polycyclic derivative **2.88** to pyridopyrimidinone **2.86** involves at least two intermediates: (i) one of them (the first identified in the mixture and labelled as **unknown nº1**) showing two doublets at δ6.44 (*J*= 8.4 Hz) and δ6.98 ppm (*J*= 8.4 Hz); (ii) the second intermediate (labelled as **unknown nº2**) shows at δ10.77 ppm and δ8.95 ppm that do not correspond to a C-H bond (according to the C-H correlation spectra), but probably to a N-H or an O-H bond. The singlet at δ 8.31 ppm, however, did correspond to a C-H bond, associated to a carbon atom at δ 102.17 ppm.
5) Although we could not perform a full characterization of the unidentified precursors observed by ^{1}H NMR, it was possible to confirm that are participating in the reaction

pathway, that leads to the formation ofpyrimidinones **2.86**. This was confirmed by the fact that, whenever these signals appear, it was possible to generate compound **2.86** as a pure product upon heating the crude mixture in either EtOH or DMSO-d_6.

Another experiment was designed to understand if polycyclic derivative **2.88a** could also be the precursor of **2.89a** when the reaction was performed in ethanol at 80 °C and in the presence of 1 equivalent of DBU (**Scheme 46**). Compound **2.88a** was used in this study, and the solid isolated after heating the mixture for 1.5 h was a mixture of **2.89a** and **2.90a** in a 1/11 ratio (**Figure 74**).



Scheme 46: Reaction of **2.88a** in ethanol and at 80 °C, in the presence of 1 equivalent of DBU, for 1.5 h

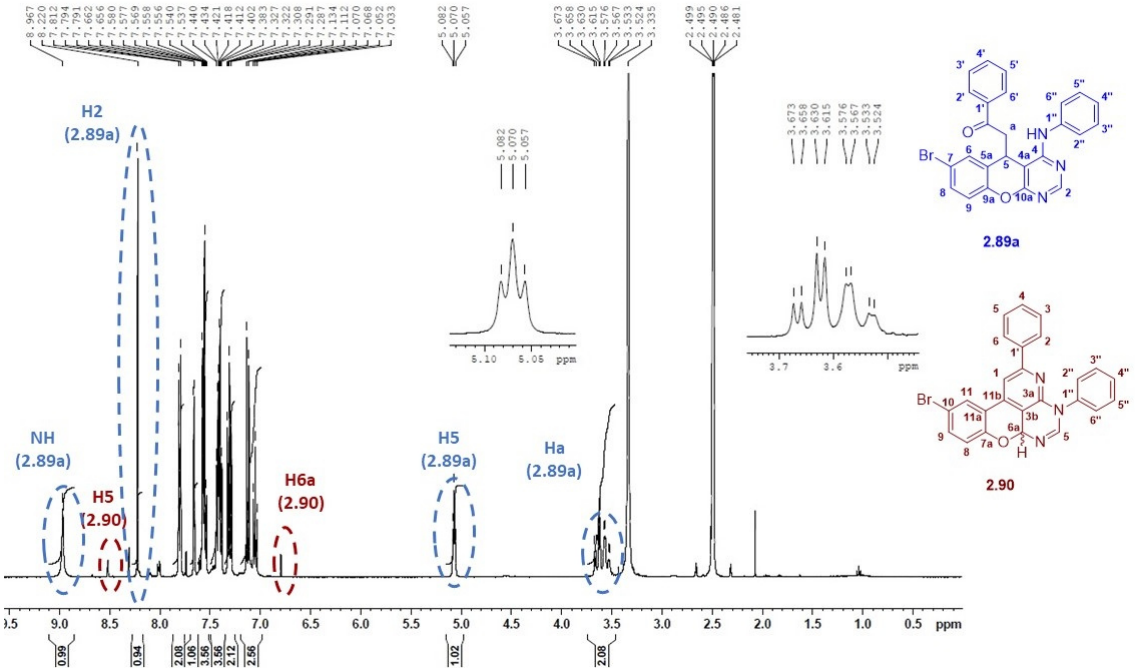
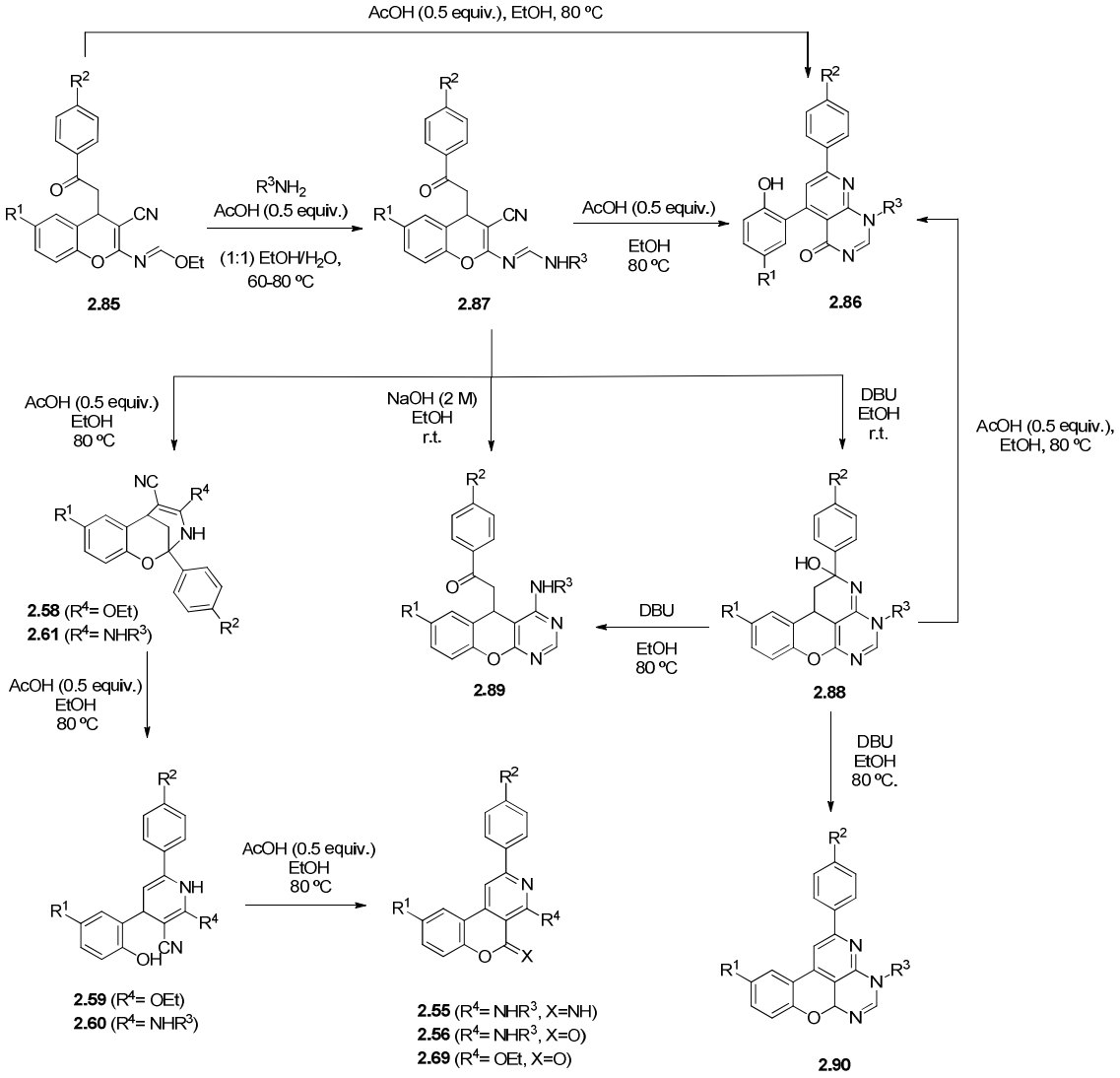


Figure 74: ^{1}H NMR (400 MHz, DMSO-d_6, δ ppm) spectrum collected from the crude product obtained after the addition of 1 equiv. of DBU to a suspension of **2.88a** in EtOH, at 80 °C, that was left stirring for 1.5 hours (400 MHz, DMSO-d_6, δ ppm)

The experiments performed in this section, involving chromenylimidate **2.85** and/or from chromenylamidine **2.87** show that several competitive reactions may operate, leading to different

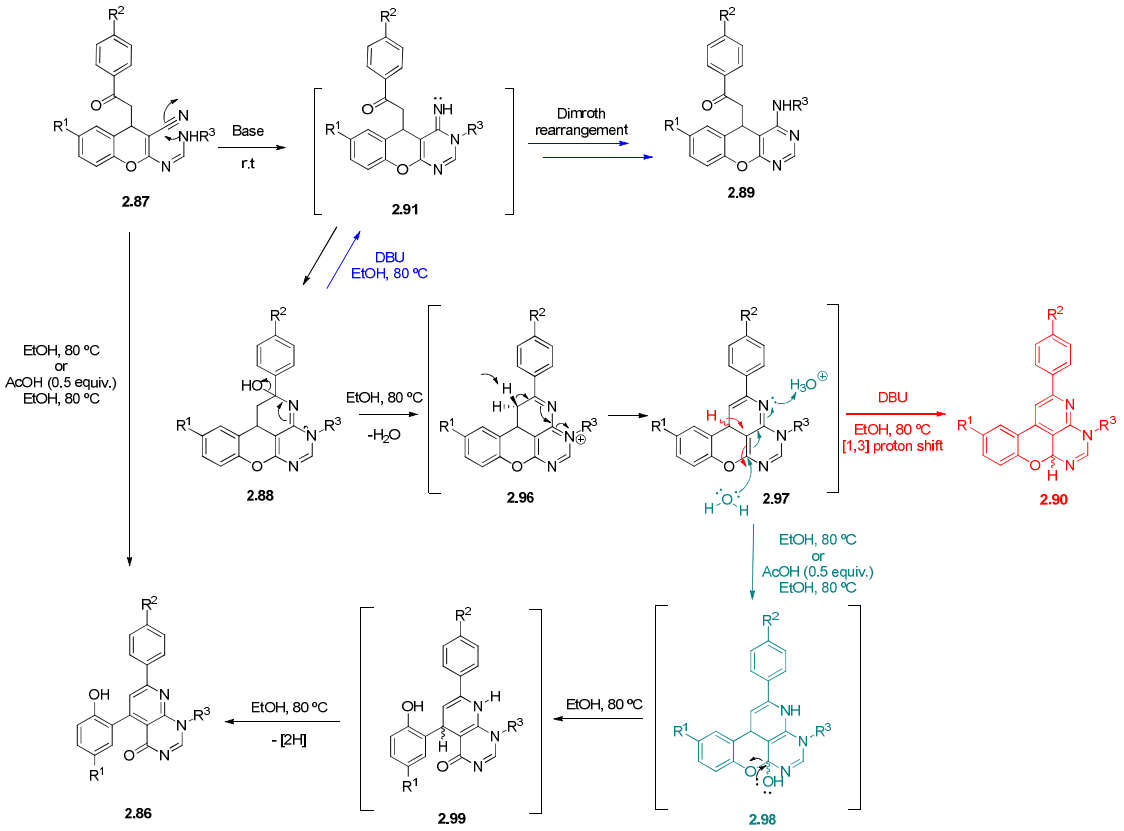
major products. **Scheme 47** summarizes the most relevant conclusions. It is evident that pyridopyrimidinones **2.86** could be isolated from imidate **2.85**, amidine **2.87** or polycyclic compounds **2.88**. The possibility of amidine **2.87** or **2.88** evolving to **2.86** through a pathway where compound **2.88** was initially formed, led us to perform a selection of experiments, where the evolution of **2.88** was studied under different experimental conditions



Scheme 47: Summary of the reaction conditions and products for the isolation of compounds **2.86**-**2.90.** The formation of compounds **2.55**, **2.56** and **2.69** was also observed

Based on these results, a mechanistic approach was proposed (Scheme 48). This proposal considers that the formation of **2.86**, isolated from the evolution of amidine in ethanol and acetic acid (0.5 equivalents), at 80 °C, could effectively follow a pathway initiated by the formation of **2.88**. The use of base at room temperature would induce intramolecular cyclization to **2.91** that

can either evolve to **2.89** by Dimroth rearrangement in the presence of NaOH, or cyclize intramolecularly to afford **2.88** using DBU, in ethanol and at room temperature. Compound **2.88** was isolated and fully characterized and could almost be quantitatively transformed into **2.86** by heating at 80 °C, in ethanol and in the presence of DBU, or in DMSO-d_6 solution.



Scheme 48: Proposed mechanism for the evolution of compound **2.87** to generate **2.86** and **2.88-2.90**

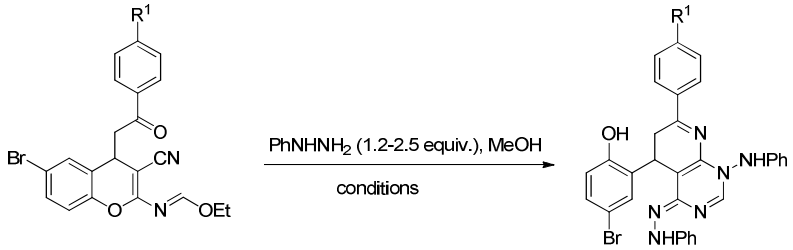
The reaction sequence must involve elimination of H_2O with formation of **2.97** (possibly **unknown nº 1** in the NMR spectra presented in **Figures 65**, **69** and **70**; **Scheme 48**). Nucleophilic attack of a water molecule on the common carbon between the chromene and the pyrimidine ring leads to **2.98**, that by ring opening affords **2.99**. Either **2.98** or **2.99** could be considered as **unknown nº2**, identified in the NMR spectra presented in **Figures 67**, **70**, **71** and **73**. Aromatization of the pyridine ring could be the driving force for the oxidation process leading to **2.86**. The formation of **2.90** from **2.97** can be envisaged by thermal or base-induced a [1,3]-proton shift.

Reaction of Ethyl *N*-(3-cyano-4-(2-oxo-2-arylethyl)-4*H*-chromen-2-yl)formimidates with phenylhydrazines

The reactivity of imidates **2.85** with hydrazines was explored under various reaction conditions. As previously described in **Scheme 30**, the reaction of **2.85** with amines involved a nucleophilic attack to the imidate moiety, which ultimately resulted in the chromene ring-opening via a water-promoted mechanism. This was also expected for the reaction with hydrazines. Phenylhydrazine was used for this study.

The treatment of compounds **2.85d-f** with 2 equivalents of phenylhydrazine in MeOH at room temperature gave compounds **2.100** in 53% yield (entry 1 - **Table 75**). When the reaction was performed at 60 °C and using only 1.2 equivalents of phenylhydrazine, the reaction yield was lower (30%). For compound **2.85f** (R^1= Br), mainly no reaction was obtained as the starting material was collected with 50% yield after 14 h stirring at room temperature.

Table 75: Reaction conditions and results obtained for the reaction of compounds **2.85d-h** with phenylhydrazine



2.85d-f **2.100**

Entry	2.85	R^1	$PhNHNH_2$(equiv.)	T (°C)	t (h)	product	η(%)
1	**2.85d**	H	2	r.t	21	**2.100a**	53
2	**2.85d**	H	1.2	60	3	**2.100a**	30
3	**2.85e**	Me	1.7	r.t	13.5	**2.100b**	32
4	**2.85f**	Br	2.5	r.t.	14	**2.85f**	50

The chemical structure of compounds **2.100** was determined by NMR spectroscopy. As an example, the ^{1}H and ^{13}C NMR spectrum of compound **2.100a**, is presented in **Figures 75** and **76**. The most relevant signals in the ^{1}H NMR spectra are four singlets, one at δ 6.85 ppm corresponding to the hydroxyl group, two at δ 11.19 ppm and δ 9.51 ppm corresponding to the hydrazine N-H moieties and at δ 8.14 ppm the relative to the CH group of the pyrimidine ring. In the ^{13}C NMR spectra three main signals are noteworthy: at δ 152.65 (pyrimidine CH), correlating

with two signals at δ156.13 (C4) and δ153.38 (C8a) ppm, and the δ 32.54 (C6) and δ 30.63 (C5) ppm signals.

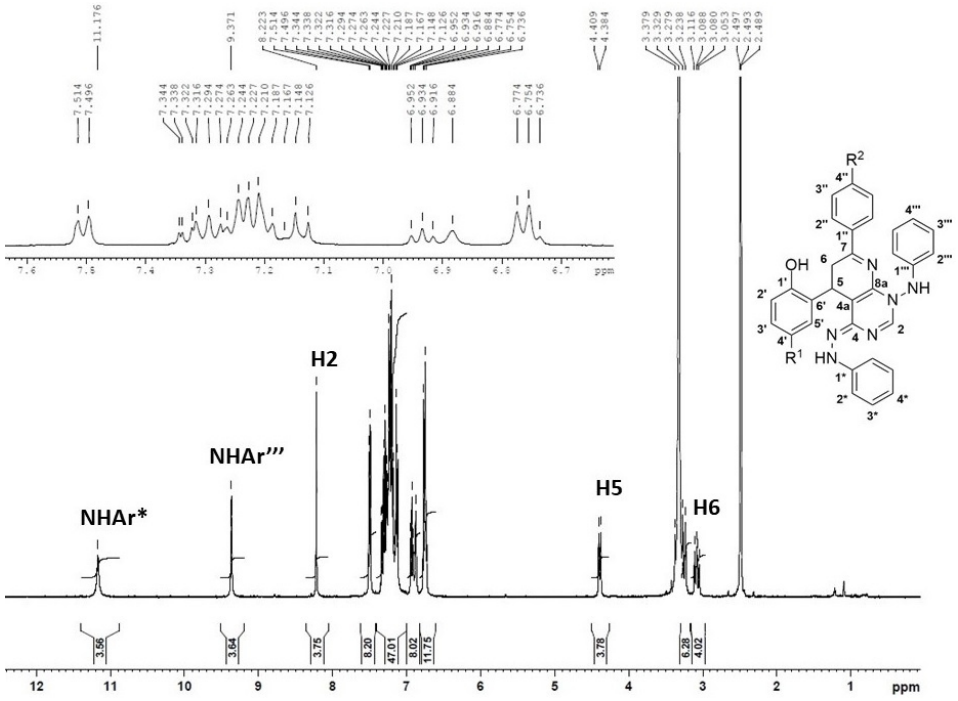


Figure 75: ^{1}H NMR (400 MHz, DMSO-d_6, δ ppm) spectrum of compound **2.100a**, in which several signals are highlighted

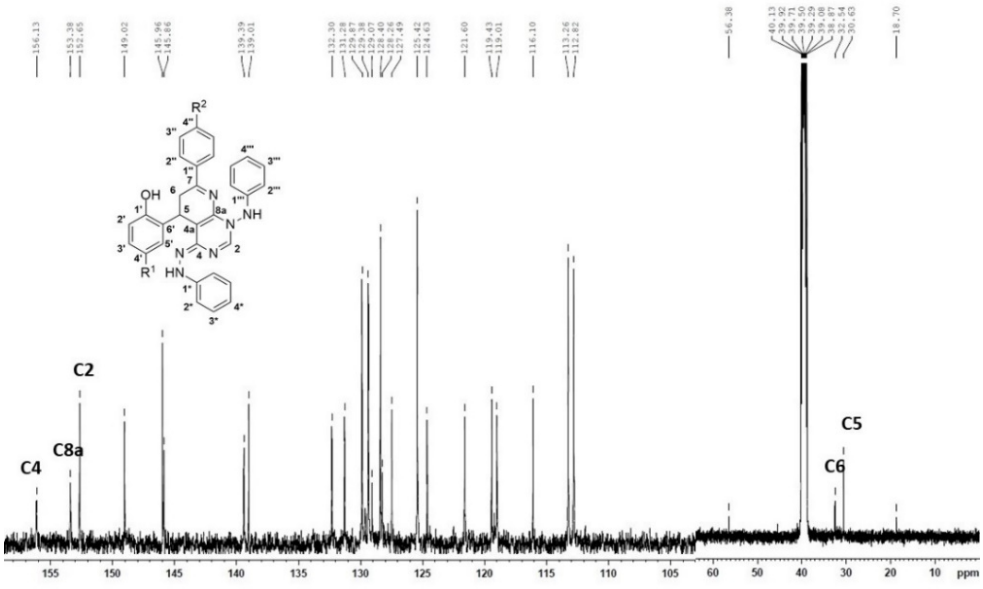
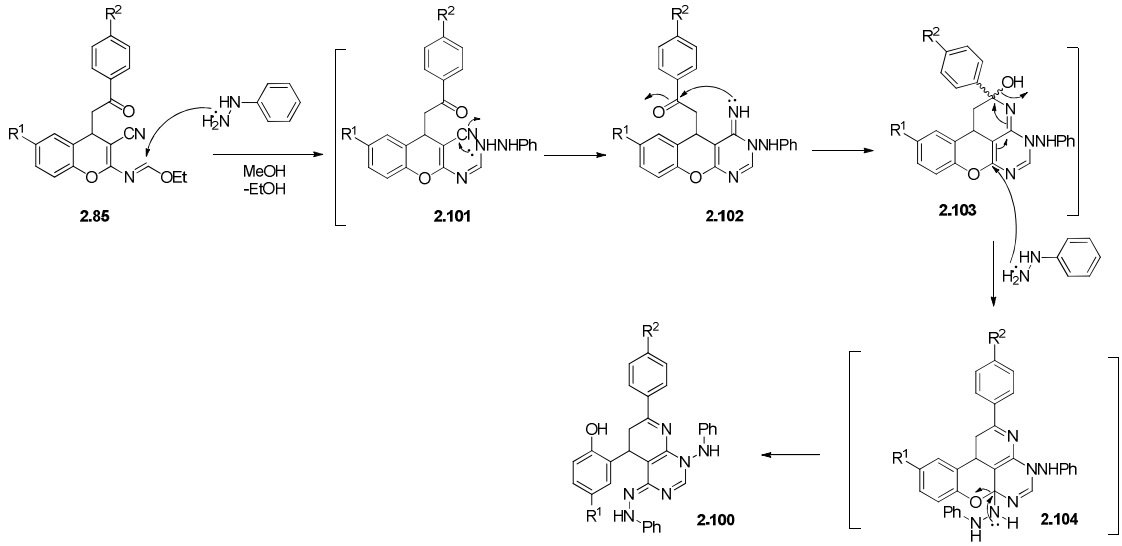


Figure 76: ^{13}C NMR (100 MHz, DMSO-d_6, δ ppm) spectrum of compound **2.100d**, in which several signals are highlighted

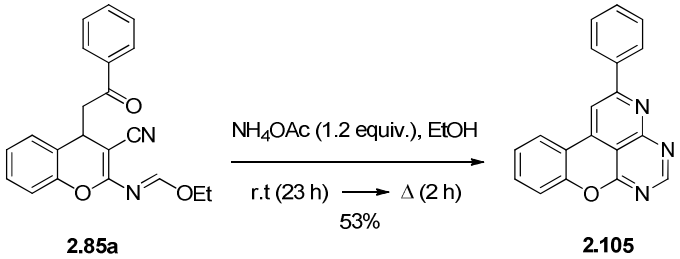
Compounds **2.100** can be formed by a similar mechanism to that described for the synthesis of pyridopyrimidines **2.86** (see **Scheme 48**) with the difference that the nucleophile that promotes the ring-opening process would now be phenylhydrazine, a highly nucleophilic amine (**Scheme 49**). The fact that the oxidation process, that leads to the formation of an aromatic ring in the pyrido[2,3-*d*]pyrimidine moiety of **2.85**, was not observed, is also noteworthy. Instead, 1,4,5,6-tetrahydropyrido[2,3-d]pyrimidin-5-yl derivatives **2.100** have been characterized.



Scheme 49: Proposed mechanism for the formation of compounds **2.100**

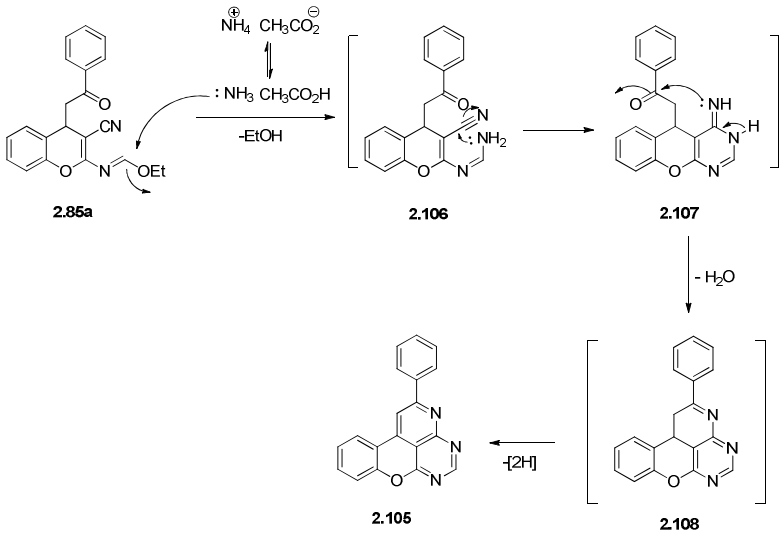
Reaction of ethyl *N*-(3-cyano-4-(2-oxo-2-arylethyl)-4*H*-chromen-2-yl)formimidates with ammonium acetate

The reaction of **2.85** with ammonium acetate was also explored. This reaction was performed in ethanol, and compound **2.105** was isolated as a pure product in 53% yield (**Scheme 50**).



Scheme 50: Synthesis of compound **2.85a** into **2.105** by treatment with ammonium acetate

The formation of this product can be explained through a similar mechanism to that described previously, but in this case the final product is fully aromatic (**Scheme 51**).



Scheme 51: Proposed mechanism for the formation of compounds **2.105** from the reaction of **2.85a** with ammonium acetate

In the ^{1}H NMR spectrum obtained for compound **2.105** stands out two singlets at δ 9.04 and δ 8.81 ppm belonging to the CH groups (**Figure 77**). In the ^{13}C NMR spectrum, a set of signals at high chemical shift values corroborate the presence of the fully aromatic system: δ 164.76, δ164.20, δ159.93, δ159.22 and δ151.67 ppm. The absence of the characteristic signals for a nitrile group also corroborates the formation of the tetracyclic ring system.

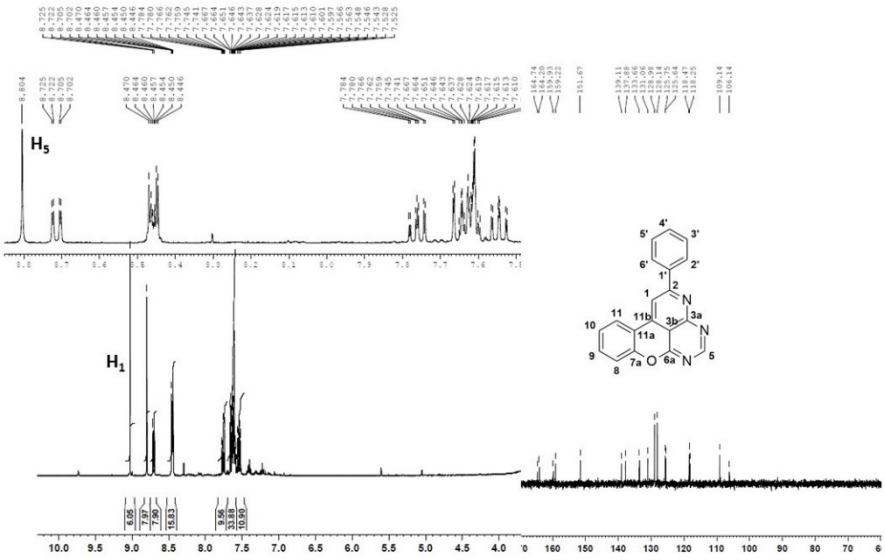


Figure 77: ^{1}H and ^{13}C NMR (400 and 100 MHz, DMSO-d_6, δ ppm) spectra of compound **2.105** with H1 and H5 signals highlighted

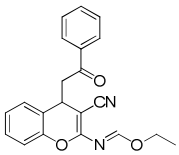
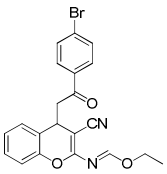
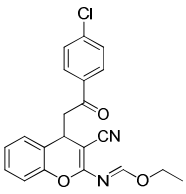
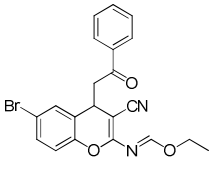
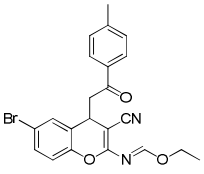
Physical, analytical and spectroscopical characterization

The structure of compounds **2.85-2.90, 2.100** and **2.105** was assigned by physical, analytical, and spectroscopic data (melting point, IR, ^{1}H and ^{13}C NMR). This information is presented in the following section.

Physical and analytical characterization

The molecular formula and molecular weight were determined based on the information obtained from the elemental analysis and are presented, along with the respective melting point values (°C), in the following **Tables 76-82**.

Table 76: Physical and analytical data obtained for imidates **2.85a-h**

Compound	structure	Mp (°C)	molecular formula/ mass (M)	calculated /obtained values (%)			
				C	H	N	O
2.85a		119-120	$C_{21}H_{18}N_2O_3$/ 346.38	72.82 –	5.24 –	8.09 –	13.86 –
2.85b		155-156	$C_{21}H_{17}BrN_2O_3$/ 425.28	59.31 –	4.03 –	6.59 –	11.29 –
2.85c		155-156	$C_{15}H_{11}ClO_2$/ 380.82	66.23 66.18	4.50 4.48	7.36 7.16	12.60 –
2.85d		164-166	$C_{21}H_{17}BrN_2O_3$/ 425.28	59.31 –	4.03 –	6.59 –	11.29 –
2.85e		160-162	$C_{22}H_{16}BrN_2O_3$/ 439.30	60.15 –	4.36 –	6.38 –	10.93 –

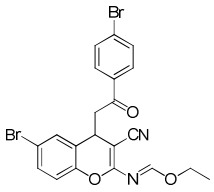
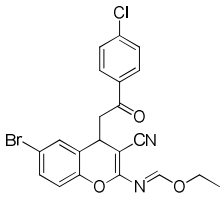
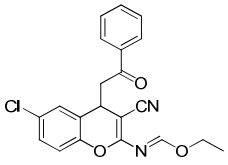
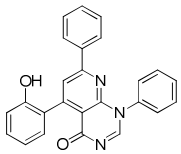
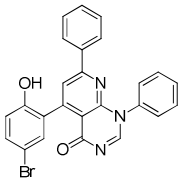
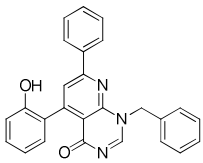
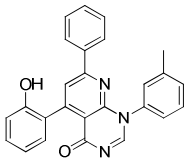
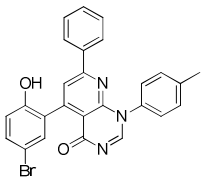
2.85f		192-194	$C_{21}H_{16}Br_2N_2O_3$/ 504.14	50.03 –	3.20 –	5.56 –	9.52 –
2.85g		178-180	$C_{21}H_{16}BrClN_2O_3$/ 459.72	54.86 –	3.51 –	6.09 –	10.44 –
2.85h		152-153	$C_{15}H_{11}ClO_2.H_2O$/ 398.45	63.24 63.51	4.76 4.37	7.02 6.49	12.60 –

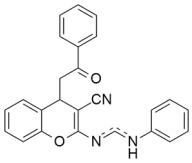
Table 77: Physical and analytical data for pyridopyrimidinones **2.86**

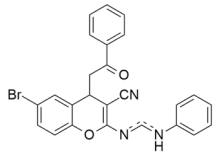
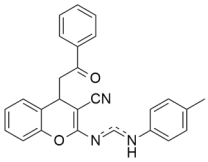
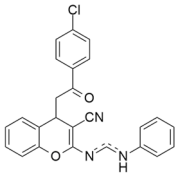
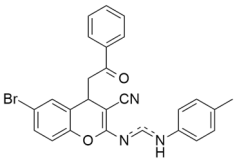
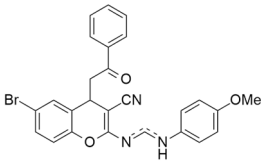
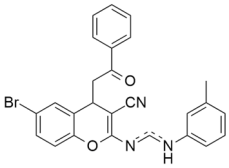
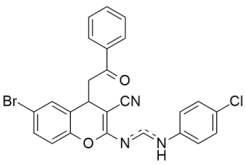
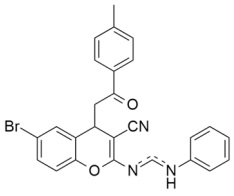
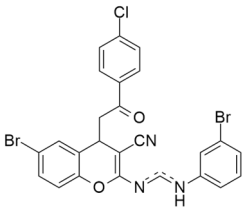
Compound	structure	Mp (°C)	molecular formula/ mass (M)	calculated /obtained values (%)			
				C	H	N	O
2.86a		228 (dec.)	$C_{25}H_{17}N_3O_2$. $0.5H_2O$/391.42	74.92 74.98	4.49 4.43	10.49 10.20	9.99 –
2.86b		275 (dec.)	$C_{25}H_{16}BrN_3O_2$ /470.32	63.84 –	3.43 –	8.93 –	6.80 –
2.86c		216 (dec.)	$C_{26}H_{19}N_3O_2$ /405.46	77.02 –	4.72 –	10.36 –	7.89 –
2.86d		>300	$C_{26}H_{19}N_3O_2$ /405.45	77.02 –	4.72 –	10.36 –	7.89 –
2.86e		232 (dec.)	$C_{26}H_{18}BrN_3O_2$. $1.5H_2O$/511.34	61.08 61.38	4.11 4.07	8.22 7.95	10.96 –

2.86f	276-278	$C_{26}H_{17}Br_2N_3O_3$ /579.24	53.91 –	2.96 –	7.25 –	8.29 –
2.86g[1]	263-266	$C_{26}H_{17}BrClN_3O_2$ /518.79	60.19 –	3.30 –	8.10 –	6.17 –
2.86h	215 (dec.)	$C_{26}H_{17}BrClN_3O_3$ /534.79	58.39 –	3.20 –	7.86 –	8.98 –
2.86k	248 (dec.)	$C_{26}H_{18}BrN_3O_3$. $0.4H_2O$/507.54	61.47 61.87	3.70 3.78	8.27 7.85	10.72 –
2.86l	215 (dec.)	$C_{25}H_{15}BrClN_3O_2$. $0.9H_2O$/520.96	57.59 57.72	3.22 3.41	8.06 7.91	8.91 –
2.86m	220 (dec.)	$C_{26}H_{18}ClN_3O_3$ /455.89	68.50 –	3.89 –	9.22 –	10.53 –

[1]Sample degraded while in storage and was not submitted for elemental analysis

Table 78: Physical and analytical data for amidines **2.87**

Comp.	structure	Mp (°C)	molecular formula/ mass (M)	calculated /obtained values (%)			
				C	H	N	O
2.87a		145-146	$C_{25}H_{19}N_3O_2$/ 393.44	76.32 76.21	4.87 4.80	10.68 10.62	8.13 –

2.87b		187-189	$C_{25}H_{18}BrN_3O_2$ /472.33	63.57 –	3.84 –	8.90 –	6.77 –
2.87c		106-108	$C_{26}H_{21}N_3O_2.0.4H_2O$ /414.66	75.24 75.32	5.26 5.19	10.13 10.01	9.26 –
2.87f		134-136	$C_{25}H_{18}ClN_3O_2$ /427.88	70.18 –	4.24 –	9.82 –	7.48 –
2.87g		189-191	$C_{26}H_{20}BrN_3O_2$ /486.36	64.21 –	4.14 –	8.64 –	6.58 –
2.87h		157-159	$C_{26}H_{20}BrN_3O_3$. $0.5H_2O$/511.36	61.08 61.38	4.11 3.88	8.21 7.94	10.95 –
2.87i		189-191	$C_{26}H_{20}BrN_3O_2$/ 489.96	63.68 63.53	4.12 3.85	8.57 8.92	6.86 –
2.87l		193-195	$C_{25}H_{17}BrClN_3O_2$/ 506.78	59.25 –	3.38 –	8.29 –	6.31 –
2.87n		165-166	$C_{26}H_{20}BrN_3O_2$. $0.4H_2O$/493.56	63.21 63.46	4.25 3.88	8.50 8.11	8.10 –
2.87y		189-191	$C_{25}H_{16}Br_2ClN_3O_2$/ 585.67	51.27 51.74	2.75 2.54	7.17 6.68	5.46 –

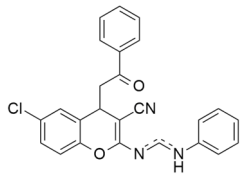
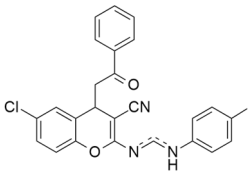
2.87z		174-176	$C_{25}H_{18}ClN_3O_2$/ 427.88	70.18 70.41	4.24 3.97	9.82 9.29	7.48 –
2.87a'		181-182	$C_{26}H_{20}ClN_3O_2$/ 441.91	70.67 –	4.56 –	9.51 –	7.24 –

Table 79: Physical and analytical data for polycyclic compounds **2.88a-c**

Compound	Structure	Mp (°C)	molecular formula/ mass (M)	calculated /obtained values (%)			
				C	H	N	O
2.88a		195-197	$C_{25}H_{18}BrN_3O_2$ /472.33	63.57 –	3.84 –	8.90 –	6.77 –
2.88b		195-196	$C_{26}H_{21}N_3O_2$/ 407.46	76.64 76.91	5.19 5.21	10.31 10.32	7.85 –
2.88c		198-200	$C_{26}H_{20}BrN_3O_2$ /486.36	64.21 –	4.14 –	8.64 –	6.58 –

Table 80: Physical and analytical data for chromenopyrimidines **2.89**

Compound	Structure	Mp (°C)	molecular formula/ mass (M)	calculated /obtained values (%)			
				C	H	N	O
2.89a		193-195	$C_{25}H_{18}BrN_3O_2$. $0.1H_2O$/474.14	63.33 63.37	3.87 3.56	8.86 8.46	7.09 –
2.89b		-	$C_{25}H_{19}N_3O_2$/ 393.44	76.32 -	4.87 -	10.68 -	8.13 -

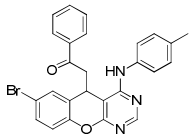
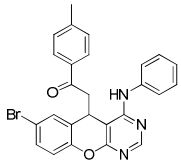
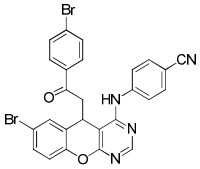
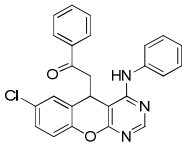
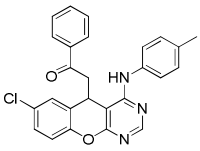
2.89c		229-231	$C_{26}H_{20}BrN_3O_2$/ 486.36	64.21 –	4.14 –	8.64 –	6.58 –
2.89d		170-172	$C_{26}H_{20}BrN_3O_2$/ 486.36	64.21 –	4.14 –	8.64 –	6.58 –
2.89e		264-265	$C_{26}H_{16}Br_2N_4O_2$/ 576.24	54.19 –	2.80 –	9.72 –	5.55 –
2.89f		181-183	$C_{25}H_{18}ClN_3O_2$/ 427.88	70.18 70.18	4.24 3.96	9.82 9.55	7.48 –
2.89g		212-214	$C_{26}H_{20}ClN_3O_2$/ 441.91	70.67 71.06	4.56 4.25	9.51 9.43	7.24 –

Table 81: Physical and analytical data for compounds **2.90** and **2.105**

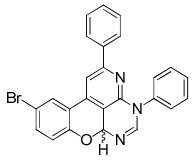
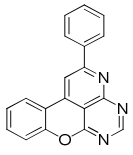
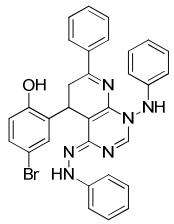
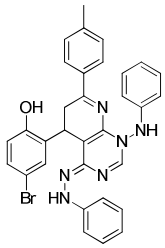
Compound	**Structure**	**Mp (°C)**	**molecular formula/ mass (M)**	**calculated /obtained values (%)**			
				C	H	N	O
2.90		290 (dec.)	$C_{25}H_{16}BrN_3O$/ 454.32	66.09 –	3.55 –	9.25 –	3.52 –
2.105		>300	$C_{19}H_{11}N_3O$/ 297.31	76.76 –	3.73 –	14.13 –	5.38 –

Table 82: Physical and analytical data obtained for compounds **2.100a,b**

Compound	Structure	Mp (°C)	molecular formula/ mass (M)	calculated /obtained values (%)			
				C	H	N	O
2.100a		215 (dec)	$C_{31}H_{25}BrN_6O$/ 577.47	64.48 –	4.36 –	14.55 –	2.77 –
2.100b		182-184	$C_{32}H_{27}BrN_6O$/ 591.50	64.98 –	4.60 –	14.21 –	2.70 –

IR spectroscopy

In **Tables 83-89**, all the IR spectroscopic data regarding compounds **2.85-2.90, 2.100a,b** and **2.105** is presented. The main characteristic of the IR spectra of these compounds is the absence of the N-H stretching vibration peaks that were present in the precursor **2.39** (**Table 83**).

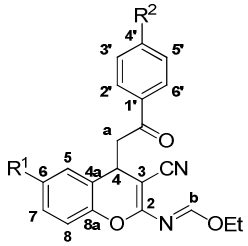


Table 83: IR spectroscopic data (Nujol, cm^{-1}) obtained for imidates **2.85a-h**

Compound	R^1	R^2	4000-3000	CN	1700-1500
2.85a	H	H	-	2203s	1682s (C=O), 1640s, 1605s, 1582sh
2.85b	H	Br	-	2202s	1683s (C=O), 1638s, 1603s, 1584sh
2.85c	H	Cl	-	2201s	1683s (C=O), 1638s, 1602s, 1585sh
2.85d	Br	H	-	2210s	1685s (C=O), 1652m, 1613s, 1577sh
2.85e	Br	Me	-	2202s	1674s (C=O), 1639m, 1606s, 1572w
2.85f	Br	Br	-	2203s	1682s (C=O), 1645m, 1609s, 1587sh
2.85g	Br	Cl	-	2201s	1679s (C=O), 1638m, 1604s, 1569sh
2.85h	Cl	H	-	2206m	1677s (C=O), 1647w, 1613s, 1572sh

The IR spectra of compounds **2.86** present a broad, or no detectable, band at around 3300 cm^{-1}, corresponding to the hydroxyl O-H stretching vibration band, and a variable and medium intensity C=O stretching vibration band in the 1700-1500 region (**Table 84**).

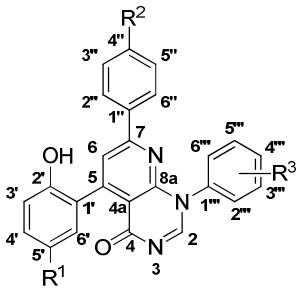
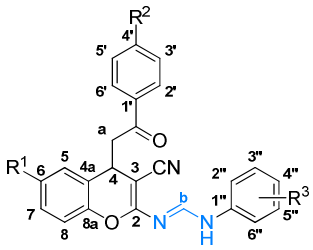


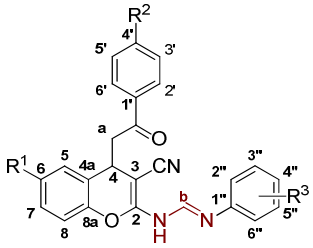
Table 84: IR spectroscopic data (Nujol, cm^{-1}) obtained for compounds **2.86**

Compound	R^1	R^2	R^3	4000-3000	1700-1500
2.86a	H	H	C_6H_5	3056w	1672m (C=O),1635w, 1611s, 1595sh, 1536m
2.86b	H	H	$CH_2C_6H_5$	3056w	1667m (C=O), 1636m, 1612s, 1570sh, 1534m
2.86c	Br	H	C_6H_5	3305w	1658m (C=O), 1637m, 1612s, 1590sh, 1569m, 1533m
2.86d	H	H	3-MeC_6H_4	3303w	1670m (C=O), 1645sh, 1608s, 1587sh, 1571sh, 1536m
2.86e	Br	H	4-MeC_6H_4	3279b	1641s (C=O), 1610m, 1574sh, 1553w, 1530m, 1511w
2.86f	Br	H	4-$OMeC_6H_4$	3540w	1673m (C=O), 1612m, 1601m, 1582sh, 1573m, 1537m, 1508w
2.86g	Br	H	4-ClC_6H_4	3374b	1655m (C=O), 1638m, 1609m, 1598sh, 1534m
2.86h	Br	Br	4-$OMeC_6H_4$	3267b	1640s (C=O), 1612m, 1578m, 1570sh, 1529m, 1511w
2.86i	Br	Cl	4-MeC_6H_4	3272b	1649s (C=O), 1608m, 1594s, 1569sh, 1530w, 1512w
2.86j	Br	Cl	4-$OMeC_6H_4$	3361b	1651sh (C=O), 1645m, 1609m, 1580sh, 1529w, 1511w
2.86k	Cl	H	4-$OMeC_6H_4$	3280b	1641s (C=O), 1611m, 1595sh, 1575w, 1532m

The IR spectra of compounds **2.87** revealed three-four bands for the stretching vibration of the N-H group, between 3300-3100 cm^{-1}. The CN stretching vibration and the C=O stretching vibration bands are identified at around 2200-2190 cm^{-1} and 1680-1660 cm^{-1}, respectively (**Table 85**).

Table 85: IR spectroscopic data (Nujol, cm^{-1}) obtained for amidines **2.87**





Compound	R^1	R^2	R^3	4000-3000	CN	1700-1500
2.87a	H	H	H	3326m, 3206b, 3144w	2195s	1682s (C=O), 1650m, 1648m, 1621s, 1614s, 1590sh, 1588s, 1556m
2.87b	Br	H	H	3387sh, 3347m, 3215w, 3141w, 3087w	2197s	1675s (C=O), 1648sh, 1632s, 1594s, 1572sh, 1533s
2.87c	H	H	4-Me	3383sh, 3307m, 3208w, 3133w	2197s	1681s (C=O), 1651s, 1618sh, 1605s, 1587s, 1582sh, 1525m
2.87f	H	Cl	H	3288w, 3249w, 3204m, 3126w, 3039w	2207s	1681s (C=O), 1647s, 1616sh, 1598s, 1587s, 1574sh
2.87g	Br	H	4-Me	3298w, 3274m, 3233w, 3057w, 3027w	2201s	1676s (C=O), 1649s, 1600s, 1585s, 1572s, 1519m
2.87h	Br	H	4-OMe	3294m, 3203w, 3135w, 3090w	2190s	1682s (C=O), 1619sh, 1603s, 1593sh, 1574sh, 1554s, 1508s
2.87i	Br	H	3-Me	3301w, 3275m, 3236w	2202s	1676s (C=O), 1650s, 1601s, 1585s, 1572s, 1519m
2.87l	Br	H	4-Cl	3321m, 3297m, 3205w, 3126w, 3068w	2197s	1676s (C=O), 1644s, 1628s, 1616s, 1603m, 1587s, 1544s
2.87n	Br	Me	H	3325m, 3210w, 3141w, 3100w	2197s	1673s (C=O), 1642m, 1621s, 1606s, 1590s, 1552s
2.87y	Br	Cl	3-Br	3283m, 3188m, 3121m	2208s	1681s (C=O),1642m, 1621sh, 1608s, 1584s, 1572sh, 1543s
2.87z	Cl	H	H	3345m, 3215w, 3141w, 3058w	2195s	1675s (C=O), 1644s, 1631sh, 1621s, 1594s, 1574sh, 1522s
2.87a'	Cl	H	4-Me	3340, 3298m, 3272m, 3170w	2200s	1678s (C=O), 1645s, 1614sh, 1601s, 1585sh, 1572s, 1551sh, 1522s

The most relevant bands in the IR spectra of compounds **2.88** are in the 4000-3000 cm^{-1} region, corresponding to the O-H stretching vibration, and in the 1700-1490 cm^{-1} region, a set of bands relative to the aromatic C=C stretching vibration (**Table 86**).

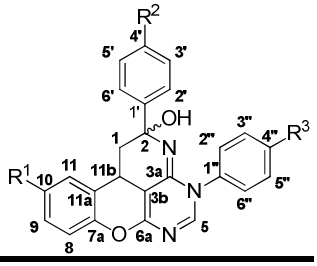


Table 86: IR spectroscopic data (Nujol, cm^{-1}) obtained for compounds **2.88a-c**

Compound	R^1	R^2	R^3	4000-3000	1700-1490
2.88a	Br	H	H	3185b, 3062w, 3026w	1646s, 1606sh, 1597m, 1593m, 1583sh, 1550s, 1491m
2.88b	H	H	Me	3307b, 3068w, 3033w	1644s, 1595m, 1577m, 1559sh, 1552m, 1510m
2.88c	Br	H	Me	3168b, 3055w, 3024w	1646s, 1595m, 1580sh, 1552s, 1510m

In the IR spectra of compounds **2.89** stands out a sharp, medium intensity band in the 3400-3300 cm^{-1} region, followed by a weak band at around 3060 cm^{-1}, which corresponds to the N-H stretching vibration (**Table 87**). The C=O stretching vibration appears between 1680-1650 cm^{-1}. The IR spectra of compounds **2.90** and **2.105** possess several bands in the 1650-1500 cm^{-1} region, assigned to the aromatic rings (C=C stretching vibration) (**Table 88**). Compounds **2.100** present several characteristic bands in the IR spectra, with 4-5 bands in the 3500-3000 cm^{-1} region, which are attributed to the N-H stretching vibration of the hydrazine moiety, as well as to the O-H stretching vibration of the hydroxyl group; also, a set of very strong bands in the region for the alkene and aromatic C=C stretching vibration appear, between 1650-1500 cm^{-1} (**Table 89**).

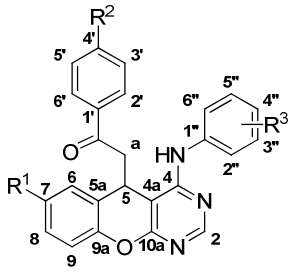
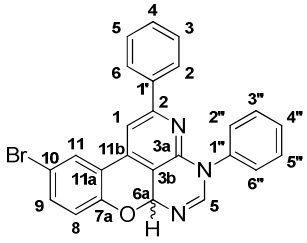


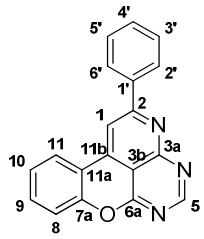
Table 87: IR spectroscopic data (Nujol, cm^{-1}) obtained for chromenopyridines **2.89**

Compound	R^1	R^2	R^3	4000-3000	CN	1700-1500
2.89a	Br	H	H	3399m, 3065w	-	1673m (C=O), 1616sh, 1603m, 1593m, 1577sh, 1560s, 1512m
2.89b[1]	H	H	H	-	-	-
2.89c	Br	H	4-Me	3407m, 3180w	-	1673m (C=O), 1614sh, 1598m, 1593m, 1577sh, 1560s, 1512m
2.89d	Br	Me	H	3391m, 3066w	-	1670m (C=O), 1601m, 1590m, 1558s, 1508m
2.89e	Br	Br	4-CN	3386m, 3097w	2217m	1669m (C=O), 1603m, 1558s, 1553s, 1509s
2.89f	Cl	H	H	3396m, 3066w	-	1674s(C=O), 1616sh, 1599s, 1580sh, 1561s, 1512m
2.89g	Cl	H	4-Me	3404m, 3065w	-	1676m (C=O), 1616sh, 1597s, 1577m, 1561s, 1515m

[1]low yield; only characterized through NMR



2.90



2.105

Table 88: IR spectroscopic data (Nujol, cm^{-1}) obtained for compounds **2.90** and **2.105**

Compound	4000-3000	1700-1490
2.90	-	1653m, 1601m, 1592m, 1577sh, 1549m
2.105	-	1651w, 1620s, 1598s, 1567s, 1541m, 1504m

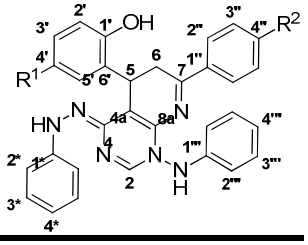


Table 89: IR spectroscopic data (Nujol, cm^{-1}) obtained for compounds **2.100a,b**

Compound	R^1	R^2	4000-3000	1700-1500
2.100a	Br	H	3309m, 3226w, 3182m, 3098m	1646s, 1602m, 1573sh, 1555m
2.105b	Br	Me	3314m, 3230m, 3102w, 3058w	1645s, 1599s, 1574m, 1555s

NMR spectroscopy

The most relevant signal in the ^{1}H NMR spectra of compounds **2.85** is a singlet at around δ8.5 ppm corresponding to the CH group of the imidate moiety. By HMBC, a set of similar correlations can be identified for each compound family (**Tables 90** and **91**). Compounds **2.85** present a correlation of the newly formed CH of the imidate and both CH_2 of the ethoxide moiety and C2. In the ^{13}C NMR spectrum, the presence of the cyano group is confirmed by a signal around δ 118 ppm. The imidate C-H shows a signal at δ 161-162 ppm.

The ^{1}H NMR spectra of compounds **2.86** possess three characteristic singlets: one at δ10-9.5 ppm, δ 8.8-8.5 ppm and δ7.9-7.7 ppm, corresponding to the OH group, H2 and H6, respectively (**Tables 92** and **93**). The pyrimidinone backbone is identified in the ^{13}C NMR spectra by signals at δ166-167 ppm (C=O), δ154-157 ppm (C2), δ121-122 ppm (C6), δ150-152 ppm (C8a) and δ 112-113 (C4a) ppm. Correlation spectra show cross peaks between H2, H6 and OH group. H2 correlates with C4, C8a and to the C1' of the R^3 group; H6 correlates with C4a, C5, C7, C1' and C1''. The OH group correlates with C2'.

The DMSO-d_6 spectra of compounds **2.87** shows the presence of two tautomers as the NH of the amidine moiety can be located at both nitrogen atoms. Two sets of characteristic signals are present in the ^{1}H and in the ^{13}C NMR spectra (**Tables 94** and **95**). Thus, the signals at δ10.7-12 ppm and δ10.2-10.5 ppm for the NH group, and at δ 8.8-9 ppm and δ 8.3-8.4 ppm for the aromatic CH group. In the ^{13}C NMR spectra, the chemical shift difference is most evident for the amidine CH group, with one set of signals around δ 151 ppm and another at δ 148-149 ppm.

The ^{1}H NMR spectra of compounds **2.88** exhibit three characteristic signals, at δ 4.21 and 2.72 ppm (both for H1), and δ 1.05 ppm and δ 5.79 for H11b and OH group, respectively (**Tables 96** and **97**). The signals of the expect pair of diastereomers are observed, with one of

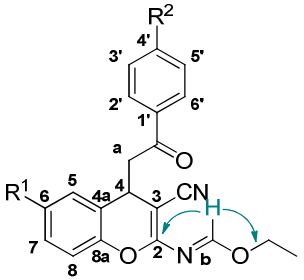
the isomers being clearly the major component (ratio ranging from 5/1 to 3/1). the ^{13}C NMR spectra highlight several signals around δ 80 ppm, mainly assigned to the aliphatic carbons, and the presence of two signals at δ 30-40 ppm and δ 20-30 ppm, assigned to C11b and C1, respectively, indicate that the aromatization of the upper ring did not occur. Two-dimensional ^{1}H-^{13}C correlation studies for compounds **2.88** showed cross peaks between H1 and C2, C11b and C1', of H11b with C1, C3a, C3b, C6a, C7a, C11 and C11a, and of H5 with C3a, C6a and C1''.

The ^{1}H NMR spectra for compounds **2.89** show two characteristic singlets at around δ 8.5-9 and δ 8.0-8.5 ppm assigned to the exocyclic amine proton and the pyrimidine C-H group (H2), respectively (**Tables 98** and **99**). Two signals at around δ 5.2 and δ 3.0-3.8 ppm, assigned to H5 and to Ha, respectively. These signals, usually present as multiplets, are often unresolved, leading to broad singlets (**2.89c**, **2.89d, 2.89j** and **2.89k**). The typical ^{13}C NMR spectrum shows three signals (C2, C4 and C10a) in the δ 150-165 ppm region, for the pyrimidine carbon atoms, and C4a is consistently present at δ 98-99 ppm. Correlation spectra for these compounds shows cross peaks between H2 and both C4 and C10a, as well as correlations of the NH group with C4, C1'' and C2''/C6''.

Compounds **2.90** and **2.105** present similar ^{1}H NMR patterns, with one singlet assigned to the CH groups of the pyridine ring, and another assigned to H5, for both, as they all share the tetracyclic backbone (**Table 100**). Compound **2.90** shows a doublet at δ 6.79 ppm (J= 2.0 Hz), which is attributed to H6a and the small coupling constant may be due to long-range coupling with H5. Correlation spectra for compounds **2.90** shows that H6a correlates with C3a, C3b, C5, C7a and C11b, and for compound **2.105** shows that H5 correlates with C3a and C6aand the pyridine H1 correlates with C1', C11a, C11 and C3b.

The ^{1}H NMR spectra for compounds **2.100** show a singlet at δ 9.5 ppm, assigned to the hydrazine NH group, but the hydroxyl group cannot be seen (**Table 101**). The presence of a doublet at δ 3.22 ppm (J= 13.2 Hz) and a doublet of doublets at δ 3.03-3.04 ppm (J_1= 13.6-14.0, J_2= 10.8 Hz) shows that the pyridine ring is not fully aromatic. It also presents two singlets at δ 8.15-8.21 ppm and δ 9.35-9.51 ppm, attributed to the H2 and NH groups, respectively. By ^{13}C NMR, C2 (around δ 152 ppm) and C4 (around δ 156 ppm) help to determine the skeleton of this group of compounds. By correlation NMR studies, the most distinctive correlation observed are of H4 and H5, C7 and C4a; of H2 and C8a and C4; and of H5 with C4a, C6, C7, C1' and C6'. The hydrazine NH protons correlate with the aromatic C1 and C2/C6 to which are linked.

Table 90: ^{1}H NMR (400 MHz, DMSO-d_6, δ ppm) spectroscopic data obtained for imidates **2.85a-h**



Compound	R^1	R^2	H5-8	H2'-6'	H4	CH2	CH	OEt
2.85a	H	H	7.30 (dd, J_1= 8.0, J_2= 1.2 Hz, 1H, H5), 7.25 (td, J_1= 8.0, J_2= 2.0 Hz, 1H, H6), 7.09 (td, J_1= 8.8, J_2= 1.2 Hz,1H, H7), 7.08 (d, J= 8.8 Hz, 1H, H8)	7.92 (dd, J_1=8.4, J_2= 1.2 Hz, 2H, H2'+ H6'), 7.61 (tt, J_1= 7.6, J_2= 1.2 Hz, 1H, H3' + H5'), 7.49 (t, J= 8.0 Hz, 2H, H4')	4.26 (t, J= 5.6 Hz, 1H)	3.66 (dd, J_1= 18, J_2= 5.6 Hz, 1H, Hα), 3.50 (dd, J_1= 18, J_2= 5.2 Hz, 1H, Hβ)	8.56 (s, 1H)	4.31 (q, J= 6.8 Hz, 2H, CH_2), 1.31 (t, J= 6.8 Hz, 3H, CH_3)
2.85b	H	Br	7.30 (dd, J_1= 7.2, J_2= 1.2 Hz, 1H, H5), 7.24 (dt, J_1= 8.0, J_2= 1.2 Hz, 1H, H7), 7.11 (dt, J_1= 8.0, J_2= 1.2 Hz, 1H, H6), 7.09 (d, J= 8.0 Hz, 1H, H8)	7.84 (dd, J_1= 8.0, J_2= 2.0 Hz 2H, H2' + H6'), 7.69 (dd, J_1= 8.0, J_2= 2.0 Hz, 2H, H3' + H5')	4.30 (t, J= 5.6 Hz, 1H)	3.64 (dd, J_1= 17.6, J_2= 5.6 Hz, 1H, Hα), 3.47 (dd, J_1= 17.6, J_2= 5.2 Hz, 1H, Hβ)	8.58 (s, 1H)	4.31 (q, J= 6.8 Hz, 2H, CH_2), 1.31 (t, J= 7.2 Hz, 3H, CH_3)
2.85c	H	Cl	7.30 (dd, J_1= 8.4, J_2= 1.6 Hz, 1H, H5), 7.24 (dt, J_1= 8.0, J_2= 1.6 Hz, 1H, H7), 7.11 (dt, J_1= 8.4, J_2= 1.2 Hz, 1H, H6), 7.09 (d, J= 7.6 Hz, 1H, H8)	7.93 (dd, J_1= 8.4, J_2= 1.6 Hz, 2H, H2' + H6'), 7.55 (dd, J_1= 8.4, J_2= 1.6 Hz, 2H, H3' + H5')	4.31 (t, J= 5.6 Hz, 1H)	3.65 (dd, J_1= 17.6, J_2= 5.6 Hz, 1H, Hα), 3.48 (dd, J_1= 17.6, J_2= 5.2 Hz, 1H, Hβ)	8.58 (s, 1H)	4.31 (q, J= 6.8 Hz, 2H, CH_2), 1.31 (t, J= 7.2 Hz, 3H, CH_3)
2.85d	Br	H	7.56 (d, J= 2.0 Hz, 1H, H5), 7.41 (dd, J_1= 8.8, J_2= 2.4 Hz, 1H, H7), 7.07 (d, J= 8.8 Hz, 1H, H8),	7.91 (dd, J_1= 8.8, J_2= 1.6 Hz, 2H, H2'+ H6'), 7.61 (t, J= 7.2 Hz, 1H, H4'), 7.49 (t, J= 8.0 Hz, 2H, H3' + H5')	4.30 (t, J= 5.6 Hz, 1H)	3.74 (dd, J_1= 18.4, J_2= 5.6 Hz, 1H, Hα), 3.53 (dd, J_1= 18.4, J_2= 5.2 Hz, 1H, Hβ)	8.58 (s, 1H)	4.31 (q, J= 6.8 Hz, 2H, CH_2), 1.30 (t, J= 7.2 Hz, 3H, CH_3)

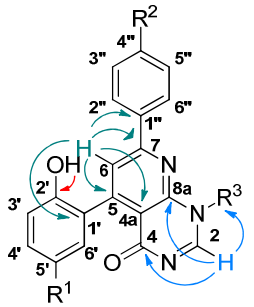
2.85e	Br	Me	7.55 (d, J= 2.0Hz, 1H, H5), 7.41 (dd, J_1= 8.8, J_2= 2.4 Hz, 1H, H7), 7.07 (d, J= 8.8 Hz, 1H, H8)	7.81 (d, J= 8.0 Hz, 2H, H2' + H6'), 7.29 (d, J_1= 8.0 Hz, 2H, H3' + H5'), 2.35 (s, 3H, Me)	4.32-4.27 (m, 3H, H4 + CH_2)	3.69 (dd, J_1= 18.0, J_2= 5.6 Hz, 1H, Hα), 3.49 (dd, J_1= 18.0, J_2= 5.2 Hz, Hz, 1H, Hβ)	8.59 (s, 1H)	4.32-4.27 (m, 3H, H4 + CH_2), 1.29 (t, J= 6.8 Hz, 3H, CH_3)
2.85f	Br	Br	7.57 (d, J= 2.0 Hz, 1H, H5), 7.42 (dd, J_1= 8.4, J_2= 2.4 Hz, 1H, H7), 7.07 (d, J_1= 8.8 Hz, 1H, H8),	7.85 (dd, J_1= 6.8, J_2= 2.4 Hz, 2H, H3' + H5'), 7.70 (dd, J_1= 6.8, J_2= 2.4 Hz, 2H, H2' + H6')	4.20 (t, J= 5.6 Hz, 1H)	3.73 (dd, J_1= 18.0, J_2= 5.6 Hz, 1H, Hα), 3.52 (dd, J_1= 18.0, J_2= 5.2 Hz, Hz, 1H, Hβ)	8.59 (s, 1H)	4.30 (q, J= 6.8 Hz, 2H, CH_2), 1.29 (t, J= 7.2 Hz, 3H, CH_3)
2.85g	Br	Cl	7.53 (d, J= 2.4 Hz, 1H, H5), 7.40 (dd, J_1= 8.8, J_2= 2.4 Hz, 1H, H7), 7.07 (d, J= 8.8 Hz, 1H, H8),	7.91 (dd, J_1= 6.8, J_2= 2.0 Hz, 2H, H2' + H6'), 7.54 (d, J_1= 6.8, J_2= 2.0 Hz, 2H, H3' + H5')	4.28 (t, J= 5.6 Hz, 1H)	3.72 (dd, J_1= 18.0, J_2= 5.6 Hz, 1H, Hα), 3.56 (dd, J_1= 18.0, J_2= 5.2 Hz, Hz, 1H, Hβ)	8.60 (s, 1H)	4.30 (q, J= 6.8 Hz, 2H, CH_2), 1.29 (t, J= 7.2 Hz, 3H, CH_3)
2.85h	Cl	H	7.45 (d, J= 2.4 Hz, 1H, H5), 7.30 (dd, J_1= 8.8, J_2= 2.8 Hz, 1H, H7), 7.13 (d, J= 8.4 Hz, 1H, H8),	7.92 (dd, J_1= 7.2, J_2= 1.2 Hz, 2H, H2'+ H6'), 7.62 (dt, J_1= 7.6, J_2= 1.2 Hz, 1H, H4'), 7.50 (dt, J_1= 8.0, J_2= 1.6 Hz, 2H, H3' + H5')	4.32 (t, J= 5.2 Hz, 1H)	3.76 (dd, J_1= 18.0, J_2= 5.6 Hz, 1H, Hα), 3.54 (dd, J_1= 18.0, J_2= 5.2 Hz, Hz, 1H, Hβ)	8.59 (s, 1H)	4.29 (q, J= 6.8 Hz, 2H, CH_2), 1.28 (t, J= 7.2 Hz, 3H, CH_3)

Table 91: ^{13}C NMR (100 MHz, DMSO-d_6, δ ppm) spectroscopic data obtained for imidates **2.85a-h**

Compound	R^1	R^2	Ar(C2-8a)	Ar(C1'-6')	CH2	CN	CH	C=O	OEt
2.85a	H	H	159.12 (C2), 149.55 (C8a), 128.20 (C5), 125.37 (C6), 128.61 (C7), 122.21 (C4a), 116.65 (C8), 78.53 (C3), 31.93 (C4)	136.59 (C1'), 133.73 (C4'), 128.95 (C3' + C5'), 128.20 (C2' + C6')	45.42	118.34	161.57	197.66	64.18 (CH_2), 14.10 (CH_3)

2.85b	H	Br	158.88 (C2), 149.35 (C8a), 128.28 (C7), 128.10 (C5), 125.12 (C6), 122.00 (C4a), 116.41 (C8), 78.34 (C3), 31.73 (C4)	135.44 (C1'), 131.77 (C3' + C5'), 130.06 (C2' + C6'), 127.57 (C4')	45.43	117.99	161.31	196.64	63.87 (CH_2), 13.88 (CH_3)
2.85c	H	Cl	158.88 (C2), 149.36 (C8a), 128.38 (C7), 128.10 (C5), 125.12 (C6), 122.01 (C4a), 116.40 (C8), 78.35 (C3), 31.73 (C4)	138.15 (C4'), 135.35 (C1'), 129.97 (C2' + C6'), 128.75 (C3' + C5')	45.55	117.99	161.31	196.43	63.87 (CH_2), 13.87 (CH_3)
2.85d	Br	H	158.66 (C2), 148.83 (C8a), 131.17 (C7), 130.63 (C5), 124.76 (C4a), 118.86 (C8), 116.85 (C6), 78.32 (C3), 31.53 (C4)	136.40 (C1'), 133.57 (C4'), 128.79 (C3' + C5'), 128.06 (C2' + C6')	44.71	117.84	161.55	197.30	64.02 (CH_2), 13.93 (CH_3)
2.85e	Br	Me	128.51 (C2), 148.75 (C8a), 130.55 (C5), 116.45 (C6), 131.02 (C7), 124.76 (C4a), 118.55 (C8), 78.35 (C3), 31.48 (C4)	143.86 (C4'), 133.93 (C1'), 129.21 (C3' + C5'), 128.11 (C2' + C6'), 21.13 (Me)	44.58	117.73	161.44	196.65	63.89 (CH_2), 13.85 (CH_3)
2.85f	Br	Br	158.60 (C2), 148.77 (C8a), 131.10 (C7), 130.62 (C5), 124.57 (C4a), 118.58 (C8), 116.50 (C6), 78.19 (C3), 31.45 (C4)	135.34 (C1'), 131.74 (C3' + C5'), 130.05 (C2' + C6'), 127.57 (C4')	44.78	117.70	161.51	197.01	63.92 (CH_2), 13.85 (CH_3)
2.85g	Br	Cl	158.83 (C2), 148.94 (C8a), 131.30 (C7), 130.73 (C5), 124.68 (C4a), 118.81 (C8), 116.70 (C6), 78.28 (C3), 31.65 (C4)	138.62 (C4'), 135.16 (C1'), 130.12 (C2' + C6'), 129.00 (C3' + C5')	44.85	117.96	161.71	196.55	64.19 (CH_2), 14.02 (CH_3)
2.85h	Cl	H	158.59 (C2), 148.30 (C8a), 128.51 (C6), 128.16 (C7), 127.70 (C5), 124.29 (C4a), 118.19 (C8), 78.20 (C3), 31.53 (C4)	136.33 (C1'), 133.45 (C4'), 128.69 (C3' + C5'), 127.99 (C2' + C6')	44.64	117.73	161.44	197.16	63.89 (CH_2), 13.84 (CH_3)

Table 92: ^{1}H NMR (400 MHz, DMSO-d_6, δ ppm) spectroscopic data obtained for pyridopyrimidines **2.86**



Comp.	R^1	R^2	R^3	H2'-6'	H2''-6''	H2'''+H6'''	H2	H6	OH
2.86a	H	H	C_6H_5	7.26-7.20 (m, 2H, H4' + H6'), 6.90 (t, J= 7.6 Hz, 1H, H5'), 6.87 (d, J= 7.6 Hz, 1H, H3')	7.94 (dd, J_1= 8.0, J_2= 1.6 Hz, 2H, H2'' + H6''), 7.65 (t, J= 7.2 Hz, 2H, H3'' + H5''), 7.41 (t, J= 7.2 Hz, 1H, H4'')	7.70 (J= 7.2 Hz, 2H, H3''' + H5'''), 7.59 (t, J= 8.4 Hz, 1H, H4'''), 7.42 (J= 7.6 Hz, 2H, H2'''+ H6''')	8.65 (s,1H)	7.83 (s, 1H)	9.48 (s, 1H)
2.86b	Br	H	C_6H_5	7.94 (dd, J_1= 8.0, J_2= 1.6 Hz, 2H, H2'' + H6''), 7.70-7.60 (m, 4H, H2''' + H6''', H3''' + H5'''), 7.59 (d, J= 6.8 Hz, 1H, H4'), 7.45-7.39 (m, 3H, H3'' + H5'', H4''), 7.38 (d, J= 2.8 Hz, 1H, H6'), 7.36-7.34 (m, 1H, H4'''), 6.91 (d, J= 8.4 Hz, 1H, H3')			8.63 (s, 1H)	7.88 (s, 1H)	10.05 (s, 1H)
2.86c	H	H	$CH_2C_6H_5$	7.20 (dt, J_1= 8.0, J_2= 1.6 Hz, 2H, H4'), 7.15 (dd, J_1= 7.6, J_2= 2.0 Hz, 2H, H6'), 6.83 (dt, J_1= 7.6, J_2= 1.6 Hz, 2H, H5'), 6.81 (d, J= 7.6 Hz, 2H, H3')	8.14 (dd, J_1= 6.8, J_2= 3.2 Hz, 2H, H2'' + H6''), 7.51 (t, J= 7.2 Hz, 1H, H4''), 7.50 (t, J= 7.2 Hz, 2H, H3'' + H5'')	7.45 (dd, J_1= 7.2, J_2= 1.6 Hz, 2H, H2''' + H6'''), 7.34 (td, J_1= 7.2, J_2= 1.6 Hz, 2H, H3''' + H5'''), 7.27 (td, J_1= 7.2, J_2= 1.6 Hz, 2H, H4'''), 5.52 (s, 2H, CH_2)	8.85 (s, 1H)	7.76 (s, 1H)	9.46 (s, 1H)
2.86d	H	H	3-MeC_6H_4	7.22 (dd, J_1= 8.0, J_2= 1.6 Hz, 1H, H6'), 7.19 (dt, J_1= 7.6, J_2= 1.6 Hz, 1H, H_4'), 6.88 (d, J= 8.0 Hz, 1H, H3'), 6.87 (dt, J_1= 7.2, J_2= 1.2 Hz, 1H, H5')	7.92 (dd, J_1= 7.2, J_2= 1.6 Hz, 2H, H2'' + H6''), 7.53-7.38 (m, 7H, H3'' + H5'', H4', H2''', H3''', H5''', H6'''), 2.48 (s, 3H, Me)		8.58 (s, 1H)	7.79 (s, 1H)	9.61 (s, 1H)

2.86e	Br	H	4-MeC_6H_4	7.36 (dd, J_1= 8.4, J_2= 2.4 Hz, 1H, H4'), 7.34 (d, J= 2.4 Hz, 1H, H6'), 6.90 (d, J= 8.4 Hz, 1H, H3')	7.96 (dd, J_1= 6.8, J_2= 2.0 Hz, 2H, H2'' + H6''), 7.55 (dd, J_1= 6.4, J_2= 2.0 Hz, 2H, H2''' + H6'''), 7.45-7.40 (m, 5H, H3'' + H5'', H4'', H3''' + H5'''), 2.44 (s, 3H, Me)		8.58 (s, 1H)	7.86 (s, 1H)	10.03 (s, 1H)
2.86f	Br	Br	4-$OMeC_6H_4$	7.37 (dd, J_1= 8.4, J_2= 2.4 Hz, 1H, H4'), 7.34 (d, J= 2.8 Hz, 1H, H6'), 6.91 (d, J= 8.8 Hz, 1H, H3')	7.92 (dd, J_1= 8.8, J_2= 2.4 Hz, 2H, H2'' + H6''), 7.59 (dd, J_1= 8.8, J_2= 1.6 Hz, 2H, H3'' + H5'')	7.64 (dd, J_1= 8.4, J_2= 1.6 Hz, 2H, H2''' + H6'''), 7.15 (dd, J_1= 9.2, J_2= 2.4 Hz, 2H, H3''' + H5'''), 3.86 (s, 3H, OMe)	8.58 (s, 1H)	7.91 (s, 1H)	10.06 (s, 1H)
2.86g	Br	Cl	4-MeC_6H_4	7.37 (dd, J_1= 8.8, J_2= 2.0 Hz, 1H, H4'), 7.34 (d, J= 2.4 Hz, 1H, H6'), 6.82 (d, J= 8.4 Hz, 1H, H3')	7.95 (dd, J_1= 8.4, J_2= 2.0 Hz, 2H, H3'' + H5''), 7.48 (dd, J_1= 8.4, J_2= 2.4 Hz, 2H, H2'' + H6'')	7.53 (dd, J_1= 8.4, J_2= 2.0 Hz, 2H, H2''' + H6'''), 7.41 (d, J= 8.4 Hz, 2H, H3''' + H5'''), 2.42 (s, 3H, Me)	8.56 (s, 1H)	7.85 (s, 1H)	9.97 (s, 1H)
2.86h	Br	Cl	4-$OMeC_6H_4$	7.37 (dd, J_1= 8.8, J_2= 2.4 Hz, 1H, H4'), 7.33 (d, J= 2.4 Hz, 1H, H6'), 6.84 (d, J= 8.4 Hz, 1H, H3')	7.96 (d, J= 8.8 Hz, 2H, H2'' + H6''), 7.59 (d, J= 8.4 Hz, 2H, H3'' + H5'')	7.57 (dd, J_1= 9.2, J_2= 2.0 Hz, 2H, H2''' + H6'''), 7.14 (d, J= 9.2 Hz, 2H, H3''' + H5'''), 3.87 (s, 3H, OMe)	8.56 (s, 1H)	7.85 (s, 1H)	9.99 (s, 1H)
2.86k	Br	H	4-$OMeC_6H_4$	7.37 (dd, J_1= 8.8, J_2= 2.4 Hz, 1H, H4'), 7.34 (d, J= 2.4 Hz, 1H, H6'), 6.81 (d, J= 8.4 Hz, 1H, H3')	7.95 (dd, J_1= 7.2, J_2= 1.6 Hz, 2H, H2'' + H6''), 7.46-7.41 (m, 3H, H3'' + H5'', H4'')	7.58 (dd, J_1= 9.2, J_2= 2.4 Hz, 2H, H2''' + H6'''), 7.15 (dd, J_1= 8.8, J_2= 2.0 Hz, 2H, H3''' + H5'''), 3.85 (s, 3H, OMe)	8.56 (s, 1H)	7.34 (s, 1H)	9.91 (s, 1H)
2.86l	Br	H	4-ClC_6H_4	7.40 (dd, J_1= 8.4, J_2= 2.4 Hz, 1H, H4'), 7.37 (d, J= 2.4 Hz, 1H, H6'), 6.21 (d, J= 8.4 Hz, 1H, H3')	7.98 (dd, J_1= 8.0, J_2= 2.8 Hz, 2H, H2'' + H6''), 7.49-7.43 (m, 3H, H3'' + H5'', H4'')	7.76 (dd, J_1= 8.4, J_2= 2.4 Hz, 2H, H2''' + H6'''), 7.15 (dd, J_1= 8.4, J_2= 2.4 Hz, 2H, H3''' + H5''')	8.63 (s, 1H)	7.89 (s, 1H)	9.85 (s, 1H)
2.86m	Cl	H	4-$OMeC_6H_4$	7.26 (dd, J_1= 8.8, J_2= 2.4 Hz, 1H, H4'), 7.25 (d, J= 2.4 Hz,	7.99 (dd, J_1= 7.2, J_2= 1.6 Hz, 2H, H2'' + H6''), 7.46-7.40 (m, 3H, H3'' + H5'', H4'')	7.60 (dd, J_1= 9.2, J_2= 2.4 Hz, 2H, H2''' + H6'''), 7.17 (dd, J_1= 8.8, J_2= 2.0 Hz, 2H, H3''' + H5'''), 3.87 (s, 3H, OMe)	8.58 (s, 1H)	7.88 (s, 1H)	9.80 (s, 1H)

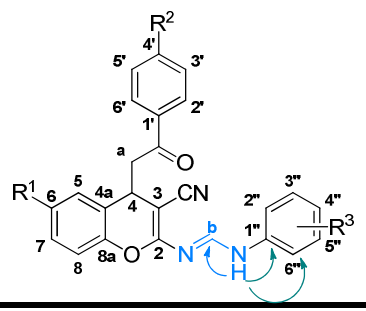
	1H, H6'), 6.86 (d, J= 8.4 Hz, 1H, H3')

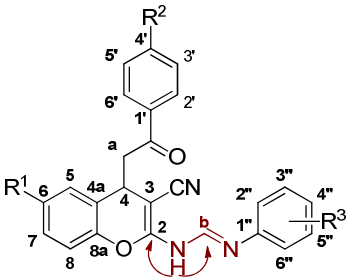
Table 93: ^{13}C NMR (100 MHz, DMSO-d_6, δ ppm) spectroscopic data for compounds **2.86**

Compound	R^1	R^2	R^3	C1-8a	C1'-6'	C1''-6''	C(R3)	C=O	C2	C6
2.86a	H	H	C_6H_5	157.82 (C7), 151.34 (C5), 150.86 (C8a), 112.27 (C4a)	154.24 (C2'), 129.20 (C4', C6'), 127.04 (C1'), 118.69 (C5'), 114.98 (C3')	136.68 (C1''), 130.56 (C4''), 128.89 (C3'' + C5''), 127.22 (C2'' + C6'')	138.02 (C1'''), 129.20 (C3''' + C5'''), 128.95 (C4'''), 128.14 (C2''' + C6''')	167.82	153.06	121.25
2.86b	Br	H	C_6H_5	158.03 (C7), 150.83 (C8a), 149.64 (C5), 112.12 (C4a)	154.23 (C2'), 131.50 (C6'), 130.70 (C4'), 129.38 (C1'), 117.08 (C3'), 109.48 (C5')	136.55 (C1''), 128.90 (C4''), 129.04 (C3'' + C5''), 127.33 (C2'' + C6'')	137.93 (C1'''), 131.07 (C3''' + C5'''), 129.24 (C4'''), 128.19 (C2''' + C6''')	167.84	153.95	121.22
2.86c	H	H	$CH_2C_6H_5$	158.12 (C7), 151.62 (C5), 149.98 (C8a), 112.92 (C4a)	154.23 (C2'), 129.31 (C6'), 129.28 (C4'), 127.08 (C1'), 118.82 (C5'), 115.06 (C3')	136.88 (C1''), 130.82 (C4''), 129.17 (C3'' + C5''), 127.58 (C2'' + C6'')	137.21 (C1'''), 128.80 (C3''' + C5'''), 127.88 (C4'''), 127.57 (C2''' + C6'''), 50.84 (CH2)	168.05	154.29	121.25
2.86d	H	H	3-MeC_6H_4	158.02 (C7), 151.62 (C5), 151.00 (C8a), 112.43 (C4a)	154.40 (C2'), 129.32 (C4'), 129.40 (C6'), 127.15 (C1'), 118.90 (C5'), 115.19 (C3')	136.83 (C1''), 130.87 (C4''), 129.77 (C3'' + C5''), 127.40 (C2'' + C6'')	139.08 (C3'''), 138.00 (C1'''), 127.17 (C4''', C6'''), 128.57 (C2'''), 125.34 (C5''')	168.08	153.26	121.49
2.86e	Br	H	4-MeC_6H_4	158.16 (C7), 150.89 (C8a),	153.95 (C2'), 131.51 (C4'), 131.09 (C6'),	136.65 (C1''), 130.71 (C3'' +	138.52 (C4'''), 135.44 (C1'''), 129.71 (C3''' +	167.88	153.46	121.29

			149.65 (C5), 112.15 (C4a)	129.43 (C1'), 117.09 (C3'), 109.50 (C5')	C5''), 128.95 (C4''), 127.38 (C2'' + C6'')	C5'''), 127.82 (C2''' + C6'''), 20.85 (Me)			
2.86f	Br	Br	4-$OMeC_6H_4$	156.88 (C7), 151.00 (C8a), 149.77 (C5), 112.35 (C4a)	153.93 (C2'), 131.48 (C4'), 131.02 (C6'), 129.27 (C1'), 117.04 (C3'), 109.41 (C5')	135.83 (C1''), 129.31 (C3'' + C5''), 129.21 (C2'' + C6''), 124.50 (C4'')	159.33 (C4'''), 130.55 (C1'''), 131.89 (C2''' + C6'''), 114.32 (C3''' + C5'''), 55.51 (OMe)	167.77	153.59	121.15
2.86g	Br	Cl	4-MeC_6H_4	157.26 (C7), 151.06 (C8a), 150.00 (C5), 112.50 (C4a)	153.98 (C2'), 131.90 (C4'), 131.33 (C6'), 129.51 (C1'), 117.24 (C3'), 109.87 (C5')	135.92 (C4''), 135.67 (C1''), 129.35 (C2'' + C6''), 129.25 (C3'' + C5'')	138.87 (C4'''), 135.49 (C1'''), 130.00 (C3''' + C5'''), 127.93 (C2''' + C6'''), 21.05 (Me)	168.09	153.75	121.55
2.86h	Br	Cl	4-$OMeC_6H_4$	157.20 (C7), 151.25 (C8a), 150.01 (C5), 112.53 (C4a)	153.99 (C2'), 131.87 (C4'), 131.31 (C6'), 129.52 (C1'), 117.25 (C3'), 109.85 (C5')	135.92 (C4''), 135.64 (C1''), 129.34 (C2'' + C6''), 129.26 (C3'' + C5'')	159.62 (C4'''), 130.52 (C1'''), 129.43 (C2''' + C6'''), 114.62 (C3''' + C5'''), 55.57 (OMe)	168.12	153.58	121.45
2.86k	Br	H	4-$OMeC_6H_4$	158.41 (C7), 151.26 (C8a), 149.75 (C5), 112.33 (C4a)	153.94 (C2'), 131.81 (C4'), 131.33 (C6'), 129.65 (C1'), 117.19 (C3'), 109.86 (C5')	136.76 (C1''), 130.96 (C3'' + C5''), 129.18 (C4''), 127.54 (C2'' + C6'')	159.59 (C4'''), 130.79 (C1'''), 129.46 (C2''' + C6'''), 114.55 (C3''' + C5'''), 55.74 (OMe)	167.88	153.46	121.29
2.86l	Br	H	4-ClC_6H_4	158.11 (C7), 150.69 (C8a), 149.55 (C5), 112.09 (C4a)	153.16 (C2'), 131.61 (C4'), 131.14 (C6'), 129.34 (C1'), 117.00 (C3'), 109.61 (C5')	136.54 (C1''), 130.71 (C3'' + C5''), 128.95 (C4''), 127.35 (C2'' + C6'')	136.79 (C1'''), 133.50 (C4'''), 130.09 (C2''' + C6'''), 129.18 (C3''' + C5''')	167.78	153.82	121.32
2.86m	Cl	H	4-$OMeC_6H_4$	158.09 (C7), 151.07 (C8a), 149.61 (C5), 112.17 (C4a)	153.36 (C2'), 128.66 (C6'), 128.47 (C4'), 128.02 (C1'), 116.46 (C3'), 122.06 (C5')	136.62 (C1''), 130.67 (C3'' + C5''), 128.92 (C4''), 127.35 (C2'' + C6'')	159.37 (C4'''), 130.67 (C1'''), 129.28 (C2''' + C6'''), 114.32 (C3''' + C5'''), 55.74 (OMe)	167.89	153.58	121.16

Table 94: ^{1}H NMR (400 MHz, DMSO-d_6, δ ppm) spectroscopic data obtained for amidines **2.87**





Compound	R^1	R^2	R^3	H5-8	H2'-6'	H4	H4	Ha	Hb	NH
2.87a (major)	H	H	H	7.92 (d, J= 8.0 Hz, 4H, H2' + H6', H3'' + H5''), 7.61 (dt, J_1= 7.6, J_2= 1.2 Hz, 1H, H4'), 7.49 (t, J= 7.6 Hz, 2H, H3' + H5'), 7.38-7.23 (m, 5H, H2'' + H6'', H5, H7, H8), 7.11-7.06 (m, 2H, H4'', H6)			4.33 (m, 1H)	3.55-3.40 (m, 2H)	8.96 (d, J= 12.0 Hz, 1H)	10.88 (d, J= 12.0 Hz, 1H)
2.87a (minor)				7.92 (d, J= 8.0 Hz, 6H, H2' + H6', H2'' + H6'', H3'' + H5''), 7.61 (dt, J_1= 7.6, J_2= 1.6 Hz, 1H, H4'), 7.48 (dt, J_1= 7.6, J_2= 1.6 Hz, 2H, H3' + H5'), 7.38-7.23 (m, 2H, H5, H7), 7.14 (d, J= 7.6 Hz, 1H, H8), 7.11-7.06 (m, 2H, H4'', H6)		4.33 (m, 1H)	3.55-3.40 (m, 2H)	8.38 (d, J= 5.2 Hz, 1H)	10.30 (d, J= 5.2 Hz, 1H)
2.87b (minor)	Br	H	H	7.40 (m, 2H, H5, H7), 7.24 (d, J= 8.4 Hz, 1H, H8)	7.94 (d, J= 8.0 Hz, 2H, H2' + H6'), 7.61 (t, J= 7.2 Hz, 1H, H4), 7.48 (t, J= 7.6 Hz, 2H, $H_{3'}$ + H5')	7.32 (d, J= 8.8 Hz, 2H, H2'' + H6''), 7.30 (t, J= 8.0 Hz, 2H, H3'' + H5''), 7.08 (t, J= 7.6 Hz, 1H, H4'')	4.29 (t, J= 5.2 Hz, 1H)	3.66 (dd, J_1=14.0, J_2= 5.2 Hz, 2H)	8.95 (d, J= 11.2 Hz, 1H)	10.90 (d, J= 12.0 Hz, 1H)
2.87b (major)				7.94 (d, J= 8.0 Hz, 4H, H2' + H6', H2'' + H6''), 7.61 (t, J= 7.2 Hz, 1H, H4), 7.54 (m, 2H, H5, H7), 7.48 (t, J= 7.6 Hz, 2H, H3' + H5'), 7.32 (t, J= 8.0 Hz, 2H, H3'' + H5''), 7.13 (d, J= 8.8 Hz, 1H, H8), 7.08 (t, J= 7.6 Hz, 1H, H4'')			4.29 (t, J= 5.2 Hz, 1H)	3.52 (dd, J_1=17.2, J_2= 4.4 Hz, 2H)	8.36 (d, J= 4.8 Hz, 1H)	10.85 (d, J= 5.2 Hz, 1H)
2.87c (major)				7.91 (dd, J_1= 8.0, J_2= 0.8 Hz 4H, H2' + H6'), 7.61 (dt, J_1= 7.6, J_2= 1.6 Hz, 1H, H4'), 7.48 (dt, J_1= 7.6, J_2= 1.6 Hz, 2H, H3' + H5'), 7.30-7.05 (m, 8H, H2''+ H6'', H3'' + H5'', H5, H6, H7, H8), 2.48 (s, 3H, Me)			4.31 (m, 1H)	3.62-3.40 (m, 2H)	8.90 (d, J= 12.4 Hz, 1H)	10.79(d, J= 12.0 Hz, 1H)

2.87c (minor)	H	H	4-Me	7.91 (dd, J_1= 8.0, J_2= 0.8 Hz, 4H, H2' + H6'), 7.78 (d, J= 8.4 Hz, 2H, H2'' + H6''), 7.48 (t, J= 7.6 Hz, 2H, H3' + H5'), 7.30-7.05 (m, 6H, H3'' + H5'', H5, H6, H7, H8), 2.41 (s, 3H, Me)	4.31 (m, 1H)	3.62-3.40 (m, 2H)	8.34 (d, J= 4.8 Hz, 1H)	10.23 (d, J= 4.8 Hz, 1H)
2.87f (major)	H	Cl	H	7.92 (d, J= 8.4 Hz, 2H, H2' + H6'), 7.90 (d, J= 8.8 Hz, 2H, H2''+H6''), 7.54 (dd, J_1= 6.8, J_2= 2.0 Hz, 2H, H3' + H5'), 7.29-7.24 (m, 5H, H5, H7, H8, H3'' + H5''), 7.11-7.06 (m, 1H, H4'')	4.31 (m, 1H)	3.62-3.38 (m, 2H)	8.95 (d, J= 12.0 Hz, 1H)	10.87 (d, J= 12.0 Hz, 1H)
2.87f (minor)				7.92 (d, J= 8.4 Hz, 2H, H2' + H6'), 7.54 (dd, J_1= 6.8, J_2= 2.0 Hz, 2H, H3' + H5'), 7.34 (d, J= 8.0 Hz, 2H, H2''+ H6''), 7.29-7.24 (m, 4H, H5, H7, H3'' + H5''), 7.13 (d, J= 8.0 Hz, 1H, H8), 7.11-7.06 (m, 1H, H4'')	4.31 (m, 1H)	3.62-3.38 (m, 2H)	8.37 (d, J= 4.8 Hz, 1H)	10.31 (d, J= 12.0 Hz, 1H)
2.87g (major)	Br	H	4-Me	7.40 (d J= 2.4 Hz, 1H, H7), 7.39 (dd, J_1= 8.8, J_2= 2.0 Hz, 1H, H5), 7.20 (d, J= 8.8 Hz, 1H, H8)	7.89 (d, J= 8.4 Hz, 2H, H2' + H6'), 7.61 (dt, J_1= 7.6, J_2= 1.2 Hz 1H, H4'), 7.48 (t, J= 7.6 Hz, 2H, H3' + H5'), 7.21-7.18 (m, 4H, H2'' + H6'', H3'' + H5''), 2.24 (s, 3H, Me)	4.25 (t, J= 5.2 Hz, 1H)	3.70-3.41 (m, 2H)	8.96 (d, J= 12.4 Hz, 1H)	10.76 (d, J= 12.0 Hz, 1H)
2.87g (minor)				7.40 (d J= 2.4 Hz, 1H, H7), 7.39 (dd, J_1= 8.8, J_2= 2.0 Hz, 1H, H5), 7.07 (d, J= 8.4 Hz, 1H, H8)	7.89 (d, J= 8.4 Hz, 2H, H2' + H6'), 7.61 (dt, J_1= 7.6, J_2= 1.2 Hz 1H, H4'), 7.48 (t, J= 7.6 Hz, 2H, H3' + H5'), 7.74 (d, J= 8.4 Hz, 2H, H2'' + H6''), 7.17 (d, J= 8.0 Hz, 2H, H3'' + H5''), 2.24 (s, 3H, Me)	4.25 (t, J= 5.2 Hz, 1H)	3.62-3.41 (m, 2H)	8.32 (d, J= 5.2 Hz, 1H)	10.25 (d, J= 4.8 Hz, 1H)
2.87h (major)	Br	H	4-OMe	7.52 (dd, J_1= 5.2, J_2= 2.4 Hz, 1H, H5), 7.39 (d, J= 8.8 Hz, 1H, H7), 7.10 (d, J= 8.8 Hz, 1H, H8)	7.90 (d, J= 7.6 Hz, 2H, H2' + H6'), 7.60 (t, J= 8.0 Hz, 1H, H4'), 7.49 (t, J= 8.0 Hz, 3H, H3' + H5')	7.25 (dd, J_1= 7.2, J_2= 2.0 Hz, 2H, H2'' + H6''), 6.92 (dd, J_1= 7.2, J_2= 2.0 Hz, 2H, H3'' + H5''), 3.75 (s, 3H, OMe)	4.27 (m, 1H)	3.70-3.52 (m, 2H)	8.81 (d, J= 12.4 Hz, 1H)	10.75 (d, J= 12.4 Hz, 1H)
2.87h (minor)	Br	H	4-OMe	7.52 (dd, J_1= 5.2, J_2= 2.4 Hz, 1H, H5), 7.39 (d, J= 8.8 Hz, 1H, H7),	7.90 (d, J= 7.6 Hz, 2H, H2' + H6'), 7.60 (t, J= 8.0 Hz, 1H,	7.81 (dd, J_1= 7.2, J_2= 2.0 Hz, 2H, H2'' + H6''), 6.88 (dd, J_1= 7.2, J_2= 2.0	4.27 (m, 1H)	3.70-3.52 (m, 2H)		

			7.10 (d, J= 8.8 Hz, 1H, H8)	H4'), 7.49 (t, J= 8.0 Hz, 3H, H3' + H5')	Hz, 2H, H3'' + H5''), 3.72 (s, 3H, OMe)			8.31 (d, J= 5.2 Hz, 1H)	10.24 (d, J= 4.8 Hz, 1H)
2.87i (major)	Br	H	3-Me	7.89 (d, J= 8.4 Hz, 2H, H2' + H6'), 7.62 (dt, J_1= 7.6, J_2= 1.2 Hz, 1H, H4'), 7.51 (d, J= 2.8 Hz, 1H, H5), 7.49 (d, J= 8.0 Hz, 2H, H3' + H5'), 7.39 (dd, J_1= 8.8, J_2= 2.4 Hz, 1H, H7), 7.23-7.17 (m, 1H, H5''), 7.12-7.08 (m, 3H, H8, H2'', H6''), 7.23-7.17 (m, 1H, H8), 6.91 (d, J=7.6 Hz, 1H, H4'')			4.23 (m, 1H)	3.70-3.50 (m, 2H)	8.88 (d, J= 12.4 Hz, 1H)	10.74 (d, J= 12.4 Hz, 1H)
2.87i (minor)				7.90 (s, 1H, H2'), 7.89 (d, J= 8.4 Hz, 2H, H2' + H6'), 7.62 (dt, J_1= 7.6, J_2= 1.2 Hz, 1H, H4'), 7.51 (d, J= 2.8 Hz, 1H, H5), 7.49 (d, J= 8.0 Hz, 2H, H3' + H5'), 7.46 (dd, J_1= 7.6, 1.6 Hz, 1H, H8), 7.39 (dd, J_1= 8.8, 2.4 Hz, 1H, H7), 7.23-7.17 (m, 2H, H5'', H6''), 6.91 (d, J= 7.6 Hz, 1H, $H_{4''}$)			4.23 (m, 1H)	3.70-3.50 (m, 2H)	8.34 (d, J= 4.8 Hz, 1H)	10.26 (d, J= 4.8 Hz, 1H)
2.87l (major)	Br	H	4-Cl	7.55 (dd, J_1= 5.2, J_2= 2.0 Hz, 1H, H5), 7.46 (dd, J_1= 8.4, J_2= 2.4 Hz, 1H, H7), 7.14 (d, J= 8.8 Hz, 1H, H8)	7.93 (d, J= 8.0 Hz, 2H, H2' + H6'), 7.62 (t, J= 7.6 Hz, 1H, H4'), 7.49 (t, J= 7.6 Hz, H3' + H5')	7.41-7.35 (m, 4H, H2'' + H6'', H3'' + H5'')	4.30 (m, 1H)	3.75-3.56 (m, 2H)	8.96 (d, J= 10.0 Hz, 1H)	10.98 (d, J= 10.0 Hz, 1H)
2.87l (minor)				7.55 (dd, J_1= 5.2, J_2= 2.0 Hz, 1H, H5), 7.24 (dd, J_1= 8.4, J_2= 2.4 Hz, 1H, H7), 7.14 (d, J= 8.8 Hz, 1H, H8)	7.93 (d, J= 8.0 Hz, 2H, H2' + H6'), 7.62 (t, J= 7.6 Hz, 1H, H4'), 7.49 (t, J= 7.6 Hz, H3' + H5')	7.96 (d, J= 8.0 Hz, 2H, H2'' + H6''), 7.41-7.35 (m, 2H, H3'' + H5'')	4.30 (m, 1H)	3.62-3.50 (m, 2H)	8.37 (d, J= 3.2 Hz, 1H)	10.82 (d, J= 4.8 Hz, 1H)
2.87n (major)	Br	Me	H	7.82 (d, J= 8.4 Hz, 2H, H2' + H6'), 7.52 (d, J= 2.4 Hz, 1H, H5), 7.43 (dd, J_1= 8.8, J_2= 2.4 Hz, 1H, H7), 7.36 (d, J= 8.8 Hz, 2H, H2'' + H6''), 7.31 (d, J= 8.0 Hz, 2H, H3' + H5'), 7.30 (d, J= 8.0 Hz, 2H, H3'' + H5''), 7.34 (d, J= 8.4 Hz, 1H, H8), 7.11-7.08 (m, 1H, H4'')			4.28 (m, 1H)	3.66-3.38 (m, 2H)	8.95 (d, J= 12.4 Hz, 1H)	10.91 (d, J= 12.0 Hz, 1H)
2.87n (minor)	Br	Me	H	7.89 (d, J= 8.0 Hz, 2H, H2'' + H6''), 7.82 (d, J= 8.4 Hz, 2H, H2' + H6'), 7.54 (d, J= 2.4 Hz, 1H, H5), 7.43 (dd, J_1= 8.8, J_2= 2.4 Hz, 1H, H7), 7.31 (d, J=			4.28 (m, 1H)	3.66-3.38 (m, 2H)	8.37 (d, J= 4.4 Hz, 1H)	10.34 (d, J= 4.8 Hz, 1H)

			8.0 Hz, 2H, H3' + H5'), 7.30 (d, J= 8.0 Hz, 2H, H3'' + H5''), 7.13 (d, J= 8.8 Hz, 1H, H8), 7.11-7.08 (m, 1H, H4'')				
2.87y (minor)	Br	Cl	3-Br	7.89 (d, J= 8.8 Hz, 2H, H2' + H6'), 7.65-7.63 (m, 1H, H6''), 7.52 (d, J= 8.4 Hz, 2H, H3' + H5'), 7.54-7.51 (m, 2H, H2'', H8), 7.39 (dd, J_1= 8.8, J_2= 2.0 Hz, 1H, H7), 7.32-7.26 (m, 2H, H4'', H5''), 7.20 (d, J= 7.6 Hz, 1H, H2'')	4.26 (m, 1H)	3.76-3.48 (m, 2H)	8.90 (d, J= 11.6 Hz, 1H)	10.88 (d, J= 11.6 Hz, 1H)
2.87y (major)				7.89 (d, J= 8.8 Hz, 2H, H2' + H6'), 7.65-7.63 (m, 1H, H6''), 7.52 (d, J= 8.4 Hz, 2H, H3' + H5'), 7.54-7.51 (m, 1H, H8), 7.39 (dd, J_1=8.8, J_2= 2.0 Hz, 1H, H7), 7.32-7.26 (m, 2H, H4'', H5''), 7.09 (d, J= 8.4 Hz, 1H, H2'')	4.26 (m, 1H)	3.76-3.48 (m, 2H)	8.34 (d, J= 3.6 Hz, 1H)	10.46 (d, J= 4.8 Hz, 1H)
2.87z (major)	Cl	H	H	7.89 (d, J= 7.2 Hz, 2H, H2' + H6'), 7.60 (dt, J_1= 7.2, J_2= 1.2 Hz, 1H, H4'), 7.48 (t, J= 8.0 Hz, 2H, H3' + H5'), 7.39 (dd, J_1= 7.6, J_2= 2.4 Hz, 1H, H5), 7.36-7.26 (m, 6H, H7, H8, H2'' + H6'', H3'' + H6''), 7.10 (dt, J_1= 8.0, J_2= 1.2 Hz, 1H, H4'')	4.27 (m, 1H)	3.76-3.47 (m, 2H)	8.92 (d, J= 11.6 Hz, 1H)	10.82 (d, J= 11.6 Hz, 1H)
2.87z (minor)				7.89 (d, J= 7.2 Hz, 2H, H2' + H6'), 7.86 (d, J= 7.6 Hz, 2H, H2'' + H6''), 7.60 (dt, J_1= 7.2, J_2= 1.2 Hz, 1H, H4), 7.48 (t, J= 8.0 Hz, 2H, H3' + H5'), 7.39 (dd, J_1= 7.6, J_2= 2.4 Hz, 1H, H5), 7.36-7.26 (m, 6H, H7, H2'' + H6'', H3'' + H6''), 7.15 (d, J= 7.6 Hz, 1H, H8), 7.10 (dt, J_1= 8.0, J_2= 1.2 Hz, 1H, H4'')	4.27 (m, 1H)	3.76-3.47 (m, 2H)	8.36 (d, J= 4.8 Hz, 1H)	10.30 (d, J= 4.8 Hz, 1H)
2.87a' (major)	Cl	H	4-Me	7.91 (d, J= 8.0 Hz, 2H, H2' + H6'), 7.61 (t, J=7.6 Hz, 1H, H4'), 7.49 (t, J= 8.0 Hz, 2H, H3'+H5'), 7.42 (d, J= 2.4 Hz, 1H, H5), 7.31-7.27 (m, 2H, H7 + H8), 7.17 (d, J= 8.4 Hz, 2H, H2'' + H6''), 7.15 (d, J= 9.2 Hz, 2H, H3''+H5''), 2.25 (s, 3H, Me)	4.28 (m, 1H)	3.70-3.47 (m, 2H)	8.90 (d, J= 12.0 Hz, 1H)	10.82 (d, J= 12.0 Hz, 1H)
2.87a' (minor)				7.91 (d, J= 8.0 Hz, 2H, H2' + H6'), 7.77 (d, J= 8.4 Hz, 2H, H2''+ H6''), 7.61 (t, J=7.6 Hz, 1H, H4'), 7.49 (t, J= 8.0 Hz, 2H, H3'+H5'), 7.41 (d, J= 2.4 Hz, 1H, H5), 7.31-7.27 (m, 2H, H7 + H8), 7.13 (d, J= 8.8 Hz, 2H, H3''+H5''), 2.26 (s, 3H, Me)	4.28 (m, 1H)	3.70-3.47 (m, 2H)	8.33 (d, J= 5.2 Hz, 1H)	10.27 (d, J= 5.2 Hz, 1H)

Table 95: ^{13}C NMR spectroscopic data obtained for amidines **2.87** (100 MHz, DMSO-d_6, δ ppm)

Compound	R^1	R^2	R^3	Ar(C2-8a)	Ar2(C1'-6')	Ar3(C2-8a)	C4	CH2	CN	CH	C=O
2.87a (major)	H	H	H	160.69 (C2), 149.74 (C8a), 129.51 (C5), 128.82 (C7), 124.65 (C6), 122.78 (C4a), 116.63 (C8), 74.02 (C3)	136.58 (C1'), 133.33 (C4'), 128.70 (C3' + C5'), 128.03 (C2' + C6')	139.17 (C1''), 128.18 (C3'' + C5''), 123.75 (C4''), 117.02 (C2'' + C6'')	32.30	45.99	119.61	151.13	197.53
2.87a (minor)				160.81 (C2), 149.62 (C8a), 129.51 (C5), 128.82 (C7), 124.73 (C6), 122.78 (C4a), 116.39 (C8), 74.71 (C3)	136.55 (C1'), 133.33 (C4'), 128.79 (C3' + C5'), 128.09 (C2' + C6')	138.87 (C1''), 127.94 (C3'' + C5''), 123.96 (C4''), 119.97 (C2'' + C6'')	31.99	45.99	119.51	148.65	197.53
2.87b (minor)	Br	H	H	160.46 (C2), 149.21 (C8a), 130.61 (C5), 130.92 (C7), 125.36 (C4a), 118.90 (C8), 116.11 (C6), 73.63 (C3)	136.51 (C1'), 133.44 (C4'), 128.73 (C3' + C5'), 128.04 (C2' + C6')	139.12 (C1''), 128.76 (C3'' + C5''), 123.96 (C4''), 117.10 (C2'' + C6'')	31.95	45.30	119.42	151.27	197.46
2.87b (major)				160.63 (C2), 149.11 (C8a), 130.46 (C5), 130.85 (C7), 125.36 (C4a), 118.64 (C8), 116.04(C6), 74.23 (C3)	136.51 (C1'), 133.44 (C4'), 128.73 (C3' + C5'), 128.04 (C2' + C6')	138.96 (C1''), 129.52 (C3'' + C5''), 123.84 (C4''), 120.04 (C2'' + C6'')	31.65	45.37	119.40	148.65	197.46
2.87c (major)	H	H	4-Me	160.86 (C2), 149.82 (C8a), 129.29 (C5), 128.28 (C7), 124.70 (C6), 122.85 (C4a), 116.69 (C8), 73.60 (C3)	136.61 (C1'), 133.44 (C4'), 128.79 (C3' + C5'), 128.09 (C2' + C6')	136.65 (C1''), 133.03 (C4''), 127.99 (C3'' + C5''), 117.02 (C2'' + C6''), 20.42 (Me)	32.30	46.05	119.80	151.16	197.65
2.87c (minor)				160.99 (C2), 149.71 (C8a), 129.29 (C5), 128.28 (C7), 124.70 (C6), 122.85 (C4a), 116.44 (C8), 74.34 (C3)	136.44 (C1'), 133.44 (C4'), 128.79 (C3' + C5'), 128.14 (C2' + C6')	136.71 (C1''), 133.19 (C4''), 129.99 (C3'' + C5''), 120.03 (C2'' + C6''), 20.52 (Me)	31.98	46.05	119.70	148.65	197.65

2.87f (major)	H	Cl	H	160.77 (C2), 149.77 (C8a), 128.27 (C7), 128.17 (C5), 124.71 (C6), 122.67 (C4a), 116.67 (C8), 73.90 (C3)	138.32 (C4'), 135.29 (C1'), 130.02 (C2' + C6'), 128.83 (C3' + C5')	139.18 (C1''), 129.55 (C3'' + C5''), 123.81 (C4''), 117.06 (C2'' + C6'')	32.31	46.05	119.63	151.20	196.68
2.87f (minor)				160.89 (C2), 149.66 (C8a), 128.27 (C7), 127.99 (C5), 124.80 (C6), 122.67 (C4a), 116.443(C8), 74.61 (C3)	138.32 (C4'), 135.26 (C1'), 130.02 (C2' + C6'), 128.83 (C3' + C5')	138.88 (C1''), 129.55 (C3'' + C5''), 124.02 (C4''), 120.01 (C2'' + C6'')	31.98	46.05	119.53	148.71	196.71
2.87g (major)	Br	H	4-Me	160.54 (C2), 149.11 (C8a), 130.88 (C7), 130.30 (C5), 125.19 (C4a), 118.78 (C8), 116.07 (C6), 72.92 (C3)	136.38 (C1'), 133.46 (C4'), 128.71 (C3' + C5'), 127.92 (C2' + C6')	136.34 (C1''), 133.32 (C4''), 129.91 (C3'' + C5''), 117.07 (C2'' + C6''), 20.42 (Me)	31.91	45.03	119.52	151.18	197.55
2.87g (minor)				160.65 (C2), 149.01 (C8a), 130.79 (C7), 130.44 (C5), 125.19 (C4a), 118.57 (C8), 115.96 (C6), 73.73 (C3)	136.41 (C1'), 133.46 (C4'), 128.71 (C3' + C5'), 127.92 (C2' + C6')	136.15 (C1''), 133.14 (C4''), 129.20 (C3'' + C5''), 119.95 (C2'' + C6''), 20.52 (Me)	31.61	45.03	119.44	148.47	197.52
2.87h (major)	Br	H	4-OMe	160.91 (C2), 149.38 (C8a), 130.99 (C7), 130.71 (C5), 125.54 (C4a), 118.76 (C8), 116.22 (C6), 72.74 (C3)	136.65 (C1'), 133.64 (C4'), 128.92 (C3' + C5'), 128.18 (C2' + C6')	156.30 (C4''), 132.35 (C1''), 118.99 (C2'' + C6''), 114.94 (C3'' + C5''), 55.52 (OMe)	32.13	45.42	119.81	151.61	197.72
2.87h (minor)				160.96 (C2), 149.28 (C8a), 131.07 (C7), 130.57 (C5), 125.54 (C4a), 118.76 (C8), 116.14 (C6), 73.55 (C3)	136.62 (C1'), 133.64 (C4'), 128.92 (C3' + C5'), 128.18 (C2' + C6')	155.92 (C4''), 132.30 (C1''), 121.60 (C2'' + C6''), 114.10 (C3'' + C5''), 55.41 (OMe)	31.86	45.42	119.72	148.37	197.70
2.87i (major)	Br	H	3-Me	160.91 (C2), 149.50 (C8a), 131.20 (C7), 130.84 (C5), 125.55 (C4a), 118.83 (C8), 116.40 (C6), 73.61 (C3)	136.72 (C1'), 133.89 (C4'), 129.13 (C3' + C5'), 128.32 (C2' + C6')	139.22 (C1''), 139.51 (C3''), 129.78 (C5''), 125.10 (C4''), 121.04 (C2''), 119.22 (C6''), 21.36 (Me)	32.30	45.36	119.80	151.61	197.93

2.87i (minor)	Br H 3-Me	160.85 (C2), 149.39 (C8a), 131.30 (C7), 130.69 (C5), 125.55 (C4a), 117.38 (C8), 116.47 (C6), 74.66 (C3)	136.77 (C1'), 133.89 (C4'), 129.13 (C3' + C5'), 128.32 (C2' + C6')	138.99 (C1''), 138.67 (C3''), 129.01 (C5''), 125.10 (C4''), 117.87 (C2''), 114.62 (C6''), 21.36 (Me)	31.95	45.36	119.88	148.83	197.98
2.87l (major)	Br H 4-Cl	160.38 (C2), 149.13 (C8a), 130.81 (C7), 130.59 (C5), 125.28 (C4a), 118.82 (C8), 116.12 (C6), 74.19 (C3)	136.46 (C1'), 133.39 (C4'), 128.67 (C3' + C5'), 128.00 (C2' + C6')	138.18 (C1''), 127.50 (C4''), 118.56 (C2'' + C6''), 128.59 (C3'' + C5'')	31.87	45.19	119.17	151.20	197.36
2.87l (minor)		160.18 (C2), 149.10 (C8a), 130.88 (C7), 130.44 (C5), 125.28 (C4a), 118.60 (C8), 116.02 (C6), 76.76 (C3)	136.46 (C1'), 133.39 (C4'), 128.67 (C3' + C5'), 128.00 (C2' + C6')	137.82 (C1''), 127.53 (C4''), 121.59 (C2'' + C6''), 129.28 (C3'' + C5'')	31.57	45.27	119.22	148.68	197.36
2.87n (major)	Br Me H	160.38 (C2), 149.19 (C8a), 130.85 (C7), 130.43 (C5), 125.41 (C4a), 118.84 (C8), 115.98 (C6), 73.69 (C3)	143.79 (C4'), 134.09 (C1'), 128.80 (C3' + C5'), 128.13 (C2' + C6')	139.08 (C1''), 129.22 (C3'' + C5''), 123.78 (C4''), 117.03 (C2'' + C6'')	31.96	45.18	119.36	151.21	196.88
2.87n (minor)		160.51 (C2), 149.05 (C8a), 130.78 (C7), 130.59 (C5), 125.41 (C4a), 118.60 (C8), 116.07 (C6), 74.41 (C3)	143.79 (C4'), 134.06 (C1'), 129.22 (C3' + C5'), 128.13 (C2' + C6')	138.80 (C1''), 129.48 (C3'' + C5''), 124.00 (C4''), 119.99 (C2'' + C6'')	31.68	45.18	119.26	149.05	196.88
2.87y (minor)	Br Cl 3-Br	160.09 (C2), 149.03 (C8a), 130.98 (C7), 130.45 (C5), 124.85 (C4a), 118.87 (C8), 116.19 (C6), 74.10 (C3)	138.42 (C4'), 134.96 (C1'), 129.86 (C2' + C6'), 128.78 (C3' + C5')	140.67 (C1''), 131.40 (C5''), 126.35 (C4''), 122.34 (C3''), 119.41 (C2''), 115.79 (C6'')	31.92	44.92	119.00	151.24	196.61
2.87y (major)		160.27 (C2), 148.90 (C8a), 130.88 (C7), 130.30 (C5), 124.85 (C4a), 118.55 (C8), 116.10 (C6), 75.09 (C3)	138.42 (C4'), 134.96 (C1'), 129.86 (C2' + C6'), 128.78 (C3' + C5')	140.06 (C1''), 130.68 (C5''), 126.65 (C4''), 121.76 (C3''), 122.40 (C2''), 118.67 (C6'')	31.61	44.92	119.22	148.85	196.61

2.87z (major)	Cl	H	H	160.88 (C2), 148.99 (C8a), 129.19 (C7), 128.52 (C6), 127.92 (C5), 125.36 (C4a), 118.77 (C8), 73.67 (C3)	136.73 (C1'), 133.83 (C4'), 129.08 (C3' + C5'), 128.37 (C2' + C6')	139.28 (C1''), 129.19 (C3'' + C5''), 124.48 (C4''), 117.40 (C2'' + C6'')	31.95	45.30	119.73	151.61	197.90
2.87z (minor)				160.98 (C2), 148.88 (C8a), 129.89 (C7), 128.44 (C6), 127.78 (C5), 125.08 (C4a), 118.52 (C8), 74.44 (C3)	136.69 (C1'), 133.83 (C4'), 129.08 (C3' + C5'), 128.37 (C2' + C6')	138.99 (C1''), 128.28 (C3'' + C5''), 124.27 (C4''), 120.32 (C2'' + C6'')	31.65	45.37	119.80	149.09	197.90
2.87a' (major)	Cl	H	4-Me	160.63 (C2), 148.81 (C8a), 128.20 (C6), 128.08 (C7), 127.62 (C5), 125.00 (C4a), 118.56 (C8), 73.15 (C3)	136.64 (C1'), 133.51 (C4'), 128.80 (C3' + C5'), 128.00 (C2' + C6')	136.53 (C4''), 133.11 (C1''), 129.99 (C3'' + C5''), 117.15 (C2'' + C6''), 20.43 (Me)	32.09	45.30	119.58	151.27	197.55
2.87a' (minor)				160.63 (C2), 148.70 (C8a), 128.20 (C6), 128.00 (C7), 127.77 (C5), 125.00 (C4a), 118.30 (C8), 73.91 (C3)	136.57 (C1'), 133.51 (C4'), 128.80 (C3' + C5'), 128.00 (C2' + C6')	136.38 (C4''), 133.29 (C1''), 129.30 (C3'' + C5''), 120.07 (C2'' + C6''), 20.53 (Me)	31.81	45.30	119.48	148.57	197.53

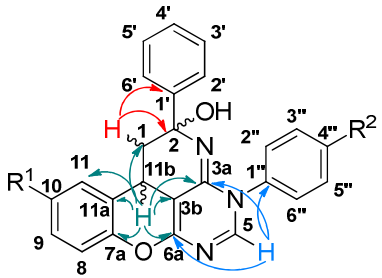


Table 96: ^{1}H NMR (400 MHz, DMSO-d_6, δ ppm) spectroscopic data obtained for compounds **2.88a-c**

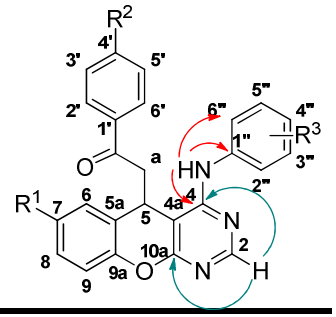
Compound	R^1	R^2	Ratio	Ar	OH	H1	H5	H11b
2.88a (major Isomer)				7.60 (d, J= 1.6 Hz, 1H, H11), 7.59 (d, J= 7.6 Hz, 2H, H2'' + H6''), 7.53-7.40 (m, 7H, H9, H11, H2'+H6', H4', H3'' + H5''), 7.24 (t, J= 7.6, 1H, H3' + H5'), 7.16 (t, J= 7.6, 1H, H4''), 7.12 (d, J= 8.8 Hz, 1H, H8)	5.79 (s, 1H)	2.72 (dd, J_1= 12.8, J_2= 4.8 Hz, 1H, Hα), 1.27 (t, J= 12.8 Hz, 1H, Hβ)	8.10 (s, 1H)	4.20 (dd, J_1= 12.8, 4.8 Hz, 1H)

2.88a (minor Isomer)	Br	H	4/1	7.60 (d, J= 1.6 Hz, 1H, H_{11}), 7.59 (d, J= 7.6 Hz, 2H, H2'' + H6''), 7.53-7.40 (m, 7H, H9, H11, H2'+H6', H4', H3'' + H5''), 7.32 (t, J= 7.6, 1H, H3' + H5'), 7.16 (t, J= 7.6, 1H, H4''), 7.07(d, J= 8.8 Hz, 1H, H8)	5.61 (s, 1H)	2.80 (dd, J_1= 12.4, J_2= 4.8 Hz, 1H, Hα), 1.76 (t, J= 12.4 Hz, 1H, Hβ)	8.04 (s, 1H)	3.30 (dd, J_1= 12.4, 4.8 Hz, 1H)
2.88b (major Isomer)	Br	Me	5/1	7.59 (d, J= 1.6 Hz, 1H, H11), 7.49 – 7.42 (m, 6H, H9, H2' + H6', H4', H2'' + H6''), 7.27 (t, J= 8.0 Hz, 2H, H3' + H5'), 7.28 (d, J= 8.0 Hz, 2H, H3'' + H5''), 7.11 (d, J= 8.8 Hz, 1H, H8), 2.33 (s, 3H, Me)	5.75 (d, J= 2.0 Hz, 1H)	2.71 (dd, J_1= 12.4, J_2= 4.8 Hz, 1H, Hα), 1.29 (dt, J_1= 12.8, J_2= 1.6 Hz, 1H, Hβ)	8.06 (s, 1H)	4.19 (dd, J_1= 12.4, 4.8 Hz, 1H)
2.88b (minor Isomer)				7.49 (d, J= 1.6 Hz, 1H, H11), 7.49 – 7.42 (m, 4H, H9, H2' + H6', H4'), 7.27 (t, J= 8.0 Hz, 2H, H3' + H5'), 7.28 (d, J= 8.0 Hz, 2H, H3'' + H5''), 7.23 (d, J= 7.6 Hz, 2H, H2'' + H6''), 7.11 (d, J= 8.8 Hz, 1H, H8), 2.32 (s, 3H, Me)	5.58 (s, 1H)	2.80 (dd, J_1= 12.4, 4.8 Hz, 1H, Hα), 1.76 (t, J= 12.4 Hz, 1H, Hβ)	8.00 (s, 1H)	3.43 (m, 1H)
2.88c (major Isomer)	H	Me	3/1	7.47-7.42 (m, 4H, H2'+H6', H2''+H6''), 7.37 (d, J= 8.0 Hz, 1H, H9), 7.34 -7.22 (m, 5H, H11, H3' + H5', H3'' + H5''), 7.19 – 7.08 (m, 3H, H8, H10, H4'), 2.33 (s, 3H, Me)	5.74 (d, J= 0.8 Hz, 1H)	2.64 (dd, J_1= 12.0, J_2= 4.8 Hz, 1H, Hα), 1.30 (dt, J_1= 12.0, J_2= 2.0 Hz, 1H, Hβ)	8.05 (d, J= 0.4 Hz, 1H)	4.18 (dd, J_1= 12.0, 4.8 Hz, 1H)
2.88c (minor Isomer)				7.47-7.42 (m, 8H, H3'+ H5', H4', H11, H2' + H6', H2''+ H6''), 7.34 - 7.22 (m, 3H, H9, H3'' + H5''), 7.19 – 7.08 (m, 2H, H8, H10), 2.32 (s, 3H, Me)	5.58 (s, 1H)	2.71 (dd, J_1= 12.4, 4.8 Hz, 1H, Hα), 1.76 (t, J= 12.8 Hz, 1H, Hβ)	7.99 (d, J= 0.8 Hz, 1H)	3.43 (m, 1H)

Table 97: ^{13}C NMR (100 MHz, DMSO-d_6, δ ppm) spectroscopic data for compounds **2.88a-c**

Compound	R^1	R^2	Ratio	C2-11a	Ar1	Ar2	C1	C5	C11b
2.88a (major Isomer)	Br	H	4/1	154.91 (C6a), 152.36 (C3a), 150.11 (C7a), 130.78 (C9), 129.16 (C11), 126.49 (C11a), 118.82 (C8), 116.66 (C10), 93.75 (C3b), 82.54 (C2)	149.26 (C1'), 127.27 (C3' + C5'), 126.38 (C4'), 125.79 (C2'+C6')	138.38 (C1''), 128.93 (C3''+ C5''), 128.43 (C4''), 127.73 (C2'' + C6'')	38.49	150.76	26.40
2.88a (minor Isomer)				154.81 (C6a), 152.86 (C3a), 150.18 (C7a), 130.93 (C9), 129.01 (C11), 126.48 (C11a), 120.12 (C8), 116.60 (C10), 93.42 (C3b), 85.50 (C2)	147.62 (C1'), 127.65 (C3' + C5'), 126.86 (C4'), 125.99 (C2'+C6')	138.53 (C1''), 128.93 (C3''+ C5''), 126.86 (C4''), 127.84 (C2'' + C6'')	38.56	151.07	27.41
2.88b (major Isomer)	Br	Me	5/1	154.90 (C6a), 152.41 (C3a), 150.11 (C7a), 130.77 (C9), 129.16 (C11), 126.46 (C11a), 118.81 (C8), 116.65 (C10), 95.66 (C3b), 82.56 (C2)	149.31 (C1'), 127.64 (C3' + C5'), 126.66 (C4'), 125.78 (C2'+C6')	137.96 (C4''), 135.85 (C1''), 129.34 (C3'' + C5''), 127.28 (C2'' + C6''), 20.61 (Me)	38.26	151.10	26.40
2.88b (minor Isomer)				154.82 (C6a), 152.41 (C3a), 150.23 (C7a), 130.92 (C9), 129.01 (C11), 126.46 (C11a), 118.81 (C8), 116.59 (C10), 93.35 (C3b), 85.48 (C2)	147.69 (C1'), 127.57 (C3' + C5'), 126.84 (C4'), 125.98 (C2'+C6')	138.05 (C4''), 135.97 (C1''), 129.60 (C3'' + C5''), 127.43 (C2'' + C6''), 20.61 (Me)	38.30	150.81	27.41
2.88c (major Isomer)	H	Me	3/1	155.11 (C6a), 152.62 (C3a), 149.51 (C7a), 127.98 (C9), 126.40 (C11), 124.84 (C10), 123.77 (C11a), 116.62 (C8), 94.00 (C3b), 82.62 (C2)	147.90 (C1'), 127.46 (C3' + C5'), 126.32 (C4'), 125.71 (C2'+C6')	137.91 (C4''), 135.90 (C1''), 129.34 (C3'' + C5''), 127.31 (C2'' + C6''), 20.61 (Me)	38.88	150.64	26.21
2.88c (minor Isomer)				155.03 (C6a), 152.62 (C3a), 150.94 (C7a), 127.67 (C9), 126.40 (C11), 123.77 (C11a), 116.62 (C8), 124.79 (C10), 93.68 (C3b), 85.50 (C2)	147.90 (C1'), 127.60 (C3' + C5'), 126.84 (C4'), 125.88 (C2'+ C6')	138.00 (C4''), 135.18 (C1''), 129.59 (C3'' + C5''), 127.02 (C2'' + C6''), 20.61 (Me)	38.88	150.78	27.21

Table 98: ^{1}H NMR (400 MHz, DMSO-d_6, δ ppm) spectroscopic data for chromenopyridines **2.89**



Compound	R^1	R^2	R^3	H6-9	H2'-6'	H2''-6''	NH	H2	H5	Ha
2.89a	Br	H	H	7.66 (d, J= 2.4 Hz, 1H, H6), 7.41 (dd, J_1= 8.4, J_2= 2.4 Hz, 1H, H8), 7.12 (d, J= 8.4 Hz, 1H, H9)	7.79 (d, J= 7.6 Hz, 2H, H2' + H6'), 7.55 (t, J= 7.6 Hz, 1H, H4'), 7.41 (t, J= 7.2 Hz, 2H, H3' + H5')	7.55 (d, J= 7.6 Hz, 2H, H2'' + H6''), 7.31 (t, J= 7.6 Hz, 2H, H3'' + H5''), 7.05 (t, J= 7.2 Hz, 1H, H4'')	8.96 (s, 1H)	8.22 (s, 1H)	5.06 (t, J= 4.8 Hz, 1H)	3.59 (m, 2H)
2.89b	H	H	H	7.45 (d, J= 7.2 Hz, 1H, H9), 7.26 (dt, J_1= 7.6, J_2= 1.6 Hz, 1H, H7), 7.14 (dd, J_1= 8.0, J_2= 1.2 Hz, 1H, H6), 7.16 (t, J= 8.0 Hz, 1H, H8)	7.75 (dd, J_1= 8.4, J_2= 1.2 Hz, 2H, H2' + H6'), 7.53 (t, J= 8.0 Hz, 1H, H4'), 7.38 (t, J= 7.6 Hz, 2H, H3' + H5')	7.54 (d, J= 7.6 Hz, 2H, H2'' + H6''), 7.31 (t, J= 7.6 Hz, 2H, H3'' + H5''), 7.05 (t, J= 7.6 Hz, 1H, H4'')	8.87 (s, 1H)	8.22 (s, 1H)	5.04 (t, J= 5.2 Hz, 1H)	3.51 (m, 2H)
2.89c	Br	H	4-Me	7.66 (d, J= 2.0 Hz, 1H, H6), 7.41 (dd, J_1= 8.8, J_2= 2.0 Hz, 1H, H8), 7.11 (d, J= 8.8 Hz, 1H, H9)	7.80 (dd, J_1= 8.0, J_2= 1.2 Hz, 2H, H2' + H6'), 7.56 (t, J= 7.6 Hz, 1H, H4'), 7.42 (t, J= 7.6 Hz, 2H, H3' + H5')	7.41 (d, J= 8.0 Hz, 2H, H2'' + H6''), 7.11 (d, J= 8.8 Hz, 2H, H3'' + H5''), 2.07 (s, 3H, Me)	8.23 (s, 1H)	8.19 (s, 1H)	4.96 (s, 1H)	3.61 (s, 2H)
2.89d	Br	Me	H	7.65 (d, J= 2.0 Hz, 1H, H6), 7.43 (dd, J_1= 8.8, J_2= 2.4 Hz, 1H, H8), 7.13 (d, J= 8.8 Hz, 1H, H9)	7.71 (d, J= 8.0 Hz, 2H, H2' + H6'), 7.20 (d, J= 8.0 Hz, 2H, H3' + H5'), 2.31 (s, 3H, Me)	7.55 (d, J= 7.6 Hz, 2H, H2'' + H6''), 7.31 (t, J= 8.0 Hz, 2H, H3'' + H5''),	8.89 (s, 1H)	8.22 (s, 1H)	4.99 (s, 1H)	3.58 (s, 2H)

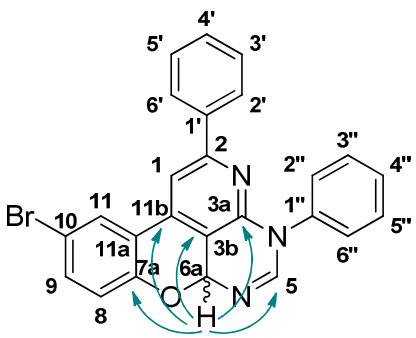
						7.05 (t, J= 7.6 Hz, 1H, H4'')				
2.89h	Br	Br	4-CN	7.68 (d, J= 2.4 Hz, 1H, H6), 7.44 (dd, J_1= 8.4, J_2= 2.4 Hz, 1H, H8), 7.14 (d, J= 8.8 Hz, 1H, H9)	7.68 (d, J= 7.2 Hz, 2H, H2' + H6'), 7.58 (dd, J_1= 8.8, J_2= 2.0 Hz, 2H, H3' + H5')	7.75 (dd, J_1= 7.2, J_2= 2.0 Hz, 2H, H3'' + H5''), 7.70 (d, J= 8.4 Hz, 2H, H2'' + H6'')	9.21 (s, 1H)	8.35 (s, 1H)	5.04 (t, J= 5.6 Hz 1H)	3.59 and 3.47 (dd, J_1= 17.2, J_2= 5.6 Hz, 2H)
2.89j	Cl	H	H	7.80 (d, J= 7.6 Hz, 2H, H2' + H6'), 7.57-7.54 (m, 4H, H6, H4', H2'' + H6''), 7.40 (t, J= 7.6 Hz, 2H, H3' + H5'), 7.32 (t, J= 7.2 Hz, 2H, H3'' + H5''), 7.29 (dd, J_1= 8.8, J_2= 2.4 Hz, 1H, H8), 7.18 (d, J= 8.4 Hz, 1H, H9), 7.05 (t, J= 7.6 Hz, 1H, H4'')			8.91 (s, 1H)	8.22 (s, 1H)	5.00 (s, 1H)	3.62 (m, 2H)
2.89k	Cl	H	4-Me	7.40 (d, J= 1.6 Hz, 1H, H6), 7.30 (dd, J_1= 8.4, J_2= 2.0 Hz, 1H, H8), 7.17 (d, J= 8.8 Hz, 1H, H9)	7.81 (d, J= 7.6 Hz, 2H, H2' + H6'), 7.53 (t, J= 8.0 Hz, 2H, H3' + H5'), 7.42 (t, J= 7.6 Hz, 1H, H4')	7.40 (d, J= 7.6 Hz, 2H, H2'' + H6''), 7.11 (d, J= 8.0 Hz, 2H, H3'' + H5''), 2.26 (s, 3H, Me)	8.83 (s, 1H)	8.19 (s, 1H)	4.97 (s, 1H)	3.63 (s, 2H)

Table 99: ^{13}C NMR (100 MHz, DMSO-d_6, δ ppm) spectroscopic data for compounds **2.89**

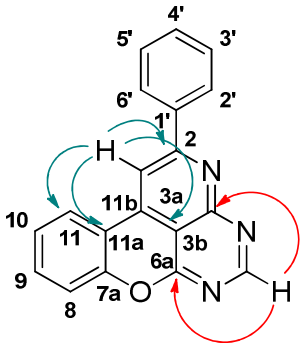
Compound	R^1	R^2	R^3	C4-10a	C1'-6'	H1''-6''	C=O	C2	C5	Ca
2.89a	Br	H	H	163.53 (C10a), 158.80 (C4), 150.02 (C9a), 131.42 (C6), 131.00 (C8), 126.85 (C5a), 118.64 (C9), 115.70 (C7), 97.53 (C4a)	136.38 (C1'), 133.38 (C4'), 128.58 (C3' + C5'), 127.95 (C2' + C6')	139.42 (C1''), 128.32 (C3'' + C5''), 123.30 (C4''), 122.29 (C2'' + C6'')	197.91	155.87	28.69	44.18
2.89b	H	H	H	163.91 (C10a), 158.93 (C4), 150.68 (C9a), 129.03 (C6), 128.44 (C8), 124.54 (C7), 124.41 (C5a), 116.52 (C9), 98.18 (C4a)	136.58 (C1'), 133.46 (C4'), 128.70 (C3' + C5'), 128.02 (C2' + C6')	139.59 (C1''), 128.49 (C3'' + C5''), 123.38 (C4''), 122.24 (C2'' + C6'')	198.16	155.90	29.05	44.70

2.89c	Br	H	4-Me	163.36 (C10a), 158.84 (C4), 150.00 (C9a), 131.42 (C6), 130.94 (C8), 126.85 (C5a), 118.60 (C9), 115.61 (C7), 97.15 (C4a)	136.36 (C1'), 133.31 (C4'), 128.53 (C3' + C5'), 127.90 (C2' + C6')	136.73 (C1''), 132.39 (C4''), 128.72 (C3'' + C5''), 122.50 (C2'' + C6''), 20.45 (Me)	197.87	155.84	28.61	44.15
2.89d	Br	Me	H	163.47 (C10a), 158.76 (C4), 149.99 (C9a), 131.42 (C6), 130.95 (C8), 126.98 (C5a), 118.64 (C9), 115.66 (C7), 97.65 (C4a)	143.74 (C1'), 133.96 (C4'), 129.08 (C3' + C5'), 128.06 (C2' + C6'), 21.05 (Me)	139.48 (C1''), 128.30 (C3'' + C5''), 123.33 (C4''), 122.22 (C2'' + C6'')	197.26	155.83	28.64	44.33
2.89h	Br	Br	4-CN	164.08 (C10a), 158.19 (C4), 149.90 (C9a), 131.48 (C6), 131.29 (C8), 126.62 (C5a), 118.83 (C9), 116.07 (C7), 99.35 (C4a)	135.28 (C4'), 127.66 (C1'), 131.67 (C3' + C5'), 130.08 (C2' + C6')	144.13 (C1''), 132.81 (C3'' + C5''), 121.04 (C2'' + C6''), 104.15 (C4''), 119.42 (CN)	197.08	155.93	28.85	44.73
2.89j	Cl	H	H	163.53 (C10a), 158.87 (C4), 149.54 (C9a), 128.55 (C6), 128.12 (C8), 127.77 (C7), 126.40 (C5a), 118.28 (C9), 97.47 (C4a)	136.38 (C1'), 133.33 (C4'), 128.55 (C3' + C5'), 127.93 (C2' + C6')	139.43 (C1''), 128.31 (C3'' + C5''), 123.29 (C4''), 122.29 (C2'' + C6'')	197.84	155.87	28.74	44.26
2.89k	Cl	H	4-Me	163.41 (C10a), 158.85 (C4), 149.55 (C9a), 128.53 (C6), 128.07 (C8), 127.69 (C7), 126.42 (C5a), 118.22 (C9), 97.12 (C4a)	136.78 (C1'), 132.37 (C4'), 128.53 (C3' + C5'), 127.90 (C2' + C6')	136.40 (C1''), 133.29 (C4''), 128.72 (C3'' + C5''), 122.50 (C2'' + C6''). 20.46 (Me)	197.80	155.86	28.71	44.18

Table 100: ^{1}H NMR (400 MHz, DMSO-d_6, δ ppm) and ^{13}C NMR (100 MHz, DMSO-d_6, δ ppm) spectroscopic data obtained for compounds **2.90** and **2.10**



2.90



2.105

Compound	NMR	H2-11b	H2'-6'	H2''-6''	H1	H5	NH
2.90	**^{1}H**	8.52 (d, *J*= 2.4 Hz, 1H, H11), 7.59 (dd, J_1= 8.4, J_2= 2.4 Hz, 1H, H9), 7.13 (d, *J*= 8.4 Hz, 1H, H8), 6.79 (d, *J*= 2.0 Hz, 1H, H6a)	8.01 (dd, J_1= 8.0, J_2= 2.8 Hz, 2H, H2' + H6'), 7.57-7.56 (m, 5H, H3' + H5', H2'' + H6'', H4''), 7.46 (t, *J*= 7.6 Hz, 1H, H4''), 7.40 (dd, J_1= 6.8, J_2= 1.6 Hz, 2H, H2'' + H6'')		8.31 (s, 1H)	7.34 (d, *J*= 2.0 Hz)	-
		C2-C11B	**C1'-C6'**	**C1''-C6''**	**C1**	**C5**	
	^{13}C	155.40 (C2), 153.59 (C7a), 146.41 (C3a),138.19 (C11b), 134.66 (C9), 127.70 or 127.77 (C11), 122.35 (C11a), 120.32 (C8), 114.27 (C10), 103.61 (C3b), 82.79 (C6a)	137.80 (C1'), 129.51 (C4'), 128.55 (C3' + C5'), 126.66 (C2' + C6')	138.31 (C1'), 129.11 (C4'), 127.70 or 127.74 (C3' + C5'), 127.34 (C2' + C6')	109.58	145.87	-
2.105		**H2-11b**	**H2'-6'**	**H2''-6''**	**H1**	**H5**	**NH**
	^{1}H	8.78 dd, J_1= 8.0, J_2= 1.2 Hz, 1H, H11), 7.77 (dt, J_1= 7.2, J_2= 1.6 Hz, 1H, H9), 7.66 (dd, J_1= 8.4, J_2= 1.2 Hz, 1H, H9), 7.58 (dt, J_1= 8.4, J_2= 1.2 Hz, 1H, $H1_0$)	8.46 (dd, J_1= 8.0, J_2= 2.4 Hz, 2H, H2' + H6'), 7.63-7.61 (m, 3H, H3' + H5', H4')	-	8.81 (s, 1H)	8.73 (s, 1H)	-
		C2-C11B	**C1'-C6'**	**C1''-C6''**	**C1**	**C5**	

	^{13}C	164.74 (C6a), 164.20 (C2), 159.93 (C3a), 151.67 (C7a), 139.11 (C11b), 133.66 (C9), 125.75 (C10), 125.64 (C11), 118.47 (C8), 118.25 (C11a), 106.14 (C3b)	137.88 (C1'), 131.06 (C4'), 128.98 (C3 + C5'), 128.14 (C2' + C6')	-		109.14	159.22	-

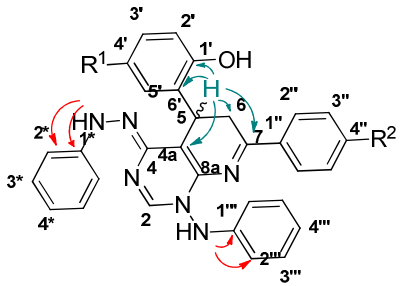


Table 101: ^{1}H NMR (400 MHz, DMSO-d_6, δ ppm) and ^{13}C NMR (100 MHz, DMSO-d_6, δ ppm) spectroscopic data obtained for compounds **2.100a,b**

Compound		**R^1**	**R^2**	**H1'-6'**	**H1''-6''**	**H1'''-6'''**	**H1*-6***	**H2-H6**	**NH**	**(C4)NNH**	**OH**
2.100a	**^{1}H**	Br	H	7.29 (dd, J_1= 8.4, J_2= 2.0 Hz, 1H, H3'), 7.09 (d, J= 8.8 Hz, 1H, H2'), 6.85 (s, 1H, H5')	7.45 (dd, J_1= 7.6, J_2= 1.2 Hz, 2H, H2'' + H6''), 7.26 (t, J= 8.4 Hz, 2H, H3''' + H5'''), 7.22-7.15 (m, 8H, H3'' + H5'', H4'', H2* + H6*, H3* + H5*, OH), 6.91 (t, J= 7.2 Hz, 1H, H4'''), 6.75 (d, J= 8.0 Hz, 2H, H2'''+ H6'''), 6.72 (dt, J_1= 6.4, J_2= 2.0 Hz, 1H, H4*)			8.15 (s, 1H, H2), 4.36 (d, J= 10.4 Hz, 1H, H5), 3.23 (d, J= 13.2 Hz, 1H, H6α) , 3.04 (dd, J_1= 10.8, J_2= 14.0 Hz, 1H, H6β)	9.51 (s, 1H)	11.11 (s, 1H)	Not seen
		R^1	**R^2**	**C1'-6'**	**C1''-6''**	**C1'''-6'''**	**C1*-6***	**C4a-8a**	**C2-C6**		
	^{13}C	Br	H	149.02 (C1'), 132.30 (C5'), 131.28 (C3'), 124.63 (C6'), 119.01 (C2'), 116.10 (C4')	139.39 (C1''), 128.40 (C3'' + C5''), 127.49 (C4''), 125.42 (C2'' + C6'')	145.86 (C1'''), 129.87 (C3''' + C5'''), 121.60 (C4'''), 113.26 (C2''' + C6''')	145.96 (C1*), 129.39 (C3* + C5*), 119.44 (C4*), 112.82 (C2* + C6*)	153.38 (C8a), 139.01 (C7), 100.20 (C4a)	152.65 (C2), 156.13 (C4), 30.63 (C5), 32.54 (C6)		

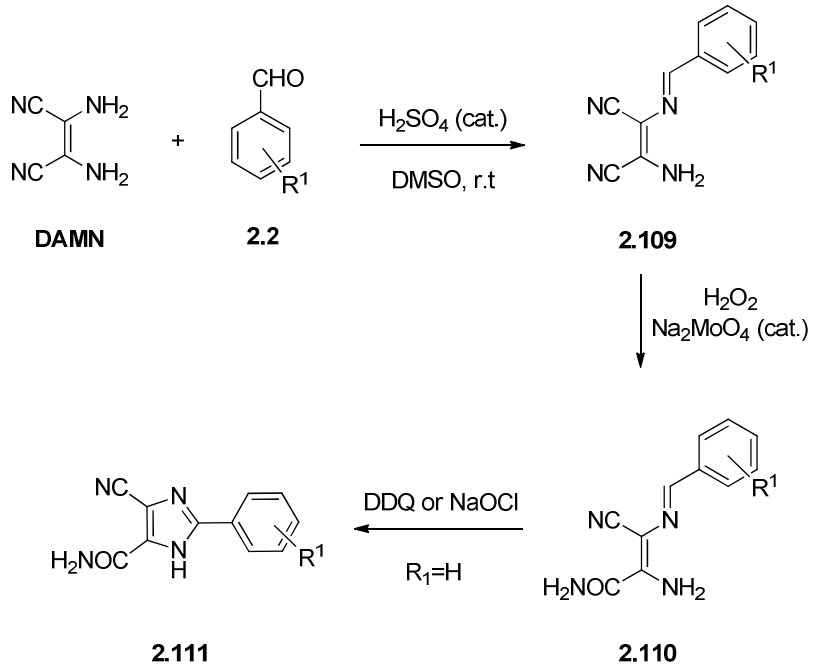
		R^1	R^2	H1'-6'	H1''-6''	H1'''-6'''	H1*-6*	H2, H5, H6	NH	(C4)NNH	OH
2.100b	^{1}H	Br	Me	7.33 (dd, J_1= 8.8, J_2= 2.0 Hz, 1H, H3'), 7.21 (m, 1H, OH), 7.13 (d, J= 8.8 Hz, 1H, H2'), 6.85 (s, 1H, H5')	7.38 (d, J= 8.0 Hz, 2H, H2'' + H6''), 7.02 (d, J= 8.8 Hz, 2H, H3''' + H5'''), 2.25 (s, 3H, Me)	7.27 (t, J= 7.2 Hz, 2H, H3''' + H5'''), 6.93 (t, J= 7.6 Hz, 2H, H4'''), 6.75 (d, J= 8.4 Hz, 2H, H2''' + H6''')	7.21 (dd, J_1= 8.0, J_2= 2.8 Hz, 2H, H2* + H6*), 7.13 (t, J= 8.0 Hz, 2H, H3* + H5*), 6.73 (t, J= 6.8 Hz, 2H, H4*)	8.21 (s, 1H, H2), 4.36 (d, J= 10.4 Hz, 1H, H5), 3.22 (d, J= 13.6 Hz, 1H, H6α), 3.03 (dd, J_1= 10.8, J_2= 13.6 Hz, 1H, H6β)	9.35 (s, 1H)	11.09 (s, 1H)	Not seen
		R^1	R^2	C1'-6'	C1''-6''	C1'''-6'''	C1*-6*	C4a-8a	C2-C6		
	^{13}C	Br	Me	148.77 (C1'), 132.13 (C5'), 130.90 (C3'), 124.39 (C6'), 118.63 (C2'), 115.79 (C4')	136.37 (C4''), 136.06 (C1''), 128.67 (C3'' + C5''), 125.15 (C2'' + C6''), 20.71 (Me)	145.56 (C1'''), 129.58 (C3''' + C5'''), 121.20 (C4'''), 112.99 (C2''' + C6''')	145.83 (C1*), 129.02 (C3* + C5*), 118.83 (C4*), 112.44 (C2* + C6*)	153.06 (C8a), 139.19 (C7), 99.99 (C4a)	152.47 (C2), 155.85 (C4), 30.38 (C5), 32.36 (C6)		

2.2. 2-Substituted 1*H*-imidazole-4-carboxamides

2.1.1 Synthesis of 2-substituted-5-cyano-1-(2-hydroxyaryl)-1*H*-imidazole-4-carboxamides

Diaminomaleonitrile as a precursor for substituted imidazoles and pyrazines

Diaminomaleonitrile (DAMN) is a tetramer of HCN with a central alkene unit substituted by two amino groups and two nitrile groups. It is generated through polymerization of hydrogen cyanide, and it was first identified by Webb *et al*[141] and Bredereck *et al*[142]. There is a large number of publications in which DAMN is used as the starting material for the preparation of diverse heterocyclic with a wide scope of applications[143–145]. Good exemples of these heterocyclic compounds are pyrazines[146–149], pyrimidines[145], adenines[145,150], purines[145,151], azepines[152], pyrroles[144] and imidazoles[143,153]. In 1979 Ohtsuka reported the preparation of different heterocycles based on DAMN[147] (**scheme 52**).

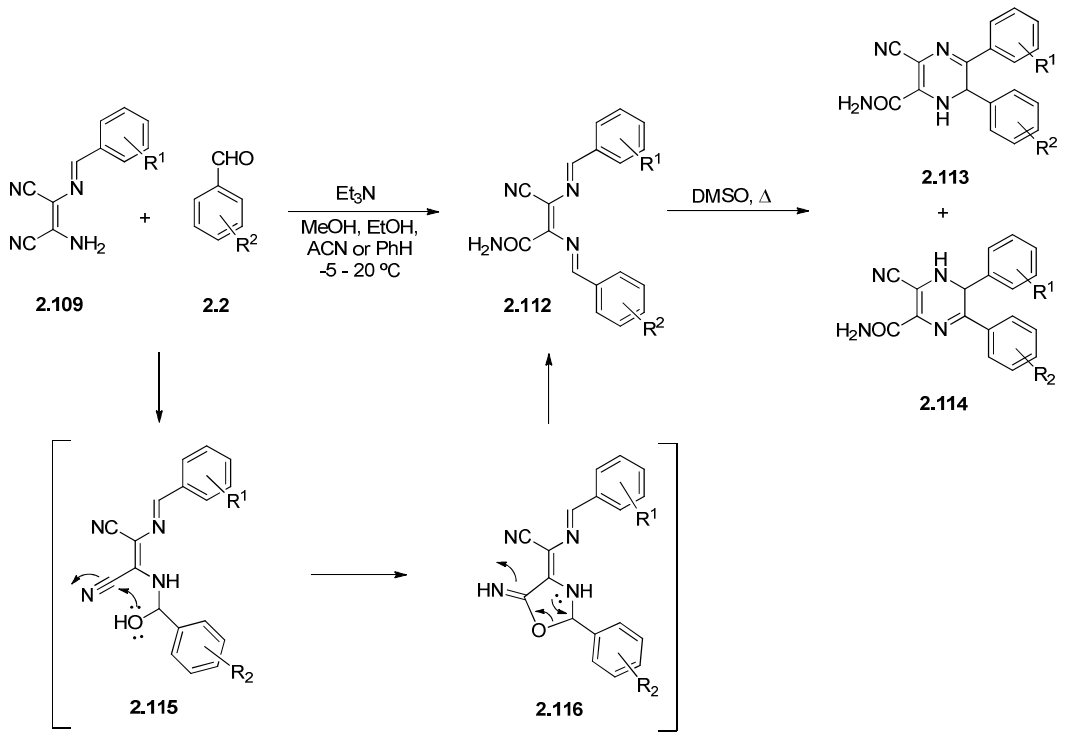


Scheme 52: Synthesis of imidazoles **2.111** from **DAMN**, as proposed by Ohtsuka *et al* [adapted from ref.147]

The Ohtsuka's approach involves three steps[147]: (i) first, the acid-catalysed reaction between diverse benzaldehydes and DAMN in DMSO to afford the Schiff base **2.109**; (ii) second, the treatment with hydrogen peroxide in the presence of a catalytic amount of Na_2MoO_4[147] to give

selectively the amide **2.110**; and (iii) finally, oxidation with dichlorodicyanobenzoquinone (DDQ) or NaOCl provides 4(5)-cyano-2-phenylimidazole-5(4)-carboxamides **2.111**.

In a later publication[148], this approach was further expanded to the synthesis of other heterocyclic compounds, particularly dihydropyrazines (**Scheme 53**). The process starts with the preparation of imines **2.109** by a similar reaction sequence as the one used in the previous publication (**Scheme 52**). Then, imines **2.109** are treated with a second benzaldehyde in basic conditions to yield diimines **2.112** in good to high yield as both a symmetrical or unsymmetrical structure. An amide group is formed when the second aromatic aldehyde is condensed under the reaction conditions that were used (triethylamine, room temperature, ethanol/acetonitrile/benzene). This was explained by an intramolecular nucleophilic addition of the hydroxyl group in the first carbonyl adduct, intermediate **2.115**, to the neighbour nitrile group, followed by ring-opening process of the obtained intermediate **2.116**.



Scheme 53: Preparation of dihydropyrazines **2.113** and **2.114** from imines **2.109**, as proposed by Ohtsuka *et al* [adapted from ref.148]

The authors refer that diimines **2.112** have marginal stabilities, and that they readily undergo intramolecular cyclization to generate the corresponding dihydropyridines **2.113** and **2.114**, which was observed during the attempts to perform purification processes by recrystallization (**Scheme 53**). Dihydropyridines **2.113** and **2.114** are easily obtained with high

yields by heating diimines **2.109** in DMSO for short periods of time (around 10 min). This methodology allowed the preparation of two distinct dihydropyridine isomers, **2.113** and **2.114** that proved to have distinct physical, chemical and spectroscopic properties, such as different melting points, solubilities in several organic solvents, and distinct reactivity with, for example, isocyanates.

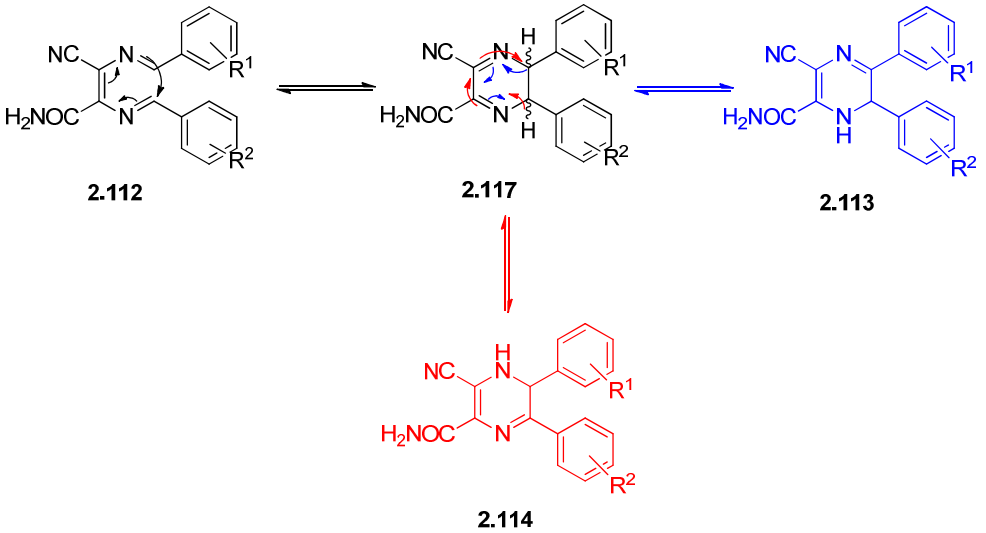
To explain this observation, the authors suggested that the cyclization reaction is substituent-directed, in order to ideally generate the «compound in which the more negatively charged substituent is located at the "methine" carbon in the dihydropyrazine ring»[148]. When both substituents are similar in terms of electronic effect, a mixture of dihydropyrazines **2.113** and **2.114** are obtained. The reaction of imine **2.109** with 4-chlorobenzaldehyde was considered a borderline case, giving a 6:4 ratio of **2.113:2.114**.

Another important aspect in the aforementioned work is that no condensation reaction between imines **2.109** and benzaldehydes containing electron-donating substituents in the *para* position (Et_2N or Me_2N) was observed, as well as between imines **2.109** containing aromatic moieties substituted with electron-withdrawing groups at the *para* position (NO_2 or CN). This was consistent with the theorical prediction that the NH_2 group of DAMN has to have the adequate nucleophilicity to react with aromatic aldehydes, in order to generate compounds **2.112**.

The formation of imines **2.112**, without intramolecular hydrolysis of the cyano group occurs at higher temperatures[154]. Thus, it was suggested that compounds **2.117** could be synthetized at low reaction temperatures because the aldehyde condensation step (which is referred by the authors as the rate-limiting step[148,155]) is favoured by the intramolecular hydrolysis the α-cyano group.

The mechanistic explanation for the formation of dihydropyrazines was also discussed in this work[148]. According to the authors, this process is an example of the diaza-Cope rearrangement[148,156], which is a [3+3]sigmatropic rearrangement, in which the final steps leading to the formation of 1,6-dihidropyrazines **2.113** or **2.114** would be a substituent-driven processes[157] (**Scheme 54**). The authors suggest that «the driving factors may be the stability of the β-cyano-acrylamide partial structure and the increase of conjugation with the aromatic substituent»[148], since no significant solvent effect was observed when the cyclization of **2.112** (R^1=R^2= Ph) was carried out in several polar solvents (MeOH, ACN, $MeNO_2$, acetone, and DMF)[148]. Another important phenomenon that was detailed in this publication was that the isomerisation between *cis* and *trans* forms of compounds **2.112**, was challenging. It is referred that all the

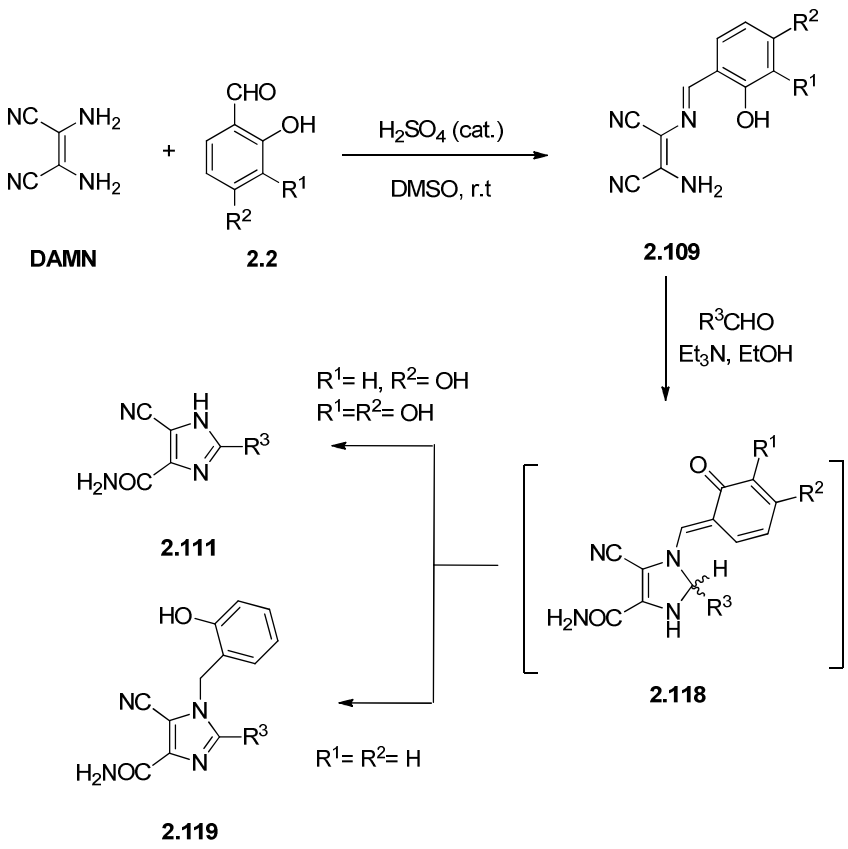
attempts to promote a conversion from the *cis* to *trans* form failed because the diaza-Cope rearrangement occurred first, and thus compounds **2.113** and **2.114** were obtained[148].



Scheme 54: Plausible mechanism for the formation of both 1,6-dihydropyrazines **2.113** and **2.114** [adapted from ref.148]

In a previously published PhD thesis[158], a series of novel imidazoles **2.111** or **2.119** have been prepared from imines **2.109**, which were obtained as previously described (**Scheme 55**). The reaction of imines **2.109** with several benzaldehydes in the presence of Et_3N at room temperature afforded imidazoles **2.111** or **2.119** depending on the type of substituents present on the starting material. Based on the results obtained, the formation of the intermediate **2.118**, resulting from the selective nucleophilic attack of N1 to the sp^2 carbon of the other imine group, as was observed experimentally, was proposed.

The present work was an attempt to make use of the vast experience in our research group on generating new heterocyclic structures from DAMN[123,125–127,129,151,158],expanding it using the reaction with other aldehydes, as well as to investigate the reaction mechanism that leads to the formation of imidazoles **2.119**, inclusively in the presence of other hydroxylated aromatic aldehydes besides the ones used in the literature[158].



Scheme 55: Reaction mechanism for the synthesis of compounds **2.111** and **2.119** from imines **2.109** [adapted from ref. 158]

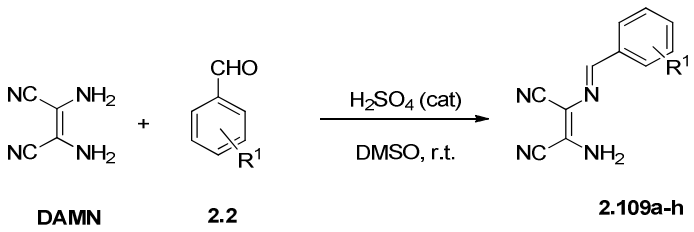
In this section, a set of milestones were defined:

1) Explore the reactivity of compounds **2.109** with different substituents in the aromatic ring, as well as the mechanistic aspects involving the preparation of imidazoles **2.119**, combining synthetic and computational tools.
2) Evaluate the biological activity of these new compounds against triple-negative breast cancer, *P. falciparum* and virulent *M. tuberculosis* strains.

Synthesis and reactivity of 2-amino-3-(arylideneamino)maleonitriles with aldehydes

The reaction between DAMN and substituted benzaldehydes **2.2** (R^1= H) was performed as previously described by Ohtsuka *et al*[146–148] in DMSO at room temperature and in the presence of a catalytic amount of H_2SO_4. This rapidly afforded imines **2.109** in an almost quantitative yield (**Table 102**).

Table 102: Reaction conditions and reagents used for the preparation of eneimines **2.109a-h** from aldehydes **2.2** and DAMN



Entry	R^1	time (min)	η (%)	Entry	R^1	time (min)	η (%)
2.109a	2-OH	3	97	**2.109e**	3-Cl	5	95
2.109b	2-OH, 5-Br	5	90	**2.109f**	4-F	6	81
2.109c	2-OH, 3-OMe	3	98	**2.109g**	4-OH	3	83
2.109d	3-OH	3	83	**2.109h**	2-OMe	5	90

The ^{1}H and ^{13}C NMR spectra of compound **2.109a** are presented in **Figures 78** and **79** as an example. The ^{1}H NMR of this compound shows three characteristic singlets at δ 10.42 ppm (OH), δ 8.58 ppm (H1') and δ7 .83 ppm (NH_2), while the signal δ 152 ppm corresponding toe the imine carbon is the most relevant in the ^{13}C NMR spectra.

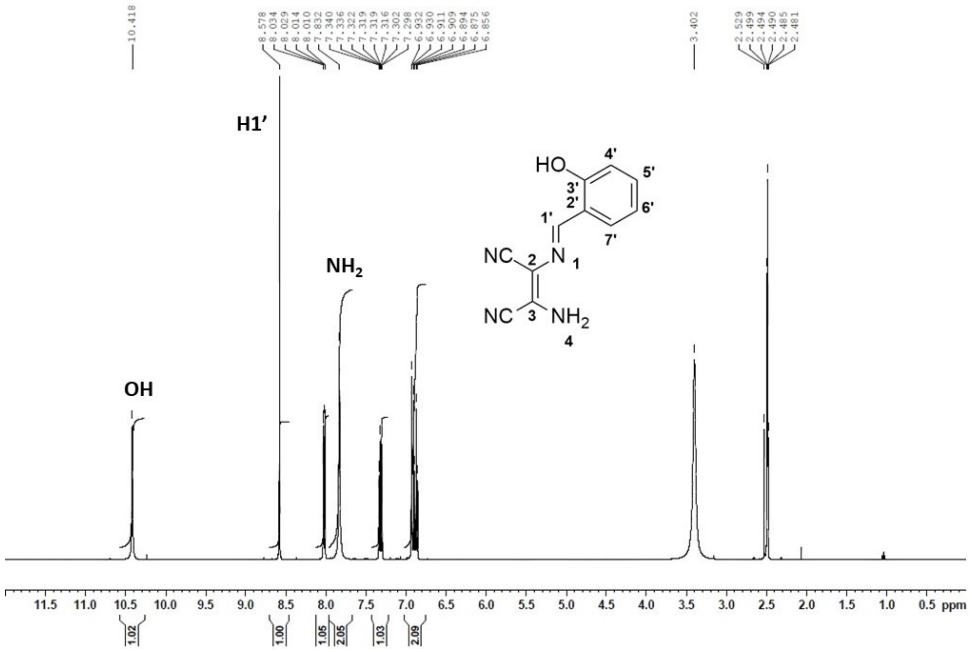


Figure 78: ^{1}H NMR (400 MHz, DMSO-d_6, δ ppm) spectrum for compound **2.109a**

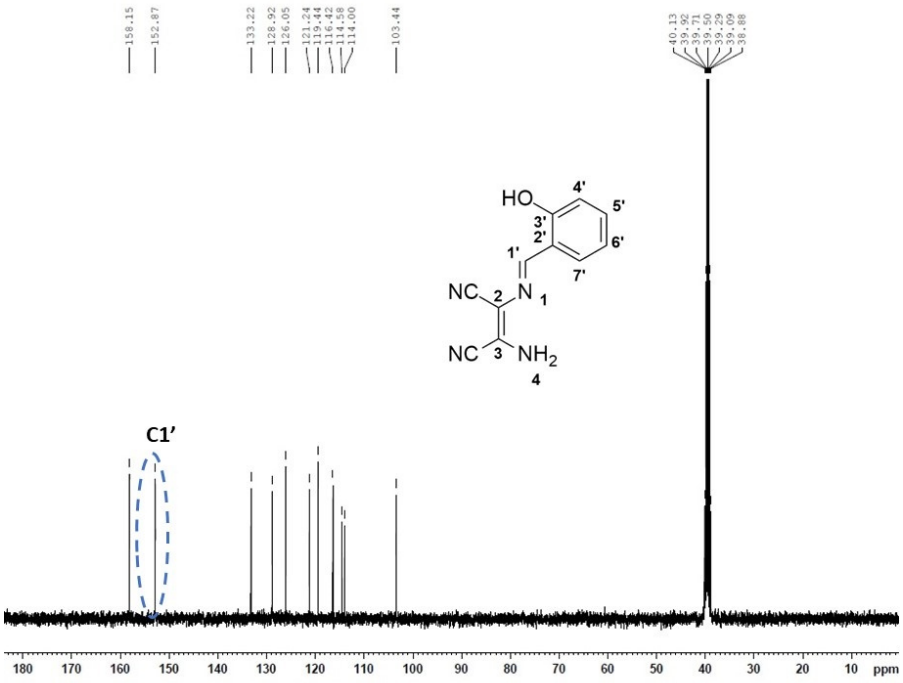
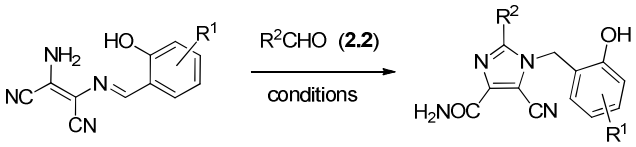


Figure 79: ^{13}C NMR (100 MHz, DMSO-d_6, δ ppm) spectrum for compound **2.114a**

Compounds **2.109** were used as starting material for the preparation of imidazoles **2.119**, using similar reaction conditions than those previously reported in the literature (Et_3N, EtOH, r.t.)[158]. The results obtained in the reactions with different benzaldehydes with a 2-hydroxyl substituent, as well as the reaction conditions used, are described in **Table 103**. When the reaction involved **2.109a** as starting material, for almost all the benzaldehydes (except for salicylaldehyde, entries 2 and 3 - **Table 103**), compound **2.119** could be isolated in good to moderate yield. Using **2.109b** as starting material did not afford the desired product **2.119**, even when the reaction was performed under heating conditions (entry 13) or in the presence of different base catalysts (Et_3N, entry 14; DBU, entry 15; NMP, entry 16). This indicates that the introduction of an electron-withdrawing substituent into the aromatic ring of Schiff base **2.109** drastically changes its reactivity towards the formation of imidazoles **2.119**.

Table 103: Experimental conditions and results obtained for the reaction of **2.109a,b** with different aldehydes **2.2**



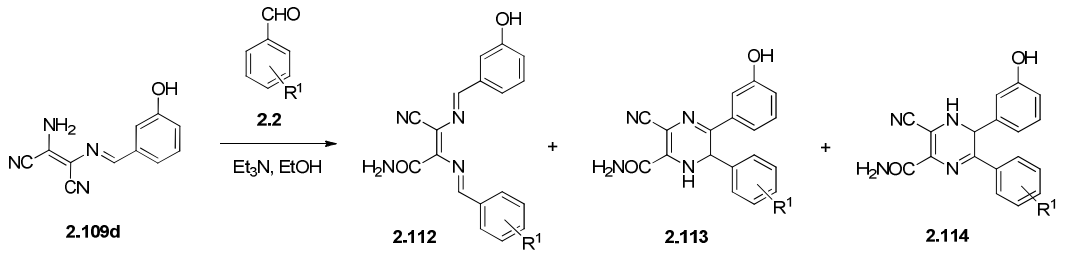
2.109a (R^1= H)
2.109b (R^1= 5-Br)

2.119

Entry	2.109	2.2		base	equiv.	solvent	T	t (h)	results	η (%)
	R^1	R^2	equiv.							
1	H	C_6H_5	1.5	Et_3N	2	EtOH	r.t.	16	**2.119a**	26
2	H	2-OHC_6H_4	1.2	Et_3N	5	EtOH	0 r.t.	15 168	complex mixture	-
3	H	2-OHC_6H_4	1.2	Et_3N	2	EtOH	60 r.t	6.5 16	complex mixture	-
4	H	2-ClC_6H_4	1.2	Et_3N	2	EtOH	60 r.t	6.5 16	**2.119b**	49
5	H	2-ClC_6H_4	1.2	Et_3N	2	EtOH	r.t.	16.5	**2.119b**	42
6	H	2-ClC_6H_4	1.2	Et_3N	2	EtOAc	r.t.	15.5	**2.119b**	43
7	H	3-ClC_6H_4	1.2	Et_3N	2	EtOH	r.t.	26	**2.119c**	74
8	H	2,5-ClC_6H_4	1.2	Et_3N	2	EtOH	r.t.	17	**2.119d**	37
9	H	C_4H_3O	1.2	Et_3N	2	EtOH	r.t.	17.5	**2.119e**	33
10	H	4-CNC_6H_4	1.2	Et_3N	2	EtOH	r.t.	15	**2.119f**	66
11	H	3-$NO_2C_6H_4$	1.2	Et_3N	2	EtOH	r.t.	19	**2.119g**	89
12	H	4-$N(Me)_2C_6H_4$	1.2	Et_3N	5	EtOH	60	1	complex mixture	-
13	5-Br	C_6H_5	1.2	Et_3N	5	EtOH	40 55	4 24	**2.109b**	24
14	5-Br	C_6H_5	1.2	Et_3N	5	EtOH	r.t.	42	**2.109b**	48
15	5-Br	C_6H_5	1.2	DBU	2 drops	EtOH	r.t.	0.90	**2.109b**	59
16	5-Br	C_6H_5	1.2	NMP	2 drops	EtOH	r.t.	120	**2.109b**	44

A similar study was carried out with substituted imines **2.109c-g** (**Table 104**). For reactions of **2.109d** (R^1= 3-OH), under comparable conditions to those that afforded imidazoles **2.119** using **2.109a** (R^1= 2-OH) were used (Et_3N, EtOH, r.t.; **Table 103**), no evidence of the formation of the corresponding imidazole **2.119** was observed. Instead, compounds **2.113a** and **2.114a** were formed through the diaza-Cope rearrangement as referred in the literature. 1,6-Dihydropyrazines **2.113** or **2.114** were identified in solution and/or in DMSO-d_6 after heating the solution containing a mixture of **2.112** and **2.113/2.114**, in the NMR tube (**Table 104**). As a full characterization could not be performed, it was not possible to distinguish which isomer, **2.113** or **2.114**, was formed. These results indicate that not only the presence of the hydroxy group in the aromatic ring of imine **2.109** is important but also its position is crucial.

Table 104: Experimental conditions and results obtained for the reaction of imine **2.109d** with benzaldehydes **2.2**, in ethanol and using triethylamine as base

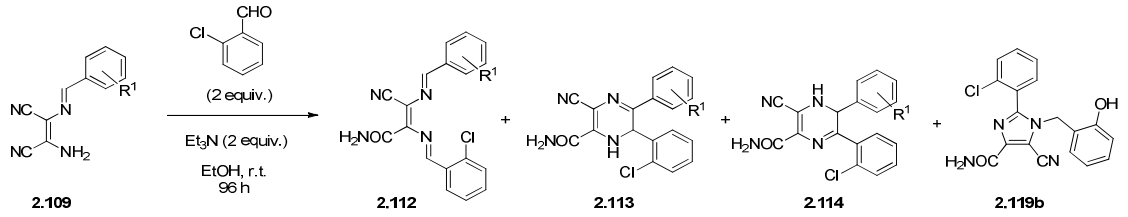


Entry	2.2		base	equiv.	T	t (h)	results (ratio)	η (%)
	R^1	equiv.						
1	H	1.5	Et_3N	5	r.t.	2	**2.112a**	85
2	H	1.5	Et_3N	2	r.t.	19	**2.112a**	59
3	2-Cl	1.2	Et_3N	5	r.t. 50	0.2 2	**2.112b + 2.113a/2.113a**[a] (6/1)	-
4	2-Cl	1.2	Et_3N	2	r.t.	19h	**2.112b + 2.113a/2.114a** (6/1)[a]	-

[a]By ^{1}H NMR; evolves to **2.113/2.114** when heated for 0.25 hours at 80 °C, in the DMSO-d_6 sample

Another set of experiments was performed, to better understand the conditions leading to imidazoles **2.119** (**Table 105**). These experiments share the same reaction time (96 h) and base molar equivalents (2 equivalents), and were performed in ethanol, with 2-chlorobenzaldehyde. The choice for 2-chlorobenzaldehyde comes from the fact that it in a liquid form at room temperature and allows for a distinctive pattern in the ^{1}H NMR spectrum to be identified.

Table 105: Selection of reactions performed with imine **2.109** and 2-chlorobenzaldehyde (2 equiv.), in the presence of triethylamine (2 equiv.), in ethanol and at room temperature for 96 h



Entry	R^1	results	ratio (2.112/2.113+2.114)	η (%)
1	2-OH	**2.119b**	-	37
2	3-OH	**2.112c + 2.113b/2.114b**[a]	1.5/1	-
3	4-OH	**2.112d + 2.113c/2.114c**[a]	4.6/1	-
4	3-Cl	**2.113d**	-	78
5	4-F	**2.113e/2.114e +** undetermined contamination	-	-
6	2-OMe	**2.109h + 2.113f/2.114f**	1/2	-

[a]By ^{1}H NMR; evolves to **2.113/2.114** when heated for 0.25 hours at 80 °C, in the DMSO-d_6 sample

The experiments described in **Table 105** reveal that when the reaction was carried out with **2.109d** (R^1= 3-OH; entry 2) under similar experimental conditions to those that were used to synthesize compound **2.119b** (entry 1) led to the isolation of compound **2.112c** as a yellow solid, mixed with dihydropyrazines **2.113b** and **2.114b** in a ratio of 1.5/1 (**Figure 80A**). When the sample was heated, in DMSO-d_6, a complete evolution to the 1,6-dihydropyrazine **2.113b** was observed (**Figure 80B**). The same results were obtained when using compound **2.109g** (R^1= 4-OH), but in a **2.112d: 2.113c/2.114c** ratio of 4.6/1 (entry 3 ; **Figure 81A**). Compound **2.113c** was also obtained after heating the mixture in DMSO-d_6 (**Figure 81B**).Using halides as substituents in the aromatic ring, as it is the case of **2.109e** (R^1= 3-Cl) and **2.109g** (R^1= 4-F), similar results were obtained: the formation of either **2.113d** (entry 4) or a mixture of **2.113d/2.114d**, together with an undetermined contamination (entry 5), allowing the NMR identification of compound **2.113d**. No evidence of the formation of the respective imidazole **2.119** was found. Using imines having an aromatic ring substituted with a 2-methoxy group, compound **2.109h**, no imidazole derivatives were formed, which confirmed that the presence of a hydroxyl group in this position is essential for the formation of imidazoles **2.119** (entry 6). A

mixture of the starting material **2.109h**, mixed with dihydropyrazines **2.113** and **2.114**, in a ratio of 1/2, was obtained.

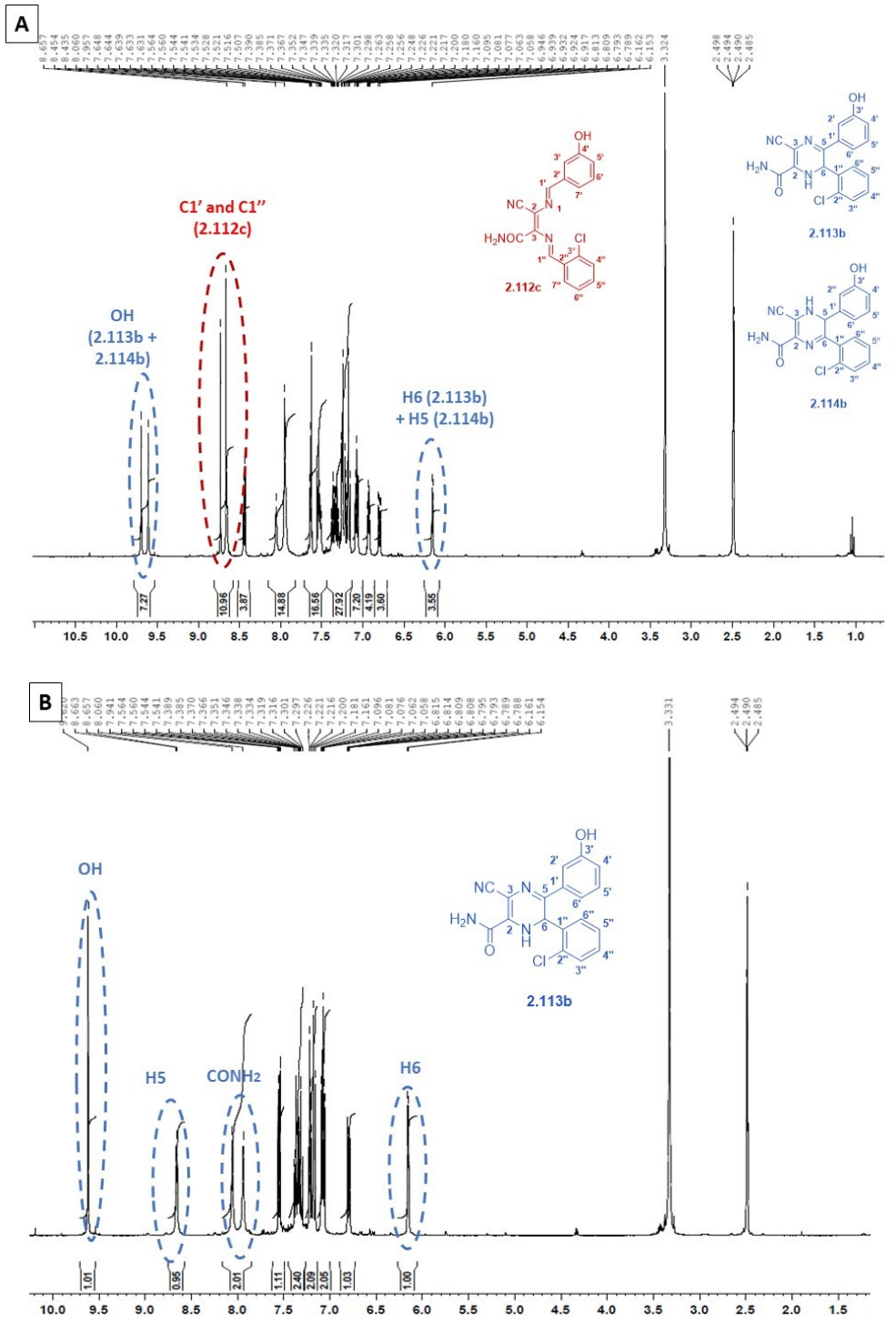


Figure 80: A: ^{1}H NMR (400 MHz, DMSO-d_6, δ ppm) spectrum of the product obtained from the reaction of **2.109c** with 2-chlorobenzaldehyde (1.2 equiv.), in EtOH and at r.t. (96 h), in the presence of Et_3N (2 equiv.). Several signals were highlighted for compounds **2.112c** (red circles) and compounds **2.113b** and **2.114b** (blue circles) (entry 2 - **Table 105**); **B:** ^{1}H NMR (400 MHz, DMSO-d_6, δ ppm) spectrum of the same product after heating the sample at 80 °C for 0.5 h, with a full conversion to **2.113b**

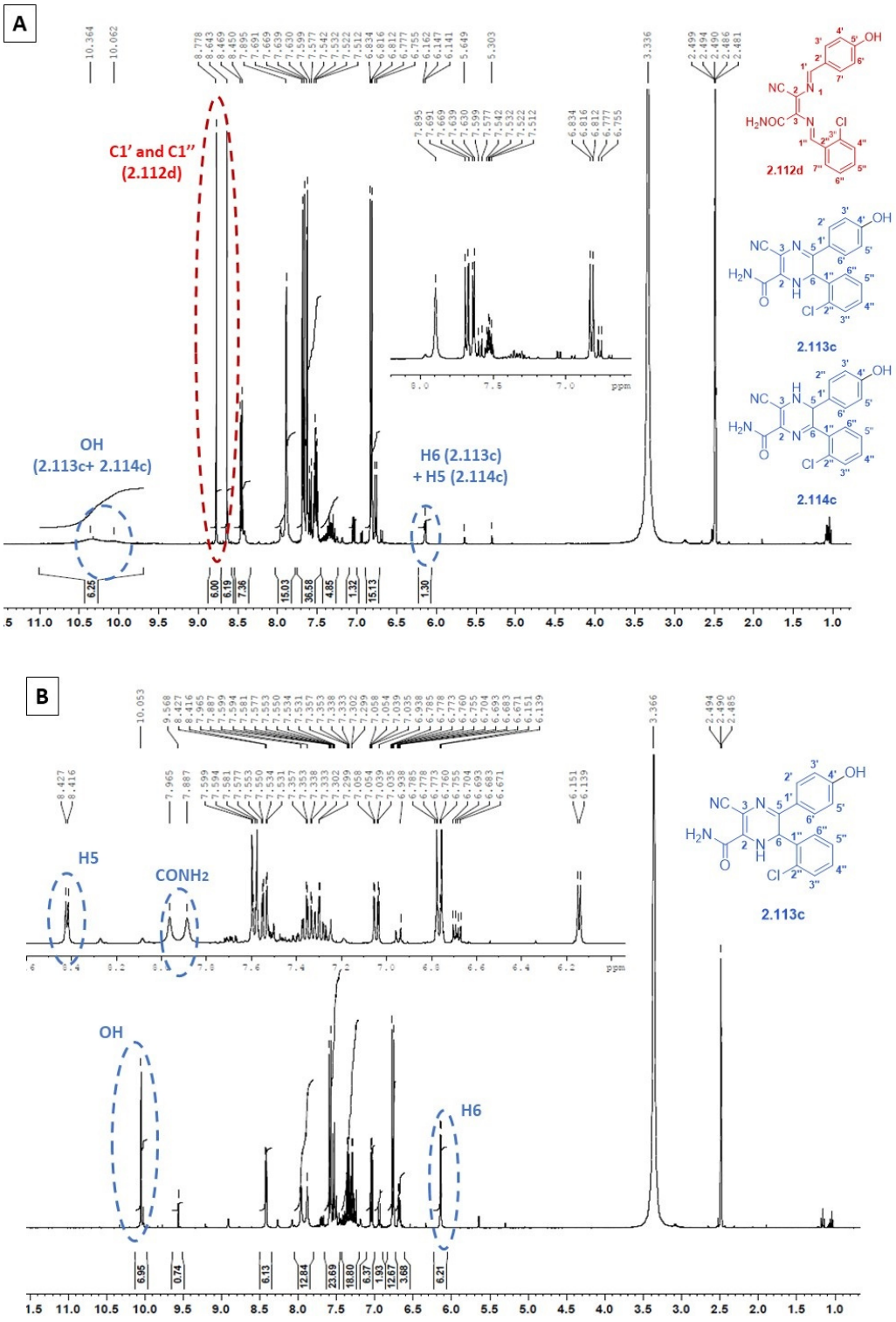


Figure 81: A: ^{1}H NMR (400 MHz, DMSO-d$_6$, δ ppm) spectrum of the product obtained from the reaction of **2.109g** with 2-chlorobenzaldehyde (1.2 equiv.), in EtOH and at r.t. (96 h), in the presence of Et$_3$N (2 equiv.). Several signals were highlighted for compounds **2.112d** (red circles) and compounds **2.113c** and **2.114c** (blue circles) (entry 3 - Table 105); **B:** ^{1}H NMR (400 MHz, DMSO-d$_6$, δ ppm) spectrum of the same product after heating the sample in the NMR tube. Several signals were highlighted

Compound **2.113d** was identified by NMR spectroscopy. The most representative peaks in the ^{1}H NMR spectra are the two signals at δ 8.87 and 6.28 ppm, corresponding to the NH group and H6, respectively (**Figure 82A**). In the ^{13}C NMR spectra highlights the signals at δ 162.18 ppm ($CONH_2$) and 48.76 ppm (C6), confirming the presence of the dihydropyrazine, supported by the correlation spectra. The correlation experiments allowed to distinguish which tautomer, **2.113** or **2.114**, was present (in this case, **2.113d**) (**Figure 82B**).

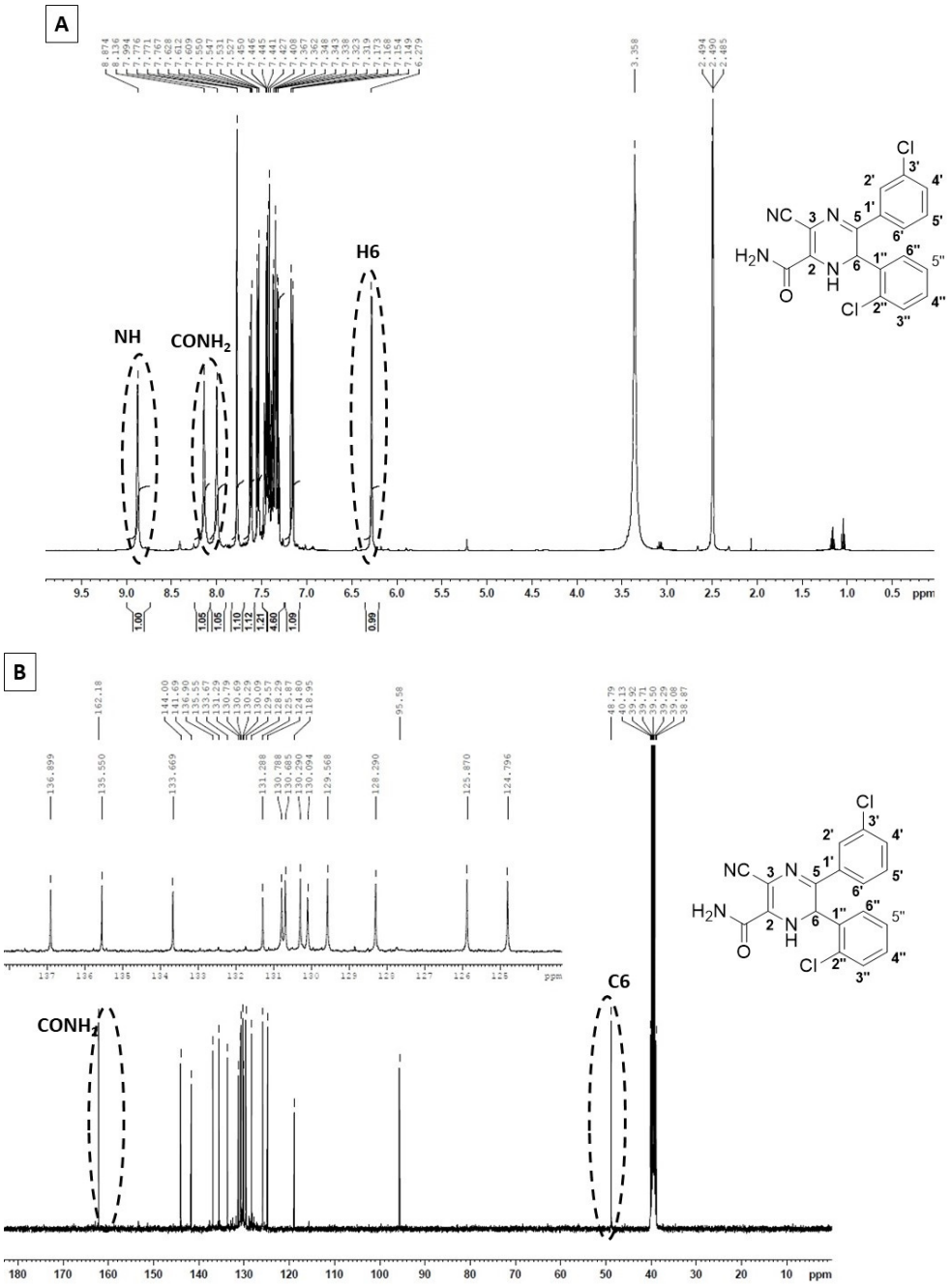
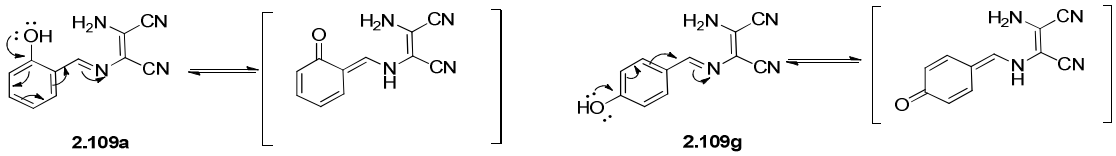


Figure 82: A: ^{1}H NMR (400 MHz, DMSO-d_6, δ ppm) spectrum obtained for compound **2.113d**, with some signals highlighted (black circles); **B**: ^{13}C NMR (100 MHz, DMSO-d_6, δ ppm) spectrum of the product obtained compound **2.113d**, with two signals highlighted (black circles)

Altogether, only imines containing a 2-OH-substituent in its aromatic ring afford imidazoles **2.119**. The reaction yield is not substantially modified by increasing the reaction time, since stirring for 16.5 h gave 42% yield while 37% was achieved for 96 h. These results indicate that it is not the electronic effect of the aromatic ring that promotes cyclization to imidazoles **2.119**, as both *ortho* and *para* substituted imines **2.109a** and **2.109d** should, theoretically, afford this product is this was the case (**Scheme 56**).



Scheme 56: Theoretical tautomeric forms of *ortho* **2.109a** and *para* substituted imines **2.109g**

Compound **2.113d** was identified by NMR spectroscopy. The most representative peaks in the ^{1}H NMR spectra are the two signals at δ 8.87 and 6.28 ppm, corresponding to the NH group and H6, respectively (**Figure 82A**). In the ^{13}C NMR spectra highlights the signals at δ 162.18 ppm ($CONH_2$) and 48.76 ppm (C6), confirming the presence of the dihydropyrazine, supported by the correlation spectra. The correlation experiments allowed to distinguish which tautomer, **2.113** or **2.114**, was present (in this case, **2.113d**) (**Figure 82B**).

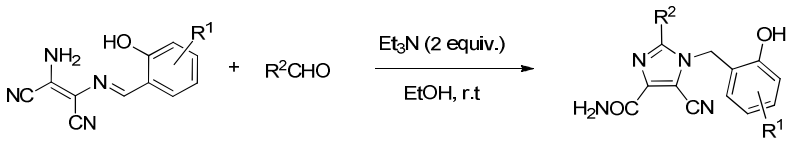
Based on these results, it became clear that imidazoles **2.119** were obtained from imines bearing a 2-hydroxyl moiety in the aromatic ring, except for **2.109b** (R^1= 5-Br). A common feature of all diimines **2.112** obtained, either as pure products or in mixtures, is that heating the sample in DMSO-d_6 accelerates the formation of dihydropyrazines **2.113/2.114**. For hydroxylated compounds **2.112a-c**, no evidence of the formation of dihydropyrazines **2.113/2.114** was found, indicating that presence of the 2-hydroxy moiety may be preferably promoting the formation of imidazoles **2.119** rather than of compounds **2.113/2.114**.

In the following studies, only compounds **2.109a** and **2.109c** were employed as starting materials for the synthesis of imidazoles **2.119**. A selection of compounds **2.113** was also prepared, but only for characterization and confirmation of the conclusions that were referred above.

Synthesis of 2-substituted 5-cyano-1-(2-hydroxyaryl)-1*H*-imidazole-4-carboxamides and cyano-5,6-diaryl-1,6-dihydropyrazine-carboxamides

Based on the studies presented in the previous section, a methodology to prepare 2-substituted 5-cyano-1-(2-hydroxyaryl)-1*H*-imidazole-4-carboxamides has been designed and optimized. The reaction sequence involves the preparation of compounds **2.109a** (97% yield) and **2.109c** (98% yield), and the subsequent reaction with diverse benzaldehydes in ethanol at room temperature, and in the presence of 2 equivalents of triethylamine. A wide variety of benzaldehydes could be used, containing either electron-drawing or electron-donating substituents. The reaction conditions leading to compounds **2.119** are summarized in **Table 106**.

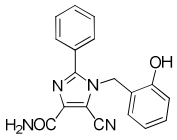
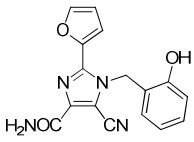
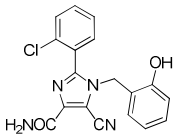
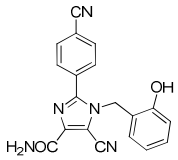
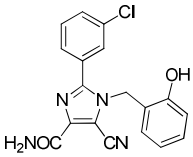
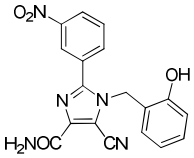
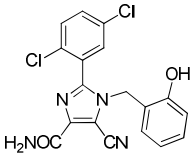
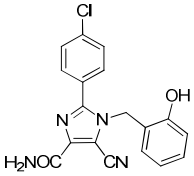
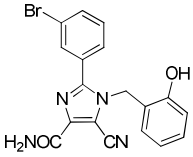
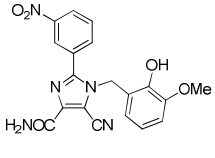
Table 106: Reaction conditions for the synthesis of imidazoles **2.119a-q**

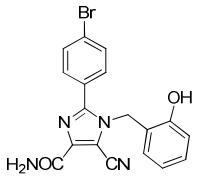
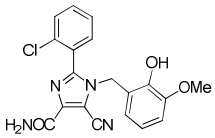
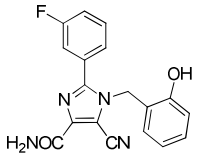
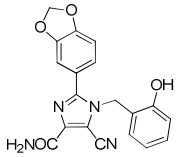
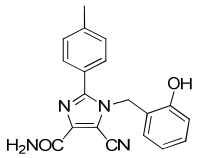
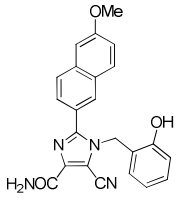
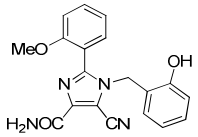


2.109a (R^1= H)
2.109c (R^1= 3-OMe)

2.2
(1.2-2 equiv)

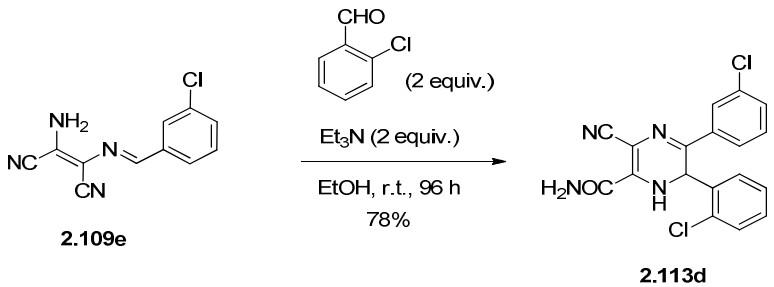
2.119a-p

Entry	Structure	t (h)	η (%)	Entry	Structure	t (h)	η (%)
2.119a		16	26	**2.119e**		17.5	33
2.119b		16.66	42	**2.119f**		15	66
2.119c		26	74	**2.119g**		17	89
2.119d		17	37	**2.119h**		25	31
2.119i		19	73	**2.119n**		66	49

2.119j		15	54	**2.119o**		68	51
2.119k		18.66	65	**2.119p**		17.5	28
2.119l		13	43	**2.119q**		16	54
2.119m		18	40				

Synthesis of cyano-5,6-diphenyl-1,6-dihydropyrazine-carboxamides

Dihydropyrazine **2.113d** was synthesized in 78% yield from imine **2.109e** and 2-chlorobenzaldehyde by stirring in the presence of 2 equivalents of Et_3N and using ethanol as solvent *via* a diaza-Cope rearrangement (**Scheme 57**). Dihydropyrazine **2.113b** was characterized by ^1H NMR after heating a solution of a mixture of **2.112c** and **2.113b/2.114b** in a ratio of 1.5/1 in DMSO-d_6 (entry 2 - **Table 105**).



Scheme 57: Synthesis of dihydropyrazine **2.113d** from imine **2.109e** and 2-chlorobenzaldehyde

Physical, analytical and spectroscopical characterization

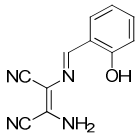
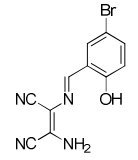
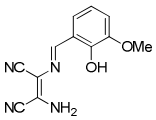
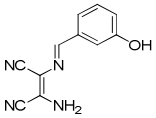
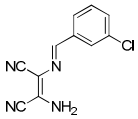
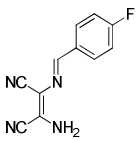
The structure of 2-amino-3-(arylideneamino)maleonitriles **2.109a-h**, cyano-5,6-diphenyl-1,6-dihydropyrazine-carboxamides **2.113b,d** and 2-substituted 5-cyano-1-(2-hydroxyaryl)-1*H*-

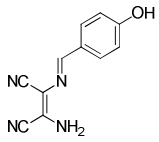
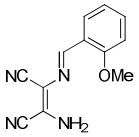
imidazole-4-carboxamides **2.119a-p** was assigned on the basis of their physical, analytical, and spectroscopic data (elemental analysis, meting point, IR, ^{1}H and ^{13}C NMR). This information is presented in the following section.

Physical and analytical characterization

The molecular formula and molecular weight were determined based on the information obtained from the elemental analysis results, and are presented, along with the respective melting point values (°C), in the following **Tables 107-109**. The elemental analysis for some of the prepared compounds **2.109** were obtained from the literature[159].

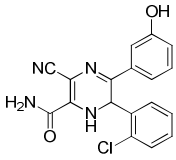
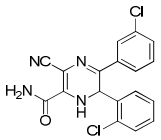
Table 107: Physical and analytical data obtained for compounds **2.109a-h**

Compound	structure	Mp (°C)	molecular formula/ mass (M)	calculated /obtained values (%)			
				C	H	N	O
2.109a[1]		240 (dec.)	$C_{11}H_8N_4O.0,9\ H_2O$/ 228.41	58.6 58.3	3.6 3.5	24.4 24.7	7.54 –
2.109b		210 (dec.)	$C_{11}H_8BrN_4O$/ 291.10	45.39 –	2.42 –	19.25 –	5.50 –
2.109c		221 (dec.)	$C_{12}H_{10}N_4O_2$/ 242.23	59.50 –	4.16 –	23.13 –	13.21 –
2.109d[1]		207-209	$C_{11}H_8N_4O.0,6\ H_2O$ / 223.01	59.8 59.6	3.5 3.3	25.0 25.3	7.54 –
2.109e		213-215	$C_{11}H_7ClN_4$/ 230.65	57.28 –	3.06 –	24.29 –	– –
2.109f		225-227	$C_{11}H_7FN_4$/ 214.20	61.68 –	3.29 –	8.87 –	26.16 –

2.109g[1]		220 (dec.)	$C_{11}H_8N_4O.1{,}9\ H_2O$/ 244.63	54.0 54.1	4.2 4.0	22.8 22.9	7.54 –
2.109h		188-190	$C_{12}H_{10}N_4O$/ 226.23	63.71 –	4.46 –	24.76 –	7.07 –

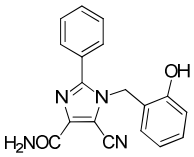
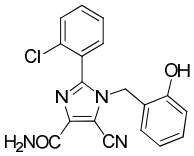
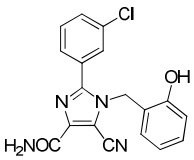
[1]data obtained from ref. 158

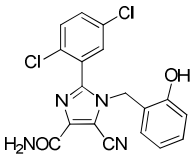
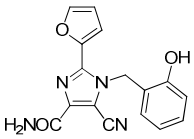
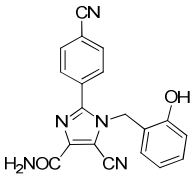
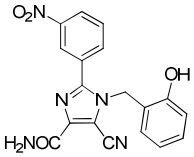
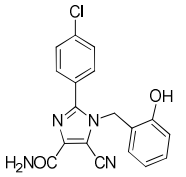
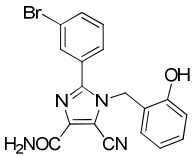
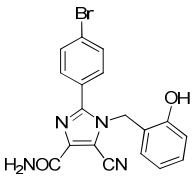
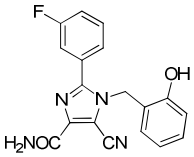
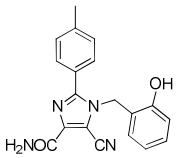
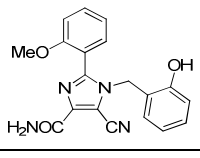
Table 108: Physical and analytical data obtained for compounds **2.113b,d**

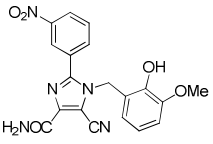
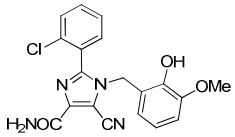
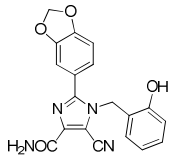
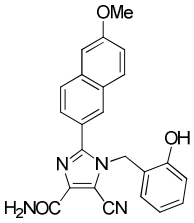
Compound	structure	Mp (°C)	molecular formula/ mass (M)	calculated /obtained values (%)			
				C	H	N	O
2.113b[1]		-	$C_{18}H_{13}ClN_4O_2$/ 352.77	61.28 –	3.71 –	15.88 –	9.07 –
2.113d		197 (dec.)	$C_{18}H_{12}Cl_2N_4O$/ 371.22	58.24 –	3.26 –	15.09 –	4.31 –

[1]Identified in DMSO-d_6 sample test tube

Table 109: Physical and analytical data obtained for compounds **2.119a-q**

Comp.	structure	Mp (°C)	molecular formula/ mass (M)	calculated /obtained values (%)			
				C	H	N	O
2.119a		202-204	$C_{18}H_{14}N_4O_2.0.25H_2O$/ 322.83	67.03 67.13	4.49 5.00	17.37 17.32	10.50 -
2.119b		230-232	$C_{18}H_{13}ClN_4O_2$/ 352.77	61.28 61.57	3.71 3.62	15.88 16.07	9.07 –
2.119c		230 (dec.)	$C_{18}H_{13}ClN_4O_2$/ 352.77	61.28 61.26	3.71 3.62	15.88 16.07	9.07 –

2.119d		225-227	$C_{18}H_{12}Cl_2N_4O_2$/ 387.22	55.83 55.74	3.12 3.19	14.47 14.41	8.26 –
2.119e		227-229	$C_{16}H_{12}N_4O_3$/ 308.29	62.33 62.15	3.92 3.97	18.17 18.09	15.57 –
2.119f		>300	$C_{19}H_{13}N_5O_2.0.5H_2O$/ 351.34	64.77 64.93	3.97 3.90	19.88 19.94	9.32 –
2.119g		>300	$C_{18}H_{13}N_5O_4$/ 367.33	59.50 –	3.61 –	19.28 –	17.61 –
2.119h		208-210	$C_{18}H_{13}ClN_4O_2.H_2O$/ 370.79	58.31 58.44	4.08 4.06	15.11 15.09	12.94 –
2.119i		220-222	$C_{18}H_{13}BrN_4O_2$/ 397.23	54.43 54.73	3.30 3.27	14.10 13.98	8.06 –
2.119j		174-175	$C_{18}H_{13}BrN_4O_2.0.7H_2O$/ 409.84	52.75 52.57	3.54 3.88	13.67 13.39	10.54 –
2.119k		>300	$C_{18}H_{13}FN_4O_2$/ 336.32	64.28 64.34	3.90 3.79	16.66 16.71	9.51 –
2.119l		238-239	$C_{19}H_{16}N_4O_2.0,5H_2O$/ 341.37	66.85 66.75	5.02 5.01	16.41 16.61	11.72 –
2.119m		212-214	$C_{19}H_{16}N_4O_3$/ 348.36	65.51 65.90	4.63 4.82	16.08 16.32	13.78 –

2.119n		203-205	$C_{19}H_{15}N_5O_5$/ 393.35	58.01 58.24	3.84 3.92	17.80 17.72	20.34 –
2.119o		260-262	$C_{19}H_{15}ClN_4O_3$/ 382.80	59.61 59.98	3.95 4.11	14.64 14.93	12.54 –
2.119p		212-214	$C_{19}H_{14}N_4O_4.H_2O$/ 376.40	61.03 60.73	4.12 4.43	14.99 14.76	17.66 –
2.119q		142-144	$C_{23}H_{18}N_4O_3.0.25H_2O$/ 402.91	68.50 68.78	4.59 5.23	13.89 13.69	12.90 –

IR spectroscopy

The IR spectra of compounds **2.109** show several characteristic bands for the NH stretching vibration of both NH and NH_2 groups (**Table 110**). The CN stretching vibration of the cyano group appear as two bands, one intense and another with a medium intensity, in the 2200-2250 cm^{-1} region.

For compounds **2.113**, the IR spectra show the NH/NH_2 stretching vibrations bands in the 3188-3461 cm^{-1} region (**Table 111**). The band corresponding to the cyano group appears at around 2210 cm^{-1}, while the carbonyl CO stretching vibration band is identified as an intense band in the 1672-1701 cm^{-1} region.

In the IR spectra of compounds **2.119** highlight the bands in the 3177-3477 cm^{-1} region corresponding to the NH and OH stretching vibrations (**Table 112**). A single medium intensity band for the stretching vibration of the cyano group appears in the 2224-2238 cm^{-1} region. The carbonyl group leads to an intense band in the 1666-1686 cm^{-1} region.

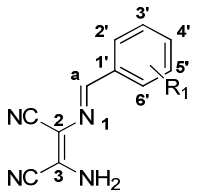


Table 110: IR spectroscopic data (Nujol, cm^{-1}) obtained for compounds **2.109a,h**

Compound	R^1	4000-3000	2300-2000	1700-1500
2.109a	2-OH	3417m, 3309s, 3194m	2233m, 2250s	1630s, 1603s, 1562m
2.109b	2-OH, 5-Br	3402m, 3301s, 3199m	2247m, 2210s	1631s, 1599s, 1550m
2.109c	2-OH, 3-OMe	3408s, 3324s, 3208sm	2245m, 2205m	1645s, 1602s, 1589m, 1526sm
2.109d	3-OH	3409s, 3301s, 3202m	2233m, 2199s	1623s, 1587m, 1561w
2.109e	3-Cl	3422s, 3297s, 3160m	2233m, 2212s	1621s,1606s, 1573m
2.109f	4-F	3427m, 3403m, 3314s, 3296s	2243m, 2201s	1616s, 1601s, 1571m
2.109g	4-OH	3463m, 3396m, 3357s	2240s, 2202m	1611s, 1593s, 1556m
2.109h	2-OMe	3425s, 3405s, 3299s, 3172m	2246m, 2201s	1602s, 1561sh

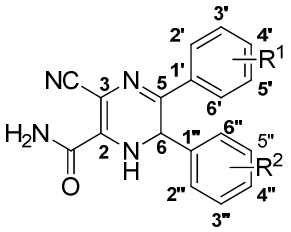
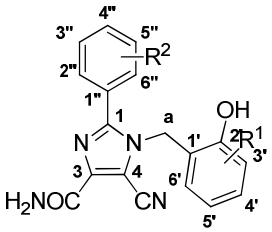


Table 111: IR spectroscopic data (Nujol, cm^{-1}) obtained for compounds **2.113a,b**

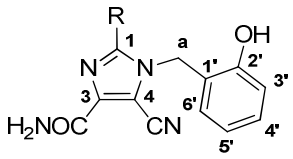
Compound	R^1	R^2	4000-3000	2300-2000	1700-1500
2.113b	3-OH	2-Cl	3475w, 3270m	2205s	1672s, 1602sm, 1558m, 1533m
2.113d	3-Cl	2-Cl	3461m, 3272w, 3188b	2208w	1701s, 1590b, 1539m

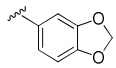
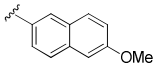
Table 112: IR spectroscopic data (Nujol, cm^{-1}) obtained for compounds **2.119a-o**



Compound	R^1	R^2	4000-3000	2300-2000	1700-1500
2.119a	H	H	3473m, 3365m, 3328m	2231m	1686m (C=O), 1669m, 1591m,1559sm, 1542sm, 1508sm
2.119b	H	2-Cl	3477m, 3348m	2238m	1668s (C=O), 1599s, 1502sm
2.119c	H	3-Cl	3479m, 3369m,3331m	2233m	1685s (C=O), 1670m, 1590m, 1511m
2.119d	H	2,5-Cl	3477m, 3370m, 3284m	2233m	1666s (C=O), 1585m, 1510sm
2.119f	H	4-CN	3394sm, 3344m, 3281sm, 3203sm	2230m, 2224m	1679s (C=O), 1597m, 1561sm, 1507sm
2.119g	H	3-NO_2	3400m, 3352sm, 3288sm, 3177m,	2228m	1685s (C=O), 1604s, 1558sm, 1522s
2.119h	H	4-Cl	3605m, 3513sm, 3439m, 3353sm, 3286sm	2230m	1688s (C=O), 1604s, 1507sm
2.119i	H	3-Br	3477m, 3367s	2233m	1683m, 1668s (C=O), 1591s, 1510sm
2.119j	H	4-Br	3633sm, 3429m, 3352sm, 3282sm, 3183m	2224m	1687s (C=O), 1601s, 1508sm
2.119k	H	3-F	3489m, 3379m, 3332m	2233m	1687m, 1672s (C=O), 1591s, 1558sm, 1520sm, 1509sm
2.119l	H	4-Me	3458m, 3295m, 3239m, 3176sm	2233m	1658s (C=O), 1597s, 1558sm, 1541sm, 1527sm, 1509sm
2.119m	H	2-OMe	3448m, 3332m	2231m	1684m, 1668s (C=O), 1597s, 1520sm
2.119n	3-OMe	3-NO_2	3483s, 3448m, 3375s, 3294m, 3075w	2226s	1683s (C=O), 1674s, 1593s, 1536s
2.119o	3-OMe	2-Cl	3487m, 3373m	2232m	1677s (C=O), 1592s, 1550sm, 1526sm

Table 113: IR spectroscopic data (Nujol, cm^{-1}) obtained for compounds **2.119e,p,q**



Compound	R	4000-3000	2300-2000	1700-1500
2.119e		3445s, 3335s	2234s	1675s (C=O), 1659s, 1596s, 1514s
2.119p		3581m, 3482sm, 3433m, 3351sm, 3266sm, 3187m	2227s	1688s (C=O), 1603s, 1499m
2.119q		3466s, 3347sm, 3278sm, 3169m, 3060sm	2226s	1683s (C=O), 1627s, 1603s, 1530sm

NMR spectroscopy

In relation to the ^{1}H NMR spectra, compounds **2.109** can be identified by two characteristic singlets, one at around δ 7.64-8.09 ppm, assigned to the NH_2 group, and the other at around δ 8.14-8.59 ppm, assigned to Ha (**Table 114**). In the ^{13}C NMR spectra, the signals of the C2 (δ 102.26-103.55 ppm) and C3 (δ 114.36-114.72 ppm) allow for a clear identification of the structure. The two cyano groups, linked to C2 and C3, present a slightly different chemical shift, with C2-CN appearing at around δ 113.72-114.00 ppm and C3-CN at δ 126.08-126.98 ppm. Ca appears at around δ 149.82-155.36 ppm (**Table 115**). By HMBC, C2 correlates to Ca and to the cyano groups, while C3 only correlates to the cyano groups. Ha also correlates with C2, C1' and C2'/C6'.

The NMR spectra of compounds **2.113** has two characteristic singlets at around δ 8.49-8.87 ppm (H1) and δ 6.16-6.28 ppm (H6) (**Table 116**). The NH_2 moiety of the amide group appears as two singlets, at around δ 8.14-8.01 and δ 7.99-7.93 ppm. The most distinguishable signals of their ^{13}C NMR spectra are the signals around δ 144.00-145.46 ppm (C5), δ 140.61-141.69 ppm (C2), δ 118.95-119.06 ppm (CN), δ 95.58-97.11 ppm (C3), δ 49.65-50.85 ppm (C6) and δ 162.18-162.34 ppm (amide carbonyl) (**Table 117**). Compounds **2.113** present correlations of and of H1 correlates to the amide carbonyl carbon and C6 correlates to C2.

The NMR spectra of compounds **2.119** can be pinpointed by their specific singlets at around δ 5.0-5.7 ppm (Ha, CH_2 group) and the OH group, which appears in an interval between δ 9.0-10.8 ppm (**Tables 118** and **119**). Compounds **2.119** can easily be identified by ^{13}C NMR for the signals at around 50-45 ppm of the Ca moiety, that correlates to C1, C3, C1', C2´ and C6'. The NH_2 moiety of the amide group correlates to C4. Lastly, the Ca moiety correlates to C1, C3, C1' and C2'/C6' (**Tables 120** and **121**).

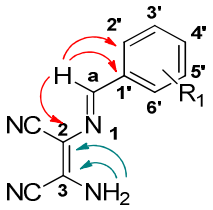


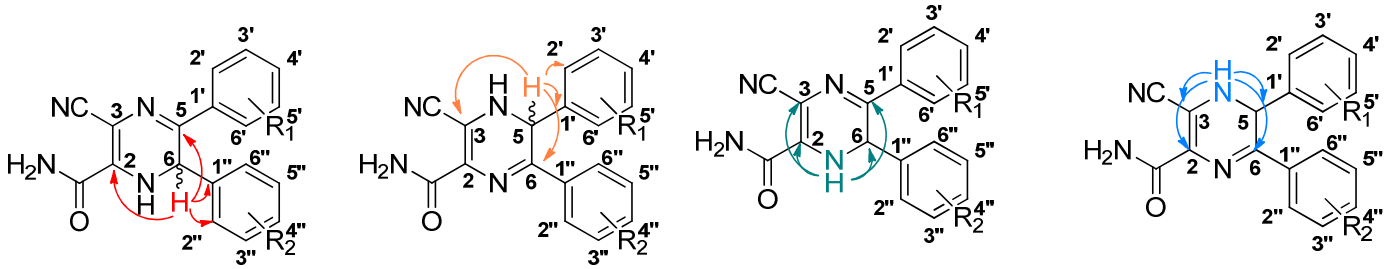
Table 114: ^1H NMR (400 MHz, DMSO-d_6, δ ppm) spectroscopic data obtained for compounds **2.109a-h**

Comp.	R^1	Ar(H1'-6')	OH	Ha	NH_2
2.109a	2-OH	8.03 (dd, J_1= 8.0, J_2= 1.6 Hz, 1H; H6'), 7.32 (dt, J_1= 8.0, J_2= 1.6 Hz; 1H; H4'), 6.92 (dd, J_1= 8.0, J_2= 0.8 Hz; 1H, H3'), 6.88 (t, J= 7.6 Hz, 1H; H5')	10,41 (s, 1H)	8.58 (s, 1H)	7.86 (s, 2H)
2.109b	2-OH, 5-Br	8.30 (d, J= 2.4 Hz, 1H, H6'), 7.43 (dd, J_1= 8.8 Hz, J_2= 2.8 Hz, 1H, H4'), 6.88 (d, J= 8.8 Hz, 1H; H3')	10.65 (s, 1H)	8.49 (s, 1H)	8.02 (s, 2H)
2.109c	2-OH, 3-OMe	7.61 (dd, J_1= 7.6, J_2= 1.2 Hz, 1H, H6'), 7.06 (dd, J_1= 7.6, J_2= 1.2 Hz, 1H, H4), 6.83 (t, J= 8.0 Hz, 1H, H5'), 3.83 (s, 3H, OMe)	9.86 (s, 1H,)	8.59 (s, 1H)	7.84 (s, 2H)
2.109d	3-OH	7.44 (d, J= 7.6 Hz, 1H, H6'), 7.37 (t, J= 2.0 Hz, 1H, H2'), 7.26 (t, J= 8 Hz, 1H, H5'), 6.90 (ddd, J_1= 8.0 Hz, J_2= 2.4 Hz, J_3= 0.8 Hz; 1H, H4')	9.64 (s, 1H)	8.16 (s, 1H)	7.88 (s, 2H)
2.109e	3-Cl	8.18 (d, J= 1.6 Hz, 1H, H2'), 7.86 (dd, J_1= 7.2, J_2= 2.4 Hz,1H, H6'), 7.49 (dd, J_1= 8.0, J_2= 1.6 Hz, 1H, H4'), 7.45 (t, J= 8.0 Hz, 1H, H5')	-	8.21 (s, 1H)	8.09 (s, 2H)
2.109f	4-F	8.10 (dd, J_1= 8.8, J_2= 2.4 Hz, 2H, H2' + H6'), 7.29 (dt, J_1= 8.8, J_2= 2.0 Hz, 2H, H3' + H5')	-	8.24 (s, 1H)	7.93 (s, 2H)
2.109g	4-OH	7.86 (dd, J_1= 6.8, J_2= 1.6 Hz, 2H, H2' + H6'), 6.83 (dd, J_1= 6.8, J_2= 2.0 Hz, 2H, H3' + H5')	10.21 (s, 1H)	8.14 (s, 1H)	7.64 (s, 2H)
2.109h	2-OMe	8.24 (dd, J_1= 8.0 Hz; J_2= 1.6 Hz, 1H; H6'), 7.46 (dt, J_1= 8.4 Hz; J_2= 2.0 Hz, 1H, H4'), 7.10 (d, J= 8.0 Hz, 1H, H3'), 7.00 (t, J= 7.6 Hz, 1H, H5'), 3.87 (s, 3H, OMe)	-	8.59 (s, 1H)	7.86 (s, 2H)

Table 115: ^{13}C NMR (100 MHz, DMSO-d_6, δ ppm) spectroscopic data obtained for compounds **2.114a.h**

Comp.	R^1	Ar(H1'-6')	C2-CN	C3-CN	Ca	C2	C3
2.114a	2-OH	158.15 (C2'), 133.32 (C4'), 128.92 (C6'), 121.24 (C1'), 119.44 (C5'), 116.42 (C3')	114.00	126.05	152.87	103.44	114.58
2.114b	2-OH, 5-Br	157.15 (C2'), 135.15 (C4'), 129.93 (C6'), 123.72 (C1'), 118.61 (C3'), 111.25 (C5')	113.88	126.77	149.88	103.06	114.45
2.114c	2-OH, 3-OMe	148.01 (C3'), 147.88 (C2'), 121.54 (C1'), 120.15 (C6'), 119.07 (C5'), 114.73 (C4')	113.95	126.08	152.84	103.34	114.53
2.114d	3-OH	157.65 (C3'), 136.81 (C1'), 129.68 (C5'), 120.26 (C6'), 118.76 (C4'), 115.74 (C2')	113.79	126.83	155.36	102.69	114.42
2.114e	3-Cl	137.70 (C1'), 134.00 (C3'), 131.11 (C4'), 130.70 (C5'), 128.39 (C6'), 127.65 (C2')	113.77	127.81	153.48	102.26	114.36
2.114f	4-F	162.55 (d, J= 249 Hz, C4'), 136.25 (d, J= 3 Hz, C1'), 131.37 (d, J= 9 Hz, 2H, C2' + C6'), 115.83 (d, J= 22 Hz, C3' + C5')	113.72	126.98	153.73	102.47	114.37
2.114g	4-OH	161.00 (C4'), 131.24 (C2' + C6'), 126.45 (C1'), 115.73 (C3' + C5')	113.95	126.94	155.14	103.46	114.72
2.114h	2-OMe	159.10 (C2'), 133.44 (C4'), 127.69 (C6'), 123.55 (C1'), 120.71 (C5'), 111.95 (C3'), 55.86 (OMe)	114.00	126.58	150.07	103.55	114.55

Table 116: ^{1}H NMR (400 MHz, DMSO-d_6, δ ppm) spectroscopic data obtained for compounds **2.113b,d**

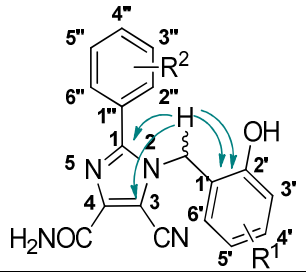


Compound	R^1	R^2	Ar(H1'-6')	Ar(H1''-6'')	H1	H6	$CONH_2$
2.113b	3-OH	2-Cl	9.62 (s, 1H, OH), 7.22 (t, J= 2.0 Hz, 1H, H2'), 7.18 (t, J= 8.0 Hz, 1H, H5'), 7.07 (dd, J_1= 7.6, J_2= 1.6 Hz, 1H, H6'), 6.78 (dd, J_1= 8.0, J_2= 2.5 Hz, 1H, H4')	7.55 (dd, J_1=7.6 Hz, J_2= 1.2 Hz, 1H, H3''), 7.37 (dt, J_1= 7.6 Hz, J_2= 1.6 Hz, 1H, H4''), 7.31 (dt, J_1= 7.6, J_2= 1.6 Hz, 1H, H5''), 7.07 (dd, J_1= 7.6, J_2= 1.6 Hz, 1H, H6'')	8.66 (d, J= 2.8 Hz, 1H)	6.16 (d, J= 2.8 Hz, 1H)	8.06 and 7.94 (s, 2H)
2.113d	3-Cl	2-Cl	7.77 (t, J= 1.6 Hz, 1H, H2'), 7.62 (dt, J_1= 7.6, J_2= 1.6 Hz, 1H, H6'), 7.41 (d, J= 7.6 Hz, 1H, H4'), 7.37 (dt, J_1= 7.6, J_2= 2.0 Hz, 1H, H5'')	7.54 (dd, J_1=8.0 Hz, J_2= 1.6 Hz, 1H, H3''), 7.46 (dt, J_1= 8.0 Hz, J_2= 1.6 Hz, 1H, H4''), 7.32 (dt, J_1= 7.2, J_2= 1.2 Hz, 1H, H5''), 7.16 (dd, J_1=7.6 Hz, J_2= 2.0 Hz, 1H, H6'')	8.87 (s, 1H)	6.28 (s, 1H)	8.14 and 7.99 (s, 2H)

Table 117: ^{13}C NMR (100 MHz, DMSO-d_6, δ ppm) spectroscopic data obtained for compounds **2.113b,d**

Compound	R^1	R^2	Ar(C1'-6')	Ar(C1''-6'')	C2	C3	C5	C6	CN	$CONH_2$
2.113b	3-OH	2-Cl	157.58 (C3'), 136.07 (C1'), 129.81 (C5'), 117.83 (C4'), 117.13 (C6'), 112.88 (C2')	135.40 (C1''), 131.42 (C2''), 130.61 (C4''), 130.27 (C3''), 129.36 (C6''), 128.10 (C5'')	140.61	96.24	145.20	48.65	119.06	162.30
2.113d	3-Cl	2-Cl	136.90 (C3'), 133.67 (C1'), 130.79 (C5'), 130.69 (C4'), 125.87 (C2'), 124.80 (C6')	135.55 (C1''), 131.29 (C2''), 130.29 (C3''), 130.09 (C4''), 129.57 (C6''), 128.29 (C5'')	141.69	95.58	144.00	48.79	118.95	162.18

Table 118: ^{1}H NMR (400 MHz, DMSO-d_6, δ ppm) spectroscopic data obtained for compounds **2.119**



Comp.	R^1	R^2	Ar(H1'-6')	Ar(H1''-6'')	Ha	$CONH_2$	OH
2.119a	H	H	7.11 (dt, J_1= 8.0, J_2= 1.6 Hz, 1H, H4'), 6.80 (dd, J_1= 8.0 Hz, J_2= 0.8 Hz, 1H, H3'), 6.70 (dt, J_1= 7.6, J_2= 1.2 Hz, 1H, H5'), 6.56 (dd, J_1= 7.6, J_2= 1.6 Hz, 1H, H6')	7.60 (dd, J_1= 7.6, J_2= 1.6 Hz, 2H. H2'' + H6''), 7.50 (t; J= 8.0 Hz; 1H, H4''), 7.48 (dt, J_1= 7.6, J_2= 1.2 Hz; 1H, H3'' + H5'')	5.28 (s, 2H)	7.80(s, 1H), 7.65 (s, 1H)	9.91 (s, 1H)
2.119b	H	2-Cl	7.06 (dt, J_1= 8.0, J_2= 0.8 Hz, 1H, H4'), 6.71 (dd, J_1= 8.0, J_2= 0.8 Hz, 1H, H3'), 6.58 (dt, J_1= 7.6, J_2= 0.8 Hz, 1H, H5'), 6.49 (dd, J_1= 7.6, J_2= 1.2 Hz, 1H, H6')	7.57 (t, J= 7.6 Hz, 1H, H4''), 7.55 (dd, J_1= 7.6, J_2= 2.0 Hz, 1H, H3''), 7.45 (dt, J_1= 8.0, J_2= 1.6 Hz, 1H, H5''), 7.43 (dd, J_1= 8.0, J_2= 2.0 Hz, 1H, H6'')	5.09 (s, 2H)	7.80 (s, 1H), 7.61 (s, 1H)	9.81 (s, 1H)
2.119c	H	3-Cl	7.11 (dt, J_1= 8.8, J_2= 1.6 Hz, 1H, H4'), 6.78 (dd, J= 8.0, J_2= 0.4 Hz, 1H, H3'), 6.70 (dt, J_1= 8.0, J_2= 0.4 Hz, 1H, H5'), 6.65 (dd, J_1= 7.6, J_2= 1.2 Hz, 1H, H6')	7.68 (t, J= 1.6 Hz, 1H, H2''), 7.57 (dt, J_1= 8.4 Hz, J_2= 1.2 Hz, 1H, H5''), 7.53 (d, J= 8.4 Hz, 1H, H6''), 7.51 (d, J= 8.0 Hz; 1H, H4'')	5.31 (s, 2H)	7.83 (s, 1H), 7.65 (s, 1H)	9.98 (s, 1H)
2.119d	H	2,5-Cl	7.07 (m, 1H, H4'), 6.70 (d, J= 7.6 Hz, 1H, H3'), 6.58 (d, J= 8.0 Hz; 1H, H6'), 6.57 (d, J= 8.0 Hz, 1H, H5')	7.60 (dd, J_1= 8.8, J_2= 2.4 Hz, 2H, H3''), 7.57 (d, J= 8.4 Hz, 1H, H4''), 7.50 (d, J= 2.4 Hz, 2H, H6'')	5.09 (s, 2H)	7.76 (s, 1H), 7.57 (s, 1H)	9.47 (s, 1H)
2.119f	H	4-CN	7.10 (m, 1H, H4'), 6.76 (d, J= 8.0 Hz, 1H, H3'), 6.68 (d, J= 4.4 Hz, 2H, H5' + H6')	7.97 (d, J= 8.0 Hz, 2H, H3'' + H5''), 7.81 (d, J= 8.0 Hz, 2H, H2'' + H6'')	5.32 (s, 2H)	7.84 (s, 1H), 7.67 (s, 1H)	9.91 (s, 1H)

2.119g	H	3-NO_2	7.10 (dt, J_1= 8.0, J_2= 1.6 Hz, 1H, H4'), 6.74 (d, J= 7.6 Hz, 1H, H3'), 6.73 (d, J= 7.6 Hz, 1H, H6'), 6.68 (dd, J_1= 7.6, J_2= 0.8 Hz, 1H, H5')	8.43 (d, J= 2.0 Hz; 1H, H2''), 8.36 (dd, J_1= 8.0, J_2= 0.8 Hz; 1H, H4''), 8.05 (dd, J_1= 8.0, J_2= 0.8 Hz, 1H, H6''), 7.79 (t, J= 8.0 Hz; 1H, H5'')	5.35 (s, 2H)	7.88 (s, 1H), 7.68 (s, 1H)	9.86 (s, 1H)
2.119h	H	4-Cl	7.10 (dt, J_1= 8.0, J_2= 0.8 Hz, 1H, H4'), 6.78 (dd, J_1= 8.0, J_2= 0.4 Hz, 1H, H3'), 6.69 (dt, J_1= 7.2, J_2= 0.8 Hz, 1H, H5'), 6.52 (dd, J_1= 7.6, J_2= 1.2 Hz, 1H, H6')	7.63 (dd, J_1= 8.8, J_2= 2.0 Hz, 2H, H2'' + H6''), 7.57 (dd, J_1= 8.8, J_2= 2.0 Hz, 2H, H3'' + H5'')	5.29 (s, 2H)	7.81(s, 1H), 7.65 (s, 1H)	9.90 (s, 1H)
2.119i	H	3-Br	7.11 (dt, J_1= 8.0 Hz, J_2= 2.0 Hz, 1H, H4'), 6.79 (d, J= 8.0 Hz, 1H, H3'), 6.71 (dt, J_1=7.6, J_2= 1.2 Hz, 1H, H5'), 6.67 (dd, J_1= 7.6 Hz, J_2= 1.2 Hz, 1H, H6')	7.83 (d, J= 1.6 Hz, 1H, H2''), 7.71 (dd, J_1= 8.0 Hz, J_2= 0.8 Hz, 1H, H6''), 7.60 (dd, J_1= 8.0, J_2= 1.2 Hz, 1H, H4''), 7.44 (t, J= 8.0 Hz, 1H, H5'')	5.31 (s, 2H)	7.84 (s, 1H), 7.65 (s, 1H)	9.92 (s, 1H)
2.119j	H	4-Br	7.11 (dt, J_1= 8.0, J_2= 1.6 Hz, 1H, H4'), 6.78 (dd, J_1= 8.0, J_2= 0.4 Hz, 1H, H3'), 6.69 (dt, J_1= 7.6, J_2= 0.8 Hz, 1H, H5'), 6.62 (dd, J_1= 7.6, J_2= 1.6 Hz, 1H, H6')	7.71 (dd, J_1= 7.6, J_2= 2.0 Hz, 2H, H3''+H5''), 7.56 (dd, J_1= 8.8, J_2= 2.0 Hz, 2H, H2'' + H6'')	5.27 (s, 2H)	7.81(s, 1H), 7.66 (s, 1H)	9.89 (s, 1H)
2.119k	H	3-F	7.11 (dt, J_1= 8.0, J_2= 1.6 Hz, 1H, H4'), 6.79 (dd, J_1= 8.0, J_2= 0.8 Hz, 1H, H3'), 6.69 (dt, J_1= 7.6, J_2= 1.2 Hz, 1H, H5'), 6.64 (dd, J_1= 7.6, J_2= 1.6 Hz, 1H, H6')	7.53 (dd, J_1= 6.4, J_2= 2.0 Hz, 1H, H5''), 7.45 (ddd, J_1= 6.8, J_2= 2.4, J_3= 1.6 Hz, 2H, H2'', H6''), 7.37 (ddt, J_1= 8.0, J_2= 2.4, J_3= 1.2 Hz, 1H, H4'')	5.33 (s, 2H)	7.82 (s, 1H), 7.67 (s, 1H)	9.90 (s, 1H)
2.119l	H	4-Me	7.07 (dt, J_1= 7.6, J_2= 0.8 Hz, 1H, H4'), 6.72 (dd, J_1= 8.0, J_2= 0.8 Hz, 1H, H3'), 6.59 (dt, J_1= 7.6, J_2= 0.8 Hz, 1H, H5'), 6.39 (dd, J_1= 7.6, J_2= 1.2 Hz, 1H, H6')	7.40 (dt, J_1= 7.6, J_2= 1.2 Hz, 1H, H3'' or H5''), 7.35 (dd, J_1= 8.0, J_2= 1.6 Hz, 1H, H2'' or H6''), 7.27 (t, J= 7.2 Hz, 2H, H3'' or H5'', H2'' or H6''), 1.95 (s, 3H, Me)	5.07 (s, 2H)	7.76 (s, 1H), 7.59 (s, 1H)	9.82 (s, 1H)
2.119m	H	2-OMe	7.05 (dt, J_1= 8.0, J_2= 1.6 Hz, 1H, H4'), 6.71 (dd, J_1= 8.0, J_2= 0.8 Hz, 1H, H3'),	7.50 (dt, J_1= 7.6, J_2= 1.6 Hz; 1H, H4''), 7.28 (dd, J_1= 7.6, J_2= 1.6 Hz, 1H, H6''), 7.11 (d, J= 8.0 Hz,	5.05 (s, 2H)	7.74 (s, 1H), 7.57 (s, 1H)	9.81 (s, 1H)

			6.61 (dt, J_1= 7.6, J_2= 0.8 Hz; 1H, H5'), 6.47 (dd, J_1= 7.6, J_2= 1.2 Hz; 1H, H6')	1H, H3''), 7.00 (dt, J_1= 7.2, J_2= 0. 8 Hz; 1H, H5''), 3.65 (s, 3H, OMe)				
2.119n	3-OMe	3-NO_2	6.90 (dd, J_1= 8.0, J_2= 0.8 Hz, 1H, H4'), 6.69 (t, J= 8.0 Hz, 1H, H5'), 6.35 (dd, J_1= 7.6, J_2= 0.8 Hz, 1H, H6'), 3.75 (s, 3H, OMe)	8.40 (t, J= 1.6 Hz, 1H, H2''), 8.33 (ddd, J_1= 7.6, J_2= 2.4, J_3= 0.8 Hz, 1H, H4'), 8.04 (d, J= 8.0 Hz, 1H, H6''), 7.78 (t, J= 8.0 Hz, 1H, H5'')	5.35 (s, 2H)	7.89 (s, 1H), 7.68 (s, 1H)	9.09 (s, 1H)
2.119o	3-OMe	2-Cl	6.85 (dd, J_1= 8.0, J_2= 1.6 Hz, 1H, H4'), 6.59 (t, J= 8.0 Hz, 1H, H5'), 6.12 (dd, J_1= 7.6, J_2= 1.2 Hz, 1H, H6'), 3.73 (s, 3H, OMe)	7.55 (dt, J_1= 8.0, J_2= 1.6 Hz, 1H, H4'), 7.54 (dd, J_1= 8.0, J_2= 1.6 Hz, 1H, H3''), 7.43 (dd, J_1= 7.2, J_2= 1.6 Hz, 1H, H6''), 7.42 (dt, J_1= 7.6, J_2= 1.6 Hz, 1H, H5'')	5.10 (s, 2H)	7.81 (s, 1H), 7.63 (s, 1H)	9.01 (s, 1H)

Table 119: ^{13}C NMR (100 MHz, DMSO-d_6, δ ppm) spectroscopic data obtained for compounds **2.119a-o**

Compound	R^1	R^2	Ar(C1'-6')	Ar(C1''-6'')	CN	C1	C3	C4	Ca	$CONH_2$
2.119a	H	H	154.53 (C2'), 129.20 (C4'), 127.01(C6'), 121.27 (C1'), 119.07 (C5'), 115.09 (C3')	130.30 (C4''), 128.88 (C2'' + C6''), 128.73 (C3'' + C5''), 128.42 (C1'')	110.87	150.48	107.74	144.02	46.17	161.52
2.119b	H	2-Cl	155.12 (C2'), 129.54 (C4'), 128.58 (C6'), 120.37 (C1'), 118.64 (C5'), 114.97 (C3')	133.42 (C1''), 132.30 (C4'', C5''), 129.60 (C3''), 127.84 (C2''), 127.33 (C6'')	110.74	147.65	107.52	143.62	46.17	161.45
2.119c	H	3-Cl	154.81 (C2'), 129.53 (C4'), 127.82 (C6'), 121.00 (C1'), 119.11 (C5'), 114.97 (C3')	133.46 (C3''), 130.73 (C4''), 130.52 (C1''), 130.26 (C5''), 128.87 (C2''), 127.53 (C6'')	110.85	148.96	108.24	144.04	46.54	161.53
			155.65 (C2'), 130.20 (C4'), 129.68 (C6'),	132.68 (C3''), 132.50 (C4''), 132.23 (C6''), 132.08 (C2''), 131.61 (C5''), 129.81 (C1'')	110.85	146.63	108.24	143.72	46.54	161.84

2.119d	H	2,5-Cl	120.38 (C1'), 119.01 (C5'), 115.37 (C3')							
2.119f	H	4-CN	154.90 (C2'), 129.58 (C4'), 128.08 (C6'), 120.85 (C1'), 119.03 (C5'), 115.19 (C3')	132.97 (C1''), 132.70 (C3'' + C5''), 129.80 (C2'' + C6''), 118.33 (CN), 112.75 (C4'')	110.75	148.73	108.60	144.16	46.67	161.42
2.119g	H	3-NO_2	154.89 (C2'), 129.52 (C4'), 128.24 (C6'), 120.75 (C1'), 118.96 (C5'), 115.16 (C3')	147.73 (C3''), 135.22 (C6''), 130.44 (C5''), 130.07 (C1''), 124.82 (C4''), 123.84 (C2'')	110.72	148.14	108.43	144.08	46.65	161.35
2.119h	H	4-Cl	154.71 (C2'), 129.37 (C4'), 127.51 (C6'), 121.05 (C1'), 119.05 (C5'), 115.14 (C3')	135.18 (C4''), 130.76 (C3'' + C5''), 128.87 (C2'' + C6''), 127.39 (C1'')	110.83	149.36	108.03	144.04	46.35	161.47
2.119i	H	3-Br	154.76 (C2'), 129.45 (C4'), 127.73 (C6'), 120.96 (C1'), 119.05 (C5'), 115.16 (C3')	133.07 (C6''), 131.67 (C2''), 130.85 (C5''), 130.67 (C1''), 127.78 (C4''), 121.83 (C3'')	110.80	148.79	108.18	144.02	46.49	161.45
2.119j	H	4-Br	154.68 (C2'), 129.34 (C4'), 127.47 (C6'), 121.03 (C1'), 119.02 (C5'), 115.12 (C3')	139.91 (C2'' + C6''), 131.77 (C3'' + C5''), 127.71 (C1''), 123.95 (C4'')	110.80	149.39	108.01	144.06	46.33	161.42
2.119k	H	3-F	154.69 (C2'), 129.37 (C4'), 127.58 (C6'), 120.98 (C1'), 119.01 (C5'), 115.12 (C3')	161.79 (d, J=244.0 Hz, C3''), 148.96 (d, J=3.0 Hz, C1''), 130.95 (d, J= 8.0 Hz, C5''), 125.07 (d, J=3.0 Hz, C6''), 117.23 (d, J=21 Hz, C4''), 115.93 (d, J= 23.0 Hz, C2'')	110.77	154.69	108.10	143.96	46.36	161.41

2.119l	H	4-Me	155.00 (C2'), 129.34 (C4'), 128.26 (C6'), 120.77 (C1'), 118.64 (C5'), 114.88 (C3')	138.11 (C4''), 130.32 (C3'' or C5''), 130.25 (C3'' or C5''), 129.79 (C2'' or C6''), 129.69 (C2'' or C6''), 18.93 (Me)	111.03	149.99	107.17	143.32	45.98	161.66
2.119m	H	2-OMe	154.86 (C2'), 129.22 (C4'), 128.04 (C6'), 121.09 (C1'), 118.78 (C5'), 114.95 (C3')	157.23 (C2''), 132.40 (C4''), 131.78 (C6''), 120.59(C5''), 117.42 (C1''), 111.65 (C3''), 55.52 (OMe)	110.97	148.69	107.21	143.97	45.95	161.74
2.119n	3-OMe	3-NO_2	147.46 (C3'), 143.49 (C2'), 121.32 (C1'), 119.95 (C6'), 119.04 (C5'), 111.90 (C4')	147.79 (C3''), 135.13 (C6''), 130.41 (C5''), 129.99 (C1''), 124.83 (C4''), 124.00 (C2'')	110.69	148.27	108.34	144.15	46.52	161.37
2.119o	3-OMe	2-Cl	147.26 (C3'), 144.04 (C2'), 120.86 (C1'), 119.71 (C6'), 118.65 (C5'), 111.89 (C4')	133.34 (C1''), 132.37 (C4''), 132.32 (C6''), 129.55 (C3''), 127.32 (C5''), 127.70 (C2'')	110.61	147.72	107.35	143.74	45.92	161.40

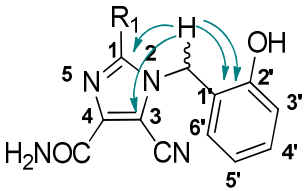


Table 120: ^{1}H NMR (400 MHz, DMSO-d_6, δ ppm) spectroscopic data obtained for compounds **2.119e,p,q**

Compound	R^1	Ar(H1'-6')	Ar(H1''-6'')	Ha	$CONH_2$	OH
2.119e		7.12 (dt, J_1= 7.2, J_2= 1.2 Hz, 1H, H4'), 6.83 (dd, J_1= 8.0, J_2= 0.4 Hz, 1H, H3'),	7.89 (d, J= 1.2 Hz; 1H, H4''), 6.95 (dd, J_1= 7.6, J_2= 0.4 Hz, 1H, H2''), 6.67 (dd, J_1= 3.6, J_2= 1.6 Hz, 1H, H3'')	5.48 (s, 2H)	7.78 (s, 1H), 7.69 (s, 1H)	9.99 (s, 1H)

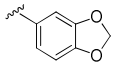
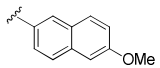
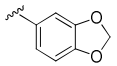
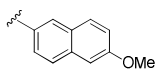
		6.71 (dt, J_1= 7.6, J_2= 0.8 Hz, 1H, H5'), 6.59 (dd, J_1= 7.6, J_2= 1.2 Hz, 1H, H6')				
2.119p		7.10 (t, J= 8 Hz, 1H, $H_{4'}$), 6.81 (d, J= 8 Hz, 1H, $H_{3'}$), 6.72 (t, J=7.6 Hz, 1H, $H_{5'}$), 6.56 (d, J= 6.8 Hz, 1H, $H_{6'}$)	7.13 (d, J= 1.6 Hz, 1H, H2''), 7.09 (dd, J_1= 8.0, J_2= 1.6 Hz, 1H, H6''), 7.02 (d, J= 8 Hz, 1H, H5''), 6.08 (s, 2H, Ha)	5.28 (s, 2H)	7.78 (s, 1H), 7.63 (s, 1H)	9.94 (s, 1H)
2.119q		7.10 (dt, J_1= 8.0, J_2= 2.0 Hz, 1H, H4'), 6.80 (dd, J_1=8.0, J_2= 1.6 Hz, 1H, H3'), 6.68 (dt, J_1= 8.0, J_2= 0.8 Hz, 1H, H5'), 6.62 (dd, J_1= 7.6, J_2= 0.8 Hz, 1H, H6')	8.09 (d, J= 1.2 Hz; 1H, H1''), 7.89 (d, J= 8.8 Hz, 1H, H8''), 7.80 (d, J= 9.2 Hz, 1H, H4''), 7.68 (dd, J_1= 8.4, J_2= 1.6 Hz, 1H, H3''), 7.37 (d, J= 2.4 Hz, 1H, H5''), 7.22 (dd, J_1= 9.2, J_2= 2.4 Hz, 1H, H7''), 3.92 (s, 3H, OMe)	5.39 (s, 2H)	7.83 (s, 1H), 7.63 (s, 1H)	10.06 (s, 1H)

Table 121: ^{13}C NMR (100 MHz, DMSO-d_6, δ ppm) spectroscopic data obtained for compounds **2.119e,p,q**

Compound	R^1	Ar(H1'-6')	Ar(H1''-6'')	CN	C1	C3	C4	Ca	$CONH_2$
2.119e		154.69 (C2'), 129.22 (C4'), 126.88 (C6'), 121.17 (C1'), 119.13 (C5'), 115.16 (C3')	145.30 (C3''), 142.70 (C1''), 113.08 (C5''), 112.10 (C4'')	110.73	141.34	107.85	144.25	46.21	161.29
2.119p		154.52 (C2'), 129.26 (C4'), 126.98 (C6'), 121.33 (C1'), 119.18 (C5'), 115.19 (C3')	148.93 (C3''), 147.53 (C4''), 123.45 (C6''), 121.95 (C1''), 109.02 (C2''), 108.75 (C5''), 101.78 (Ca)	110.95	150.23	107.49	143.90	46.16	161.58
2.119q		154.61 (C2'), 129.26 (C4'), 127.17 (C6'), 121.36 (C1'), 119.09 (C5'), 115.15 (C3')	158.53 (C6''), 134.81 (C2''), 129.98 (C4''), 128.64 (C1''), 127.62 (C10''), 127.17 (C8''), 126.17 (C3''), 123.41 (C9''), 119.69 (C7''), 105.97 (C5'')	111.03	150.68	107.85	144.10	46.22	161.61

References:

[1] O'Callaghan, C. N. "Anticancer Agents: VIII. Synthesis of Substituted Benzopyranom- [2, 3-d] Pyrimidines from 3-Carbamoyl-2-Iminochromens." *Proc. R. Irish Acad. Sect. B Biol. Geol. Chem. Sci. JSTOR* . **73**. 291–297 (1973).

[2] O'Callaghan, C. N. Isomerisation of 2-aryl-4-oxo-2,3-dihydrobenzopyrano[2,3-*d*]pyrimidines to 2-aryl-4-hydroxy-5*H*-benzopyrano[2,3-*d*]pyrimidines. *J. Chem. Soc. Perkin Trans. 1* 1335–1337 (1980). doi:10.1039/p19800001335.

[3] Hadfield, J. A. *et al.* Synthesis and anticancer activities of 4-oxobenzopyrano[2,3-*d*]pyrimidines. *Anti-Cancer Drugs* vol. 10 591–595 (1999).

[4] Borisov, A. V., *et al.* Parallel liquid-phase synthesis of benzopyrano[2,3-d]pyrimidine libraries. *J. Comb. Chem.* **9**, 5–8 (2007).

[5] Proença, F. & Costa, M. A simple and eco-friendly approach for the synthesis of 2-imino and 2-oxo-2*H*-chromene-3-carboxamides. *Green Chem.* **10**, 995–99 (2008).

[6] Costa, M. Síntese de derivados de cromeno para screening como agentes antipsicóticos. (University of Minho, 2010).

[7] O'Callaghan, C. N. *et al.*. Isomerisation of benzopyran-2-imines in [2H6]dimethyl sulfoxide. *J. Chem. Soc. Perkin Trans.* **2**, 425–429 (1998).

[8] Gutierrez, M. C. *et al*. Abiotic elicitation of coumarin phytoalexins in sunflower. *Phytochemistry* **38**, 1185–1191 (1995).

[9] Maes, D. *et al.* Synthesis and structural revision of naturally occurring ayapin derivatives. *Tetrahedron* **61**, 2505–2511 (2005).

[10] Ribeiro, A. B. *et al.* Chemical characterization of Citrus sinensis grafted on C. limonia and the effect of some isolated compounds on the growth of Xylella fastidiosa. *J. Agric. Food Chem.* **56**, 7815–7822 (2008).

[11] Chiang, C. C. *et al.* Prenyl coumarins from Fatoua pilosa. *J. Nat. Prod.* **73**, 1718–1722 (2010).

[12] Liang, D. *et al.* Lysilactones A-C, three 6*H*-dibenzo[*b,d*]pyran-6-one glycosides from Lysimachia clethroides, total synthesis of Lysilactone A. *Tetrahedron* **69**, 2093–2097 (2013).

[13] Robe, K. *et al.* The Coumarins: Secondary Metabolites Playing a Primary Role in Plant Nutrition and Health. *Trends Plant Sci.* **26**, 248–259 (2021).

[14] Salehian, F. *et al.* A review: Biologically active 3,4-heterocycle-fused coumarins. *Eur. J. Med. Chem.* **212**, 113034 (2021).

[15] Guilet, D. *et al*. Cytotoxic coumarins from Calophyllum dispar. *Phytochemistry* **58**, 571–575 (2001).

[16] Holiyachi, M. *et al.* Design and synthesis of new series of dipyrromethane-coumarin and porphyrin-coumarin derivatives: Excellent anticancer agents. *J. Mol. Struct.* **1237**, 130424

(2021).

[17] Al-Abbas, N. S. & Shaer, N. A. Combination of coumarin and doxorubicin induces drug-resistant acute myeloid leukemia cell death. *Heliyon* **7**, e06255 (2021).

[18] Dong, Y., Morris-Natschke, S. L. & Lee, K. H. Biosynthesis, total syntheses, and antitumor activity of tanshinones and their analogs as potential therapeutic agents. *Nat. Prod. Rep.* **28**, 529–542 (2011).

[19] Rath, B. *et al.* Design, synthesis and molecular modeling studies of novel mesalamine linked coumarin for treatment of inflammatory bowel disease. *Bioorg. Med. Chem. Lett.* **41**, 128029 (2021).

[20] Reddy, D. S., Kongot, M. & Kumar, A. Coumarin hybrid derivatives as promising leads to treat tuberculosis: Recent developments and critical aspects of structural design to exhibit anti-tubercular activity. *Tuberculosis* **127**, 102050 (2021).

[21] Hu, Y. Q. *et al.* Recent developments of coumarin-containing derivatives and their anti-tubercular activity. *Eur. J. Med. Chem.* **136**, 122–130 (2017).

[22] Kumbar, S. S. *et al.* Design, synthesis, molecular docking and biological activity studies of novel coumarino-azetidinones. *J. Mol. Struct.* **1231**, 130016 (2021).

[23] Li, Z. *et* al. Pharmacological perspectives and molecular mechanisms of coumarin derivatives against virus disease. *Genes Dis.* 103307 (2021). doi:https://doi.org/10.1016/j.gendis.2021. 03.007.

[24] Hu, Y. *et al.* Synthesis and antiviral activity of coumarin derivatives against infectious hematopoietic necrosis virus. *Bioorg. Med. Chem. Lett.* **29**, 1749–1755 (2019).

[25] Mishra, S., Pandey, A. & Manvati, S. Coumarin: An emerging antiviral agent. *Heliyon* **6**, e03217 (2020).

[26] Xu, Z., Chen, Q., Zhang, Y. & Liang, C. Coumarin-based derivatives with potential anti-HIV activity. *Fitoterapia* **150**, 104863 (2021).

[27] Mohr, F. *et al.* Synthesis and SAR evaluation of coumarin derivatives as potent cannabinoid receptor agonists. *Eur. J. Med. Chem.* 113354 (2021) doi:10.1016/j.ejmech.2021.113354.

[28] Sariyer, E. *et al.* In vitro inhibition studies of coumarin derivatives on Bos taurus enolase and elucidating their interaction by molecular docking, molecular dynamics simulations and MMGB(PB)SA binding energy calculation. *Bioorg. Chem.* **110**, 104796 (2021).

[29] Setena, S. M. & Shah, N. M. The chemistry of coumarins. *Chem. Rev.* **36**, 1–62 (1945)

[30] Murray, R. D. H. Coumarins. *Nat. Prod. Rep.* 477–505 (1995).

[31] Shockravi, A., Valizadeh, H. & Heravi, M. M. A one-pot and convenient synthesis of coumarins in solventless system. *Phosphorus, Sulfur.* **178**, 501–504 (2003).

[32] Kaye, P. T. *et al.* Does the DABCO-catalysed reaction of 2-hydroxybenzaldehydes with methyl acrylate follow a Baylis-Hillman pathway? *Org. Biomol. Chem.* **1**, 1133–1138 (2003).

[33] Sun, P. & Hu, Z. Gallium triiodide-catalyzed organic reaction: A convenient procedure for the synthesis of coumarins. *Synth. Commun.* **35**, 1875–1880 (2005).

[34] Manhas, M. S.. *et al.* Microwave initiated reactions: Pechmann coumarin synthesis, Biginelli reaction, and acylation. *Tetrahedron Lett.* **47**, 2423–2425 (2006).

[35] Ulgheri, F., Marchetti, M. & Piccolo, O. Enantioselective synthesis of (*S*)- and (*R*)-tolterodine by asymmetric hydrogenation of a coumarin derivative obtained by a Heck reaction. *J. Org. Chem.* **72**, 6056–6059 (2007).

[36] Borah, K. J. & Borah, R. Poly(4-vinylpyridine)-supported sulfuric acid: An efficient solid acid catalyst for the synthesis of coumarin derivatives under solvent-free conditions. *Monatshefte fur Chemie* **142**, 1253–1257 (2011).

[37] Khaligh, N. G. Synthesis of coumarins via Pechmann reaction catalyzed by 3-methyl-1-sulfonic acid imidazolium hydrogen sulfate as an efficient, halogen-free and reusable acidic ionic liquid. *Catal. Sci. Technol.* **2**, 1633–1636 (2012).

[38] Kalita, P. & Kumar, R. Solvent-free coumarin synthesis via Pechmann reaction using solid catalysts. *Micropor. Mesopor. Mat.* **149**, 1–9 (2012).

[39] Augustine, J. K. *et al.* An efficient one-pot synthesis of coumarins mediated by propylphosphonic anhydride (T3P) via the Perkin condensation. *Tetrahedron Lett.* **53**, 4422–4425 (2012).

[40] Albadi, J. *et al.* A green, efficient and recyclable poly(4-vinylpyridine)-supported copper iodide catalyst for the synthesis of coumarin derivatives under solvent-free conditions. *Comptes Rendus Chim.* **16**, 407–411 (2013).

[41] Costa, M., Rodrigues, A. I., F. P. & Proença, M. F. Synthesis of 3-aminochromenes : the Zincke reaction revisited. *Tetrahedron* **70**, 4869–4875 (2014).

[42] Vahabi, V. & Hatamjafari, F. Microwave assisted convenient one-pot synthesis of coumarin derivatives via Pechmann condensation catalyzed by FeF3 under solvent-free conditions and antimicrobial activities of the products. *Molecules* **19**, 13093–13103 (2014).

[43] Das, D. K. *et al.* A mild and efficient method for large scale synthesis of 3-aminocoumarins and its further application for the preparation of 4-bromo-3-aminocoumarins. *Tetrahedron Lett.* **55**, 4869–4874 (2014).

[44] S. Zambare, A. *et al.* Recent advances in the synthesis of coumarin derivatives via Pechmann condensation. *Curr. Org. Chem.* **20**, 798–828 (2015).

[45] Detsi, A., Kontogiorgis, C. & Hadjipavlou-Litina, D. Coumarin derivatives: an updated patent review (2015-2016). *Expert Opin. Ther. Pat.* **27**, 1201–1226 (2017).

[46] Pornsatitworakul, S. *et al.* The coumarin synthesis: a combined experimental and theoretical study. *Monatshefte fur Chemie* **148**, 1245–1250 (2017).

[47] Chaudhari, H. K., Pahelkar, A. & Takale, B. S. Preparative-scale synthesis of amino coumarins through new sequential nitration and reduction protocol. *Tetrahedron Lett.* **58**, 4107–4110 (2017).

[48] Li, H. *et al.* Anticancer carbazole alkaloids and coumarins from Clausena plants: A review. *Chin. J. Nat. Med.* **15**, 881–888 (2017).

[49] Ibrar, A. *et al.* Developing hybrid molecule therapeutics for diverse enzyme inhibitory action: Active role of coumarin-based structural leads in drug discovery. *Bioorgan. Med. Chem.* **26**, 3731–3762 (2018).

[50] Singh, H. *et al.* Rational approaches, design strategies, structure activity relationship and mechanistic insights for therapeutic coumarin hybrids. *Bioorgan. Med. Chem.* **27**, 3477–3510 (2019).

[51] Kumar, K. A. *et al*. Comprehensive review on coumarins: Molecules of potential chemical and pharmacological interest. *J. Chem. Pharm. Res.* **7**, 67–81 (2015).

[52] Costa, M., Dias, T. A., Brito, A. & Proença, F. Biological importance of structurally diversified chromenes. *Eur. J. Med. Chem.* **123**, 487–507 (2016).

[53] Burlison, J. A. & Blagg, B. S. J. Synthesis and evaluation of coumermycin A1 analogues that inhibit the Hsp90 protein folding machinery. *Org. Lett.* **8**, 4855–4858 (2006).

[54] Burlison, J. A. *et al.* Development of novobiocin analogues that manifest anti-proliferative activity against several cancer cell lines. *J. Org. Chem.* **73**, 2130–2137 (2008).

[55] Musa, M. A. *et al*. *In Vitro* cytotoxicity of benzopyranone derivatives with basic side chain against human lung cell lines. *Anticancer Res.* **30**, 4613–4617 (2010).

[56] Alt, S. *et al*. An artificial pathway to 3,4-dihydroxybenzoic acid allows generation of new aminocoumarin antibiotic recognized by catechol transporters of E. coli. *Chem. Biol.* **18**, 304–313 (2011).

[57] Thakur, A., Singla, R. & Jaitak, V. Coumarins as anticancer agents: A review on synthetic strategies, mechanism of action and SAR studies. *Eur. J. Med. Chem.* **101**, 476–495 (2015).

[58] Emami, S. & Dadashpour, S. Current developments of coumarin-based anti-cancer agents in medicinal chemistry. *Eur. J. Med. Chem.* **102**, 611–630 (2015).

[59] Skoczynska, A. *et al.* Synthesis, structural analysis, redox properties and in vitro antitumor evaluation of half-sandwich complexes of Ru(II) with aminocoumarins. *Polyhedron* **127**, 307–314 (2017).

[60] Bisi, A. *et al.* Coumarin derivatives as potential antitumor agents: Growth inhibition, apoptosis induction and multidrug resistance reverting activity. *Eur. J. Med. Chem.* **127**, 577–585 (2017).

[61] Elshemy, H. A. H. & Zaki, M. A. Design and synthesis of new coumarin hybrids and insight into their mode of antiproliferative action. *Bioorgan. Med. Chem.* **25**, 1066–1075 (2017).

[62] Alblewi, F. F. *et al.* Antiproliferative effect, cell cycle arrest and apoptosis generation of novel synthesized anticancer heterocyclic derivatives based 4*H*-benzo[*h*]chromene. *Bioorg. Chem.* **87**, 560–571 (2019).

[63] Rodríguez-Cerrato, V. *et al.* Comparative efficacy of novobiocin and amoxicillin in experimental sepsis caused by β-lactam-susceptible and highly resistant pneumococci. *Int. J. Antimicrob. Agents* **35**, 544–549 (2010).

[64] Matts, R. L. *et al.* A systematic protocol for the characterization of Hsp90 modulators. *Bioorgan. Med. Chem.* **19**, 684–692 (2011).

[65] Azelmat, J. *et al.* Synthesis and evaluation of antibacterial and anti-inflammatory properties of naturally occurring coumarins. *Phytochem. Lett.* **13**, 399–405 (2015).

[66] Angelova, V. T. *et al.* Antimycobacterial activity of novel hydrazide-hydrazone derivatives with 2*H*-chromene and coumarin scaffold. *Bioorgan. Med. Chem. Lett.* **27**, 223–227 (2017).

[67] Mbaba, M. *et al.* Ferrocenyl and organic novobiocin derivatives: synthesis and their in vitro biological activity. *J. Inorg. Biochem.* **172**, 88–93 (2017).

[68] Jaswal, S. *et al.* Recent advancements in the medicinal chemistry of bacterial type II topoisomerase inhibitors. *Bioorg. Chem.* **104**, 104266 (2020).

[69] Mani Chandrika, K. V. S. & Sharma, S. Promising antifungal agents: A minireview. *Bioorgan. Med. Chem.* **28**, (2020).

[70] Singh, O. M. *et al.* Novel 3-alkanoyl/aroyl/heteroaroyl-2*H*-chromene-2-thiones: Synthesis and evaluation of their antioxidant activities. *Eur. J. Med. Chem.* **45**, 2250–2257 (2010).

[71] Patil, P. O. *et al.* A comprehensive review on synthesis and designing aspects of coumarin derivatives as monoamine oxidase inhibitors for depression and Alzheimer's disease. *Bioorgan Med. Chem.* **21**, 2434–2450 (2013).

[72] Matos, M. J. *et al.* Novel (coumarin-3-yl)carbamates as selective MAO-B inhibitors: Synthesis, in vitro and in vivo assays, theoretical evaluation of ADME properties and docking study. *Eur. J. Med. Chem.* **63**, 151–161 (2013).

[73] Anand, A. *et al.* A click chemistry approach for the synthesis of mono and bis aryloxy linked coumarinyl triazoles as anti-tubercular agents. *Eur. J. Med. Chem.* **105**, 194–207 (2015).

[74] Subbareddy, C. V., Subashini, R. & Sumathi, S. Synthesis of substituted 2*H*-chromenes by a three-component reaction as potential antioxidants. *Mol. Divers.* **21**, 841–848 (2017).

[75] de Souza, L. G., Rennã, M. N. & Figueroa-Villar, J. D. Coumarins as cholinesterase inhibitors: A review. *Chem. Biol. Interact.* **254**, 11–23 (2016).

[76] Gonçalves, G. A. *et al.* Natural and synthetic coumarins as antileishmanial agents: A review. *Eur. J. Med. Chem.* **203**, (2020).

[77] Thacker, P. S. *et al.* Synthesis and biological evaluation of some coumarin hybrids as selective carbonic anhydrase IX and XII inhibitors. *Bioorg. Chem.* **104**, 104272 (2020).

[78] Smith, C. G. *et al.* Streptonivicin, a new antibiotic. I. Discovery and biologic studies. *Antibiot Chemother (Northfield)* **6**, 135–142 (1956).

[79] Hoeksema, H., Johnson, J. L. & Hinman, J. W. Structural srudies on streptonivicin, a new antibiotic. *J. Am. Chem. Soc.* **77**, 6710–6711 (1955).

[80] Hooper, D. C. *et al.* Effects of novobiocin, coumermycin Al, clorobiocin, and their analogs on Escherichia coli DNA Gyrase and bacterial growth. *Antimicrob. Agents Chemother.* **22**, 662–671 (1982).

[81] Marcu, M. G. *et al.* The heat shock protein 90 antagonist novobiocin interacts with a previously unrecognized ATP-binding domain in the carboxyl terminus of the chaperone. *J. Biol. Chem.* **275**, 37181–37186 (2000).

[82] Yu, X. M. *et al.* Hsp90 inhibitors identified from a library of novobiocin analogues. *J. Am. Chem. Soc.* **127**, 12778–12779 (2005).

[83] Burlison, J. A. *et al.* Novobiocin: Redesigning a DNA gyrase inhibitor for selective inhibition of Hsp90. *J. Am. Chem. Soc.* **128**, 15529–15536 (2006).

[84] Le Bras, G. *et al.* New novobiocin analogues as antiproliferative agents in breast cancer cells and potential inhibitors of heat shock protein 90. *J. Med. Chem.* **50**, 6189–6200 (2007).

[85] Shawna, B. C. *et al.* Characterization of a novel novobiocin analogue as a putative C-terminal inhibitor of heat shock protein 90 in prostate cancer cells. *Prostate* **70**, 27–36 (2011).

[86] Eskew, J. D. *et al.* Development and characterization of a novel C-terminal inhibitor of Hsp90 in androgen dependent and independent prostate cancer cells. *BMC Cancer* **11**, 468 (2011).

[87] Zhao, H. *et al.* 3-arylcoumarin derivatives manifest anti-proliferative activity through Hsp90 inhibition. *ACS Med. Chem. Lett.* **3**, 327–331 (2012).

[88] Gunaherath, G. M. K. B. *et al.* Synthesis and biological evaluation of novobiocin analogues as potential heat shock protein 90 inhibitors. *Bioorgan Med. Chem.* **21**, 5118–5129 (2013).

[89] Zhao, H. *et* al.3D-QSAR-assisted design, synthesis, and evaluation of novobiocin analogues. *ACS Med. Chem. Lett.* **4**, 57–62 (2013).

[90] Garg, G., Khandelwal, A. & Blagg, B. S. J. *Anticancer Inhibitors of Hsp90 Function: Beyond the Usual Suspects*. *Advances in Cancer Research* vol. 129 (Elsevier Inc., 2016).

[91] Byrd, K. M. *et al.* Synthesis and biological evaluation of novobiocin core analogues as Hsp90 inhibitors. *Chem-Eur. J.* **22**, 6921–6931 (2016).

[92] Zhao, H. *et al.* Engineering an antibiotic to fight cancer: optimization of the novobiocin scaffold to produce anti-proliferative agents. *J. Med. Chem.* **54**, 3839–3853 (2011).

[93] Kusuma, B. R., Duerfeldt, A. S. & Blagg, B. S. J. Synthesis and biological evaluation of arylated novobiocin analogs as Hsp90 inhibitors. *Bioorgan. Med. Chem. Lett.* **21**, 7170–7174 (2011).

[94] Linch, F. W. CLXXXVII.-3-Aminocoumain. *J. Chem. Soc. Trans.* **101**, 1758–1765 (1925).

[95] Donnelly, A. C. *et al.* The design, synthesis, and evaluation of coumarin ring derivatives of the novobiocin scaffold that exhibit antiproliferative activity. *J. Org. Chem.* **73**, 8901–8920 (2008).

[96] Kudale, A. A. *et al.* Hydrolysis-free synthesis of 3-aminocoumarins. *Tetrahedron Lett.* **48**, 5077–5080 (2007).

[97] Proença, M. F. & Costa, M. One-pot approach to the synthesis of novel 12*H*-chromeno[2′,3′:4,5]imidazo[1,2-*a*]pyridines in aqueous media. *Tetrahedron* **66**, 4542–4550 (2010).

[98] Reis, J. *et al.* Chromone as a privileged scaffold in drug discovery: recent advances. *J. Med. Chem.* **60**, 7941–7957 (2017).

[99] Raj, V. & Lee, J. 2*H*/4*H*-Chromenes- A versatile biologically attractive scaffold. *Front. Chem.* **8**, 1–23 (2020).

[100] Zhao, W. *et al.* Design, synthesis, and biological evaluation of novel 4*H* -chromen-4- one derivatives as antituberculosis agents against multidrug-resistant tuberculosis. *Eur. J. Med. Chem.* **189**, 112075 (2020).

[101] Thanh, N. D. *et al.* Efficient click chemistry towards novel 1*H*-1,2,3-triazole-tethered 4*H*-chromene−*D*-glucose conjugates: Design, synthesis and evaluation of in vitro antibacterial, MRSA and antifungal activities. *Eur. J. Med. Chem.* **167**, 454–471 (2019).

[102] Chitreddy, S. V & Shanmugam, S. Solvent free-synthesis of highly functionalized 4*H*-chromene-3-carboxamide derivatives using cerium ammonium nitrate and their antioxidant, antibacterial and solvatochromism studies. *J. Mol. Liq.* **243**, 494–502 (2017).

[103] Carr, M. *et al.* Optimisation of estrogen receptor subtype-selectivity of a 4-Aryl-4*H*-chromene scaffold previously identified by virtual screening. *Bioorg. Med. Chem.* **28**, 115261 (2020).

[104] Pontes, O. *et al.* Exploitation of new chalcones and 4*H*-chromenes as agents for cancer treatment. *Eur. J. Med. Chem.* **157**, 101–114 (2018).

[105] Anthony, S. P. *et al.* EPC2407, a new beta-tubulin vascular disrupting agent with potent apoptosis and cell growth inhibition. *J. Clin. Oncol.* **25**, 14043 (2007).

[106] Wang, H. *et al.*. Regioselective synthesis and evaluation of 2-amino 3-cyano chromene-chrysin hybrids as potential anticancer agents. *Bioorg. Med. Chem. Lett.* **30**, 127087 (2020).

[107] Spasov, A. A. *et al.* Synthesis, in vitro and in vivo evaluation of 2-aryl-4*H*-chromene and 3-aryl-1*H*-benzo[*f*]chromene derivatives as novel α-glucosidase inhibitors. *Bioorg. Med. Chem. Lett.* **29**, 119–123 (2019).

[108] Manouchehrizadeh, E. *et al.* Alignment-independent 3D-QSAR and molecular docking studies of tacrine–4-oxo-4*H*-Chromene hybrids as anti-Alzheimer' s agents. *Comput. Biol. Chem.* **80**, 463–471 (2019).

[109] Dige, N. C. *et al.* Synthesis and characterization of new 4*H*-chromene-3-carboxylates ensuring potent elastase inhibition activity along with their molecular docking and chemoinformatics properties. *Bioorg. Chem.* **100**, 103906 (2020).

[110] A Phase I/II Trial of Crolibulin (EPC2407) Plus Cisplatin in Adults With Solid Tumors With a Focus on Anaplastic Thyroid Cancer (ATC).URL: https://clinicaltrials.gov/ct2/show/NCT01240590 (2021).

[111] Yin, S. Q. *et al.* Preparation of S14161 and its analogues and the discovery of 6-bromo-8-ethoxy-3-nitro-2H-chromene as a more potent antitumor agent in vitro. *Bioorgan. Med. Chem. Lett.* **23**, 3314–3319 (2013).

[112] Saha, P. *et al.* Enantioselective Synthesis of Highly Substituted Chromans via the Oxa-Michael-Michael Cascade Reaction with a Bifunctional Organocatalyst. *J. Org. Chem.* **80**, 11115–11122 (2015).

[113] Tashrifi, Z. *et al. Synthesis and pharmacological properties of polysubstituted 2 - amino-4H-pyran-3-carbonitrile derivatives*. *Molecular Diversity* vol. 24 (Springer International Publishing, 2020).

[114] Halawa, A. H. *et al.* Synthesis, biological evaluation and molecular docking studies of 4*H*-benzo[*h*]chromenes, 7*H*-benzo[h]chromeno[2,3-*d*]pyrimidines as antitumor agents. *Lett. Drug Des. Discov.* **13**, 77–88 (2016).

[115] Alblewi, F. F. *et al.* Antiproliferative effect, cell cycle arrest and apoptosis generation of novel synthesized anticancer heterocyclic derivatives based 4*H*-benzo[*h*]chromene. *Bioorg. Chem.* **87**, 560–571 (2019).

[116] El-Agrody, A. M., Fouda, A. M. & Al-Dies, A. A. M. Studies on the synthesis, in vitro antitumor activity of 4*H*-benzo[*h*]chromene, 7*H*-benzo[*h*]chromene[2,3-*d*]pyrimidine derivatives and structure-Activity relationships of the 2-,3- and 2,3-positions. *Med. Chem. Res.* **23**, 3187–3199 (2014).

[117] Okasha, R. M. *et al.* Design of new Benzo[*h*]chromene derivatives: antitumor activities and structure-activity relationships of the 2,3-positions and fused rings at the 2,3-positions. *Molecules* **22**, (2017).

[118] Minch, M. J. Orientational dependence of vicinal proton-proton NMR coupling constants: The Karplus relationship. *Concepts Magn. Reson.* **6**, 41–56 (1994).

[119] Aydin, R., Loux, J.-P. & Günther, H. Karplus Curve for 3J(13C,1H) in Hydrocarbons. *Angew. Chemie Int. Ed. English* **21**, 449 (1982).

[120] Davey, S. Analysing the α-effect. *Nat. Chem.* **3**, 753–753 (2011).

[121] Pontes, O. New chromene-based drug candidates for cancer treatment. (University of Minho, 2016).

[122] Khademi, Z. & Nikoofar, K. Applications of alkyl orthoesters as valuable substrates in organic transformations, focusing on reaction media. *RSC Adv.* **10**, 30314–30397 (2020).

[123] Alves, M. J., Booth, B. & Proença, M. F. J. R. P. Synthesis of 5-Amino-4-(cyanoformimidoyl)-1*H*-imidazole: a reactive intermediate for the synthesis of 6-carbamoyl-I2-dihydropurines and 6- carbamoylpurines. *1. CHEM. SOC. PERKIN TRANS* 1705–1712 (1990).

[124] Booth, B. L. *et al.* Synthesis of 1-(N-benzyloxyformimidoyl)-2-aryl-4,5-dicyanoimidazoles: A new and efficient method from diaminomaleonitrile derivatives. *Synthesis (Stuttg).* 1269–1278 (2000) doi:10.1055/s-2000-6420.

[125] Alves, M. J. *et al.* (*Z*)-N3-(2-Amino-1,2-dicyanoviny1)formamidrazone: a precursor in the synthesis of 1,5-diaminoimidazoles and 6-carbamoyl-1,2-dihydropurines. *J. CHEM. SOC. PERKIN TRANS. I* 913–917 (1992).

[126] Alves, M. J., Proença, M. F. J. R. P. & Booth, B. L. Synthesis of 4- and 5-disubstituted 1-benzylimidazoles, important precursors of purine analogs. *J. Heterocycl. Chem.* **31**, 345–350 (1994).

[127] Alves, M. J. *et al.* Synthesis of 4-substituted 8-amino-4,5-dihydro-3*H*-pyrrolo[3,4-f]-1,3,5-triazepin-6-ones and 5-amino-2-aryl-4-(1-aryl-5-alkylideneaminoimidazol-4-yl)-1,3-oxazoles. *J. Chem. Soc. Peerkin Trans I* 3571–3577 (1994).

[128] Booth, B. L. *et al*. Synthesis of (*Z*)-*N*-(2-aniino-l,2-dicyanovmyl)forniamide O-alkyloximes and a study of their cyclization in the presence of base. *J. Chem. Soc. - Perkin Trans. 1* 1853–1858 (1999) doi:10.1039/a901332f.

[129] Alves, M. J. *et al*. Synthesis and mechanism of formation of novel 2,5-dihydro-2,5-diimino-3,4-di[(N,N-dimethylamino)methylideneamino]pyrroles and 5-Amino-3,4-di[(N,N-dimethylamino) methylideneamino]-2*H*-2-iminopyrroles. *J. Heterocycl. Chem.* **36**, 193–199 (1999).

[130] Fadda, A. A. & Youssif, E. H. E. Synthesis of some new chromene derivatives, Part 6. *Synth. Commun.* **41**, 677–694 (2011).

[131] El-Wahab, A. H. F. A. Synthesis, reactions and evaluation of the antimicrobial activity of some 4-(*p*-Halophenyl)-4*H*-naphthopyran, pyranopyrimidine and pyranotriazolopyrimidine derivatives. *Pharmaceuticals* **5**, 745–757 (2012).

[132] Abd El-Wahab *et* al. Synthesis and reactions of some new benzylphthalazin-1-ylaminophenols, 2*H*-chromene and 5*H*-chromeno[2,3-*d*]pyrimidine derivatives with promising antimicrobial activities. *Lett. Org. Chem.* **9**, 360–367 (2012).

[133] Youssef, M. S. K., Abeed, A. A. O. & El-Emary, T. I. Synthesis and evaluation of chromene-based compounds containing pyrazole moiety as antimicrobial agents. *Heterocycl. Commun.* **23**, 55–64 (2017).

[134] Figueiredo, P. *et al*. Adenine derivatives: promising candidates for breast cancer treatment. *Eur. J. Org. Chem.* **2018**, 3943–3956 (2018).

[135] L'abbé, G. Molecular rearrangements of five-membered ring heteromonocycles. *J. Heterocycl. Chem.* **21**, 627–638 (1984).

[136] El Ashry, E. S. H. *et al*. Chapter 5 - *Recent advances in the Dimroth Rearrangement: a valuable tool for the synthesis of heterocycles*. in *Advances in Heterocyclic Chemistry* (ed. Katritzky, A. R.) vol. 101 161–228 (Academic Press, 2010).

[137] L'Abbé, G. & Vanderstede, E. Dimroth rearrangement of 5-hydrazino-1,2,3-thiadiazoles. *J. Heterocycl. Chem.* **26**, 1811–1814 (1989).

[138] Mamedov, V. A. *et al*/The Dimroth rearrangement in the synthesis of condensed pyrimidines – structural analogs of antiviral compounds. **57**, 342–368 (2021).

[139] Loakes, D., Brown, M. & Salisbury, S. A. A Dimroth rearrangement of pyrimidine nucleosides. 1333–1337 (1999).

[140] Loakes, D. & Road, H. Cyclisation and rearrangement of *N*-4-acylaminodeoxycytidines. **39**, 3865–3868 (1998).

[141] Webb, R. L., Frank, S. & Schneider, W. C. The structure of Hcn tetramer. *J. Am. Chem. Soc.* **77**, 3491–3493 (1955).

[142] Bredereck, H. & Becher, G. S. H. Zur Konstitution der tetrameren Blausäure und ihrer Acyl-Derivate. *J. Ann.* **600**, 87–95 (1956).

[143] Al-Azmi, A., Elassar, A. Z. A. & Booth, B. L. The chemistry of diaminomaleonitrile and its utility in heterocyclic synthesis. *Tetrahedron* **59**, 2749–2763 (2003).

[144] MacLachlan, M. J., Park, M. K. & Thompson, L. K. Coordination compounds of Schiff-Base ligands derived from diaminomaleonitrile (DAMN): mononuclear, dinuclear, and macrocyclic derivatives. *Inorg. Chem.* **35**, 5492–5499 (1996).

[145] Booth, B. L. *et al.* The reactions of diaminomaleonitrile with isocyanates and either aldehydes or ketones revisited. *J. Org. Chem.* **66**, 8436–8441 (2001).

[146] Ohtsuka, Y. Chemistry of diaminomaleonitrile. II. Preparation of the open-chain adduct with ketone in phosphorus pentoxide-ethanol system. *J. Org. Chem.* **41**, 629–633 (1976).

[147] Ohtsuka, Y. Chemistry of diaminomaleonitrile. 4. Nitrile hydration of the Schiff bases. *J. Org. Chem.* **44**, 827–830 (1979).

[148] Ohtsuka, Y. & Tohma, E. Chemistry of diaminomaleonitrile. 5.' Dihydropyrazine synthesis. *J. Org. Chem* **44**, 4871–4876 (1979).

[149] Shirai, K., Matsuoka, M. & Fukunishi, K. New syntheses and solid state fluorescence of azomethine dyes derived from diaminomaleonitrile and 2,5-diamino-3,6-dicyanopyrazine. *Dye. Pigment.* **47**, 107–115 (2000).

[150] Sun, Z. & Hosmane, R. S. An improved synthesis of 9-benzyladenine: A model for adenosine and its analogues. *Synth. Commun.* **31**, 549–554 (2001).

[151] Correia, C., Carvalho, M. A. & Proença, M. F. Synthesis and in vitro activity of 6-amino-2,9-diarylpurines for *Mycobacterium tuberculosis*. *Tetrahedron* **65**, 6903–6911 (2009).

[152] Horiguchi, E. *et al.* New syntheses and spectral properties of diazepine flourescent dyes with non-planar molecular structure. *Dye. Pigment.* **50**, 99–107 (2001).

[153] Ribeiro, A. I. *et al.* Synthesis and antimicrobial activity of novel 5-aminoimidazole-4-carboxamidrazones. *Bioorgan. Med. Chem. Lett.* **24**, 4699–4702 (2014).

[154] Begland, R. W. US. Patent 3 914 276. (1976).

[155] Patai, S. & Jacob, Z. *The chemistry of the carbonyl group*. (1966).

[156] Padwa, A. & Glazer, E. Photochemical Reorganizations in the 1,3-Diazabicyclo[3.1 .O] hex-3-ene System. *J. Am. Chem. Soc.* **94**, 7788–7797 (1972).

[157] R., K. A. & Boulton, A. J. *Advances in Heterocyclic Chemistry*. (1972).

[158] Pereira, C. B. B. C. Síntese e avaliação da actividade antioxidante e micobacteriana de novos derivados de imidazole e purina. (University of Minho, 2010).

[159] Areias, F. M. F. de M. Novos compostos heterocíclicos de Azoto com unidades fenólicas: Síntese e actividade biológica. (University of Minho, 2006).

Chapter 3

Biological evaluation and computational studies

3.1 Triple-negative breast Cancer (TNBC)

3.1.1 Introduction

Cancer – relevance, incidence, and impact on human health

According to the World Health Organization (WHO) "the cancer burden continues to grow globally, exerting tremendous physical, emotional and financial strain on individuals, families, communities and health systems"[1]. Considering the Global Cancer observatory GLOBOCAN report (International Agency for Research on Cancer, 2020, WHO[2]), cancer has become one of the leading cause of death globally, with an accounted 9.9 million deaths in 2020, which corresponds to 1 in 6 human deaths. The most lethal types of cancer are lung cancer (1.79 million cases), breast cancer (684.996 cases), colorectal cancer (935 173 cases) and liver cancer (830 180 cases) (**Figure 83**).

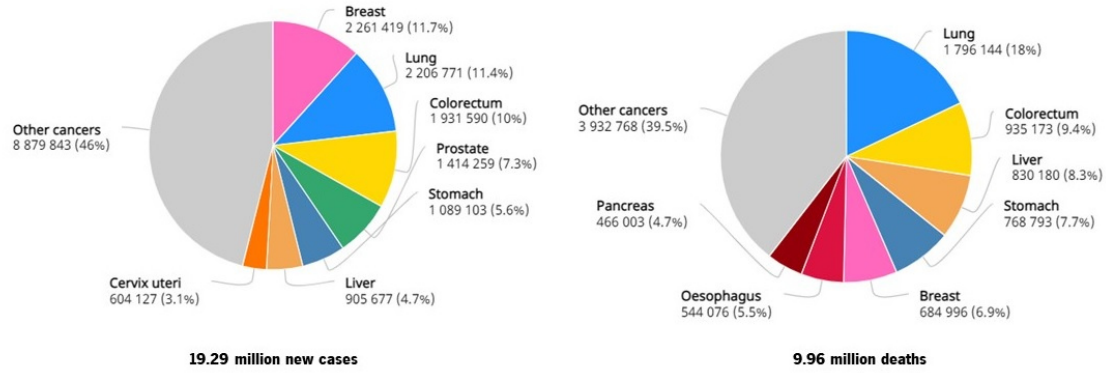


Figure 83: Charts presenting the distribution of cases and deaths for the 10 most common cancers for both sexes in 2020, according to GLOBOCAN 2020 [Arnold M, Rutherford M, Lam F, Bray F, Ervik M, Soerjomataram I (2019). ICBP SURVMARK-2 online tool: International Cancer Survival Benchmarking. Lyon, France: International Agency for Research on Cancer. Available from: http://gco.iarc.fr/survival/survmark, accessed [12th/June/2021]

In terms of incidence, the most frequent types of cancer diseases among 19.2 million new cases identified in 2020 are breast cancer (2.26 million cases), lung cancer (2.21 million cases), colorectal cancer (1.93 million cases), prostate cancer (1.41 million cases) and stomach cancer (1.09 million cases)[2]. In addition, when analyzed separately, each sex has different percentages of incidence and mortality. Thus, for males, lung cancer (14.5%) and prostate cancer (13.5%) are the most diagnosed types, with lung cancer (22%) and liver cancer (10.2%) being the deadliest. For women, breast cancer (24.2%) and colorectal cancer (9.5%) are the most common types, with breast cancer (15%) and lung cancer (13.8%) being the most lethal types.

Although not fully understood, cancer seems to be the consequence of a multifactorial process that converts a normal cell into a tumor cell, which usually progresses from a non-cancerous lesion to a malignant tumor[1]. This evolution is driven by the combination of individual's genetic factors with external factors (carcinogens), which can be classified into three major categories[1]:

A) Physical carcinogens (ultraviolet, ionizing radiation, etc)
B) Chemical carcinogens (asbestos, components of tobacco smoke, arsenic, etc)
C) Biological carcinogens (infections from certain viruses, bacteria, or parasites, such as Human Papilomavirus)

Molecular mechanisms and biochemical features of cancer

Cancer is described as a group of diseases that relate to each other by an uncontrolled cell division, acquired and replicative immortality, loss of function and resistance to cell death[3]. Cancer cells typically grow into an abnormal cell mass (tumor)[3]. An exception for this is hematologic tumors, for which cancer cells grow and spread throughout the blood, lymph systems and the bone marrow[3,4].

The process typically starts by the occurrence of damage or mutation on proto-oncogenes coding for proteins implicated in regulating cell proliferation and differentiation, and/or on tumor suppressor genes coding for proteins that stimulate inhibitory signals of cell growth and/or stimulate apoptosis. Alterations in both onco-genes and tumor suppressor genes are necessary for tumor development and are favored by mutations in the tumor susceptibility genes, which encode for a family of proteins that control DNA damage. With each cloning, there is a selection of mutations that induce aberrant and uncontrolled cell division, avoid regulation of excessive cell growth, cloaking from the immune system, accumulation of erratic genetic mutations and further transmission[3,5–11].

In 2000, Hanahan and Weinberg summarized the most important hallmarks for cancer development, highlighting the most relevant factors involved in cell survival, growth and proliferation[12]. In 2011, the same authors further amplified the idea, to include two more hallmarks[13], resulting in the graphic included in **Figure 84**. Later, Floor *et al* expanded this concept in order to include the loss of differentiation as an essential hallmark to be considered. The authors justified this inclusion because these events occur through deregulation of several intertwined signaling pathways and biochemical alterations within the cell.



Figure 84: The cancer hallmarks according to Hananah and Weinberg [Reprinted from ref.12, copyright 2021, with permission from Elsevier]

One of the most recognized mechanisms that tumoral cells are able to alter and manipulate is apoptosis[14]. This process differentiates from necrosis[15] because of its origin, morphology and biochemical patterns[16]. Typically, the term necrosis is used when a trauma or unprogrammed event occurs, leading to the loss of the integrity of cells and tissues, which is due to the lack of blood perfusion or other occurencies[15,17,18]. On the contrary, apoptosis is considered a regulated cell death process[15–18] to which cells recur as an evolutionary conservative mean to avoid the propagation of DNA or organelle errors and mutations[16–18]. Some authors refer that necrotic or apoptotic process can occur depending on the dosage or extension of the aggression[19–21]. Usually, apoptosis occurs during cell development and aging and as a homeostatic mechanism to maintain cell populations in tissues[19], as well as a defense mechanism such as in immune reactions or in cellular damage by disease or noxious agents[19]. Although there are some doubts, as to the specific function of some of its components, or the biochemical process by which apoptosis proceeds is well-known[19,22–24]. There are two main pathways for apoptosis: (i) intrinsic or mitochondrial pathway; and (ii) extrinsic or death receptor pathway. Although interconnection between them is possible[19,25,26], it is recognized that the extrinsic pathway is activated by the binding to death receptors of members of the tumor necrosis factor (TNF) superfamily of cytokines (as for example TNF-α, fibroblast-associated cell surface (Fas) ligand (FasL) and TNF-related apoptosis-inducing ligand (TRAIL))[26]. On the contrary, the intrinsic pathway alters on the mitochondrial activity, whereby caspase-8 cleaves the pro-apoptotic B-cell lymphoma 2 (Bcl-2) homology (BH) domain BH-3 interacting-domain death agonist (Bid), leading to mitochondrial permeabilization and release of cytochrome c and other apoptosis inducing factors[26].

On the other hand, nowadays, the general knowledge about carcinogenesis has been increasing, and at the present, two models are accepted to describe the development of cancer cells: (i) the stochastic model defends that any type of cell is able to initiate and promote tumour development; and (ii) the cancer stem cell (CSC) model that suggests that tumours are hierarchically structured and cancer-promoting potential is only present in CSCs[27,28].

Breast cancer and triple-negative breast cancer

Breast cancer is described as one of the most nefarious cancer types. According to GLOBOCAN 2020[2], it is the most diagnosed cancer type worldwide and is the main cause of cancer-related deaths in women (684.996 deaths, 6.9% of the total cancer-related deaths). Following the same tendency as verified for almost all types of cancer, it was most frequently diagnosed in Asia (45.4%), Europe (23.5%) and North America (12.5%), but the majority of deaths occurred in Asia (50.5%), Europe (20.7%) and Africa (12.5 %)[29]. In 2020, an increase of 29.011 deaths in comparison to 2018 was verified, which had 2.1 million newly diagnosed cases. It is estimated that it represents 1 in 4 cases of cancer in women[30], and that 1 in every 8-10 women develops breast cancer[31,32].

The survival rate of breast cancer patients, in both the developed and developing countries, have significant variations[33]. According to incomplete statistical data, for the developed countries, the 5-year survival rate of patients with breast cancer can reach 80%, while is lower than 40% in developing countries[33,34]. Unfortunately, despite the mortality rate is decreasing[33], the problem is far from being solved. Thus, GCO predicts that, in the next 20 years, the incidence of breast cancer in women, of all ages, will rise from 2 179 457 cases and 655 690 deaths in 2020 to 3 059 829 cases and 991 904 deaths in 2040.

Despite existing a hereditary and genetic predisposition for developing breast cancer, this only represents about 5-10% of breast cancer cases. In fact, studies of migration patterns have shown that non-hereditary factors are indeed the major contributors of the observed international and interethnic differences in breast cancer incidence[30]. By studying the low-risk populations migration to high-risk populations it was possible to understand that breast cancer incidence rates rise in successive generations[30,35].

High incidence rates in countries with higher Human Developing Index (HDI) are attributed to an elevated prevalence of known risk factors. On the contrary, elevated incidence rates in transitioned countries result from known risk factors that arise from menstruation (early age at menarche, later age at menopause), reproduction (late age at first birth, nulliparity and fewer descendants), hormonal intake (oral contraceptive use and hormone replacement therapy), anthropometry (weight gain during adulthood, body fat distribution and increased weight) and dietary habits (alcohol intake). By contrast, it is documented that breastfeeding and physical activity act as protective factors[30,36]. Although epidemiological tracing and risk factors assessment is still a challenge to overcome and fully understand, as they most likely reflect an interaction of demographic, social and economic development factors, an awareness arose from this knowledge. In several developed countries (United States, the United Kingdom, France, Australia and Canada), a decrease in the number of incidences in the early 2000s was correlated with a declining usage of postmenopausal hormonal treatment, as revealed a trial from Women's Health Initiative that proved a linkage between these drugs and an increase of breast cancer risk[30,37].

According to the St. Gallen Consensus report, published in 2011, breast cancer is considered an heterogeneous disease with multiple molecular subtypes (Luminal A, Luminal B, HER2-enriched and Basal-Like or Triple Negative), which are summarized in **Table 122**[38–40]. This molecular diversity results in different responses to treatment, prognosis and risk factors, which in turns means that it is a pathology that requires an adapted therapy for each case[40–43], encompassing all immunohistochemical differences that each one have.

Table 122: Molecular subtypes of breast cancer, according to the St. Gallen Consensus summary [adapted from ref.41][a]

Intrinsic subtype	IHC Classification
Luminal A	ER and/or PR positive, HER2 negative; Ki-67 <14%
Luminal B	"luminal B negative (HER2-" (ER and/or PR positive, HER2 negative; Ki-67 >14%) "luminal B positive (HER2+" (ER and/or PR positive, HER2 over-expressed or amplified; any Ki-67)
HER2-enriched	"HER2 positive (non-luminal)" HER2 over-expressed or amplified; ER and PR absent
Basal-like	"Triple-negative" ER and PR absent, HER2 negative

[a]PR – Progesterone receptor; ER – Estrogen receptor; HER2- Human epidermal growth factor receptor 2

The major factors that are recognized as being responsible for the occurrence and development of breast cancer are:

a) Reproductive factors: Premature menarche, late menopause, no breastfeeding and nulliparity lead to higher probability of developing breast cancer[33,44–46].
b) Genetic factors: Chances of developing breast cancer double if the mother has/had breast cancer[47].
c) Dietary and lifestyle-related factors: Obesity, smoking and drinking are related to the development of breast cancer[48,49].
d) Environmental factors: Exposure to exogenous estrogen for a long period of time increases the risk of developing breast cancer[50].

Presently, in a first step, breast cancer is treated by surgical resection and chemotherapy[51,52]. Chemotherapeutic drugs are generally highly toxic, and traditional pharmaceutical dosage cannot reduce toxicity, resulting in severe side effects. On the other hand, conventional pharmaceutical preparations lack specificity for the tumorous cells, and only a small fraction of the drug is targeted to the tumor tissues following entry into the systemic circulation. For this reason, the drug utilization rate of conventional pharmaceutical preparations is in decrease. Therefore, selecting effective and safe drugs treatment of patients with breast cancer is of vital importance[33].

Triple-negative breast cancer (TNBC) represents about 12-17% of all breast cancers[53–55] and is considered the most aggressive subtype[56–59]. Although new targeted therapies are being developed for the treatment of patients with HR+ or HER2+ phenotypic expression, chemotherapy is the only systemic therapy for patients with breast cancer types that do not express these markers[56], and unfortunately, with very limited results[60]. The majority of TNBCs share common histological and molecular traits, which include a set of frequent p53 and BRCA1 mutations, an elevated proliferative index, and frequent expression of a basal-like gene expression signature[54,61]. TNBCs are also characterized by extensive inter- and intra-tumoral heterogenicity, which leads to various biological and clinical subgroups that are formed[54], as well as high tumor recurrence rates and poor overall survival[55]. It is also characterized by an earlier onset of metastatic disease, visceral metastases, short response duration to available therapies, rapidly progressive disease and less favourable survival outcomes[62,63]. This aggressiveness is well illustrated by the fact that the peak risk of recurrence happens between the first and third years and almost all deaths occur in the first 5 years, after therapy[56,64,65]. These findings along with the fact that

TNBC more frequently affect younger patients (<50 years)[56,64–67], suggest that TNBC has similarities to basal-like cancers. This type of cancer is more prevalent in African-American women[67–69].

A series of modified molecular pathways that are involved in the development of TNBC have already been identified[53,70]. Thus, it is well established the connection between BRCA1 gene disfunction and the triple negative status of TNBC, as hereditary BRCA1-mutated breast cancer usually exhibits basal-like gene expression patters, and sporadic TNBC often carries BRCA1 mutations[71]. Since BRCA1 is strictly involved in DNA double-strand break repair, it has been postulated, and later corroborated by experimental data[72], that is particularly sensitive to DNA-damaging agents. Diverse signaling pathways are damaged and/or altered in TNBC, such as the PI3K/AKT/mTOR pathway, the RAF/MEK/ERK pathway, the JAK/STAT pathway and the PARP-dependent DNA repair pathway[63,70,73–75]. Also, several targets involved in DNA repair pathways and cell cycle checkpoint appear to be affected as well, such as p53 (which is mutated in about 80%, in TNBC[70,74]) and the Myc gene family (which showed a gene amplification that can be as high as 40%[74]). ErbB1, also known as epidermal growth factor receptor (EGFR), is a trans-membrane glycoprotein encoded by a proto-oncogene located at 7p12-p13, which is involved, among other biological functions, in the regulation of normal breast cells growth and development[53]. EGFR is closely involved in cell migration, proliferation, and protection against apoptosis, mediated by subsequent activation of intracellular pathways. Similarly to HER2, EGFR is a potent cell-growth-activating pathways promoter, via which it stimulates tumor growth when activated[53,76]. It is referred, in several studies, that EGFR is overexpressed in at least 20% of the total breast cancer cases[77,78], as well as being correlated with TNBC, with percentages ranging from 42 to 71% of EGFR expression being found in these cancer subtype[79,80].

In the search for effective drugs against TNBC, several targets are currently being studied, such as phosphoinositide 3-kinase (PI3K), mitogen-activated protein kinase (MEK), poly-ADP ribose polymerase (PARP) and epidermal growth factor receptor (EGFR), with diverse compounds targeting these biological objectives being already at different phases of clinical trials[70]. Moreover, despite its role in TNBC is not fully understood, the androgen receptor (AR) has also been investigated with promising results[53,74,81]. The outcomes of this effort is a set of clinical trials, at different clinical phases, that are ongoing for TNBC treatment[63,73,82,83].

Current therapies and treatment

The extensive research effort devoted to the identification of small-molecule inhibitors in the last years has led to the approval by the Food and Drug Administration (FDA) of several new anticancer drugs. These are relatively low molecular weight compounds (less than 900 Da) that are able to penetrate into cancer cells and target specific protein within the cells[84–86]. Some examples include inhibitors of tyrosine kinases, serine/threonine kinases, human epidermal growth factor receptor 2 (HER2), epidermal growth factor receptor (EGFR) and vascular endothelial growth factor (VEGF), BRAF and Akt[87]. Non-receptor tyrosine kinases (nRTKs) have also been explored as anti-cancer agents[87]. In addition, compounds targeting signalling pathways, which are dysregulated during carcinogenesis, proteasomes, cyclin-dependent kinases (CDKs), and poly ADP-ribose polymerase (PARP), which activate cell-cycle checkpoint, trigger apoptosis, and promote DNA repair[86,88], have also been studied.

Developing new therapeutic approaches against TNBC is a challenge due to its biological and biochemical characteristics, and the little knowledge available about this type of cancer, in particular its genomic sequencing, and its molecular characterization[62,63,89]. The lack of expression of the estrogen receptor (ER), progesterone receptor (PR) and human epidermal growth factor 2-receptor (HER2), combined with a more aggressive biology, harden the task of tackling this disease efficiently is an issue for clinicians[62,63,89]. In fact, there is no efficient treatment for TNBC that has been approved by either FDA or EMA[54], with lumpectomy and standard chemotherapy being used nowadays[70,71]. Some of the solutions that has been studied in the context of TNBC are miRNA therapy[90] and imunotherapy[91], in a similar fashion to what is already applied for other types of cancers. Fortunately, there have also been significant advances on the characterization of different subclonal heterogeneity and biological differences[54,73,92], which allows for the improvement of targeted therapies for each TNBC subtypes.

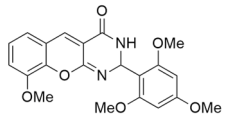
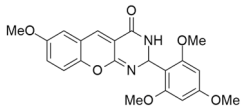
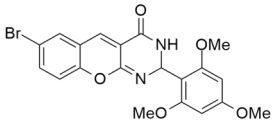
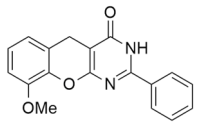
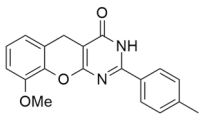
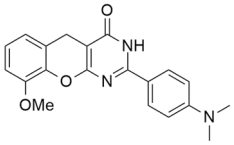
3.1.2 Biological evaluation of chromene-based and imidazole-based compounds activity against TNBC cell lines

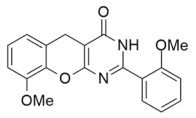
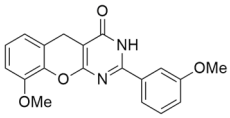
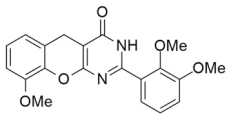
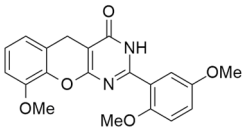
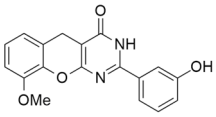
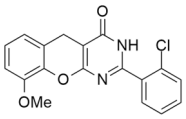
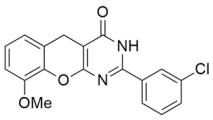
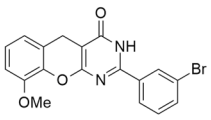
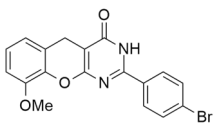
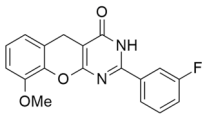
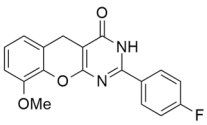
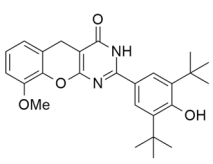
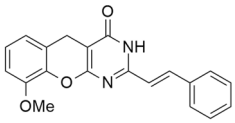
In this PhD thesis, the activity of compounds **2.3**, **2.6**, **2.50**, **2.55**, **2.69**, **2.86**, **2.87**, **2.90** and **2.109** against diverse TNBC cancer cell lines was evaluated by a series of assays performed by Luísa Carvalho, under the supervision of Doctor Marta Costa (published on her Master thesis named ''Exploitation of new chromene-based compounds as promising agents for cancer treatment'')[93]. In this

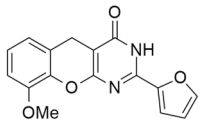
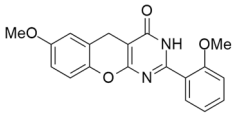
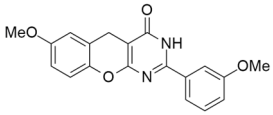
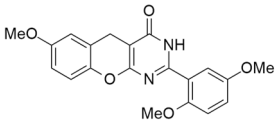
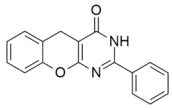
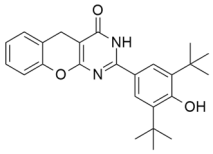
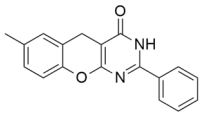
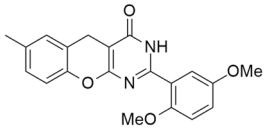
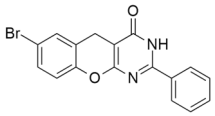
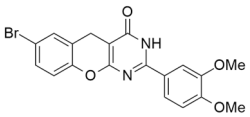
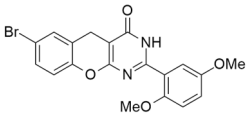
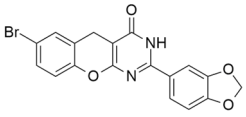
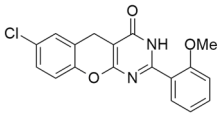
work, the ability of compounds' **2.3** and **2.6** to reduce cancer cell viability was measured at 10 and 30 μM concentrations, employing three cell lines, specifically MDA-MB-231 (triple negative), Hs578t (triple negative) and MCF-7 (luminal subtype). The percentage of cell survival was calculated after 72 h of treatment, by using Sulforhodamine B assay (SRB).

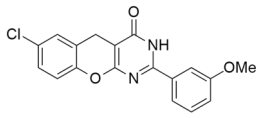
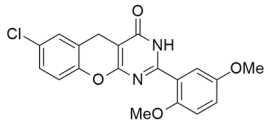
For a first screening, MDA-MB-231 cell lines were employed with a selection of compounds, which were tested at 10 μM and 30 μM concentrations. In these assays, the best results were obtained with compounds **2.6p** and **2.6d'**, for both concentrations studied, while the remaining compounds showed no significant anticancer activity (Table 123). The same assay was performed using Hs578t cell lines and a larger batch of compounds. In the latter case, compounds **2.6p** and **2.6d'** were also among the most promising anticancer agents, along with compounds **2.6l**, **2.6h'** and **2.6j'** (Table 123).

Table 123: Percentage (%) of cell viability, in Hs578t, MDA-MB-231 and MCF-7 breast cancer cell lines, after 72 h of treatment with compounds **2.3** and **2.6** at 10 and 30 μM concentrations

Compound		**MDA-MB-231**		**Hs578t**		**MCF-7**	
Ref.	**Structure**	10 μM	30 μM	10 μM	30 μM	10 μM	30 μM
2.3d		n.d	n.d	94.8	86.0	n.d	n.d
2.3h		n.d	n.d	100.3	96.	n.d	n.d
2.3i		n.d	n.d	96.9	79.5	n.d	n.d
2.6a		91.8	89.2	91.1	75.8	n.d	n.d
2.6b		99.2	91.1	86.8	63.3	n.d	n.d
2.6c		109.9	103.1	97.4	87.5	n.d	n.d

2.6d		n.d	n.d	86.0	80.2	n.d	n.d
2.6e		n.d	n.d	99.3	85.3	n.d	n.d
2.6f		87.1	88.4	72.7	73.9	n.d	n.d
2.6g		93.7	98.4	74.7	61.9	n.d.	n.d
2.6i		101.5	101.8	75.9	67.3	n.d	n.d
2.6j		92.5	90.1	81.7	72.5	n.d	n.d
2.6k		80.8	76.9	72.0	49.9	n.d	n.d
2.6l		92.0	80.7	66.8	40.6	78.4	52.4
2.6m		83.7	80.4	97.7	84.4	n.d	n.d
2.6n		81.2	71.2	95.3	60.8	n.d	n.d
2.6o		105.2	97.8	97.5	84.4	n.d	n.d
2.6p		68.1	58.6	30.0	18.7	59.8	43.5
2.6q		99.2	92.5	99.8	97.9	n.d	n.d

2.6r		n.d	n.d	99.8	90.7	n.d	n.d
2.6s		n.d	n.d	87.5	65.6	n.d	n.d
2.6t		n.d	n.d	88.0	77.0	n.d	n.d
2.6u		n.d	n.d	95.9	96.5	n.d	n.d
2.6x		n.d	n.d	76.3	65.4	n.d	n.d
2.6y		n.d	n.d	80.2	81.0	n.d	n.d
2.6b'		n.d	n.d	96.0	73.3	n.d	n.d
2.6c'		n.d	n.d	61.2	40.5	n.d	n.d
2.6d'		62.3	52.1	40.2	21.1	39.2	36.7
2.6f'		85.3	77.8	86.1	78.5	n.d	n.d
2.6g'		102.6	95.0	94.1	93.6	n.d	n.d
2.6h'		88.2	64.9	78.4	38.7	80.0	57.3
2.6i'		n.d	n.d	80.2	90.5	n.d	n.d

2.6j'		n.d	n.d	54.7	33.9	n.d	n.d
2.6k'		n.d	n.d	91.7	92.0	n.d	n.d

Based on the obtained results for these two cancer cell lines, compounds **2.6l**, **2.6p**, **2.6d'** and **2.6h'** were also tested in MCF-7 cancer cell lines. The results afforded a pattern that was consistent with the results that were obtained for MDA-MB-231 and Hs578t cell lines (**Table 123, Figure 85**).

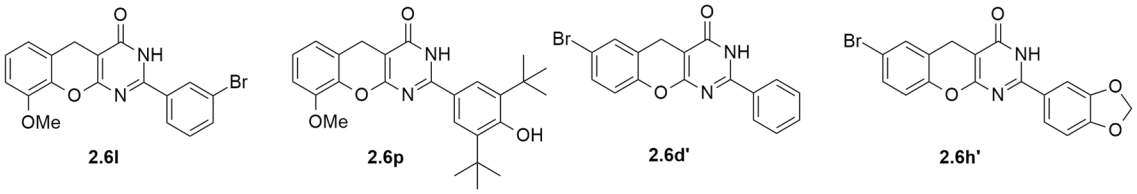
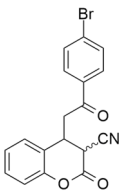
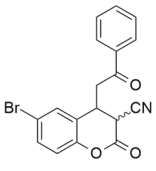
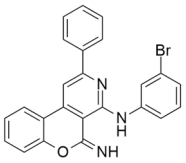
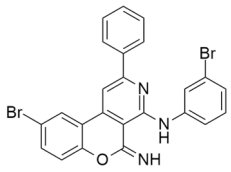
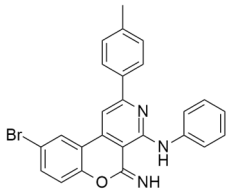
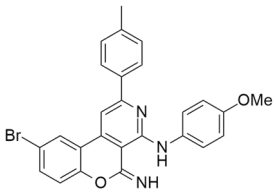
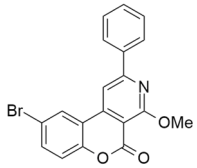
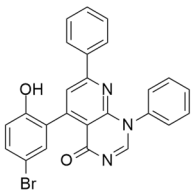
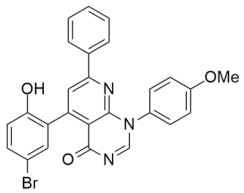
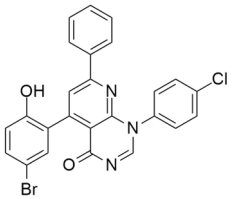
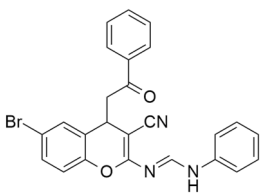


Figure 85: Compounds employed in assays with MCF-7 cancer cell lines

Compounds **2.50**, **2.55**, **2.69b**, **2.86**, **2.87** and **2.90** were also tested for their anticancer activity in Hs578t cancer cell lines (**Tables 124** and **125**). Among them, compounds **2.86b**, **2.86g**, and **2.90** proved to be the most active, while compounds **2.119** did not show any relevant anticancer activity against this cancer cell line (**Table 125**).

Table 124: Percentage (%) of cell viability in Hs578t cancer cell line, after 72h of treatment with compounds **2.50**, **2.55, 2.69b**, **2.86**, **2.87** and **2.90** at 10 μM and 30 μM concentrations

Compound		**Hs578t**	
Ref.	**Structure**	10 μM	30 μM
2.50c		107.7	104.5
2.50d		99.7	95.1

2.55e		111.2	101.2
2.55m		92.0	67.1
2.55n		99.9	97.2
2.55q		101.0	97.5
2.69b		95.7	97.7
2.86b		80.6	46.9
2.86f		101.9	52.9
2.86g		56.9	38.3
2.87b		96.1	89.9

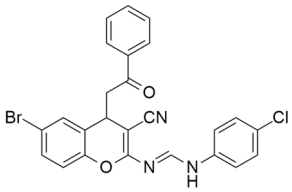
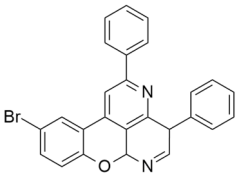
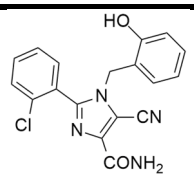
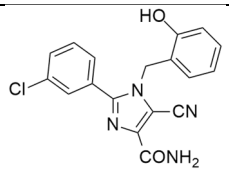
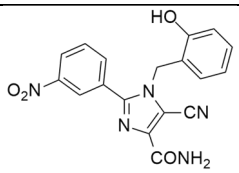
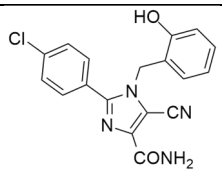
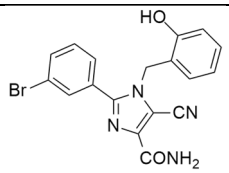
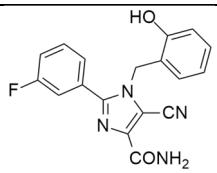
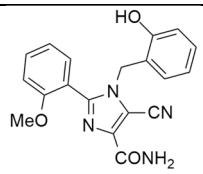
2.87l		99.1	91.9
2.90		50.4	32.6

Table 125: Percentage (%) of cell viability in Hs578t cancer cell lines, after 72 h of treatment with compounds **2.119** at 10 μM and 30 μM concentrations

Compound		**Hs578t**	
Ref.	**Structure**	10 μM	30 μM
2.119b		95.0	77.6
2.119c		96.0	81.0
2.119g		89.5	78.3
2.119h		86.1	77.3
2.119i		88.8	77.1
2.119k		98.2	74.3

2.119m		103.8	100.7

Hence, based on their induced low survival rates in the tested cancer cell lines, compounds **2.6p**, **2.6d'**, **2.6j'**, **2.86g** and **2.90** were selected for further studies. In addition, the effect of compounds **2.6p** and **2.6d'** on cell survival was also assessed in a non-neoplastic cell line (MCF-10A) to determine the potential *in vitro* toxicity of these compounds, as well as their selectivity towards cancer cell lines. These are relevant assays since most of the conventional therapies, such as chemotherapy, involve severe side-effects associated with compound toxicity and off-target effects. The half maximal inhibitory concentration (IC_{50}) values of the selected derivatives **2.6p**, **2.6d'**, **2.6j'**, **2.86g** and **2.90** against Hs578t cancer cell lines were determined by using the Sulforhodamine B (SRB) cytotoxicity assay, using doxorubicin and quercetin (a naturally occurring chromene) as reference compounds (**Table 126**). Seven different concentrations (40, 30, 10, 5, 1, 0.1 and 0.05 μM) of these compounds were studied. The IC_{50} values of compounds **2.6p** and **2.6d'** were also determined for MCF-10A cell lines, measurements taken at slightly higher concentrations, specifically 60, 45, 30, 10, 5, 1 and 0.1 μM.

Table 126: IC_{50} values of compounds **2.6p**, **2.6d'**, **2.6j'**, **2.86g** and **2.90**, doxorubicin and quercetin against Hs578t and MCF-10A cell lines after 72 h of treatment and selectivity index

Compounds[a]	**Breast cancer cell lines**		
	Hs578t IC_{50} **(μM) ± SD**[b]	**MCF-10A** IC_{50} **(μM) ± SD**[b]	**SI**[c]
2.6p	9.08 ± 0.10	> 60	> 5.61
2.6d'	4.50 ± 0.29	> 60	> 12.33
2.6j'	13.10 ± 0.05	n.d.	n.d.
2.86g	26.28 ± 0.08	n.d.	n.d.
2.90	8.63 ± 0.04	n.d.	n.d.
Doxorubicin	0.52 ± 0.01	1.54 ± 0.08	1.96
Quercetin	50.54 ± 0.12	n.d.	n.d.

[a]Each compound was tested at least in triplicate and the data are presented as mean values; [b]Standard Deviation; [c]Selectivity index of tested compounds against Hs578t *vs* MCF-10A cell lines

Altogether, the biological results indicate that **2.6d'**, **2.96** and **2.6p** represent the most promising compounds of the series, as they possess good IC_{50} values and high selectivity indexes in relation to non-neoplastic cell lines (MCF-10A). Thus, these compounds are between 6-fold and 11-fold more active than the natural chromene quercetin, and their selectivity indexes are over 40-fold higher than that of the standard doxorubicin.

3.1.3 Structure-activity relationship of chromeno[2,3-*d*]pyrimidin-4(5*H*)-ones 2.3 and 2.6

The results obtained for MDA-MB-231 cancer cell line follow a consistent pattern to those obtained for Hs578t cancer cell line for the same compounds. For this reason, and because it was possible to obtain a larger, better, and more consistent set of results for Hs578t cell line, these data were used to construct a general structure-activity relationship (SAR) model for this family of compounds against TNBC. To this end, all tested compounds, pyridopyrimidinones **2.3** and **2.6**, were clustered into seven groups according to their different substituents in positions 2, 7 and 9 (**Figure 86**).

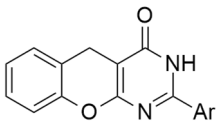


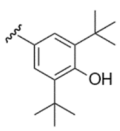
2.3 **2.6**

Figure 86: Ring nomenclature for compounds **2.3** and **2.6**

(1) Group 1 - Compounds with no substituents in ring A (**Table 127**). This group includes compounds **2.6y** and **2.6z** and serves as a standard value.

Table 127: Compounds included in group 1



Entry	Compound	Ar	Cell viability @10 µM	Cell viability @30 µM
1	**2.6x**		76.3%	65.4%
2	**2.6y**		80.2%	81.0%

(2) Group 2 – Compounds with a methoxy substituent in ring A (**Table 128**). This group includes 17 compounds, including **2.6s** where ring C is substituted by a 2-furyl group.

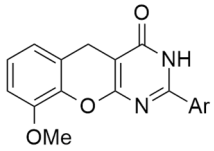
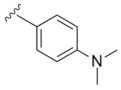
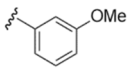
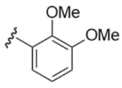
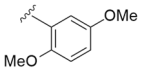
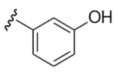
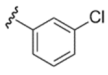
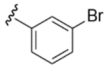
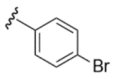
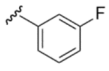
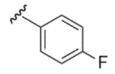
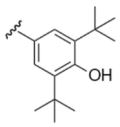
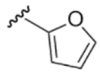


Table 128: Compounds included in group 2

Entry	Compound	Ar	Cell viability @10 µM	Cell viability @30 µM
1	**2.6a**		91.1%	75.8%
2	**2.6b**		86.8%	63.3%
3	**2.6c**		97.4%	87.5%
4	**2.6d**		86.0%	80.2%
5	**2.6e**		99.3%	85.3%
6	**2.6f**		72.7%	73.9%
7	**2.6g**		74.7%	61.9%
8	**2.6i**		75.9%	67.2%
9	**2.6j**		81.7%	72.5%
10	**2.6k**		72.0%	49.8%
11	**2.6l**		66.8%	40.6%
12	**2.6m**		97.7%	84.4%
13	**2.6n**		95.3%	60.8%

14	**2.6o**		97.5%	84.4%
15	**2.6p**		30.0%	18.7%
16	**2.6r**		99.8%	90.7%

There are several conclusions that can be taken from this group:

a) The activity increases when the position 2 (ring C) is substituted with an electron-withdrawing group, specifically chlorophenyl, bromophenyl or fluorophenyl (entries 11 and 13 *vs* 5 – **Table 128**). The major enhancement effect occurs for *meta* substituted halophenyl derivatives, as it is the case with compounds **2.6j**, **2.6l** and **2.6n** (entries 10, 11 and 13 – **Table 128**), followed by *ortho* substituted compounds (entry 9 – **Table 128**). Among the *meta* substituents, the trend is Br > Cl > F.

b) Compounds having a phenol substituent in position 2 (ring C) do not follow the previous trend, suggesting an alternative mechanism of action for those ones, such as radical processes (entry 8 – **Table 128**). Thus, the excellent activity achieved with compound **2.6p** (entry 15 – **Table 128**), which has a *para* phenol group flanked by two bulky groups, suggests that these substituents would stabilize a plausible radical generated in this position, thus increasing its lifetime.

(3) Group 3 – Compounds substituted with a methoxy group in position 7 (**Table 129**).

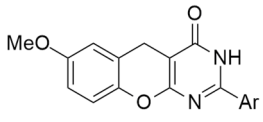
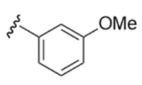
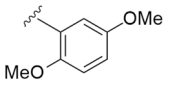


Table 129: Compounds included in group 3

Entry	Compound	Ar	Cell viability @10 µM	Cell viability @30 µM
1	**2.6s**		87.5%	65.6%
2	**2.6t**		86.6%	63.3%

3	**2.6u**		97.4%	87.5%

The comparison of these results with compounds **2.6d**, **2.6e** and **2.6g**, in which the methoxy group is located on position 9, suggests that the activity is enhanced up to about 80% when this group is on position 7, unless when the phenyl group in position 2 is substituted in both *meta* and *ortho* positions.

(4) Group 4 – Compounds substituted with a methyl group in position 7 (**Table 130**).

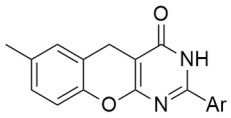
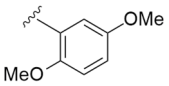


Table 130: Compounds included in group 4

Entry	Compound	Ar	Cell viability @10 µM	Cell viability @30 µM
1	**2.6b'**		96.0%	73.3%
2	**2.6c'**		61.2%	40.5%

From these results, some conclusions can be drawn:

a) When position 2 (ring C) is substituted by a phenyl group, the introduction of a methyl substituent in position 7 (ring A) slightly reduces the activity (entry 1 – **Table 127** *vs* entry 1 – **Table 130**).

b) On the contrary, when the substituent on position 2 (ring C) is a 2,5-dimethoxyphenyl group, the introduction of a methyl group in position 7 (ring A) significantly enhances the activity up to about 65%. In addition, for compounds substituted with a 2,5-dimethoxyphenyl group in position 2 (ring C), the functionalization of position 7 (ring A) is the one that most contributes to an improvement in activity among the compounds explored (entry 2 – **Table 130** *vs* entry 7 – **Table 128** and entry 3 – **Table 129**).

(5) Group 5 – Compounds substituted with a bromide in position 7 (**Table 131**).

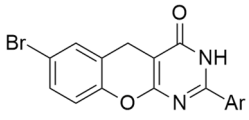
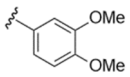
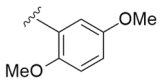
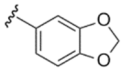


Table 131: Compounds included in group 5

Entry	Compound	Ar	Cell viability @10 μM	Cell viability @30 μM
1	**2.6d'**		40.2%	21.1%
2	**2.6f'**		86.1%	78.5%
3	**2.6g'**		94.1%	93.6%
4	**2.6h'**		78.4%	38.7%

From the results, it is possible to conclude that:

a) When the position 2 (ring C) is substituted by a phenyl ring, the introduction of a bromide substituent in position 7 (ring A) significantly enhances the activity. Thus, a 3-fold increase on the activity was obtained with compound **2.6d'** vs compound **2.6x** (entry 1 **– Table 131** *vs* entry 1 – **Table 127**).

b) On the contrary, no significant effect was observed for those compounds where the substituent in position 2 (ring C) is an electron-rich aromatic ring.

c) An exception of that is compound **2.6h'**, having a benzo[*d*][1,3]dioxol-5-yl moiety in position 2 (ring C). However, only good activity was obtained at 30 μM concentration.

(6) Group 6 – Compounds substituted with a chloride in position 7 (**Table 132**).

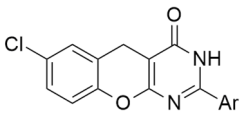
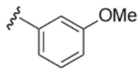
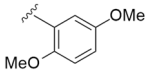


Table 132: Compounds included in group 6

Entry	Compound	Ar	Cell viability @10 μM	Cell viability @30 μM
1	**2.6i'**		80.2%	90.5%

2	**2.6j'**		39.8%	33.9%
3	**2.6k'**		91.7%	92.0%

A series of conclusions can be taken from these results:

a) The results obtained with compound **2.6j'** and its comparison with the activity obtained with compound **2.6t**, having a methoxy group at the same position 7, reveals the positive effect (2-fold enhancement) of reducing the electron density of ring A (entry 2 – **Table 132** *vs* entry 2 – **Table 129**).

b) However, the latter effect strongly depends on the existing aromatic substituent on position 2 (ring C). Thus, comparing compounds **2.6c'**, **2.6g'** and **2.6k'**, all bearing a 2,5-dimethoxyphenyl group at this position, but having a methyl, a bromine, and a chlorine substituent, respectively, at position 7 (ring A), did not follow this trend (entry 3 – **Table 132** *vs* entry 2 – **Table 130** and entry 3– **Table 131**). Compound **2.6c'** was the most potent compound of the three, suggesting that either they target distinct biological objectives, or the relative disposition of the chromeno[2,3*d*]pyrimidin-4-one moiety *vs* the aryl group at position 2 (ring C) controls the binding of the ligand, and therefore its efficacy. Regarding the latter, the analysis of the minimum energy conformation of compounds **2.6j'** and **2.6k'** reveals that the methoxy group in *ortho* position would interact by hydrogen bonding with the NH group of the pyrimidinone moiety, thus fixing the relative arrangement of both rings (**Figure 87**). On the contrary, in the absence of this substituent, free rotation around the C2-C1' bond was predicted to occur, suggesting that upon binding, this ligand could more easily achieve the optimal conformation of both rings to maximize the interaction with the target.

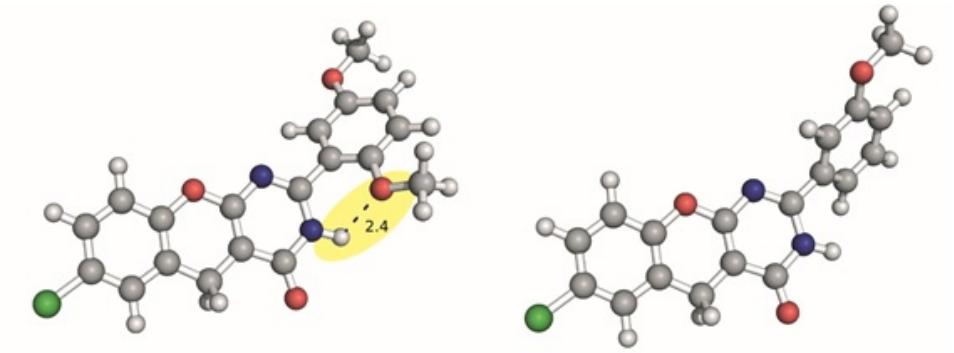


Figure 87: Minimum energy conformations of compounds **2.6j'** (left) and **2.6k'** (right). Note how for compound **2.6j'** a strong hydrogen bonding between the NH group of the pyrimidinone ring and the oxygen atom of the methoxy substituent at position 2 was identified, which would control the relative arrangement between the rings

(7) Group 7 – Tested compounds **2.3** (**Table 133**).

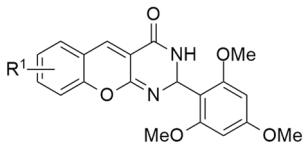
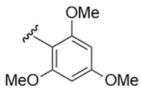
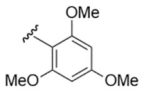
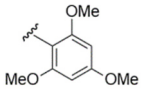


Table 133: Compounds included in group 7

Entry	Compound	Ar	Cell viability @10 μM	Cell viability @30 μM
1	**2.3d**		94.8%	86.0%
2	**2.3g**		100.3%	96.5%
3	**2.3i**		98.4%	83.0%

The fact that none of these compounds **2.3** were significantly active suggests that:

a) An almost planar geometry of the chromenepyrimidinone core seems to be important for good activity. Thus, the analysis of the relative arrangement of the two aromatic rings in the minimum energy conformation revealed that the migration of the double bond from ring C to ring B would cause a significant change in the overall shape of these compounds. As it is shown in **Figure 88**, compound **2.3i** would have a folded arrangement, mainly caused by the sp^3 form of C2, while a more linear conformation would be established when the sp^2 form of C2 is present in ring C.

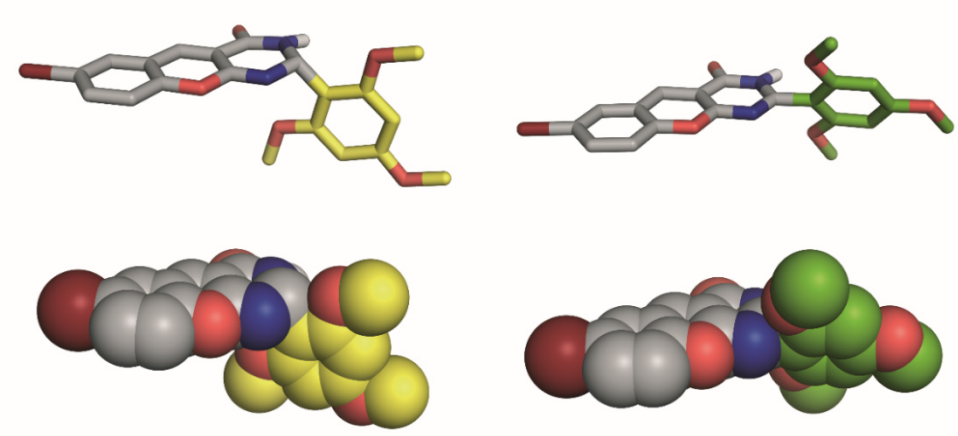


Figure 88: Minimum energy conformations of compound **2.3i** (left) and its counterpart with C2 being a sp^2 carbon (right). Each compound is represented in sticks (up) and in spheres (down). The carbon atoms of the aryl substituent in position C2 of the chromenepyrimidinone moiety are highlighted in yellow and green colours. Note the significant change in the overall conformation of the compounds when the position C2 change from the sp^3 to sp^2 hybridized forms

In conclusion, the biological results obtained with the chromene[2,3-*d*]pyrimidin-4(5*H*)-one derivatives **2.3** and **2.6** synthesized in this doctoral thesis revealed that the antitumor activity of these compounds is enhanced by: (i) the functionalization of position 7 (ring A) with an electron-withdrawing groups (halide); (ii) the introduction of an electron-deficient aromatic ring in position 2 (ring C), in particular in *meta* position, such as 3-bromobenzene or 3-chlorobenzene; (iii) the free rotation around the bond that joins the tricyclic system and the aromatic ring; and (iv) an overall planar arrangement of the scaffold, which is mainly achieved by a planar disposition of ring C (**Figure 89**).

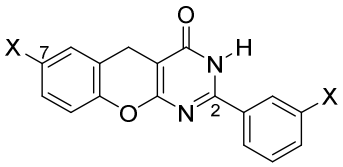


Figure 89: Positions and substituents promoting the activity of chromene[2,3-*d*]pyrimidin-4(5*H*)-one derivatives studied against TNBC cell lines. X = halide

3.1.4 *In silico* study of the potential of chromene[2,3-*d*]pyrimidin-4(5*H*)-ones 2.6 as PARP inhibitors

Importance of BRCA genes and PARP inhibition in TNBC

As previously mentioned, TNBC comprises a set of peculiar characteristics that contribute its aggressiveness and hardens the therapeutic process for the disease it promotes[58,59]. Despite the huge efforts devoted to achieve new anti-TNBC[94–98] drugs in the last years, the current therapies involve highly toxic and nonspecific chemotherapeutic agents, without the desired levels of efficacy. Therefore, it is urgent to search for new drugs to face this challenge. Among these peculiar characteristics, deficient expression of estrogen, progesterone, and HER2 are included, along with a well-documented relation with BRCA1/2 mutations[40,56,57,99].

The BRCA1 and 2 genes have a very well documented relation with several tumor suppression functions, in which are included the reparation of double strand DNA breaks via a process called homologous recombination repair[100–102]. In this way, an homologous DNA sequence is used to guide repair at the DNA breaks, and is considered a "conservative" mechanism as it restores the original DNA sequence at the site of DNA damage[102,103]. When this mechanism is compromised, as for example in the event of BRCA1/2 mutations, genomic instability and patients' predisposition to hereditary breast cancer is observed[100,104]. In addition, as the cell tends to recur to other DNA repair, like non-homologous end

joining and base excision repair[102,105]. These processes either fuse broken DNA ends at the DNA breaks without using a homologous DNA sequence to assist reparations, or fuse regions of DNA that exhibit short regions of DNA sequence homology and that are close to the site of the DNA break, deleting the intervening DNA sequence[102], and often leading to several DNA modifications such as genetic material deletion. Several of these alterations promote tumoral initiation, development and progression, partially explaining the BRCA-associated cancer risk[102], and generate spontaneous and DNA damage-induced genetic instability, which often leads to tumorigenesis[104].

The poly(ADP-ribose) polymerase (PARP) family comprises a group of 17 enzymes that are involved in a series of relevant cellular functions. PARP1 is an enzyme that uses β-NAD+ as a cofactor to synthesise poly(ADP-ribose) (PAR) chains on target proteins, and has a well-established role in the repair of single-strand DNA breaks through base excisional repair and non-homologous end joining[106–108] (**Figure 90**). When PARP is inhibited, unrepaired DNA single-strand break accumulate in BRCA-deficient cells, leading to DNA breaks that homologous recombination and non-homologous end joining cannot repair and thus generating continuous and fatal DNA damage. Therefore, mutations in BRCA1/2 genes will result in homologous repair deficiency and over sensitise cancer cells to PARP inhibitors[105]. This is also true to tumour phenotypes that are included in the "BRCAness" type[109]. This concept includes all somatic and induced phenotypes that promote homologous recombination repair deficiency, and that can also promote a response to the inhibition of PARP.

Farmer *et al*[110] and Bryant *et al*[111] were the first authors to propose that small molecule inhibitors of PARP caused accentuated cell inhibition of BRCA1/2 mutant tumour cells with minimal effects on wild-type cells with functional homologous recombination repair processes. Initially, it was suggested that the inhibition of PARP was caused by the amplification of DNA damage that required homologous repair for its restoration[110,111], but a few years later Murai *et al*[112,113] proposed that PARP inhibitors (PARPi) activity was mediated by what was called "PARP-trapping", a mechanism in which PARP binds to damaged DNA and then initiates a series of PARylation events. The latter is a series of cascade post-translational modifications promoted by PARP, in which can be included autoPARylation, that causes the release of PARP once its role in the initial phase of DNA repair is complete[104,107]. "PARP-trapping" promoted by PARPi impedes autoPARylation and thus stopping the decoupling of PARP from DNA (**Figure 90**). Based on this background, a possible strategy to target these BRCA-mutated cancer cells involves the promotion of replication fork damage, that forces homologous recombination repair to occur. As the cells are BRCA-deficient, this process cannot occur, leading to the inability to repair this defect and subsequent cell

death[104]. This process, in which a single mutation do not compromise cell functionality, but when combined with a mutation in another gene, cell viability becomes compromised, is called **synthetic lethality**, and such relation has been proposed between PARP and BRCA gene[108].

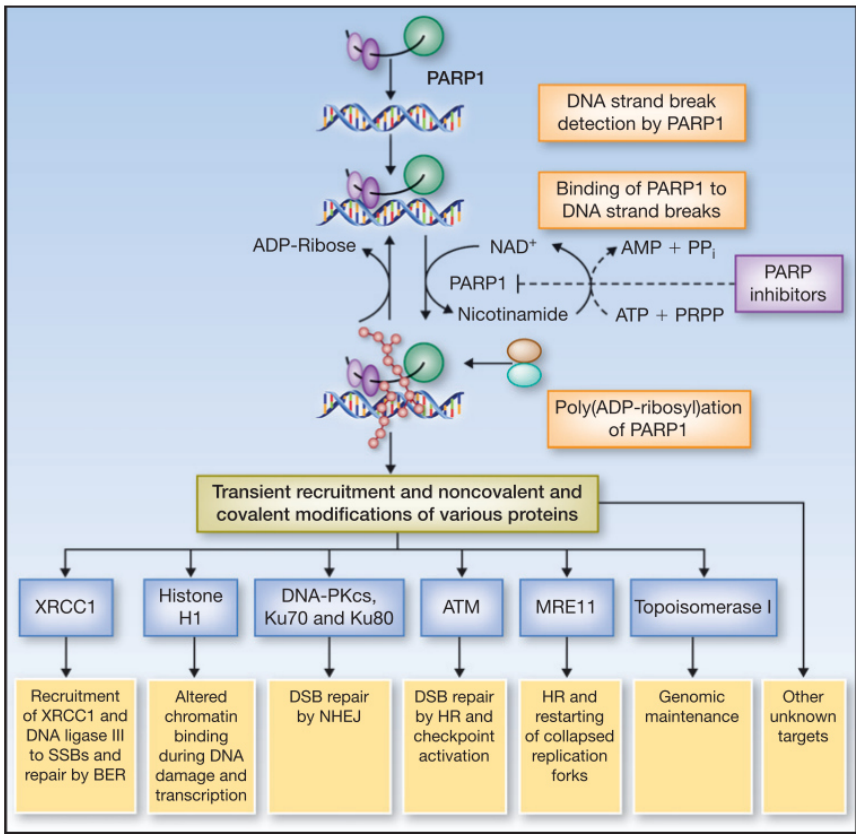


Figure 90: Schematic representation of PARP1 biological function. After binding to SSBs, PARP1 transfers the ADP-ribosyl moiety from NAD^+ to acceptor proteins, generating long chains of poly (ADP-ribosylated polymers. This allows for the recruitment of DNA repair proteins such as DNA polymerase b, DNA ligase III, and scaffolding protein XRCC1 to sites of SSBs. PARP may also facilitate homologous recombination via recruitment of factors like ATM, Mre11, and Nbs1 to sites of double-stranded DNA damage and has been shown to interact with the DNA protein kinase complex involved with nonhomologous end-joining. ATM, ataxia telangiectasia-mutated; BER, base excision repair; DNA-PKcs, DNA-protein kinase catalytic subunit; DSB, double-strand break; HR, homologous recombination; Mre11, mitotic recombination 11; Nbs1, Nijmegen breakage syndrome 1; NHEJ, nonhomologous end-joining; PPi, inorganic pyrophosphate; SSB, single-strand break; XRCC1, X-ray cross-complementing protein [Reprinted from ref. 107, with permission from AACR]

Based on the concept of synthetic lethality, much effort has been devoted to the development of PARP inhibitors for the treatment of a series of BRCA mutated cancer cells, in particular in the last decade[105,114–119]. Olaparib (AstraZeneca and Merck & Co) was the first PARP inhibitor to be approved by the FDA and EMA (2014), as a monotherapy, for germline BRCA-mutated advanced ovarian cancer patients that have received three or more prior chemotherapy treatments. In 2018, olaparib was also approved by FDA as a second-line treatment for human epidermal growth factor receptor-2 (HER2)-negative metastatic breast cancer[120]. After that, several compounds were launched on the market for the

treatment of different types of cancer: (i) rucaparib (Agouron Pharmaceuticals, approved by FDA, 2016); (ii) niraparib (GSK, approved by FDA and EMA, 2017); (iii) talazoparib (Pfizer, approved in 2018 by FDA and in 2019 by EMA) (**Figure 91**)[120].

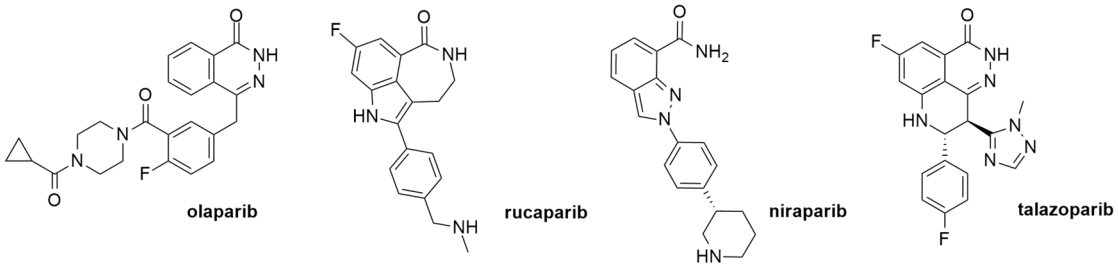


Figure 91: Chemical structures of olaparib, rucaparib, niraparib and talazoparib

Moreover, PARP inhibition has also been investigated as a potential therapeutic pathway for the treatment of TNBC patients based on the evidences reported that correlates PARP inhibition with improved therapeutic results for TNBC patients[120–122]. It has also been reported that more than half of the BRCA1 gene carriers have TNBC subtype[123], and several patients suffering from TNBC possess either BRCA1 mutation or "BRCAness"[120].

Structure-activity relationships in PARP inhibitors

In the 1980s, nicotinamide and 3-aminobenzamide were very useful as a proof of concept for PARPi, as they were able to inhibit PARP1 as expected[123]. The idea to test these two compounds came from PARP1 natural substrate, nicotinamide adenine dinucleotide (NAD^+), which bounds to the 55 kD catalytic domain and serves as building blocks for the poly-ADP ribose polymerization function. Later, Ueda and Banasik screened over 100 structurally diverse compounds and found a series of structural motifs, namely several bicyclic and tricyclic lactams, with inhibitory activity in the submicromolar range[123]. This work paved the road for the discovery of several other structural motifs, such as isoquinolinones, dihydroisoquionlinones, phthalazinones, quinazolinones, quinazolinediones, among others (**Figure 92**).

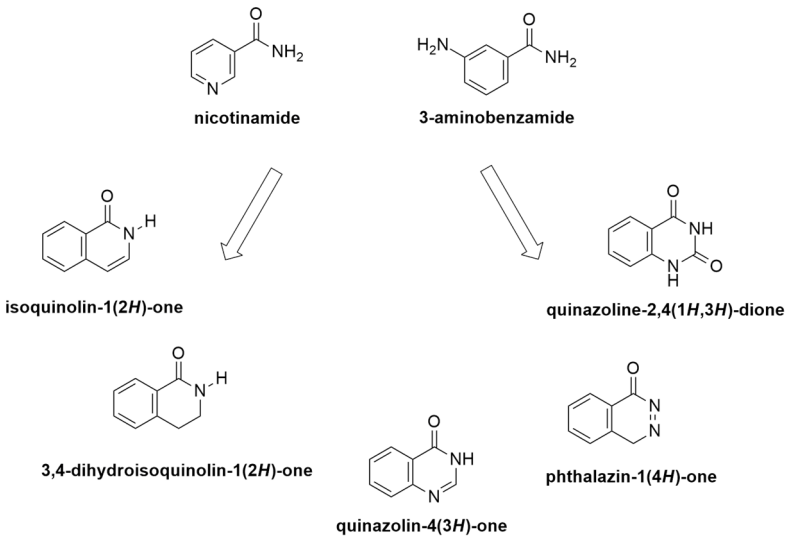


Figure 92: Structural motifs in reported PARP inhibitors

These studies were key for improving the PARP1 pharmacophore model, as it demonstrated that the inhibitory capacity of the compounds was increased by the presence of conformationally constrained amide groups (lactams) in the scaffold[123]. After several years of study and numerous contributions[115,124–126], it was possible to confirm that the lactam moiety plays a pivotal role in the enzyme-ligand interaction in a similar fashion to that happens in the natural ligand, NAD^+ (**Figure 93**)[123].

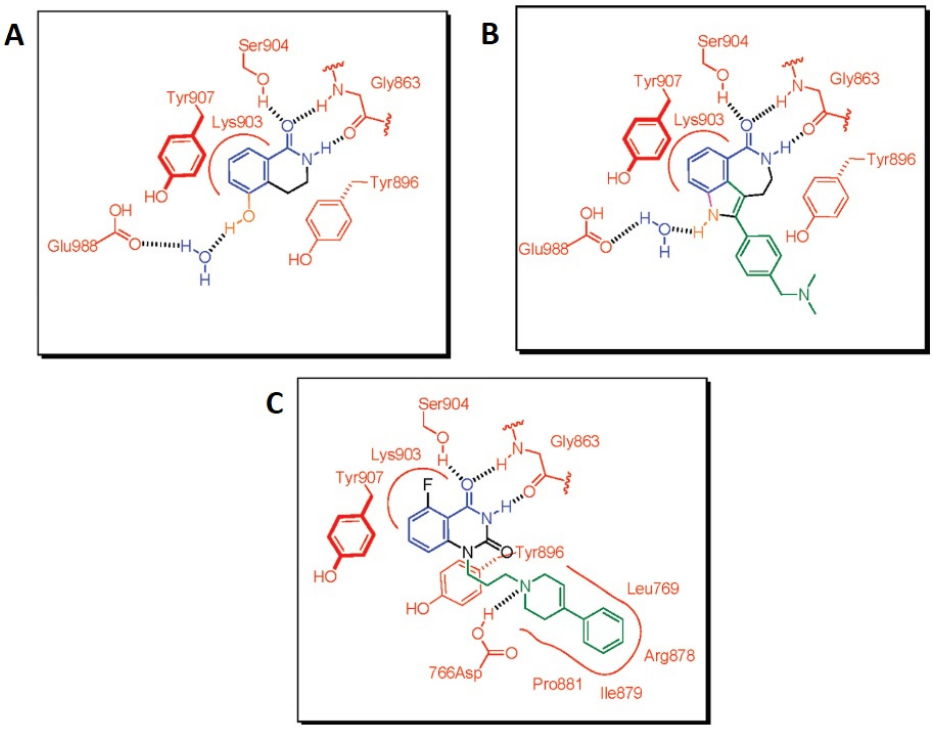


Figure 93: Schematic representation of the binding mode of several PARP-1 inhibitors in the nicotinamide binding pocket of PARP1: (A) 5-hydroxy-3,4-dihydroisoquinolin-1(2H)-one; (B) rucaparib; (C) quinazoline derivative [Reprinted with permission from ref.123, copyright 2021 American Chemical Society]

As it is shown in **Figure 93**, the lactam moiety of all the inhibitors is anchored in the nicotinamide binding pocket of PARP1 by three strong hydrogen bonding interactions, one with the side chain of residue Ser904, and two with the main NH and carbonyl groups of residue Gly863, which is similar to the observed for the nicotinamide moiety in NAD^+ (PDB 6BHV, 2.3 Å). The presence of an aromatic ring fused to the lactam group is also important since it is involved in π-π interactions with the phenol groups of residues Tyr896 and Tyr907, explaining the increased potency often observed with arylamides *vs* saturated amides. In addition, the tight and small pocket involving the side chains of the residues Ala898 and Lys903, tolerate small substituents (e.g., CH_3, F, Cl) on the benzamide-containing ring[123]. In some cases, the presence of a hydrogen bond donor group (OH, NH) enhances the inhibitory potency since the ligand is able to form an additional hydrogen bonding interaction with the side chain of residue Glu988 via a water molecule[123]. Finally, the large hydrophobic pocket adjacent to the nicotinamide binding site, which is often referred to as the adenine-ribose binding site, can also be exploited to improve the potency, the solubility, and other important pharmacodynamic and pharmacokinetic properties of the ligand by the introduction of long chains (**Figures 93B** and **93C**)[123]. Based on these findings, the pharmacophore model for PARP1 inhibitors shown in **Figure 94** has been constructed[123].

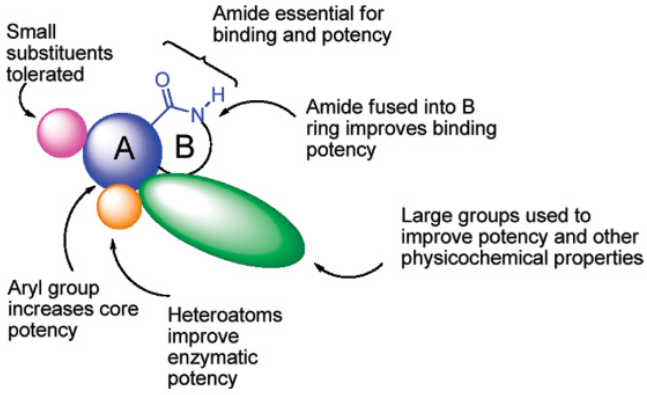


Figure 94: Pharmacophore model for PARP1 inhibitors [derivative [Reprinted with permission from ref.123, copyright 2021 American Chemical Society]

Considering these precedents, the possible inhibition of PARP1 by compounds **2.6** was explored *in silico*. This hypothesis was based on the structural similarities identified on these compounds relative to the drugs currently in clinical use, specifically, the presence of the pyrimidinone group and the restricted conformation of the tricyclic moiety. To this end, the following objectives were defined:

1) Explore the binding mode of the most potent compounds against the TNBC cell lines by molecular docking using the program GOLD.

2) Analyse the GOLD-predicted binding modes of the most relevant compounds by Molecular Dynamics (MD) simulation studies on the resulting ligand@PARP1 binary complexes.
3) Calculate the binding free energy of the selected ligands via the MM/PBSA approach implemented in Amber, for analysing the plausible correlation between the calculated binding and the experimentally obtained results.

Molecular docking studies

Molecular docking is an important computational tool to explore the binding mode and affinity of a ligand to a given target. For these studies, the ligand is considered flexible while the macromolecule is taken as a rigid template (lock-key model). The protein binding area of study is selected by the user, usually based on existing pharmacological information and/or biochemical studies with the isolated target, such as enzyme kinetics, inhibitory assays, etc. The docking program identifies the most suitable conformations of the ligands studied to fit in the selected area and estimates its binding affinity, which allows to compare a series of compounds. This comparison is reliable for a set of a family of compounds, which all have the same scaffold, to account for the positive/negative effect of the substituents. The binding strongly depends on the size and the overall structure of the ligands, and therefore the comparison of structurally very different compounds must be taken as a trend rather than quantitatively. In addition, the resulting affinity values are determined by the score fitness function used, since each one can give different weight to the hydrogen bonding, electrostatic and hydrophobic interactions in the overall binding energy, as well as other factors, such as the inclusion of other terms obtained by regression of experimental binding affinity data.

The binding modes of a selection of compounds **2.3** and **2.6** (**Figure 95**) in the nicotinamide pocket of PARP1 were analysed by Molecular Docking using the program GOLD version 2020.2.0, and the coordinates obtained in the available crystal structure of PARP1 enzyme in complex with (**2-{3-[4-(4-fluorophenyl)-3,6-dihydro-1(2*H*)-pyridinyl]propyIL}-8-methyl-4(3*H*)-quinazolinone,** namely FR257517) (PDB ID 1UK0[127], 3.00 Å). The selection of compounds **2.3** and **2.6** shown in **Figure 95** was based on the results obtained from the *in vitro* activity against Hs578t cancer cell lines. Compound **2.6l'** was also included in this study for comparison with the results obtained with compounds **2.6d'** and **2.6j'**, the two most active derivatives, as it possesses a bromide substituent and a 3-methoxyphenyl group in positions 7 and 2, respectively. For docking studies, the position of ligand FR257517 in PDB ID

1UK0[127] was selected for matching the ligand conformation and residues within 6.0 Å were selected. GOLDScore fitness function was employed.

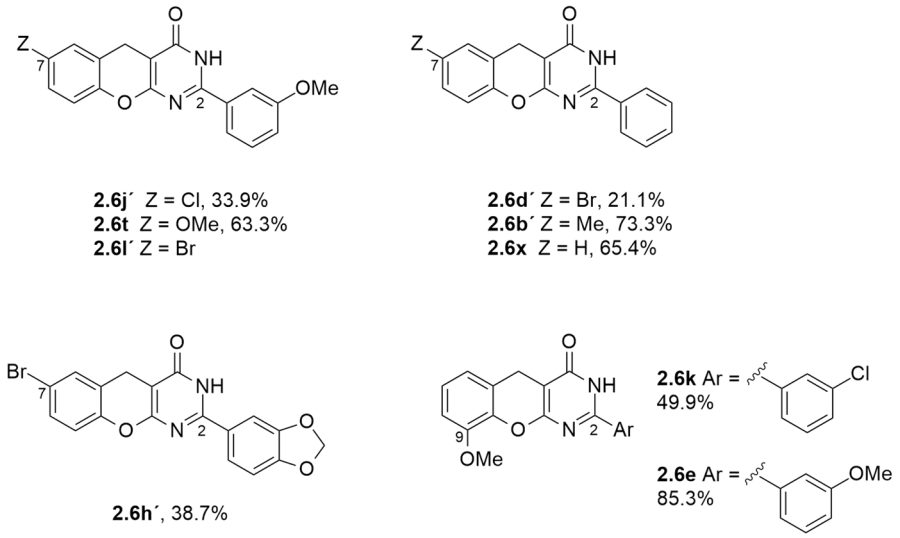


Figure 95: Compounds used in the molecular docking studies. The percentage of cell viability in Hs578t cancer cell lines after 72 h of treatment and at 30 μM concentration of the compound is also included

The results of these studies revealed that, for the halides **2.6d'**, **2.6h'**, **2.6j'** and **2.6l'**, the highest score solutions showed similar binding as for FR257517 (**Figure 96A** and **B**). Thus, the ligands would be anchored in the pocket by three hydrogen bonding interactions with the main NH and carbonyl groups of residue Gly863, and the side chain of residue Ser904. Besides, these ligands are tricyclic systems and therefore larger than FR257517, some π-π interaction between the ligand and the phenol group of Tyr907 was identified, mainly involving rings B and C.

The proposed binding mode for compounds **2.6t** and **2.6b'**, and **2.6x** showed some differences between them (**Figure 97**). While for compound **2.6t** a similar binding to halides **2.6d'**, **2.6h'**, **2.6j'** and **2.6l'** was obtained, less efficient anchoring was observed for compounds **2.6b'**, and **2.6x**. Thus, for the latter compounds the orientation of the lactam group is predicted to be less suitable for maximizing the polar contacts with the enzyme, mainly due to the introduction of bulkier substituents (MeO, Me) in position 7, which might explain their weaker efficacy.

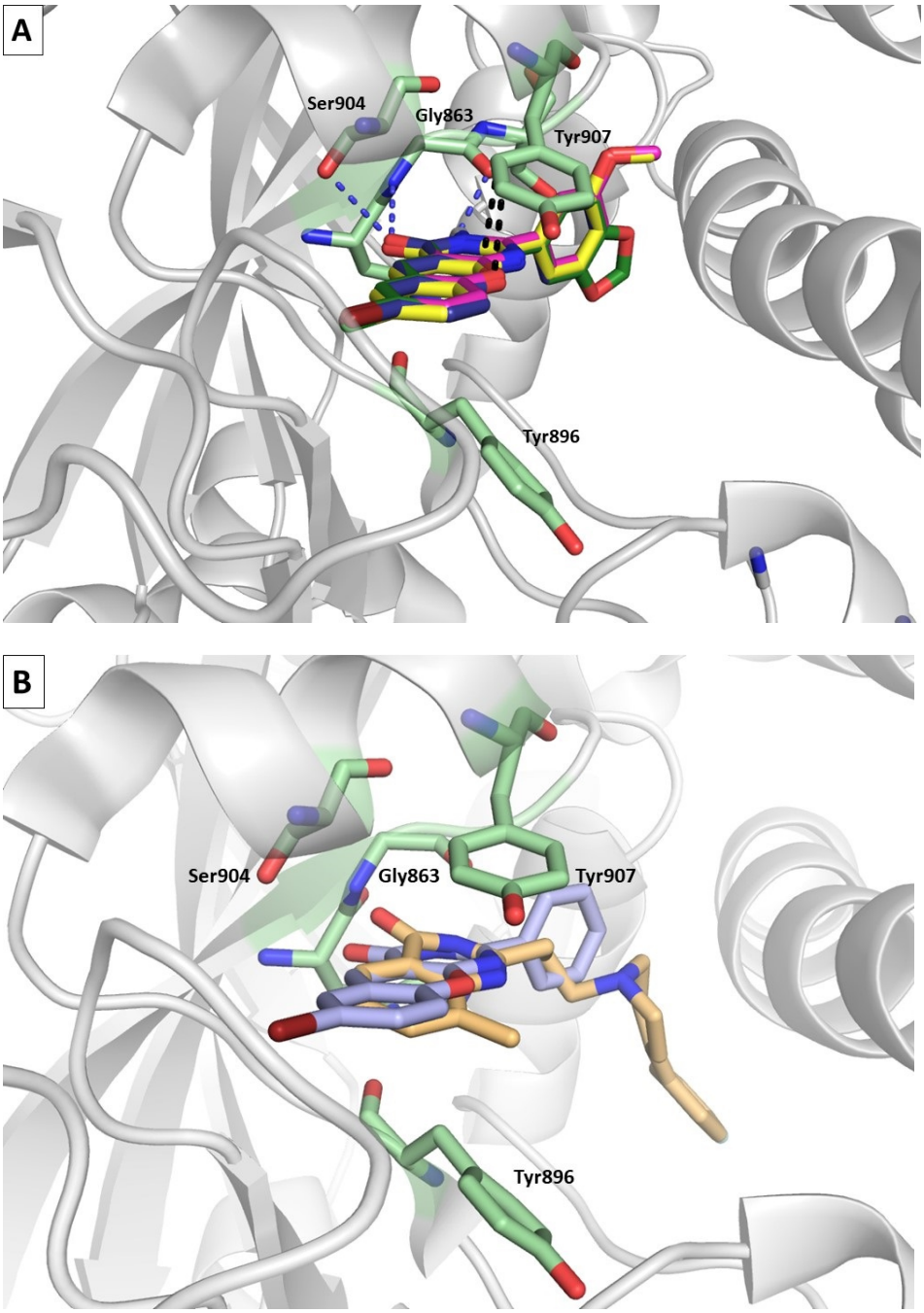


Figure 96: (A) Comparison of the highest score solutions obtained by molecular docking for compounds **2.6d'** (blue), **2.6h'** (green), **2.6j'** (yellow) and **2.6l'** (magenta) in the nicotinamide binding pocket of PARP1. (B) Superposition of the proposed binding mode for bromide **2.6d'** (blue) and inhibitor FR257517 (orange) as observed in PDB 1UK0. Relevant side chain residues are shown and labelled. The most relevant interactions are indicated as blue (polar) and black (apolar) dashed lines.

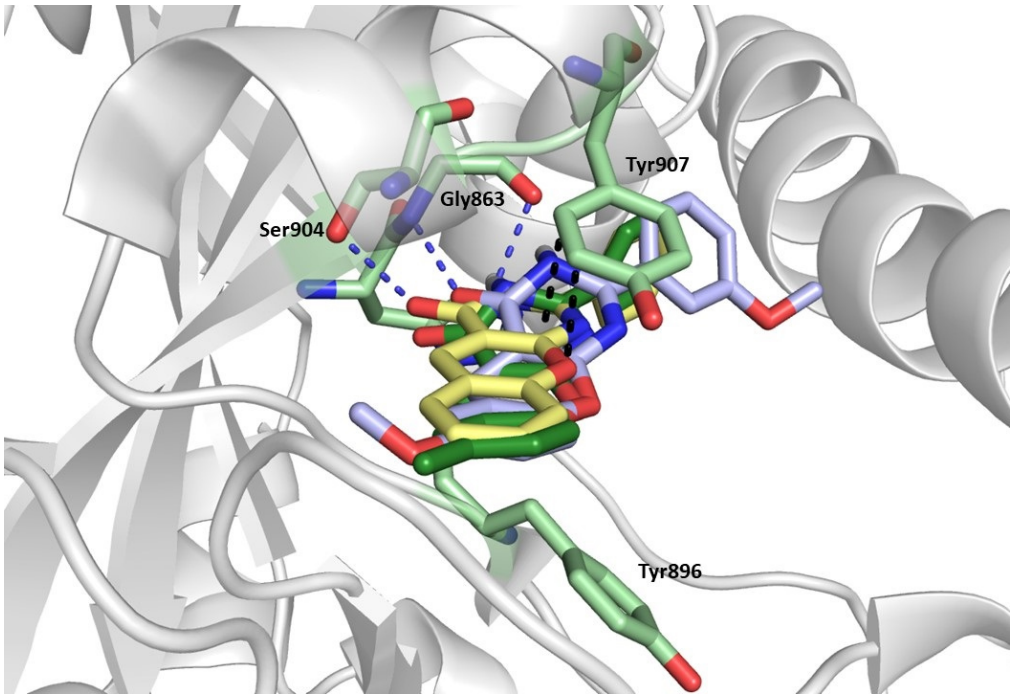


Figure 97: Comparison of the highest score solutions obtained by molecular docking for compounds **2.6t** (blue), **2.6x** (yellow) and **2.6b'** (green) in the nicotinamide binding pocket of PARP1. Relevant side chain residues are shown and labelled. The most relevant interactions are indicated as blue (polar) and black (apolar) dashed lines.

For compounds **2.6e** and **2.6k**, the results revealed a less conformational selection for a particular pose (**Figure 98A** and **B**). A variety of arrangements were obtained, in some cases even with a 180° rotation. For the latter ligands, the aforementioned hydrogen bonding interactions could not be established. These outcomes suggested that a relevant conformational adjustment of the enzyme would be necessary for binding this pocket, which would be greater than in the previous cases, since they have a bulky group (MeO) in a position equivalent to an *ortho* substitution. Hence, to perform MD simulation studies, in which both the ligand and the macromolecule are flexible, would be particularly relevant in these cases to assess whether this arrangement is real, or an artifact derived from the conformation of the macromolecule used.

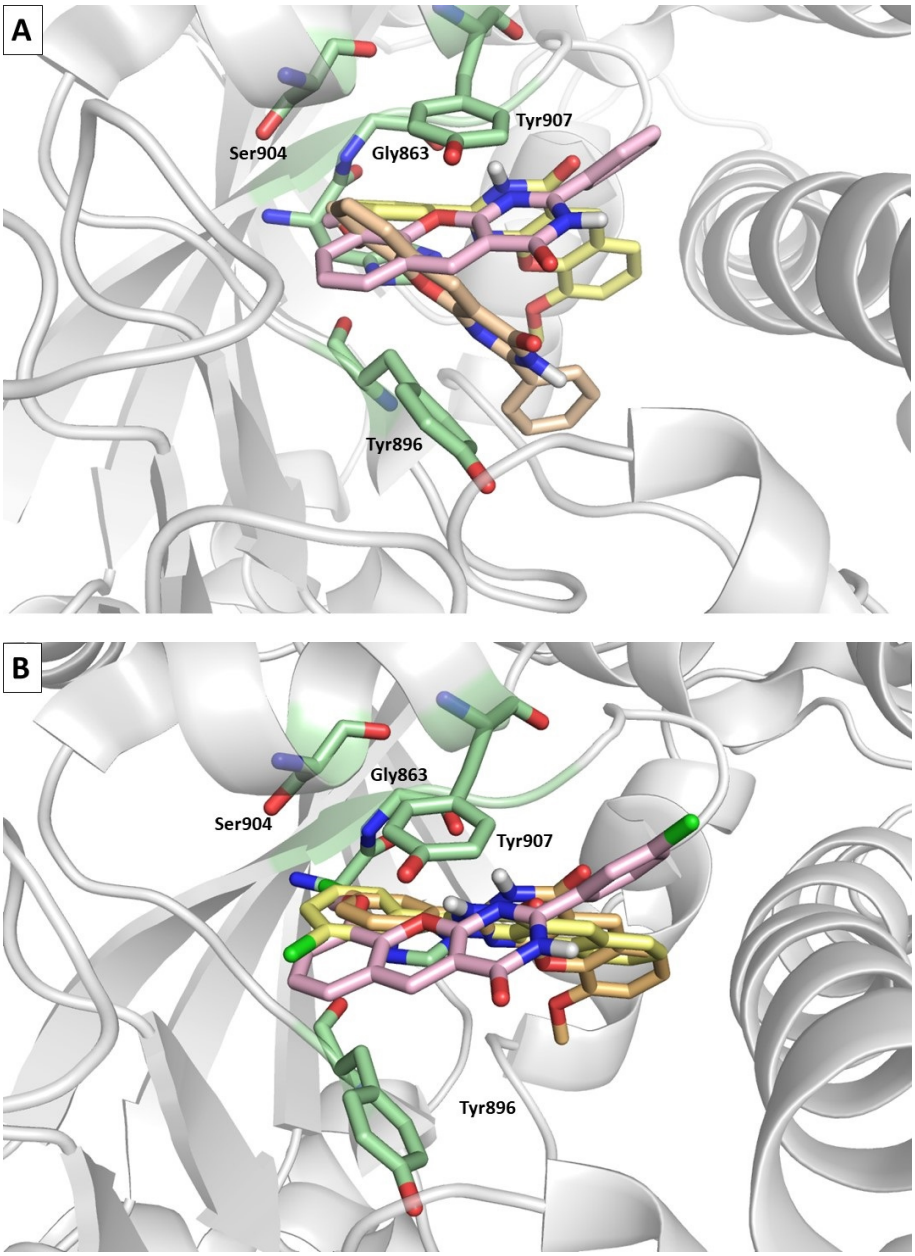


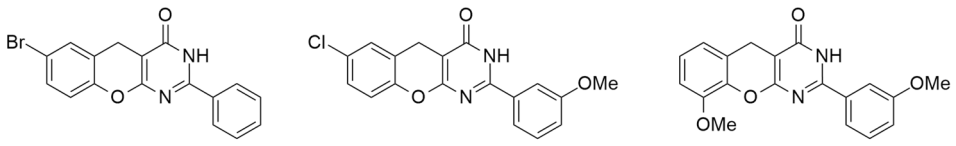
Figure 98: Superposition of some of the arrangements for compounds **2.6e** (A) and compound **2.6k** (B) obtained by molecular docking.

To explore further the relevance of the binding interactions identified for the most relevant compounds and to corroborate its proposed binding in the PARP1 nicotinamide binding site, simulation studies on the ligand@PARP1 binary complexes obtained by molecular docking were performed, which will be discussed in the next section.

Molecular Dynamics simulations

These types of computational studies, in which both the ligand and the enzyme are considered flexible, are complementary tools widely used in drug discovery to validate potential binding modes obtained via molecular docking studies. For the latter type of studies, the macromolecule is considered as a rigid template (lock-key model) and therefore the outcomes of these studies will be driven by the target conformation employed. This requirement has the advantage of being easily performed in a laptop, using programs that do not require extensive knowledge on computational chemistry. However, they also have the disadvantage that: (i) the protein arrangement might not be optimal for the compounds under study (available area for binding, arrangement of the residues side chains, etc.) or (ii) the proposed binding obtained by molecular docking could be an artifact of this arrangement. This is because the enzyme conformation is generally induced by the ligand/substrate that it recognizes, thereby maximizing the ligand–enzyme interactions (induced-fit model), which may be markedly different from that adopted with the compounds used for crystallization, or in the unbound form. In fact, the biological function of an enzyme depends on both its three-dimensional structure and its intrinsic-shape motion for turnover. As a result, the ligand-binding mode proposed by docking studies using unrealistic enzyme conformations for the ligands under study may be an artifact, or quite different from the real ligand@enzyme complex, since the plasticity of the macromolecule has not been considered. Hence, the study of the ligand@enzyme complexes obtained by docking using dynamic simulations allows false binding modes, in which case the ligand would escape from the pocket (unstable), to be ruled out, and a more realistic picture of the effects caused by the ligand on an atomic scale to be obtained.

For this reason, MD simulations were performed on a selection of the ligand@enzyme complexes obtained by molecular docking (Figure 18). In particular, the binary complexes **2.6d'**@PARP1, **2.6j'**@PARP1 and **2.6e**@PARP1 were analysed according to the biological results obtained for Hs578t cancer cell lines. Thus, compounds **2.6d'** and **2.6j'** were among the most active, with **2.6d'** being the most active of the two (**Figure 99**). Compound **2.6e**, which was among the least active compounds for all cell lines tested (MDA-MB-231 and Hs578t), was selected for comparison. For compounds **2.6d'** and **2.6j'**, the coordinates of the highest score solution obtained by Molecular Docking results were used, while compound **2.6e** was manually docked to match the same arrangement as ligands **2.6d'** and **2.6j'**.

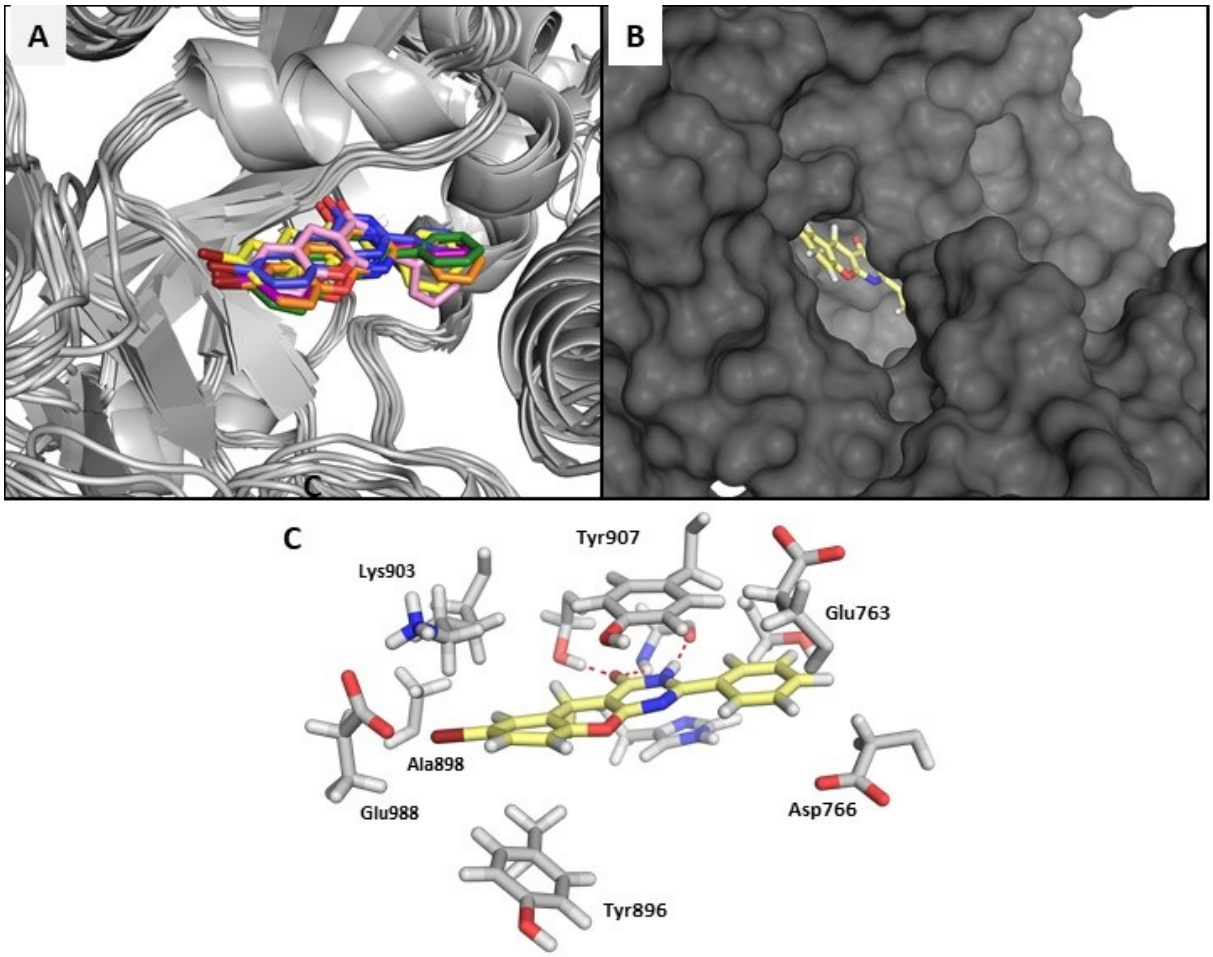


2.6d' **2.6j'** **2.6e**

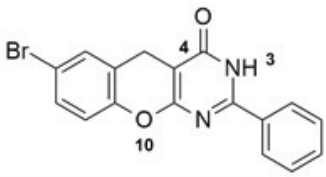
Figure 99: Compounds used for MD simulation studies

- ***2.6d'**@PARP1 binary complex*

The compound **2.6d'** proved to be stable within the pocket as no relevant changes were observed during the whole simulation (**Figure 100**). This ligand would be deeply embedded in the nicotinamide binding pocket (**Figure 100A**). Three strong polar interactions between the ligand and the enzyme were identified: (i) two hydrogen bonding interactions between the carbonyl group of the ligand and the side chain of residue Ser904 and another with the main NH group of residue Gly863; and (ii) a hydrogen bonding interaction between the main carbonyl group of residue Gly863 and the NH group of the ligand (**Figure 100B**). In addition, diverse lipophilic contacts were identified, such as halogen-CH interactions with the carbon side chain of residues Ala898 and Glu988; CH-π interactions with residues Tyr896, Asp766 (carbon chain) and Glu763 (carbon chain); and π-π interactions between the tricyclic moiety of the ligand and the phenol ring of residue Tyr907. It is important to highlight that the analysis of the frequency with which the hydrogen bonding interactions between **2.6d'** and PARP1 are observed during the whole simulation clearly showed their strength and impact on the binding (**Figure 100C**). Thus, these polar interactions were identified during 71% and 99% of the simulation with average distances between 2.8 Å and 2.9 Å, when this interaction was detected. Altogether, these computational studies suggested that compound **2.6d'** could interact favorably with the nicotinamide binding site of PARP1, whose inhibition could justify the *in vitro* results obtained. Biochemical studies with the isolated enzyme would be required to validate this hypothesis.



D



2.6d'
40.2 % (10 μM)
21.1 % (30 μM)

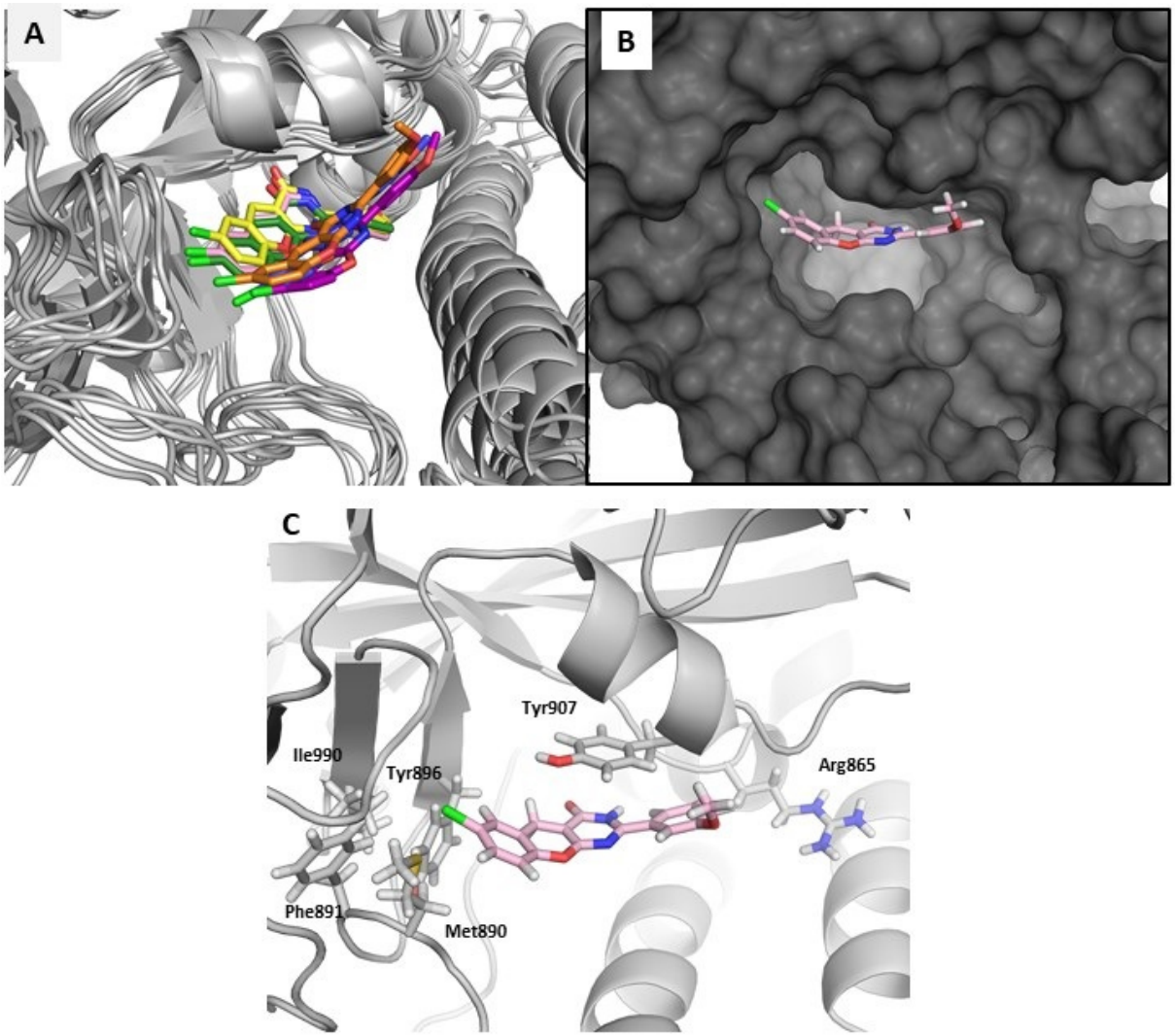
H Donor	Acceptor	Frequency (%)	Av. Distance (Å)
Gly863(NH)	O4	77	2.90
Ser904 (OH)	O4	91	2.84
N3-H	Gly863(C=O)	99	2.93

Figure 100: (**A**) Superposition of several snapshots [0 ns (yellow), 20 ns (pink), 40 ns (green); 60 ns (blue), 80 ns (orange), 100 ns (purple)] from the 100 ns of MD simulation on the **2.6d'**@PARP1 binary complex. (**B**) Overall view of the binding mode of compound **2.6d'** against PARP1 obtained by MD simulation studies. Snapshot taken after 80 ns of simulation. (**C**) Detailed view of the main contacts for **2.6d'** in the **2.6d'**@PARP1 binary complex. The relevant residues and side chains involved are shown and labeled. Hydrogen bonding interactions are indicated as red dashed lines. (**D**) Frequency (%) and enzyme atoms with which the hydrogen bonding interactions between **2.6d'** and PARP1 are observed during whole simulation. Average distances (Å) between the donor/acceptor atoms involved when the hydrogen bond is observed are also shown.

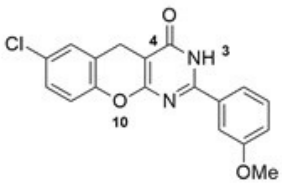
- ***2.6j'**@PARP1 binary complex*

The simulation studies performed on the **2.6j'**@PARP1 binary complex showed that the interaction of this ligand within the nicotinamide binding site of PARP1 would be less efficient than for compound **2.6d'** (**Figure 101**). Thus, the results revealed that: (i) during the simulation, the ligand moves away from the pocket involving residues Gly863 and Ser904, which is responsible for the anchoring of inhibitor FR257517 as well as compound **2.6d'** (**Figure 101A**); (ii) as a result of (i), the ligand would be more exposed to the water environment than compound **2.6d'** (**Figure 101B**); and (iii) after 50 ns of simulation the hydrogen bonding interactions between the ligand and the enzyme residues were quite weak (**Figure 101C**). In contrast to compound **2.6d'**, only the hydrogen bonding interaction between the main carbonyl group of residue Gly863 and the NH group in **2.6j'** was identified during a significant part of the simulation (71%) and the geometry of this interaction showed to be less efficient than for **2.6d'** because the other two hydrogen bonds were absent (**Figure 101D**).

It seems that the ligand moves away from the Gly863/Ser904 site due to the free rotation of the 3-methoxyphenyl ring, which would be located on a narrow and rigid pocket. The presence of a chlorine atom in position 7 would also reduce the possible adjustments since the pocket that surrounds this area of the ligand is also narrow. As a result, the 3-methoxyphenyl ring does not seem to find an optimal position for maximizing the interactions of its methoxy group in the vicinity of the Gly863/Ser904 site. The introduction of steric hindrance in both positions 7 and 2 seems to trigger the displacement of the ligand towards wider sites of the protein. In doing so, the apolar interactions of the tricyclic moiety would be maximized, especially of the halide-containing ring, with the pocket composed by residues Met890, Tyr896, Ile990 and Phe891. Without considering the different permeability properties that compounds **2.6j'** and **2.6d'** might have, all these outcomes suggested that the interaction between compound **2.6d'** and the nicotinamide binding site of PARP1 would be weaker than for compound **2.6j'**, which would explain the weaker *in vitro* potency obtained with this compound. These results also suggested that the functionalization of position 7 would have a huge impact on the substitution of the phenyl group of position 2, since both positions are flanked by pockets of limited plasticity.



D



2.6j'
39.8 % (10 μM)
33.9 % (30 μM)

H Donor	Acceptor	Frequency (%)	Av. Distance (Å)
Gly863(NH)	O4	36	2.92
Ser904 (OH)	O4	26	2.93
N3-H	Gly863(C=O)	71	2.96

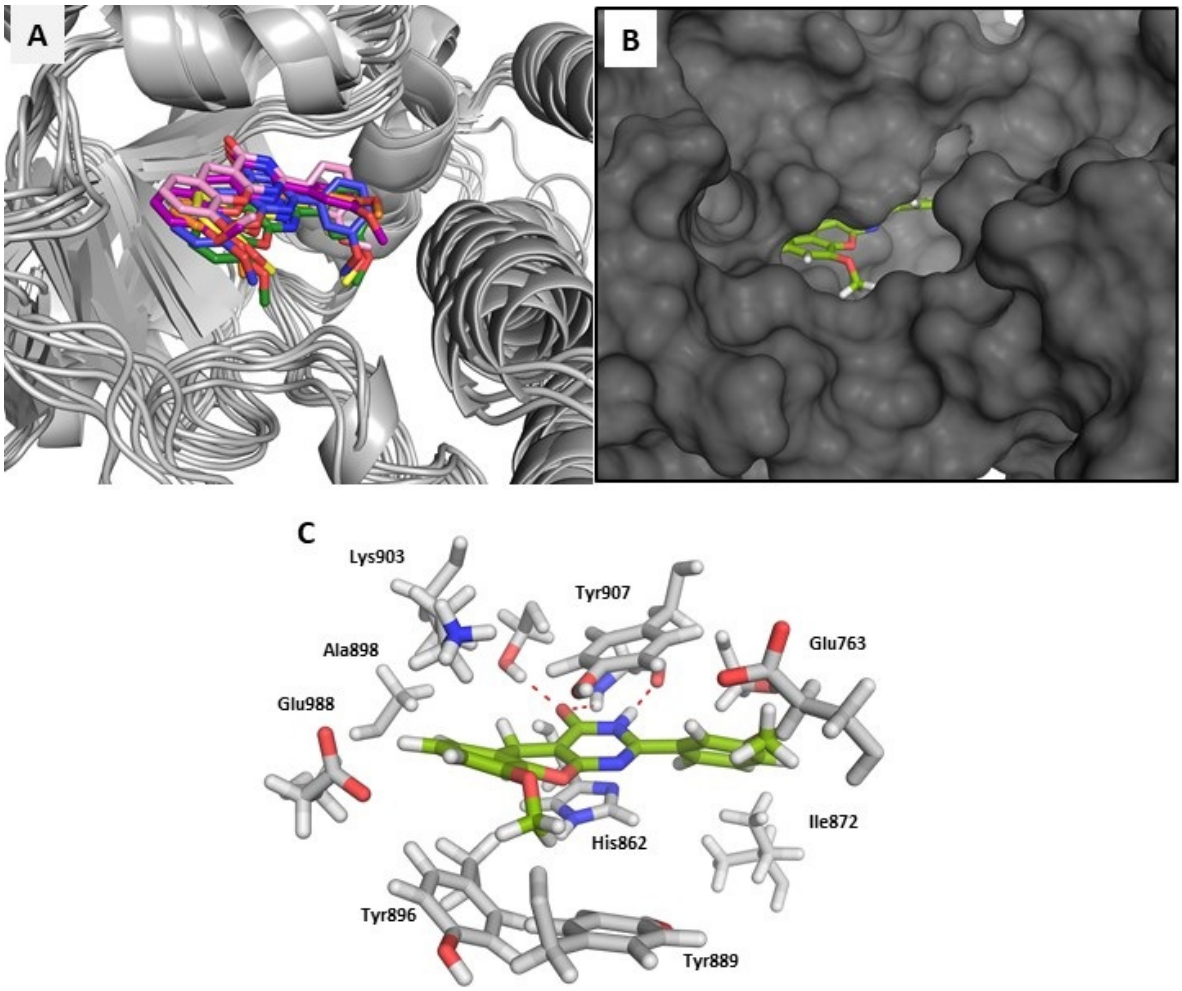
Figure 101: (**A**) Superposition of several snapshots [0 ns (yellow), 20 ns (pink), 40 ns (green); 60 ns (blue), 80 ns (orange), 100 ns (purple)] from the 100 ns of MD simulation on the **2.6j'**@PARP1 binary complex. (**B**) Overall view of the binding mode of compound **2.6j'** against PARP1 obtained by MD simulation studies. Snapshot taken after 80 ns of simulation. (**C**) Detailed view of the main contacts for **2.6j'** in the **2.6j'**@PARP1 binary complex at 50 ns. (**D**) Frequency (%) and enzyme atoms with which the hydrogen bonding interactions between **2.6j'** and PARP1 are observed during whole simulation. Average distances (Å) between the donor/acceptor atoms involved when the hydrogen bond is observed are also shown.

- ***2.6e**@PARP1 binary complex*

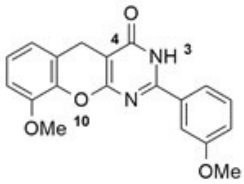
Compound **2.6e** showed a similar behaviour as for compound **2.6d'**, having a great stability in the nicotinamide binding pocket of PARP1 (**Figure 102A**). This ligand would also be deeply embedded in the pocket, with its lactam moiety interacting with residue Gly863 by hydrogen bonding during most of the simulation (**Figures 102B and 102D**). The hydrogen bonding interaction between the carbonyl group of the ligand and the side chain of residue Ser903 also proved to be relevant, as it was observed during 53% of the simulation. Based on the length of the hydrogen bonding interactions promoted by compounds **2.6e** and **2.6d'**, the overall strength of the interaction of derivative **2.6e** with the enzyme is predicted to be less efficient than for compound **2.6d'**. As for compound **2.6d'**, the ligand would be also stabilized by numerous apolar interactions within the pocket, particularly CH-π interactions with residues Tyr907, Tyr889, Lys903 (carbon chain) and Ser864 (carbon chain); π-π interactions between the tricyclic moiety of the ligand and residues Tyr907 and His862; and lipophilic interactions with residues Ile872, Glu988 (carbon chain) and Glu762 (carbon chain) (**Figure 102C**).

Comparing the results obtained with compounds **2.6e** and **2.6j'**, which only differ in the position and type of substituent on the tricyclic moiety, thus the first has a methoxy group in position 9 and the second a chloride in position 7, suggested that the lack of substitution in position 7 facilitates the introduction of substituents in the aryl group in position 2. On the other hand, since the position 9 of the scaffold would not interact with the internal part of the site, the substitution of the phenyl ring would not have a negative impact on the binding, because the ligand would be able to reach an arrangement where the polar interactions are the most numerous and favorable. However, the limited inhibitory capacity of compound **2.6e** experimentally observed suggested that either its internalization in cancer cells is low, as this compound does not have halide substituents that facilitate it, or else the therapeutic target of these types of compounds is another.

To further compare the interaction of the selected compounds **2.6d'**, **2.6j'** and **2.6e** in the nicotinamide binding pocket of PARP1, the binding free energy for these compounds was calculated, as discussed in the next section.



D



2.6e
99.3 % (10 μM)
85.3 % (30 μM)

H Donor	Acceptor	Frequency (%)	Av. Distance (Å)
Gly863(NH)	O4	87	3.88
Ser904 (OH)	O4	53	2.93
N3-H	Gly863(C=O)	98	2.89

Figure 102: (**A**) Superposition of several snapshots [0 ns (yellow), 20 ns (pink), 40 ns (green); 60 ns (blue), 80 ns (orange), 100 ns (purple)] from the 100 ns of MD simulation on the **2.6e**@PARP1 binary complex. (**B**) Overall view of the binding mode of compound **2.6** against PARP1 obtained by MD simulation studies. Snapshot taken after 80 ns of simulation. (**C**) Detailed view of the main contacts for **2.6e** in the **2.6e**@PARP1 binary complex obtained by MD simulation studies. Snapshot taken after 80 ns of simulation. The relevant residues and side chains involved are shown and labeled. Hydrogen bonding interactions are indicated as red dashed lines. (**D**) Frequency (%) with which the hydrogen bonding interactions between **2.6e** and PARP1 are observed during whole simulation and average distance (Å) between the donor/acceptor atoms involved.

MMPBSA calculations

Calculating binding free energies between protein and ligand (or two proteins) using computational methods is not an easy task. Much research effort has been devoted to this goal but finding a definitive method for these calculations remains elusive. Conceptually, it is a very simple calculation, thus the difference between the energy of the ligand@protein complex and the energy of both the ligand and the protein in their unbound forms. However, this can only be calculated precisely by computational methods in vacuum (or in gas phases assuming high dilution), which is of no suitable for biological systems. In solution, water molecules are constantly forming and breaking hydrogen bonds with other molecules, and the energy variation associated to this process is so high, that the error associated to the energy calculation is of a higher magnitude than the value of binding free energy. Molecular mechanics Poisson-Boltzmann surface area (MM/PBSA) calculations is one of the most popular approaches used for binding free energy calculation, which has been shown to effectively balance computational cost against accuracy. It is based on MD simulations of the ligand@macromolecule complex and have been applied to large number of systems with varying success[128–130]. Using this method, binding free energy in solvated media is calculated using the thermodynamical cycle showed in **Figure 103**, using the following **equation 1**:

$$\Delta Gbinding, solvated = \Delta Gbinding, vaccum + \Delta Gcomplex, solvation - \Delta Gligand, solvation - \Delta Gprotein, solvation$$

Equation 1: Equation used in the MM/PBSA method

For the calculation of the solvation energies, MM/PBSA uses implicit solvation methods generalized Born (GB) and Poisson-Boltzmann (PB). This approach implies that any effects that water molecules can have in the binding process are not considered, because all water molecules are replaced with a continuous equation term along the surface. This allows for a low computational cost, which makes it quite popular. For the calculation, either Monte Carlo or MD simulations can be used to provide structures for the complex, protein, and ligand, with multiple snapshots along the simulated trajectories used for the calculation of the binding free energy. When the binding does not induce big conformational changes, a single trajectory can be used, allowing for faster calculations. In this case, the trajectory for the ligand@protein complex is also used to provide trajectories for the protein and the ligand in unbound form, simply by removing coordinates of the ligand and protein respectively. The theory of this type of calculation assumes that it is possible to obtain an approximation of the free energy of the ligand@protein

interaction by calculating the free energy values for each step individually and without solvent, and then calculate the free energy involved in the solvation (**Figure 103**).

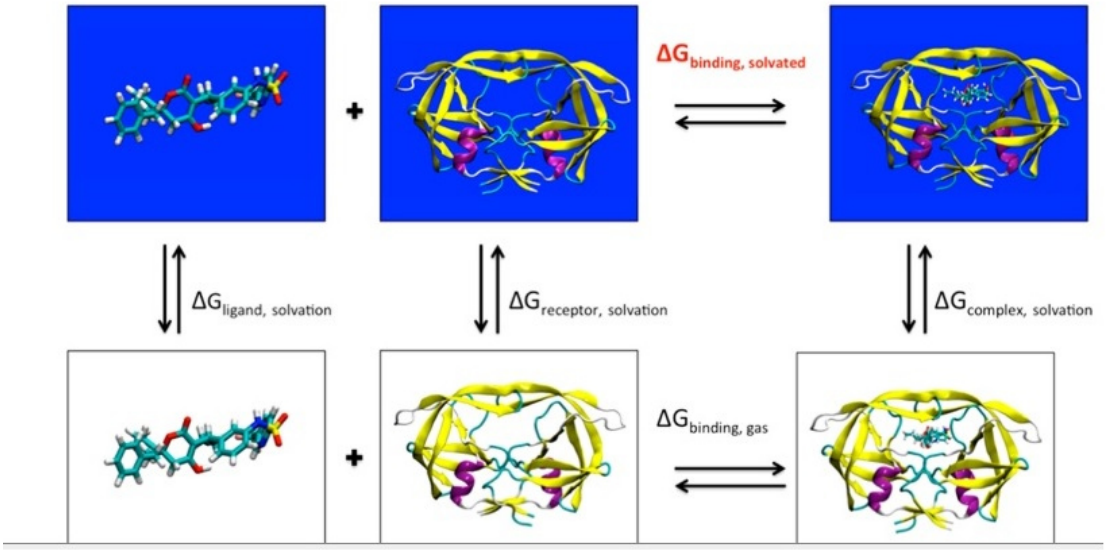


Figure 103: Schematic representation of the MM/PBSA approach. Thermodynamic cycles for binding free energy calculations for a protein–ligand complex. Solvated systems are shown in blue boxes, while systems in the gas phase are in white boxes. Free energies that are directly calculated are shown in black, while the free energy of interest is shown in red [Reprinted with permission from ref.130. Copyright 2021 American Chemical Society]

Typically, it is in the solvation free energy calculations that the procedure may differ: this process can be calculated through a generalized Born method or using a PB distribution[128–130]. For this reason, the calculation of the free energy of the ligand@protein complex in solution ($\Delta G_{binding,\ solvated}$), which tends to be a difficult process, is simplified to the calculation of the ligand-complex binding free energy while considering it to be in a non-interactable gas ($\Delta G_{binding,\ vacuum}$), to which the solvation is further added ($\Delta G_{complex,\ solvation}$). The ligand and protein free energy values are estimated by removing the solvation from the previously performed end-point calculation, which can be obtained from Monte Carlo or, as in the case of the present study, MD calculations, using the final trajectory files as starting point.

The binding free energy for compounds **2.6d'**, **2.6j'** and **2.6e** was calculated by the MM/PBSA approach implemented in Amber Tools 1.5. ante-MMPBSA.py module was used to create topology files for the ligand@enzyme complex, enzyme and ligands and binding free energies were calculated with the MMPBSA.py module. A single trajectory approach was used to calculate binding free energies considering only the last 80 ns of the 100 ns MD trajectories. The Poisson-Boltzmann (PB) and Generalized Born (GB) implicit solvation models were employed. The results are summarized in **Table 134**.

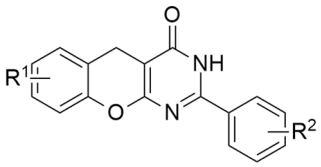


Table 134: Calculated binding free energies (kcal mol^{-1}) for compounds **2.6d'**, **2.6j'** and **2.6e** using MM/PBSA method

Compounds	Substituents		GB		PB	
	R^1	**R^2**	$\Delta G_{binding,\ solvated}$	$\Delta\Delta G$	$\Delta G_{binding,\ solvated}$	$\Delta\Delta G$
2.6d'	7-Br	H	-42.51	0	-7.67	0
2.6j'	7-Cl	3-OMe	-30.16	12.35	0.92	8.59
2.6e	9-OMe	3-OMe	-39.98	2.53	-2.85	4.82

As expected, the results revealed the higher affinity of compound **2.6d'** (lowest $\Delta G_{binding,solvation}$) than compounds **2.6j'** and **2.6e** by the PARP1 enzyme with calculated binding energy differences up to 12.3 kcal mol^{-1}, considering the GB model, which are in line with the results that were obtained for its biological activity *in vitro*. However, the binding affinity of the least active compound **2.6e** is estimated to also be good, as for compound **2.6d'**, with calculated binding energy differences between them of 2.5 kcal mol^{-1}, considering the GB model. These results can be understood when other non-calculated factors are considered, such as compounds' permeability, or the interaction with other targets as no specific binding assay on the interaction of these compounds with the isolated PARP1 enzyme was performed to corroborate that is the biological target. However, these results show that the reported chromenopyrimidinones could be PARP1 inhibitors, and therefore a good starting point for the design of novel PARP1 inhibitors.

3.2 Tuberculosis

3.2.1 Tuberculosis – challenges and impact on human health

Tuberculosis (TB) is a disease caused by the bacillus, *Mycobacterium tuberculosis*, which is easily spread through the air by cough, sneeze or spit, from an infected person[131,132]. It mainly affects the lungs (pulmonary TB) but can also affect other parts of the body (extrapulmonary TB)[132]. It is presently a detectable and curable disease and can affect anyone anywhere, but the main target of this disease are adults, with a prevalence of men over women[132]. The 30 high-burden countries (a list that comprises the

most affected countries in terms of tuberculosis infections) account for almost 90% of those who fall sick with TB each year[132]. It is also considered a disease associated with poverty[132]. According to the WHO Global Tuberculosis Report 2020, in the majority of cases, "economic distress, vulnerability, marginalization, stigma and discrimination are often faced by people affected by TB"[132].

Nowadays, TB is the leading cause of death for people infected with HIV and a major contributor to bacterial resistance to antibiotics, being responsible for one-third of global antimicrobial resistance related deaths[132,133]. According to WHO global Tuberculosis report 2020, TB is still the leading cause of death from an infectious disease among adults worldwide, with more than 10 million TB-infected cases each year for the last years, being among the top 10 causes of death worldwide and the leading cause of death from a single infectious agent (ranking above HIV/AIDS)[131,132]. According to the same report, 8.7 million (87%) of these individuals reside in the 30 high-burden countries and only 6.4 million were diagnosed and officially notified, among which 1.3 million are expected to perish annually[131,132]. There were an estimated 1.2 million (range, 1.1–1.3 million) deaths, due to TB, among HIV-negative people in 2019 (a decrease from 1.7 million in 2000), as well as 208.000 deaths (range, 177.000–242.000) amidst HIV-positive people (a decrease from 678.000 in 2000)[132]. In 2019, 56% of the total number of TB cases were men (aged ≥15 years), 32% were women and 12% children (aged <15 years), and 8.2% of the total cases were among people living with HIV[132].

Most newly developed TB cases (2019) came from the WHO regions of South-East Asia (44%), Africa (25%) and the Western Pacific (18%), Eastern Mediterranean (8.2%), the Americas (2.9%) and Europe (2.5%)[132] (**Figure 104**). An asymmetry in case distribution can be perceived, with eight countries representing two thirds of the global total: India (26%), Indonesia (8.5%), China (8.4%), the Philippines (6.0%), Pakistan (5.7%), Nigeria (4.4%), Bangladesh (3.6%) and South Africa (3.6%)[132]. The remaining 22 countries in WHO's list of 30 high TB burden countries accounted for 21% of the global total[132].

Since 2000, TB treatment has averted more than 60 million deaths, but because proper health coverage is still not accessible to every infected person, many millions have also missed out on diagnosis and care[132]. Preventive treatment is available for people with TB infection, and the number of people developing infection and disease (and thus the number of deaths) can also be reduced through multisectoral action that attend to recognized TB risk factors such as poverty, undernutrition, HIV infection, smoking and diabetes[131,132].

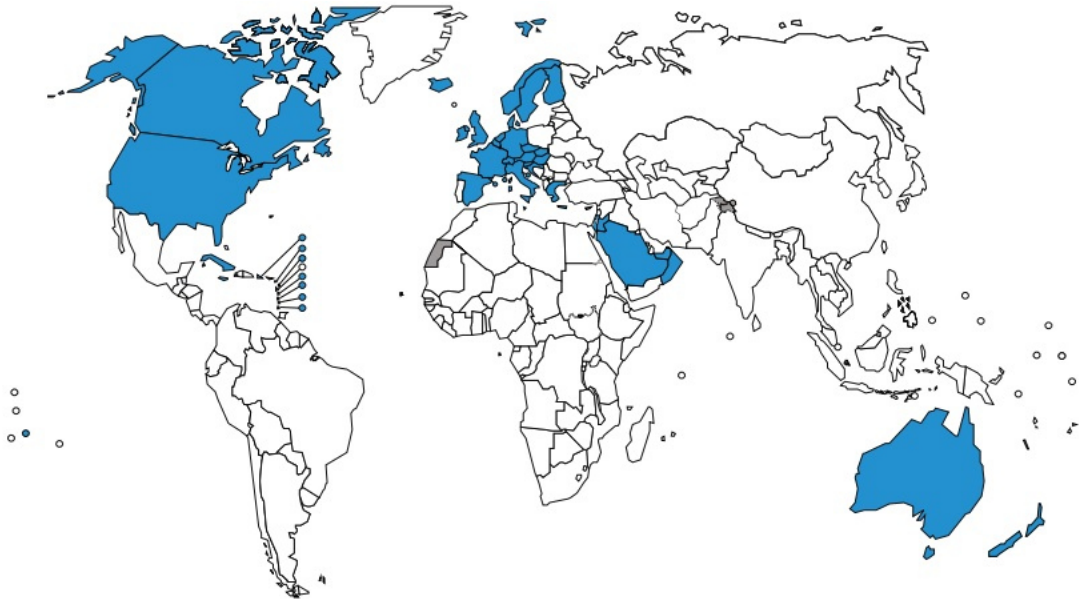


Figure 104: Countries (in blue) that had an estimated TB incidence rate of less than 10 per 100 000 population in 2019 [obtained from ref.132; license: https://creativecommons.org/licenses/by-nc-sa/3.0/igo/]

Although significant improvements in treatment and diagnosis have been achieved in the last decades, multidrug-resistant strains of *M. tuberculosis* are currently on course to be the world's deadliest pathogens, being responsible for 25% of deaths due antimicrobial resistance (**Figure 105**)[131,132]. It is considered a completely curable disease but it is understood as a last century pathology, and in spite of its high-ranked mortality numbers and drug resistance, R&D investment has not been responding accordingly[131]. In the last decades, and after years of stagnation, R&D for new anti-TB drugs, and in particular against multidrug-resistant and extremely-resistant strains of TB, have been reinforced, with several repurposed and newly developed drugs entering clinical trials[134].

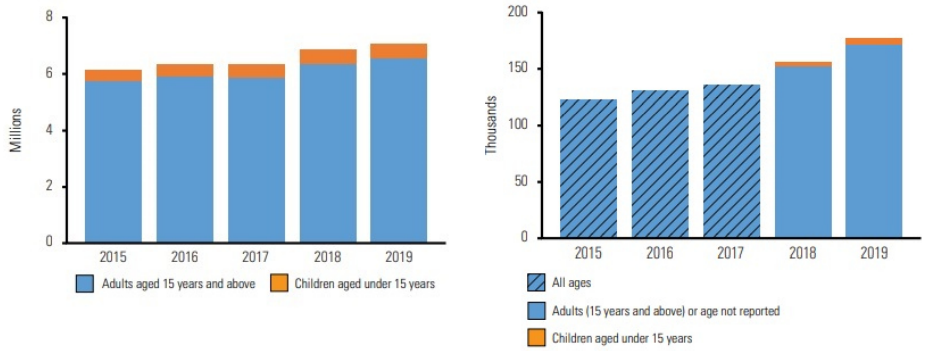


Figure 105: Global number of people reported to have been treated for TB disease, 2015–2019 (left) and the global number of people reported to have been enrolled on treatment for MDR/RR-TB, 2015–2019 (Global data disaggregated by age are not available for the years before 2018) (right) [obtained from ref. 132; license: https://creativecommons.org/licenses/by-nc-sa/3.0/igo/]

Current therapies and treatment

To engage the ongoing worldwide tuberculosis outbreak, the WHO proposed a series of guidelines[132,135,136] to achieve the End TB Strategy (a 90% decrease in TB incidence and 95% decrease in TB mortality by 2035 compared with 2015), which involve not only a series of protocols to improve funding, testing and diagnosis, but also to improve the existing treatment options and the discovery of new anti-TB agents[132,136,137].

The first-line TB therapy consists on a 4-drug treatment with rifampicin, isoniazid, pyrazinamide and either ethambutol or streptomycin, for 2 months, followed by 4 up to 24 months of treatment with rifampicin and isoniazid[138]. It is a very prolonged therapy, which favors its non-compliance and the emergence of new resistant strains. Thus, these strains, namely multidrug-resistant tuberculosis (MDR-TB), do not respond to the first-line anti-TB drugs, isoniazid and rifampicin, and are developed in previously treated TB patients (secondary resistance). For those cases, the second-line therapy is employed, which includes drugs such as linezolid, bedaquiline, moxifloxacin, levofloxacin, cycloserine, clofazimine, kanamicin, capreomycin, amikacin, viomycin, ethionamide, *p*-amino salicylic acid, cycloserine, and some macrolides[138]. Their applicability, conjugation and duration of treatment varies with the clinical status and bacterial characteristics. The most serious form of MDR-TB is the extensively drug-resistant tuberculosis (XDR-TB), which is caused by strains that do not respond to any second-line drug, which leaves, in many cases, many patients without therapeutic options[135].

The eradication of the tuberculosis is difficult, because in addition to the special characteristics of the bacteria itself, the currently available therapy is so long that it favors the emergence of resistant strains. It is therefore not surprising that, in recent years, the main focus within the scientific community has been to search for shorter and more efficient therapies[137]. Another important issue that has been increasingly been considered is the impact of TB among immunocompromised individuals, such as those infected with HIV, suffering from diabetes, undergoing organ transplantations, among others[132,138]; for example, as of 2019, 2.2 and 0.35 million TB cases could be attributed to HIV and diabetes , respectively[132]. MDR and XDR forms of TB are extraordinarily difficult to treat in patients of this type with a compromised immune system.

There is already an extensive knowledge about the molecular mechanism and targets of the available antibacterial drugs currently available and approved for the treatment of TB[138]. Rifampicin binds to the β-subunit of RNA polymerase and blocks elongation of the RNA strand, which in turn interferes

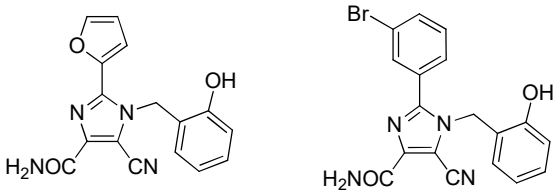
with the transcription process[138]; isoniazid undergoes oxidation once inside the cell by the catalase peroxidase enzyme KatG to afford the isonicotinoyl radical, which in the presence of NADH-dependent reductase enzyme and its cofactor NADH/NAD^+ leads to the deactivation of the reductase enzyme by modification of the cofactor[138]; ethambutol inhibits arabinosyltransferase and disrupts the arabinogalactam biosynthesis in the cell wall, increasing its permeability[138]; streptomycin acts is an inhibitor of the protein biosynthesis[138]. Moreover, fluoroquinoline, a second-line drug, blocks the Mycobacterial DNA replication and transcription by inhibiting the topoisomerase II (DNA gyrase) enzyme[138]; ethionamide is activated by the mono oxygenase enzyme and inhibits the NADH dependent ACP reductase enzyme via disruption of the mycolic acid biosynthesis[138].

In spite of having achieved further insight of the molecular processes and drug-resistant mechanisms, inherent to the TB infection and disease progression, as well as on the genomic sequence of *M. tuberculosis* and some resistant strains, there is still an urgent need of new therapeutic agents in order to achieve the End TB Strategy[139]. In the last years, there have been some investment in drug repurposing to treat *M. tuberculosis* infection[140], as well as in new drugs such as bedaquiline, delamanid and protamanid. This investment has been helpful in the treatment of MDR-TB and the more nefarious XDR-TB, but the prognosis of the disease promoted by these two conditions remain unfavorable and the solutions unsufficient[138]. Adding to this, bedaquiline possesses severe secondary effects, being only prescribed as a last resort treatment[141], and delaquinine has showed less efficacy than previously predicted[142]. Although some improvements have been made in the search for a vaccine, in the last decade, only one vaccine has been approved to this date, which is the BCG vaccine[143,144].

3.2.2 Biological evaluation of chromene-based and imidazole-based compounds activity against *M.tuberculosis*

To explore the potential of the compounds described in this doctoral thesis against infections caused by *M. tuberculosis*, the *in vitro* activity of a selection of the previously synthesised chromene and imidazole derivatives was assayed against virulent strains of *M. tuberculosis* (H37Rv). The assays consisted on the measurement of the MIC (μg/mL) values using the Alamar Blue assay[145] and resazurin as standard. The studies were performed in a collaboration with Prof. José Antonio Aínsa from the Faculty of Medicine of the University of Zaragoza, Spain.

The results of these studies showed that no significant activity was found (>160 μg/mL) for the tested compounds **2.3**, **2.6**, **2.50**, **2.55**, **2.69**, **2.86** and **2.87**, as well as for compound **2.105**. The best results were obtained with the imidazoles **2.119** that showed MIC vales in the range 40-80 μg/mL, specifically 40 μg/mL for compound **2.119e** and 80 μg/mL for compound **2.119i** (**Figure 106**).



2.119e
40 μg/mL

2.119i
80 μg/mL

Figure 106: Chemical structure of compounds **2.119e** and **2.119i** and their *in vitro* [MIC (μg/mL)] activity against virulent *M. tuberculosis*

3.3 Malaria

3.3.1 Malaria - Challenges and impact on human health

According to the 2020 edition of the WHO´s World Malaria Report, malaria can be defined as a ''life-threatening disease caused by parasites that are transmitted to people through the bites of infected female *Anopheles* mosquitoes. It is preventable and curable''[146]. It causes acute fever, chills, headaches, nausea, and can progress into a severe clinical disease if left untreated, with the first symptoms typically manifesting, in a non-immune individual, up to 10-15 days after the infection[146].

The female *Anopheles* mosquitoes act as **malaria vectors**, as they are able to spread a parasite through their bites[146,147]. according to WHO, ''There are 5 recognized parasitical species that can cause malaria in humans, from which 2 of them – *Plasmodium falciparum* and *Plasmodium vivax* – constitute the greatest threat''[146]. Also according to WHO[146,147], *P. falciparum* was responsible, in 2019, for 99.7% of the total malaria cases in the WHO African Region, 71% of the cases in the Eastern Mediterranean region, 65% of the cases in the Western Pacific region and 50% of the cases in WHO South-East Asia region; as for *P. vivax*, it was the predominant parasitic agent in the WHO Region of the Americas, being responsible for 75% of the total cases[146,147].

Although being defined as a curable disease, malaria is still a health challenge nowadays. In 2019, nearly half of the world's population was at risk of contracting malaria, and an estimated 229 million cases have been identified in 2019 alone (in comparison with 228 million cases in 2018)[146]. The number of deaths in 2019 ascended to 409.000, and although not climbing, in comparison with 2018, it is still a concerning number[146,147]. Also, between 2015 and 2017, and opposing a consecutive decrease between 2000 and 2015, 55 countries had an increase in cases and 38 countries had an increase in deaths, which, despite not being clear to whether this is a real epidemiological trend, is still indicative that this problem is far from over[148].

Current therapies and treatment

The eradication of the malaria endemics would require the extinction of the four main parasite species: *P. falciparum*, *P. vivax*, *P. ovale* and *P. malariae*[148]. As this goal has not yet been achieved, malarian parasites have had the opportunity to adapt and develop drug resistance to some of the clinically used antimalarial drugs, and for this reason, the development of new antimalarial drugs have been supported by a series of project and institutions[148,149]. In 1820, quinine (**Figure 107**) started to be used as an effective antimalarial treatment, based on which a series of other compounds were designed and prepared[149]. However, several of these compounds are not in clinical use nowadays, either because drug resistance has been confirmed or have been related to undesirable side effects such as cardiotoxicity or toxic psychosis[149].

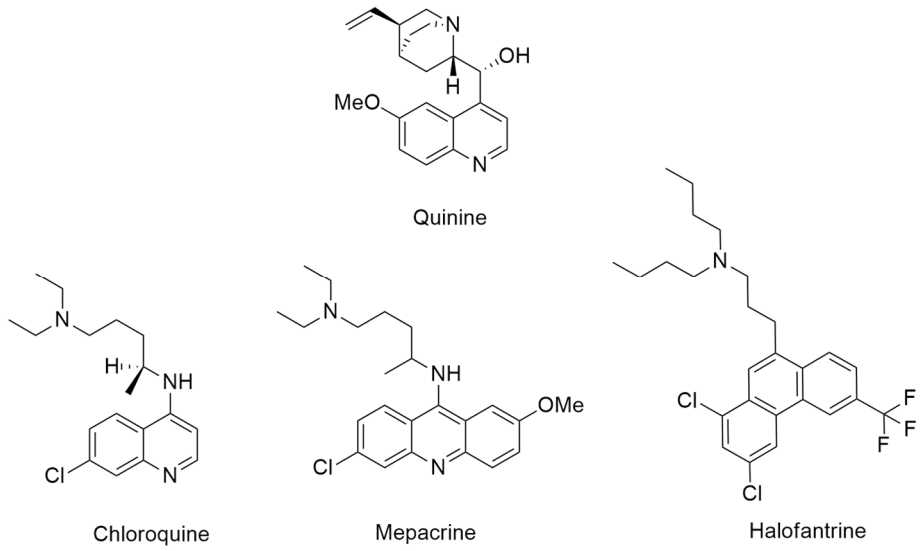


Figure 107: Examples of quinine-derived antimalarial drugs, developed between 1820 and the 1980s

Isolated for the first time in 1971, from *Artemisia annua*, a plant most used in Chinese traditional medicine, the sesquiterpene artemisinin (**Figure 108**) has proven to be effective against all drug-resistant variants of *P. falsiparum*[149]. Nowadays, several pro-drugs derived from artemisinin (such as artemether, artesunate and artemotil) are commercially available, and all share the same active compound, dihydroartemisinin[149]. The mechanism of action of artemisinin-derived compounds is still unclear, but the most accepted theory involves the generation of free radical species via haem-catalysed activation, leading to the unrepairable damage of several proteins that are vital for the parasites' survival[149,150]. However, other possible mechanisms of action have also been identified: in 2013, a computational study revealed that not only haem is involved in the mechanism but also PfATP6 (a Ca^{2+} transporter) could be involved[151]; others, for example, identify PfPI3K as a potential target of artemisinin, with the evidence pointing to the possibly of it acting as an inhibitor of said enzyme[152].

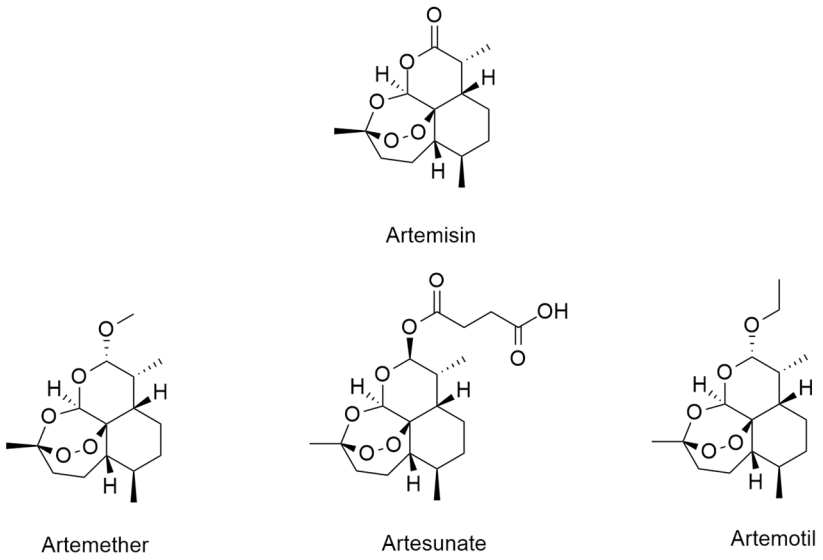


Figure 108: Examples of artemisinin-derived antimalarial drugs

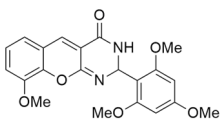
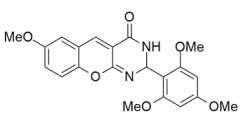
Nowadays, many other drugs have been approved for the treatment of malaria, such as lumefantrine, proguanil, tafenoquine, and others. However, there are still a necessity for new anti-malarial drugs, as drug-resistance phenomenon is still an occurring event: In the past 62 years, we have suffered three outbreaks of *P. falciparum* drug resistance. From 1957 to the late 1970s, chloroquine-resistant variants spread from southeast Asia to several parts of the world[147,148]. Sulfadoxine-pyrimethamine was introduced in 1981, but a rapid spread of drug-resistant forms of *Plasmodium* was identified worldwide in a 20-year period[148]. Even to the artemisinin-based drugs, designed to overcome drug resistance, resistance is now common and is a huge concern in the Greater Mekong Subregion, which led to an

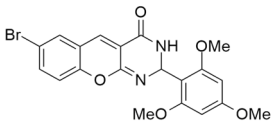
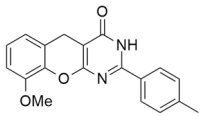
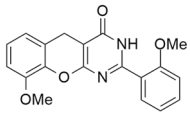
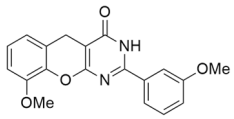
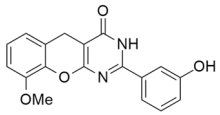
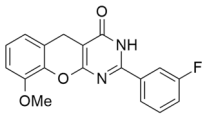
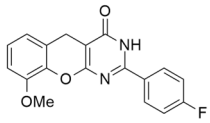
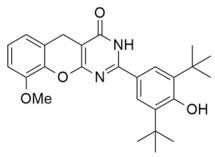
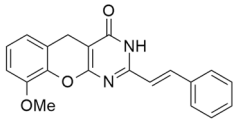
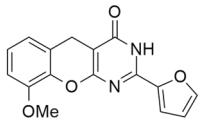
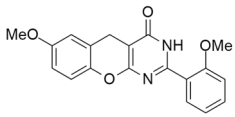
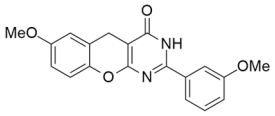
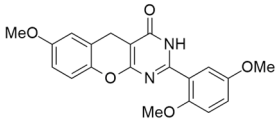
emergency response by WHO[146,148]. With *P. vivax*, many chloroquine-resistant forms have been pinpointed in the Americas, Asia, and Africa[146,148]. For this reason, the research and development of new therapeutic agents is still a health necessity, and is still included as one of the priorities of the WHO[146].

3.3.2 Biological evaluation of chromene-based and imidazole-based compounds activity against *Plasmodium falciparum*

To explore the potential of the targeted compounds against malaria, their possible antimalarial activity was assayed by Dr. Carla Calçada, form the University of Minho, Braga, Portugal, in a collaboration with Isabel Veiga's laboratory. The 3d7 and Dd2 parasite lines were obtained from MR4-Malaria Resources and maintained at about 4% haematocrit with human red blood cells in RPMI-1640, supplemented with 2 mM L-glutamine, 200 μM hypoxanthine, 0.25 μg/mL gentamycin, 25 mM HEPES, 0.2% $NaHCO_3$, and 0.25% Albumax II (Invitrogen; ThermoFisher Scientific). Parasite cultures were maintained at 37°C under a humidified controlled atmosphere of 5% O_2/5% CO_2/90% N_2. Parasite growth was monitored through Giemsa-stained blood smears. Parasite synchronization was performed with 5% sorbitol for 15 minutes at 37°C. For an initial screening of each compound and the respective drug susceptibility assays a fluorimeter plate reader was used. Briefly, for the initial screening, each compound was diluted and used at concentration of 2 μM/well. Only compounds that inhibited the parasite growth compared with control condition (without compound) at this concentration were used in the next step for IC_{50} determination. The results are presented in the following **Tables 135-137**.

Table 135: Survival rate percentage of *Plasmodium falciparum* (% mean value) parasites after treatment with a selection of compounds **2.3** and **2.6**

Compound	Structure	% survival (mean value)	
		Dd2	3D7
2.3d		87.4	82.5
2.3h		76.4	79.8

2.3i		88.1	65.6
2.6b		94.2	86.6
2.6d		93.1	94.8
2.6e		101.2	77.5
2.6i		101.1	83.0
2.6n		107.5	92.0
2.6o		107.6	86.8
2.6p		103.8	81.5
2.6q		94.8	99.4
2.6r		94.8	73.6
2.6s		96.4	80.4
2.6t		78.8	81.6
2.6u		103.1	87.6

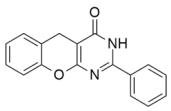
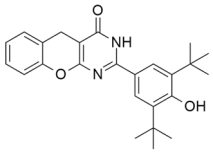
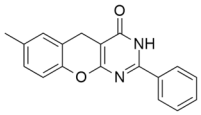
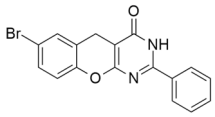
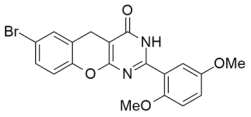
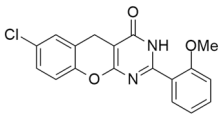
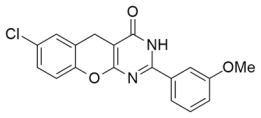
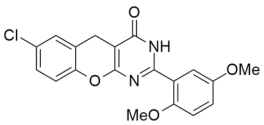
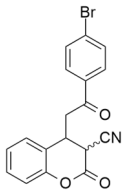
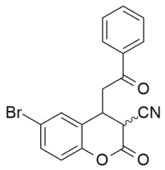
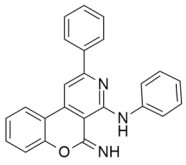
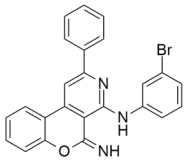
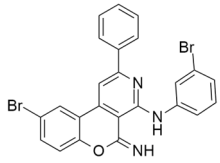
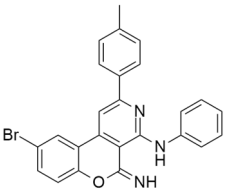
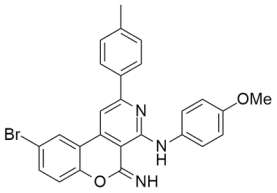
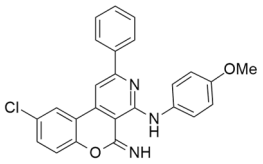
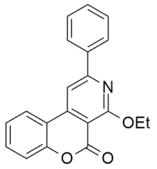
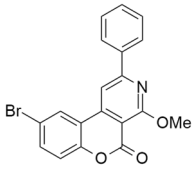
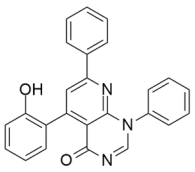
2.6x		94.5	75.6
2.6y		41.3	64.9
2.6b'		98.7	92.8
2.6d'		116.7	88.2
2.6g'		109.7	81.0
2.6i'		80.6	86.2
2.6j'		103.2	95.7
2.6m'		96.4	77.7

Table 136: Survival rate percentage of *Plasmodium falciparum* (% mean value) parasites after treatment with a selection of compounds **2.50**, **2.55**, **2.69**, **2.86**, **2.87**, **2.90** and **2.105**

Compound	**Structure**	**% survival (mean value)**	
		Dd2	**3D7**
2.50c		115.3	81.4
2.50d		118.0	92.3

2.55b		113.9	91.2
2.55e		102.2	92.4
2.55m		106.1	99.7
2.58n		103.5	91.8
2.58q		98.5	99.5
2.58b'		103.8	96.7
2.69a		125.7	84.4
2.69b		80.4	47.2
2.86a		95.9	68.2

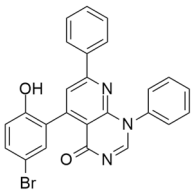
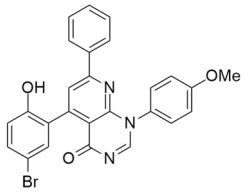
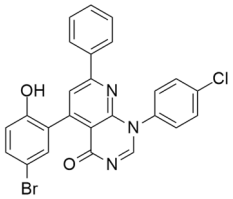
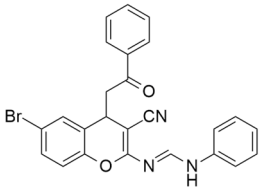
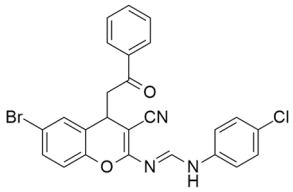
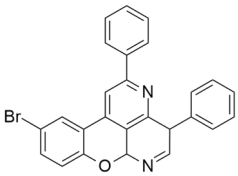
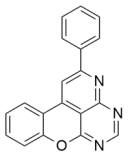
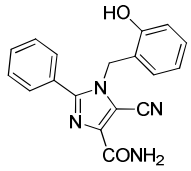
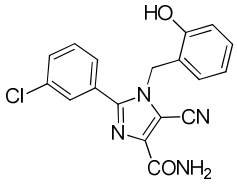
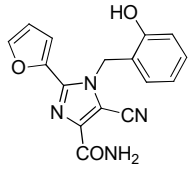
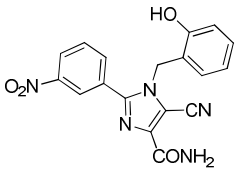
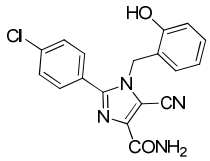
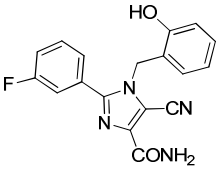
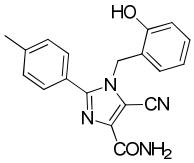
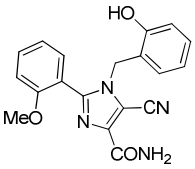
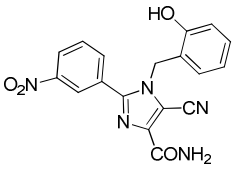
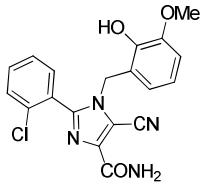
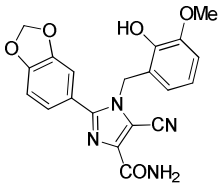
2.86b		96.6	64.8
2.86f		99.8	97.0
2.86g		23.6	7.45
2.87b		24.5	13.2
2.87l		20.3	13.2
2.90		119.9	79.6
2.105		110.1	90.3

Table 137: Survival rate percentage of *Plasmodium falciparum* (% mean value) parasites after treatment with a selection of compounds **2.119**

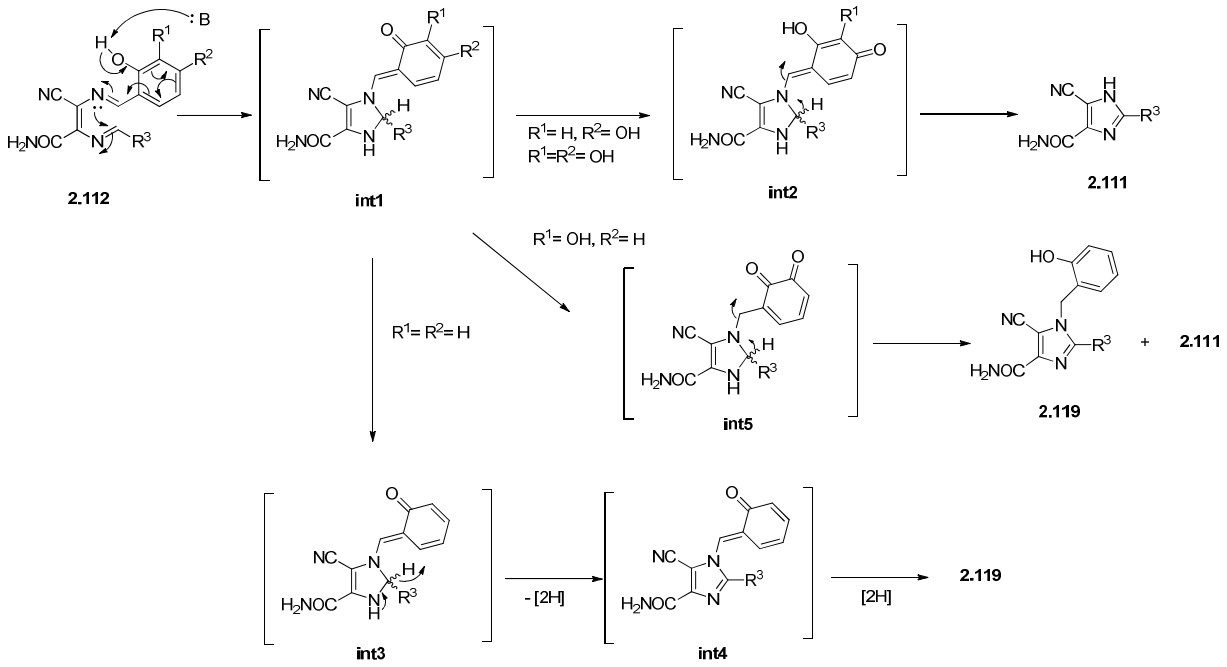
Compound	Structure	% survival (mean value)	
		Dd2	Dd2
2.119a		110.9	103.1
2.119c		108.0	102.7
2.119e		106.7	95.4
2.119g		92.0	82.6
2.119h		106.8	99.8
2.119k		93.8	95.6
2.119l		110.4	93.9
2.119m		111.6	88.5

2.119n		113.5	102.9
2.119o		116.3	90.2
2.119p		109.7	99.4

From the presented results (**Tables 135-137**), it is possible to observe that the best results were obtained for compounds **2.6y**, **2.86g**, **2.87b** and **2.87l**. None of the tested imidazoles **2.119** presented relevant results. Notably, two of the best results were obtained with both the precursor amidine **2.87l** (R^1=Br, R^2=H, R^3=4-Cl) and the pyridopyrimidinone **2.86g**, which was originated from amidine **2.87l**. Based on the present results, further studies are proceeding to evaluate the potential of amidines **2.87** and pyridopirimidinones **2.86** as new classes of antimalarial bioactive compounds.

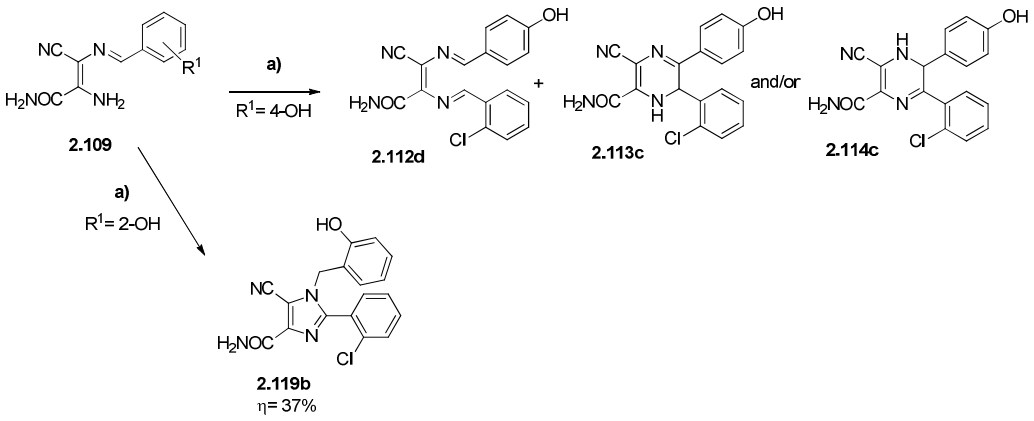
3.4 Computational studies on the reaction mechanism of 2-substituted 5-cyano-1-(2-hydroxybenzyl)-1*H*-imidazole-4-carboxamides

As previously discussed in chapter 2, Pereira[153] suggested a reaction mechanism for the synthesis of 1*H*-imidazoles **2.119** from benzylidene acrylamides **2.112**. In this publication, which were only focused on 2-hydroxybenzylidene acrylamides, the authors did not explore the case of conversions using 4-hydroxybenzylidene acrylamides, but rather included other polyhydroxylated systems (2,3-dihydroxy- or 2,3,4-trihydroxybenzylidene substituents), which in any case were also all substituted in *ortho* position (**Scheme 58**).



Scheme 58: Reaction mechanism for the synthesis of compounds **2.119** and side reaction obtained from hydroxylated derivatives of **2.112** [adapted from ref. 153]

This led the authors to postulate that the reaction involves the removal of the proton from the phenol group on the readily generated diimine intermediate. This triggers the delocalization of the resulting negative charge through the aromatic ring, generating a negatively charged nitrogen atom at position N1, which then conducts a nucleophilic attack on the second imine group. The selectivity of the reaction is therefore explained by the authors assuming the greater nucleophilicity of the N1 nitrogen atom than its counterpart N4. However, this statement would be equally true with 4-hydroxybenzylidene acrylamides, but, under the same reaction conditions, the formation of imidazole derivatives was not experimentally observed (**Scheme 59**).

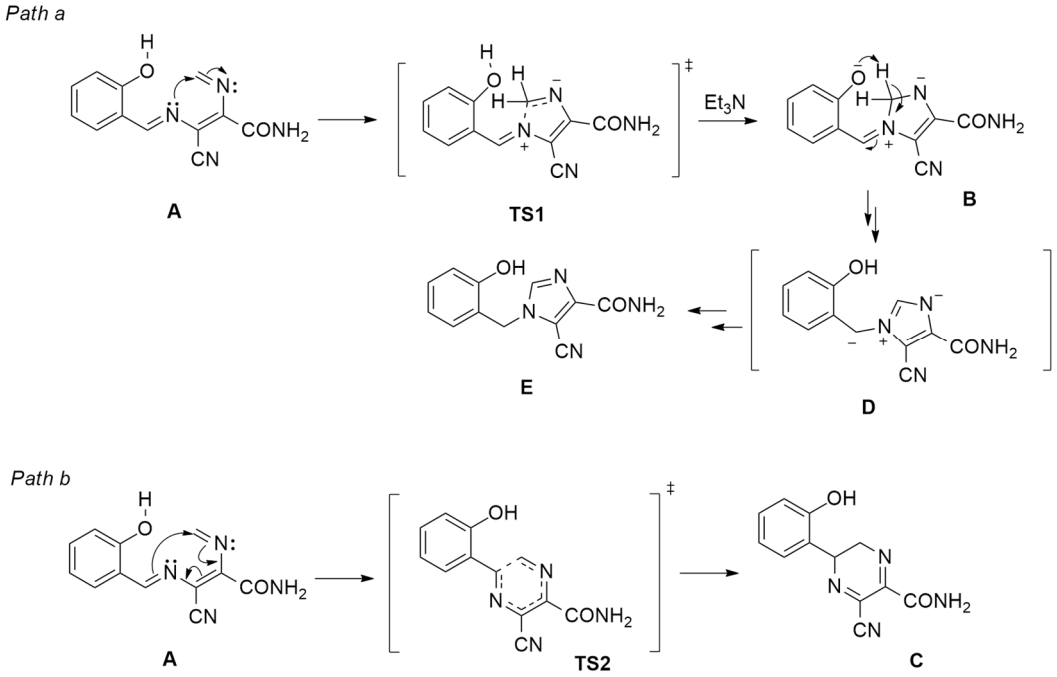


Scheme 59: Results obtained from the reaction of **2.109a** (R^1= 2-OH) and **2.109g** (R^1= 4-OH) with 2-chlorobenzaldehyde; **a)** 2-chlorobenzaldehyde (1.2 equiv.), Et_3N (2 equiv.), EtOH, r.t., 96h

This led us to believe that the selectivity of the 2-hydroxybenzylidene derivatives **2.109a** towards the formation of compounds **2.119** could be explained by an alternative mechanism, particularly by a self-catalysed process mediated by the 2-phenol group acting as a base, which would be absent in the 3- and 4-hydroxybenzylidene derivatives. To get further insights into this hypothesis, the reaction mechanism of 2-, 3- and 4-hydroxybenzylidene acrylamides was studied *in silico*, in particular to clarify the following points:

a) Why only 2-hydroxybenzylidene derivatives afford imidazole derivatives like **2.119**?
b) How is the 2-phenol group controlling the reaction path?
c) Is it an electronic effect or a self-catalysed process?

It is worth highlighting that the nucleophilic attack of the N1 nitrogen atom to the second imine moiety, considering the tautomeric form of the starting material as suggested by Pereira[153], was ruled out based on the very high activation barriers obtained on our preliminary studies exploring this idea. The tetrahedral geometry of the nucleophile (NH group) in this mechanism, and the presence of the hydrogen atom on the nitrogen would make the nucleophilic attack more difficult than for a sp^2 nitrogen atom (imine moiety). These initial results led us to explore other more suitable reaction paths. To this end, two plausible mechanisms were explored (**Scheme 60**): (i) *path a* - the formation of five-membered heterocycles (imidazoles) by nucleophilic attack of the N1 nitrogen atom (step 1), followed by aromatization catalysed by the phenolate form of the 2-phenol moiety (step 2); and (ii) *path b* - the formation of six-membered heterocycles (pyrazines) *via* an aza-Claisen-like cyclization. No substituents were included in the second imine moiety to reduce the number of isomers to study. This mechanism also assumes that a diamine is generated during the reaction.



Scheme 60: Plausible mechanisms studied for the formation of 1H-imidazole **E** and pyrazine derivative **C** from 2-hydroxybenzylidene acrylamide **A**

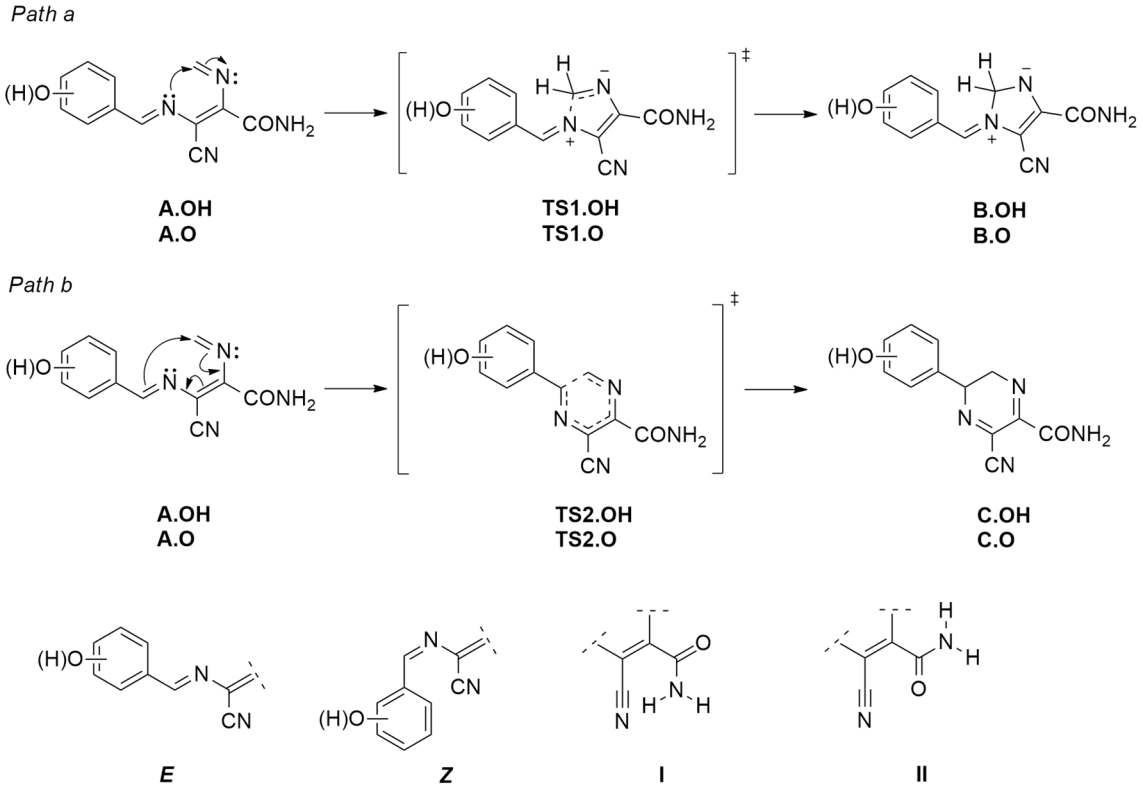
The calculation methodology involved the following steps:

1) **Identify the most suitable transition states** (**TS**) involved in the mechanism.
2) **Find the conformers of the reactant and product of the reaction**.
3) Determine the global **energy profile** of the conversion.

These computational studies were performed considering the three isomeric forms of the starting structure (**A**), TS (**TS1** and **TS2**) and products (**C** and **E**), thus, 2-, 3- and 4-hydroxybenzylidene derivatives, and for all these structures, the phenoxide and phenol forms were also considered. The most relevant results of both paths and each step are discussed in the next sections.

3.4.1 Step 1: intramolecular cyclization

First, we studied the intramolecular cyclization reaction that would lead to the formation of the 5-membered compound **B** from diimine **A**, and the 6-membered compound **C**, through the respective TS, **TS1** and **TS2** (**Scheme 61**). The structures in which the phenol group is in the neutral form are indicated as "**.OH**" and with "**.O**" for those using phenolate forms.



Scheme 61: Schematic representation of the reaction paths for the formation of 5- and 6-membered compounds **B** and **C**, respectively. The different types of isomers studied are also indicated. The structures in which the phenol group is in the neutral form are indicated as "**.OH**" and with "**.O**" for those using phenolate forms.

For both reaction paths the 2-, 3- and 4-hydroxyl isomers in the neutral form and the corresponding phenolate forms, as well as the E/Z isomers of the benzylidene group in the dimine **A** were studied (**Scheme 61**). In addition, for each of these structures, two possible conformers of the $CONH_2$ group were considered. Thus, one with the -NH_2 group in the $CONH_2$ substituent pointing towards the CN substituent (**I**, **Scheme 61**), and the another with the CO group in the $CONH_2$ substituent pointing towards the CN substituent (**II**, **Scheme 61**). The results of these studies considering the phenol moiety in the neutral and the phenolate forms are summarized in **Figure 109**. When the neutral form of the phenol group was employed, the activation free energies obtained for the formation of 5-membered compounds range between 12.3 kcal mol^{-1} (*ortho* substitution) and 14.3 kcal mol^{-1} (*para* substitution), while values between 23.9 kcal mol^{-1} (*ortho* substitution) and 26.1 kcal mol^{-1} (*para* substitution) were obtained for the formation of the 6-membered derivatives (**Figure 109A**). When the phenolate form was considered, the activation free energies varied between 12.4 kcal mol^{-1} (*meta* substitution) and 17.8 kcal mol^{-1} (*para* substitution) for the formation of 5-membered compounds and between 16.4 kcal mol^{-1} (*ortho* substitution) and 23.3 kcal mol^{-1} (*meta* substitution) for the 6-membered derivatives (**Figure 109B**).

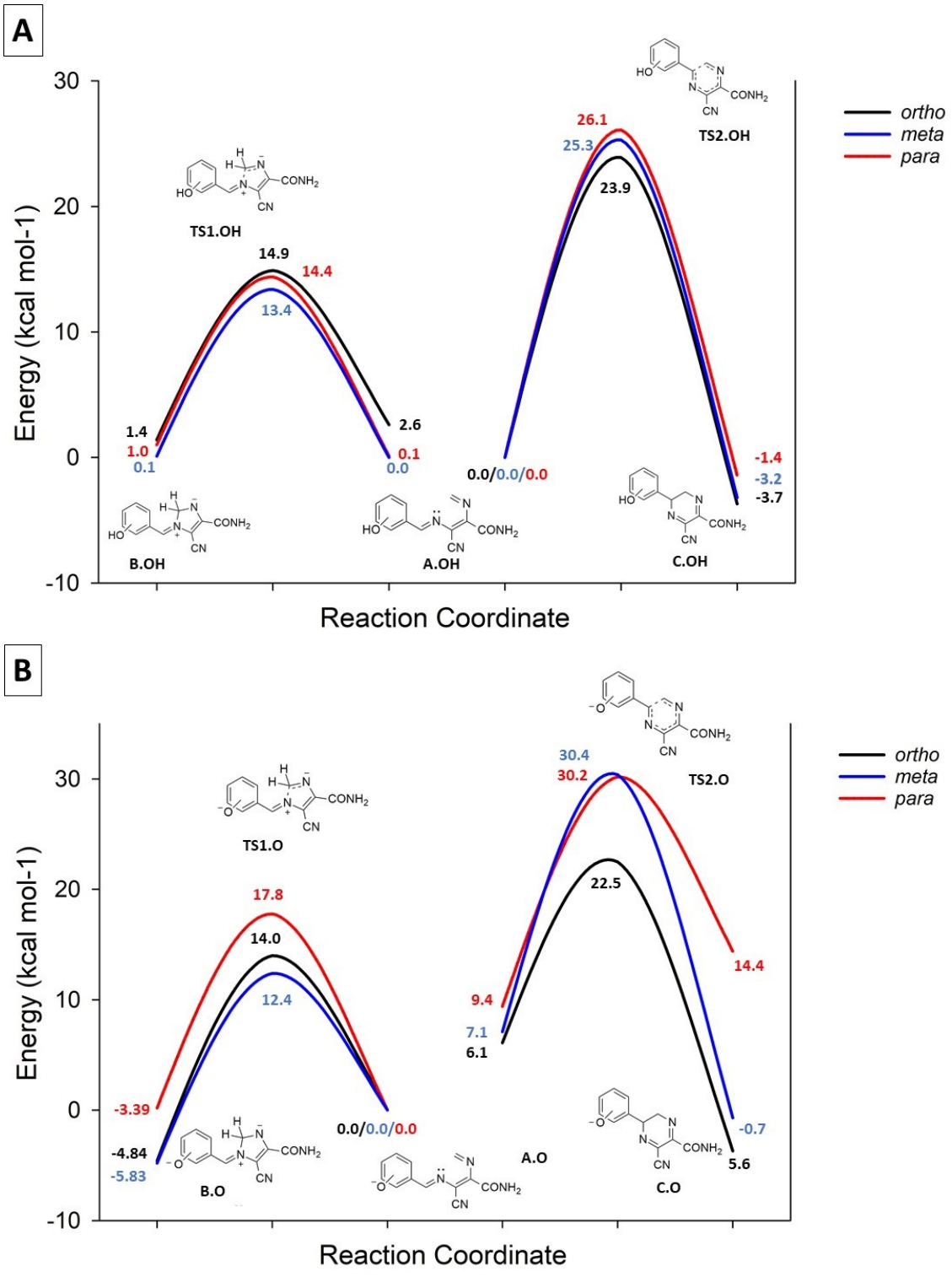


Figure 109: Free energy profiles for the cyclization steps to afford 5- and 6-membered derivatives substituted with 2-, 3- and 4-hydroxylphenyl groups

For both cases, the formation of 5-membered derivatives predicted to be more favourable than for the 6-membered ones, and this effect was significantly relevant when the neutral phenol form was considered. In the latter case, no significant differences were identified among the three isomers (*ortho,*

meta, para) studied, showing energy differences of about 12 kcal mol^{-1}. However, when the phenolate form was employed, these energy differences were only identified for the *meta* isomer (~11 kcal mol^{-1}), since for *ortho* and *para* isomers only differences of 2–3 kcal mol^{-1} were obtained. These findings highlighted a strong contribution of the electronic effects on the intramolecular cyclization step, and, based on the low energy barriers differences obtained, both paths would be possible. Therefore, the reason for explaining the different regioselectivity obtained may lie in the subsequent evolution of the intermediates generated in step 1 (**Figure 109**).

On the other hand, the analysis of the geometries of the transition states **TS1.OH**/**TS1.O (Figure 110**) and **TS2.OH**/**TS2.O** (**Figure 111**) revealed that for all the transition states, the NH_2 group in the $CONH_2$ substituent would be pointing towards the N4 nitrogen atom to stablish a hydrogen bonding interaction. The latter contact seems to help to achieve the best arrangement for cyclization. However, as these calculations were performed in vacuum, the relevance of this interaction may be lost in solution. In addition, some differences among the **TS1** for the three isomers explored were identified. Thus, the relative arrangement of the phenolic ring in relation to the 5-membered formed in the cyclization showed to be distinct for the *ortho* isomer compared with the *meta* and *para* isomers, which followed a similar architecture. For the *ortho* isomer, the phenolic ring showed to be almost coplanar to the new 5-membered ring generated.

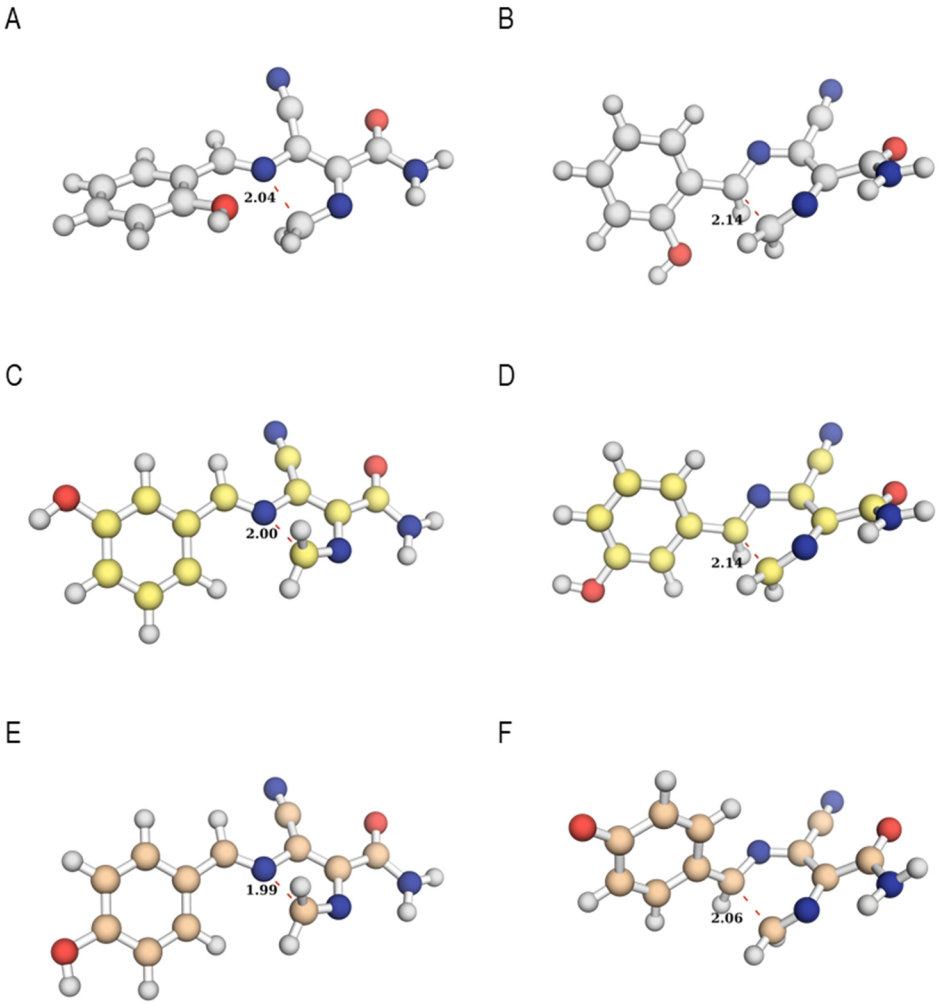


Figure 110: Geometries of the transition states **TS1.OH** (A, C and E) and **TS2.OH** (B, D, F). The ortho (A, B), meta (C, D) and para (E, F) isomers of each TS are shown

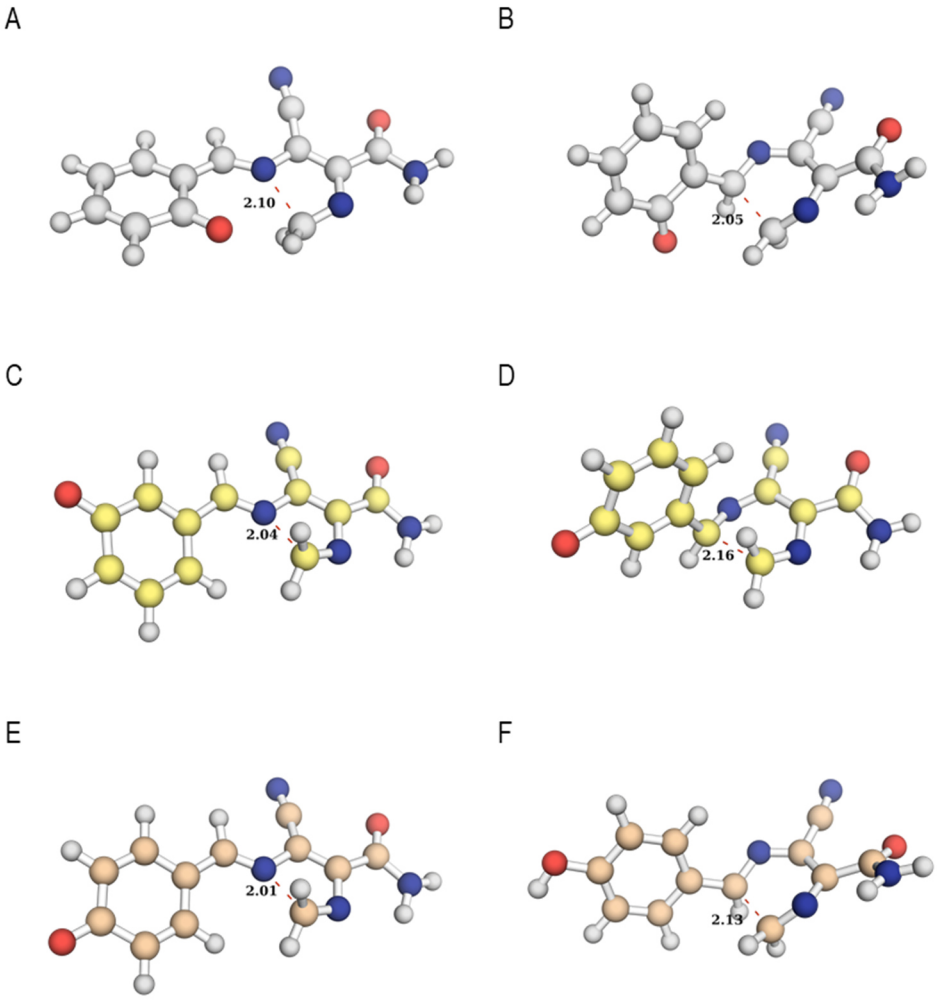
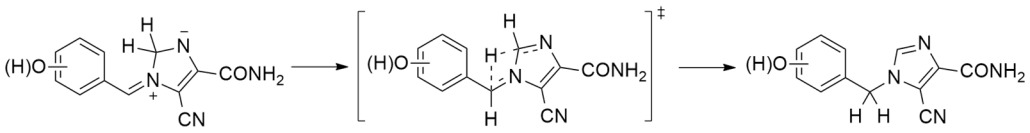


Figure 111: Geometries of the transition states **TS1.O** (A, C and E) and **TS2.O** (B, D, F). The ortho (A, B), meta (C, D) and para (E, F) isomers of each TS are shown

3.4.2 Step 2: aromatization

The intramolecular hydrogen transfer between the methylene moiety and the benzylidene group in intermediates **B.OH**/**B.O** was first explored (**Scheme 62**). However, for all the isomers (*ortho, meta, para*), energy barriers higher than 49 kcal mol^{-1} were obtained, with no significant differences between isomers. Such a high value of activation energy rules out this possibility.



Scheme 62: Schematic representation of the possible conversion of intermediates **B.OH** and **B.O** in imidazoles **E.OH** and **E.O** through [1,3]-hydrogen shift reaction

An inspection of the intermediates **B.OH** and **B.O**, which were obtained in the step 1 of the 5-membered ring formation mechanism, showed remarkable differences in their spatial disposition depending on the position of the substituent in the aromatic ring (**Figure 112**).

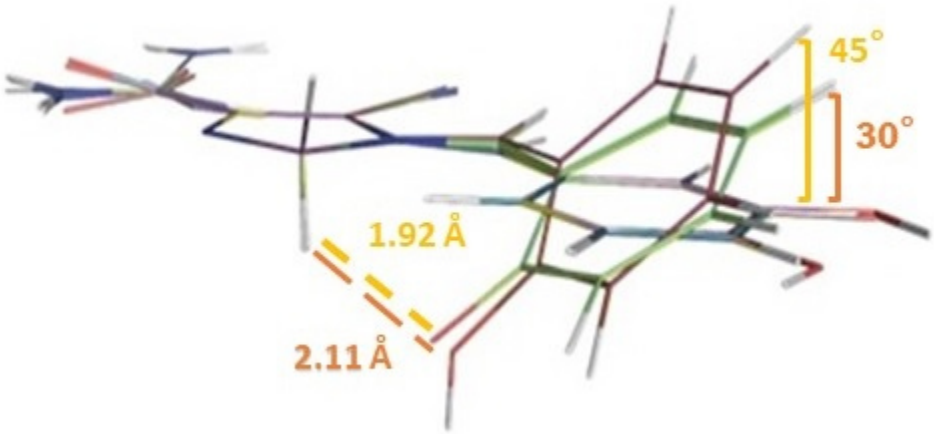
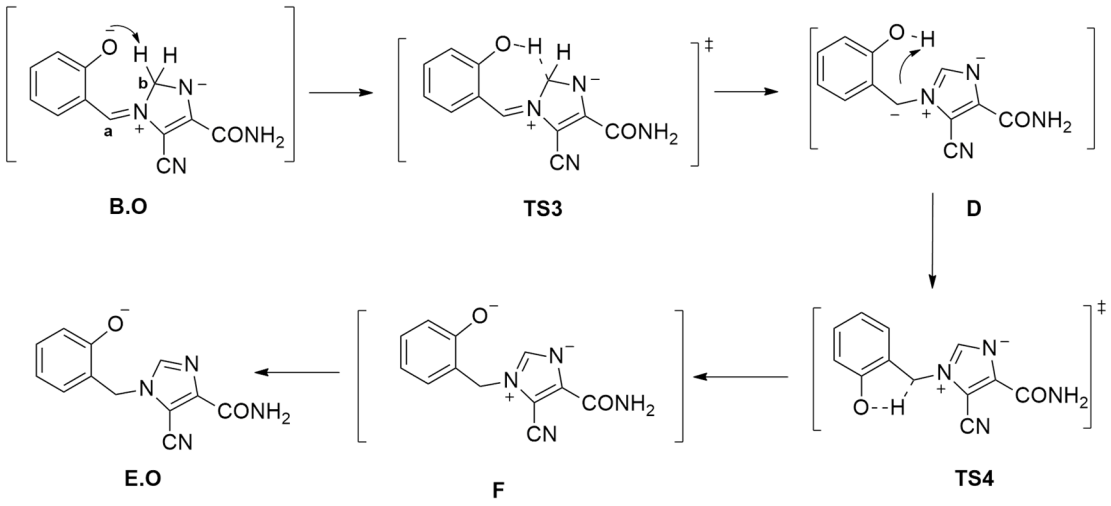


Figure 112: Geometries of the intermediates **B.OH** and **B.O**. Note how for the ortho isomers, no planar arrangements were observed. The phenol/phenolate moieties are located on a suitable arrangement for the removal of one of the hydrogen atoms of the methylene group. The distances between the oxygen atom of the phenol/phenolate group and the methylene hydrogen atom are highlighted

For the *meta* and *para* isomers, an overall planar arrangement was obtained with the newly formed 5-membered ring and the phenol moiety in the same plane. However, for the *ortho* isomers, the phenol/phenolate ring is arranged about 30° and 45°, respectively, from the coplanar disposition. As a result, the oxygen atom in the phenol/phenolate moiety would be close to one of the hydrogen atoms in the methylene group of the 5-membered ring, with distances of 2.11 Å and 1.92 Å for the phenol and phenolate derivatives, respectively. This disposition for the *ortho* intermediates **B.OH** and **B.O** suggests that the phenol/phenolate group could be involved in the final aromatization of the 5-membered ring generated to afford the experimentally observed imidazole derivatives. These finding led us to explore this intramolecular abstraction reaction, which would be geometrically difficult for the *meta* and *para* isomers (**Scheme 63**). As the intermediate **B.OH** could also be converted into **B.O** by reaction with the Et_3N employed in the reaction, our next calculations were focused in intermediate **B.O**.

In **TS4**, the transferred proton was located at 1.53 Å to the benzylic carbon atom and at 1.16 Å to the phenolic oxygen atom (**Figure 114**). Additionally, this step should be irreversible, as a high $\Delta G^{\ddagger}$ (24.1 kcal mol^{-1}) was obtained.



Scheme 63: Schematic representation of the possible conversion of intermediate **B.O** in imidazole **E.O** through an intramolecular hydrogen abstraction and a subsequent proton transfer reaction

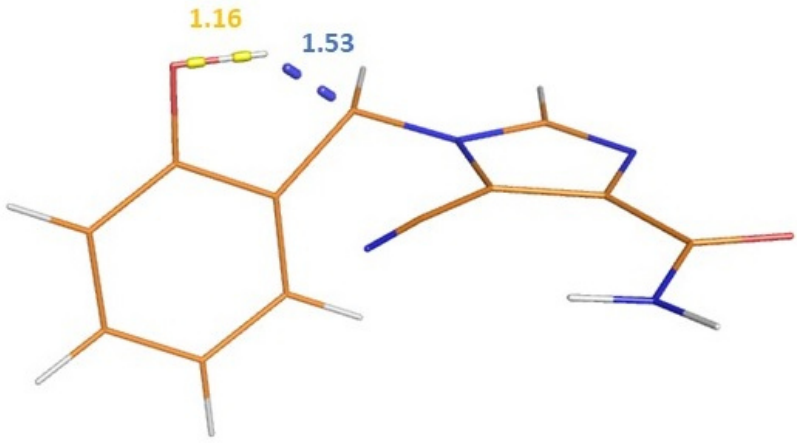


Figure 113: Geometry of the **TS4**. The distances (Å) of the formed (blue) and broken (yellow) bond are indicated.

The full energy landscape is presented in **Figure 114**. In contrast to **TS1.0**, in the TS of this transformation, **TS4**, the carbonyl group of the amide was pointing towards the heterocyclic nitrogen atom (**Figure 114**). The activation energy calculated for the intramolecular hydrogen abstraction by the 2-phenoxide group proved to be low, 10.8 kcal mol^{-1}. The energy barrier calculated for the protonation of the resulting anion **D** was very low of only 0.6 kcal mol^{-1}, indicating that the generation of **F** would be very fast.

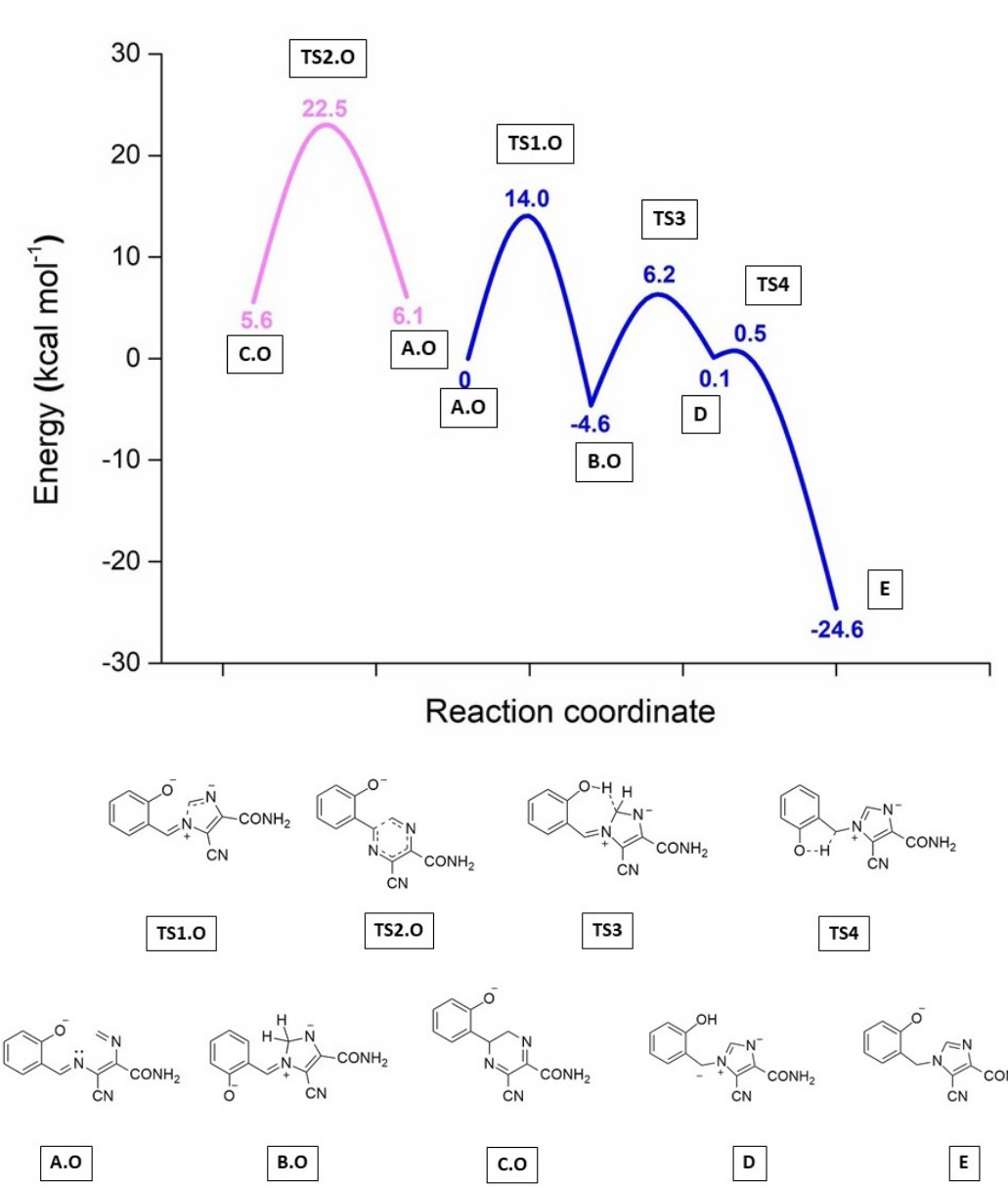


Figure 114: Free energy profiles for the formation of 5- and 6-membered derivatives substituted with 2-, 3- and 4-hydroxylphenyl groups. Only the phenolate forms of the starting material, intermediates and TS are considered.

From the full energy landscape obtained for the diamine **A.O** (**Figure 114**) we can conclude that the intramolecular cyclization for the formation of both the 5- and 6-membered derivatives would be: (i) an energetically favorable process; (ii) as both reactions have similar energy barriers of 14.0 and 16.4 kcal mol^{-1}, respectively, they are competitive process and reversible. For the 3- and 4-hydroxybenzylidene derivatives **2.138d** and **2.138g**, since the generated intermediates **B.OH**/**B.O** cannot evolve, the process reverses, favoring the formation of the 6-membered systems. However, for the *ortho* derivatives, as this type of substitution promotes the intramolecular abstraction of one of the methylene hydrogens of the 5-membered system **B.O**, the evolution of the reaction towards the formation of imidazole derivatives

is triggered. The low energy barriers of the abstraction and protonation steps (globally a [1,3]-hydrogen sift) and the $\Delta G^{\ddagger}$ calculated for the global process leading to the imidazole derivative **E** of -24.6 kcal mol^{-1} would make this reaction highly favorable. According to the calculations performed here, the intramolecular cyclization reaction would be the rate determining step.

References:

[1] World Health Organization (WHO). *Cancer. WHO*. URL: https://www.who.int/health-topics/cancer #tab= tab_1 (2021), last accessed in 24th October 2021.

[2] International Agency for Research on Cancer (IARC), World Healt Organization (WHO). Cancer. G*LOBOCAN* (2020).

[3] Pérez-Herrero, E. & Fernández-Medarde, A. Advanced targeted therapies in cancer: Drug nanocarriers, the future of chemotherapy. *Eur. J. Pharm. Biopharm.* **93**, 52–79 (2015).

[4] Stein, G. S. & Pardee, A. B. *Cell cycle and Growth Control: Biomolecular Regulation and Cancer*. (Springer, 2004).

[5] McKinnell, R. G., Parchment, R. E., Perantoni, A. O., Pierce, G. B. & Damjanov, I. *The Biological Basis of Cancer*. (Cambridge University Press, 1998).

[6] Pollock, P. M. & Meltzer, P.S. Cancer: lucky draw in the gene raffle. *Nature* **417**, 906–907 (2002).

[7] Floor, S. L. *et al*. Hallmarks of cancer: Of all cancer cells, all the time? *Trends Mol. Med.* **18**, 509–515 (2012).

[8] Fearon, E. R. & Bommer, G. T. *Progressing from gene mutations to cancer*. (Clinical Oncology, Churchill Livingstone, Elsevier, 2008).

[9] Croce, C. M. Oncogenes and cancer. *Science* **267**, 1408–1409 (1995).

[10] Krug, U., Ganser, A. & Koeffler, H. P. Tumor suppressor genes in normal and malignant hematopoiesis. *Oncogene* **21**, 3475–3495 (2002).

[11] Park, B. H. & Vogelstein, B. Tumor-suppressor genes. in *Holland-Frei Cancer Medicine* (eds. Kufe, D. W. *et al.*) 86–102 (BC Decker Inc, 2003).

[12] Hanahan, D. & Weinberg, R. The Hallmarks of cancer. *Cell* **100**, 57–70 (2000).

[13] Hanahan, D. & Weinberg, R. A. Hallmarks of cancer: The next generation. *Cell* **144**, 646–674 (2011).

[14] Kerr, J.F.R., Wyllie, A. H. & Currie, A. R. Apoptosis: a basic biological phenomenon with wide-ranging implications in tissue kinetics. *Br. J. Cancer* **26**, 239–257 (1972).

[15] Walker, N. I. *et al.*. Patterns of cell death. *Methods Achiev Exp Pathol* **1**, 18–54 (1988).

[16] Hong, S. J., Dawson, T. M. & Dawson, V. L. Nuclear and mitochondrial conversations in cell death: PARP-1 and AIF signaling. *Trends Pharmacol. Sci.* **25**, 259–264 (2004).

[17] Proskuryakov, S. Y., Konoplyannikov, A. G. & Gabai, V. L. Necrosis: A specific form of programmed cell death? *Exp. Cell Res.* **283**, 1–16 (2003).

[18] Blagosklonny, M. V. Cell death beyond apoptosis. *Leukemia* **14**, 1502–1508 (2000).

[19] Elmore, S. Apoptosis: a review of programmed cell death. *Toxicol. Pathol.* **35**, 495–516 (2007).

[20] Hirsch, T. *et al.* The apoptosis-necrosis paradox. Apoptogenic proteases activated after mitochondrial permeability transition determine the mode of cell death. *Oncogene* **15**, 1573–1581 (1997).

[21] Zeiss, C. J. The apoptosis-necrosis continuum: Insights from genetically altered mice. *Vet. Pathol.* **40**, 481–495 (2003).

[22] Li, P. *et al.* Caspase-9: structure, mechanisms and clinical application. *Oncotarget* **8**, 23996–24008 (2017).

[23] Dawson, V. L. & Dawson, T. M. Deadly conversations: nuclear-mitochondrial cross-talk. *J. Bioenerg. Biomembr.* **36**, 287–294 (2004).

[24] Majno, G. & Joris, I. Apoptosis, oncosis, and necrosis: An overview of cell death. *Am. J. Pathol.* **146**, 3–15 (1995).

[25] Igney, F. H. & Krammer, P. H. Death and anti-death: tumour resistance to apoptosis. *Nat. Rev. Cancer* **2**, 277–288 (2002).

[26] Morris, G. *et al.* Cell death pathways: a novel therapeutic approach for neuroscientists. *Mol. Neurobiol.* **55**, 5767–5786 (2018).

[27] Tannishtha, R. *et al.* Stem cells, cancer, and cancer stem cells. *Nature* **414**, 105–111 (2001).

[28] Beug, H. Breast cancer stem cells: eradication by differentiation Therapy? *Cell* **138**, 623–625 (2009).

[29] International Agency for Research on Cancer (IARC), World Healt Organization (WHO). Breast cancer. G*LOBOCAN* (2020

[30] Bray, F. *et al.* Global cancer statistics 2018: GLOBOCAN estimates of incidence and mortality worldwide for 36 cancers in 185 countries. *CA. Cancer J. Clin.* **68**, 394–424 (2018).

[31] Tao, Z. Q. *et al.* Breast cancer: epidemiology and Etiology. *Cell Biochem. Biophys.* **72**, 333–338 (2015).

[32] Haghighat, S. *et al.* Standardized breast cancer mortality rate compared to the general female population of iran. *Asian Pacific J. Cancer Prev.* **13**, 5525–5528 (2012).

[33] Fang, X., Cao, J. & Shen, A. Advances in anti-breast cancer drugs and the application of nano-drug delivery systems in breast cancer therapy. *J. Drug Deliv. Sci. Technol.* **57**, 101662 (2020).

[34] Coleman, M. P. *et al.* Cancer survival in five continents: a worldwide population-based study (CONCORD). *Lancet* **9**, 730–752 (2008).

[35] Ziegler, R. *et al.* Migration patterns and breast cancer risk in asian-american women. *J. Natl. Cancer Inst.* **85**, 1819–1827 (1993).

[36] Brinton, L.A, Gaudet, M.M, Gierach, G.L. Breast cancer. In: Thun, M.J., Linet, M.S., Cerhan, J.R., Haiman, C.A., Schottenfeld, D., eds. Cancer Epidemiology and Prevention (4th ed. New York: Oxford University Press. 861-888. 2018).

[37] Rossouw, J.E. *et al.* Risks and benefits of estrogen plus pro- gestin in healthy postmenopausal women: principal results from the Women's Health Initiative randomized controlled trial. *JAMA* **288**. 321-333 (2002).

[38] Goldhirsch, A. *et al.* Strategies for subtypes-dealing with the diversity of breast cancer: Highlights of the St Gallen international expert consensus on the primary therapy of early breast cancer 2011. *Ann. Oncol.* **22**, 1736–1747 (2011).

[39] Viale, G. The current state of breast cancer classification. *Ann. Oncol.* **23** (2012).

[40] Prat, A. *et al.* Clinical implications of the intrinsic molecular subtypes of breast cancer. *Breast* **24**, S26–S35 (2015).

[41] Onitilo, A. *et al.* Breast Cancer Subtypes Based on ER/PR and Her2. *Clin. Med. Res.* **7**, 4–13 (2009).

[42] Santos, C. *et al.* Intrinsic cancer subtypes-next steps into personalized medicine. *Cell. Oncol.* **38**, 3–16 (2015).

[43] Niu, M. *et al.* Tumor-associated macrophage-mediated targeted therapy of triple-negative breast cancer. *Mol. Pharm.* **13**, 1833–1842 (2016).

[44] Hanf, V. & Hanf, D. Reproduction and breast cancer risk. *Breast Care* **9**, 398–405 (2014).

[45] Wielsøe, M., Gudmundsdottir, S. & Bonefeld-Jørgensen, E. C. Reproductive history and dietary habits and breast cancer risk in Greenlandic Inuit: a case control study. *Public Health* **137**, 50–58 (2016).

[46] Namiranian, N. *et al.* Risk factors of breast cancer in the eastern mediterranean region: a systematic review and meta-analysis. *Asian Pac. J. Cancer Prev.* **15**, 9535–9541 (2014).

[47] Mansfield, C. M. A review of the etiology of breast cancer. *J. Natl. Med. Assoc.* **85**, 217–221 (1993).

[48] Wang, X. *et al.* The association between body size and breast cancer in han women in northern and eastern china. *Oncologist* **21**, 1362–1368 (2016).

[49] Shield, K. D., Soerjomataram, I. & Rehm, J. Alcohol use and breast cancer: a critical review. *Alcohol Clin. Exp. Res.* **40**, 1166–1181 (2016).

[50] Pastor-Barriuso, R. *et al.* Total effective xenoestrogen burden in serum samples and risk for breast cancer in a population-based multicase–control study in Spain. *Environ. Health Perspect.* **124**, 1575–1582 (2016).

[51] Buchholz, T. A. Radiation therapy for early-stage breast cancer after breast-conserving surgery. *N. Engl. J. Med.* **360**, 63–70 (2009).

[52] Florescu, A. *et al.* Immune therapy for breast cancer in 2010 — hype or hope? *Curr. Oncol.* **18**, 9–18 (2011).

[53] Kallel, I. *et al*. What common biomarkers characterize a triple-negative profile in breast cancer? *Pathol. Biol.* **63**, 224–229 (2015).

[54] Karaayvaz, M. *et al.* Unravelling subclonal heterogeneity and aggressive disease states in TNBC through single-cell RNA-sequiv. *Nat. Commun.* **9**, (2018).

[55] Ozretic, P. *et al.* Apoptosis regulator Bcl-2 is an independent prognostic marker for worse overall survival in triple-negative breast cancer patients. *Int. J. Biol. Markers* **33**, 109–115 (2018).

[56] Reis-Filho, J. S. & Tutt, A. N. J. Triple negative tumours: a critical review. *Histopathology* **52**, 108–118 (2008).

[57] Foulkes, W. D., Smith, I.E. & Reis-Filho, J. S. Triple-negative breast cancer. *N. Engl. J. Med* **363**, 1938–1948 (2010).

[58] Garrido-Castro, A.C., Lin, N.U. & Polyak, K. Insights into molecular classifications of triple-negative breast cancer: Improving patient selection for treatment. *Cancer Discov.* **9**, 176–198 (2019).

[59] Lee, K.L. *et al.* Triple-negative breast cancer: current understanding and future therapeutic breakthrough targeting cancer stemness. *Cancers (Basel).* **11**, (2019).

[60] Ajithkumar, T. V. & Hatcher, H. M. *Specialist Training in oncology*. (2011).

[61] Shah, S. P. *et al.* The clonal and mutational evolution spectrum of primary triple-negative breast cancers. *Nature* **486**, 395–399 (2012).

[62] Lyons, T. G. & Traina, T. A. Emerging novel therapeutics in triple-negative breast cancer. in *Breast cancer metastasis and drug resistance: challenges and progress* (ed. Ahmad, A.) 377–399 (Springer International Publishing, 2019). doi:10.1007/978-3-030-20301-6_20.

[63] Lyons, T. G. Targeted therapies for triple-negative breast cancer. *Curr. Treat. Options Oncol.* **20**, (2019).

[64] Dent, R. *et al.* Triple-negative breast cancer: clinical features and patterns of recurrence. *Clin. Cancer Res.* **13**, 4429–4434 (2007).

[65] Tischkowitz, M. *et al.* Use of immunohistochemical markers can refine prognosis in triple negative breast cancer. *BMC Cancer* **7**, 1–11 (2007).

[66] Haffty, B. G. *et al.* Locoregional relapse and distant metastasis in conservatively managed triple negative early-stage breast cancer. *J. Clin. Oncol.* **24**, 5652–5657 (2006).

[67] Bauer, K. R. *et al.* Descriptive analysis of estrogen receptor (ER)-negative, progesterone receptor (PR)-negative, and HER2-negative invasive breast cancer, the so-called triple-negative phenotype: A population-based study from the California Cancer Registry. *Cancer* **109**, 1721–1728 (2007).

[68] Harris, L. N. *et al.* Molecular subtypes of breast cancer in relation to paclitaxel response and outcomes in women with metastatic disease: Results from CALGB 9342. *Breast Cancer Res.* **8**, 1–12 (2006).

[69] Morris, G. J. *et al.* Differences in breast carcinoma characteristics in newly diagnosed African-American and Caucasian patients: A single-institution compilation compared with the national

cancer institute's surveillance, epidemiology, and end results database. *Cancer* **110**, 876–884 (2007).

[70] Chang-Qing, Y. *et al.* Recent treatment progress of triple negative breast cancer. *Prog. Biophys. Mol. Biol.* **151**, 40–53 (2020).

[71] De Laurentiis, M. *et al.* Treatment of triple negative breast cancer (TNBC): Current options and future perspectives. *Cancer Treat. Rev.* **36**, S80–S86 (2010).

[72] Quinn, J. E. *et al.* BRCA1 Functions as a Differential Modulator of Chemotherapy-induced Apoptosis 1. 6221–6228 (2003).

[73] Lebert, J. M. *et al.* Advances in the systemic treatment of triple-negative breast cancer. *Curr. Oncol.* **25**, S142–S150 (2018).

[74] Azim, H. A. *et al.* Personalized treatment in metastatic triple-negative breast cancer: The outlook in 2020. *Breast J.* **26**, 69–80 (2020).

[75] Wang, X. *et al.* Emerging therapeutic modalities of PARP inhibitors in breast cancer. *Cancer Treat. Rev.* **68**, 62–68 (2018).

[76] Burgess, A. W. EGFR family: Structure physiology signalling and therapeutic targets†. *Growth Factors* **26**, 263–274 (2008).

[77] Kurebayashi, J. *et al.* Inhibition of HER1 signaling pathway enhances antitumor effect of endocrine therapy in breast cancer. *Breast Cancer* **11**, 38–41 (2004).

[78] Tsutsui, S. *et al.* Prognostic value of epidermal growth factor receptor (EGFR) and its relationship to the estrogen receptor status in 1029 patients with breast cancer. *Breast Cancer Res. Treat.* **71**, 67–75 (2002).

[79] Cheang, M. C. U. *et al.* Basal-like breast cancer defined by five biomarkers has superior prognostic value than triple-negative phenotype. *Clin. Cancer Res.* **14**, 1368–1376 (2008).

[80] Dogu, G. G. *et al.* Triple-negative breast cancer: Immunohistochemical correlation with basaloid markers and prognostic value of survivin. *Med. Oncol.* **27**, 34–39 (2010).

[81] Jhan, J. R. & Andrechek, E. R. Triple-negative breast cancer and the potential for targeted therapy. *Pharmacogenomics* **18**, 1595–1609 (2017).

[82] Denkert, C. *et* al. Molecular alterations in triple-negative breast cancer—the road to new treatment strategies. *Lancet* **389**, 2430–2442 (2017).

[83] Bergin, A. R. T. & Loi, S. Triple-negative breast cancer: recent treatment advances. *F1000Research* **8**, 1–11 (2019).

[84] Duk, W., Visintin, I. & Mor, G. Targeted cancer therapy – Are the days of systemic chemotherapy numbered ? *Maturitas* **76**, 308–314 (2013).

[85] Nwibo, D. D., Levi, C. A. & Nwibo, M. I. Small molecule drugs; down but not out: a future for medical research and therapeutics. *J. Dent. Med. Sci.* **14**, 70–77 (2015).

[86] Lee, Y. T., Tan, Y. J. & Oon, C. E. Molecular targeted therapy: Treating cancer with specificity. *Eur. J. Pharmacol.* **834**, 188–196 (2018).

[87] Seebacher, N. A., Stacy, A. E., Porter, G. M. & Merlot, A. M. *Clinical development of targeted and immune based anti-cancer therapies*. *Journal of Experimental and Clinical Cancer Research* **vol. 38** (Journal of Experimental & Clinical Cancer Research, 2019).

[88] Lheureux, S., *et* al. Molecularly targeted therapies in cancer: a guide for the nuclear medicine physician. *Eur J Nucl. Med. Mol. Imaging*. **44** (Suppl 1). 41-54 (2017). doi: 10.1007/s00259-017-3695-3**44**.

[89] Al-Mahmood, S. *et al.* Metastatic and triple-negative breast cancer: Challenges and treatment options. *Drug Deliv. Transl. Res.* **8**, 1483–1507 (2018).

[90] Sabit, H. *et al.* Triple negative breast cancer in the era of miRNA. *Crit. Rev. Oncol. Hematol.* **157**, 103196 (2021).

[91] Marra, A., Viale, G. & Curigliano, G. Recent advances in triple negative breast cancer: The immunotherapy era. *BMC Med.* **17**, 1–9 (2019).

[92] Yeo, S. K. & Guan, J.-L. Breast cancer: multiple subtypes within a tumor? *Trends in Cancer* **3**, 753–760 (2017).

[93] Carvalho, L. Exploitation of new chromene-based compounds as promising agents for cancer treatment. (University of Minho, 2020).

[94] He, J. *et al.* Molecularly engineering triptolide with aptamers for high specificity and cytotoxicity for triple-negative breast cancer. *J. Am. Chem. Soc.* **142**, 2699–2703 (2020).

[95] Zhou, W. X. *et al.* Discovery and optimization of withangulatin A derivatives as novel glutaminase 1 inhibitors for the treatment of triple-negative breast cancer. *Eur. J. Med. Chem.* **210**, 112980 (2021).

[96] Zhang, L. *et al.* Discovery of a small molecule targeting ULK1-modulated cell death of triple negative breast cancer in vitro and in vivo. *Chem. Sci.* **8**, 2687–2701 (2017).

[97] Zhang, W. *et al.* A new synthetic derivative of cryptotanshinone KYZ3 as STAT3 inhibitor for triple-negative breast cancer therapy. *Cell Death Dis.* **9**, (2018).

[98] Yang, G.-J. *et al.* Selective inhibition of lysine-specific demethylase 5A (KDM5A) using a rhodium(III) complex for triple-negative breast cancer therapy. *Angew. Chemie Int. Ed.* **57**, 13091–13095 (2018).

[99] Koboldt, D. C. *et al.* Comprehensive molecular portraits of human breast tumours. *Nature* **490**, 61–70 (2012).

[100] Scully, R. & Puget, N. The role of BRCA1 and BRCA2 in hereditary breast cancer. *Biochimie* 95–102 (2002).

[101] Scully, R., Xie, A. & Nagaraju, G. Molecular functions of BRCA1 in the DNA damage response. *Cancer Biol. Ther.* **3**, 521–527 (2004).

[102] Lord, C. J. & Ashworth, A. PARP inhibitors: synthetic lethality in the clinic. *Science (80-.).* **355**, 1152–1158 (2017).

[103] Moynahan, M. E. & Jasin, M. Mitotic homologous recombination maintains genomic stability and suppresses tumorigenesis. *Nat. Rev. Mol. Cell Biol.* **11**, 196–207 (2010).

[104] Dhillon, K. K., Bajrami, I., Taniguchi, T. & Lord, C. J. Synthetic lethality: The road to novel therapies for breast cancer. *Endocr. Relat. Cancer* **23**, T39–T55 (2016).

[105] Wang, J. *et al.* Discovery of novel PARP/PI3K dual inhibitors with high efficiency against BRCA-proficient triple negative breast cancer. *Eur. J. Med. Chem.* 113054 (2020) doi:10.1016/j.ejmech.2020.113054.

[106] Hottiger, M. O. *et al*. Toward a unified nomenclature for mammalian ADP-ribosyltransferases. *Trends Biochem. Sci.* **35**, 208–219 (2010).

[107] Do, K. & Chen, A. P. Molecular pathways: targeting PARP in cancer treatment. *Clin. Cancer Res.* **19**, 977–984 (2013).

[108] Turk, A. A. & Wisinski, K. B. PARP inhibitors in breast cancer: bringing synthetic lethality to the bedside. *Cancer* **124**, 2498–2506 (2018).

[109] Papadimitriou, M., Mountzios, G. & Papadimitriou, C. A. The role of PARP inhibition in triple-negative breast cancer: unraveling the wide spectrum of synthetic lethality. *Cancer Treat. Rev.* **67**, 34–44 (2018).

[110] Farmer, H. *et al.* Targeting the DNA repair defect in BRCA mutant cells as a therapeutic strategy. *Nature* **434**, 917–921 (2005).

[111] Bryant, H. E. *et al.* Specific killing of BRCA2-deficient tumours with inhibitors of poly(ADP-ribose) polymerase.[erratum appears in Nature. 2007 May 17;447(7142):346]. *Nature* **434**, 913–917 (2005).

[112] Murai, J. *et al.* Stereospecific PARP trapping by BMN 673 and comparison with olaparib and rucaparib. *Mol. Cancer Ther.* **13**, 433–443 (2014).

[113] Murai, J. *et al.* Trapping of PARP1 and PARP2 by clinical PARP inhibitors. *Cancer Res.* **72**, 5588–5599 (2012).

[114] Chadha, N. & Silakari, O. Identification of low micromolar dual inhibitors for aldose reductase (ALR2) and poly (ADP-ribose) polymerase (PARP-1) using structure based design approach. *Bioorgan. Med. Chem. Lett.* **27**, 2324–2330 (2017).

[115] Zhu, G. D. *et al.* Discovery and SAR of orally efficacious tetrahydropyridopyridazinone PARP inhibitors for the treatment of cancer. *Bioorganic Med. Chem.* **20**, 4635–4645 (2012).

[116] Elmasry, G. F. *et al.* Design and synthesis of novel PARP-1 inhibitors based on pyridopyridazinone scaffold. *Bioorg. Chem.* **87**, 655–666 (2019).

[117] Lin, S. *et al.* Synthesis of novel dual target inhibitors of PARP and HSP90 and their antitumor activities. *Bioorgan. Med. Chem.* **28**, 115434 (2020).

[118] Dai, Q. *et al.* Design, synthesis and biological evaluation of novel phthalazinone acridine derivatives as dual PARP and Topo inhibitors for potential anticancer agents. *Chinese Chem. Lett.* **31**, 404–408 (2020).

[119] Zheng, F. *et al.* Mechanism and current progress of Poly ADP-ribose polymerase (PARP) inhibitors in the treatment of ovarian cancer. *Biomed. Pharmacother.* **123**, 109661 (2020).

[120] Han, Y. *et al.* New Perspectives for Resistance to PARP Inhibitors in Triple-Negative Breast Cancer. *Front. Oncol.* **10**, 1–14 (2020).

[121] Geenen, J. J. J. *et al.* PARP Inhibitors in the Treatment of Triple-Negative Breast Cancer. *Clin. Pharmacokinet.* **57**, 427–437 (2018).

[122] O'Shaughnessy, J. *et al.* Efficacy of BSI-201, a poly(ADP-ribose)polymerase-1 (PARP1) inhibitor, in combination with gemcitabine/carboplatin (G/C) in patients with metastatic triple-negative breast cancer (TNBC): Results of a randomized phase II trial. *J. Clin. Oncol.* **27**, 3 (2009).

[123] Ferraris, D. V. Evolution of poly(ADP-ribose)polymerase-1 (PARP-1) inhibitors: from concept to clinic. *J. Med. Chem.* **53**, 4561–4584 (2010).

[124] Giannini, G. *et al.* Novel PARP-1 inhibitors based on a 2-propanoyl-3*H*-quinazolin-4-one scaffold. *Bioorgan. Med. Chem. Lett.* **24**, 462–466 (2014).

[125] Dawicki-McKenna, J. M. *et al.* PARP-1 activation requires local unfolding of an autoinhibitory domain. *Mol. Cell* **60**, 755–768 (2015).

[126] Bellocchi, D. *et al.* Docking studies on PARP-1 inhibitors: Insights into the role of a binding pocket water molecule. *Bioorgan. Med. Chem.* **13**, 1151–1157 (2005).

[127] Kinoshita, T. *et al.* Inhibitor-induced structural change of the active site of human poly(ADP-ribose) polymerase. *FEBS Lett.* **556**, 43–46 (2004).

[128] Wang, E. *et al.* End-Point binding free energy calculation with MM/PBSA and MM/GBSA: strategies and applications in drug design. *Chem. Rev.* **119**, 9478–9508 (2019).

[129] Wang, C. *et al.* Recent developments and applications of the MMPBSA method. *Front. Mol. Biosci.* **4**, 1–18 (2018).

[130] Miller, B. R. *et al.* MMPBSA.py: An Efficient Program for End-State Free Energy Calculations. (2012).

[131] Furin, J., Cox, H. & Pai, M. Tuberculosis. *Lancet* **393**, 1642–1656 (2019).

[132] World Healt Organization (WHO). *Global Tuberculosis Report* (2020).

[133] Shetye, G. S., Franzblau, S. G. & Cho, S. New tuberculosis drug targets, their inhibitors, and potential therapeutic impact. *Transl. Res.* **220**, 68–97 (2020).

[134] Dheda, K., Barry, C. E. & Maartens, G. Tuberculosis. *Lancet* **387**, 1211–1226 (2016).

[135] Maitr, T. *et al.*, Multidrug and extensively drug-resistant tuberculosis, *Med. Mal. Infect.* **47**, 3-10 (2016). doi: 10.1016/j.medmal.2016.07.006.

[136] World Health Organization (WHO).*Consolidated Guidelines on Dru-resitant tuberculosis treatment* (2019).

[137] Lee, A. *et al.* Current and future treatments for tuberculosis. *BMJ* **368** (2020).

[138] Khawbung, J. L., Nath, D. & Chakraborty, S. Drug resistant Tuberculosis: A review. *Comp. Immunol. Microbiol. Infect. Dis.* **74**, 101574 (2021).

[139] Reid, M. J. A. *et al.* Building a tuberculosis-free world: The Lancet Commission on tuberculosis. *Lancet* **393** 1331–1384 (2019).

[140] An, Q. *et al.* Repurposed drug candidates for antituberculosis therapy. *Eur. J. Med. Chem.* **192**, (2020).

[141]Tiberi, S. *et al.* The challenge of the new tuberculosis drugs. *Press. Medicale* **46**, e41–e51 (2017).

[142] von Groote-Bidlingmaier, F. *et al.* Efficacy and safety of delamanid in combination with an optimised background regimen for treatment of multidrug-resistant tuberculosis: a multicentre, randomised, double-blind, placebo-controlled, parallel group phase 3 trial. *Lancet Respir. Med.* **7**, 249–259 (2019).

[143] Whitlow, E., Mustafa, A. S. & Hanif, S. N. M. An overview of the development of new vaccines for tuberculosis. *Vaccines* **8**, 1–13 (2020).

[144] Fatima, S. *et al.* Tuberculosis vaccine: A journey from BCG to present. *Life Sci.* **252**, 117594 (2020).

[145] Palomino, J.C. *et al.* Resazurin Microtiter Assay Plate: Simple and Inexpensive Method for Detection of Drug Resistance in Mycobacterium tuberculosis. *Antimicrob. Agents Chemother.* **46**, 2720–2722 (2002).

[146] World Health Organization (WHO). Malaria. URL: https://www.who.int/news-room/fact-sheets/detail/malaria (2021) last accessed in 19th September 2021.

[147] World Health Organization (WHO). *World Malaria Report*. (2020). doi:10.1002/(SICI)1096-8628(19971128)73:1<1::AID-AJMG1>3.0.CO;2-Y.

[148] Feachem, R. G. A. *et al.* Malaria eradication within a generation: ambitious, achievable, and necessary. *Lancet* **394**, 1056–1112 (2019).

[149] Tse, E. G., Korsik, M. & Todd, M. H. The past, present and future of anti-malarial medicines. *Malar. J.* **18**, 1–21 (2019).

[150] Tilley, L. *et al.* Artemisinin Action and Resistance in *Plasmodium falciparum*. *Trends Parasitol.* **32**, 682–696 (2016).

[151] Shandilya, A. *et al.* A plausible mechanism for the antimalarial activity of artemisinin: A computational approach. *Sci. Rep.* **3**, 1–7 (2013).

[152] Mbengue, A. *et al.* A molecular mechanism of artemisinin resistance in *Plasmodium falciparum* malaria. *Nature* **520**, 683–687 (2015).

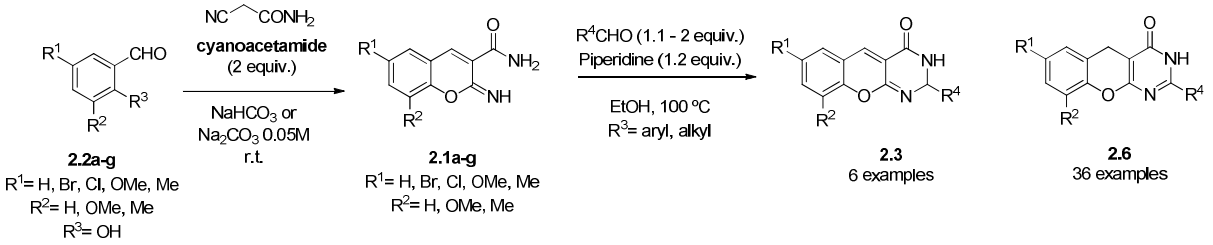
[153] Pereira, C.B.B.C. Síntese e avaliação da actividade antioxidante e micobacteriana de novos derivados de imidazole e purina. (University of Minho, 2010).

Chapter 4

Conclusion and final remarks

Derivatives of 3-Aryl-2,3-dihydro-1*H*-chromeno[3,2-*c*]pyridin-1-ones 2.3 and 2-aryl-3*H*-chromeno[2,3-*d*]pyrimidin-4(5*H*)-ones 2.6

A series of 3-aryl-2,3-dihydro-1*H*-chromeno[3,2-c]pyridin-1-ones (**2.3**) and 2-aryl-3*H*-chromeno[2,3-d]pyrimidin-4(5*H*)-ones (**2.6**) were prepared from the reaction of salicylaldehydes **2.2** and cyanoacetamide (**Scheme 64**).



Scheme 64: Synthetic route for the preparation of compounds **2.3** and **2.6**

The synthesis of a vast selection of compounds **2.3** and **2.6** and testing them in the Hs578t cancer cell line allowed to identify compound **2.6d'** (R^1=Br, X=H) as the most active. The results for the biological activity enabled the construction of a structure-activity relationship model for the PARP1 enzyme. The computational studies indicated that the presence of an electron withdrawing group (R^1=Br, Cl) in position 7, and a *meta*-substituted phenyl ring in the position 2 (X=Br, Cl) was important for the anticancer activity (**Figure 115**).

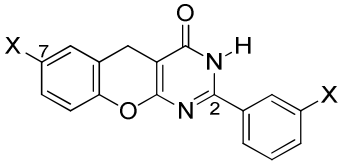


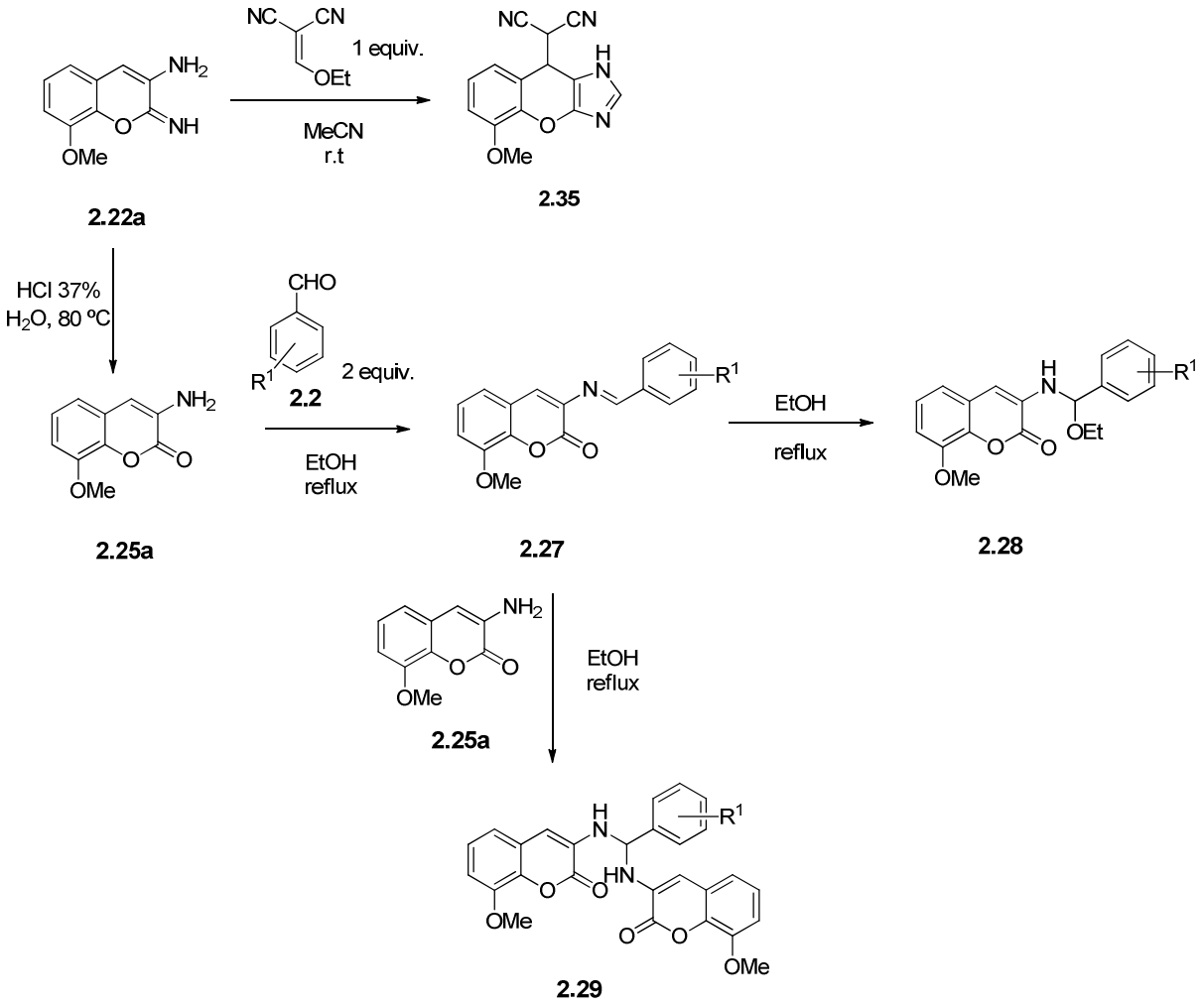
Figure 115: Substituents and positions (X=halide) promoting the activity of chromene[2,3-*d*]pyrimidin-4(5*H*)-one derivatives (**2.6**) studied against TNBC cell lines, considering the interaction with the PARP1 enzyme

The molecular docking simulations revealed that compounds **2.6** can interact favorably with the PARP1 nicotinamide binding pocket. However, their interaction with the binding site depends on the substituents present in position 7 and in position 2 of the phenyl ring. These two positions cannot be substituted simultaneously, because when the anchorage with the Gly863/Ser904 is achieved, both positions 2 and 7 are located in narrow pockets. As a future prospective, the insertion of hydrophilic groups in position 9 may improve the low solubility of this scaffold in aqueous medium. The substitution of position 2 with other substituted phenyl groups, or even with non-aromatic substituents, may allow for

an improved placement of these structures in the binding pocket, and thus lead to the development of novel PARP1 inhibitors.

Derivatives of 2-imino-8-methoxy-2*H*-chromen-3-amine 2.22a and 2-oxo-8-methoxy-2*H*-chromen-3-amine 2.25a

Compounds **2.27**, **2.28** and **2.29** could be prepared in satisfactory yields from 2-aminochromene **2.25a** (**Scheme 65**). Additionally, a simple synthetic route that leads to chromenoimidazole **2.35**, has been developed. This compound may be an interesting scaffold to explore the anticancer activity, by incorporating different substituents in the imidazole moiety (**Scheme 65**).

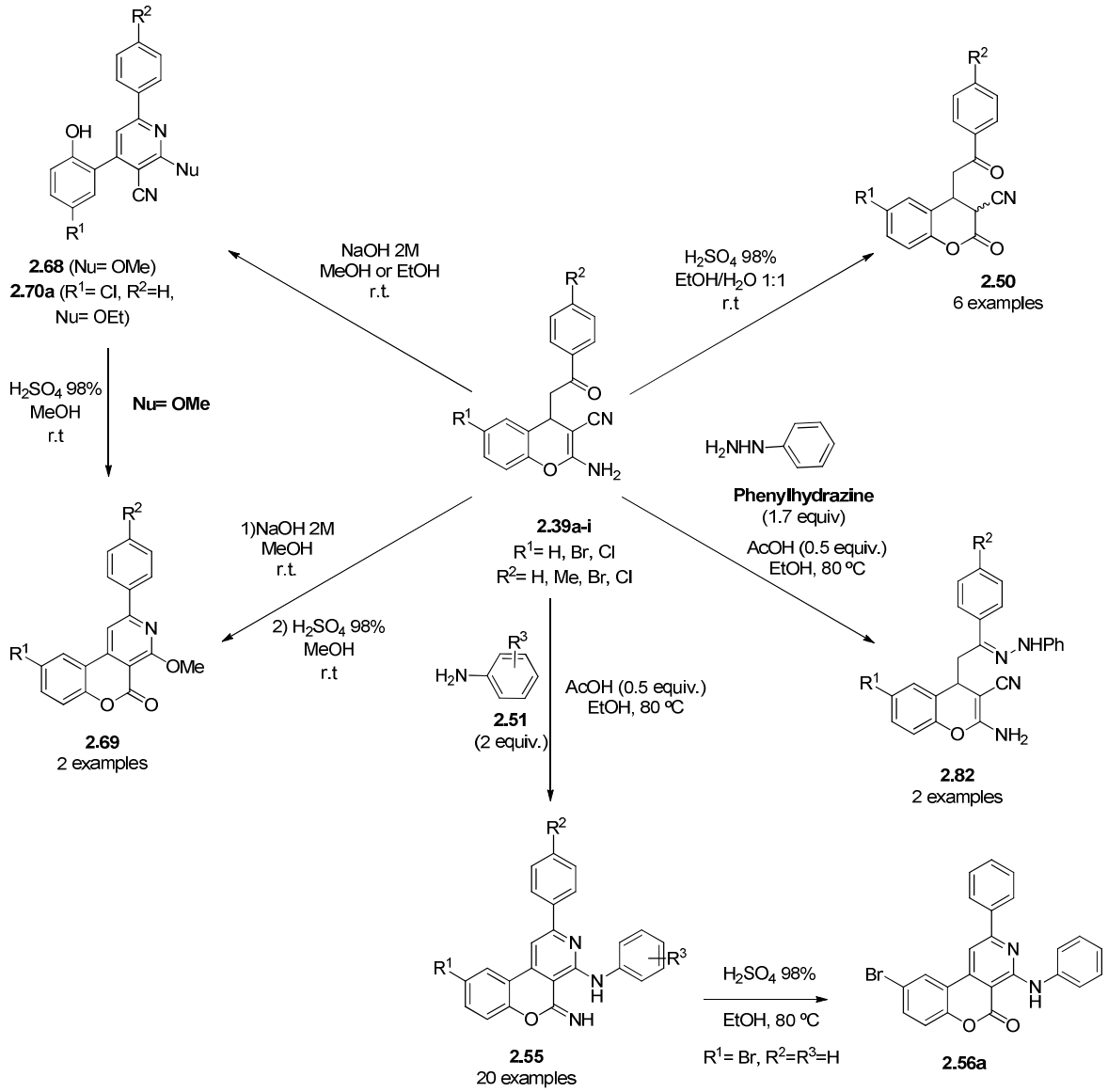


Scheme 65: Synthetic route for the preparation of compounds **2.27-2.29** and **2.35**

Derivatives of 2-amino-4-(2-oxo-2-arylethyl)-4*H*-chromene-3-carbonitriles 2.39

The work on the reactivity of compounds **2.39** led to novel chromene-based scaffolds. Compounds **2.39** mainly reacted by nucleophilic attack to position 2, followed by ring-opening processes. The weak nucleophilicity of the amino group in position 2 may be responsible for the chemical versatility of compounds **2.39**, as they led to the formation of different products under different reaction conditions: (i) the use of aqueous sulfuric acid allowed the preparation of compounds **2.50**, probably through protonation of the amino group and further nucleophilic attack of a water molecule to position 2; (ii) the use of aqueous sodium hydroxide led to nucleophilic attack to position 2 and subsequent opening of the chromene ring, followed by nucleophilic attack to the carbonyl group of the 2-oxo-2-arylethyl moiety, resulting in the formation of pyridines **2.68** and **2.70**; compounds **2.68** could be engaged in an acid-catalysed (with sulfuric acid) ring-closing step to afford chromenopyridines **2.69**; (iii) the reaction with primary aromatic amines (**2.51**) led to a similar process as described in (ii), and compound **2.39** further evolved to the formation of the chromenopyridine moiety, leading to chromenes **2.55**; compound **2.56a** (R^1= Br, R^2=H, R^3=H) could be prepared from a mixture containing **2.55a**, in aqueous sulfuric acid; (iv) performing the reaction with phenyl hydrazine led to the formation of compounds **2.82** by nucleophilic attack to the carbonyl group of the 2-oxo-2-arylethyl moiety and not to position 2 of the chromene nucleus (**Scheme 66**).

For future work on this topic, the synthesis of compounds **2.55** could be explored using different solvents or solvent mixtures, and different primary amines. The preparation of compounds **2.69** could also be improved by selecting the optimal basic conditions to promote the preferential formation of compounds **2.68**. Another exploratory work could involve the use of pyridines **2.68** and **2.70** as pH sensors or colorimetric structures, as it was observed that these pyridines were highly affected by pH variations. Such sensitivity was accompanied by a clear change in colour, ranging from violet to red depending on the substituents present in both aromatic rings.

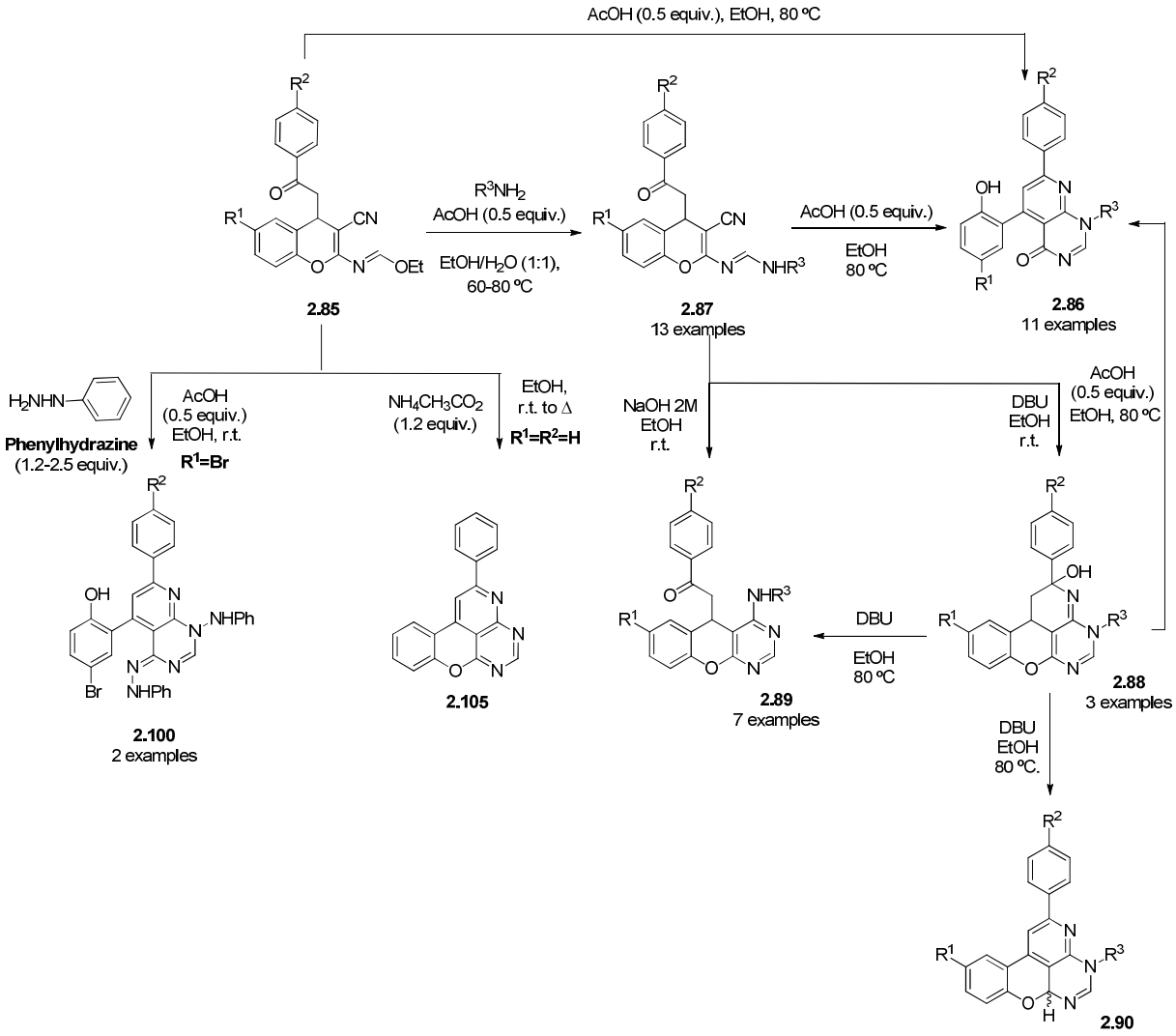


Scheme 66: Synthetic route for the preparation of compounds **2.50**, **2.55**, **2.56**, **2.68**, **2.69**, **2.70** and **2.82**

Derivatives of ethyl *N*-(3-cyano-4-(2-oxo-2-arylethyl)-4*H*-chromen-2-yl)formimidate 2.98

The reactions involving imidates **2.85** led to novel scaffolds, mainly by an ANRORC-type mechanism involving both the imidate and the carbonyl moieties. The evolution of amidines **2.87**, generated from imidates **2.85** by reaction with primary amines, strongly depends on the reaction conditions used. It was observed that (i) performing the reaction of imidates **2.85** with primary amines, in a EtOH/H_2O 1:1 system, afforded amidines **2.87** in good to high yields; (ii) pyridopyrimidines **2.86** could be prepared either from the reaction of imidates **2.85** with primary amines, or from the pure amidine **2.87** (or a crude mixture containing this compound), in ethanol at 80 °C, with or without the

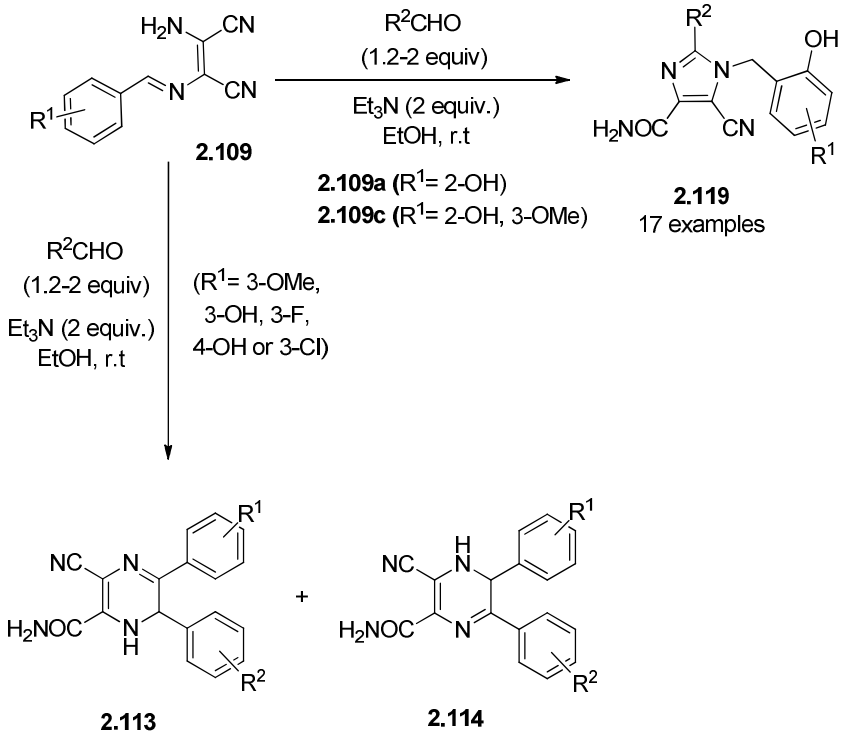
addition of a catalytic amount of acetic acid (0.5 equivalents); (iii) polycyclic compounds **2.88** could be prepared from amidine **2.87** by intramolecular cyclization at room temperature, in the presence of 1 equivalent of DBU or in an aqueous mixture of NaOH 0.05M/EtOH 1:1 (v/v); (iv) intramolecular cyclization, followed by Dimroth rearrangement, occurred when amidines **2.87** were allowed to stir in an NaOH 2M (1.2-4.5 equivalents)/EtOH mixture; (v) adding DBU to a mixture of amidine **2.87** or **2.88** ultimately led to the formation of the tetracyclic product **2.90**; (vii) compounds **2.100** could be prepared by the reaction of imidates **2.85** with 1.2-2.5 equivalents of phenylhydrazine, at room temperature; (viii) compounds **2.105** could be prepared from the reaction of imidate **2.85a** with ammonium acetate, at room temperature; (ix) compounds **2.88** were also identified as precursors in the synthesis of **2.86** (**Scheme 67**). Several of these novel scaffolds were tested for their biological activity in triple-negative breast cancer, malaria and tuberculosis, with compounds **2.86l**, **2.87l** and **2.90** presenting the most promising results.



Scheme 67: Synthetic route for the preparation of compounds **2.86-2.90**, **2.100** and **2.105**

2-Substituted-5-cyano-1-(2-hydroxyaryl)-1*H*-imidazole-4-carboxamides 2.119

A series of 2-substituted-5-cyano-1-(2-hydroxyaryl)-1*H*-imidazole-4-carboxamides **2.119** were prepared and evaluated for their biological activity against triple-negative breast cancer, malaria and tuberculosis, with no relevant results. However, exploring the reaction mechanism that led to imidazoles **2.119** showed that the presence of the 2-hydroxyl moiety affects the mechanism of reaction, guiding it mainly through a self-catalysed proton shift (**Scheme 68**).



Scheme 68: Synthetic route for the preparation of imidazoles **2.119**

These conclusions were based on the reactions performed with eneimine derivatives **2.109**, where it was observed that (i) only eneimines with a 2-hydroxyl moiety in the aromatic ring evolved to imidazoles **2.119** (except **2.109b** where R^1= 2-OH, 5-Br); eneimines **2.109d** (R^1= 3-OH) and **2.109g** (R^1= 4-OH), led to the formation of pyrazines **2.113** and **2.114** via a Diaza-Cope reaction (**Scheme 68**). The synthesis of imidazoles 2.119 was supported by computational studies, where the most energetically favourable mechanism involved a hydroxyl-assisted proton shift. This explains the selectivity of 2-hydroxylated aromatic eneimines in the formation of the imidazole ring.

Chapter 5

Experimental section

All chemicals, reagents and solvents for synthesis were analytical grade, purchased from commercial sources and used without further purification, unless otherwise specified. The reactions were followed by Thin Layer Chromatography, TLC, in glass plates coated with silica gel 60 and fluorescent indicator (Macherey-Nagel, DC-Fertigplotten Duresil 25 UV254) or in aluminium plates coated with silica gel 60 and fluorescent indicator (Macherey-Nagel, DC-Fertigfolien ALUGRAM Xtra SIL G/UV254). The spots were observed under ultraviolet (UV) light using a UV chamber (CN-6 Vilber Lourmat) with a 254nm lamp and in an iodine chamber. For dry-flash chromatography, silica gel MN Kieselgel 60 (230 ASTM, particle size <0.063 mm) was used. Some of the reactions were carried out in an IKAMAG RCT equipment with a magnetic stirring of 400 RPM under variable temperatures. The solvent was evaporated in a rotary evaporator Buchi RE III or Buchi R 114.

^{1}H NMR spectra were recorded at room temperature in a Varian Unity Plus 300 MHz or a Brucker Avance III 400 MHz spectrometer and deuterated dimethyl sulfoxide (DMSO) was used as solvent. The chemical shifts were registered in ppm using the signal of the deuterated solvent as internal reference. The *J* values were registered in Hz. ^{13}C NMR spectra were performed in the same equipment at 75 or 100 MHz, respectively.

The identification of the novel compounds was supported by analysis of the chemical shifts, peak multiplicities and *J* values and was supported by bidimensional heteronuclear correlation techniques HMQC and HMBC. The elemental analysis was purchased as an external service from CACTI Vigo. IR spectra were recorded in a FT-IR BomemMB using nujol mulls and NaCl cells. The melting points were determined with a Stuart SMP3 melting point apparatus and are uncorrected.

The commercial starting materials were acquired from Sigma-Aldrich, Merck, Riedel or Acros Organics. The solvents were designated as pure and distilled water was used in the reactions performed in aqueous solution.

Molecular Docking studies

Ligand geometries were minimized using the AM1 Hamiltonian as implemented in the program Gaussian 03w and used as MOL2 files. The Molecular Docking studies were carried out using the program GOLD[1] version 5.8. Each ligand was docked in 25 independent genetic algorithm (GA) runs, and for each of these a maximum number of 100000 GA operations were performed on a single population of 100 individuals. Operator weights for crossover, mutation and migration in the entry box were used as default parameters (95, 95, and 10, respectively), as well as the hydrogen bonding (6.0 Å) and van der Waals (3.0 Å) parameters. The position of the co-crystallyzed ligand (FR257517 inhibitor, PDB ID 1UK0, 3.00

Å)[2] was used to define the active site and the radius was set to 10 Å. The "flip ring corners" flag was switched on, while all the other flags were off. The GOLD scoring function was used to rank the ligands by fitness.

Molecular Dynamics simulations

Ligand minimization: The ligand geometries were minimized using Gaussian 03w using a restricted Hartree–Fock (RHF) method, at a B3LYP level of theory and a 6–31G(d) basis set, as implemented in the ab initio program Gaussian 03w. Partial charges were derived by quantum mechanical calculations using Gaussian 03w, as implemented in the R.E.D. Server (version 3.0)[3,4] according to the RESP[5] model. The missing bonded and nonbonded parameters were attributed, by analogy or through interpolation, from those already available in the AMBER[6] database (GAFF)[7,8].

Minimization of the protein-ligand complex: The protein coordinates were obtained from the crystal structure of PARP1 (PARP1, *Homo sapiens*, PDB ID 1UK0, 3 Å). Ligands were manually docked into the nicotinamide pocket to fit the coordinates of the co-crystallized ligand in the PDB file (**2-{3-[4-(4-fluorphenyl)-3,6-dihydro-1(2*H*)-pyridinyl]propyl}-8-methyl-4(3*H*)-quinazolinone)**.Computation of the protonation state of titratable groups at pH 7.0 was carried out using the H^{++} Web server[9]. As a result of this analysis, His742, His822, His826, His855, His862, His909, His934, His937 and His946 were protonated in the ε position. Addition of hydrogen and molecular mechanics parameters from the ff14SB[10] and GAFF force fields were allocated to the protein and the ligands using the LEaP module of AMBER Tools 16. The protein was immersed in a truncated octahedron of ∼12.000-12.300 TIP3P water molecules The system was minimized in four stages: a) Ligand minimization (1000 steps, steepest descent in the first half and then a conjugate gradient); b) solvent minimization (5000 steps, steepest descent in the first half and then a conjugate gradient); c) side chain residues, waters, and ions minimization (5000 steps, steepest descent in the first half and then a conjugate gradient); d) final minimization of the whole system (5000 steps, steepest descent in the first half and then a conjugate gradient). A positional restraint force of 50 kcal mol^{-1} $Å^{-2}$ was applied to the whole protein, and α carbons, during the first two stages (a and b), respectively.

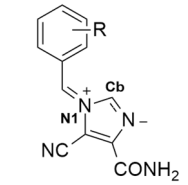
Molecular Dynamics simulations: Molecular Dynamics simulations were performed using the pmemd.cuda_SPFP[11–13] module in the AMBER 16 suite of programs. Periodic boundary conditions were

applied, and electrostatic interactions were calculated using the smooth particle mesh Ewald method (PME)[14], with a grid spacing of 1 Å. The cut-off distance for the non-bonded interactions was 9 Å. The SHAKE algorithm[15] was applied to all hydrogen-containing bonds, using a 10^{-5} Å, and an integration step of 2.0 fs. The minimized system was then heated from 0 to 300 K, over 100 ps, at 1 atm of pressure, and was then kept at 300 K for another 100 ps, applying a positional restraint force of 50 Kcal mol^{-1} $Å^{-2}$, to α carbon atoms, during the heating stage. Finally, an equilibration of the system at a constant volume (200 ps, with positional restraints of 5 Kcal mol^{-1} $Å^{-2}$ to all α carbons) and constant pressure (another 100 ps with positional restraints of 5 Kcal mol^{-1} $Å^{-2}$ to α carbons) was performed. The applied positional restraints were gradually decreased from 5 to 1 mol^{-1} $Å^{-2}$ (5 steps, 100 ps each), and the resulting systems were allowed to equilibrate without any restriction (100 ps). Unrestrained Molecular Dynamics simulation were carried out for 100 ns, and the system coordinates were collected every 10 ps for further analysis. The visualization of structural information was performed using the molecular graphics program PyMOL[16]. The cpptraj module in AMBER 16 was used to analyse the trajectories and to calculate the root mean square deviation (RMSD) of the protein-ligand complex during the simulation, as well as to measure the distance between a selection of residues and the ligands inside the binding pocket. The visualization of the results obtained from the Molecular Dynamics simulations was performed using VMD-Visual Molecular dynamics[17].

MMPBSA and MMGBSA calculations: The binding free energy for **2.6e, 2.6d'** and **2.6j'** was calculated by the MM/PBSA approach[18] implemented in Amber Tools 1.7. ante-MMPBSA.py module was used to generate the topology files for the complex, enzyme, and ligands, while the binding free energies were calculated using the MMPBSA.py module. A single trajectory approach was used to calculate the binding free energies considering the final 80 ns (801 snapshots) of the MD trajectories (PARP1/Ligand) (L= **2.6e, 2.6d', 2.6j'**). The Poisson-Boltzmann (PB) and Generalized Born (GB) implicit solvation models were used.

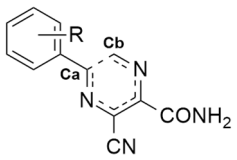
Mechanistic studies:

All calculations were performed in vacuum using the program Gaussian 09 at the B3LYP level of theory and the basis set 6-31G(d).



TS1
R = 2-OH, 2-O⁻, 3 -OH, 3 -O⁻, 4 -OH, 4 -O⁻

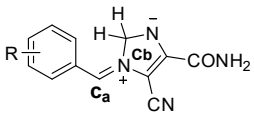
Study of the formation of the 5-membered ring structures: All structures **TS1** were minimized using Gaussian 09, using a restricted Hartree–Fock (RHF) method, as implemented in the program Gaussian 09. To find a starting point for the transition state (TS) calculations, a relaxed potential energy surface (PES) was calculated for each one of these compounds, elongating the N1-Cb distance from 1.6 to 2.5 Å, always taking the last step of the previous distance as the starting point of the next one. Then, the highest energy points of these PES were used as the starting point for the calculation of the TS, using a restricted Hartree–Fock (RHF) method, as implemented in the ab initio program Gaussian 09. To these structures, CN and amide groups were added, considering 2 possible conformations with NH_2 or O of the amide group close to the CN group, and the TS structures were also found for these new structures. All the TS were characterized by having an imaginary frequency that corresponds to the formation of the N1-Cb bond. Once the TS were found, an IRC calculation was performed in both the forward and reverse direction, to obtain both the starting and end points of the reaction. In all cases, the final step of the IRC calculation was further minimized to obtain a local minimum for the compounds.



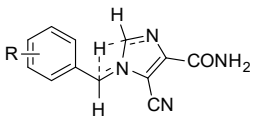
TS2
R = 2-OH, 2-O⁻, 3 -OH, 3 -O⁻, 4 -OH, 4 -O⁻

Study of the formation of the 6-membered ring structures:

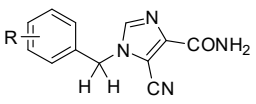
The procedure used was the same as applied for the 5-membered ring structures, performing the Ca-Cb bond elongation of the **TS2** structures. All the TS were characterized by having an imaginary frequency that corresponds to the formation of the Ca-Cb bond. Once the TS were found, an IRC calculation was performed in both the forward and reverse direction, to obtain both the starting and end points of the reaction. In all cases, the final step of the IRC calculation was further minimized to obtain a local minimum for the compounds.



B



TS3

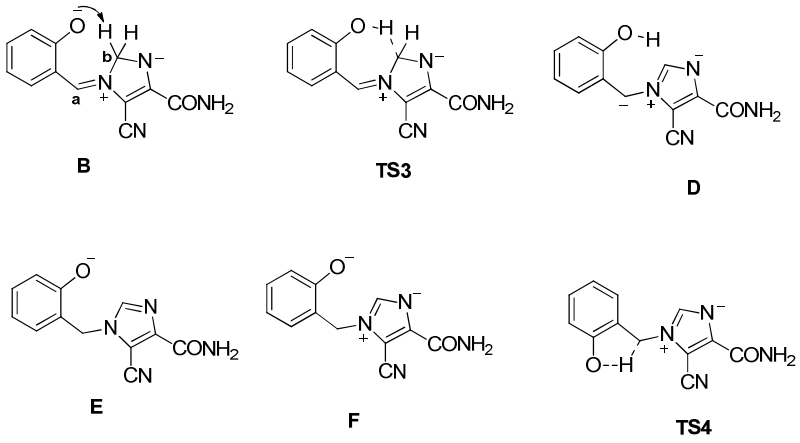


E

R= 2-OH, 2-O⁻, 3-OH, 3-O⁻,4-OH, 4-O⁻

1,3-proton shift: The procedure used was the same as applied for the 5-membered ring structures. The elongation of the Ca-Hb was performed from 1.0 to 3.0 Å, starting from a previously generated Cb-H bond (**structure B**) and Ca-H bond (**structure E**) structures and performing the calculus in both forward and reverse directions to obtain **TS3**. All the TS were characterized by having an imaginary frequency

that corresponds to the formation of the Cb-H bond. Once the TS were found, an IRC calculation was performed in both the forward and reverse direction, to obtain both the starting and end points of the reaction. In all cases, the final step of the IRC calculation was further minimized to obtain a local minimum for the compounds.



Hydroxyl-assisted proton transfer: The procedure used was the same as applied for the 5-membered ring structures, but performed in two stages: a) proton abstraction by the phenoxide group; b) transfer of the proton from the resulting hydroxyl group to Ca. The elongation was performed from 1.3 to 3.0 Å, starting from a previously generated Cb-H bond (**structure B**) and O-H bond (**structure D**) structures, and performed in both forward and reverse directions to obtain **TS3**. All the TS were characterized by having an imaginary frequency that corresponds to the formation of the Cb-H bond. The elongation was then performed from 1.3 to 3.0 Å, starting from a previously generated O-H bond (**structure D**) and Ca-H bond (**structure F**) structures, and performed in both forward and reverse directions to obtain **TS4**. All the TS were characterized by having an imaginary frequency that corresponds to the formation of the O-H bond (**TS3**) or of the Ca-H bond (**TS4**). Once both TS were found, an IRC calculation was performed in both the forward and reverse direction, to obtain both the starting and end points of the reaction. In all cases, the final step of the IRC calculation was further minimized to obtain a local minimum for the compounds.

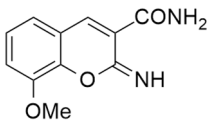
Synthesis and reaction conditions

General procedure for the synthesis of 2-imino-2*H*-chromene-3- carboxamides (2.1):

The synthesis of compounds **2.1** was performed according to the procedure described in the literature (**ref. 6**, chapter 2). Cyanoacetamide **2.13a** was added to a suspension of the appropriate salicylaldehyde

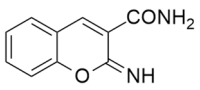
2.14, in aqueous $NaHCO_3$ (0.05 M, 2.00 ml), and the mixture was stirred at room temperature for 17-61 h. The obtained suspension was then removed from stirring and cooled in an ice bath for 1-3h, filtered and washed with water, and a few drops of diethyl ether, affording the desired product **2.1**. Compounds **2.1a** and **2.15a** were previously prepared and fully characterized (**ref. 6**, chapter 2).

2-imino-8-methoxy-2*H*-chromene-3-carboxamide(**2.1a**):



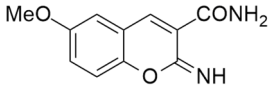
2-Cyanoacetamide (0.500 g, 6.0 mol) was added to a suspension of 3-methoxysalicylaldehyde (0.913 g, 6.0 mol) in aqueous $NaHCO_3$ (0.05 M, 5.00 ml) and the reaction mixture was stirred at room temperature for a further 22 h. After this time, the stirring was stopped, and the beige suspension was allowed to cool in an ice bath for 2h. The white solid was then filtered and washed with cold water and a few drops of diethyl ether leading to the pure product **2.1a** (1.316g, 4.9 mol, 82%), which was identified by IR, ^{1}H, ^{13}C, Mp. and elemental analysis.

2-imino-2*H*-chromene-3-carboxamide (**2.1b**):



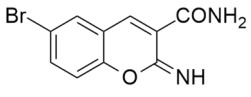
2-Cyanoacetamide (0.500 g, 6.0 mol) was added to a suspension of salicylaldehyde (0.913 g, 627 µL, 6.0 mol) in aqueous $NaHCO_3$ (0.05 M, 5.00 ml) and the reaction mixture was stirred at room temperature for 17 h. After this time, the stirring was stopped, and the beige suspension was allowed to cool in an ice bath for 2 h. The white solid was filtered and washed with cold water and a few drops of diethyl ether leading to the pure, white product **2.1b** (1.172 g, 5.9 mol, 99%), which has been identified by IR, ^{1}H, ^{13}C, Mp. and elemental analysis.

2-imino-6-methoxy-2*H*-chromene-3-carboxamide (**2.1c**):



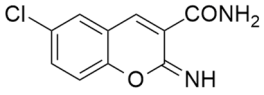
2-Cyanoacetamide (0.840 g, 10 mmol) was added to a suspension of 5-methoxysalicylaldehyde (1.522 g, 1.25 mL, 10 mmol) in aqueous $NaHCO_3$ (0.05 M, 8.00 ml) and the reaction mixture was stirred at room temperature for 61 h. After this time, the stirring was stopped, and the beige suspension was allowed to cool in an ice bath for 2h. The white solid was filtered and washed with cold water and a few drops of diethyl ether leading to the pure product **2.1c** (2.012 g, 9.8 mol, 98%), which was identified by IR, ^{1}H, ^{13}C and Mp.

6-bromo-2-imino-2*H*-chromene-3-carboxamide (**2.1d**):



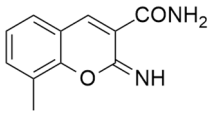
2-Cyanoacetamide (0.500 g, 6.0 mmol) was added to a suspension of 5-bromosalicylaldehyde (1.206 g, 6.0 mmol) in aqueous $NaHCO_3$ (0.05 M, 6.00 ml) and the reaction mixture was stirred at room temperature for 22 h. After this time, the stirring was stopped, and the beige suspension was allowed to cool in an ice bath for 2h. The beige solid was filtered and washed with cold water and a few drops of diethyl ether leading to the pure product **2.1d** (1.080 g, 4.0 mmol, 67%), which was identified by IR, ^{1}H, ^{13}C, Mp. and elemental analysis.

6-chloro-2-imino-2*H*-chromene-3-carboxamide (**2.1e**):



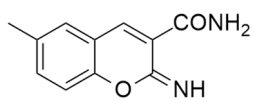
2-Cyanoacetamide (0.280 g, 3.3 mmol) was added to a suspension of 5-chlorosalicylaldehyde (0.518g, 3.3 mmol) in aqueous $NaHCO_3$ (0.05 M, 4.00 ml) and the reaction mixture was stirred at room temperature for 22 h. After this time, the stirring was stopped, and the beige suspension was allowed to cool in an ice bath for 2h. The white solid was filtered and washed with cold water and a few drops of diethyl ether leading to the pure product **2.1e** (0.697 g, 3.1 mmol, 95 %), which was identified by IR, ^{1}H, ^{13}C, Mp. and elemental analysis.

2-imino-8-methyl-2*H*-chromene-3-carboxamide (**2.1f**):



2-Cyanoacetamide (0.185 g, 2.2 mmol) was added to a suspension of 3-methylsalicylaldehyde (0.272 g, 242 µL, 2.2 mmol) in aqueous $NaHCO_3$ (0.05 M, 1.00 ml) and EtOH (200 µL) and the reaction mixture was stirred at room temperature for 24 h. After this time, the stirring was stopped, and the beige suspension was allowed to cool in an ice bath for 2h. The white solid was filtered and washed with cold water and a few drops of diethyl ether. The product was recrystallized from EtOH/*n*-hexane 1:1, leading to the pure product **2.1f** (0.197 g, 0.97 mmol, 44 %), which was identified by IR, ^{1}H, ^{13}C, Mp. and elemental analysis.

2-imino-6-methyl-2*H*-chromene-3-carboxamide (**2.1g**):



2-Cyanoacetamide **2.13a** (0.185 g, 2.2 mmol) was added to a suspension of 5-methylsalicylaldehyde **2.14f** (0.300 g, 2.2 mmol) in aqueous $NaHCO_3$ (0.05 M, 1.00 ml) and EtOH (200 µL) and the reaction mixture was stirred at room temperature for 23 h. After this time, the stirring was stopped, and the beige suspension was allowed to cool in an ice bath for 2h. The white solid was filtered and washed with cold water and a few drops of diethyl ether. The product

was recrystallized from EtOH/*n*-hexane 1:1, leading to the pure product **2.1g** (0.325 g, 1.6 mmol, 73%), which was identified by IR, ^{1}H, ^{13}C, Mp. and elemental analysis.

General procedure for the synthesis of 2-oxo-2*H*-chromene-3- carboxamides (2.15):

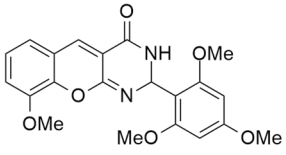
Compounds **2.1** were prepared according to the procedure described in the literature[19]. Full characterization and synthesis were described in this reference.

General procedure for the synthesis of 3-aryl-2,3-dihydro-1*H*-chromeno[3,2-*c*]pyridin-1-ones (2.3) and 2-aryl-3*H*-chromeno[2,3-*d*]pyrimidin-4(5*H*)-ones (2.6):

Method A: Used for the preparation of compound **2.6q**. *N*-Methylpiperazine (1.2 equiv.) was added to a suspension of the appropriate chromene **2.1a** and aryl aldehyde (1.2-1.5 equiv.), kept at 100 °C. After stirring at 100 °C, the suspension was allowed to cool to room temperature, and then was left in an ice bath for 1 hour. The solid was filtered and washed with cold EtOH and cold diethyl ether. The product was dried, and identified as **2.6q**.

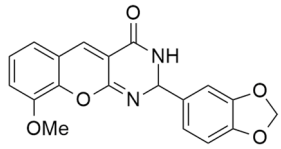
Method B: Piperidine (1.2 equiv.) was added to a suspension of the appropriate chromene **2.1** and aryl aldehyde (1.2 equiv.), at 100 °C. After stirring at 100 °C, the suspension was cooled to room temperature. Diethyl ether (5 mL) was added and the suspension was allowed to stand in an ice bath for 1 hour. The solid was filtered and washed with cold EtOH and cold diethyl ether. The product was dried, and identified as the corresponding **2.3** or **2.6.**

9-Methoxy-2-(2,4,6-trimethoxyphenyl)-2,3-dihydro-1*H*-chromeno[3,2-*c*]pyri- dine-1-one (**2.3d**):



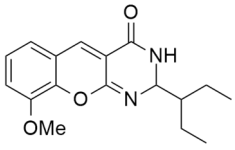
2,4,6-Trimethoxybenzaldehyde (1.2 equiv.; 0.216 g, 1.10 mmol) was added to a suspension of **2.1a** (0.20 g; 0.91 mmol) in EtOH (2.00 mL), and the mixture was stirred at 100 °C. Then, piperidine (1.2 equiv.; 109 µL) was added to the suspension, which gradually turned the beige suspension into a red solution after 2 minutes. After 20 minutes, the red solution started to turn gradually into an orange suspension, that slowly kept turning into a beige, thick suspension. After 3 hours and 30 minutes at 100 °C, the stirring was stopped, and the suspension was allowed to cool to room temperature for 5 minutes. Diethyl ether (5 mL) was added, and the suspension was allowed to stand in an ice bath for 1 hour. The solid was filtered and washed with cold EtOH and cold diethyl ether. The light-yellow solid was dried, and identified by IR, ^{1}H, ^{13}C, Mp., as the pure product **2.3d** (0.231 g, 0.58 mmol, 63%).

2-(Benzo[*d*][1,3]dioxol-5-yl)-9-methoxy-2*H*-chromeno[2,3-*d*]pyrimidin-4(3*H*)-one (**2.3e**):



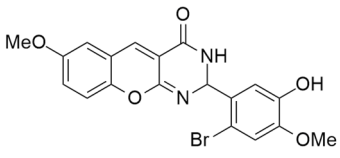
Piperonal (1.2 equiv.; 0.165 g, 1.10 mmol) was added to a suspension of **2.1a** (0.20 g; 0.91 mmol) in EtOH (2.00 mL), and the mixture was stirred at 100 °C. Then, piperidine (1.2 equiv.; 109 µL) was added to the suspension, which gradually turned the beige suspension into a red solution after 2 minutes. After 15 minutes, the red solution started to turn gradually into an orange suspension that slowly turned into a beige, thick suspension. After 2 hours and 30 minutes at 100 °C, the stirring was stopped, and the suspension was allowed to cool to room temperature for 5 minutes. Diethyl ether (5 mL) was added and the suspension was allowed to stand in an ice bath for 1 hour. The solid was filtered and washed with cold EtOH and cold diethyl ether. The crude solid was recrystallized from a 1:1 mixture of EtOH/n-hexane, leading to a yellow solid that was filtered, dried, and identified by IR, ^{1}H, ^{13}C and Mp, as the pure product **2.3e** (0.100 g, 0.29 mmol, 31%).

9-Methoxy-2-(pentan-3-yl)-2*H*-chromeno[2,3-*d*]pyrimidin-4(3*H*)-one (**2.3f**):



2-Ethylbutanal (1.2 equiv.; 0.100 g, 104 µL, 1.10 mmol) was added to a suspension of **2.1a** (0.20 g; 0.91 mmol) in EtOH (2.00 mL), and the mixture was stirred at 100 °C. Then, piperidine (1.2 equiv.; 109 µL) was added to the beige suspension, which gradually turned into a red solution after 2 minutes. After 30 minutes, the red solution started to turn gradually into an orange suspension that slowly turned into a beige, thick suspension. After 6 hours and 30 minutes at 100 °C, the stirring was stopped, and the suspension was allowed to cool to room temperature for 5 minutes. Diethyl ether (5 mL) was added and the suspension was allowed to stand in an ice bath for 1 hour. The solid was filtered and washed with cold EtOH and cold diethyl ether. The light-yellow solid was dried and identified by IR, ^{1}H, ^{13}C, Mp. and elemental analysis, as the pure product **2.3f** (0.068 g, 0.22 mmol, 25%).

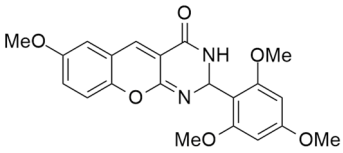
2-(2-Bromo-5-hydroxy-4-methoxyphenyl)-7-methoxy-2,3-dihydro-1*H*-chromeno [3,2-*c*]pyridin-1-one(**2.3g**):



2-Bromo-5-hydroxy-4-methoxybenzaldehyde (1.2 equiv.; 0.254 g, 1.10 mmol) was added to a suspension of **2.1c** (0.20 g; 0.91 mmol) in EtOH (2.00 mL), and the mixture was stirred at 100 °C. Then, piperidine (1.2 equiv.; 109 µL) was added to the beige suspension, which gradually turned into a red solution after 2 minutes. After 20 minutes, the red solution started to turn gradually into an orange suspension that slowly turned into a beige, thick suspension. After 4 hours at 100 °C, the stirring was stopped, and the

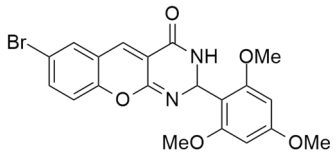
suspension was allowed to cool to room temperature for 5 minutes. Diethyl ether (5 mL) was added and the suspension was allowed to stand in an ice bath for 2 hours. The solid was filtered and washed with cold EtOH and cold diethyl ether. The yellow solid was dried and identified by IR, ^{1}H, ^{13}C and Mp., as the pure product **2.3g** (0.192 g, 0.44 mmol, 48%).

7-Methoxy-3-(2,4,6-trimethoxyphenyl)-2,3-dihydro-1*H*-chromeno[3,2-*c*] pyridin-1-one (**2.3h**):



2,4,6-Trimethoxybenzaldehyde (1.2 equiv.; 0.216 g, 1.10 mmol) was added to a suspension of **2.1c** (0.20 g; 0.91 mmol) in EtOH (2.00 mL) and the mixture was stirred at 100 °C. Then, piperidine (1.2 equiv.; 109 µL) was added to the beige suspension, which gradually turned into a red solution after 2 minutes. After 20 minutes, the red solution started to turn gradually into an orange suspension that slowly turned into a beige, thick suspension. After 1 hour and 30 minutes at 100 °C, the stirring was stopped, and the suspension was allowed to cool to room temperature for 5 minutes. Diethyl ether (5 mL) was added and the suspension was allowed to stand in an ice bath for 1 hour. The solid was filtered and washed with cold EtOH and cold diethyl ether. The lime green solid was dried and identified by IR, ^{1}H, ^{13}C, Mp. and elemental analysis, as the pure product **2.3h** (0.287 g, 0.72 mmol, 79%).

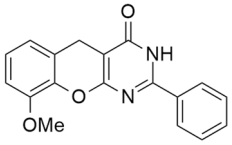
7-Bromo-2-(2,4,6-trimethoxyphenyl)-2*H*-chromeno[2,3-*d*]pyramid din-4(3*H*)-one (**2.3i**):



2,4,6-Trimethoxybenzaldehyde (1.2 equiv.; 0.159 g, 0.81 mmol) was added to a suspension of **2.1d** (0.20 g; 0.67 mmol) in EtOH (2.00 mL) and the mixture was stirred at 100 °C. Then, piperidine (1.2 equiv.; 80 µL) was added to the beige suspension, which gradually turned into a red solution after 2 minutes. After 20 minutes, the red solution started to turn gradually into an orange suspension that slowly turned into a beige, thick suspension. After 10 hours and 30 minutes at 100 °C, the stirring was stopped, and the suspension was allowed to cool to room temperature for 5 minutes. Diethyl ether (5 mL) was added and the suspension was allowed to stand in an ice bath for 1 hour. The solid was filtered and washed with cold EtOH and cold diethyl ether. The light-yellow solid was dried and identified by IR, ^{1}H, ^{13}C and Mp., as the pure product **2.3i** (0.083 g, 0.19 mmol, 28%).

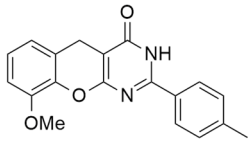
9-Methoxy-2-phenyl-3*H*-chromeno[2,3-*d*]pyrimidin-4(5*H*)-one (**2.6a**):

Benzaldehyde (1.2 equiv.; 0.117 g, 120 µL, 1.10 mmol) was added to a suspension of **2.1a** (0.20 g; 0.91 mmol) in EtOH (2.00 mL) and the mixture was stirred at 100 °C. Then, piperidine (1.2 equiv.; 109 µL) was added to the beige suspension, which gradually turned into a red solution after 2 minutes. After



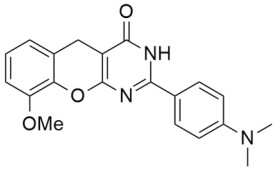
20 minutes, the red solution started to turn gradually into an orange suspension that slowly turned into a beige, thick suspension. After 3 hours at 100 °C, the stirring was stopped, and the suspension was allowed to cool to room temperature for 5 minutes. Diethyl ether (5 mL) was added, and the suspension was allowed to stand in an ice bath for 1 hour. The solid was filtered and washed with cold EtOH and cold diethyl ether. The beige solid was dried and identified by IR, ^{1}H, ^{13}C and Mp., as the pure product **2.6a** (0.100 g, 0.32 mmol, 35%).

9-Methoxy-2-(p-tolyl)-3*H*-chromeno[2,3-*d*]pyrimidin-4(5*H*)-one (**2.6b**):



p-Tolualdehyde (1.2 equiv.; 0.132 g, 130 µL, 1.10 mmol) was added to a suspension of **2.1a** (0.20 g; 0.91 mmol) in EtOH (2.00 mL) and the mixture was stirred at 100 °C. Then, piperidine (1.2 equiv.; 109 µL) was added to the beige suspension, which gradually turned into a red solution after 2 minutes. After 20 minutes, the red solution started to turn gradually into an orange suspension that slowly turned into a beige, thick suspension. After 3 hours and 20 minutes at 100 °C, the stirring was stopped, and the suspension was allowed to cool to room temperature for 5 minutes. Diethyl ether (5 mL) was added, and the suspension was allowed to stand in an ice bath for 1 hour. The solid was filtered and washed with cold EtOH and cold diethyl ether. The light-yellow solid was dried and identified by IR, ^{1}H, ^{13}C, Mp. and elemental analysis, as the pure product **2.6b** (0.125 g, 0.39 mmol, 42%).

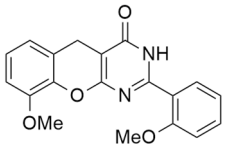
2-(4-(Dimethylamino)phenyl)-9-methoxy-3*H*-chromeno[2,3-*d*]pyrimidin-4(5*H*) -one (**2.6c**):



p-Dimethylaminobenzaldehyde (1.2 equiv.; 0.164 g, 1.10 mmol) was added to a suspension of **2.1a** (0.20 g; 0.91 mmol) in EtOH (2.00 mL) and the mixture was stirred at 100 °C. Then, piperidine (1.2 equiv.; 109 µL) was added to the beige suspension, which gradually turned into a red solution after 2 minutes. After 20 minutes, the red solution started to turn gradually into an orange suspension that slowly turned into a beige, thick suspension. After 28 hours at 100 °C, the stirring was stopped, and the suspension was allowed to cool to room temperature for 5 minutes. Diethyl ether (5 mL) was added, and the suspension was allowed to stand in an ice bath for 1 hour. The solid was filtered and washed with cold EtOH and cold diethyl ether. The light-yellow solid was dried and further identified by IR, ^{1}H, ^{13}C and Mp., as the pure product **2.6c** (0.146 g, 0.42 mmol, 45%).

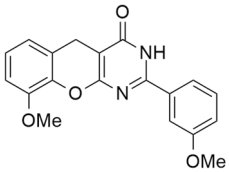
9-Methoxy-2-(2-methoxyphenyl)-3*H*-chromeno[2,3-*d*]pyrimidin-4(5*H*)-one (**2.6d**):

o-Anisaldehyde (1.2 equiv.; 0.150 g, 1.10 mmol) was added to a suspension of **2.1a** (0.20 g; 0.91



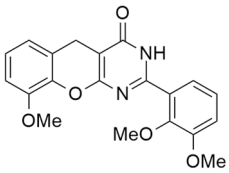
mmol) in EtOH (2.00 mL) and the mixture was stirred at 100 °C. Then, piperidine (1.2 equiv.; 109 µL) was added to the beige suspension, which gradually turned into a red solution after 2 minutes. After 20 minutes, the red solution started to turn gradually into an orange suspension that slowly turned into a beige, thick suspension. After 3 hours and 30 minutes at 100 °C, the stirring was stopped, and the suspension was allowed to cool to room temperature for 5 minutes. Diethyl ether (5 mL) was added, and the suspension was allowed to stand in an ice bath for 1 hour. The solid was filtered and washed with cold EtOH and cold diethyl ether. The light-yellow solid was dried, and identified by IR, ^{1}H, ^{13}C and Mp., as the pure product **2.6d** (0.194 g, 0.58 mmol, 63%).

9-Methoxy-2-(3-methoxyphenyl)-3*H*-chromeno[2,3-*d*]pyrimidin-4(5*H*)-one (**2.6e**):



m-Anisaldehyde (1.2 equiv.; 0.150 g, 134 µL, 1.10 mmol) was added to a suspension of **2.1a** (0.20 g; 0.91 mmol) in EtOH (2.00 mL), and the mixture was stirred at 100 °C. Then, piperidine (1.2 equiv.; 109 µL) was added to the beige suspension, which gradually turned into a red solution after 2 minutes. After 20 minutes, the red solution started to turn gradually into an orange suspension that slowly turned into a beige, thick suspension. After 3 hours and 30 minutes at 100 °C, the stirring was stopped, and the suspension was allowed to cool to room temperature for 5 minutes. Diethyl ether (5 mL) was added, and the suspension was allowed to stand in an ice bath for 1 hour. The solid was filtered and washed with cold EtOH and cold diethyl ether. The beige solid was dried and further identified by IR, ^{1}H, ^{13}C and Mp, as the pure product **2.6e** (0.106 g, 0.32 mmol, 34 %).

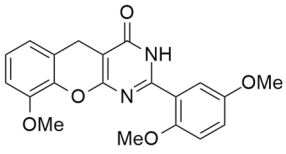
2-(2,3-Dimethoxyphenyl)-9-methoxy-3*H*-chromeno[2,3-*d*]pyrimidin-4(5*H*)-one (**2.6f**):



2,3-Dimethoxybenzaldehyde (1.2 equiv.; 0.183 g, 1.10 mmol) was added to a suspension of **2.1a** (0.20 g; 0.91 mmol) in EtOH (2.00 mL) and the mixture was stirred at 100 °C. Then, piperidine (1.2 equiv.; 109 µL) was added to the beige suspension, which gradually turned into a red solution after 2 minutes. After 20 minutes, the red solution started to turn gradually into an orange suspension that slowly turned into a beige, thick suspension. After 3 hours and 40 minutes at 100 °C, the stirring was stopped, and the suspension was allowed to cool to room temperature for 5 minutes. Diethyl ether (5 mL) was added, and the suspension was allowed to stand in an ice bath for 1 hour. The solid was filtered and washed with cold EtOH and cold diethyl ether. The crude solid was then recrystallized in an EtOH/n-hexane 1:1 mixture, after which the cream solid

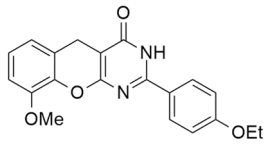
was filtered, dried and identified, by IR, ^{1}H, ^{13}C and Mp., as the pure product **2.6f** (0.200 g, 0.55 mmol, 59 %).

2-(2,5-Dimethoxyphenyl)-9-methoxy-3*H*-chromeno[2,3-*d*]pyrimidin-4(5*H*)-one (**2.6g**):



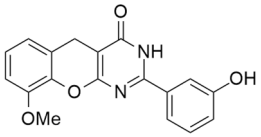
2,5-Dimethoxybenzaldehyde (1.2 equiv.; 0.183 g, 1.10 mmol) was added to a suspension of **2.1a** (0.20 g; 0.91 mmol) in EtOH (2.00 mL) and the mixture was stirred at 100 °C. Then, piperidine (1.2 equiv.; 109 µL) was added to the beige suspension, which gradually turned into a red solution after 2 minutes. After 15 minutes, the red solution started to turn gradually into an orange suspension that slowly turned into a beige, thick suspension. After 4 hours and 40 minutes at 100 °C, the stirring was stopped, and the suspension was allowed to cool to room temperature for 5 minutes. Diethyl ether (5 mL) was added, and the suspension was allowed to stand in an ice bath for 1 hour. The solid was filtered and washed with cold EtOH and cold diethyl ether, after which the cream solid was dried and identified by IR, ^{1}H, ^{13}C and Mp., as the pure product **2.6g** (0.200 g, 0.55 mmol, 59 %).

2-(4-Ethoxyphenyl)-9-methoxy-3*H*-chromeno[2,3-*d*]pyrimidin-4(5*H*)-one (**2.6h**):



p-Ethoxybenzaldehyde (1.2 equiv.; 0.150 g, 118 µL, 1.10 mmol) was added to a suspension of **2.1a** (0.20 g; 0.91 mmol) in EtOH (2.00 mL) and the mixture was stirred at 100 °C. Then, piperidine (1.2 equiv.; 109 µL) was added to the suspension, which gradually turned the beige suspension into a red solution after 2 minutes was added to the beige suspension, which gradually turned into a red solution after 2 minutes. After 30 minutes, the red solution started to turn gradually into an orange suspension that slowly turned into a beige, thick suspension. After 17 hours at 100 °C, the stirring was stopped, and the suspension was allowed to cool to room temperature for 5 minutes. Diethyl ether (5 mL) was added, and the suspension was allowed to stand in an ice bath for 1 hour. The solid was filtered and washed with cold EtOH and cold diethyl ether, after which the white solid was dried and identified by IR, ^{1}H, ^{13}C, Mp. and elemental analysis, as the pure product **2.6h** (0.119 g, 0.34 mmol, 37 %).

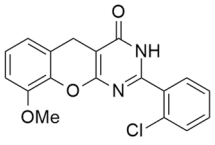
2-(3-Hydroxyphenyl)-9-methoxy-3*H*-chromeno[2,3-*d*]pyrimidin-4(5*H*)-one (**2.6i**):



m-Hydroxybenzaldehyde (1.2 equiv.; 0.122 g, 1.10 mmol) was added to a suspension of **2.1a** (0.20 g; 0.91 mmol) in EtOH (2.00 mL) and the mixture was stirred at 100 °C. Then, piperidine (1.2 equiv.; 109 µL) was added to the beige suspension, which gradually turned into a red solution after 2 minutes. After 30 minutes, the red

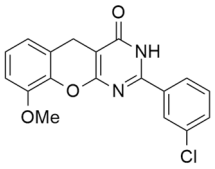
solution started to turn gradually into an orange suspension that slowly turned into a beige, thick suspension. After 10 hours at 100 °C, the stirring was stopped, and the suspension was allowed to cool to room temperature for 5 minutes. Diethyl ether (5 mL) was added, and the suspension was allowed to rest on an ice bath for 1 hour. The solid was filtered and washed with cold EtOH and cold diethyl ether, after which the white solid was dried and further identified, by IR, ^{1}H, ^{13}C and Mp., as the pure product **2.6i** (0.158 g, 0.49 mmol, 54 %).

2-(2-Chlorophenyl)-9-methoxy-3*H*-chromeno[2,3-*d*]pyrimidin-4(5*H*)-one (**2.6j**):



o-Chlorobenzaldehyde (1.2 equiv.; 0.155 g, 124 µL, 1.10 mmol) was added to a suspension of **2.1a** (0.20 g; 0.91 mmol) in EtOH (2.00 mL), and the mixture was stirred at 100 °C. Then, piperidine (1.2 equiv.; 109 µL) was added to the beige suspension, which gradually turned into a red solution after 2 minutes. After 15 minutes, the red solution started to turn gradually into an orange suspension that slowly turned into a beige, thick suspension. After 9 hours at 100 °C, the stirring was stopped, and the suspension was allowed to cool to room temperature for 5 minutes. Diethyl ether (5 mL) was added, and the suspension was allowed to stand in an ice bath for 1 hour. The solid was filtered and washed with cold EtOH and cold diethyl ether, after which the beige solid was dried and further identified by IR, ^{1}H, ^{13}C, Mp. and elemental analysis, as the pure product **2.6j** (0.112 g, 0.33 mmol, 36 %).

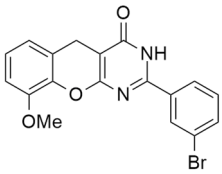
2-(3-Chlorophenyl)-9-methoxy-3*H*-chromeno[2,3-*d*]pyrimidin-4(5*H*)-one (**2.6k**):



m-Chlorobenzaldehyde (1.2 equiv.; 0.155 g, 125 µL, 1.10 mmol) was added to a suspension of **2.1a** (0.20 g; 0.91 mmol) in EtOH (2.00 mL) and the mixture was stirred at 100 °C. Then, piperidine (1.2 equiv.; 109 µL) was added to the beige suspension, which gradually turned into a red solution after 2 minutes. After 15 minutes, the red solution started to turn gradually into an orange suspension that slowly turned into a beige, thick suspension. After 16 hours at 100 °C, the stirring was stopped, and the suspension was allowed to cool to room temperature for 5 minutes. Diethyl ether (5 mL) was added, and the suspension was allowed to stand in an ice bath for 1 hour. The solid was filtered and washed with cold EtOH and cold diethyl ether, after which the white solid was dried, and further identified, by IR, ^{1}H, ^{13}C, Mp. and elemental analysis, as the pure product **2.6k** (0.084 g, 0.25 mmol, 27 %).

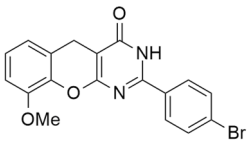
2-(3-Bromophenyl)-9-methoxy-3*H*-chromeno[2,3-*d*]pyrimidin-4(5*H*)-one (**2.6l**):

m-Bromobenzaldehyde (1.2 equiv.; 0.186 g, 118 µL, 1.10 mmol) was added to a suspension of **2.1a**



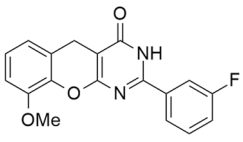
(0.20 g; 0.91 mmol) in EtOH (2.00 mL), and the mixture was stirred at 100 °C. Then, piperidine (1.2 equiv.; 109 µL) was added to the beige suspension, which gradually turned into a red solution after 2 minutes. After 20 minutes, the red solution started to turn gradually into an orange suspension that slowly turned into a beige, thick suspension. After 14 hours at 100 °C, the stirring was stopped, and the suspension was allowed to cool to room temperature for 5 minutes. Diethyl ether (5 mL) was added, and the suspension was allowed to stand in an ice bath for 1 hour. The solid was filtered and washed with cold EtOH and cold diethyl ether, after which the beige solid was dried, and further identified, by IR, ^{1}H, ^{13}C and Mp., as the pure product **2.6l** (0.074 g, 0.19 mmol, 22 %).

2-(4-Bromophenyl)-9-methoxy-3*H*-chromeno[2,3-*d*]pyrimidin-4(5*H*)-one (**2.6m**):



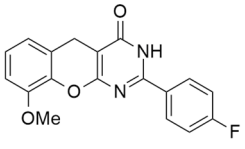
p-Bromobenzaldehyde (1.2 equiv.; 0.186 g, 1.10 mmol) was added to a suspension of **2.1a** (0.20 g; 0.91 mmol) in EtOH (2.00 mL), and the mixture was stirred at 100 °C. Then, piperidine (1.2 equiv.; 109 µL) was added to the beige suspension, which gradually turned into a red solution after 2 minutes. After 20 minutes, the red solution started to turn gradually into an orange suspension that slowly turned into a beige, thick suspension. After 16 hours at 100 °C, the stirring was stopped, and the suspension was allowed to cool to room temperature for 5 minutes. Diethyl ether (5 mL) was added, and the suspension was allowed to stand in an ice bath for 1 hour. The solid was filtered and washed with cold EtOH and cold diethyl ether, after which the beige solid was collected and dried, and further identified, by IR, ^{1}H, ^{13}C and Mp., as the pure product **2.6m** (0.136 g, 0.35 mmol, 39 %).

2-(3-Fluorophenyl)-9-methoxy-3*H*-chromeno[2,3-*d*]pyrimidin-4(5*H*)-one (**2.6n):**



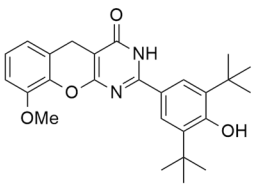
m-Fluorbenzaldehyde (1.2 equiv.; 0.124 g, 106 µL, 1.10 mmol) was added to a suspension of **2.1a** (0.20 g; 0.91 mmol) in EtOH (2.00 mL), and the mixture was stirred at 100 °C. Then, piperidine (1.2 equiv.; 109 µL) was added to the beige suspension, which gradually turned into a red solution after 2 minutes. After 20 minutes, the red solution started to turn gradually into an orange suspension that slowly turned into a beige, thick suspension. After 8 hours at 100 °C, the stirring was stopped, and the suspension was allowed to cool to room temperature for 5 minutes. Diethyl ether was added, and the suspension was allowed to stand in an ice bath for 1 hour. The solid was filtered and washed with cold EtOH and cold diethyl ether, after which the white solid was dried and identified, by IR, ^{1}H, ^{13}C and Mp., as the pure product **2.6n** (0.051 g, 0.15 mmol, 17 %).

2-(4-Fluorophenyl)-9-methoxy-3*H*-chromeno[2,3-*d*]pyrimidin-4(5*H*)-one (**2.6o**):



p-Fluorbenzaldehyde (1.2 equiv.; 0.124 g, 106 µL, 1.10 mmol) was added to a suspension of **2.1a** (0.20 g; 0.91 mmol) in EtOH (2.00 mL), and the mixture was stirred at 100 °C. Then, piperidine (1.2 equiv.; 109 µL) was added to the beige suspension, which gradually turned into a red solution after 2 minutes. After 20 minutes, the red solution started to turn gradually into an orange suspension that slowly turned into a beige, thick suspension. After 2 hours and 20 minutes at 100 °C, the stirring was stopped, and the suspension was allowed to cool to room temperature for 5 minutes. Diethyl ether (5 mL) was added, and the suspension was allowed to stand in an ice bath for 1 hour. The solid was filtered and washed with cold EtOH and cold diethyl ether, after which the white solid was dried, and identified by IR, ^{1}H, ^{13}C and Mp. and elemental analysis, as the pure product **2.6o** (0.066 g, 0.20 mmol, 23 %).

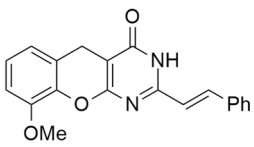
2-(3,5-Di-tert-butyl-4-hydroxyphenyl)-9-methoxy-3*H*-chromeno[2,3-*d*]pyrimidin-4(5*H*)-one (**2.6p**):



3,5-Di-*t*-butyl-4-hydroxybenzaldehyde (1.2 equiv.; 0.244 g, 1.10 mmol) was added to a suspension of **2.1a** (0.20 g; 0.91 mmol) in EtOH (2.00 mL), and the mixture was stirred at 100 °C. Then, piperidine (1.2 equiv.; 109 µL) was added to the beige suspension, which gradually turned into a red solution after 2 minutes. After 20 minutes, the red solution started to turn gradually into an orange suspension that slowly turned into a beige, thick suspension. After 7 hours and 30 minutes at 100 °C, the stirring was stopped, and the suspension was allowed to cool to room temperature for 5 minutes. Diethyl ether (5 m) was added, and the suspension was allowed to stand in an ice bath for 1 hour. The solid was filtered and washed off with cold EtOH and cold diethyl ether, after which the olive green solid was dried, and identified, by IR, ^{1}H, ^{13}C and Mp., as the pure product **2.6p** (0.068 g, 0.16 mmol, 17 %).

9-Methoxy-2-styryl-3*H*-chromeno[2,3-*d*]pyrimidin-4(5*H*)-one (**2.6q**):

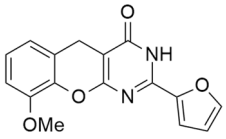
Cinnamaldehyde (1.2 equiv.; 0.145 g, 138 µL, 1.10 mmol) was added to a suspension of **2.1a** (0.20 g; 0.91 mmol) in EtOH (2.00 mL) and the mixture was stirred at 100 °C. Then, *N*-methylpiperazine (1.2



equiv.; 122 µL) was added to the beige suspension, which gradually turned into a red solution after 2 minutes. After 20 minutes, the red solution started to turn gradually into an orange suspension that slowly turned into a beige, thick suspension. After 4 hours at 100 °C, the stirring was stopped, and the suspension was allowed to cool to room temperature for 5 minutes. Diethyl ether (5 mL) was added, and the suspension was allowed to

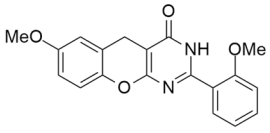
stand in an ice bath for 1 hour. The solid was filtered and washed with cold EtOH and cold diethyl ether, after which the light brown solid was dried, and identified, by IR, ^{1}H, ^{13}C, Mp. and elemental analysis, as the pure product **2.6q** (0.058 g, 0.17 mmol, 19 %).

2-(Furan-2-yl)-9-methoxy-3*H*-chromeno[2,3-*d*]pyrimidin-4(5*H*)-one (**2.6r**):



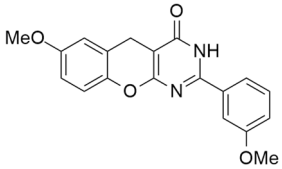
Furfural (1.2 equiv.; 0.106 g, 91 µL, 1.10 mmol) was added to a suspension of **2.1a** (0.20 g; 0.91 mmol) in EtOH (2.00 mL) and the mixture was stirred at 100 °C. Then, piperidine (1.2 equiv.; 109 µL) was added to the beige suspension, which gradually turned into a red solution after 2 minutes. After 15 minutes, the red solution started to turn gradually into an orange suspension that slowly turned into a beige, thick suspension. After 2 hours at 100 °C, the stirring was stopped, and the suspension was allowed to cool to room temperature for 5 minutes. Diethyl ether (5 mL) was added, and the suspension was allowed to stand in an ice bath for 1 hour. The solid was filtered and washed with cold EtOH and cold diethyl ether, after which the dark brown solid was collected and dried, and further identified, by IR, ^{1}H, ^{13}C and Mp., as the pure product **2.6r** (0.090 g, 0.31 mmol, 33 %).

7-Methoxy-2-(2-methoxyphenyl)-3*H*-chromeno[2,3-*d*]pyrimidin-4(5*H*)-one (**2.6s**):



o-Anisaldehyde (1.2 equiv.; 0.150 g, 1.10 mmol) was added to a suspension of **2.1c** (0.20 g; 0.91 mmol) in EtOH (2.00 mL) and the mixture was stirred at 100 °C. Then, piperidine (1.2 equiv.; 109 µL) was added to the beige suspension, which gradually turned into a red solution after 2 minutes. After 15 minutes, the red solution started to turn gradually into an orange suspension that slowly turned into a beige, thick suspension. After 1 hour and 10 minutes at 100 °C, the stirring was stopped, and the suspension was allowed to cool to room temperature for 5 minutes. Diethyl ether (5 mL) was added, and the suspension was allowed to stand in an ice bath for 1 hour. The solid was filtered and washed with cold EtOH and cold diethyl ether, after which the beige solid was collected and dried, and further identified, by IR, ^{1}H, ^{13}C, Mp. and elemental analysis, as the pure product **2.6s** (0.251 g, 0.75 mmol, 81 %).

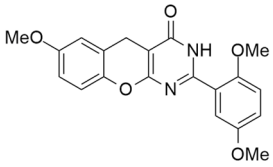
7-Methoxy-2-(3-methoxyphenyl)-3*H*-chromeno[2,3-*d*]pyrimidin-4(5*H*)-one (**2.6t**):



m-Anisaldehyde (1.2 equiv.; 0.150 g, 134 µL,1.10 mmol) was added to a suspension of **2.1c** (0.20 g; 0.91 mmol) in EtOH (2.00 mL) and the mixture was stirred at 100 °C. Then, piperidine (1.2 equiv.; 109 µL) was added to the beige suspension, which gradually turned into a red solution after 2 minutes. After 15 minutes, the red

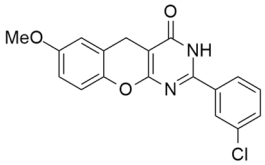
solution started to turn gradually into an orange suspension that slowly turned into a beige, thick suspension. After 1 hour and 10 minutes at 100 °C, the stirring was stopped, and the suspension was allowed to cool to room temperature for 5 minutes. Diethyl ether (5 m) was added, and the suspension was allowed to stand in an ice bath for 1 hour. The solid was filtered and washed with cold EtOH and cold diethyl ether, after which the light-yellow solid was dried and identified by IR, ^{1}H, ^{13}C, Mp. and elemental analysis, as the pure product **2.6t** (0.177 g, 0.60 mmol, 65 %).

2-(2,5-Dimethoxyphenyl)-7-methoxy-3*H*-chromeno[2,3-*d*]pyrimidin-4(5*H*)-one (**2.6u**):



2,5-Dimethoxybenzaldehyde (1.2 equiv.; 0.183 g, 1.10 mmol) was added to a suspension of **2.1c** (0.20 g; 0.91 mmol) in EtOH (2.00 mL), and the mixture was stirred at 100 °C. Then, piperidine (1.2 equiv.; 109 µL) was added to the beige suspension, which gradually turned into a red solution after 2 minutes. After 15 minutes, the red solution started to turn gradually into an orange suspension that slowly turned into a beige, thick suspension. After 1 hour and 40 minutes at 100 °C, the stirring was stopped, and the suspension was allowed to cool to room temperature for 5 minutes. Diethyl ether (5 mL) was added, and the suspension was allowed to stand in an ice bath for 1 hour. The solid was filtered and washed with cold EtOH and cold diethyl ether, after which the cream solid was dried, and identified by IR, ^{1}H, ^{13}C and Mp., as the pure product **2.6u** (0.252 g, 0.69 mmol, 74 %).

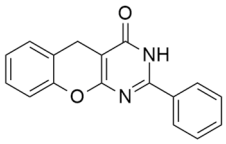
2-(3-Chlorophenyl)-7-methoxy-3*H*-chromeno[2,3-*d*]pyrimidin-4(5*H*)-one (**2.6v**):



m-Chlorobenzaldehyde (1.2 equiv.; 0.155 g, 125 µL, 1.10 mmol) was added to a suspension of **2.1a** (0.20 g; 0.91 mmol) in EtOH (2.00 mL), and the mixture was stirred at 100 °C. Then, piperidine (1.2 equiv.; 109 µL) was added to the beige suspension, which gradually turned into a red solution after 2 minutes. After 15 minutes, the red solution started to turn gradually into an orange suspension that slowly turned into a beige, thick suspension. After 2 hours and 30 minutes at 100 °C, the stirring was stopped, and the suspension was allowed to cool to room temperature for 5 minutes. Diethyl ether (5 mL) was added, and the suspension was allowed to stand in an ice bath for 1 hour. The solid was filtered and washed with cold EtOH and cold diethyl ether, after which the beige solid was dried, and identified by IR, ^{1}H, ^{13}C, Mp. and elemental analysis, as the pure product **2.6v** (0.121 g, 0.35 mmol, 39 %).

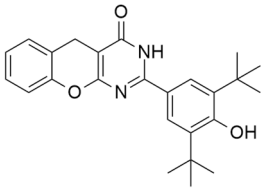
2-Phenyl-3*H*-chromeno[2,3-*d*]pyrimidin-4(5*H*)-one (**2.6x**):

Benzaldehyde (1.2 equiv.; 0.169 g, 162 µL, 1.27 mmol) was added to a suspension of **2.1b** (0.20 g;



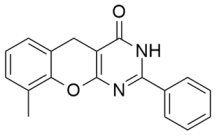
1.06 mmol) in EtOH (2.00 mL), and the mixture was stirred at 100 °C. Then, piperidine (1.2 equiv.; 126 µL) was added to the beige suspension, which gradually turned into a red solution after 2 minutes. After 15 minutes, the red solution started to turn gradually into an orange suspension that slowly turned into a beige, thick suspension. After 5 hours at 100 °C, the stirring was stopped, and the suspension was allowed to cool to room temperature for 5 minutes. Diethyl ether (5 mL) was added, and the suspension was allowed to stand in an ice bath for 1 hour. The solid was filtered and washed with cold EtOH and cold diethyl ether, after which the beige solid was dried and identified by IR, ^{1}H, ^{13}C, Mp. and elemental analysis, as the pure product **2.6x** (0.113 g, 0.41 mmol, 39 %).

2-(3,5-Di-tert-butyl-4-hydroxyphenyl)-3*H*-chromeno[2,3-*d*]pyrimidin-4(5*H*)-one (**2.6y**):



3,5-Di-*t*-butyl-4-hydroxybenzaldehyde (1.2 equiv.; 0.309 g, 1.27 mmol) was added to a suspension of **2.1b** (0.20 g; 1.06 mmol) in EtOH (2.00 mL), and the mixture was stirred at 100 °C. Then, piperidine (1.2 equiv.; 126 µL) was added to the beige suspension, which gradually turned into a red solution after 2 minutes. After 15 minutes, the red solution started to turn gradually into an orange suspension that slowly turned into a beige, thick suspension. After 5 hours at 100 °C, the stirring was stopped, and the suspension was allowed to cool to room temperature for 5 minutes. Diethyl ether (5 mL) was added, and the suspension was allowed to stand in an ice bath for 1 hour. The solid was filtered and washed with cold EtOH and cold diethyl ether, after which the beige solid was dried, and identified by IR, ^{1}H, ^{13}C, Mp. and elemental analysis, as the pure product **2.6y** (0.090 g, 0.22 mmol, 21 %).

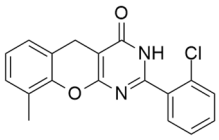
9-Methyl-2-phenyl-3*H*-chromeno[2,3-*d*]pyrimidin-4(5*H*)-one (**2.6z**):



Benzaldehyde (1.2 equiv.; 0.126 g, 120 µL, 1.18 mmol) was added to a suspension of **2.1f** (0.200 g; 0.98 mmol) in EtOH (2.00 mL), and the mixture was stirred at 100 °C. Then, piperidine (1.2 equiv.; 116 µL) was added to the beige suspension, which gradually turned into a red solution after 2 minutes. After 10 minutes, the red solution started to turn gradually into an orange suspension that slowly turned into a beige, thick suspension. After 4 hours and 45 minutes at 100 °C, the stirring was stopped, and the suspension was allowed to cool to room temperature for 5 minutes. Diethyl ether (5 mL) was added, and the suspension was allowed to stand in an ice bath for 1 hour. The solid was filtered and washed with cold EtOH and cold diethyl ether, after

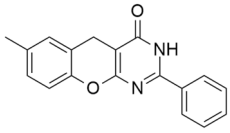
which the beige solid was dried, and identified by IR, ^{1}H, ^{13}C, Mp. and elemental analysis, as the pure product **2.6z** (0.159 g, 0.55 mmol, 56%).

2-(2-Chlorophenyl)-9-methyl-3*H*-chromeno[2,3-*d*]pyrimidin-4(5*H*)-one (**2.6a'**):



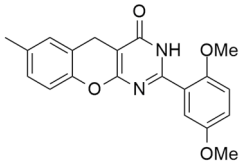
o-Chlorobenzaldehyde (1.2 equiv.; 0.165 g, 132 µL, 1.18 mmol) was added to a suspension of **2.1f** (0.20 g; 0.98 mmol) in EtOH (2.00 mL), and the mixture was stirred at 100 °C. Then, piperidine (1.2 equiv.; 116 µL) was added to the beige suspension, which gradually turned into a red solution after 2 minutes. After 20 minutes, the red solution started to turn gradually into an orange suspension that slowly turned into a beige, thick suspension. After 17 hours and 40 minutes at 100 °C, the stirring was stopped, and the suspension was allowed to cool to room temperature for 5 minutes. Diethyl ether (5 mL) was added, and the suspension was allowed to stand in an ice bath for 1 hour. The solid was filtered and washed with cold EtOH and cold diethyl ether, after which the beige solid was dried, and identified, by IR, ^{1}H, ^{13}C and Mp., as the pure product **2.6a'** (0.106 g, 0.33 mmol, 34 %).

7-Methyl-2-phenyl-3*H*-chromeno[2,3-*d*]pyrimidin-4(5*H*)-one (**2.6b'**):



Benzaldehyde (1.2 equiv.; 0.126 g, 120 µL, 1.18 mmol) was added to a suspension of **2.1g** (0.200 g; 0.98 mmol) in EtOH (2.00 mL), and the mixture was stirred at 100 °C. Then, piperidine (1.2 equiv.; 116 µL) was added to the beige suspension, which gradually turned into a red solution after 2 minutes. After 10 minutes, the red solution started to turn gradually into an orange suspension that slowly turned into a beige, thick suspension. After 4 hours and 45 minutes at 100 °C, the stirring was stopped, and the suspension was allowed to cool to room temperature for 5 minutes. Diethyl ether (5 mL) was added, and the suspension was allowed to stand in an ice bath for 1 hour. The solid was filtered and washed with cold EtOH and cold diethyl ether, after which the beige solid was collected and dried, and further identified, by IR, ^{1}H, ^{13}C, Mp. and elemental analysis, as the pure product **2.6b'** (0.159 g, 0.55 mmol, 62%).

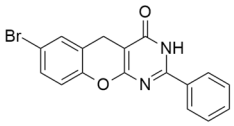
2-(2,5-Dimethoxyphenyl)-7-methyl-3*H*-chromeno[2,3-*d*]pyrimidin-4(5*H*)-one (**2.6c'**):



2,5-Dimethoxybenzaldehyde (1.2 equiv.; 0.196 g, 1.18 mmol) was added to a suspension of **2.1g** (0.200 g; 0.98 mmol) in EtOH (2.00 mL), and the mixture was stirred at 100 °C. Then, piperidine (1.2 equiv.; 116 µL) was added to the beige suspension, which gradually turned into a red solution after 2 minutes. After 10 minutes, the red solution started to turn gradually into an orange suspension that slowly turned into a beige, thick

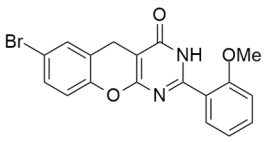
suspension. After 4 hours and 45 minutes at 100 °C, the stirring was stopped, and the suspension was allowed to cool to room temperature for 5 minutes. Diethyl ether (5 mL) was added, and the suspension was allowed to rest on an ice bath for 1 hour. The solid was filtered and washed with cold EtOH and cold diethyl ether, after which the white solid was dried, and identified by IR, ^{1}H, ^{13}C, Mp. and elemental analysis, as the pure product **2.6c'** (0.213 g, 0.61 mmol, 73%)

7-Bromo-2-phenyl-3*H*-chromeno[2,3-*d*]pyrimidin-4(5*H*)-one (**2.6d'**):



Benzaldehyde (1.2 equiv.; 0.085 g, 81 µL, 0.80 mmol) was added to a suspension of **2.1d** (0.20 g; 0.67 mmol) in EtOH (2.00 mL), and the mixture was stirred at 100 °C. Then, piperidine (1.2 equiv.; 54 µL) was added to the beige suspension, which gradually turned into a red solution after 2 minutes. After 10 minutes, the red solution started to turn gradually into an orange suspension that slowly turned into a beige, thick suspension. After 5 hours and 30 minutes at 100 °C, the stirring was stopped, and the suspension was allowed to cool to room temperature for 5 minutes. Diethyl ether (5 mL) was added, and the suspension was allowed to stand in an ice bath for 1 hour. The solid was filtered and washed with cold EtOH and cold diethyl ether. The beige solid was dried, and identified by IR, ^{1}H, ^{13}C and Mp., as the pure product **2.6d'** (0.053 g, 0.15 mmol, 22%).

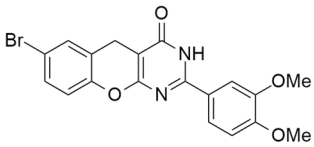
7-Bromo-2-(2-methoxyphenyl)-3*H*-chromeno[2,3-*d*]pyrimidin-4(5*H*)-one (**2.6e'**):



o-Anisaldehyde (1.2 equiv.; 0.109 g, 0.80 mmol) was added to a suspension of **2.1d** (0.20 g; 0.67 mmol) in EtOH (2.00 mL), and the mixture was stirred at 100 °C. Then, piperidine (1.2 equiv.; 54 µL) was added to the beige suspension, which gradually turned into a red solution after 2 minutes. After 10 minutes, the red solution started to turn gradually into an orange suspension that slowly turned into a beige, thick suspension. After 3 hours and 40 minutes at 100 °C, the stirring was stopped, and the suspension was allowed to cool to room temperature for 5 minutes. Diethyl ether (5 mL) was added, and the suspension was allowed to stand in an ice bath for 1 hour. The solid was filtered and washed with cold EtOH and cold diethyl ether. The beige solid was dried, and identified by IR, ^{1}H, ^{13}C, Mp. and elemental analysis, as the pure product **2.6e'** (0.065 g, 0.17 mmol, 25%).

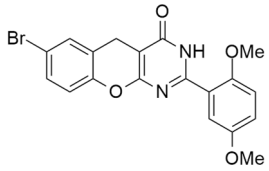
7-Bromo-2-(3,4-dimethoxyphenyl)-3*H*-chromeno[2,3-*d*]pyrimidin-4(5*H*)-one (**2.6f'**):

3,4-Dimethoxybenzaldehyde (1.2 equiv.; 0.133 g, 0.80 mmol) was added to a suspension of **2.1d** (0.20



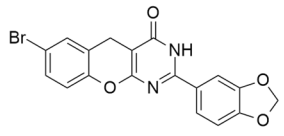
g; 0.67 mmol) in EtOH (2.00 mL), and the mixture was stirred at 100 °C. Then, piperidine (1.2 equiv.; 54 µL) was added to the beige suspension, which gradually turned into a red solution after 2 minutes. After 10 minutes, the red solution started to turn gradually into an orange suspension that slowly turned into a beige, thick suspension. After 12 hours and 30 minutes at 100 °C, the stirring was stopped, and the suspension was allowed to cool to room temperature for 5 minutes. Diethyl ether (5 mL) was added, and the suspension was allowed to stand in an ice bath for 1 hour. The solid was filtered and washed with cold EtOH and cold diethyl ether. The beige solid was dried, and identified by IR, ^{1}H, ^{13}C, Mp. and elemental analysis, as the pure product **2.6f'** (0.067 g, 0.16 mmol, 24%).

7-Bromo-2-(2,5-dimethoxyphenyl)-3*H*-chromeno[2,3-*d*]pyrimidin-4(5*H*)-one (**2.6g'**):



2,5-Dimethoxybenzaldehyde (1.2 equiv.; 0.133 g, 0.80 mmol) was added to a suspension of **2.1d** (0.20 g; 0.67 mmol) in EtOH (2.00 mL), and the mixture was stirred at 100 °C. Then, piperidine (1.2 equiv.; 54 µL) was added to the beige suspension, which gradually turned into a red solution after 2 minutes. After 10 minutes, the red solution started to turn gradually into an orange suspension that slowly turned into a beige, thick suspension. After 11 hours at 100 °C, the stirring was stopped, and the suspension was allowed to cool to room temperature for 5 minutes. Diethyl ether (5 mL) was added, and the suspension was allowed to stand in an ice bath for 1 hour. The solid was filtered and washed with cold EtOH and cold diethyl ether. The yellow solid was dried and identified by IR, ^{1}H, ^{13}C and Mp., as the pure product **2.6g'** (0.122 g, 0.29 mmol, 44%).

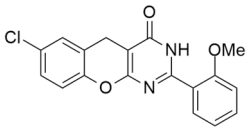
2-(Benzo[*d*][1,3]dioxol-5-yl)-7-bromo-3*H*-chromeno[2,3-*d*]pyrimidin-4(5*H*)-one (**2.6h'**):



Piperonal (1.2 equiv.; 0.120 g, 0.80 mmol) was added to a suspension of **2.1d** (0.20 g; 0.67 mmol) in EtOH (2.00 mL), and the mixture was stirred at 100 °C. Then, piperidine (1.2 equiv.; 54 µL) was added to the beige suspension, which gradually turned into a red solution after 2 minutes. After 10 minutes, the red solution started to turn gradually into an orange suspension that slowly turned into a beige, thick suspension. After 5 hours and 30 minutes at 100 °C, the stirring was stopped, and the suspension was allowed to cool to room temperature for 5 minutes. Diethyl ether (5 mL) was added, and the suspension was allowed to stand in an ice bath for 1 hour. The solid was filtered and washed with cold EtOH and cold diethyl ether.

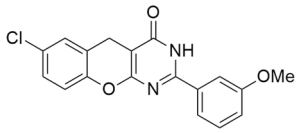
The beige solid was dried, and identified by IR, ^{1}H, ^{13}C and Mp., as the pure product **2.6h'** (0.059 g, 0.14 mmol, 21%).

7-Chloro-2-(2-methoxyphenyl)-3*H*-chromeno[2,3-*d*]pyrimidin-4(5*H*)-one (**2.6i'**):



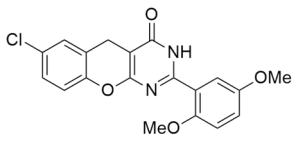
o-Methoxybenzaldehyde (1.2 equiv.; 0.146 g, 1.07 mmol) was added to a suspension of **2.1e** (0.20 g; 0.90 mmol) in EtOH (2.00 mL), and the mixture was stirred at 100 °C. Then, piperidine (1.2 equiv.; 106 µL) was added to the beige suspension, which gradually turned into a red solution after 2 minutes. After 15 minutes, the red solution started to turn gradually into an orange suspension that slowly turned into a beige, thick suspension. After 3 hours and 40 minutes at 100 °C, the stirring was stopped, and the suspension was allowed to cool to room temperature for 5 minutes. Diethyl ether (5 mL) was added, and the suspension was allowed to stand in an ice bath for 1 hour. The solid was filtered and washed with cold EtOH and cold diethyl ether. The light-yellow solid was dried and further identified by IR, ^{1}H, ^{13}C and Mp., as the pure product **2.6i'** (0.260 g, 0.70 mmol, 65%).

7-Chloro-2-(3-methoxyphenyl)-3*H*-chromeno[2,3-*d*]pyrimidin-4(5*H*)-one (**2.6j'**):



m-Methoxybenzaldehyde (1.2 equiv.; 0.146 g, 1.07 mmol) was added to a suspension of **2.1e** (0.20 g; 0.90 mmol) in EtOH (2.00 mL), and the mixture was stirred at 100 °C. Then, piperidine (1.2 equiv.; 106 µL) was added to the beige suspension, which gradually turned into a red solution after 2 minutes. After 15 minutes, the red solution started to turn gradually into an orange suspension that slowly turned into a beige, thick suspension. After 3 hours and 40 minutes at 100 °C, the stirring was stopped, and the suspension was allowed to cool to room temperature for 5 minutes. Diethyl ether (5 mL) was added, and the suspension was allowed to stand in an ice bath for 1 hour. The solid was filtered and washed with cold EtOH and cold diethyl ether. The light-yellow solid was dried and identified by IR, ^{1}H, ^{13}C and Mp., as the pure product **2.6j'** (0.126 g, 0.34 mmol, 32%).

7-Chloro-2-(2,5-dimethoxyphenyl)-3*H*-chromeno[2,3-*d*]pyrimidin-4(5*H*)-one (**2.6k'**):



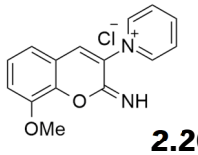
m-Methoxybenzaldehyde (1.2 equiv.; 0.178 g, 1.07 mmol) was added to a suspension of **2.1e** (0.20 g; 0.90 mmol) in EtOH (2.00 mL), and the mixture was stirred at 100 °C. Then, piperidine (1.2 equiv.; 106 µL) was added to the beige suspension, which gradually turned into a red solution after 5 minutes. After 15 minutes, the red solution started to turn gradually into an orange suspension that slowly turned into a beige, thick

suspension. After 3 hours and 40 minutes at 100 °C, the stirring was stopped, and the suspension was allowed to cool to room temperature for 5 minutes. Diethyl ether (5 mL) was added, and the suspension was allowed to stand in an ice bath for 1 hour. The solid was filtered and washed with cold EtOH and cold diethyl ether. The light-yellow solid was dried and identified by IR, ^{1}H, ^{13}C and Mp., as the pure product **2.6k'** (0.245 g, 0.66 mmol, 62%).

Synthesis of 2-imino-8-methoxy-2*H*-chromen-3-amine (2.22a) and 2-oxo-8-methoxy-2*H*-chromen-3-amine (2.25a):

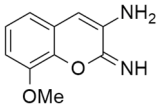
Compounds **2.22a** and **2.25a** were prepared according to the procedure described in the literature (ref. 6 and 41, chapter 2), where full characterization and procedure was already detailed. The obtained spectra were compared with the information presented in the literature.

1-(2-Imino-8-methoxy-2*H*-chromen-3-yl)pyridinium chloride (**2.21a**):



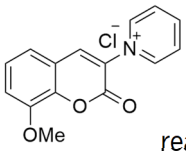
1-Methylpiperazine (0.10 g; 1.00 mmol; 115 μL) was added to a solution of 3-methoxysalicylaldehyde (0.16 g; 1.05 mmol) and 1-(cyanomethyl)pyridinium chloride **2.20** (0.15 g; 0.97 mmol) in a mixture of ethanol (0.4 mL) and acetone (1.2 mL), which led to a brown solution that was stirred on an ice bath. After 7 minutes, a red suspension was formed, and after 23 minutes, the yellow solid was filtered and washed with acetone, dried and identified by IR, ^{1}H and ^{13}C as 1-(2-imino-8-methoxy-2*H*-chromeno-3-yl)pyridinium chloride **2.21a** contaminated with NH_4Cl in a 1:1 ratio (0.09 g; 0.33 mmol; 43%), and its identification was confirmed by comparison with the information presented in the literature (ref. 6 and 41, chapter 2).

2-Imino-8-methoxy-2*H*-3-amine (**2.22a**):



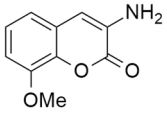
N-Methylpyperazine (0.1 g; 1.59 mmol; 181 μL) to a suspension of 1-(2-imino-8-methoxy-2*H*-chromen-3-yl)pyridinium chloride **2.21a** (0.09 g; 0.33 mmol, contaminated with NH_4Cl) in acetone (10 mL), and the yellow suspension was stirred at room temperature. The salt slowly solubilized, generating a red solution. After 20 hours, the solvent was removed on the rotary evaporator and the red oil was purified by flash chromatography using ethyl acetoacetate as eluent. 2-Imino-8-methoxy-2*H*-3-amine **2.22a** was obtained as an orange solid (0.03 g, 0.16 mmol, 50%), and its identification was confirmed by comparison with the information presented in the literature (ref. 6 and 41, chapter 2).

1-(2-Oxo-8-methoxy-2*H*-chromen-3-yl)pyridinium chloride (**2.24a**):



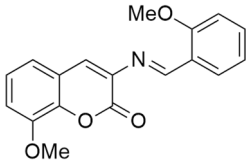
Concentrated HCl (1.8 mmol, 3 equiv.) was added to a solution of 1-(2-imino-2*H*-chromen-3-yl)pyridinium chloride **2.21a** (0.18 g; 0.76 mmol) in water (4 ml) and the reaction mixture was stirred on a water bath at 80 °C. After 2 h, the solvent was removed in the rotary evaporator and acetone was added to the crude mixture to precipitate a solid that was filtered and washed with acetone. The yellow solid was identified as 1-(2-oxo-2*H*-cromen-3-yl)pyridinium chloride **2.24a**, contaminated with NH_4Cl 1:1 ratio (0.18 g; 0.76 mmol; 65 %), and its identification was confirmed by comparison with the information presented in the literature (ref. 6 and 41, chapter 2).

2-Oxo-8-methoxy-2*H*-3-amine (**2.25a**):



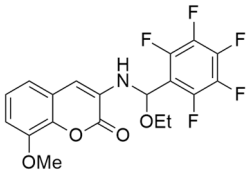
N-Methylpiperazine (0.11 g, 1.65 mmol, 200 μL) was added to a suspension of 1-(2-oxo-2*H*-cromen-3-yl)pyridinium chloride **2.24a** (0.09 g; 0.33 mmol, contaminated with NH_4Cl) in acetone (10 ml) and an orange/red suspension was formed and stirred at room tempera- ture. After 2 h, a red solution was obtained and after 24 h, the solvent was removed in the rotary evaporator, leading to a red oil. Flash chromatography was performed using ethyl acetate as eluent. Several crops were isolated, all containing the pure product by TLC. The crops were combined and the solvent was removed in the rotary evaporator. The solid was collected and identified as 3-amino-2*H*-chromen-2-one derivative **2.25a** (0.05 g; 0.26 mmol; 80 %), and its identification was confirmed by comparison with the information presented in the literature (ref. 6 and 41, chapter 2).

Synthesis of 8-methoxy-3-((2-methoxybenzylidene)amino)-2*H*-chromen-2-one 2.27:



o-Methoxybenzaldehyde (2 equiv.; 0.14 g, 1.04 mmol) was added to a suspension of **2.25a** (0.10 g, 0.52 mmol) in ethanol (2.00 mL). The mixture was refluxed for 27 hours, after which the suspension was cooled to room temperature for 5 minutes, and then in an ice bath for 1 hour. The beige suspension was filtered and washed with cold ethanol and diethyl ether, from which a light-brown solid was collected, dried, and identified, by ^{1}H, ^{13}C, IR, Mp. and elemental analysis, as the pure product **2.27** (0.05 g, 0.16 mmol, 30%).

Synthesis of 3-((ethoxy(perfluorophenyl)methyl)amino)-8-methoxy-2*H*-chromen-2-one 2.28:

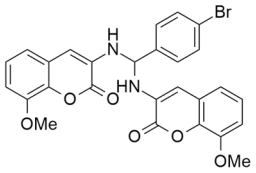


2,3,4,5-Pentafluorbenzaldehyde (1 equiv.; 0.10 g, 64 μL, 0.52 mmol) was added to a suspension of **2.25a** (0.10 g, 0.52 mmol) in ethanol (2.00 mL). The mixture was refluxed for 4 hours, after which the suspension was cooled to

room temperature for 5 minutes, and then in an ice bath for 1 hour. The beige suspension was filtered and washed with cold ethanol and diethyl ether, from which a light-brown solid was collected, dried and identified, by ^{1}H, ^{13}C, IR, Mp. and elemental analysis, as the pure product **2.28** (0.11 g, 0.27 mmol, 51%).

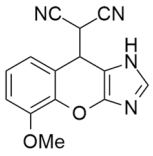
Synthesis of 3-((ethoxy(perfluorophenyl)methyl)amino)-8-methoxy-2H-chromen-2-one 2.29:

o-Methoxybenzaldehyde (1 equiv.; 0.10 g, 64 μL, 0.52 mmol) was added to a suspension of **2.25a** (0.10



g, 0.52 mmol) in ethanol (2.00 mL). The mixture was refluxed for 1 hour, after which the suspension was cooled to room temperature for 5 minutes, and then in an ice bath for 1 hour. The beige suspension was filtered and washed with cold ethanol and diethyl ether, from which a beige solid was collected, dried and identified, by ^{1}H, ^{13}C, IR, Mp. and elemental analysis, as the pure product **2.29** (0.11 g, 0.27 mmol, 13%).

Synthesis of 3-((ethoxy(perfluorophenyl)methyl)amino)-8-methoxy-2*H*-chromen-2-one 2.35:

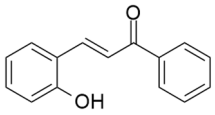


Ethoxymethylene malononitrile **2.31** (1 equiv.; 0.06 g, 0.52 mmol) was added to a suspension of **2.22a** (0.10 g, 0.52 mmol) in acetonitrile (2.00 mL). The mixture was stitted at room temperature for 5 days. Then, the beige suspension was cooled in an ice bath for 3 hours. The beige suspension was filtered and washed with cold acetonitrile and diethyl ether, from which a light brown was collected, dried, and identified, by ^{1}H and ^{13}C as compound **2.35** (0.04 g, 0.16 mmol, 31%).

General procedure for the synthesis of 3-(2-hydroxyaryl)-1-arylprop-2-en-1-ones (2.37): Compounds **2.37** were prepared according to the procedure described in the literature (ref. 104, chapter 2), where full characterization of compounds **2.37a, 2.37e, 2.37f, 2.37g, 2.37h** and **2.37i** was already detailed.

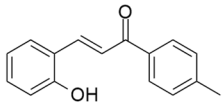
Aqueous 3M NaOH was added to a solution of the appropriate salicylaldehyde **2.2** (1.2 equiv.) and acetophenone **2.36** in ethanol. The solution was stirred at room temperature (4-31 h). The solution was neutralized with concentrated HCl (37%) and a yellow suspension was obtained, cooled in an ice bath for 1-2 h. The solid was filtered and washed with cold ethanol and water, leading to the corresponding α,β-unsaturated carbonyl compound **2.37**.

3-(2-Hydroxyphenyl)-1-(phenyl)prop-2-en-1-one (**2.37a**):



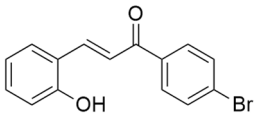
Aqueous 3M NaOH was added to a solution of salicylaldehyde (1.26 mL, 1.474 g, 1.2 equiv.) and acetophenone (1.17 mL, 1.20 g, 1.0 equiv.) in ethanol. The solution was stirred at room temperature for 24 h. Then, the solution was neutralized with concentrated HCl (37%) and a yellow suspension was obtained. After cooling in an ice bath for 2 h, the yellow solid was filtered and washed with cold ethanol and water, leading to the α,β-unsaturated carbonyl compound **2.37a**, slightly contaminated with salicylaldehyde (1.67 g, 6.2 mmol, 62 %), and was characterized by ^{1}H, ^{13}C, IR and M.p.

3-(2-Hydroxyphenyl)-1-(*p*-tolyl)prop-2-en-1-one (**2.37b**):



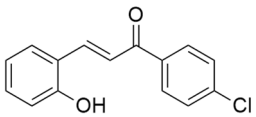
Aqueous 3M NaOH was added to a solution of salicylaldehyde (1.26 mL, 1.474 g, 1.2 equiv.) and *p*-methylacetophenone (1.34 mL, 1.34 g, 1.0 equiv.) in ethanol. The solution was stirred at room temperature for 30 h. Then, the solution was neutralized with concentrated HCl (37%) and a yellow suspension was obtained. After cooling in an ice bath for 2 h, the yellow solid was filtered and washed with cold ethanol and water, leading to the α,β-unsaturated carbonyl compound **2.37b** (1.82 g, 6.8 mmol, 68 %), and was characterized by ^{1}H, ^{13}C, and IR.

1-(4-Bromophenyl)-3-(2-hydroxyphenyl)prop-2-en-1-one (**2.37c**):



Aqueous 3M NaOH was added to a solution of salicylaldehyde (1.26 mL, 1.474 g, 1.2 equiv.) and *p*-bromoacetophenone (1.99 g, 1.0 equiv.) in ethanol. The solution was stirred at room temperature for 72 h. Then, the solution was neutralized with concentrated HCl (37%) and a yellow suspension was obtained. After cooling on an ice bath for 2 h, the yellow solid was filtered and washed with cold ethanol and water, leading to the respective α,β-unsaturated carbonyl compound **2.37c** (3.05 g), contaminated with aldehyde (by ^{1}H NMR) in a ratio of 0.17:1.0 of salicylaldehyde: **2.37c**, and was used without further purification as starting material for the next synthetic step.

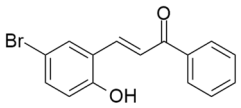
1-(4-Chlorophenyl)-3-(2-hydroxyphenyl)prop-2-en-1-one (**2.37d**):



Aqueous 3M NaOH was added to a solution of salicylaldehyde (1.26 mL, 1.474 g, 1.2 equiv.) and *p*-chloroacetophenone (1.30 mL, 1.546 g, 1.0 equiv.) in ethanol. The solution was stirred at room temperature for 22 h. Then, the solution was neutralized with concentrated HCl (37%) and a yellow suspension was obtained. After cooling on an ice bath for 2 h, the

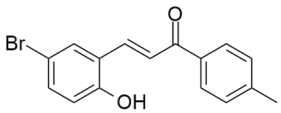
yellow solid was filtered and washed with cold ethanol and water, leading to the respective α,β-unsaturated carbonyl compound **2.37d** (1.65 g, 5.3 mmol, 53 %), and was characterized by ^{1}H, ^{13}C and IR-

3-(5-Bromo-2-hydroxyphenyl)-1-phenylprop-2-en-1-one (**2.37e**):



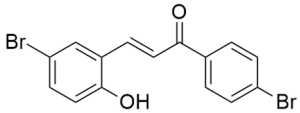
Aqueous 3M NaOH was added to a solution of 5-bromosalicylaldehyde (2.01 g, 1.2 equiv.) and acetophenone (1.17 mL, 1.20 g, 1.0 equiv.) in ethanol. The solution was stirred at room temperature for 3 h. Then, the solution was neutralized with concentrated HCl (37%) and a yellow suspension was obtained. After cooling on an ice bath for 1 h, the yellow solid was filtered and washed with cold ethanol and water, leading to the respective α,β-unsaturated carbonyl compound **2.37e** (2.06 g, 6.8 mmol, 68 %), and was identified by comparison with the information presented in the literature (ref. 104, chapter 2).

3-(5-Bromo-2-hydroxyphenyl)-1-(4-bromophenyl)prop-2-en-1-one (**2.37f**):



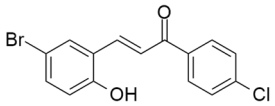
Aqueous 3M NaOH was added to a solution of 5-bromosalicylaldehyde (2.01 g, 1.2 equiv.) and *p*-methylacetophenone (1.34 mL, 1.34 g, 1.0 equiv.) in ethanol. The solution was stirred at room temperature for 3 h. Then, the solution was neutralized with concentrated HCl (37%) and a yellow suspension was obtained. After cooling in an ice bath for 1 h, the yellow solid was filtered and washed with cold ethanol and water, leading to the α,β-unsaturated carbonyl compound **2.37f** (1.68 g, 5.3 mmol, 53 %), and was identified by comparison with the information presented in the literature (ref. 104, chapter 2).

3-(5-Bromo-2-hydroxyphenyl)-1-(*p*-)prop-2-en-1-one (**2.37g**):



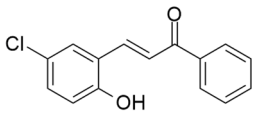
Aqueous 3M NaOH was added to a solution of 5-bromosalicylaldehyde (2.01 g, 1.2 equiv.) and *p*-bromoacetophenone (1.99 g, 1.0 equiv.) in ethanol. The solution was stirred at room temperature for 1.66 h. Then, the solution was neutralized with concentrated HCl (37%) and a yellow suspension was obtained. After cooling on an ice bath for 1 h, the yellow solid was filtered washed with cold ethanol and water, leading to the α,β-unsaturated carbonyl compound **2.37g** (2.45 g, 6.4 mmol, 64 %), and was identified by comparison with the information presented in the literature (ref. 104, chapter 2).

1-(4-Chlorophenyl)-3-(2-hydroxyphenyl)prop-2-en-1-one (**2.37h**):



Aqueous 3M NaOH was added to a solution of 5-bromosalicylaldehyde (2.01 g, 1.2 equiv.) and *p*-chloroacetophenone (1.30 mL, 1.546 g, 1.0 equiv.) in ethanol. The solution was stirred at room temperature for 3 h. Then, the solution was neutralized with concentrated HCl (37%) and a yellow suspension was obtained. After cooling on an ice bath for 1 h, the yellow solid was filtered and washed with cold ethanol and water, leading to the respective α,β-unsaturated carbonyl compound **2.37h** (3.05 g), contaminated with aldehyde (by ^{1}H NMR) in a ratio of 0.6:1 of 5-bromosalicylaldehyde:**2.37h**, and was used without further purification as starting material for the next synthetic step. Compound **2.37h** was identified by comparison with the information presented in the literature (ref. 104, chapter 2).

3-(5-Chloro-2-hydroxyphenyl)-1-phenylprop-2-en-1-one (**2.37i**):



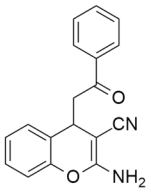
Aqueous 3M NaOH was added to a solution of 5-chlorosalicylaldehyde (1.57 g, 1.2 equiv.) and acetophenone (1.17 mL, 1.20 g, 1.0 equiv.) in ethanol. The solution was stirred at room temperature for 24 h. Then, the solution was neutralized with concentrated HCl (37%) and a yellow suspension was obtained. After cooling on an ice bath for 1 h, the yellow solid was filtered and washed with cold ethanol and water, leading to the respective α,β-unsaturated carbonyl compound **2.37i**, slightly contaminated with 5-chlorosalicylaldehyde (2.10 g, 8.1 mmol, 81 %), and was characterized by ^{1}H, ^{13}C, IR and Mp..

General procedure for the synthesis of 2-amino-4-(2-oxo-2-arylethyl)-4*H*-chromene-3-carbonitriles (2.39):

Compounds **2.39** were prepared according to the procedure described in the literature (ref. 104, chapter 2), where full characterization of compounds **2.39a, 2.39f** and **2.39g** is already detailed.

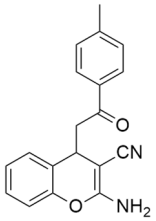
Triethylamine (2-5 equiv) was added to a solution of the appropriate α,β-unsaturated carbonyl compound **2.37** and malononitrile (2 equiv.) in ethanol. The solution was stirred for 2-23 h, at room temperature, and filtered or first cooled, on an ice bath or at 4 °C, for 1 h to 7 days and then filtered. After washing with cold ethanol and diethyl ether, the obtained solid was dried and further identified as being the desired compound **2.39**.

2-amino-4-(2-oxo-2-phenylethyl)-4*H*-chromene-3-carbonitrile (**2.39a**):



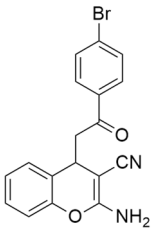
Triethylamine (4 equiv.; 4.20 mL) was added to a solution of **2.37a** (1.67 g, 7.44 mmol) and 2 equivalents of malononitrile (0.98 g, 14.9 mmol) in ethanol (5.00 mL). The solution was stirred at room temperature for 2 hours and then was cooled in an ice bath for 2 hours. The suspension was filtered and washed with cold ethanol and diethyl ether, after which the white solid was dried, and was identified by comparison with the information presented in the as **2.39a** (0.639 g, 2.2 mmol, 30 %).

2-Amino-4-(2-oxo-2-(*p*-tolyl)ethyl)-4*H*-chromene-3-carbonitrile (**2.39b**):



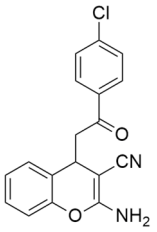
Triethylamine (4 equiv.; 4.20 mL) was added to a solution of **2.37b** (1.82 g, 7.63 mmol) and 2 equivalents of malononitrile (1.00 g, 15.3 mmol) in ethanol (6.00 mL). The solution was stirred at room temperature for 2 hours and then was cooled in an ice bath for 2 hours. The suspension was filtered and washed with cold ethanol and diethyl ether, after which the white solid was dried and identified, by ^{1}H,^{13}C and IR, as **2.39b** (1.15 g, 3.8 mmol, 50 %).

2-Amino-4-(2-(4-bromophenyl)-2-oxoethyl)-4*H*-chromene-3-carbonitrile (**2.39c**):



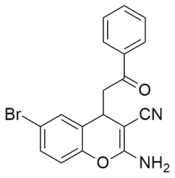
Triethylamine (5 equiv.; 3.22 mL) was added to a solution of the crude product **2.37c** (1.40 g, 4.62 mmol) and 2 equivalents of malononitrile (0.61 g, 9.30 mmol) in ethanol (6.00 mL). The solution was stirred at room temperature for 3 hours and 20 minutes and then was cooled in an ice bath for 2 hours. The suspension was filtered and washed with cold ethanol and diethyl ether, after which the white solid was dried and identified, by ^{1}H,^{13}C and IR, as **2.39c** (0.873 g, 2.36 mmol, 51 %).

2-Amino-4-(2-(4-chlorophenyl)-2-oxoethyl)-4*H*-chromene-3-carbonitrile (**2.39d**):



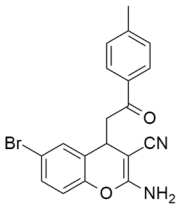
Triethylamine (4 equiv.; 3.60 mL) was added to a solution of **2.37d** (1.68 g, 6.49 mmol) and 2 equivalents of malononitrile (0.85 g, 13.0 mmol) in ethanol (6.00 mL). The solution was stirred at room temperature for 5 hours and 30 minutes, and then was cooled in an ice bath for 2 hours. The suspension was filtered and washed with cold ethanol and diethyl ether, after which the white solid was dried and identified, by ^{1}H,^{13}C and IR, as **2.39d** (1.11 g, 3.4 mmol, 53 %).

2-Amino-6-bromo-4-(2-oxo-2-phenylethyl)-4*H*-chromene-3-carbonitrile (**2.39e**):



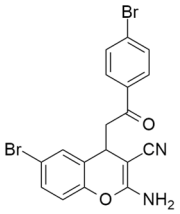
Triethylamine (4 equiv.; 7.61 mL) was added to a solution of **2.37e** (4.132 g, 13.6 mmol) and 2 equivalents of malononitrile (1.81 g, 27.4 mmol) in ethanol (8.00 mL). The solution was stirred at room temperature for 1 hour and then was cooled in an ice bath for 1 hour. The suspension was filtered and washed with cold ethanol and diethyl ether, after which the white solid was dried and identified, by ^{1}H,^{13}C, IR and Mp., as **2.39e** (2.71 g, 7.36 mmol, 54 %).

2-Amino-6-bromo-4-(2-oxo-2-(*p*-tolyl)ethyl)-4*H*-chromene-3-carbonitrile (**2.39f**):



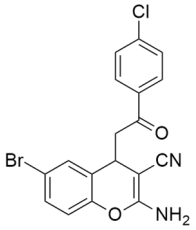
Triethylamine (4 equiv.; 4.20 mL) was added to a solution of **2.37f** (1.68, 5.3 mmol) and 2 equivalents of malononitrile (0.70 g, 10.6 mmol) in ethanol (5.00 mL). The solution was stirred at room temperature for 1.5 hours and then was cooled in an ice bath for 2 hours. The suspension was filtered and washed with cold ethanol and diethyl ether, after which the white solid was dried, and was identified by comparison with the information presented in the literature (ref. 104, chapter 2) as **2.39f** (0.93 g, 2.4 mmol, 46 %).

2-Amino-6-bromo-4-(2-oxo-2-(*p*-tolyl)ethyl)-4*H*-chromene-3-carbonitrile (**2.39g**):



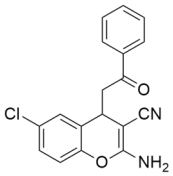
Triethylamine (4 equiv.; 4.20 mL) was added to a solution of **2.37g** (2.45, 6.4 mmol) and 2 equivalents of malononitrile (0.85 g, 12.8 mmol) in ethanol (6.00 mL). The solution was stirred at room temperature for 1 hours and then was cooled in an ice bath for 2 hours. The suspension was filtered and washed with cold ethanol and diethyl ether, after which the white solid was dried, and was identified by comparison with the information presented in the literature (ref. 104, chapter 2) as **2.39g** (1.15 g, 2.56 mmol, 40 %).

2-amino-6-bromo-4-(2-(4-chlorophenyl)-2-oxoethyl)-4H-chromene-3-carbonitrile (**2.39h**):



Triethylamine (2.28 equiv.; 5.62 mL) was added to a solution of **2.38e** (5.96 g, 17.7 mmol) and 2 equivalents of malononitrile (1.59 g, 24.0 mmol) in ethanol (8.00 mL). The solution was stirred at room temperature for 3 hour and then was cooled in an ice bath for 1 hour. The suspension was filtered and washed with cold ethanol and diethyl ether, after which the white solid was dried and identified, by ^{1}H,^{13}C and IR, as **2.40h** (2.99 g, 7.44 mmol, 42 %).

2-amino-6-bromo-4-(2-oxo-2-phenylethyl)-4*H*-chromene-3-carbonitrile (**2.39i**):

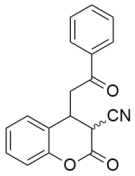


Triethylamine (3.96 equiv.; 1.36 mL) was added to a solution of **2.38e** (2.53 g, 9.78 mmol) and 2 equivalents of malononitrile (1.29 g, 19.6 mmol) in ethanol (6.00 mL). The solution was stirred at room temperature for 1 hour and then was cooled in an ice bath for 1 hour. The suspension was filtered and washed with cold ethanol and diethyl ether, after which the white solid was dried and identified, by ^{1}H,^{13}C, IR and Mp., as **2.40i** (1.63 g, 5.02 mmol, 51 %).

General procedure for the synthesis of 2-oxo-4-(2-oxo-2-arylethyl)chroman-3-carbonitriles (2.50):

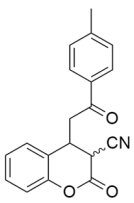
Concentrated H_2SO_4 (98%) (50-300 μL) was added to a suspension of the adequate chromene **2.39** in a 1:1 mixture of EtOH/H_2O (1:4 for **2.39c**), at room temperature (50 °C for **2.39c**). The beige suspension gradually turned into a beige solution, and after 1-2 hours, a new suspension gradually started to form. The thick suspension was then allowed to stand in an ice bath for 2-4 hours, or at 4 °C overnight. The beige solid was filtered, washed with cold water and ethanol, dried and identified as the corresponding chroman **2.50**, in a diastereoisomeric mixture.

2-Oxo-4-(2-oxo-2-phenylethyl)chroman-3-carbonitrile (**2.50a**):



1.7 Equivalents of H_2SO_4 (98%) was added to a suspension of chromene **2.39a** (0.35 g, 1.20 mmol) in a 1:1 mixture of EtOH/H_2O (4 mL) and the mixture was stirred at room temperature. The beige suspension gradually turned into a beige solution, and after 2 hours, a suspension gradually started to form. After 4 hours at room temperature, the thick suspension was allowed to cool in an ice bath for 2 hours. The solid was filtered, washed with cold water and ethanol, dried and identified by ^{1}H,^{13}C, IR and Mp., as chroman **2.50a** (0,214 g, 0.73 mmol, 61%) in an isomeric ratio of 2.1/1.

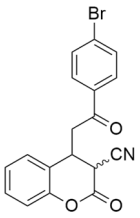
2-Oxo-4-(2-oxo-2-(p-tolyl)ethyl)chroman-3-carbonitrile (**2.50b**):



1.7 Equivalents of H_2SO_4 (98%) was added to a suspension of chromene **2.39b** (0.33 g, 1.08 mmol) in a 1:1 mixture of EtOH/H_2O (4 mL) and the mixture was stirred at room temperature. The beige suspension gradually turned into a beige solution, and after 2 hours, a suspension gradually started to form. After 4 hours at room temperature, the suspension was allowed to cool in an ice bath for 2 hours. The solid was filtered, washed with cold water

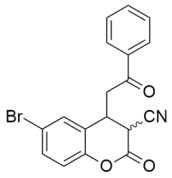
and ethanol, dried and identified, by ^{1}H,^{13}C, IR and Mp., as chroman **2.50b** (0.28 g, 0.92 mmol, 84 %), in an isomeric ratio of 2.5/1.

4-(2-(4-Bromophenyl)-2-oxoethyl)-2-oxochroman-3-carbonitrile (**2.50c**):



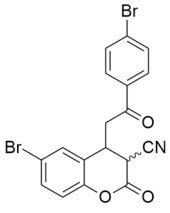
3.7 Equivalents of H_2SO_4 (98%) was added to a suspension of chromene **2.39c** (0.20 g, 0.54 mmol) in a 1:4 mixture of EtOH/H_2O (2.5 mL) and the mixture was stirred at 50 °C. The beige suspension gradually turned into a beige solution, and after 10 minutes, a suspension gradually started to form from. After 1 hour, the suspension was allowed to cool in an ice bath for 2 hours. The solid was filtered, washed with cold water and ethanol, dried and identified by ^{1}H,^{13}C, IR and Mp., as chroman **2.50c** (0.155 g, 0.42 mmol, 78 %), in an isomeric ratio of 2.7/1.

6-Bromo-2-oxo-4-(2-oxo-2-phenylethyl)chroman-3-carbonitrile (**2.50d**):



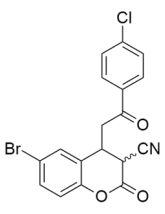
3.0 Equivalents of H_2SO_4 (98%) was added to a suspension of the chromene **2.39e** (0.25 g, 0.68 mmol) in a 1:1 mixture of EtOH/H_2O (2 mL) and the mixture was stirred at room temperature. The beige suspension gradually turned into a beige solution, and after 1 hour, a suspension gradually started to form. After 4 hours, the suspension was allowed to cool in an ice bath for 2 hours. The solid was filtered, washed with cold water and ethanol, dried and identified, by ^{1}H,^{13}C, IR and Mp., as chroman **2.50d** (0.14 g, 0.38 mmol, 57 %), in an isomeric ratio of 2.7/1.

6-Bromo-4-(2-(4-bromophenyl)-2-oxoethyl)-2-oxochroman-3-carbonitrile (**2.50e**):



4.5 Equivalents of H_2SO_4 (98%) was added to a suspension of chromene **2.39g** (0.20 g, 0.45 mmol) in a 1:1 mixture of EtOH/H_2O (2 mL) and the mixture was stirred at room temperature. The beige suspension gradually turned into a beige solution, and after 30 minutes, a suspension gradually started to form from. After 2 hours, the suspension was allowed to cool in an ice bath for 2 hours. The solid was filtered, washed with cold water and ethanol, dried and identified by ^{1}H,^{13}C, IR and Mp., as chroman **2.50e** (0.03 g, 0.07 mmol, 17 %), in an isomeric ratio of 2.9/1.

6-Bromo-4-(2-(4-chlorophenyl)-2-oxoethyl)-2-oxochroman-3-carbonitrile (**2.50f**): 4.0 Equivalents of H_2SO_4 (98%) was added to a suspension of chromene **2.39h** (0.20 g, 0.50 mmol) in a 1:1 mixture of EtOH/H_2O (2 mL) and the mixture was stirred at room temperature. The beige suspension gradually turned into a beige solution, and after 30 minutes, a suspension

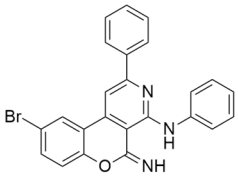


gradually started to form. After 1 hour and 40 minutes, the suspension was allowed to cool in an ice bath for 2 hours. The solid was filtered, washed with cold water and ethanol, dried and identified by ^{1}H,^{13}C, IR and Mp., as chroman **2.50f** (0.03 g, 0.08 mmol, 16 %), in an isomeric ratio of 2.9/1.

General procedure for the synthesis of 5-imino-*N*,2-diaryl-5*H*-chromeno[3,4-c]pyridin-4-amines (2.55):

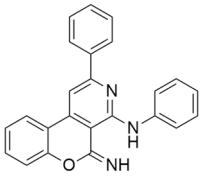
The amine (2-3 equiv.) was added to a suspension of the appropriate chromene **2.39** in ethanol, kept stirring at 80°C. Acetic acid (0.5 equiv.) was also added. The suspension gradually turned into a solution and after 1-3 hours, a yellow solid started to precipitate from the reaction mixture. After the starting material was consumed, as evidenced by TLC (AcOEt/*n*-hexane 1:1), the suspension was cooled to room temperature for 5 minutes and then in an ice bath for 2-5 hours or at 4 °C for 24-72 hours. The yellow suspension was filtered, washed with cold ethanol, a few drops of diethyl ether and dried. The solid was characterized, by ^{1}H,^{13}C, IR and Mp., and identified as the appropriate chromenopyridine **2.55**.

9-Bromo-5-imino-*N*,2-diphenyl-5*H*-chromeno[3,4-*c*]pyridin-4-amine (**2.55a**):



Aniline (3 equiv.; 111 μL, 0.12 g, 1.23 mmol) was added to a suspension of chromene **2.39e** (0.15 g, 0.41 mmol) in ethanol (2.00 mL), with stirring at 80°C, followed by addition of acetic acid (0.5 equiv.; 12 μL, 0.01 g, 0.21 mmol). The suspension gradually turned into a solution, and after 2 hours, a yellow solid started to precipitate from the reaction mixture. The reaction was complete after 63 hours, as evidenced by TLC (AcOEt/ *n*-hexane 1:1). The yellow suspension was cooled to room temperature for 5 minutes, and then in an ice bath for 3 hours. The product was filtered and washed with cold ethanol and a few drops of diethyl ether and dried. The yellow solid was characterized by ^{1}H, ^{13}C and IR, as being chromenopyridine **2.55a** (0.06 g, 0.13 mmol, 31 %).

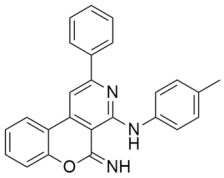
5-Imino-*N*,2-diphenyl-5*H*-chromeno[3,4-*c*]pyridin-4-amine (**2.55b**):



Aniline (2 equiv.; 94 μL, 0.10 g, 1.03 mmol) was added to a suspension of chromene **2.39a** (0.15 g, 0.52 mmol) in ethanol (2.00 mL), with stirring at 80°C, followed by addition of acetic acid (0.5 equiv.; 15 μL, 0.02 g, 0.26 mmol). The suspension gradually turned into a solution, and after 2 hours, a yellow solid started to precipitate from the reaction mixture. The reaction was complete after 22 hours, as evidenced by TLC (AcOEt/ *n*-hexane 1:1). The yellow suspension was cooled to room temperature for 5 minutes, and then in an ice bath for 2 hours. The product was filtered and washed with cold ethanol and a few drops of diethyl ether, and dried. The

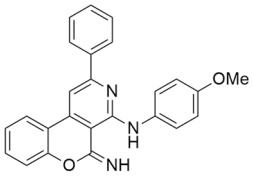
yellow solid was characterized, by ^{1}H,^{13}C, IR and Mp., and identified by ^{1}H, ^{13}C and IR, and identified as the chromenopyridine **2.55b** (0.11 g, 0.31 mmol, 61 %).

5-Imino-2-phenyl-*N*-(p-tolyl)-5*H*-chromeno[3,4-*c*]pyridin-4-amine (**2.55c**):



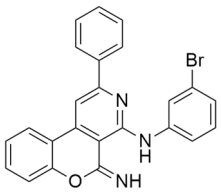
p-Toluidine (2 equiv.; 0.11 g, 1.03 mmol) was added to a suspension of chromene **2.40a** (0.15 g, 0.52 mmol) in ethanol (2.00 mL), with stirring at 80°C, followed by the addition of acetic acid (0.5 equiv.;15 μL, 0.02 g, 0.26 mmol). The suspension gradually turned into a solution, and after 2 hours, a yellow solid started to precipitate from the reaction mixture. The reaction was complete after 22 hours and 45 minutes, as evidenced by TLC (AcOEt/*n*-hexane 1:1). The yellow suspension was cooled to room temperature for 5 minutes, and then in an ice bath for 2 hours. The product was filtered and washed with cold ethanol and a few drops of diethyl ether, and dried. The light-yellow solid was characterized by ^{1}H, ^{13}C and IR, and identified as the chromenopyridine **2.55c** (0.13 g, 0.31 mmol, 66%; 3.6 % contamination with the oxo form **2.56b**, by ^{1}H NMR).

5-Imino-*N*-(4-methoxyphenyl)-2-phenyl-5*H*-chromeno[3,4-c]pyridin-4-amine (**2.55d**):



p-Methoxyaniline (2 equiv.; 0.13 g, 1.03 mmol) was added to a suspension of chromene **2.39a** (0.15 g, 0.52 mmol) in ethanol (2.00 mL), with stirring at 80°C, followed by the addition of acetic acid (0.5 equiv.; 15 μL, 0.02 g, 0.26 mmol). The suspension gradually turned into a solution, and after 2 hours, a yellow solid started to precipitate from the reaction mixture. The reaction was complete after 22 hours and 15 minutes, as evidenced by TLC (AcOEt/ *n*-hexane 1:1). The yellow suspension was cooled to room temperature for 5 minutes, and then in an ice bath for 2 hours. The yellow suspension was filtered and washed with cold ethanol and a few drops of diethyl ether, and dried. The light-yellow solid was characterized by ^{1}H,^{13}C and IR, and identified as the chromenopyridine **2.55d** (0.14 g, 0.35 mmol, 68 %).

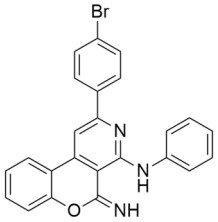
5-Imino-*N*-(3-bromophenyl)-2-phenyl-5*H*-chromeno[3,4-*c*]pyridin-4-amine (**2.55e**):



m-Bromoaniline (2 equiv.; 0.18 g, 1.03 mmol) was added to a suspension of chromene **2.39a** (0.15 g, 0.52 mmol) in ethanol (2.00 mL), with stirring at 80°C, followed by the addition of acetic acid (0.5 equiv.; 15 μL, 0.02 g, 0.26 mmol). The suspension gradually turned into a solution, and after 4 hours, a yellow solid started to precipitate from the reaction mixture. The reaction was complete after 22 hours and 15 minutes, as evidenced by TLC (AcOEt/ *n*-hexane 1:1). The yellow suspension was cooled to room temperature for 5

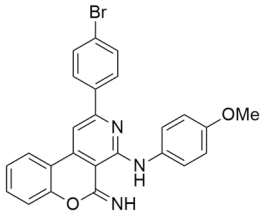
minutes, and then in an ice bath for 3 hours. The product was filtered and washed with cold ethanol and a few drops of diethyl ether, and dried. The light-yellow solid was characterized, by ^{1}H, ^{13}C and IR, and identified as he chromenopyridine **2.55e** (0.07 g, 0.35 mmol, 48%; 4.8 % contamination with the oxo form **2.59c**, by ^{1}H NMR).

5-Imino-*N*-(3-bromophenyl)-2-phenyl-5*H*-chromeno[3,4-*c*]pyridin-4-amine (**2.55f**):



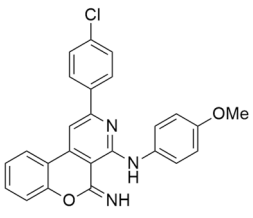
Aniline (3 equiv.; 113 μL, 0.11 g, 1.22 mmol) was added to a suspension of chromene **2.39c** (0.15 g, 0.41 mmol) in ethanol (2.00 mL), with stirring at 80°C, followed by the addition of acetic acid (0.5 equiv.;12 μL, 0.01 g, 0.21 mmol). The suspension gradually turned into a solution, and after 4 hours, a yellow solid started to precipitate from the reaction mixture. The reaction was complete after 14 hours, as evidenced by TLC (AcOEt/ *n*-hexane 1:1). The yellow suspension was cooled to room temperature for 5 minutes, and then in an ice bath for 3 hours. The product was filtered and washed with cold ethanol and a few drops of diethyl ether, and dried. The light-yellow solid was characterized, by ^{1}H, ^{13}C and IR, and identified as the chromenopyridine **2.55f** (0.006 g, 0.02 mmol, 5 %).

2-(4-Bromophenyl)-5-imino-*N*-(4-methoxyphenyl)-5*H*-chromeno[3,4-*c*]pyridin-4-amine (**2.55g**):



p-Methoxyaniline (3 equiv.; 0.15 g, 1.22 mmol) was added to a suspension of chromene **2.39c** (0.15 g, 0.41 mmol) in ethanol (2.00 mL), with stirring at 80°C, followed by the addition of acetic acid acid (0.5 equiv.; 12 μL, 0.01 g, 0.21 mmol). The suspension gradually turned into a solution, and after 4 hours, a yellow solid started to precipitate from the reaction mixture. The reaction was complete after 14 hours, as evidenced by TLC (AcOEt/*n*-hexane 1:1). The yellow suspension was cooled to room temperature for 5 minutes, and then in an ice bath for 3 hours. The product was filtered and washed with cold ethanol and a few drops of diethyl ether, and dried. The light-orange solid was characterized by ^{1}H, ^{13}C and IR, and identified as chromenopyridine **2.55g** (0.04 g, 0.09 mmol, 22 %).

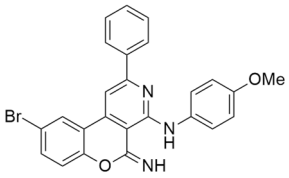
2-(4-Chlorophenyl)-5-imino-*N*-(4-methoxyphenyl)-5*H*-chromeno[3,4-*c*]pyridin-4-amine (**2.55j**):



p-Methoxyaniline (3 equiv.; 0.17 g, 1.39 mmol) was added to a suspension of chromene **2.39d** (0.15 g, 0.46 mmol) in ethanol (2.00 mL), with stirring at 80°C, followed by the addition of acetic acid (0.5 equiv.; 13 μL, 0.01 g, 0.23 mmol). The suspension gradually turned into a solution and after 30 minutes, a yellow solid started to precipitate from the reaction mixture. The reaction was complete after 6 hours and 30

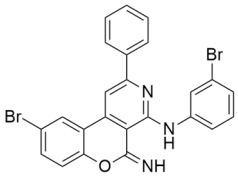
minutes, as evidenced by TLC (AcOEt/ *n*-hexane 1:1). The yellow suspension was cooled to room temperature for 5 minutes and then at 4 °C for 24 hours. The product was then filtered and washed with cold ethanol and a few drops of diethyl ether, and dried. The light-yellow solid was characterized by ^{1}H, ^{13}C and IR, and identified as the chromenopyridine **2.55j** (0.02 g, 0.04 mmol, 8 %).

9-Bromo-5-imino-*N*-(4-methoxyphenyl)-2-phenyl-5*H*-chromeno[3,4-*c*]pyridin-4-amine (**2.55i**):



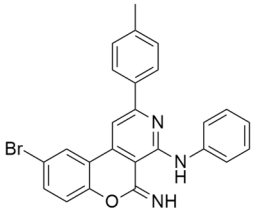
p-Methoxyaniline (2 equiv.; 0.10 g, 0.82 mmol) was added to a suspension of chromene **2.39e** (0.15 g , 0.41 mmol) in ethanol (2.00 mL), with stirring at 80°C, followed by the addition of acetic acid (0.5 equiv. ;12 μL, 0.01 g, 0.21 mmol). The suspension gradually turned into a solution, and after 1 hour, a yellow solid started to precipitate from the reaction mixture. The reaction was complete after 22 hours, as evidenced by TLC (AcOEt/*n*-hexane 1:1). The yellow suspension was cooled to room temperature for 5 minutes, and then in an ice bath for 3 hours. The product was then filtered and washed with cold ethanol and a few drops of diethyl ether, and dried. The yellow solid was characterized by ^{1}H, ^{13}C and IR, and identified as the chromenopyridine **2.55i** (0.11 g, 0.22 mmol, 55%, with traces of the oxo form **2.56f**, by ^{1}H NMR).

9-Bromo-*N*-(3-bromophenyl)-5-imino-2-phenyl-5*H*-chromeno[3,4-*c*]pyridin-4-amine (**2.55m**):



m-Bromoaniline (3 equiv.; 0.14 g, 0.82 mmol) was added to a suspension of chromene **2.39e** (0.15 g, 0.41 mmol) in ethanol (2.00 mL), with stirring at 80°C, followed by the addition of acetic acid (0.5 equiv.; 12 μL, 0.01 g, 0.21 mmol). The suspension gradually turned into a solution, and after 2 hours, a yellow solid started to precipitate from the reaction mixture. The reaction was complete after 19 hours, as evidenced by TLC (AcOEt/ *n*-hexane 1:1). The yellow suspension was cooled to room temperature for 5 minutes, and then in an ice bath for 3 hours. The product was then filtered and washed with cold ethanol and a few drops of diethyl ether, and dried. The yellow solid was characterized, by ^{1}H, ^{13}C and IR, and identified as the chromenopyridine **2.55m** (0.04 g, 0.08 mmol, 19 %).

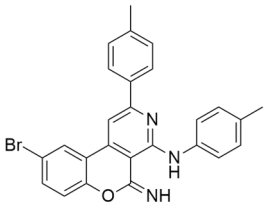
9-Bromo-5-imino-*N*-phenyl-2-(*p*-tolyl)-5*H*-chromeno[3,4-*c*]pyridin-4-amine (**2.55n**):



Aniline (2 equiv.; 72 μL, 0.07 g, 0.79 mmol) was added to a suspension of chromene **2.39f** (0.15 g, 0.39 mmol) in ethanol (2.00 mL), with stirring at 80°C, followed by the addition of acetic acid (0.5 equiv.; 11 μL, 0.01 g, 0.20 mmol). The suspension gradually turned into a solution, and after 3 hours, a yellow solid

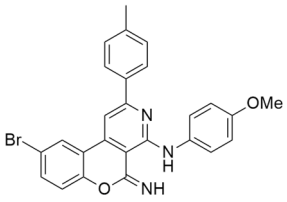
started to precipitate from the reaction mixture. The reaction was complete after 22 hours, as evidenced by TLC (AcOEt/*n*-hexane 1:1). The yellow suspension was cooled to room temperature for 5 minutes, and then at 4 °C for 26 hours. The product was then filtered, washed with cold ethanol and few drops of diethyl ether and dried. The yellow solid was characterized by ^{1}H, ^{13}C and IR, and identified as chromenopyridine **2.55n** (0.03 g, 0.06 mmol, 15 %).

9-Bromo-5-imino-*N*,2-di-*p*-tolyl-5*H*-chromeno[3,4-c]pyridin-4-amine (**2.55p**):



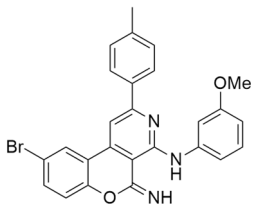
p-Toluidine (3 equiv.; 0.08 g, 0.78 mmol) was added to a suspension of chromene **2.39f** (0.15 g, 0.39 mmol) in ethanol (2.00 mL), with stirring at 80°C, followed by the addition of acetic acid (0.5 equiv.; 11 μL, 0.01 g, 0.20 mmol). The suspension gradually turned into a solution, and after 2 hours, a yellow solid started to precipitate from the reaction mixture. The reaction was complete after 22 hours, as evidenced by TLC (AcOEt/*n*-hexane 1:1). The yellow suspension was cooled to room temperature for 5 minutes and then in an ice bath for 3 hours. The product was then filtered and washed with cold ethanol and a few drops of diethyl ether, and dried. The yellow solid was characterized by ^{1}H, ^{13}C and IR, and identified as the chromenopyridine **2.55p** (0.07 g, 0.15 mmol, 37 %).

9-Bromo-5-imino-*N*-(4-methoxyphenyl)-2-(*p*-tolyl)-5*H*-chromeno[3,4-*c*]pyridin-4-amine (**2.55q**):



-Methoxyaniline (2 equiv.; 0.15 g, 1.18 mmol) was added to a suspension of chromene **2.39f** (0.15 g, 0.39 mmol) in ethanol (2.00 mL), with stirring at 80°C, followed by the addition of acetic acid (0.5 equiv.; 11 μL, 0.01 g, 0.20 mmol). The suspension gradually turned into a solution, and after 2 hours, a yellow solid started to precipitate from the reaction mixture. The reaction was complete after 17 hours and 15 minutes, as evidenced by TLC (AcOEt/*n*-hexane 1:1). The yellow suspension was cooled to room temperature for 5 minutes and then in an ice bath for 3 hours. The product was then filtered and washed with cold ethanol and a few drops of diethyl ether, and dried. The yellow solid was characterized by ^{1}H, ^{13}C and IR, and identified as the chromenopyridine **2.55q** (0.06 g, 0.13 mmol, 32 %).

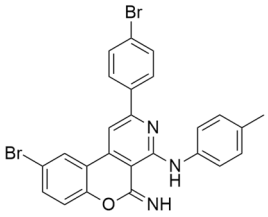
9-Bromo-5-imino-*N*-(3-methoxyphenyl)-2-(*p*-tolyl)-5*H*-chromeno[3,4-*c*]pyridin-4-amine (**2.55r**):



m-Methoxyaniline (2 equiv.; 95 μL,0.09 g, 0.79 mmol) was added to a suspension of chromene **2.39f** (0.15 g, 0.39 mmol) in ethanol (2.00 mL), with stirring at 80°C, followed by the addition of acetic acid (0.5 equiv.; 11 μL, 0.01 g, 0.20 mmol). The suspension gradually turned into a solution, and after 4

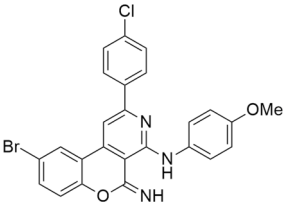
hours, a yellow solid started to precipitate from the reaction mixture. The reaction was complete after 22 hours and 45 minutes, as evidenced by TLC (AcOEt/*n*-hexane 1:1). The yellow suspension was cooled to room temperature for 5 minutes and then at 4°C for 18 hours. The product was then filtered and washed with cold ethanol and a few drops of diethyl ether, and dried. The yellow solid was characterized, by ^{1}H, ^{13}C and IR, as being chromenopyridine **2.55r** (0.06 g, 0.12 mmol, 31 %).

9-Bromo-2-(4-bromophenyl)-5-imino-*N*-(*p*-tolyl)-5*H*-chromeno[3,4-*c*]pyridin-4-amine (**2.55u**):



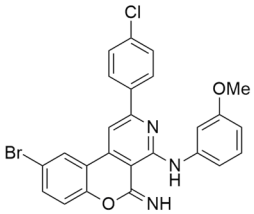
p-Toluidine (3 equiv.; 0.11 g, 1.00 mmol) was added to a suspension of chromene **2.39g** (0.15 g, 0.34 mmol) in ethanol (2.00 mL), with stirring at 80°C, followed by the addition of acetic acid (0.5 equiv.; 10 μL, 0.01 g, 0.17 mmol). The suspension gradually turned into a solution, and after 5 hours, a yellow solid started to precipitate from the reaction mixture. The reaction was complete after 32 hours and 15 minutes, as evidenced by TLC (AcOEt/*n*-hexane 1:1). The yellow suspension was cooled to room temperature for 5 minutes and then at 4°C for 26 hours. The product was then filtered and washed with cold ethanol and a few drops of diethyl ether, and dried. The yellow solid was characterized, by ^{1}H, ^{13}C and IR, and identified as the chromenopyridine **2.55u** (0.03 g, 0.06 mmol, 17 %).

9-Bromo-2-(4-chlorophenyl)-5-imino-*N*-(4-methoxyphenyl)-5*H*-chromeno[3,4-*c*]pyridin-4-amine (**2.55b'**):



p-Methoxyaniline (3 equiv.; 0.14 g, 1.12 mmol) was added to a suspension of chromene **2.39h** (0.15 g, 0.37 mmol) in ethanol (2.00 mL), with stirring at 80°C, followed by the addition of acetic acid (0.5 equiv.;10 μL, 0.01 g, 0.17 mmol). The suspension gradually turned into a solution, and after 4 hours, a yellow solid started to precipitate from the reaction mixture. The reaction was complete after 27 hours and 25 minutes, as evidenced by TLC (AcOEt/*n*-hexane 1:1). The yellow suspension was cooled to room temperature for 5 minutes and then at 4°C for 27 hours. The product was then filtered and washed with cold ethanol and a few drops of diethyl ether, and dried. The yellow solid was characterized by ^{1}H, ^{13}C and IR, and identified as the chromenopyridine **2.55b'** (0.04 g, 0.08 mmol, 21 %; with traces of **2.60d**).

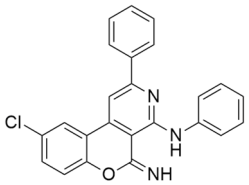
9-Bromo-2-(4-chlorophenyl)-5-imino-*N*-(3-methoxyphenyl)-5*H*-chromeno[3,4-*c*]pyridin-4-amine (**2.55c'**):



m-Methoxyaniline (2 equiv.; 90 μL, 0.09 g, 0.74 mmol) was added to a suspension of chromene **2.39h** (0.15 g, 0.37 mmol) in ethanol (2.00 mL), with stirring at 80°C, followed by the addition of acetic acid (0.5 equiv.; 10 μL, 0.01 g, 0.17 mmol). The suspension gradually turned into a

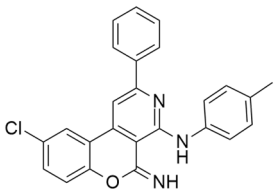
solution, and after 4 h, a yellow solid started to precipitate from the reaction mixture. The reaction was complete after 39 hours, as evidenced by, by TLC (AcOEt/*n*-hexane 1:1). The yellow suspension was cooled to room temperature for 5 minutes, and then at 4°C for 30 hours. The product was then filtered and washed with cold ethanol and a few drops of diethyl ether, and dried. The yellow solid was characterized by ^{1}H, ^{13}C and IR, and identified as the chromenopyridine **2.55c'** (0.01 g, 0.01 mmol, 4 %).

9-Chloro-5-imino-*N*,2-diphenyl-5*H*-chromeno[3,4-*c*]pyridin-4-amine (**2.55d'**):



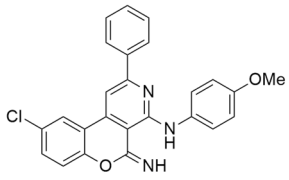
Aniline (3 equiv.; 126 μL, 0.13 g, 1.38 mmol) was added to a suspension of chromene **2.39i** (0.15 g, 0.46 mmol) in ethanol (2.00 mL), with stirring at 80°C, followed by the addition of acetic acid (0.5 equiv.; 13 μL, 0.01 g, 0.23 mmol). The suspension gradually turned into a solution, and after 3 hours, a yellow solid started to precipitate from the reaction mixture. The reaction was complete after 22 hours, as evidenced by TLC (AcOEt/*n*-hexane 1:1). the yellow suspension was cooled to room temperature for 5 minutes, and then in an ice bath for 4 hours. The product was then filtered and washed with cold ethanol and a few drops of diethyl ether, and dried. The yellow solid was characterized by ^{1}H, ^{13}C and IR, as being chromenopyridine **2.55d'** (0.101 g, 0.25 mmol, 55 %).

9-chloro-5-imino-2-phenyl-N-(p-tolyl)-5H-chromeno[3,4-c]pyridin-4-amine (**2.55f'**):



Aniline (2 equiv.; 0.10 g,0.92 mmol) was added to a suspension of chromene **2.39i** (0.15 g, 0.46 mmol)in ethanol (2.00 mL), with stirring at 80°C, followed by the addition of 0.5 equivalents of acetic acid (13 μL, 0.01 g, 0.23 mmol). The suspension gradually turned into a solution, and after 3 hours, a yellow solid started to precipitate from the reaction mixture. The reaction was complete after 22 hours, as evidenced by TLC (AcOEt/*n*-hexane 1:1). The yellow suspension was cooled to room temperature for 5 minutes, and then in an ice bath for 4 hours. The product was then filtered and washed with cold ethanol and a few drops of diethyl ether, and dried. The yellow solid was characterized by ^{1}H, ^{13}C and IR, and identified as the chromenopyridine **2.55f'** (0.04 g, 0.10 mmol, 22 %).

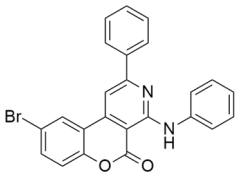
9-chloro-5-imino-2-phenyl-N-(p-methoxyphenyl)-5H-chromeno[3,4-c]pyridin-4-amine (**2.55g'**):



p-Methoxyaniline (2 equiv.; 0.11 g, 0.92 mmol) was added to a suspension of chromene **2.39i** (0.15 g, 0.46 mmol) in ethanol (2.00 mL), with stirring at 80°C, followed by the addition of acetic acid (0.5 equiv.; 13 μL, 0.01 g,

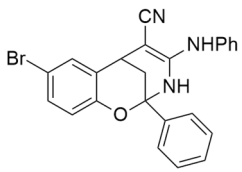
0.23 mmol). The suspension gradually turned into a solution, and after 2 hours, a yellow solid started to precipitate from the reaction mixture. The reaction was complete after 39 hours and 15 minutes, as evidenced by TLC (AcOEt/*n*-hexane 1:1). The yellow suspension was cooled to room temperature for 5 minutes, and then in an ice bath for 4 hours. The product was then filtered and washed with cold ethanol and a few drops of diethyl ether, and dried. The collected yellow solid was characterized by ^{1}H, ^{13}C and IR, and identified as the chromenopyridine **2.55g'** (0.11 g, 0.26 mmol, 55 %).

Synthesis of 9-bromo-2-phenyl-4-(phenylamino)-5H-chromeno[3,4-c]pyridin-5-one (2.56a):



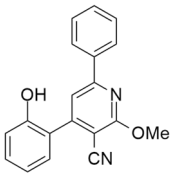
H_2SO_4 (2.5 equiv.) was added to a mixture of compounds **2.55a**, **2.56a, 2.60a** and **2.61a** (0.19 g) in ethanol/water (2.5 mL), with stirring at 80 °C. The reaction was complete after 3 hours and 30 minutes, as evidenced by TLC (AcOEt/*n*-hexane 1:1). The suspension was filtered and washed with cold ethanol and water, and a few drops of diethyl ether, and dried. The yellow solid was characterized by ^{1}H, ^{13}C and IR, and identified as the chromenopyridine **2.56a** (0.05 g, 0.12 mmol).

Synthesis of 8-Bromo-2-phenyl-4-(phenylamino)-3,6-dihydro-2*H*-2,6-methanobenzo[g][1,3] oxazocine-5-carbonitrile (2.61a):



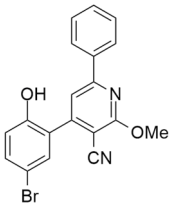
Aniline (2 equiv.; 74 μL, 0.08 g, 0.82 mmol) was added to a suspension of chromene **2.39e** (0.15 g, 0.41 mmol) in a 1:1 mixture of ethanol/water (2 mL), with stirring at 80 °C, generating a beige suspension. Then acetic acid (0.5 equiv.; 12 μL, 0.01 g, 0.21 mmol) was added, generating a light-yellow suspension. After 1 hour and 30 minutes, the yellow suspension was allowed to stand at 4 °C for 18 hours. The yellow solid was filtered and washed with cold ethanol. After drying, the product was identified, by ^{1}H, ^{13}C and IR, and identified as compound **2.61a** (0.12 g, 0.26 mmol, 65 %).

Synthesis of 2-ethoxy-4-(2-hydroxy-5-methylphenyl)-6-phenylnicotino-nitrile (2.68a):



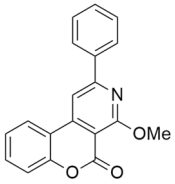
Aqueous NaOH 2M (2 mL) was added to a suspension of chromene **2.39i** (0.250 g, 0.86 mmol) in methanol (4 mL). while stirring at room temperature. The orange solution gradually turned into a red solution. After stirring for 64 hours, the light-brown suspension was filtered and washed with cold methanol and water, and dried. The product was identified, by ^{1}H, ^{13}C and IR, and identified as compound **2.68a** (0.05 g, 0.18 mmol, 21 %).

Synthesis of 2-ethoxy-4-(2-hydroxy-5-methylphenyl)-6-phenylnicotino-nitrile (2.68b):



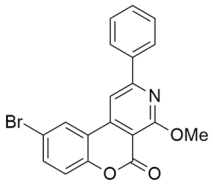
Aqueous NaOH 2M (2 mL) was added to a suspension of chromene **2.39e** (0.150 g, 0.40 mmol) in methanol (4 mL). while stirring at room temperature. The orange solution gradually turned into a red solution. After stirring for 41 hours, the dark-yellow suspension was filtered and washed with cold methanol and water, and dried. The product was identified, by ^{1}H, ^{13}C and IR, and identified as compound **2.68b** (0.07 g, 0.19 mmol, 46 %).

4-methoxy-2-phenyl-5*H*-chromeno[3,4-c]pyridin-5-one (**2.69a**):



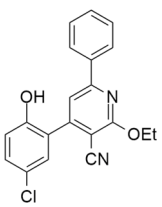
Compound **2.68a** (0.06 g, 0.18 mmol) was combined with 1 mL of ethanol and H_2SO_4 (4 equiv.; 12 μL, 0.021 g, 0.72 mmol). After stirring for 1 hour at room temperature, a white solid was formed. The product was filtered, washed with cold methanol and a few drops of diethyl ether and dried. The white solid was characterized by ^{1}H, ^{13}C and IR, and was identified as 4-methoxy-2-phenyl-5*H*-chromeno[3,4-*c*]pyridin-5-one **2.69a** (0.012 g, 0.04 mmol, 21 %).

9-bromo-4-methoxy-2-phenyl-5*H*-chromeno[3,4-c]pyridin-5-one (**2.69b**):



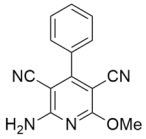
Aqueous NaOH 2M (1 mL)) was added to a suspension of chromene **2.39e** (0.2 g, 0.55 mmol) in methanol (1 mL), while stirring at room temperature. The orange suspension gradually turned into a red solution. The reaction was complete after 1 hours and 20 minutes, as evidenced by TLC (AcOEt/*n*-hexane 1:1). The red solution was neutralized with H_2SO_4 (followed by pH strip), generating a light-brown suspension which was left stirring at room temperature for 20 minutes at room temperature. A beige solid was collected from the reaction mixture, by filtration, and was recrystallized from ethanol/*n*-hexane 1:1, a white solid was collected and further identified, by ^{1}H, ^{13}C and IR, as 9-bromo-4-methoxy-2-phenyl-5*H*-chromeno[3,4-c]pyridin-5-one **2.69b** (0.08 g, 0.21 mmol 38%).

Synthesis of 2-ethoxy-4-(2-hydroxy-5-methylphenyl)-6-phenylnicotinonitrile (2.70a):



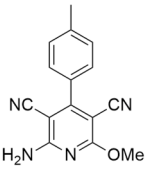
Aqueous NaOH 2M (1 mL) was added to a suspension of chromene **2.39i** (0.200 g, 0.62 mmol) in ethanol (1 mL), leading to an orange solution that gradually turned into a red solution. After stirring for 2 hours at room temperature, the solution was neutralized with H_2SO_4 (followed by pH strip), leading to a light-brown suspension that was stirred at room temperature for 1 hour and 10 minutes. The suspension was filtered, washed with cold ethanol and water and dried. The beige solid was identified, by ^{1}H, ^{13}C and IR, as compound **2.70a** (0.19 g, 0.52 mmol, 84 %).

Synthesis of 2-amino-6-methoxy-4-(phenyl)pyridine-3,5-dicarbonitrile(2.71a):



Malononitrile (2 equiv.; 0.435 g, 6.60 mmol) was added to a suspension of **2.37e** (1.00 g, 3.29 mmol in 9 mL of methanol and the mixture was stirred at room temperature. Aqueous NaOH 3M (1.5 mL) was added to the suspension, that was left stirring at room temperature. The brown suspension rapidly turned into a red solution, but after 30 seconds gradually turned into a yellow suspension. Ethanol (4 mL) was added to the thick suspension, that was stirred at room temperature for an additional 2 hours. From the yellow suspension, a white solid was filtered, washed with cold methanol and diethyl ether and dried. The product was identified by ^{1}H, ^{13}C and IR, as **2.71a** (0.17 g, 0.67 mmol, 20 %).

Synthesis of 2-amino-6-methoxy-4-(*p*-tolyl)pyridine-3,5-dicarbonitrile (2.71b):

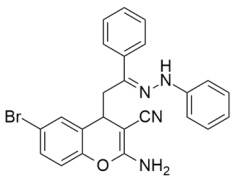


Aqueous NaOH 2M (1 mL) was added to a suspension of chromene **2.39b** (0.2 g, 0.66 mmol) in methanol (1 mL), leading to a red solution. After stirring for 3 hours and 40 minutes, at room temperature, TLC indicated the absence of the starting material **2.39b**. The red solution was neutralized with H_2SO_4 (followed by pH strip), leading to a light-brown suspension which was stirred at room temperature for 4 hours. The white solid was filtered, washed with cold methanol and dried. The product was identified, by ^{1}H, ^{13}C and IR, as compound **2.71b** (0.02 g, 0.07 mmol, 10 %).

General procedure for the synthesis of 2-amino-4-(2-aryl-2-(2-phenylhydrazono)ethyl)-4*H*-chromene-3-carbonitriles (2.82):

Phenylhydrazine (1.7 equiv.) and acetic acid (0.5 equiv.) were added to a suspension of the appropriate chromene **2.39** in ethanol and the mixture was stirred at 80 °C for 1-2 hours. After confirming the consumption of the starting material **2.39** (by TLC, AcOEt/*n*-hexane 1:1), the suspension was cooled in an ice bath for 1-2 hours. The white solid was filtered, washed with cold ethanol and a few drops of diethyl ether and dried. The product was identified, by ^{1}H, ^{13}C and IR, as the pure compound **2.82**.

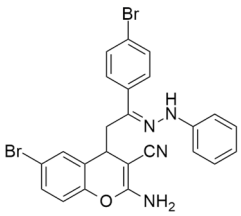
2-Amino-6-bromo-4-(2-phenyl-2-(2-phenylhydrazono)ethyl)-4*H*-chrome ne-3-carbonitrile **(2.82a):**



Phenylhydrazine (1.7 equiv.) and acetic acid (0.5 equiv.) were added to a suspension of chromene **2.39e** (0.150 g, 0.41 mmol) in 2 mL of ethanol and the mixture was stirred at 80 °C for 2 hours. After confirming the consumption of the starting material **2.39** (by TLC, AcOEt/*n*-hexane 1:1), the suspension was cooled in an ice bath for 1

hour. The white solid was filtered, washed with cold ethanol and a few drops of diethyl ether and dried. The product was identified, by ^{1}H, ^{13}C and IR, as the pure compound **2.82a** (0.10 g, 0.22 mmol, 53 %).

2-amino-6-bromo-4-(2-phenyl-2-(2-phenylhydrazono)ethyl)-4*H*-chrome ne-3-carbonitrile **(2.82b):**

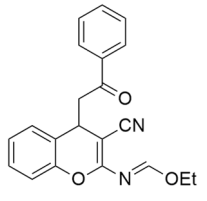


Phenylhydrazine (1.7 equiv.) and acetic acid (0.5 equiv.) were added to a suspension of chromene **2.39g** (0.150 g, 0.33 mmol) in 2 mL of ethanol and the mixture was stirred at 80 °C for 1 hour. After confirming the consumption of the starting material **2.39** (by TLC, AcOEt/*n*-hexane 1:1), the obtained suspension was left cooling on an ice bath for 1 hour, after which the white solid was filtered and washed off with cold ethanol and drops of diethyl ether. The obtained white solid was dried and further identified, by ^{1}H, ^{13}C and IR, as the pure compound **2.82b** (0.10 g, 0.22 mmol, 45 %).

General procedure for the synthesis of ethyl *N*-(3-cyano-4-(2-oxo-2-arylethyl)-4*H*-chromen-2-yl)formimidates (2.85):

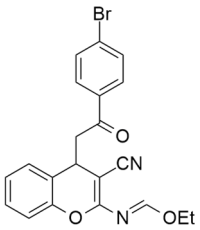
Triethyl orthoformate (8 equiv.) and acetic anhydride (3 equiv.) were added to the appropriate chromene **2.39** (1 equiv.) and the mixture was refluxed for 10-40 minutes. After consumption of the starting material **2.39** (confirmed by TLC, AcOEt/*n*-hexane 1:1), 8-10 mL of *n*-hexane were added to the mixture. The brown solution led to a suspension after standing in an ice bath for 1-2 hours. The solid was filtered, washed with cold *n*-hexane and dried. The product was identified by ^{1}H, ^{13}C, IR and Mp., as the corresponding compound **2.85**.

Ethyl *N*-(3-cyano-4-(2-oxo-2-phenylethyl)-4*H*-chromen-2-yl)formimidate (**2.85a**):



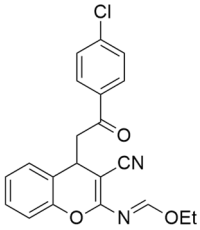
Triethyl orthoformate (8 equiv.; 1.22 g, 16.5 mmol, 2.74 mL) and acetic anhydride (3 equiv.; 0.32 g, 3.09 mmol, 586 µL), were added to chromene **2.39a** (0.60 g, 2.06 mmol) and the mixture was refluxed for 30 minutes. After consumption of the starting material **2.39a** (confirmed by TLC, AcOEt/*n*-hexane 1:1), 8 mL of *n*-hexane were added to the mixture. The brown solution led to a suspension after standing in an ice bath for 2 hours. The beige solid was filtered, washed with cold *n*-hexane and dried. The product was identified by ^{1}H, ^{13}C and IR, as compound **2.85a** (1.96 mmol, 0.68 g, 95%).

Ethyl *N*-(4-(2-(4-bromophenyl)-2-oxoethyl)-3-cyano-4*H*-chromen-2-yl)formimidate (**2.85b**):



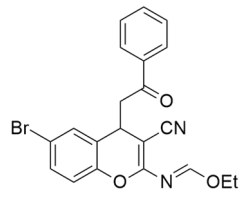
Triethyl orthoformate (8 equiv.; 2.59 g, 17.5 mmol, 2.91 mL) and acetic anhydride (3 equiv.; 0.67 g, 6.57 mmol, 621 μL), were added to chromene **2.39c** (0.81 g, 2.19 mmol and the mixture was refluxed for 20 minutes. After consumption of the starting material **2.39c** (confirmed by TLC, AcOEt/*n*-hexane 1:1), 8 mL of *n*-hexane were added to the mixture. The brown solution led to a suspension after standing in an ice bath for 2 hours. The beige solid was filtered, washed with cold *n*-hexane and dried. The product was identified by ^{1}H, ^{13}C and IR, as compound **2.85b** (1.95 mmol, 0.83 g, 89 %).

Ethyl *N*-(4-(2-(4-chlorophenyl)-2-oxoethyl)-3-cyano-4*H*-chromen-2-yl)formimidate (**2.85c**):



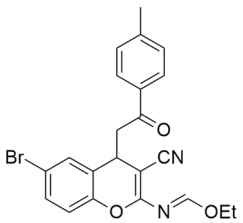
Triethyl orthoformate (8 equiv.; 1.80 g, 12.2 mmol, 2.03 mL) and acetic anhydride (3 equiv.; 0.47 g, 4.59 mmol, 434μL), were added to chromene **2.39d** (0.50 g, 1.53 mmol and the mixture was refluxed for 30 minutes. After consumption of the starting material **2.39d** (confirmed by TLC, AcOEt/*n*-hexane 1:1), 8 mL of *n*-hexane were added to the mixture. The brown solution led to a suspension after standing in an ice bath for 1 hour. The beige solid was filtered, washed with cold *n*-hexane and dried. The product was identified by ^{1}H, ^{13}C and IR, as compound **2.85c** (1.45 mmol, 0.55 g, 95 %).

Ethyl *N*-(6-bromo-3-cyano-4-(2-oxo-2-phenylethyl)-4*H*-chromen-2-yl)formimidate (**2.85d**):



Triethyl orthoformate (8 equiv.; 2.58 g, 17.4 mmol, 2.90 mL) and acetic anhydride (3 equiv.; 0.66 g, 6.51 mmol, 615 μL), were added to chromene **2.39e** (0.82 g, 2.17 mmol), and the mixture was refluxedfor 35 minutes. After consumption of the starting material **2.39e** (confirmed by TLC, AcOEt/*n*-hexane 1:1), 10 mL of *n*-hexane were added to the mixture. The brown solution led to a suspension after standing in an ice bath for 2 hours. The light-pink solid was filtered, washed with cold *n*-hexane and dried. The product was identified by ^{1}H, ^{13}C and IR, as compound **2.85d** (2.07 mmol, 0.88 g, 96 %).

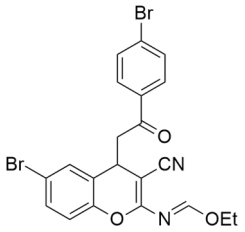
Ethyl *N*-(6-bromo-3-cyano-4-(2-oxo-2-(*p*-tolyl)ethyl)-4*H*-chromen-2-yl)formimidate (**2.85e**):



Triethyl orthoformate (8 equiv.; 4.30 g, 28.5 mmol, 4.75 mL) and acetic anhydride (3 equiv.; 1.09 g, 10.7 mmol, 1.01 mL), were added to chromene **2.39f** (1.42 g, 3.57 mmol), and the mixture was refluxed for 40 minutes. After consumption of the starting material **2.39f** (confirmed by TLC, AcOEt/*n*-hexane 1:1), 10 mL of *n*-

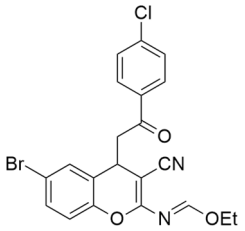
hexane were added to the mixture. The brown solution led to a suspension after standing in an ice bath for 2 hours. The light-brown solid was filtered, washed with cold *n*-hexane and dried. The product was identified by ^{1}H, ^{13}C and IR, as compound **2.85e** (3.08 mmol, 1.35 g, 86 %).

Ethyl *N*-(6-bromo-4-(2-(4-bromophenyl)-2-oxoethyl)-3-cyano-4*H*-chromen -2-yl)formimidate (**2.85f**):



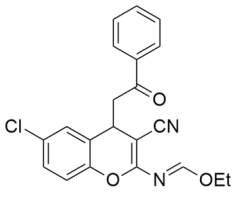
Triethyl orthoformate (8 equiv.; 6.00 g, 40.5 mmol, 6.75 mL) and acetic anhydride (3 equiv.; 1.55 g, 15.2 mmol, 1.43 mL), were added to chromene **2.39g** (2.27 g, 5.06 mmol), and the mixture was refluxed for 30 minutes. After consumption of the starting material **2.39** (confirmed by TLC, AcOEt/*n*-hexane 1:1), 10 mL of *n*-hexane were added to the mixture. The brown solution led to a suspension after standing in an ice bath for 2 hours. The white solid was filtered, washed with cold *n*-hexane and dried. The product was identified by ^{1}H, ^{13}C and IR, as compound **2.85f** (4.60 mmol, 2.32 g, 91 %).

Ethyl *N*-(6-bromo-4-(2-(4-chlorophenyl)-2-oxoethyl)-3-cyano-4*H*-chromen-2-yl) formimidate (**2.85g**):



Triethyl orthoformate (8 equiv.; 4.02 g, 27.2 mmol, 4.50 mL) and acetic anhydride (3 equiv.; 1.55 g, 10.2 mmol, 961 μL), were added to chromene **2.39h** (1.37 g, 3.39 mmol) and the mixture was refluxed for 30 minutes. After consumption of the starting material **2.39h** (confirmed by TLC, AcOEt/*n*-hexane 1:1), 10 mL of *n*-hexane were added to the mixture. The brown solution led to a suspension after standing in an ice bath for 2 hours. The beige solid was filtered, washed with cold *n*-hexane and dried. The product was identified by ^{1}H, ^{13}C and IR, as compound **2.85g** (3.09 mmol, 1.42 g, 91 %).

Ethyl *N*-(6-chloro-3-cyano-4-(2-oxo-2-phenylethyl)-4*H*-chromen-2-yl)formi midate (**2.85h**):



Triethyl orthoformate (8 equiv.; 3.56 g, 24.0 mmol, 4.00 mL) and acetic anhydride (0.92 g, 9.0 mmol, 851 μL), were added to chromene **2.39i** (0.97 g, 3.00 mmol), and the mixture was refluxed for 30 minutes. After consumption of the starting material **2.39i** (confirmed by TLC, AcOEt/*n*-hexane 1:1), 10 mL of *n*-hexane were added to the mixture. The brown solution led to a suspension after standing in an ice bath for 2 hours. The beige solid was filtered, washed with cold *n*-hexane and dried. The product was identified by ^{1}H, ^{13}C and IR, as compound **2.85g** (2.61 mmol, 1.00 g, 87 %).

General procedure for the synthesis of 1-substituted 5-(2-hydroxyaryl)-7-arylpyrido[2,3-*d*]pyrimidin-4(1*H*)-ones (2.86):

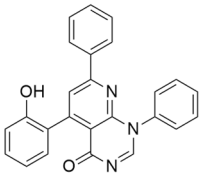
Method A: A suspension of the appropriate imidate **2.85** in ethanol (2 mL), was combined with 1-2 equivalents of the appropriate amine and 0.2-0.5 equivalents of acetic acid, and the mixture was stirred at 40-80 °C. After 1-20 hours, the suspension was cooled to room temperature for 5 minutes, and than in an ice bath for 2 hours or at 4 °C overnight. The suspension was filtered, washed with cold ethanol and dried. The product was identified, by ^{1}H, ^{13}Cand IR, as the corresponding pyridopyrimidinone **2.86.**

Method B: A suspension of the appropriate imidate **2.85** in ethanol (2 mL), was combined with 1-2 equivalents of the appropriate amine and the mixture was stirred at 40-80 °C. After 1-142 hours, the suspension was cooled to room temperature for 5 minutes, and then in an ice bath for 2 hours or at 4 °C overnight. The suspension was filtered, washed with cold ethanol, and dried. The product was identified, by ^{1}H, ^{13}Cand IR, as the corresponding pyridopyrimidinone **2.86.**

Method C: A suspension of the appropriate amidine **2.87** in ethanol (2 mL), was combined with 0.5 equivalents of acetic acid, and the mixture was stirred at 40-80 °C for 1-20 hours. the suspension was cooled to room temperature for 5 minutes, and then in an ice bath for 2 hours or at 4 °C overnight. The suspension was filtered, washed with cold ethanol and dried. The product was identified, by ^{1}H, ^{13}C and IR, as the corresponding pyridopyrimidinone **2.86.**

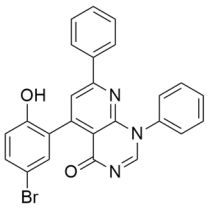
For method C, the product (mmol), as well as the reaction yield presented, are calculated assuming that all the crude product used as starting material was the corresponding amidine **2.87**.

5-(2-Hydroxyphenyl)-1,7-diphenylpyrido[2,3-*d*]pyrimidin-4(1*H*)-one (**2.86a**):



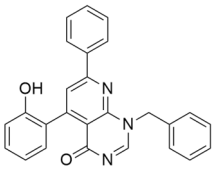
Compound **2.86a** was prepared using method B. A suspension of imidate **2.85a** (0.15 g, 0.43 mmol) in ethanol (2 mL), was combined with 1.2 equivalents of aniline (0.05 g, 052 mmol, 47 μL) and the mixture was stirred at 40 °C. After 142 hours, the light-brown suspension was cooled to room temperature for 5 minutes, and then in an ice bath for 2 hours. The light-yellow suspension was filtered, washed with cold ethanol and dried. The light-yellow solid was identified by ^{1}H, ^{13}C and IR, as pyridopyrimidinone **2.86a** (0.07 g, 0.18 mmol, 41 %)**.**

5-(5-Bromo-2-hydroxyphenyl)-1,7-diphenylpyrido[2,3-*d*]pyrimidin-4(1*H*)-one (**2.86b**):



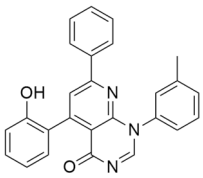
Compound **2.86b** was prepared using method A. A suspension of imidate **2.85d** (0.15 g, 0.35 mmol) in ethanol (2 mL) was combined with 1.5 equivalents of aniline (0.05 g, 0.51 mmol, 48 μL) and 0.5 equivalents of acetic acid (10 μL, 0.01 g, 0.18 mmol) and the mixture was stirred at 80 °C. After 4 hours and 30 minutes, the yellow suspension was cooled to room temperature for 5 minutes, and then in an ice bath for 2 hours. The suspension was filtered, washed with cold ethanol and dried. The yellow solid was identified, by ^{1}H, ^{13}C and IR, as pyridopyrimidinone**2.86b** (0.03 g, 0.06 mmol, 16 %)**.**

1-Benzyl-5-(2-hydroxyphenyl)-7-phenylpyrido[2,3-*d*]pyrimidin-4(1*H*)-one (**2.86c**):



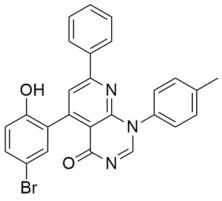
Compound **2.86c** was prepared using method A. A suspension of imidate **2.85a** (0.15 g, 0.43 mmol) in ethanol (2 mL), was combined with 1 equivalent of benzylamine (0.04 g, 0.43 mmol, 45 μL) and 0.5 equivalents of acetic acid (12 μL, 0.01 g, 0.21 mmol) and the mixture was stirred at 80 °C. After 5 hours and 30 minutes, the light-brown suspension was cooled to room temperature for 5 minutes, and then in an ice bath for 2 hours. The suspension was filtered, washed with cold ethanol and dried. The product was identified, by ^{1}H, ^{13}C and IR, as pyridopyrimidinone **2.86c** (0.03 g, 0.08 mmol, 19 %)**.**

5-(2-Hydroxyphenyl)-7-phenyl-1-(*m*-tolyl)pyrido[2,3-*d*]pyrimidin-4(1*H*)-one (**2.86d**):



Compound **2.86d** was prepared using method A. A suspension of imidate **2.85d** (0.15 g, 0.43 mmol) in ethanol (2 mL), was combined with 1.2 equivalents of m-toluidine (0.07 g, 0.52 mmol, 71 μL) and 0.5 equivalents of acetic acid (13 μL, 0.01 g, 0.17 mmol) and the mixture was stirred at 80 °C. After 2 hours and 15 minutes, the light-brown suspension was cooled to room temperature for 5 minutes, and then at 4 °C overnight. The suspension was then filtered, washed with cold ethanol, and dried. The light-brown solid was identified, by ^{1}H, ^{13}C and IR, as pyridopyrimidinone **2.86d** (0.04 g, 0.09 mmol, 27 %)**.**

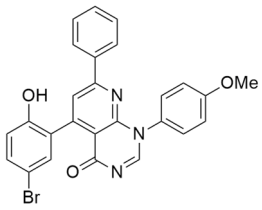
5-(5-Bromo-2-hydroxyphenyl)-7-phenyl-1-(*p*-tolyl)pyrido[2,3-*d*]pyrimidin-4(1*H*)-one (**2.86e**):



Compound **2.86e** was prepared using method A. A suspension of imidate **2.85d** (0.15 g, 0.35 mmol) in ethanol (2 mL), was combined with 1.2 equivalents of *p*-toluidine (0.05 g, 0.43 mmol) and 0.5 equivalents of acetic acid (10 μL, 0.01 g, 0.18 mmol) and the mixture was stirred at 80 °C. After 3 hours and 30 minutes,

the yellow suspension was cooled to room temperature for 5 minutes, and then in an ice bath for 2 hours. The suspension was filtered, washed with cold ethanol and dried. The yellow solid was identified, by ^{1}H, ^{13}C and IR, as pyridopyrimidinone **2.86e** (0.05 g, 0.10 mmol, 28 %)**.**

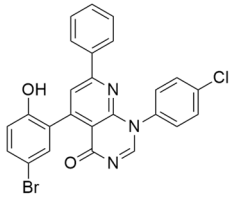
5-(5-Bromo-2-hydroxyphenyl)-1-(4-methoxyphenyl)-7-phenylpyrido[2,3-*d*]pyrimidin-4(1*H*)-one (**2.86f**):



Compound **2.86f** was prepared using method C. A suspension of the crude product isolated in the synthesis of amidine **2.87f** (0.12 g, 0.24 mmol) in ethanol (2 mL) was stirred at 80 °C for 18 hours and 15 minutes. The yellow suspension was cooled to room temperature for 5 minutes, and then in an ice bath for 2 hours. The suspension was filtered, washed with cold ethanol, and dried. The yellow solid was identified, by ^{1}H, ^{13}C and IR, as pyridopyrimidinone **2.86f** (0.06 g, 0.12 mmol, 49%)**.**

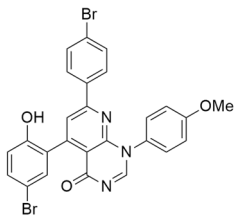
5-(5-Bromo-2-hydroxyphenyl)-1-(4-chlorophenyl)-7-phenylpyrido[2,3-*d*]pyrimidin-4(1*H*)-one (**2.86g**):

Compound **2.86g** was prepared using method C. A suspension of the crude product isolated in the



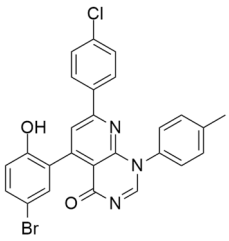
synthesis of amidine **2.87h** (0.09 g, 0.17 mmol) in ethanol (2 mL), was stirred at 80 °C for 14 hours and 40 minutes. The yellow suspension was cooled to room temperature for 5 minutes, and then in an ice bath for 2 hours. The suspension was filtered, washed with cold ethanol, and dried. The light-yellow solid was identified, by ^{1}H, ^{13}C and IR, as pyridopyrimidinone **2.86g** (0.01 g, 0.02 mmol, 13 %)**.**

5-(5-Bromo-2-hydroxyphenyl)-7-(4-bromophenyl)-1-(4-methoxyphenyl)pyrido[2,3-*d*]pyrimidin-4(1*H*)-one (**2.86h**):



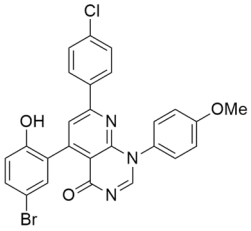
Compound **2.86h** was prepared using method A. A suspension of imidate **2.85f** (0.15 g, 0.30 mmol) in ethanol (2 mL), was combined with 2 equivalents of *p*-methoxyaniline (0.07 g, 0.60 mmol) and 0.5 equivalents of acetic acid (9 μL, 0.01 g, 0.15 mmol) and the mixture was stirred at 80 °C. After 2 hours, the light-brown suspension was cooled to room temperature for 5 minutes, and then at 4 °C overnight. The suspension was filtered, washed with cold ethanol, and dried. The light-grey solid was identified by ^{1}H,^{13}C and IR, as pyridopyrimidinone **2.86h** (0.05 g, 0.08 mmol, 26 %)**.**

5-(5-Bromo-2-hydroxyphenyl)-7-(4-chlorophenyl)-1-(*p*-tolyl)pyrido[2,3-*d*]pyrimidin-4(1*H*)-one (**2.86i**):



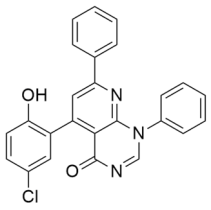
Compound **2.86i** was prepared using method A. A suspension of imidate **2.85g** (0.15 g, 0.33 mmol) in ethanol (2 mL) was combined with 1.5 equivalents of *p*-toluidine (0.05 g, 0.49 mmol) and 0.5 equivalents of acetic acid (9 μL, 0.01 g, 0.16 mmol) and the mixture was stirred at 80 °C. After 22 hours, the light-brown suspension was cooled to room temperature for 5 minutes, and then at 4 °C overnight. The suspension was filtered, washed with cold ethanol, and dried. The light-yellow solid was identified by ^{1}H,^{13}C and IR, as pyridopyrimidinone**2.86i** (0.05 g, 0.09 mmol, 27 %)**.**

5-(5-bromo-2-hydroxyphenyl)-7-(4-chlorophenyl)-1-(4-methoxyphenyl)pyrido[2,3-*d*]pyrimidin-4(1*H*)-one (**2.86j**):



Compound **2.86j** was prepared using method A. A suspension of imidate **2.85g** (0.15 g, 0.33 mmol) in ethanol (2 mL), was combined with 1.5 equivalents of *p*-methoxyaniline (0.05 g, 0.60 mmol) and 0.5 equivalents of acetic acid (9 μL, 0.01 g, 0.16 mmol) and the mixture was stirred at 80 °C. After 2 hours and 30 minutes, the orange suspension was cooled to room temperature for 5 minutes, and then at 4 °C overnight. The suspension was filtered, washed with cold ethanol, and dried. The light-orange solid was identified by ^{1}H, ^{13}C and IR, as pyridopyrimidinone **2.86j** (0.04 g, 0.07 mmol, 22 %).

5-(5-chloro-2-hydroxyphenyl)-1-(4-methoxyphenyl)-7-phenylpyrido[2,3-*d*]pyrimidin-4(1*H*)-one (**2.86k**):



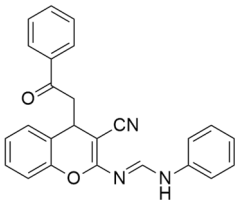
Compound **2.86k** was prepared using method C. A suspension of the crude product from the synthesis of amidine **2.87m** (0.17 g, 0.38 mmol) in ethanol (2 mL) was stirred at 80 °C for 4 hours, in the presence of 0.2 equivalents of acetic acid (0.001 g, 0.04 mmol, 2 μL). The yellow suspension was cooled to room temperature for 5 minutes, and then in an ice bath for 2 hours. The suspension was filtered, washed with cold ethanol and dried. The light-yellow solid was identified by ^{1}H,^{13}C and IR, as pyridopyrimidinone **2.86k** (0.12 g, 0.25 mmol, 65 %).

General procedure for the synthesis of N-(3-cyano-4-(2-oxo-2-arylethyl)-4*H*-chromen-2-yl)-*N*-arylformimidamides (2.87):

A suspension of the selected imidate **2.85** in ethanol/water 1:1 was combined with 2 equivalents of the appropriate amine and 0.5 equivalents of acetic acid, and the mixture was stirred at 50-80 °C. After the

consumption of the starting material **2.85** (by TLC, AcOEt/*n*-hexane 1:1), the dense suspension was cooled to room temperature for 5 minutes, and then in an ice bath for 1-2 hours. The suspension was filtered, washed with cold ethanol and water and a few drops of diethyl ether, and dried. The solid was identified as the corresponding pure amidine **2.87**, by ^{1}H, ^{13}C, IR and Mp..

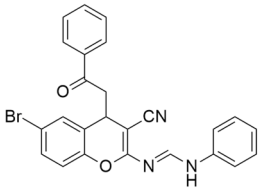
N-(3-Cyano-4-(2-oxo-2-phenylethyl)-4*H*-chromen-2-yl)-*N*-phenylformimidamide (**2.87a**):



A suspension of imidate **2.85a** (0.15 g, 0.43 mmol), in ethanol/water 1:1 (2 mL), was combined with 2 equivalents of aniline (0.08 g, 0.87 mmol, 79 μL) and 0.5 equivalents of acetic acid (0.01 g, 0.22 mmol, 12 μL) and the mixture was stirred at 60 °C. After 25 minutes, the dense suspension was cooled to room temperature for 5 minutes, and then in an ice bath for 2 hours. The suspension was filtered, washed with cold ethanol and water, and a few drops of diethyl ether, and dried. The white solid was identified as the pure amidine **2.87a** (0.06 g, 0.14 mmol, 33%), by ^{1}H, ^{13}C, IR and Mp.

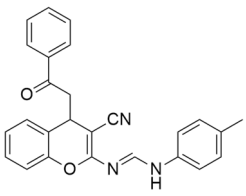
N-(6-Bromo-3-cyano-4-(2-oxo-2-phenylethyl)-4*H*-chromen-2-yl)-*N*-phe nylformi midamide (**2.87b**):

A suspension of imidate **2.85d** (0.15 g, 0.35 mmol), in ethanol/water 1:1 (2 mL), was combined with 2 equivalents of aniline (0.07 g, 0.71 mmol, 65 μL) and 0.5 equivalents of acetic acid (0.01 g, 0.18



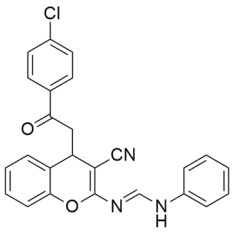
mmol, 12 μL) and the mixture was stirred at 80 °C. After 5 hours, the dense suspension was cooled to room temperature for 5 minutes, and then in an ice bath for 2 hours. The suspension was filtered, washed with cold ethanol and water, and a few drops of diethyl ether, and dried. The beige solid was identified as the pure amidine **2.87b** (0.14 g, 0.30 mmol, 85%), by ^{1}H, ^{13}C, IR and Mp..

N-(3-Cyano-4-(2-oxo-2-phenylethyl)-4*H*-chromen-2-yl)-*N*-(*p*-tolyl)formimidamide (**2.87c**):



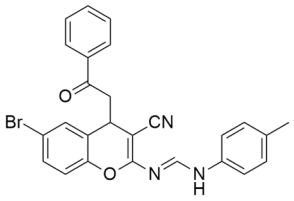
A suspension of imidate **2.85a** (0.15 g, 0.43 mmol in ethanol/water 1:1 (2 mL), was combined with 2 equivalents of *p*-toluidine (0.09 g, 0.87 mmol) and 0.5 equivalents of acetic acid (0.01 g, 0.22 mmol, 12 μL) and the mixture was stirred at 60 °C. After 25 minutes, the dense suspension was cooled to room temperature for 5 minutes, and then in an ice bath for 2 hours. The suspension was filtered, washed with cold ethanol and water, and a few drops of diethyl ether, and dried. The beige solid was identified as the pure amidine **2.87c** (0.09 g, 0.24 mmol, 56%), by ^{1}H, ^{13}C, IR and Mp..

N-(4-(2-(4-Chlorophenyl)-2-oxoethyl)-3-cyano-4*H*-chromen-2-yl)-*N*-phenyl formimidamide (**2.87f**):



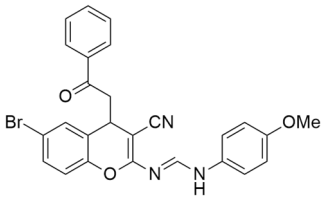
A suspension of imidate **2.85c** (0.15 g, 0.39 mmol), in ethanol/water 1:1 (2 mL), was combined with 2 equivalents of amidine (0.07 g, 0.78 mmol, 72 μL) and 0.5 equivalents of acetic acid (0.01 g, 0.22 mmol, 10 μL) and the mixture was stirred at 60 °C. After 2 hours, the dense suspension was cooled to room temperature for 5 minutes, and then in an ice bath for 2 hours. The suspension was filtered, washed with cold ethanol and water, and a few drops of diethyl ether, and dried. The beige solid was identified as the pure amidine **2.87f** (0.13 g, 0.30 mmol, 77%), by ^{1}H, ^{13}C, IR and Mp..

N-(6-Bromo-3-cyano-4-(2-oxo-2-phenylethyl)-4*H*-chromen-2-yl)-*N*-(*p*-tolyl)formimidamide (**2.87g**):



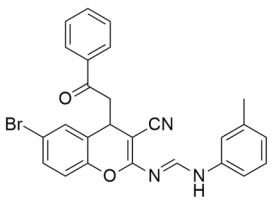
A suspension of imidate **2.85d** (0.15 g, 0.35 mmol), in ethanol/water 1:1 (2 mL), waqs combined with 2 equivalents of *p*-toluidine (0.08 g, 0.71 mmol) and 0.5 equivalents of acetic acid (0.01 g, 0.18 mmol, 12 μL) and the mixture was stirred at 60 °C. After 30 minutes, the dense suspension was cooled to room temperature for 5 minutes, and then in an ice bath for 2 hours. The suspension was filtered, washed with cold ethanol and water, and a few drops of diethyl ether, and dried. The beige solid was identified as the pure amidine **2.87g** (0.12 g, 0.24 mmol, 68%), by ^{1}H, ^{13}C, IR and Mp..

N-(6-Bromo-3-cyano-4-(2-oxo-2-phenylethyl)-4*H*-chromen-2-yl)-*N*-(4-methoxyphenyl)formimidamide (**2.87h**):



A suspension of imidate **2.85d** (0.15 g, 0.35 mmol), in ethanol/water 1:1 (2 mL), was combined with 2 equivalents of *p*-methoxyaniline (0.09 g, 0.71 mmol) and 0.5 equivalents of acetic acid (0.01 g, 0.18 mmol, 12 μL) and the mixture was stirred at 50 °C. After 2 hours, the dense suspension was cooled to room temperature for 5 minutes, and then in an ice bath for 2 hours. The suspension was filtered, washed with cold ethanol and water and a few drops of diethyl ether, and dried. The beige solid was identified as the pure amidine **2.87h** (0.14 g, 0.27 mmol, 77%), by ^{1}H, ^{13}C, IR and Mp.

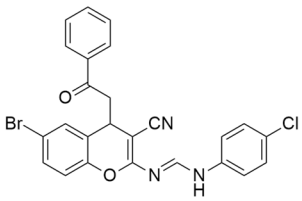
N-(6-Bromo-3-cyano-4-(2-oxo-2-phenylethyl)-4*H*-chromen-2-yl)-*N*-(m-to lyl)formimidamide (**2.87i**):



A suspension of imidate **2.85d** (0.15 g, 0.35 mmol), in ethanol/water 1:1 (2 mL), was combined with 2 equivalents of *m*-toluidine (0.08 g, 0.71 mmol, 76 μL) and 0.5 equivalents of acetic acid (0.01 g, 0.18 mmol, 12 μL) and the

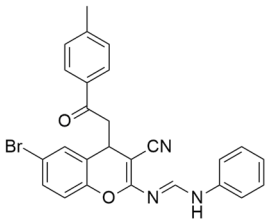
mixture was stirred at 50 °C. After 1 hour and 40 minutes, the dense suspension was cooled to room temperature for 5 minutes, and then in an ice bath for 2 hours. The suspension was filtered, washed with cold ethanol and water and a few drops of diethyl ether, and dried. The beige solid was identified as the pure amidine **2.87i** (0.13 g, 0.27 mmol, 77%), by ^{1}H, ^{13}C, IR and Mp..

N-(6-Bromo-3-cyano-4-(2-oxo-2-phenylethyl)-4*H*-chromen-2-yl)-*N*-(4-chlorophenyl)formimidamide (**2.87l**):



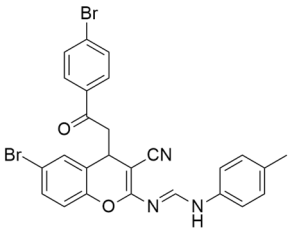
A suspension of imidate **2.85d** (0.15 g, 0.35 mmolin ethanol/water 1:1 (2 mL), was combined with 2 equivalents of *p*-chloroaniline (0.09 g, 0.71 mmol) and 0.5 equivalents of acetic acid (0.01 g, 0.18 mmol, 12 μL) and the mixture was stirred at 80 °C. After 20 minutes, the dense suspension was cooled to room temperature for 5 minutes, and then in an ice bath for 2 hours. The suspension was filtered, washed with cold ethanol and water and a few drops of diethyl ether, and dried. The beige solid was identified as the pure amidine **2.87l** (0.12 g, 0.24 mmol, 67%), by ^{1}H, ^{13}C, IR and Mp..

N-(6-Bromo-3-cyano-4-(2-oxo-2-(*p*-tolyl)ethyl)-4*H*-chromen-2-yl)-*N*-phe nylformi midamide (**2.87n**):



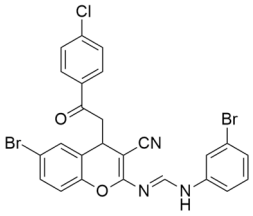
A suspension of imidate **2.85e** (0.15 g, 0.34 mmolin ethanol/water 1:1 (2 mL), was combined with 2 equivalents of aniline (0.06 g, 0.68 mmol, 62 μL) and 0.5 equivalents of acetic acid (0.01 g, 0.17 mmol, 10 μL) and the mixture was stirred at 60 °C. After 1 hour and 40 minutes, the dense suspension was cooled to room temperature for 5 minutes, and then in an ice bath for 2 hours. The suspension was filtered, washed with cold ethanol and water and a few drops of diethyl ether, and dried. The light-brown solid was identified as the pure amidine **2.87n** (0.08 g, 0.16 mmol, 48%), by ^{1}H, ^{13}C, IR and Mp..

N-(6-Bromo-4-(2-(4-bromophenyl)-2-oxoethyl)-3-cyano-4*H*-chromen-2-yl)-*N*-(*p*-tolyl)formimidamide (**2.87q**):



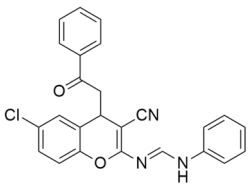
A suspension of imidate **2.85f** (0.15 g, 0.30 mmol), in ethanol/water 1:1 (2 mL), was combined with 2 equivalents of *p*-toluidine (0.06 g, 0.60 mmol) and 0.5 equivalents of acetic acid (0.01 g, 0.15 mmol, 9 μL) and the mixture was stirred at 80 °C. After 2 hours, the dense suspension was cooled to room temperature for 5 minutes, and then in an ice bath for 2 hours. The suspension was filtered, washed with cold ethanol and water, and a few drops of diethyl ether, and dried. The light-yellow solid was identified as the pure amidine **2.87q** (0.11 g, 0.20 mmol, 68%), by ^{1}H, ^{13}C, IR and Mp..

N-(6-Bromo-4-(2-(4-chlorophenyl)-2-oxoethyl)-3-cyano-4*H*-chromen-2-yl)-*N*-(3-bromophenyl) formimidamide (**2.87y**):



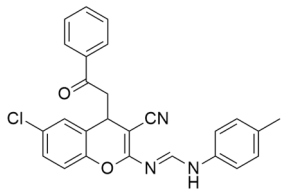
A suspension of imidate **2.85g** (0.15 g, 0.33 mmol), in ethanol/water 1:1 (2 mL), was combined with 1.5 equivalents of *m*-bromoaniline (0.08 g, 0.49 mmol, 53 μL) and 0.5 equivalents of acetic acid (0.01 g, 0.16 mmol, 9 μL) and the mixture was stirred at 80 °C. After 15 hours and 30 minutes, the dense suspension was cooled to room temperature for 5 minutes, and then in an ice bath for 2 hours. The suspension was filtered, washed with cold ethanol and water, and a few drops of diethyl ether, and dried. The light-yellow solid was identified as the pure amidine **2.87y** (0.11 g, 0.19 mmol, 57%), by ^{1}H, ^{13}C, IR and Mp..

N-(6-Chloro-3-cyano-4-(2-oxo-2-phenylethyl)-4*H*-chromen-2-yl)-*N*-phenylformimidamide (**2.87z**):



A suspension of imidate **2.85h** (0.15 g, 0.39 mmol), in ethanol/water 1:1 (2 mL), was combined with 2 equivalents of aniline (0.07 g, 0.79 mmol, 72 μL) and 0.5 equivalents of acetic acid (0.01 g, 0.20 mmol, 11 μL) and the mixture was stirred at 80 °C. After 3 hours and 10 minutes, the dense suspension was cooled to room temperature for 5 minutes, and then in an ice bath for 2 hours. The suspension was filtered and washed with cold ethanol and water and a few drops of diethyl ether, and dried. The beige solid was identified as the pure amidine**2.87z** (0.12 g, 0.29 mmol, 75%), by ^{1}H, ^{13}C, IR and Mp.

N-(6-Chloro-3-cyano-4-(2-oxo-2-phenylethyl)-4*H*-chromen-2-yl)-*N*-(*p*-tolyl)formimidamide (**2.87a'**):



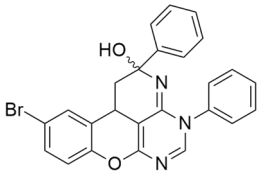
A suspension of imidate **2.85h** (0.15 g, 0.39 mmol),), in ethanol/water 1:1 (2 mL), was combined with 2 equivalents of *p*-toluidine (0.08 g, 0.79 mmol) and 0.5 equivalents of acetic acid (0.01 g, 0.20 mmol, 11 μL) and the mixture was stirred at 80 °C. After 3 hours, the dense suspension was cooled to room temperature for 5 minutes, and then in an ice bath for 2 hours. The suspension was filtered, washed with cold ethanol and water, and a few drops of diethyl ether, and dried. The beige solid was identified as the pure amidine **2.87a'** (0.10 g, 0.23 mmol, 59 %), by ^{1}H, ^{13}C, IR and Mp..

General procedure for the synthesis of 2,4-diaryl-1,2,4,11b-tetrahydro-7-oxa-3,4,6-triazabenzo[*de*]anthracen-2-ol(2.88):

A suspension of the appropriate amidine **2.87** in ethanol was combined with 1 equivalent of DBU and the suspension was stirred at room temperature for 15.5-19.5 hours. The suspension slowly turned into

an orange solution and then into an orange suspension. The suspension was cooled in an ice bath for 2-5 hours. The solid was filtered, washed with cold ethanol and a few drops of diethyl ether and dried. The product was identified, by ^{1}H, ^{13}C and IR, as the corresponding compound **2.88**, in a diastereoisomeric mixture.

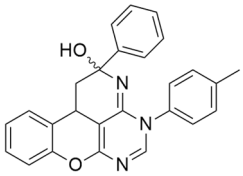
10-Bromo-2,4-diphenyl-1,2,4,11b-tetrahydro-7-oxa-3,4,6-triazabenzo[*de*]anthracen-2-ol (**2.88a**):



A suspension of amidine **2.87b** (0.13 g, 0.28 mmol) in ethanol (2 mL) was combined with 1 equivalent of DBU (0.04 g, 0.28 mmol, 31 μL) and the suspension was stirred at room temperature for 19 hours and 30 minutes The suspension slowly turned into an orange solution and then into an orange suspension. The suspension was cooled in an ice bath for 2 hours. The solid was filtered, washed with cold ethanol and a few drops of diethyl ether and dried. The beige solid was identified, by ^{1}H, ^{13}C and IR, as compound **2.88a** (0.08 g, 0.17 mmol, 60 %) in a diastereoisomeric mixture.

2-phenyl-4-(*p*-tolyl)-1,2,4,11b-tetrahydro-7-oxa-3,4,6-triazabenzo[*de*]anthracen-2-ol (**2.88b**):

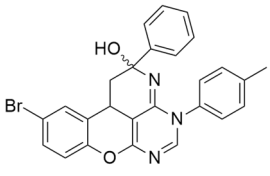
A suspension of amidine **2.87c** (0.03 g, 0.08 mmol) in ethanol (1 mL) was combined with 1 equivalent of DBU (0.01 g, 0.08 mmol, 12 μL) and the suspension was stirred at room temperature for 15 hours



and 30 minutes The suspension slowly turned into an orange solution and then into an orange suspension. The suspension was cooled in an ice bath for 5 hours. The solid was filtered, washed with cold ethanol and a few drops of diethyl ether and dried. The beige solid was identified, by ^{1}H, ^{13}C and IR, as compound **2.88a** (0.01 g, 0.03 mmol, 41%) in a diastereoisomeric mixture.

10-Bromo-2-phenyl-4-(*p*-tolyl)-1,2,4,11b-tetrahydro-7-oxa-3,4,6-triazabenzo[*de*]anthracen-2-ol (**2.88c**):

A suspension of amidine **2.87g** (0.10 g, 0.31 mmol) in ethanol (2 mL) was combined with 1 equivalent



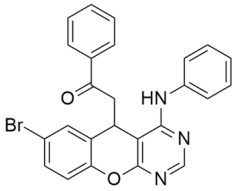
of DBU (0.05 g, 0.28 mmol, 42 μL) and the suspension was stirred at room temperature for 16 hours and 30 minutes. The suspension slowly turned into an orange solution and then into an orange suspension. The suspension was cooled in an ice bath for 2 hours. The solid was filtered, washed with cold ethanol and a few drops of diethyl ether and dried. The beige solid was identified by ^{1}H, ^{13}C and IR, as compound **2.88c** (0.06 g, 0.13 mmol, 42 %) in a diastereoisomeric mixture.

General procedure for the synthesis of 1-aryl-2-(4-(arylamino)-5*H*-chromeno[2,3-*d*]pyrimidin-5-yl)ethanones (2.89):

A suspension of either the appropriate pure amidine **2.87** or the crude product from the synthesis of amidine **2.87**, in ethanol, was combined with a 2M aqueous solution of NaOH and the mixture was stirred at room temperature for 3-24 hours. The consumption of the starting material **2.87** was confirmed by TLC (AcOEt/*n*-hexane 2:1), and the suspension was filtered, washed with a mixture of cold ethanol and water (1:1 v/v), and a few drops of diethyl ether. After drying overnight, the solid was identified as the desired product **2.89**, by ^{1}H, ^{13}C, IR and Mp.

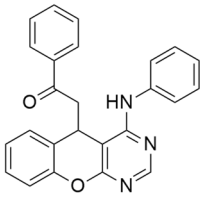
For the cases where the crude product from the synthesis of amidine was used, the reaction yield was calculated assuming that the amidine was pure.

2-(7-Bromo-4-(phenylamino)-5*H*-chromeno[2,3-*d*]pyrimidin-5-yl)-1-phenylethanone (**2.89a**):



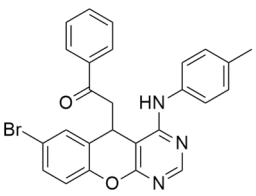
A suspension of amidine **2.87b** (0.14 g, 0.29 mmol) in ethanol (0.5 mL), was combined with a 2M aqueous solution of NaOH (1.5 mL) and the mixture was stirred at room temperature for 7 hours and 30 minutes. The suspension was filtered, washed with a mixture of cold ethanol and water (1:1 v/v) and a few drops of diethyl ether. After drying overnight, the white solid was identified as **2.89a** (0.07 g, 0.15 mmol, 53 %), by ^{1}H, ^{13}C, IR and Mp..

1-Phenyl-2-(4-(phenylamino)-5*H*-chromeno[2,3-*d*]pyrimidin-5-yl)ethanone (**2.89b**):



A suspension of amidine **2.87a** (0.02 g, 0.05 mmol) in ethanol (150 μL) was combined with a 2M aqueous solution of NaOH (600 μL) and the mixture was stirred at room temperature for 16 hours and 30 minutes. The suspension was filtered, washed with a mixture of cold ethanol and water (1:1 v/v) and a few drops of diethyl ether. After drying overnight, the light-orange solid was identified as **2.89b** (3 mg, 0.008 mmol, 17%), by ^{1}H and ^{13}C.

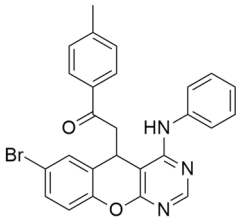
2-(7-Bromo-4-(phenylamino)-5*H*-chromeno[2,3-*d*]pyrimidin-5-yl)-1-phenyletha none (**2.89c**):



A suspension of amidine **2.87g** (0.02 g, 0.05 mmol) in ethanol (200 μL), was combined with a 2M aqueous solution of NaOH (200 μL) and the mixture was stirred at room temperature for 14 hours and 20 minutes. The suspension was filtered, washed with a mixture of cold ethanol and water (1:1 v/v) and a few

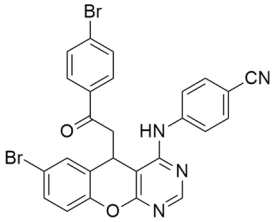
drops of diethyl ether. After drying overnight, the white solid was identified as **2.89c** (0.02 g, 0.03 mmol, 65 %), by ^{1}H, ^{13}C, IR and Mp.

2-(7-Bromo-4-(phenylamino)-5*H*-chromeno[2,3-*d*]pyrimidin-5-yl)-1-(*p*-tolyl)etha none (**2.89d**):



A suspension of amidine **2.87n** (0.05 g, 0.11 mmol) in ethanol (1 mL), was combined with a 2M aqueous solution of NaOH (330 μL) and the mixture was stirred at room temperature for 13 hours and 30 minutes. The suspension was filtered, washed with a mixture of cold ethanol and water (1:1 v/v) and a few drops of diethyl ether. After drying overnight, the white solid was identified as **2.89d** (0.02 g, 0.04 mmol, 42 %), by ^{1}H, ^{13}C, IR and Mp.

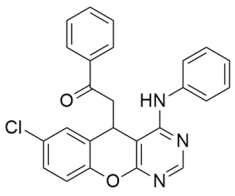
4-((7-Bromo-5-(2-(4-bromophenyl)-2-oxoethyl)-5*H*-chromeno[2,3-*d*]pyrimidin-4-yl)amino)benzonitrile (**2.89h**):



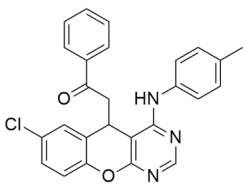
A suspension of the crude product from the synthesis of *N*-(6-bromo-4-(2(4-bromophenyl)-2-oxoethyl)-3-cyano-4*H*-chromen-2-yl)-*N*-(4-cyanophenyl)formimidamide (0.07 g, 0.11 mmol) in ethanol (1 mL), was combined with a 2M aqueous solution of NaOH (330 μL) and the mixture was stirred at room temperature for 14 hours. The suspension was filtered, washed with a mixture of cold ethanol and water (1:1 v/v) and a few drops of diethyl ether. After drying overnight and recrystallization from DCM/*n*-hexane 3:1, the light-yellow solid was identified as **2.89h** (0.02 g, 0.03 mmol, 23 %), by ^{1}H, ^{13}C, IR and Mp.

2-(7-chloro-4-(phenylamino)-5*H*-chromeno[2,3-*d*]pyrimidin-5-yl)-1-phenyletha none (**2.89j):**

A suspension of amidine **2.87z** (0.09 g, 0.21 mmol) in ethanol (500 μL), was combined with a 2M aqueous solution of NaOH (500 μL) and the mixture was stirred at room temperature for 1 hour and 40 minutes. The suspension was filtered, washed with a mixture of cold ethanol and water (1:1 v/v) and a few drops of diethyl ether. After drying overnight, the white solid was identified **2.89j** (0.06 g, 0.13 mmol, 62 %), by ^{1}H, ^{13}C, IR and Mp..



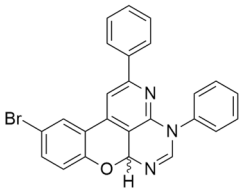
2-(7-chloro-4-(*p*-tolylamino)-5*H*-chromeno[2,3-*d*]pyrimidin-5-yl)-1-phenylethanone(**2.89k**):



A suspension of amidine **2.87a'** (0.11 g, 0.23 mmol) in ethanol (1 mL), was combined with a 2M aqueous solution of NaOH (330 μL) and the mixture was stirred at room temperature for 15 hours. The suspension was filtered, washed

with a mixture of cold ethanol and water (1:1 v/v) and a few drops of diethyl ether. After drying overnight, the white solid was identified as **2.89k** (0.06 g, 0.12 mmol, 53 %), by ^{1}H,^{13}C, IR and Mp..

Synthesis of 10-bromo-2,4-diphenyl-4,6*a*-dihydro-7-oxa-3,4,6-triazabenzo [*de*]anthra cene (2.90):

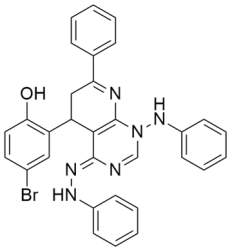


A mixture of amidine **2.87b** (0.10 g, 0.21 mmol) was added to 2 mL of ethanol and heated to 80 °C for 4 hours. The beige suspension slowly turned yellow after 30 minutes. Then, 1 equivalent of DBU (0.03 g, 0.21 mmol, 26 μL) was added to the yellow suspension that turned orange after 30 minutes. After 2 hours and 30 minutes, the dark-orange suspension was allowed to cool to room temperature for 5 minutes, and then in an ice bath for 3 hours. The light-yellow solid was filtered, washed with cold ethanol and dryied overnight. The product was identified, by ^{1}H,^{13}C and IR, as compound **2.90** (0.04 g, 0.09 mmol, 42 %).

General procedure for the synthesis of substituted 2-(7-aryl-1-(phenylamino)-4-(2-phenylhydrazono)-1,4,5,6-tetrahydropyrido[2,3-*d*]pyrimidin-5-yl)phenols (2.100):

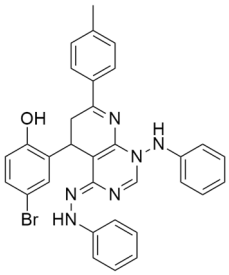
A suspension of the appropriate imidate **2.85** in methanol was combined with 1.2-2.5 equivalents of phenyl hydrazine and the mixture was stirred at room temperature for 15-21 hours. The suspension was cooled in an ice bath for 2-3 hours. The product was filtered, washed with cold methanol and a few drops of diethyl ether and dried. The solid was identified, by ^{1}H, ^{13}C and IR, as the corresponding compound **2.100.**

4-bromo-2-(7-phenyl-1-(phenylamino)-4-(2-phenylhydrazono)-1,4,5,6-tetrahydro pyrido[2,3-*d*]pyrimidin-5-yl)phenol (**2.100a**):



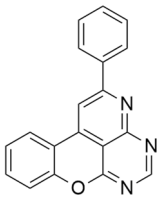
A suspension of imidate **2.85d** (0.10 g, 0.24 mmol) in methanol (1 mL), was combined with 2 equivalents of phenyl hydrazine (0.05 g, 0.48 mmol, 46 μL) and the mixture was stirred at room temperature for 21 hours. The suspension was cooled in an ice bath for 2 hours. The solid was filtered, washed with cold methanol and a few drops of diethyl ether, and was dried. The product was identified by ^{1}H, ^{13}C and IR, as compound **2.100a** (0.07 g, 0.13 mmol, 53 %).

4-bromo-2-(1-(phenylamino)-4-(2-phenylhydrazono)-7-(*p*-tolyl)-1,4,5,6-tetrahy dropyrido[2,3-*d*]pyrimidin-5-yl)phenol (**2.100b**):



A suspension of imidate **2.85e** (0.15 g, 0.34 mmol) in methanol (2 mL), was combined with 1.2 equivalents of phenyl hydrazine (0.04 g, 0.41 mmol, 40 μL) and the mixture was stirred at room temperature for 13 hours and 30 minutes. The suspension was cooled in an ice bath for 3 hours and was filtered, washed with cold methanol and a few drops of diethyl ether. The solid was dried and identified by ^{1}H,^{13}C and IR, as compound **2.100b** (0.06 g, 0.11 mmol, 32 %).

Synthesis of 2-phenyl-7-oxa-3,4,6-triazabenzo[*de*]anthracene (2.105):

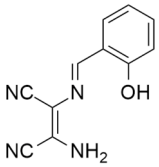


A suspension of imidate **2.85a** (0.15 g, 0.43 mmol) in ethanol (2 mL), was combined with 1.2 equivalents of ammonium acetate (0.04 g, 0.52 mmol) and the mixture was stirred at room temperature for 23 hours. The white suspension was then refluxed for 2 hours, leading to a grey suspension. The mixture was cooled to room temperature for 5 minutes, and then the solvent was removed in the rotatory evaporator. Addition diethyl ether (3 mL) to the crude product led to a grey suspension that was filtered, washed with cold ethanol and diethyl ether and dried. The product was identified by ^{1}H, ^{13}C and IR, as **2.105** (0.06 g, 0.28 mmol, 56 %).

General procedure for the preparation of 2-amino-3-(arylideneamino)maleo nitriles (2.109):

The experimental procedure was adapted from the information published in the literature (ref. 158, chapter 2). Diaminomaleonitrile was combined with 1 equivalent of the appropriate aldehyde in the minimum amount of DMSO. A catalytic amount of H_2SO_4 was added, while the mixture was vigorously stirred. A solid precipitate was generated almost instantaneously. The mixture was diluted with 15 mL of water and the dense suspension was cooled in an ice bath for 2 hours. The solid was filtered, thoroughly washed with water, ethanol and diethyl ether, and dried for 3 days. The product was identified by ^{1}H, ^{13}C, IR and Mp., as the expected imine **2.109.**

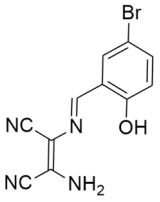
2-Amino-3-((2-hydroxybenzylidene)amino)maleonitrile (**2.109a**):



Diaminomaleonitrile (0.54 g, 5.0 mmol) and 1 equivalent of salicylaldehyde (0.61 g, 525 μL, 5.0 mmol) were combined in the minimum amount of DMSO. A catalytic amount of H_2SO_4 was added while the mixture was vigorously stirred. A solid precipitate was

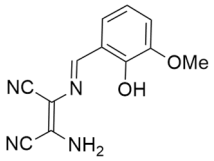
generated almost instantaneously. The mixture was diluted with 15 mL of water and the dense suspension was cooled in an ice bath for 2 hours. The solid was filtered, thoroughly washed with water, ethanol and diethyl ether, and dried for 3 days. The dark-yellow solid was identified as **2.109a** (1.03 g**,** 0.49 mmol, 97 %) by comparison with the information presented in the literature (ref. 158, chapter 2)

2-Amino-3-(5-bromo-2-hydroxybenzylidene)amino)maleonitrile (**2.109b**):



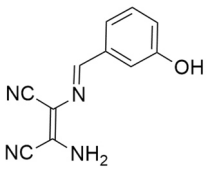
Diaminomaleonitrile (0.54 g, 5.0 mmol) and 1 equivalent of 5-bromosalicylaldehyde (1.01 g, 5.0 mmol) were combined in the minimum amount of DMSO. A catalytic amount of H_2SO_4 was added while the mixture was vigorously stirred. A solid precipitate was generated almost instantaneously. The mixture was diluted with 15 mL of water and the dense suspension was cooled in an ice bath for 2 hours. The solid was filtered, thoroughly washed with water, ethanol and diethyl ether, and dried for 3 days. The light-brown solid was identified by ^{1}H, ^{13}C and IR as **2.109b** (1.31 g**,** 0.45 mmol, 90 %).

2-Amino-3-(2-hydroxy-3-methoxybenzylidene)amino)maleonitrile (**2.109c**):



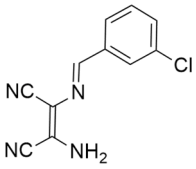
Diaminomaleonitrile (0.54 g, 5.0 mmol) and 1 equivalent of 3-methoxy salicylaldehyde (0.76 g, 5.0 mmol) were combined in the minimum amount of DMSO. A catalytic amount of H_2SO_4 was added while the mixture was vigorously stirred. A solid precipitate was generated almost instantaneously. The mixture was diluted with 15 mL of water and the dense suspension was cooled in an ice bath for 2 hours. The solid was filtered, thoroughly washed with water, ethanol and diethyl ether, and dried for 3 days. The dark-yellow solid was identified by ^{1}H, ^{13}C and IR, as **2.109c** (1.19 g**,** 0.49 mmol, 98 %).

2-Amino-3-(3-hydroxybenzylideneamino)maleonitrile (**2.109d**):



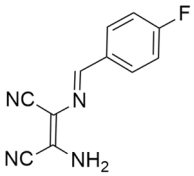
Diaminomaleonitrile (0.54 g, 5.0 mmol) and 1 equivalent of *m*-hydroxybenzaldehyde (0.61 g, 5.0 mmol) were combined in the minimum amount of DMSO. A catalytic amount of H_2SO_4 was added while the mixture was vigorously stirred. A solid precipitate was generated almost instantaneously. The mixture was diluted with 15 mL of water and the dense suspension was cooled in an ice bath for 2 hours. The solid was filtered, thoroughly washed with water, ethanol and diethyl ether, and dried for 3 days. The dark-yellow solid was identified as **2.109d** (0.88 g**,** 0.42 mmol, 83 %) by comparison with the information presented in the literature (ref. 158, chapter 2).

2-Amino-3-(3-chlorobenzylidene)amino)maleonitrile (**2.109e**):



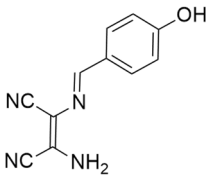
Diaminomaleonitrile (0.54 g, 5.0 mmol) and 1 equivalent of *m*-chlorobenzaldehyde (0.70 g, 5.0 mmol, 567 μL) were combined in the minimum amount of DMSO. A catalytic amount of H_2SO_4 was added while the mixture was vigorously stirred. A solid precipitate was generated almost instantaneously. The mixture was diluted with 15 mL of water and the dense suspension was cooled in an ice bath for 2 hours. The solid was filtered, thoroughly washed with water, ethanol and diethyl ether, and dried for 3 days. The dark-yellow solid was identified by ^{1}H, ^{13}C and IR, as **2.109e** (1.10 g**,** 0.48 mmol, 95 %).

2-amino-3-(4-fluorobenzylidene)amino)maleonitrile (**2.109f**):



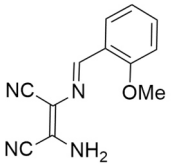
Diaminomaleonitrile (0.54 g, 5.0 mmol) and 1 equivalent of *p*-fluorbenzaldehyde (0.62 g, 5.0 mmol, 528 μL) were combined in the minimum amount of DMSO. A catalytic amount of H_2SO_4 was added while the mixture was vigorously stirred. A solid precipitate was generated almost instantaneously. The mixture was diluted with 15 mL of water and the dense suspension was cooled in an ice bath for 2 hours. The solid was filtered, thoroughly washed with water, ethanol and diethyl ether, and dried for 3 days. The dark-yellow solid was identified by ^{1}H, ^{13}C and IR, as **2.109f** (0.89 g**,** 0.42 mmol, 83 %).

2-Amino-3-(3-hydroxybenzylideneamino)maleonitrile (**2.109g**):



Diaminomaleonitrile (0.54 g, 5.0 mmol) and 1 equivalent of *p*-hydroxybenzaldehyde (0.61 g, 5.0 mmol) were combined in the minimum amount of DMSO. A catalytic amount of H_2SO_4 was added while the mixture was vigorously stirred. A solid precipitate was generated almost instantaneously. The mixture was diluted with 15 mL of water and the dense suspension was cooled in an ice bath for 2 hours. The solid was filtered, thoroughly washed with water, ethanol and diethyl ether, and dried for 3 days. The dark-yellow solid was identified as **2.109g** (0.88 g**,** 0.42 mmol, 83 %) by comparison with the information presented in the literature (ref. 158, chapter 2).

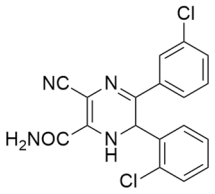
2-amino-3-(2-methoxybenzylidene)amino)maleonitrile (**2.109h**):



Diaminomaleonitrile (0.54 g, 5.0 mmol) and 1 equivalent of *o*-methoxybenzaldehyde (0.68 g, 5.0 mmol) were combined in the minimum amount of DMSO. A catalytic amount of H_2SO_4 was added while the mixture was vigorously stirred. A solid precipitate was

generated almost instantaneously. The mixture was diluted with 15 mL of water and the dense suspension was cooled in an ice bath for 2 hours. The solid was filtered, thoroughly washed with water, ethanol and diethyl ether, and dried for 3 days. The dark-yellow solid was identified by ^{1}H, ^{13}C and Ir as **2.109h** (1.02 g**,** 0.45 mmol, 90 %).

Synthesis of 6-(2-chlorophenyl)-5-(3-chlorophenyl)-3-cyano-1,6-dihydropyrazine-2-carboxamide (**2.113d**):

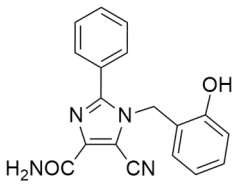


A suspension of benzylideneamine **2.109e** (0.20 g, 0.88 mmol) in ethanol (2 mL) was combined with 2 equivalents 2-chlorobenzaldehyde (0.25 g, 1.77 mmol, 199 μL) and 2 equivalents of triethylamine (0.18 g, 1.77 mmol, 246 μL) and the mixture was stirred at room temperature for 3 days. The suspension was cooled in an ice bath for 2 hours and the dark-yellow solid was filtered, washed with cold ethanol and a few drops of diethyl ether and dried. The product was identified, by ^{1}H, ^{13}C and IR as dihydropyrazine **2.113d** (0.18 g, 0.47 mmol, 53%).

General procedure for the synthesis of *2*-substituted 5-cyano-1-(2-hydroxybenzyl)-1*H*-imidazole-4-carboxamides (2.119):

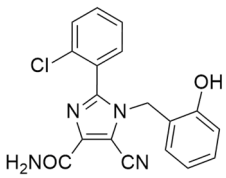
A suspension of the selected benzylideneamine **2.109** in ethanol, was combined with 1.2 equivalents of an aldehyde and 2 equivalents of triethylamine and the mixture was stirred at room temperature for 13-22 hours. The suspension was cooled in an ice bath for 2 hours. The solid was filtered, washed with cold methanol, ethanol and diethyl ether, and dried. The product was identified as the substituted imidazole **2.119**.

5-Cyano-1-(2-hydroxybenzyl)-2-phenyl-1*H*-imidazole-4-carboxamide (**2.119a**):



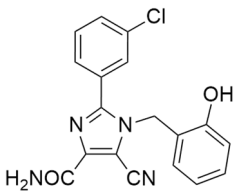
A suspension of benzylideneamine **2.109a** (0.20 g, 0.94 mmolin ethanol, was combined with 1.2 equivalents of benzaldehyde (0.12 g, 1.13 mmol, 115 μL) and 2 equivalents of triethylamine (0.19 g, 1.88 mmol, 262 μL) and the mixture was stirred at room temperature for 16 hours. The suspension was cooled in an ice bath for 2 hours. The light-brown solid was filtered, washed with cold methanol, ethanol and diethyl ether, and dried. The product was identified by ^{1}H, ^{13}C, IR and Mp, as the substituted imidazole **2.119a** (0.08 g, 0.25 mmol, 26 %).

2-(2-Chlorophenyl)-5-cyano-1-(2-hydroxybenzyl)-1*H*-imidazole-4-carboxamide (**2.119b**):



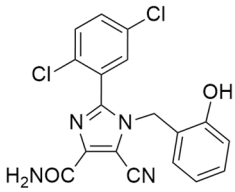
A suspension of benzylideneamine **2.109a** (0.20 g, 0.94 mmol) in ethanol, was combined with 1.2 equivalents of 2-chlorobenzaldehyde (0.16 g, 1.13 mmol, 128 μL) and 2 equivalents of triethylamine (0.19 g, 1.88 mmol, 262 μL) and the mixture was stirred at room temperature for 16 hours and 40 minutes. The suspension was cooled in an ice bath for 2 hours. The light-pink solid was filtered, washed with cold methanol, ethanol and diethyl ether, and dried. The product was identified by ^{1}H, ^{13}C, IR and Mp, as the substituted imidazole **2.119b** (0.14 g, 0.40 mmol, 42 %).

2-(3-Chlorophenyl)-5-cyano-1-(2-hydroxybenzyl)-1*H*-imidazole-4-carboxamide (**2.119c**):



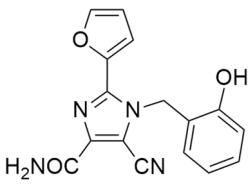
A suspension of benzylideneamine **2.109a** (0.20 g, 0.94 mmol) in ethanol, was combined with 1.2 equivalents of 3-chlorobenzaldehyde (0.16 g, 1.13 mmol, 128 μL) and 2 equivalents of triethylamine (0.19 g, 1.88 mmol, 262 μL) and the mixture was stirred at room temperature for 25 hours. The suspension was cooled in an ice bath for 2 hours. The light-pink solid was filtered, washed with cold methanol, ethanol and diethyl ether, and dried. The product was identified by ^{1}H, ^{13}C, IR and Mp, as the substituted imidazole**2.119c** (0.25 g, 0.71 mmol, 73 %).

2-(2,5-Dichlorophenyl)-5-cyano-1-(2-hydroxybenzyl)-1*H*-imidazole-4-carboxamide (**2.119d**):



A suspension of benzylideneamine **2.109a** (0.20 g, 0.94 mmol) in ethanol, was combined with 1.2 equivalents of 3-chlorobenzaldehyde (0.20 g, 1.13 mmol) and 2 equivalents of triethylamine (0.19 g, 1.88 mmol, 262 μL) and the mixture was stirred at room temperature for 17 hours. The suspension was cooled in an ice bath for 2 hours. The light-brown solid was filtered, washed with cold methanol, ethanol and diethyl ether, and dried. The product was identified by ^{1}H, ^{13}C, IR and Mp, as the substituted imidazole **2.119d** (0.14 g, 0.35 mmol, 37 %).

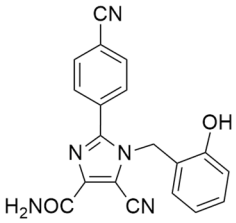
5-Cyano-2-(furan-2-yl)-1-(2-hydroxybenzyl)-1*H*-imidazole-4-carboxamide (**2.119e**):



A suspension of benzylideneamine **2.109a** (0.20 g, 0.94 mmol)) in ethanol, was combined with 1.2 equivalents of furfural (0.11 g, 1.13 mmol, 94 μL) and 2 equivalents of triethylamine (0.19 g, 1.88 mmol, 262 μL) and the mixture was stirred at room temperature for 66 hours and 30 minutes. The suspension was

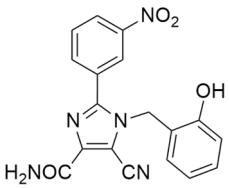
cooled in an ice bath for 2 hours. The light-brown solid was filtered, washed with cold methanol, ethanol and diethyl ether, and dried. The product was identified by ^{1}H, ^{13}C, IR and Mp, as the substituted imidazole **2.119e** (0.10 g, 0.31 mmol, 33 %).

5-cyano-2-(4-cyanophenyl)-1-(2-hydroxybenzyl)-1*H*-imidazole-4-carboxamide (**2.119f**):



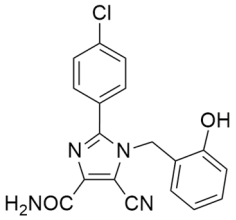
A suspension of benzylideneamine **2.109a** (0.20 g, 0.94 mmol) in ethanol, was combined with 1.2 equivalents of 4-cyanobenzaldehyde (0.15 g, 1.13 mmol) and 2 equivalents of triethylamine (0.19 g, 1.88 mmol, 262 μL) and the mixture was stirred at room temperature for 15 hours. The suspension was cooled in an ice bath for 2 hours. The grey solid was filtered, washed with cold methanol, ethanol and diethyl ether, and dried. The product was identified by ^{1}H, ^{13}C, IR and Mp, as the substituted imidazole **2.119f** (0.21 g, 0.62 mmol, 66 %).

5-Cyano-1-(2-hydroxybenzyl)-2-(3-nitrophenyl)-1*H*-imidazole-4-carboxamide (**2.119g**):



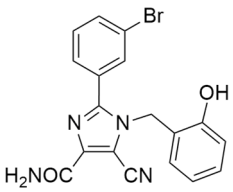
A suspension of benzylideneamine **2.109a** (0.20 g, 0.94 mmol) in ethanol, was combined with 1.2 equivalents of 3-nitrobenzaldehyde (0.17 g, 1.13 mmol) and 2 equivalents of triethylamine (0.19 g, 1.88 mmol, 262 μL) and the mixture was stirred at room temperature for 15 hours. The suspension was cooled in an ice bath for 2 hours. The grey solid was filtered, washed with cold methanol, ethanol and diethyl ether, and dried. The product was identified by ^{1}H, ^{13}C, IR and Mp, as the substituted imidazole **2.119g** (0.30 g, 0.83 mmol, 89 %).

2-(4-Chlorophenyl)-5-cyano-1-(2-hydroxybenzyl)-1*H*-imidazole-4-carboxamide (**2.119h**):



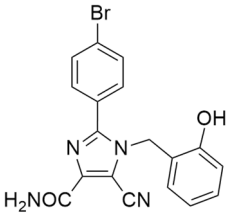
A suspension of benzylideneamine **2.109a** (0.20 g, 0.94 mmol) in ethanol, was combined with 1.2 equivalents of 3-chlorobenzaldehyde (0.16 g, 1.13 mmol) and 2 equivalents of triethylamine (0.19 g, 1.88 mmol, 262 μL) and the mixture was stirred at room temperature for 25 hours. The suspension was cooled in an ice bath for 2 hours. The light-pink solid was filtered, washed with cold methanol, ethanol and diethyl ether, and dried. The product was identified by ^{1}H, ^{13}C, IR and Mp, as the substituted imidazole **2.119h** (0.11 g, 0.30 mmol, 31 %).

2-(3-Bromophenyl)-5-cyano-1-(2-hydroxybenzyl)-1*H*-imidazole-4-carboxamide (**2.119i**):



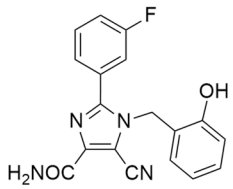
A suspension of benzylideneamine **2.109a** (0.20 g, 0.94 mmol) in ethanol, was combined with 1.2 equivalents of 3-bromobenzaldehyde (0.21 g, 1.13 mmol, 132 μL) and 2 equivalents of triethylamine (0.19 g, 1.88 mmol, 262 μL) and the mixture was stirred at room temperature for 19 hours. The suspension was cooled in an ice bath for 2 hours. The light-pink solid was filtered, washed with cold methanol, ethanol and diethyl ether, and dried. The product was identified by ^{1}H, ^{13}C, IR and Mp, as the substituted imidazole**2.119i** (0.27 g, 0.68 mmol, 73 %).

2-(4-Bromophenyl)-5-cyano-1-(2-hydroxybenzyl)-1*H*-imidazole-4-carboxamide (**2.119j**):



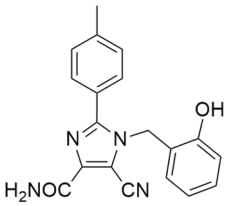
A suspension of benzylideneamine **2.109a** (0.20 g, 0.94 mmol) in ethanol, was combined with 1.2 equivalents of 3-bromobenzaldehyde (0.21 g, 1.13 mmol, 132 μL) and 2 equivalents of triethylamine (0.19 g, 1.88 mmol, 262 μL) and the mixture was stirred at room temperature for 19 hours. The suspension was cooled in an ice bath for 2 hours. The light-pink solid was filtered, washed with cold methanol, ethanol and diethyl ether, and dried. The product was identified by ^{1}H, ^{13}C, IR and Mp, as the substituted imidazole **2.119j** (0.27 g, 0.68 mmol, 73 %).

2-(4-Fluorphenyl)-5-cyano-1-(2-hydroxybenzyl)-1*H*-imidazole-4-carboxamide (**2.119k**):



A suspension of benzylideneamine **2.109a** (0.20 g, 0.94 mmol) in ethanol, was combined with 1.2 equivalents of 3-fluorobenzaldehyde (0.14 g, 1.13 mmol, 126 μL) and 2 equivalents of triethylamine (0.19 g, 1.88 mmol, 262 μL) and the mixture was stirred at room temperature for 19 hours. The suspension was cooled in an ice bath for 2 hours. The light-brown solid was filtered, washed with cold methanol, ethanol and diethyl ether, and dried. The product was identified by ^{1}H, ^{13}C, IR and Mp, as the substituted imidazole **2.119k** (0.20 g, 0.61 mmol, 65 %).

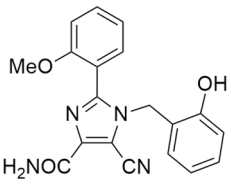
5-Cyano-1-(2-hydroxybenzyl)-2-(p-tolyl)-1*H*-imidazole-4-carboxamide (**2.119l**):



A suspension of benzylideneamine **2.109a** (0.20 g, 0.94 mmol) in ethanol, was combined with 1.2 equivalents of *p*-tolualdehyde (0.14 g, 1.13 mmol, 133 μL) and 2 equivalents of triethylamine (0.19 g, 1.88 mmol, 262 μL) and the mixture was stirred at room temperature for 13 hours. The suspension was cooled in an ice bath

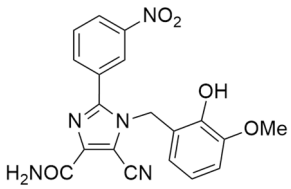
for 2 hours. The brown solid was filtered, washed with cold methanol, ethanol and diethyl ether, and dried. The product was identified by ^{1}H, ^{13}C, IR and Mp, as the substituted imidazole **2.119l** (0.14 g, 0.40 mmol, 43 %).

5-Cyano-1-(2-hydroxybenzyl)-2-(2-methoxyphenyl)-1*H*-imidazole-4-carboxamide (**2.119m**):



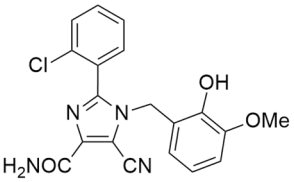
A suspension of benzylideneamine **2.109a** (0.20 g, 0.94 mmol) in ethanol, was combined with 1.2 equivalents of 2-methoxybenzaldehyde (0.15 g, 1.13 mmol) and 2 equivalents of triethylamine (0.19 g, 1.88 mmol, 262 μL) and the mixture was stirred at room temperature for 18 hours and 20 minutes. The suspension was cooled in an ice bath for 2 hours. The light-orange solid was filtered, washed with cold methanol, ethanol and diethyl ether, and dried. The product was identified by ^{1}H, ^{13}C, IR and Mp, as the substituted imidazole **2.119m** (0.13 g, 0.37 mmol, 40 %).

5-Cyano-1-(2-hydroxy-3-methoxybenzyl)-2-(3-nitrophenyl)-1*H*-imidazole-4-carboxamide (**2.119n**):



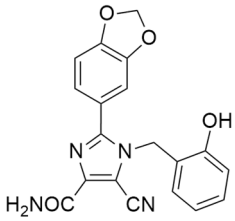
A suspension of benzylideneamine **2.109c** (0.20 g, 0.83 mmol) in ethanol, was combined with 1.2 equivalents of 3-nitrobenzaldehyde (0.15 g, 1.00 mmol, and 2 equivalents of triethylamine (0.17 g, 1.66 mmol, 230 μL) and the mixture was stirred at room temperature for 66 hours. The suspension was cooled in an ice bath for 2 hours. The beige solid was filtered, washed with cold methanol, ethanol and diethyl ether, and dried. The product was identified by ^{1}H, ^{13}C, IR and Mp, as the substituted imidazole **2.119n** (0.16 g, 0.41 mmol, 49 %).

2-(2-Chlorophenyl)-5-cyano-1-(2-hydroxy-3-methoxybenzyl)-1*H*-imi dazole-4-carboxamide (**2.119o**):



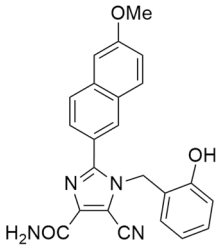
A suspension of benzylideneamine **2.109c** (0.20 g, 0.83 mmol) in ethanol, was combined with 1.2 equivalents of 2-chlorobenzaldehyde (0.14 g, 1.00 mmol, 113 μL) and 2 equivalents of triethylamine (0.17 g, 1.66 mmol, 230 μL) and the mixture was stirred at room temperature for 68 hours. The suspension was cooled in an ice bath for 2 hours. The beige solid was filtered, washed with cold methanol, ethanol and diethyl ether, and dried. The product was identified by ^{1}H, ^{13}C, IR and Mp, as the substituted imidazole **2.119o** (0.16 g, 0.42 mmol, 51 %).

2-(Benzo[*d*][1,3]dioxol-5-yl)-5-cyano-1-(2-hydroxybenzyl)-1*H*-imidazole-4-carboxamide (**2.119p**):



A suspension of benzylideneamine **2.109a** (0.20 g, 0.94 mmol) in ethanol, was combined with 1.2 equivalents of piperonal (0.17 g, 1.13 mmol) and 2 equivalents of triethylamine (0.19 g, 1.88 mmol, 262 μL) and the mixture was stirred at room temperature for 17 hours and 20 minutes. The suspension was cooled in an ice bath for 2 hours. The light-brown solid was filtered, washed with cold methanol, ethanol and diethyl ether, and dried. The product was identified by ^{1}H, ^{13}C, IR and Mp, as the substituted imidazole **2.119p** (0.09 g, 0.26 mmol, 28 %).

5-Cyano-1-(2-hydroxybenzyl)-2-(6-methoxynaphthalen-2-yl)-1*H*-imidazole-4-carboxamide (**2.119q**):



A suspension of benzylideneamine **2.109a** (0.20 g, 0.94 mmol) in ethanol, was combined with 1.2 equivalents of 6-methoxy-2-naphthaldehyde (0.21 g, 1.13 mmol) and 2 equivalents of triethylamine (0.19 g, 1.88 mmol, 262 μL) and the mixture was stirred at room temperature for 16 hours. The suspension was cooled in an ice bath for 2 hours. The light-purple solid was filtered, washed with cold methanol, ethanol and diethyl ether, and dried. The product was identified by ^{1}H, ^{13}C, IR and Mp, as the substituted imidazole **2.1191** (0.20 g, 0.51 mmol, 54 %).

References:

[1] Verdonk, M. L. *et al.* Improved protein-ligand docking using GOLD. *Proteins Struct. Funct. Genet.* **52**, 609–623 (2003).

[2] Kinoshita, T. *et al.* Inhibitor-induced structural change of the active site of human poly(ADP-ribose) polymerase. *FEBS Lett.* **556**, 43–46 (2004).

[3] Frisch, M. J. *et al.* Gaussian 09, Revision B.01. *Gaussian 09, Revis. B.01, Gaussian, Inc., Wallingford CT* 1–20 (2009).

[4] Vanquelef, E. *et al.* R.E.D. Server: a web service for deriving RESP and ESP charges and building force field libraries for new molecules and molecular fragments. *Nucleic Acids Res.* **39**, 511–517 (2011).

[5] Dupradeau, F. Y. *et al.* The R.E.D. tools: Advances in RESP and ESP charge derivation and force field library building. *Phys. Chem. Chem. Phys.* **12**, 7821–7839 (2010).

[6] Case, D. A. *et al.* The Amber biomolecular simulation programs. *J. Comput. Chem.* **26**, 1668–1688 (2005).

[7] Wang, J. *et al.* Development and testing of a general Amber force field. *J. Comput. Chem.* **25**,

1157–1174 (2004).

[8] Wang, J *et al.* Automatic atom type and bond type perception in molecular mechanical calculations. *J. Mol. Graph. Model.* **25**, 247–260 (2006).

[9] Gordon, J. C. *et al.* H++: A server for estimating pKas and adding missing hydrogens to macromolecules. *Nucleic Acids Res.* **33**, 368–371 (2005).

[10] Maier, J. A. *et al.* ff14SB: Improving the accuracy of protein side chain and backbone parameters from ff99SB. *J. Chem. Theory Comput.* **11**, 3696–3713 (2015).

[11] Götz, A. W. *et al.* Routine microsecond molecular dynamics simulations with AMBER on GPUs. 2. Explicit Solvent Particle Mesh Ewald. *J. Chem. Theory Comput.* **8**, 1542–1555 (2012).

[12] Götz, A. W. *et al.* Routine microsecond molecular dynamics simulations with AMBER on GPUs. 1. generalized born. *J. Chem. Theory Comput.* **8**, 1542–1555 (2012).

[13] Le Grand, S., Götz, A. W. & Walker, R. C. SPFP: Speed without compromise - a mixed precision model for GPU accelerated molecular dynamics simulations. *Comput. Phys. Commun.* **184**, 374–380 (2013).

[14] Darden, T., York, D. & Pedersen, L. Particle mesh Ewald: An N·log(N) method for Ewald sums in large systems. *J. Chem. Phys.* **98**, 10089–10092 (1993).

[15] Ryckaert, J.P., Ciccotti, G. & Berendsen, H. J. C. Numerical integration of the cartesian equations of motion of a system with constraints: molecular dynamics of n-alkanes. *J. Comput. Phys.* **23**, 327–341 (1977).

[16] DeLano, W. L. The PyMOL Molecular Graphics System (acessed on February, 2021). (2008).

[17] Humphrey, W., Dalke, A. & Schulten, K. VMD - Visual Molecular Dynamics. *J. Molec. Graph.* **14**, 33–38 (1996).

[18] Miller, B. R. *et al.* MMPBSA.py : an efficient program for end-state free energy calculations. *J. Chem. Theor. Comput.* **8** 3314–3321 (2012).doi:10.1021/ct300418h.

[19] Proença, F. & Costa, M. A simple and eco-friendly approach for the synthesis of 2-imino and 2-oxo-2H-chromene-3-carboxamides. *Green Chem.* **10**, 995–99 (2008).